Seismic design repair and retrofit strategies for steel roof deck diaphragms

By

John-Edward Franquet

Department of Civil Engineering and Applied Mechanics

McGill University, Montreal, Canada

October 2009

A thesis submitted to the Faculty of Graduate and

Postdoctoral Studies in partial fulfillment of the requirements

of the degree of Master of Engineering

ABSTRACT

Structural engineers will often rely on the roof diaphragm to transfer lateral seismic loads to the bracing system of single-storey structures. The implementation of capacity-based design in the NBCC 2005 has caused an increase in the diaphragm design load due to the need to use the probable capacity of the bracing system, thus resulting in thicker decks, closer connector patterns and higher construction costs.

Previous studies have shown that accounting for the in-plane flexibility of the diaphragm when calculating the overall building period can result in lower seismic forces and a more cost-efficient design. However, recent studies estimating the fundamental period of single storey structures using ambient vibration testing showed that the in-situ approximation was much shorter than that obtained using analytical means. The difference lies partially in the diaphragm stiffness characteristics which have been shown to decrease under increasing excitation amplitude. Using the diaphragm as the energy-dissipating element in the seismic force resisting system has also been investigated as this would take advantage of the diaphragm's ductility and limited overstrength; thus, lower capacity based seismic forces would result.

An experimental program on 21.0m by 7.31m diaphragm test specimens was carried out so as to investigate the dynamic properties of diaphragms including the stiffness, ductility and capacity. The specimens consisted of 20 and 22 gauge panels with nailed frame fasteners and screwed sidelap connections as well a welded and button-punch specimen. Repair strategies for diaphragms that have previously undergone inelastic deformations were devised in an attempt to restitute the original stiffness and strength and were then experimentally evaluated. Strength and stiffness experimental estimations are compared with those predicted with the Steel Deck Institute (SDI) method.

A building design comparative study was also completed. This study looks at the difference in design and cost yielded by previous and current design practice with EBF braced frames. Two alternate design methodologies, where the period is not restricted by code limitations and where the diaphragm force is limited to the equivalent shear force calculated with R_dR_o = 1.95, are also used for comparison. This study highlights the importance of incorporating the diaphragm stiffness in design and the potential cost savings.

RÉSUMÉ

Les ingénieurs en structures vont souvent compter sur l'effet diaphragme du pontage métallique du toit en acier pour transférer les charges latérales vers les contreventements dans la conception d'un bâtiment de faible hauteur. L'implantation de la méthode de conception basée sur la capacité dans le Code National du Bâtiment du Canada CNBC 2005 a causé une augmentation de la charge sismique que les diaphragmes doivent soutenir. La demande sismique n'est plus limitée à la charge statique équivalente définie dans le code ; le diaphragme doit maintenant être conçu pour la capacité nominale du système de contreventement. Cette augmentation de charge force les ingénieurs à concevoir des diaphragmes avec des tôles plus épaisses et plus de connecteurs ; ceux-ci deviennent donc plus coûteux.

Des études précédentes ont démontré que l'inclusion de la flexibilité du diaphragme dans le calcul de la période fondamentale du bâtiment contribue à réduire la demande sismique, ainsi que le coût du bâtiment. Cependant, des recherches récentes, qui estimaient la période du bâtiment en utilisant des vibrations ambiantes, ont montré que la période obtenue avec ces mesures est beaucoup plus courte que celle obtenue par calcul. Cette différence est liée en partie à la rigidité du diaphragme qui diminue en fonction de l'amplitude de l'excitation dynamique. D'autres études ont aussi considéré l'utilisation du diaphragme en tant que dissipateur d'énergie dans le système de résistance latérale. Cette méthode prendrait en considération la ductilité et l'écrouissage réel du diaphragme.

Une étude expérimentale à été mise sur pied avec des spécimens de diaphragmes en acier de 21m de long et 7.31m de large. Cette étude avait pour but d'évaluer les caractéristiques dynamiques des spécimens ; ainsi que la rigidité, ductilité et résistance des diaphragmes. La liste d'essais comportait des diaphragmes cloués et vissés de 0.76 et 0.91 mm d'épaisseur ainsi qu'un spécimen soudé et poinçonné avec un outil de sertissage. Des stratégies de réparation ont été conçues pour récupérer la résistance et rigidité du diaphragme original. Ces méthodes de réparation ont été testées expérimentalement pour évaluer leur viabilité.

Une étude comparative de conception d'un bâtiment typique de faible hauteur a aussi été complétée, examinant la différence de coût entre les méthodes de conception antérieures au CNBC 2005 et actuelles. Deux méthodes alternatives sont aussi proposées. La première ne limite pas la période à l'estimation empirique donnée par le CNB et la deuxième méthode limite la charge du diaphragme à celle évaluée avec la force équivalente statique et R_dR_o = 1.95. Cette étude démontre l'importance d'incorporer la flexibilité du diaphragme dans la conception des bâtiments et compare les épargnes éventuelles.

ACKNOWLEDGEMENTS

There are too many people that need to be thanked for all the help and support I received throughout my degree; this is just a small token of my gratitude as I know I owe you a lot more. I'd like to express my sincere gratefulness to my supervisors, Prof. Colin A. Rogers and Prof. Robert Tremblay, who embarked me on this journey and made sure, through constant moral and technical support, that I would accomplish this work with success, pride and knowledge. Thank you very much, I'll never forget it.

I have to extend my thanks to the whole diaphragm team, Robert Massarelli, Kishor Shrestha, David Ek, Derek Kozak, and William Franquet for all their help, even very late at night, during the experimental testing; everyone's input was really indispensable and the team spirit in the laboratory made it just that more pleasant to be there. Thanks to all my colleagues who were always there to offer their help when needed: Nisreen Balh, Kostadin Velchev, Gilles Comeau, Denise Morello and Damien Gilles. I couldn't have worked with a better group of individuals and I'm very grateful for this.

Thanks to all the technical staff at École Polytechnique, Patrice Bélanger, Viacheslav Koval, Denis Fortier, Marc Charbonneau who helped us with our setup and were able to bear our constant noise for the time we moved in. Thanks to Anthony Caruso, Gabriele Rotili and JF Groulx for their help in the initial construction of the setup. I can't forget to acknowledge Camelia Nedisan, who started this project and Charles-Philippe Lamarche, who was really helpful with the initial signal processing.

I'd like to recognize the financial support from several institutions without which any of this research would not have been possible: The Natural Sciences and Engineering Research Council of Canada, the Steel Structures Education Foundation, the Canadian Sheet Steel Building Institute and the Vancouver Steel Deck Diaphragm Committee (See next page). I also wish to thank the materials providers: Hilti, CANAM, Sofab and Lainco.

Lastly, I'd like to thank my family and friends who supported me throughout my whole degree without ever doubting in me. I couldn't have accomplished this without any of you. To everyone: Thank you, Merci, Dank U Well!

VANCOUVER DIAPHRAGM COMMITTEE

Structural Engineering Companies

Bianco Lam Consultants

Bogdonov Pao Associates Ltd.

Bush Bohlman

CA Boom

CWMM

Glotman Simpson Consulting Engineers

John Bryson & Partners

Krahn Engineering

Lang Structural Engineering Inc.

Mainland Engineering

Omicron Consulting Group

PJB Engineering Ltd.

Phoenix Structural Designs Ltd.

RDJ Structural

Pomeroy Engineering

Read Jones Christoffersen Ltd.

Reliable Equipment Rentals

Siefken Engineering Ltd.

Tabet Engineering Ltd.

Thomas Leung Structural Engineering Inc.

Weiler Smith Bowers Consulting Structural Engineers

Decking Installers

Rite-Way Metals Ltd.
Continental Steel Ltd.
The Beedie Group
Teck Construction LLP
Opus Building Canada Inc.
Wales McLelland Construction Co. (1988) Ltd.
ICC Integrated Cons Concepts Ltd.
Prism Construction Ltd.
Ventana Construction Corporation
Rockwell Pacific
Dominion Construction Company Inc.
Contura Building Corp.
Sun Life Financial (Real Estate Investment Division)
Porte Realty Ltd.
Overon Designs

Architectural Design

Sanford Designs Ltd.
D Forcier Designs

TABLE OF CONTENTS

LIST OF FIGURES

LIST OF TABLES

CHAPTER 1

1.0 INTRODUCTION

1.1. General Overview

Canada possesses two active seismic regions, namely the Ottawa River & St. Lawrence Valley and the Cascadia Subduction Zone, which necessitate the consideration of seismic design when conceiving new buildings or retrofitting existing structures. The latest edition of the National Building Code of Canada (NRCC, 2006) specifies that buildings must be designed using capacity design principles to resist an earthquake with a probability of exceedance of 2% in 50 years, as opposed to 10% in the previous 1995 edition (NRCC, 1995). These implementations have a large effect on the design of single-storey steel buildings.

Engineers following the most recent building code will often rely on the steel roof deck to act as a diaphragm in the seismic force resisting system (SFRS) of a single-storey building (Figure 1.1). The diaphragm would thus be designed to transfer the inertia loads induced from the roof weight, through shearing action, to the bracing bents of the structure. This in-plane load transferring capability is achieved by connecting the steel deck sheets together as well as to the underlying frame. The chord and collector elements also greatly contribute to the load transferring system. Many recent studies have been completed at École Polytechnique on steel roof deck diaphragms (Martin, 2002; Essa, 2001 ;Yang, 2003) but uncertainties concerning the dynamic characteristics and capabilities have culminated in the research project presented herein. Dissimilarities between the overall building periods obtained through ambient vibration (Tremblay *et al.*, 2008a), analysis (Lamarche, 2005) and with equations that incorporate diaphragm flexibility (Tremblay,

2002) still exist and no consensus has yet been reached on which value to use for the purpose of seismic analysis.

Single-storey buildings with roof steel decks represent a large portion of buildings in Canada and there is therefore significant interest in understanding their behaviour. Due to the increase in cost of constructing the SFRS obtained through the use of the current NBCC (NRCC, 2006) and the lack of information regarding the dynamic properties of single-storey buildings, there came a need to further previous research in the context of the new Building Code to better understand the seismic behaviour of these types of buildings as well as to devise new cost-effective design procedures that would not economically penalize single-storey structures with steel roof deck diaphragms. The overall objective of this research program is therefore to propose simple yet cost-effective design provisions in the next versions of the NBCC that result from a better comprehension of the performance of diaphragms.

1.2. Statement of Problem

The need for this testing program arose from the changes to the National Building Code of Canada, which in 2005 was revised such that capacity design principles were implemented in the code. This amendment, along with the fact that the seismic load now needs to be determined from a Uniform Hazard Spectrum with a probability of exceedance of 2% in 50 years as opposed to the peak ground acceleration with a probability of exceedance of 10% in 50 years, greatly increased the forces that the diaphragm needs to withstand. Following capacity design principles, the diaphragm needs to have sufficient elastic strength so that the means of energy dissipation in the SFRS can be sustained. Consequently, it is now required to design the diaphragm to resist the full probable resistance of the bracing system which is shown in Figure 1.1.

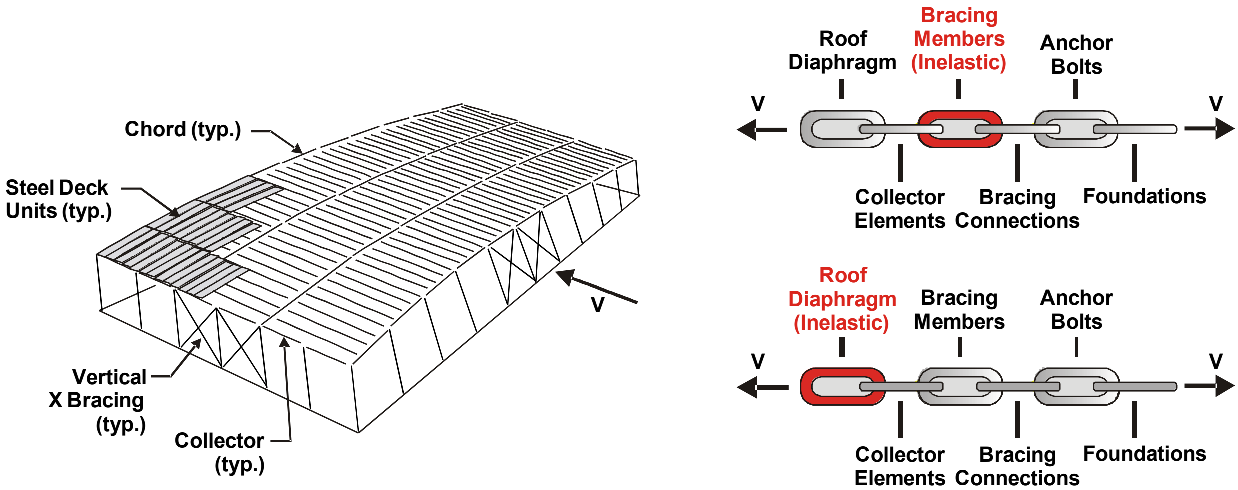

Figure 1.1 – Typical single-storey steel building structure; Weak brace design (Top); Weak diaphragm design (Bottom) (Rogers & Tremblay, 2010)

Due to the overstrength of the bracing system and the fact that slenderness often governs the design of the braces in such single-storey structures, a significant increase in fastener pattern, deck thickness and as a result, cost has resulted. The main incentive behind this research program is that modern codes fail to account for the in-plane flexibility of the diaphragm when calculating the fundamental building period. The period calculated by methods of mechanics, assuming bare frame and accounting for the in-plane flexibility of the diaphragm, could be longer than the period calculated with the empirical formula from the NBCC 2005 (NRCC, 2006) and much longer than that determined from ambient vibration tests performed on single-storey buildings. Preliminary testing performed in the context of this research project (Tremblay *et al.*, 2008) showed that the diaphragm period elongates with increasing excitation amplitude and that current design methodologies (Lutrell, 2004; CSSBI, 2006) underestimate the stiffness of diaphragms under high-amplitude excitations. Many tests have been performed on diaphragms to assess their strength and stiffness using a cantilever setup; these utilized static or pseudo-static loading and are therefore not representative of dynamic loading conditions. Investigations were consequently required to observe and characterize the dynamic and seismic behaviour of full-scale diaphragms. Specifically, examinations of the dynamic change in the period and stiffness, the distribution of inertia forces and the inelastic performance of the diaphragms were necessary.

Rogers & Tremblay (2005) have investigated the current design practice along with another methodology where a weak diaphragm, strong brace system, as shown in Figure 1.1 (Bottom), would be adopted. This could decrease the seismic load as the overstrength present in the diaphragm is very minimal. In this design methodology, energy dissipation would be achieved in a ductile manner through the diaphragm while the bracing system would be designed to carry the full probable capacity of the diaphragm. Some experimental programs, and analytical evaluations were performed to assess the viability of this design procedure as well as the ductile characteristics of diaphragms (Tremblay *et al.*, 2004; Essa *et al.*, 2001) but full-scale dynamic tests had never been performed.

Rogers & Tremblay (2003a; 2003b) investigated the inelastic performance of frame and sidelap fasteners as the inelastic behaviour of diaphragms is directly dependent on the fasteners. It was shown that nail frame fasteners and screwed sidelaps were preferred given their satisfactory performance under cyclic loading which resulted in pinched hysteretic behaviour. Button-punched sidelaps, on the other hand, would not be able to withstand large shear deformations. This is worrisome as many buildings in Canada have been built with welded and button-punched diaphragms and no retrofitting or repair strategies have yet been tested. In addition, if a design methodology is adopted where the diaphragm is used as a fuse, repair schemes must be devised so that the building can be repaired following an earthquake.

1.3. Objectives

The general objective is to develop seismic design methodologies which take into account the ductility and flexibility of steel roof deck diaphragms. The specific objectives of this research are the following:

1. Characterize the dynamic properties of the diaphragms using full-scale dynamic diaphragm testing;
2. Evaluate the effect of non-structural materials on a large-scale diaphragm test setup and compare the results with those obtained by Mastroguiseppe *et al.* (2008);
3. Develop and experimentally evaluate seismic design repair strategies for diaphragms that have previously undergone inelastic deformations;
4. Establish new seismic building design methodologies that incorporate the actual stiffness of the diaphragm, or that utilize the diaphragm as the energy-dissipating element in the SFRS;
5. Perform a comparative analysis of the new methodologies with a single-storey building with eccentric braced frames.

1.4. Scope

The research comprised dynamic and seismic tests on 10 different diaphragm configurations that replicated the most commonly found nailed and screwed fastener patterns in typical North American construction for 22 (0.76mm) and 20 (0.91mm) gauge corrugated steel roof deck diaphragms. Their inelastic load-carrying capacity, along with their dynamic characteristics, was evaluated. This thesis contains a summary of the measured parameters and the computed properties. Parameters such as the deformed shape (Appendix H & I), load-carrying capacity (Appendix F & G) and damage patterns (Appendix E) are listed. From the experimental measurements, the dynamic change in stiffness (Appendix B & C), the damping (Appendix J) and the shear force profile (Appendix H & I) were calculated for all the different configurations.

Repair procedures were devised in an attempt to recuperate the stiffness and strength of the original diaphragm and were then experimentally evaluated. The same parameters as for the new specimens are presented in this thesis. Comparisons of the measurements of stiffness and strength with the SDI predictions are also made.

The diaphragm frequency results were compared with current design equations that are used to calculate the fundamental frequency of single-storey buildings with flexible steel roof deck diaphragms. A comparative analysis for the design of a single-storey building with eccentric braced frames according to NBCC 2005 (NRCC, 2006) and CSA-S16 (2005) was accomplished by incorporating the in-plane flexibility of the diaphragm. A number of design strategies were contrasted and the comparisons are presented.

1.5. Literature Review – Building Design

The design of the seismic force resisting system for single-storey buildings involves the calculation of the earthquake loading, as per the National Building Code of Canada (NRCC, 2006), the analysis and design of the braces and other collector elements as per the Canadian Standards Association (CSA) Steel Design Standard S16 (2005) and the design of the diaphragm. Three design methodologies are currently utilized for diaphragm design. These include the Steel Deck Institute (Luttrell, 1995), the Tri-services method which is covered in the Canadian Sheet Steel Building Institute manual (CSSBI, 2006) and the Stressed Skin Diaphragm Design approach (Davies & Bryan, 1982).

1.5.1. National Building Code of Canada - 2005 Edition

The National Building Code of Canada prescribes the minimum earthquake loading that the seismic force resisting system (SFRS) must be able to withstand, which is dependent on the geographical location and soil conditions, as well as the intended use and importance of the building.

1.5.1.1. General Requirements

All elements in the SFRS must be able to withstand the earthquake loading by behaving elastically, or by having enough non-linear capacity to support the gravity loads while undergoing the inelastic deformations induced by the earthquake motion. Two methods are presented in the NBCC as acceptable for the determination of loading. These methods are the equivalent static force procedure and the dynamic analysis. However, stringent regularity conditions regarding the stiffness, mass, discontinuities and out of plane offsets in the SFRS have to be satisfied in order to use the first procedure.

1.5.1.2. Design Spectrum

The NBCC 2005 includes values of the 5% damped spectral response acceleration, $S_a(T)$, for different soil classifications where T represents the fundamental lateral period of vibration of the building or structure. The soil classification needs to be determined from the average shear wave velocity, the energy-corrected average standard penetration resistance or the average soil undrained shear strength. Site Class C $S_a(T)$ values correspond to a probability of exceedance of 2% in 50 years. To obtain the design spectral acceleration values, $S(T)$, the NBCC also specifies that an acceleration-based coefficient, F_a, and a velocity-based coefficient, F_v, [Cl. 4.1.8.4.] (NRCC, 2006) be used as follows (Equation 1-1 to 1-5):

$$S(T) = F_a S_a(0.2)\ for\ T \leq 0.2s \tag{1-1}$$

$$= F_V S_a(0.5)\ or\ F_a S_a(0.2), whichever\ is\ smaller\ for\ T = 0.5\ s \tag{1-2}$$

$$= F_V S_a(1.0)\ for\ T = 1.0\ s \tag{1-3}$$

$$= F_V S_a(2.0)\ for\ T = 2.0\ s \tag{1-4}$$

$$= \frac{F_V S_a(2.0)}{2} for\ T \geq 4.0\ s \tag{1-5}$$

These factors, F_a and F_v, are functions of the site class and the intensity of the ground motion. They account for the seismic amplification resulting from to the underlying soil profile at the building location.

1.5.1.3. Equivalent Static Force Procedure (ESFP)

The NBCC states that the minimum lateral earthquake force, V, acting on regular structures shall be calculated using Equation 1-6:

$$V = \frac{S(T_a)M_v I_E W}{R_d R_o} \tag{1-6}$$

Where:

M_v – is a factor to take into account higher mode effects on the minimum lateral earthquake force; 1.0 for low-rise buildings

I_E – is the earthquake importance factor of the structure which depends on the criticality of the designed structure

W – represents the seismic weight or permanent load on the building. This load shall be taken as the summation of 100 % of the dead load, 25% of the snow loads, 60% of the storage loads and all of the reservoir loads in the building.

R_d – Ductility-related force modification factor which reflects the ability of the structure to dissipate energy inelastically through ductile behaviour.

R_o – Overstrength-related force modification factor which accounts for the reserve in strength that the structure may exhibit.

However, the minimum lateral earthquake force may not be less than that calculated by Equation 1-7:

$$V \geq \frac{S(2.0)M_v I_E W}{R_d R_o} \tag{1-7}$$

And if the lateral resisting system displays any ductility (R_d = 1.5 or higher), there also exists an upper bound limit for the shear that is equal to Equation 1-8:

$$V \leq \frac{(\frac{2}{3})S(0.2)I_E W}{R_d R_o} \tag{1-8}$$

The lateral period that must be used to calculate this force is directly related to the type of SFRS used. In the ESFP, approximations may be used to calculate the fundamental lateral periods. In the case of steel, the following formulas (Equations 1-9 and 1-10) may be used where h_n is the height of the building:

- Moment resisting frame $T_a = 0.085(h_n)^{\frac{3}{4}}$ (1-9)
- Steel braced frames: $T_a = 0.025h_n$ (1-10)

Methods of mechanics may also be employed to determine the period of the structure but the NBCC sets a limit where the period determined using the latter shall not exceed 1.5 times, for moment-resisting frames, and 2.0 times, for braced frames, the value determined using Equations 1-9 and 1-10 respectively.

The last requisite defined in the NBCC is that of accidental torsion. Unless the building is sensitive to torsion, in which case dynamic analysis is required, it is specified that additional loads that account for accidental torsion must be distributed so that they are resisted by the SFRS. Two separate load cases must be considered with the following torsional moments (Equations 1-11 and 1-12):

$$T_x = F_X(e_x + 0.10D_{nx}) \tag{1-11}$$

$$T_x = F_X(e_x - 0.10D_{nx}) \tag{1-12}$$

Where:

T_x – is the force to be applied which takes into account accidental torsion

F_x – is the elastic base shear

e_x – is the existent eccentricity between the centre of mass and the centre of rigidity

D_{nx} – is the in-plan dimension of the building considered which causes the eccentricity (ie. The dimension perpendicular to the direction of the lateral earthquake force)

1.5.1.4. Dynamic Analysis Procedure

Dynamic analysis may be used to determine the earthquake force by means of the following procedures:

1. Linear Dynamic Analysis
    a. Modal Response Spectrum Method
    b. Numerical Integration Linear Time History Method
2. Nonlinear Dynamic Analysis

However, the spatial distribution and magnitude of the mass must be well-representative of actual conditions. Any factor that may influence the lateral stiffness of the building has to be taken into account as well as the effect of finite sizes and joints. P-Δ effects must also be considered due to the large inter-storey deflections that may arise due to the earthquake motion.

In the case where a time-history method is used in the dynamic analysis, the ground motion record used must be equal or exceed the *S(T)* design values given by the NBCC for the building site.

1.5.1.5. Deflection and Drift Limits

The NBCC states that the deflections shall be computed using linear elastic analysis using any of the procedures mentioned above. However, these methods must reflect the effect of torsion and shall be multiplied by R_dR_o/I_E to take into account the ductility (inelastic behaviour) in the system. Limits for interstorey drifts have been tabulated (Table 1.1).

Table 1.1 – Largest inter-storey deflection according to building type [Cl. 4.1.8.13.] (NRCC, 2006)

Type of Building	Largest Inter-storey Deflection
Post-Disaster Buildings	$0.01h_s$
Schools	$0.02h_s$
All other buildings	$0.025h_s$

\\\

1.5.1.6. Diaphragm Design Provisions

The NBCC provides certain provisions [Cl. 4.1.8.15.] for diaphragms in which it states that diaphragms, along with their connections, shall be designed so as not to yield. The load path must be entirely defined and must take into account the shape of the diaphragm and any openings or discontinuities. The NBCC also specifies that the diaphragm be designed for the governing load case as determined from the regulations below.

a) The diaphragm must be designed for the load capacity of the SFRS as determined from the ESFP or the Dynamic Analysis Procedure together with any additional loading that will be experienced due to the transfer of loads between elements of the SFRS attributable to the lateral capacity of those elements and taking into account any discontinuity or change in stiffness.

b) The diaphragm must be designed at any floor level (x) for a minimum force that is obtained by dividing the design-based shear by the number of storeys (N).

1.5.2. CAN/CSA-S16

The CSA-S16 Standard (2005) addresses the limit states design of steel structures; its Clause 27 is dedicated to the seismic resistance of buildings using a capacity-based design approach. This standard provides the seismic design guidelines and detailing requisites related to the design of the seismic force resisting system elements. Table 1.2 summarizes the types of systems that are covered in the standard along with their ductility and overstrength-related seismic force reduction factors.

Table 1.2 – Ductility and overstrength seismic force reduction factors according to SFRS type [Cl. 27]

Type of SFRS	R_d	R_o
Ductile Moment Resisting Frame	5.0	1.5
Moderately Ductile Moment Resisting Frame	3.5	1.5
Limited Ductility Moment Resisting Frame	2.0	1.3
Moderately Ductile Concentrically Braced Frame	3.0	1.3
Limited-Ductility Concentrically Braced Frame	2.0	1.3
Ductile Eccentrically Braced Frames	4.0	1.5
Ductile Plate Walls	5.0	1.6
Limited-Ductility Plate Walls	2.0	1.5
Conventional Construction	1.5	1.3

Though the standard provides very little information about diaphragms, it does specify that if decking is to be used to transfer the loads to the lateral bracing system, all the connection and attachments pertinent to the diaphragm action must be clearly indicated on the design drawings. In addition, capacity design methodology necessitates that the diaphragms and collector elements are able to transfer the inertia forces generated at each level to the SFRS. No changes pertinent to diaphragms are to be implemented in the 2009 version of CSA-S16 (2008).

Clause 27.11 in this section of the standard is dedicated to special seismic construction. It allows for the use of different framing systems as long as there have been thorough investigations to quantify their seismic performance and the level of safety they can attain. In current practice, only the braces of concentrically braced frame (CBF) buildings are allowed to reach the inelastic range. An objective of the full-scale dynamic testing program is to evaluate design methodologies where the diaphragm could be used as the fuse in the SFRS.

1.5.3. Steel Deck Institute Diaphragm Design Manual

This procedure was developed at West Virginia University following the research of Dr. Larry D. Luttrell (1981). In excess of 150 diaphragms with different types of fasteners and fastener spacings were subjected to static loading to determine diaphragm design formulae. The manual is composed of two major sections; the first section deals with the shear strength of diaphragms and the second section is focused on the shear stiffness of the diaphragm. The former research conducted by Luttrell (1981) has been heavily investigated in the diaphragm testing program presented herein as the shear stiffness was determined to have very different static and dynamic characteristics.

1.5.3.1. Shear Strength

The shear strength is attributed to four different factors, the lower of which will control the design and define the overall shear strength of the diaphragms. The expressions for shear strength are in terms of the fastener type, strength, spacing and the geometry of the deck. The four possible failure mechanisms are the following:

1. The fastener failure in the end panels of the diaphragm;
2. The allowable forces generated by the fasteners in the interior panels;
3. The limitations of the fasteners in the end members due to possibility of additional loading in the corner connections; and
4. Overall shear buckling of the diaphragm

Resistance factors of $\phi = 0.50$ to 0.70, depending on the type of fastener, have been decided upon for the Limit States Design of diaphragms in CSA-S136. Such low factors exist due to the high variance in fastener strength.

1.5.3.2. Shear Stiffness

The shear stiffness, G', is defined as the ability of the diaphragm to deform in its plane under loading. Figure 1.2 displays an idealized deformation of the diaphragm as represented in the SDI manual. To determine the influential factors related to the shear strength of diaphragms, the SDI Manual begins by considering the idealized stiffness of a flat plate, and then elaborates on the different deformational comportment of a steel deck diaphragm.

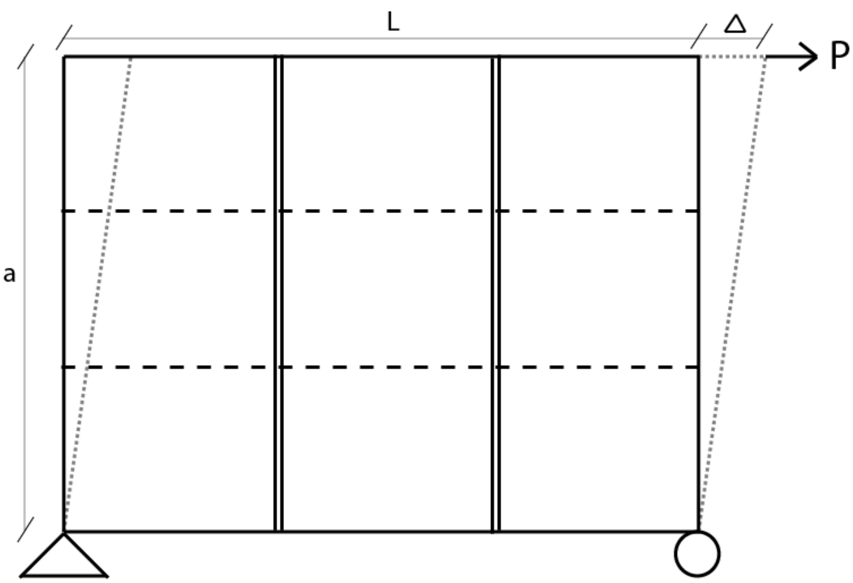

Figure 1.2 – Diagram depicting notion of diaphragm stiffness

The effective shear modulus is given by Equation 1-13:

$$G_{eff} = \frac{\tau}{\gamma} \tag{1-13}$$

Where τ is the shear stress and γ is the shear strain.

This equation turns into the subsequent Equation 1-14 for the general formulation of the diaphragm in-plane shear stiffness:

$$G' = \frac{Pa/L}{\Delta_s + \Delta_d + \Delta_c} \tag{1-14}$$

Where L and a represent the length and width of the shear panel respectively; all the other deformation components are explained for Equation 1-15. To examine G', Δ is derived while keeping the load P constant. In the case of diaphragms, the SDI method separates the deflection into 5 different independent components which contribute to the shear stiffness. The deflection may be expressed as follows (Equation 1-15):

$$\Delta = \Delta_s + \Delta_d + \Delta_c + \Delta_e + \Delta_m \tag{1-15}$$

Where Δ_s corresponds to the shear displacement of a perfect diaphragm and all other values correspond to the contribution to the displacement by the panel warping, interior sidelap, edge panel slip and miscellaneous effects respectively.

1.5.4. CSSBI Design Manual

The manual includes both the SDI and Tri-Services methods for designing diaphragms. Section 1.5.3 explains the SDI design procedure. The Tri-Services methodology is empirical in nature and only applies to diaphragms with welded deck-to-frame connections and button punch side-lap connections. Similarly to the SDI method, it is composed of two distinct categories, one for strength and one for deflection, which are both used to complete the design of the diaphragm. In the third edition of the CSSBI manual, tables are provided with the strength and flexibility of the diaphragm in terms of the connection pattern and spacing and the joist span.

1.5.4.1. Strength Design

The diaphragm is considered as a flat beam in the tri-services procedure but only two failure modes are considered. The governing case is given by the lowest value of:

1. The overall elastic shear buckling
2. The connection failure which is itself a combination of:
    a. The shear resistance of the transverse welds at the end of the panel
    b. The contribution of the sidelap connectors to the diaphragm strength

A limit is also placed on the contribution from sidelap connectors so that it is not overestimated in the design approach.

1.5.4.2. Deflection Design

In this methodology, the diaphragm in-plane deflection needs to be calculated by considering both the flexural deflection experienced by the eave members in addition to the shear deflection experienced by the deck. Typical beam deflection formulae are used to calculate the flexural deflection while another equation that is dependent on the in-plane flexibility of the diaphragm is used to calculate the shear deflection as can be seen in Equation 1-16 and Figure 1.3.

$$\Delta_{Total} = \Delta_{Flange} + \Delta_{Web} = \frac{5wL^4}{384EI} + \frac{q_{AVG}LF}{2x10^6} \tag{1-16}$$

Where

w – The uniformly applied load along the length of the diaphragm

L – The diaphragm length

E – Modulus of elasticity of the eave beams

I – Inertia of the deep beam given by the perimeter beams alone

q_{AVG} – Average shear per unit length

F – Flexibility factors for the diaphragm

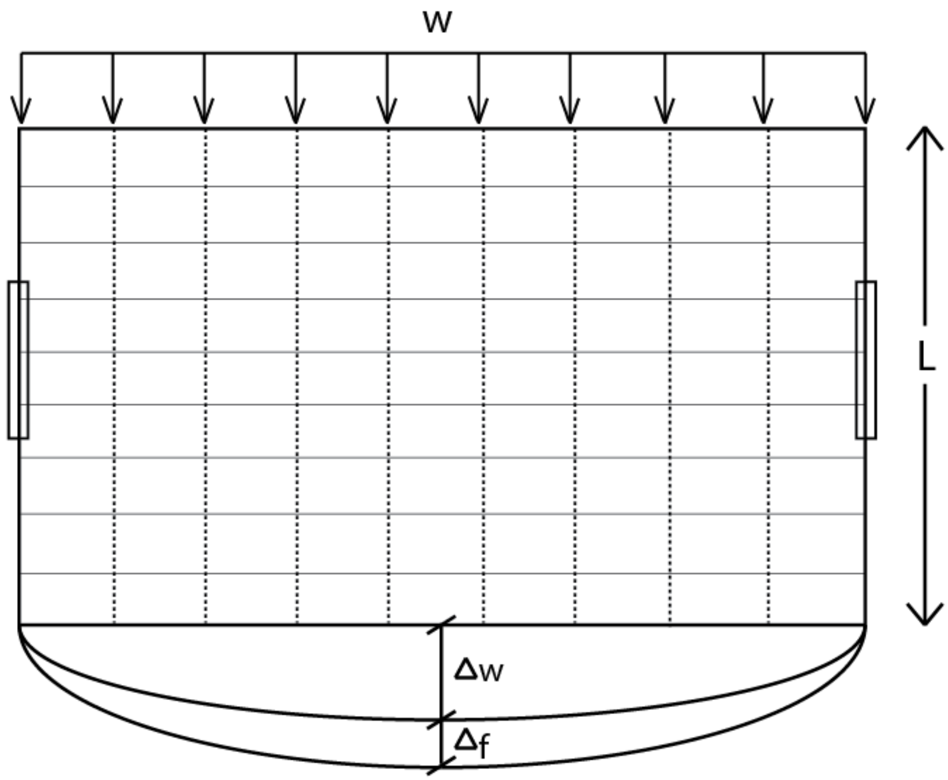

Figure 1.3 – Plan view of typical building: Diaphragm deformation

The flexibility factor is the variable that takes into account the in-plane stiffness of the diaphragm for deflection calculations. Unlike the SDI Method, only three factors are included for flexibility in the Tri-Services procedure. The first factor corresponds to the idealized stiffness of a diaphragm acting as a flat plate. The second factor incorporates the flexibility due to fastener deformation and sheet distortion. The last factor takes into account the number of spans that one deck sheet will extend over since increasing spans will significantly increase the stiffness by reducing the warping distortion of the panel.

1.5.5. Manual of Stressed Skin Diaphragm Design

This methodology is the most extensive of the three presented as it is has existed for the longest amount of time; but also because more influential factors were taken into account in the research. This methodology is not restricted to using steel sheet decking on joists as is most often done in the Canadian industry; it allows for the design of diaphragms with different types of supporting frames. Special attention is also given to the change in flexibility and strength given the orientation of the sheeting compared to the loading. This methodology is widely used in Europe since it had been adopted by the European Convention for Constructional Steelwork of European Recommendations for the Stressed Skin Design of Steel Structures (ERSSDSS) in 1977. The basic shear panel that was considered can be seen in Figure 1.4.

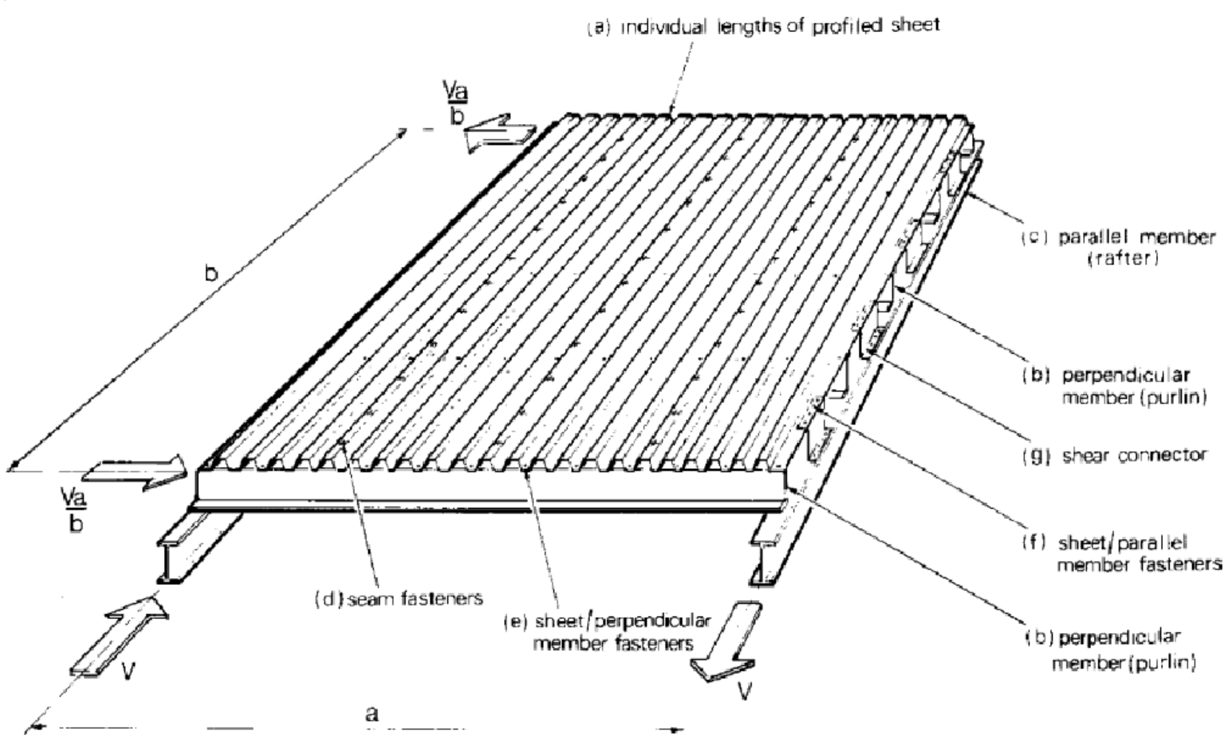

Figure 1.4 – Basic shear panel (Davies, 2006)

1.5.5.1. Diaphragm Strength

Six failure modes are considered to determine the diaphragm strength. As requested by the ERSSDSS, all failure modes must exhibit a ductile behaviour. In contrast, the governing failure mode must have an additional strength of 25% to ensure that non-ductile failure does not occur. This has been directly incorporated in the design equations of this manual. Davies & Bryan (1982) considered the following failure modes:

1. Failure along a line of seam fasteners
2. Failure in the sheet to parallel member (shear connector) fasteners
3. Failure in the sheet to perpendicular member fasteners near the gables or rafters for diaphragms fastened on two sides only. This failure occurs in a direction parallel to the span of the sheeting
4. Overall shear buckling of the sheeting
5. Failure in the sheet to perpendicular member (purlin) fasteners in a direction perpendicular to the span of the sheeting; and
6. Failure at the edge member in compression or combined compression and bending

1.5.5.2. Diaphragm Flexibility

Similarly to the diaphragm strength, the estimation of the flexibility (Equations 1-17 and 1-18) is much more elaborate than the two other diaphragm design methodologies. There are six different flexibility contributions that need to computed and added together in the following way for cantilever panels.

$Sheeting\ Perpendicular\ to\ Span\ of\ Diaphragm$:

$$c = c_{1,1} + c_{1,2} + c_{2,1} + c_{2,2} + c_{2,3} + c_3 \tag{1-17}$$

$Sheeting\ Parallel\ to\ Span\ of\ Diaphragm$:

$$c = \left(\frac{L}{a}\right)^2 (c_{1,1} + c_{1,2} + c_{2,1} + c_{2,2} + c_{2,3}) + c_3 \tag{1-18}$$

The different components of the flexibility have been tabulated below (Table 1.3).

Table 1.3 – Different flexibility components in stressed skin approach (Davies & Bryan, 1982)

Variable	Component
$c_{1,1}$	Flexibility due to distortion of the sheeting profile
$c_{1,2}$	Flexibility due to shear strain in the sheet
$c_{2,1}$	Flexibility due to movement at the sheet to perpendicular member fasteners
$c_{2,2}$	Flexibility due to movement in the seams
$c_{2,3}$	Flexibility due to movement in the sheet to parallel member fasteners (four sides fastened) or flexibility due to movement at the perpendicular member to parallel member (purlin to rafter) connections (two sides fastened)
c_3	Flexibility due to axial strain in the edge members (treated as an equivalent shear flexibility)

1.5.6. FEMA 273 & FEMA 274 (Commentary)

FEMA 273 – NEHRP Guidelines for the Seismic Rehabilitation of Buildings (1997), along with its commentary, FEMA 274 (1997), provide seismic rehabilitation guidelines for steel structures.

Measures for the rehabilitation or retrofit of bare steel deck diaphragms are provided for stiffness, strength and deformation. However, these guidelines were created assuming an elastic behaviour of the diaphragm which is only used as a means to transfer lateral forces to the bracing system and its strength should therefore not be exceeded. Hence, these directives may not necessarily be applicable if the diaphragm is used as the energy-dissipating element in the SFRS of the building. No additions have been made in the new edition of the standard, FEMA 356 – Prestandard and Commentary for the Seismic Rehabilitation of Buildings (2000).

1.5.6.1. Stiffness

In terms of stiffness for a linear static design procedure, the FEMA guidelines state that the diaphragm shall be modelled as flexible and that the appropriate flexibility factors shall be obtained from manufacturers' catalogues or the Steel Deck Institute Manual. Interpolations are allowed if the values for a specific system are not available. The criteria mentioned above only apply to stiffened or strengthened diaphragms where the diaphragm must remain elastic and where the load transfer mechanism between new and existing diaphragm components must be considered so as to ensure stiffness compatibility (FEMA 273, 1997).

In the case of a nonlinear static design procedure, the guidelines suggest that the non-linearity of steel deck diaphragms is generally not included in such an analysis. However, since extremely flexible diaphragms may be forced to behave inelastically, suggestions are provided to obtain the non-linear response. The first suggests that the procedure for wood diaphragms in masonry buildings be used to obtain the non-linear behaviour while the second suggests using a post-elastic strength hardening modulus of 3% for the diaphragm. In addition, the FEMA 273 guidelines assert that diaphragm fastener connection non-linearity cannot be modelled in any case.

1.5.6.2. Strength and Deformation

Four common types of deficiencies are listed in the guidelines which would impact the overall strength of the diaphragm in the SFRS. Different rehabilitation methods are suggested so the structure complies with the existing standards. Table 1.4 lists the most-commonly found deficiencies and measures to satisfy the rehabilitation acceptance criterion.

Table 1.4 – Deficiencies and rehabilitation measures for bare steel deck diaphragms (FEMA 273, 1997)

Common Deficiencies	Rehabilitation Measures
1. Inadequate connection between metal deck and chord or collector components	a. Adding shear connectors for chord or collector forces
2. Inadequate strength of chord or collector components	b. Strengthening existing chords or collectors by the addition of new steel plates to existing frame components
3. Inadequate attachment of deck to supporting members	c. Adding puddle welds or other shear connectors at panel perimeters
4. Inadequate strength and/or stiffness of the metal deck	d. Adding diagonal steel bracing to supplement diaphragm strength
	e. Replacing non-structural fill with structural concrete
	f. Adding connections between deck and supporting members

1.5.7. Tremblay & Stiemer

Tremblay & Stiemer (1996) incorporated 36 nonlinear numerical models in the evaluation of typical single-storey buildings with flexible roof diaphragms; these models were subjected to historical accelerogram earthquake records. The size, weight and stiffness characteristics were varied as well as the location of the buildings. All of the buildings were designed according to the NBCC 1995 (NRCC, 1995). The time-history analyses were conducted in DRAIN-2DX (Prakash & Powell, 1993) to determine the inelastic in-plane deformations of the diaphragm. The study revealed the conservativeness of the NBCC 1995 especially when ignoring the in-plane flexibility of the diaphragm. In addition, though the maximum shear force observed in the diaphragm did not exceed the strength assigned to the braces, the moment recorded numerically at midspan exceeded the moment calculated from statics by a factor of up to 2.3. This was attributed to the fact that the linear variation in force assumed in design is not representative of dynamic loading conditions. Thus, the authors recommend that a dynamic amplification factor of 2.3 be applied to the static bending moment and the in-plane roof deformation to obtain more tangible values.

1.5.8. Medhekar & Kennedy

Medhekar & Kennedy (1999a) performed a seismic evaluation for single-storey buildings. The evaluation consisted of assessing a building designed as per the NBCC 1995 through numerous analytical studies. These included free vibration analysis, response spectrum analysis, nonlinear static analysis and nonlinear dynamic time history analyses for 5 different seismic zones. Observations were made that if the diaphragm is not designed with the capacity design principles, it will experience inelastic deformations. It was recommended to exercise caution when assuming a linear variation in diaphragm forces as is often done in current practice since the response spectrum analysis and dynamic time history analyses resulted in nonlinear variation of maximum shear forces along the width of the diaphragm. Inelastic diaphragm response was also considered unsatisfactorily; thus a strong diaphragm-weak frame approach was suggested. The incorporation of the stiffness from non-structural elements in a numerical model proved to alleviate the seismic demand on the braces though it increased the response of the roof diaphragm. A significant reduction in the fundamental building period was also computed due to the inclusion of the diaphragm stiffness, particularly in low seismic zones.

In addition, a simplified estimate of the building period (Equation 1-19) which incorporates the stiffness of flexible diaphragms (Equation 1-20) was suggested.

$$T = 2\pi\sqrt{\frac{(K_B + K_D)}{K_B K_D}\frac{W}{g}} \tag{1-19}$$

Where

$$K_D = \frac{\pi^2}{\frac{L^3}{\pi^2 EI} + \frac{L}{G'b}} \tag{1-20}$$

Where:

K_B, K_D – are the brace and diaphragm stiffness respectively

L, b – represents the length and width of the diaphragm, respectively, in the direction considered

W – is the seismic weight of the single-storey building

G', EI – are the shear stiffness and the flexural rigidity of the diaphragm respectively

1.5.9. Nedisan

The purpose of this study was to verify through numerical modelling the applicability of the most recent SDI method for use in seismic design. Nedisan (2002) used methods of static equilibrium and the software DRAIN (Prakash and Powell, 1993) to validate the SDI methodology. It was determined that unless the ratio between the rigidity of deck to deck and deck to frame fasteners was equal to two, and the number of deck panels greater than four, the results obtained SDI, DRAIN and static equilibrium did not coincide. This comparison was made for the distribution of forces, the panel shear deformation and the fastener deformation. Static non-linear analyses were also completed that determined that the diaphragm resistance was dependent on the rigidity ratio of the connectors. Thus, Nedisan (2002) recommended that weak connectors not be used as SDI bases its expressions on the ultimate capacity of the connectors.

In addition, static and dynamic analyses were also compared for single-storey buildings with flexible diaphragms. The flexibility of the diaphragm was found to increase the forces and displacements in the braces. Hence, the static-equivalent method underestimates the ductility demand in the braces. Similar analyses were run with an eccentricity in the brace stiffness. Again, the NBCC underestimated the forces in the braces as it was shown that the ductility demand in the weaker braces was augmented while the stronger braces had a decreased ductility demand. (Tremblay *et al.*, 2003)

1.5.10. Lamarche

This project was comprised of in-situ ambient vibration modal analysis of buildings to determine the actual fundamental period of single-storey steel structures so a comparison could be made with the estimate expressions provided in the NBCC 2005. The equation for a steel braced frame is provided in Section 2.1.3 and it is entirely dependent on the building height. The in-situ results did not coincide with the approximation and consequently, Lamarche (2006) proposed 10 more representative regressions that are dependent on the building height as well as its width. It is important to realize that these periods were calculated at very low excitations. As Tremblay *et al.* (2008a; 2008b) stated in later studies, the dynamic characteristics under earthquake related deformation demand may vary significantly from the static properties of single-storey buildings.

1.5.11. Moanda

This study looked at the effect of roof diaphragm flexibility on the seismic behaviour of single-storey buildings through numerical modeling in SAP90. The main conclusions were that the flexibility of the diaphragm did not have a significant impact on the load distribution between the different braced walls. The difference in load distribution between flexible and rigid diaphragms was inferior than 10%. However, the deformation of a flexible roof has to be accounted for as it represented up to 400% of the deformation of the building with a rigid roof which was considered in this study. It was also confirmed that the period of a building varies dependently of the diaphragm flexibility. The latter must therefore be taken into account when calculating the seismic demand for appropriate results and proper detailing (Moanda, 2000).

1.5.12. Other Analytical Studies

The effect of diaphragm flexibility has been the topic of many studies. Reports exist that offer solutions for the flexibility of profiled sheeting (Davies, 1986a & 1986b). Some studies have looked at the difference in building response due to diaphragm flexibility through analytical studies (e.g. Kim & White, 2002 & 2004; Ju & Lin, 1999; Jain 1984; Masi *et al.*, 1997; Naman & Goodno, 1986) and also considered the incidence of inelasticity in the diaphragm (Dolce *et al.*, 1994), while others have looked at building irregularities and their performance with flexible diaphragms (e.g. Basu & Jain, 2004). A review of all the initial work done in the context of diaphragm panel behaviour can be found in the paper by Wright & Manbeck (1992).

1.6. Literature Review – Experimental Investigations

There have been numerous experimental studies on roof diaphragms. However, only the most recent studies that are pertinent to the ductile behaviour of diaphragms will be covered in Section 1.6.

1.6.1. Essa

The purpose of this study by Essa *et al.* (2001) was to investigate the ability of diaphragms to dissipate energy through inelastic behaviour in the event of an earthquake. In total, 18 cantilever diaphragm specimens were tested under monotonic and reversed cyclic loading (Figure 1.5).

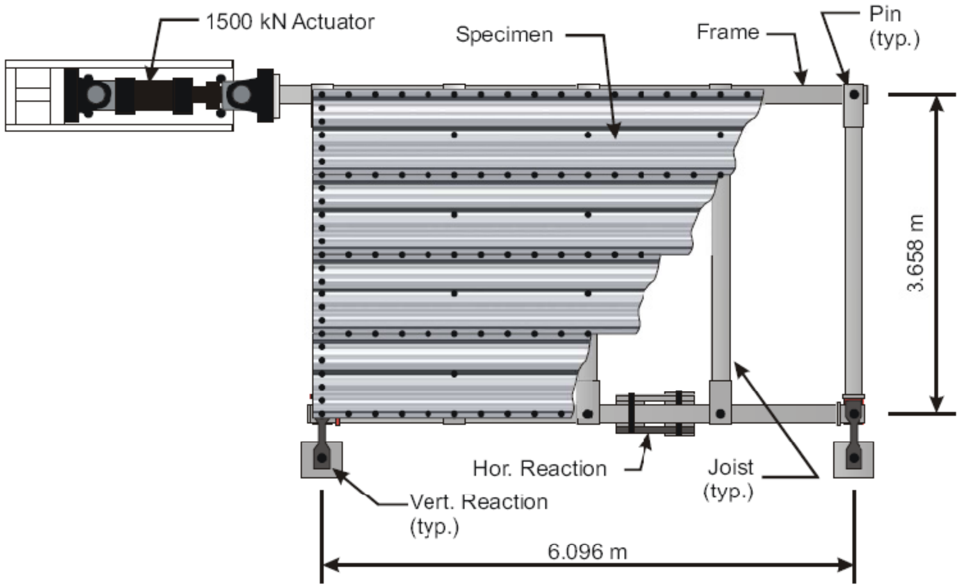

Figure 1.5 – Cantilever test configuration used by Essa *et al.* (2001)

The same fastening pattern, namely frame fasteners at every two flutes and sidelap spacing of 305 mm [1 ft], was maintained for all the experiments but nine different assemblies of deck-to-frame and deck-to-deck fasteners were tested. The panel thickness of all but the last two diaphragms was 0.76 mm; the remaining two were composed of 0.91 mm thick deck panels. The main conclusion was that the level of hysteretic behaviour, the ductility and the energy-dissipation capabilities are largely dependent on the fastener type. Diaphragms with welded-with-washers or Hilti nail deck-to-frame fasteners and screw sidelap fasteners exhibited the greatest ductility and could sustain large displacements under cyclic loading. The 0.91 mm thick deck panel with Hilti nails and screws revealed to be 50% more efficient than the 0.76 mm thick diaphragm with the same fasteners. A maximum plastic rotation of 0.01 radians for the 0.76 mm deck and 0.012 radians for the 0.91 mm deck was recommended so that the strength does not degrade below 80% level of the peak monotonic load.

1.6.2. Martin

The main objective of Martin's research (Martin, 2002; Tremblay *et al.,* 2004) was to evaluate the seismic demand on the most common types of diaphragms and to observe the dynamic response of the latter. To do so, non-linear time-history models were created in Ruaumoko (Carr, 1994) to determine the demand on three different buildings subjected to earthquakes in Victoria, British Columbia and Quebec City, Quebec. From the results, loading protocols were devised to reproduce the inelastic behaviour on 19 full-scale specimens using the same setup as the one by Essa *et al* (2001). The buildings had been designed according to CSA-S16 and the NBCC 2004, the preliminary version of NBCC 2005, with tentative values of ductility-related modification factors, R_d of 2.0 for the eastern Canada region and 3.0 for both the eastern and the western Canadian regions. Figure 1.6 shows one of the protocols which was determined from the numerical modeling for the experimental part of the study.

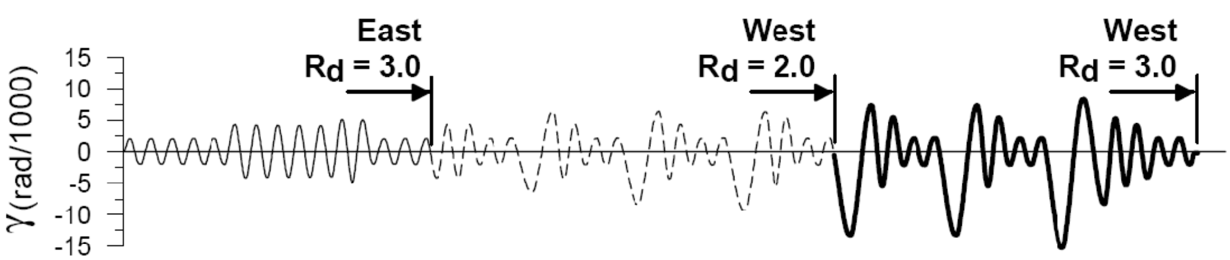

Figure 1.6 – Loading protocol for different ductility demands (Martin, 2006)

The Ruaumoko results demonstrated that the East part of the protocols did not bring the diaphragm into inelastic behaviour, but ultimate shear deformations of 0.068 and 0.0108 radians were recorded for R_d equal to 2.0 and 3.0 respectively for the West part of the protocol. The results confirmed the initial conclusions from Essa *et al.* (2001) that welded and button-punch diaphragms do not perform satisfactorily under seismic loading. Martin also proposed preliminary ductility-related factors for each set of fastener combination as listed in Table 1.5.

Table 1.5 – Ductility and overstrength factors for different fastener combinations (Martin, 2006)

Fastener Combination	R_d	R_o
Weld | Button Punch	1.0	1.0
Weld with Washer | Weld with Washer	1.5	$1/\phi$
Nail | Weld with Washer	1.5	$1/\phi$
Nail | Screw	2.0	$1/\phi$

1.6.3. Yang

The study completed by Yang (2003) investigated the influence of different manufactured nails in terms of ductility as well as the stiffening effect of non-structural components and the deck overlap at panel ends. The same cantilever setup as Essa and Martin was again used to complete 12 full-scale diaphragm tests. A finite element model was also created to examine the effect of diaphragm flexibility and stiffness eccentricity on the brace force. Diaphragms with Hilti and ITW Buildex nails were compared and it was determined that the diaphragm with Hilti fasteners was stiffer. This confirmed the results from the connection tests by Rogers & Tremblay (2000). Diaphragms with two smaller overlapping panels were found to be more flexible than the full panel length diaphragm. A decrease in shear stiffness of 39% and 29% were recorded for the nailed and screwed diaphragm and the welded and button-punched diaphragm respectively. This was attributed to the warping deformations that are restricted with the full panel but are released with the deck overlap.

The tests with non-structural components allowed for a quantification of the increase in stiffness due to the roofing components placed on top of the steel deck panels. An increase in shear stiffness was mainly attributed to the gypsum boards which experienced significant deformations during the tests. Notable strength and stiffness augmentations of 24% and 49% respectively were observed from the tests. Yang remarked that this could have serious implications on the design methodology which utilizes the predicted shear stiffness of the steel deck diaphragm. Where the diaphragm is used as the energy-dissipating element, omitting this increase in shear resistance due to non-structural components could result in other elements in the SFRS yielding prior to the diaphragm and failing. Further research on the subject was recommended.

The analytical results obtained for the inelastic deck responses confirmed the deductions made by Martin (2002). A satisfactory ductile response was witnessed for a nail and screwed deck designed with a value of R_d of 2. A ductility-response modification factor of 3.0 was proven to be acceptable for decks with either end overlap or non-structural components. In addition, from the finite element modelling, it was determined that a flexible diaphragm would relieve the effect of torsion. However, storey drifts would increase 2 to 4 times and there would also be an increased ductility demand on the braces.

1.6.4. Mastrogiuseppe

Mastrogiuseppe's main objective was to investigate the effects of non-structural components on the diaphragm characteristics through experimental testing and numerical modeling (Mastrogiuseppe *et al.*, 2008; Mastrogiuseppe, 2006). The non-structural component attributes were also studied as well as the connections between the decking and the roofing material. The

Young's modulus and in-plane shear stiffness were determined for the gypsum and fibreboard materials as well as the stiffness of the connections. Gypsum was proved to be the stiffest component, which coincided with Yang's (2003) finding that it was the most influential material in terms of the deck flexibility. The increase in stiffness in terms of thickness and fastener spacing is displayed in Table 1.6.

Table 1.6 – Increase in stiffness due to gypsum boards for different diaphragm configurations and thicknesses (Mastrogiuseppe, 2006)

Thickness (mm)	Fastener Spacing			
	305/305	305/152	152/305	152/152
0.76	46.4 %	38.1 %	15.3 %	11.9 %
0.91	25.0 %	30.6 %	11.0 %	8.8 %
1.22	18.1 %	16.7 %	7.8 %	5.6 %
1.51	10/1 %	10.0 %	6.5 %	4.7 %

Mastrogiuseppe *et al.* (2008) performed a parametric study to predict the linear elastic behaviour of bare sheet steel diaphragms and diaphragms constructed with non-structural materials. It was found that there was very little difference in the fundamental period of vibration of buildings computed using diaphragm characteristics with and without non-structural roofing components.

1.6.5. Tremblay, Berair & Filiatrault

This paper depicts experimental shake table tests that were conducted on a 1:7.5 scale model of a low-rise steel building at École Polytechnique de Montreal. These tests were performed to examine the seismic performance of single-storey buildings with flexible diaphragms. In particular, the stiffness of the diaphragm and mass, stiffness and strength eccentricities were investigated.

The tests confirmed the validity of the equation proposed by Medhekar & Kennedy (1999a) for the period of a single-storey building with a flexible diaphragm. As well, it was noticed that the shear demand on the diaphragm was very high due to the increased strain rate, and yield strength, experienced by the braces. Lastly, strength eccentricities were shown to have a significant impact on the ductility demand of the braces. The NBCC only considers an eccentricity between the centre of rigidity and the centre of mass but does not look at the redistribution of the load following inelastic behaviour (Tremblay *et al.*, 2000).

1.6.6. Other Experimental Studies

Other laboratory and field experimental studies were carried out on structures with flexible diaphragms. Cohen *et al.* (2006) and Tena-Colunga *et al.* (1996) investigated the seismic behaviour of masonry buildings with flexible diaphragms. Field ambient vibration testing has also been completed on many single storey structures (e.g. Lamarche *et al.*, 2009; Tremblay *et al.*, 2008a; Turek & Ventura, 2005). Studies that examined the hysteretic behaviour of shear panel connections have also been conducted to evaluate their inelastic performance (Rogers & Tremblay, 2008a; 2008b; De Matteis & Landolfo, 1999)

1.7. Literature Review – Conclusions

The design information mentioned in Section 1.5 of this chapter was incorporated in the study to define the diaphragm characteristics and relate the results with current building design. The SDI method (Luttrell, 2004) was used to define the shear strength and stiffness of each of the diaphragm specimens. All the strength and flexibility comparisons were related to the properties obtained with this procedure. The NBCC 2005 (NRCC, 2006) was used to relate all the results to current building design in Canada by incorporating the diaphragm stiffness into the overall building period using the equation proposed by Medhekar & Kennedy (1999a). The NBCC 2005, along with CSA-S16 (2005), was used for the comparative analysis to calculate the seismic forces and apply capacity-based design for each of the building designs.

The experimental investigation conclusions were compared with those obtained in this study. Specifically, those obtained by Yang (2003) and Tremblay *et al.* (2004) for the effect of non-structural materials were contrasted. The results of in-situ ambient vibration studies (Lamarche, 2006; Lamarche *et al.*, 2009; Tremblay *et al.*, 2008a) were also compared and put into context with the results of the experimental part of the research program.

CHAPTER 2

2.0 LARGE-SCALE DYNAMIC DIAPHRAGM EXPERIMENTS

2.1. General

The testing program included large-scale dynamic diaphragm testing along with numerical modelling to characterize the behaviour of metal roof diaphragms. These tests were intended to determine the fundamental frequency of flexible steel deck diaphragms as well as to evaluate their dynamic response under seismic loading. The ductility demand and capacity of the diaphragm was also assessed though these full-scale experiments. However, more specifically, since the diaphragms could be considered as a fuse element, there was a need to evaluate repair schemes once the diaphragm has undergone inelastic deformations. Hence, various configurations were devised and evaluated in terms of strength, stiffness, ductility and dynamic response. Repair scenarios were also evaluated for diaphragms which are attached to the underlying frame with arc-spot welds and together with button-punched sidelaps. Two series of tests, Phase I and Phase II, were conducted at École Polytechnique during the summer of 2007 and 2009 respectively.

2.2. Large-Scale Dynamic Experimental Testing

2.2.1. Procedure and Test Setup

The test setup consisted of a 21.02 m wide by 7.31 m long rectangular roof frame structure with overlying steel decking as shown in Figure 2.1 and Figure 2.2. The frame was dynamically shaken in-plane and in-phase using two hydraulic actuators. Each test comprised 24 corrugated steel deck sheets to cover the diaphragm frame setup in its entirety.

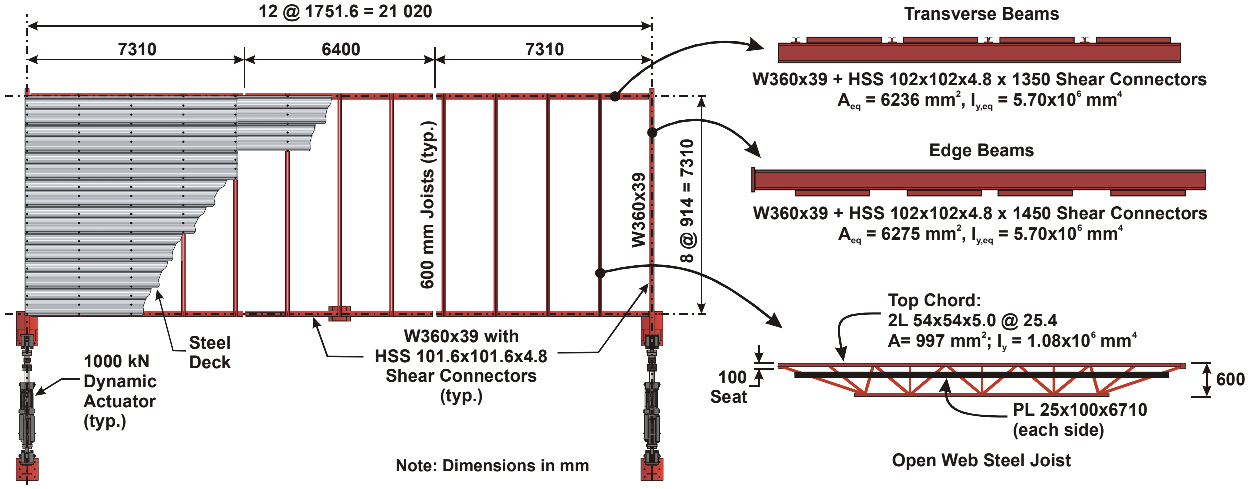

Figure 2.1 – Plan view and detail of test setup

Figure 2.2 – Diaphragm test assembly in construction

Two 1000 kN high performance dynamic MTS actuators were used to induce movement into the frame by simulating random vibration, sine signals, ground motion and other displacement protocols as well as to act as the lateral force resisting system on either side of the steel frame. Consequently, each actuator would theoretically carry half of the seismic force induced in the diaphragm. The concurrent and identical accelerations inputted by the actuators generated inertia forces along the length of the diaphragm due to the self-weight of the diaphragm assembly and the additional masses; thereby, dynamic loading occurred. The actuators were controlled by means of displacements; protocols ranged from 0 Hz to 25 Hz, dependent on the diaphragm configuration being tested.

2.2.1.1. Frame

The frame consisted of W360x39 perimeter beams along with typical interior open web steel joists which were spaced evenly over the width of the frame. The joists were designed for a specified dead load of 2.12 kN/m and a specified live load of 3.8 kN/m. A design depth of 600 mm was also used to mimic typical joists in long span building applications. These also had a 100 mm seat for direct support on the W-Beams. Shear connectors made up of HSS 102x102x4.8 were welded onto the eave beams between the joists to allow for frame fastener connections, and consequently shear flow, at those locations. At edge beam fastener locations, connections were made directly on the W-Beams. The other shear connections welded onto the bottom of edge beams depicted in Figure 2.1 were meant for another setup layout. Deck sheets were placed directly on the joists and covered four spans perpendicular to the direction of loading. Shear resistance was achieved by mechanically fastening the deck onto the underlying frame.

2.2.1.2. Supports

The actuators were anchored onto a reaction column, which was itself secured to the strong floor using pre-tensioned filleted rods so as to prevent any upwards movement or sliding of the base. The connection between the actuator and the column was done through a connection plate and four 25.4 mm [1 in.] A325 bolts which were each pre-tensioned to avoid any detachment of the bolts from the plate avoided during the tests. Lastly, the anchorage between the beam and the actuators was made by extending the edge beams and having a 51 mm connection plate welded at the end of it (Figure 2.3).

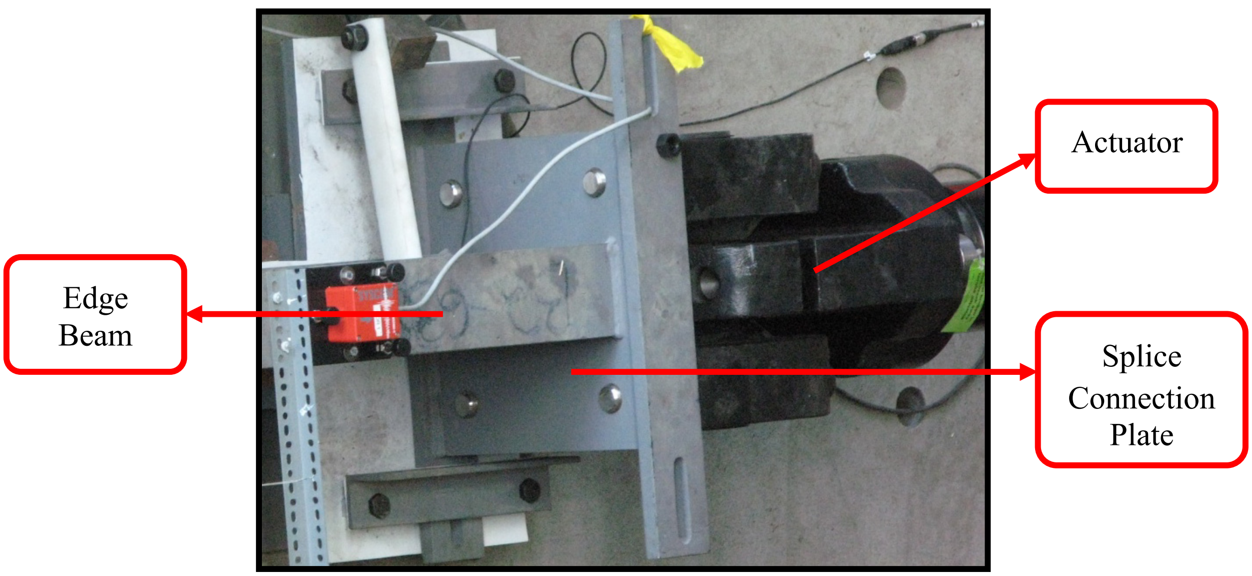

Figure 2.3 – Close-up of beam-actuator splice connection

Four 38.1 mm [1 ½ in.] diameter socket head cap screws were used to attach the actuator swivel to the beam. Two supports illustrated in Figure 2.4 were placed at the actuator locations. These supports served as vertical and horizontal guiders for the beam by restraining its direction of movement.

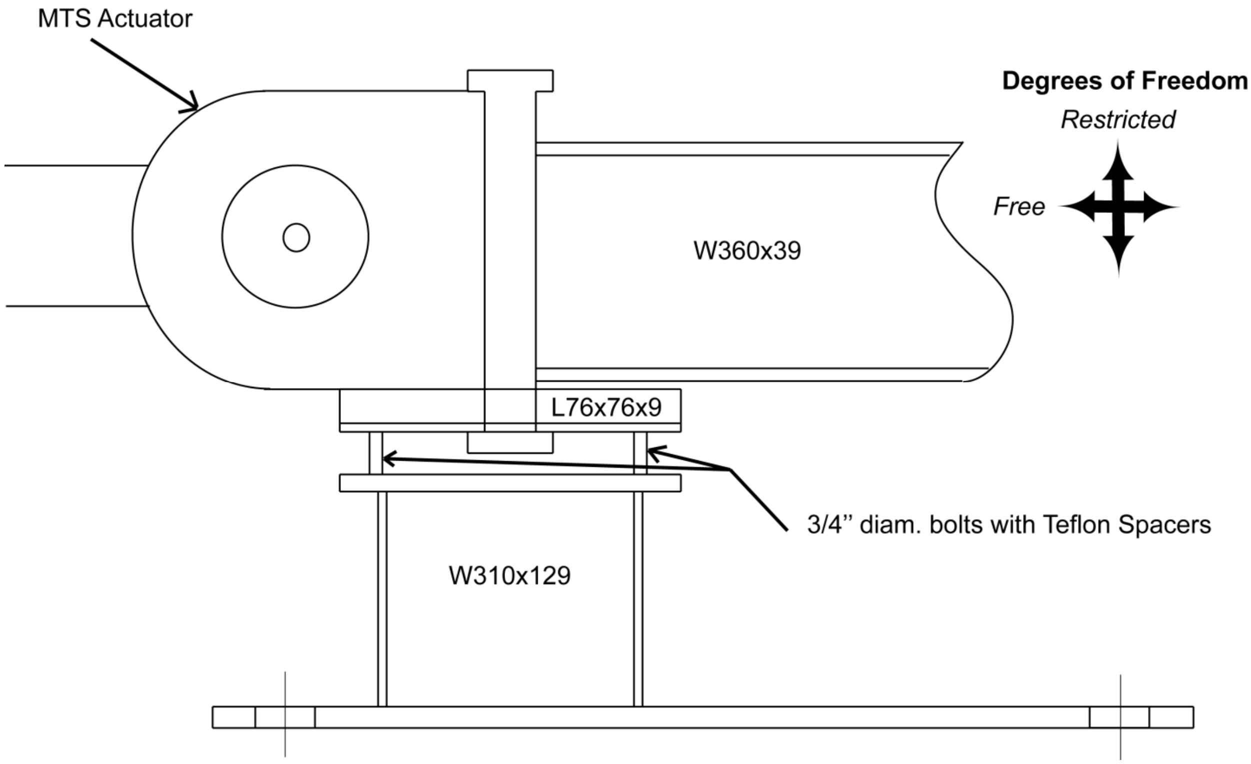

Figure 2.4 – Schematic representation of free and restricted degrees of freedom at splice connection

Two 25 mm plates were welded onto the beam connection plate to be able to control the direction of movement of the edge beams. Two L76x76x9 angles were placed on either side of the connection so as to restrain the plates vertically and prevent any excessive lateral movement of the beams.

Two sets of servo-valves were required to run the tests due to the large variation in amplitude of the applied displacement. In addition, for the more sensitive white noise tests, external LVDTs were used to precisely control the actuators (Figure 2.5). A large metal base was used along with a steel and Teflon extension to hold the displacement transducer in place. The support was heavy enough to not be influenced by any external disturbance and the extension was bolted tightly so that no movement would occur during the tests. The actuators were controlled using their internal LVDTs for the large displacement tests.

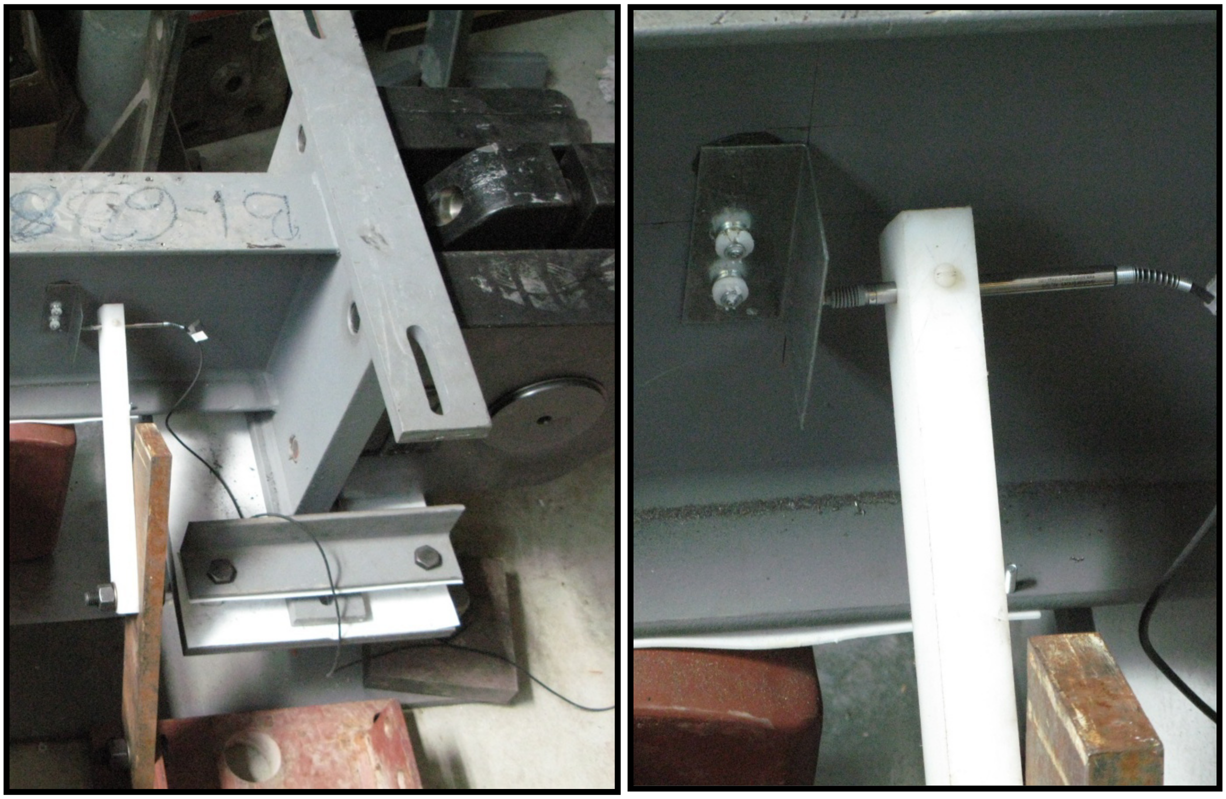

Figure 2.5 – External Controlling LVDT (left) with close-up (right)

The frame was supported symmetrically at eight locations. Rockers made up of welded HSS 203x203x13 sections, as seen in Figure 2.6, were used at the extremities and at third points along the width of the frame while rollers, also shown in Figure 2.6, were used in the middle of the frame.

Figure 2.6 – HSS rocker (left) and roller support (right)

The HSS rockers were underlain by a galvanized steel plate and two metal rods which allowed for any lateral movement to occur without interference. Teflon sheeting was also used at the interface between the rockers and the beams to minimize any energy loss due to friction that would have been incurred from lateral movement of the frame.

2.2.1.3. Masses & Weight

The mass on a typical diaphragm was simulated by adding steel plates and bars to the specimen. The square steel bars, which measured 762 mm [30 in.] in length and 31.75 mm [1.25 in.] in width, were distributed evenly across the roof width to replicate the evenly distributed load that would be present on the roof in the event of an earthquake. These bars were glued using epoxy (Hilti RE500) and screwed onto the deck after having cleaned the deck with acetone. Two mass distribution patterns were used for Phase I and Phase II respectively. The mass distributions for one deck length are shown in Figure 2.7 and Figure 2.8 where the transverse lines represent the joists and the rectangles represent the masses.

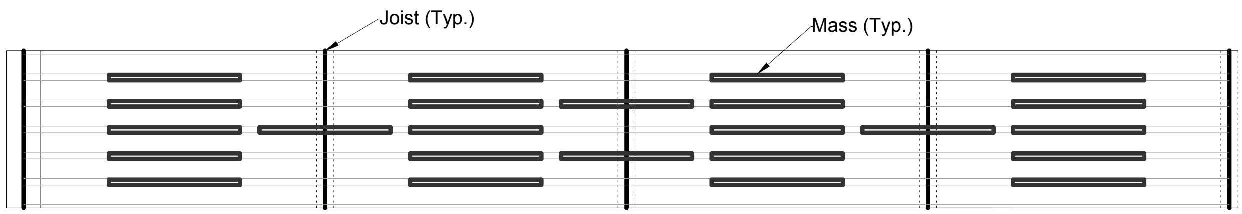

Figure 2.7 – Mass layout on a single deck panel for Phase I tests

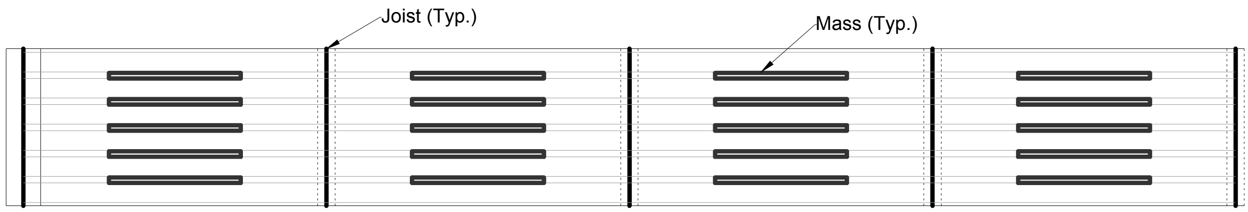

Figure 2.8 – Mass layout on a single deck panel for Phase II tests

Welded to each of the joists were 22 foot long, 4 inch wide and 1 inch thick steel plates. These masses did not represent the dead load on the roof; rather, they were used to attain the force required to bring the diaphragm into the inelastic range of behaviour and to reach its ultimate resistance. The placement of plates for Phase I can be seen in Figure 2.9. Phase II of the testing, due to the increased capacity of the diaphragms, required 4 pairs of steel plates (Figure 2.10) welded on each side of the joists to achieve a force great enough to force the diaphragm into inelastic behaviour. This was due to the closer fastener spacing and thicker deck encountered in Phase II of the testing program.

Figure 2.9 – Additional masses on joist for Phase I specimens

Figure 2.10 – Additional masses on joists for Phase II specimens

The total weight of a single specimen used in Phase I was 120 kN while the second layout amounted to a total weight of 202.3 kN for specimens with 0.76 mm deck sheets or 204.7 kN for specimens with 0.91 mm deck sheets. The breakdown of these values can be found in Table 2.1 to 2.4.

Table 2.1 – Weight distribution for Phase I specimens

	Weight [kN]	**Tributary Weight / Joist [kN]**	**Tributary Weight / End Beam [kN]**
Steel Deck	13.00	1.08	0.54
Steel Bars	34.10	2.84	1.42
Transverse Eave Beams	20.20	1.68	0.84
Open Web Steel Joists	13.70	1.25	
Steel Plates	29.30	2.66	
Total	**110.30**	**9.52**	**2.80**
Seismic Weight Not Carried By The Diaphragm (kN)			
Actuator Load Cell + Swivel	11.00	5.50	
End Beams	9.70	4.85	
Total	**20.70**	**10.35**	

Table 2.2 – Weight distribution for Phase II specimens with t = 0.76mm

	Weight [kN]	Tributary Weight / Joist [kN]	Tributary Weight / End Beam [kN]
Steel Deck	13.00	1.08	0.54
Steel Bars	28.40	2.37	1.18
Transverse Eave Beams	20.20	1.68	0.84
Open Web Steel Joists	13.70	1.25	
Steel Plates	117.30	10.66	
Total	**192.60**	**17.04**	**2.57**
Seismic Weight Not Carried By The Diaphragm (kN)			
Actuator Load Cell + Swivel	11.00	5.50	
End Beams	9.70	4.85	
Total	**20.70**	**10.35**	

Table 2.3 – Weight distribution for Phase II specimens with t = 0.76mm with gypsum

	Weight [kN]	Tributary Weight / Joist [kN]	Tributary Weight / End Beam [kN]
Steel Deck	13.00	1.08	0.54
Steel Bars	28.40	2.37	1.18
Gypsum	16.90	1.41	0.70
Transverse Eave Beams	20.20	1.68	0.84
Open Web Steel Joists	13.70	1.25	
Steel Plates	117.30	10.66	
Total	**209.50**	**18.45**	**3.27**
Seismic Weight Not Carried By The Diaphragm (kN)			
Actuator Load Cell + Swivel	11.00	5.50	
End Beams	9.70	4.85	
Total	**20.70**	**10.35**	

Table 2.4 – Weight distribution for Phase II specimens with t = 0.91mm

	Weight [kN]	**Tributary Weight / Joist [kN]**	**Tributary Weight / End Beam [kN]**
Steel Deck	15.40	1.28	0.64
Steel Bars	28.40	2.37	1.18
Transverse Eave Beams	20.20	1.68	0.84
Open Web Steel Joists	13.70	1.25	
Steel Plates	117.30	10.66	
Total	**195.00**	**17.24**	**2.67**
Seismic Weight Not Carried By The Diaphragm (kN)			
Actuator Load Cell + Swivel	11.00	5.50	
End Beams	9.70	4.85	
Total	**20.70**	**10.35**	

2.2.1.4. Specimens

The diaphragms used in the first sets of dynamic tests consisted of 0.76 mm thick Z275 (G90) galvanized steel decking complying to ASTM A653M SS Grade 230 with powder-driven nail fasteners for the deck to frame connections and self-tapping screws for the sidelap connections. The deck was rolled by the company CANAM from sheet steel with a minimum specified F_y = 230 MPa and F_u = 310 MPa. All specimens consisted of 38 mm deep by 914 mm wide corrugated deck sheets as shown in Figure 2.11. The type of sidelap deck profile depended on the type of fastener used. For nailed and screwed diaphragms, only an overlap was required but welded and button-punched diaphragms required a special interlocking profile for the connection. The test nomenclature is listed in Table 2.5 and Table 2.6.

Table 2.5 – Phase I diaphragm specimen configurations

Test No.	Deck Profile	Sheet Thickness (mm)	Frame Fasteners	Fastener Pattern	Sidelap Fasteners	Lap Spacing (mm)	End Overlap
DIA1	38x914	0.76	ENDK22 Nails	36/4	#12 Screws	305	yes
DIA1R	38x914	0.76	ENDK22 Nails	36/4	#12 Screws	305	yes
DIA2	38x914	0.76	ENDK22 Nails	36/4	#12 Screws	305	no

Note: R suffix refers to repaired specimen configuration; For nailed frame fasteners, X-EDNK22 THQ12 nails were used at edge beam locations in all cases; Fastener patterns are explained in Figure 2.15

Table 2.6 – Phase II diaphragm specimen configurations

Deck Profile	Deck Profile	Sheet Thickness (mm)	Frame Fasteners	Fastener Pattern	End Overlap	Sidelap Fasteners	Lap Spacin g (mm)
DIA3	38x914	0.76	ENDK22 Nails	36/4	36/7	#12 Screws	152
DIA3R				36/7	36/7	#12 Screws	152
DIA4	38x914	0.76	ENDK22 Nails	36/7	36/7	#12 Screws	152
DIA4R				36/9	36/9	#12 Screws	152
DIA5	38x914	0.76	ENDK22 Nails	36/9	36/9	#12 Screws	152
DIA5R				36/9	36/9	#12 Screws	102
DIA6	38x914	0.76	ENDK22 Nails	36/11	36/11	#12 Screws	152
DIA6R				36/11	36/11	#12 Screws	102
DIA7	38x914	0.91	ENDK22 Nails	36/7	36/7	#12 Screws	152
DIA7R				36/7	36/7	Rivets	152
DIA8	38x914	0.91	ENDK22 Nails	36/9	36/9	#12 Screws	152
DIA8R				36/9	36/9	#12 Screws	102
DIA9	38x914	0.91	ENDK22 Nails	36/11	36/11	#12 Screws	152
DIA9R				36/11	36/11	#12 Screws	102
DIA10	38x914	0.76	16 mm welds	36/4	36/4	Button punch	305
DIA10R	38x914	0.76	ENDK22 Nails	36/4	36/4	#12 Screws	305

Note: R suffix refers to repaired specimen configuration; For nailed frame fasteners, X-EDNK22 THQ12 nails were used at edge beam locations in all cases; Fastener patterns are explained in Figure 2.15

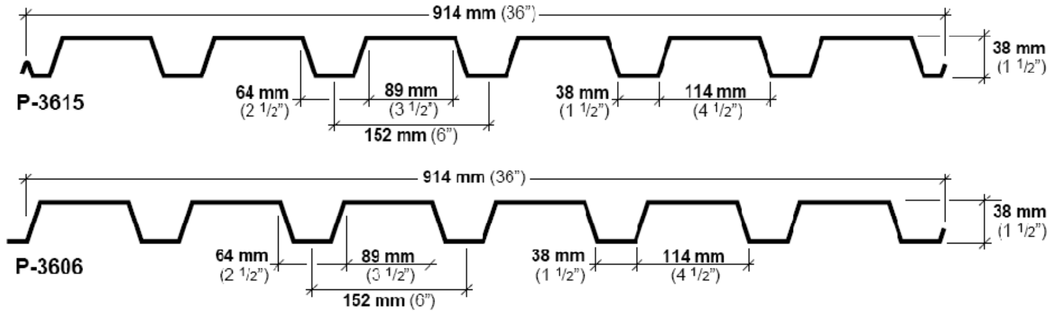

Figure 2.11 – P-3606 (top) and P-3615 (bottom) deck profile (CANAM, 2009)

The powder-driven nail fasteners used for the tests were X-EDNK22 THQ12 for all the joist and eave beam fastener locations. Edge beams required X-EDN 19 THQ 12M nail fasteners to satisfy the metal thickness requirements. For the screwed sidelap locations, Hilti S-MD 12 self drilling screws were used in all test scenarios. All the mechanical fastener types are shown in Figure 2.12 and all the types of frame fasteners are shown in Figure 2.13. Installed sidelap fasteners are displayed in Figure 2.14.

Figure 2.12 – X-EDN 19 THQ 12M nail, X-EDNK22 THQ12 nail and #12 Self tapping screw (left to right)

Figure 2.13 – Installed frame fasteners: X-EDN 19 THQ 12M nail, X-EDNK22 THQ12 nail and weld (left to right)

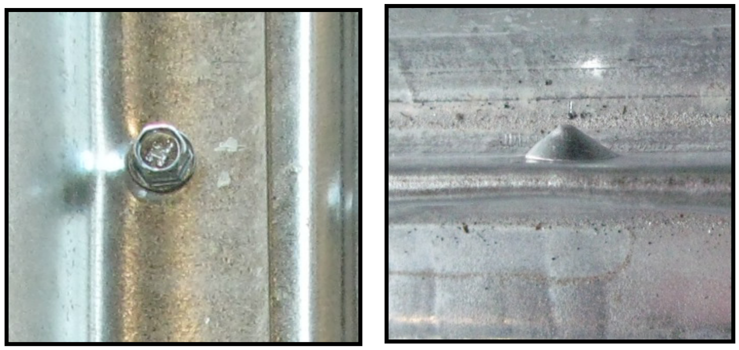

Figure 2.14 – Installed sidelap fasteners: #12 self-tapping screw and button punch (left to right)

Phase I of the test program, which was conducted during the summer of 2007, consisted of three sets of tests. The properties of the diaphragms used for first phase of the diaphragm testing program are included in Table 2.5. The fastener patterns refer to those defined by the SDI (Luttrell, 2004) as shown in Figure 2.15.

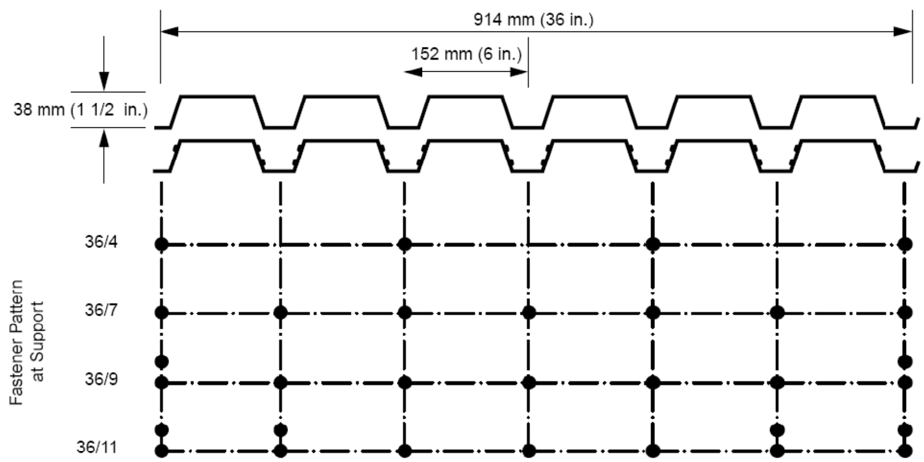

Figure 2.15 – Fastener configurations (CANAM, 2007; Luttrell, 2004)

The only difference between the two sets of dynamic tests conducted on new diaphragms in Phase I was that there was no overlapping at the end joints in test DIA2 whereas DIA1 included a 50mm overlap to restrain the warping at sheet extremities (Figure 2.16 & Figure 2.17). This allowed for a quantitative measurement of the stiffness contribution and the limitation of slip due to the constriction of warping.

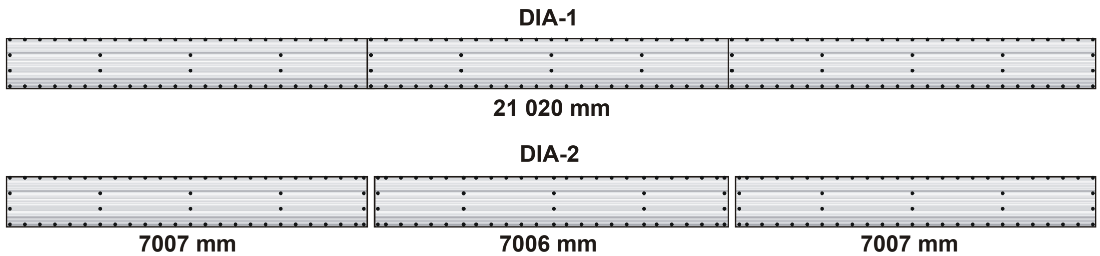

Figure 2.16 – Illustration of overlap and non-overlapped diaphragm scenarios

Figure 2.17 – Overlapped DIA1 specimen (left) and non-overlapped DIA2 specimen (right) comparison

Phase II was planned to cover screwed and nailed fastener patterns for 0.76 and 0.91 mm decks. Each diaphragm in Phase II was constructed with end overlaps; this represents the common detail used in practice. As opposed to repairing the diaphragms with the same fastener pattern after they have undergone inelastic deformations as was done in Phase I, Phase II test specimens were repaired using diverse methods as explained in Section 2.3. An investigation into the effect of non-structural gypsum and different end and interior overlap fastener patterns was also investigated with DIA3.

Lastly, Phase II of the diaphragm testing program involved a welded and button punched diaphragm (DIA-10) which in past years in Canada has been the most common approach to connecting the roof deck panels. Based on previous static cantilever tests, diaphragms of this construction do not perform well in the inelastic range (Rogers & Tremblay, 2003a; 2003b). Nonetheless, this specimen was included to evaluate the response of a welded/button punch diaphragm under dynamic and seismic loading and thus provide information on what could be expected in terms of seismic performance of existing buildings constructed with similar diaphragm assemblies. A repair scheme was devised for the weld / button punch configuration as described in Section 2.3. In the event of an earthquake, where damage to the diaphragm would have occurred, there is no information regarding possible repair procedures that would permit the diaphragm to perform satisfactorily as a component in the SFRS if it were subjected to seismic activity again.

Specimen DIA10 comprised 16 mm arc-spot welds which were installed by a certified welder using E6011 electrodes. To ensure that the specified weld diameter had been met, all welds were measured and an average of 17mm was recorded. In addition, the welder was also timed to be able to compare with the timing of welders in the field. The record of all the weld diameters and the timing are included in Appendix E. The average time per weld was recorded to be 7.7 seconds.

A seam locking / clinching tool (Figure 2.18) was used to install the button punched connections at sidelap locations. The connection thus relies entirely on the mechanical friction and locking generated from the deformed steel sheet.

Figure 2.18 – Seam-locking tool

The strengths and stiffnesses for Phase I and II, determined using the SDI methodology and the nominal thickness and material properties, are included in Table 2.7. Two cases were considered for the test setup. Case A refers to the values obtained for a single panel length (7006 mm), and Case B refers to the instance where the full diaphragm length (21020mm) was considered for the calculation of stiffness and strength. The nominal resistance, S_n, is based on the lowest of the resistance of the panel end, resistance of the interior panel and the resistance of the corner connection. The overall shear buckling failure mode was not considered as it is more critical for shallow depth decks with closely spaced fastener connections. All the parameters for the calculation of the shear resistance according to the SDI (2004) methodology are included in Appendix A.

Table 2.7 – Predicted Phase I & II specimen strengths and stiffnesses using the SDI design method

Test No	Case A		Case B	
	S_n (kN/m)	G' (kN/mm)	S_n (kN/m)	G' (kN/mm)
1	13.03	4.21	12.52	12.98
1R	13.03	4.21	12.52	12.98
2	13.03	4.21	12.52	12.98
3*	23.52	4.45	22.61	15.72
3R	24.41	16.99	23.72	24.99
4	24.41	16.99	23.72	24.99
4R	29.18	17.38	27.98	25.77
5	29.18	17.38	27.98	25.77
5R	35.29	18.33	34.29	28.09
6	31.84	17.61	29.62	25.98
6R	38.55	18.48	37.23	28.41
7	29.16	21.83	28.35	29.49
7R**	34.85	22.42	33.43	30.49
8	34.85	22.42	33.43	30.49
8R	42.15	23.88	40.96	33.48
9	38.03	22.77	36.24	31.10
9R	46.05	24.11	44.48	33.89
10	8.50	3.55	7.91	7.78
10R***	14.08	4.22	13.44	13.09

*** Capacity calculated assuming alternate nailed spacing**
**** Capacity calculated using #12 screwed sidelap characteristics**
*****Capacity calculated using 16mm weld and #12 screw characteristics**

2.2.1.5. Gypsum

In addition to the steel deck diaphragm test series, gypsum was installed on specimen DIA3 to investigate the stiffness increase due to non-structural materials. The other components typically found in a roofing membrane were ignored as previous studies had shown that they did not influence the stiffness of the steel roof deck diaphragm (Mastrogiussepe, 2006). The non-structural gypsum used in the testing program was standard ProRocType X 5/8 inch gypsum board with a mass of 11.2 kg/m^2 (CertainTeed, 2009). The gypsum sheets were attached to the underlying decking using 38.1 mm [1 ½ in.] screws and 76.2 mm [3 in.] diameter plates (Figure 2.19); this is the only connection method currently sanctioned by Factory Mutual to obtain satisfactory uplift resistance.

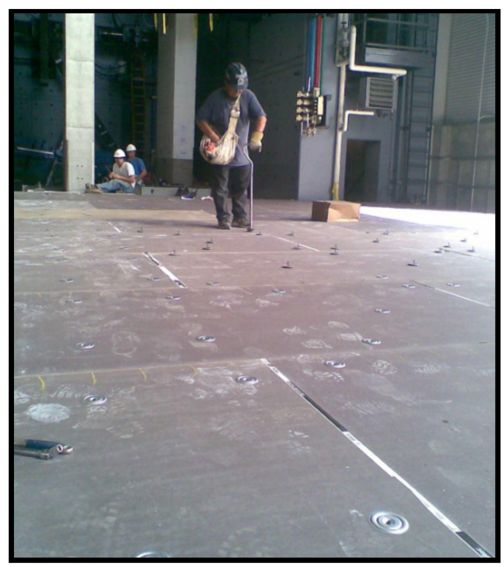

Figure 2.19 – Screw and plate connection (left) (OMG, Inc., 2009) and gypsum installation (right)

Factory Mutual also specifies that a minimum of 8 screws per 4 ft by 8 ft (1.2 by 2.4 m) sheet must be installed for an uplift resistance of 1.4 kPa or 11 screws per sheet for an uplift resistance between 1.4 and 2.2 kPa (Canadian Roofing Contractors' Association, 1993). The typical screw quantities were respected except that 12 screws were used around the perimeter of the diaphragm test specimen to resist the greater bending deformations. Thus, an upper bound solution would be obtained for the increase in shear stiffness due to gypsum. The patterns used for DIA3G can be seen in Figure 2.20. The overall layout of the gypsum, along with the number of fasteners used per board, is displayed in Figure 2.21.

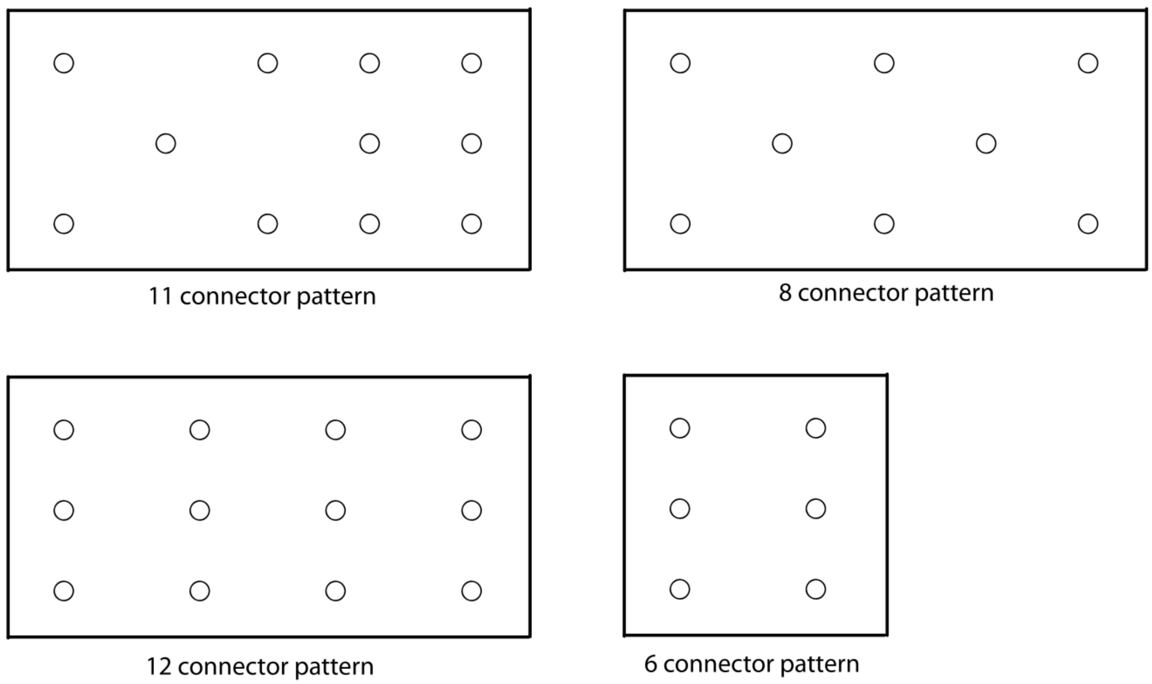

Figure 2.20 – Gypsum fastener patterns

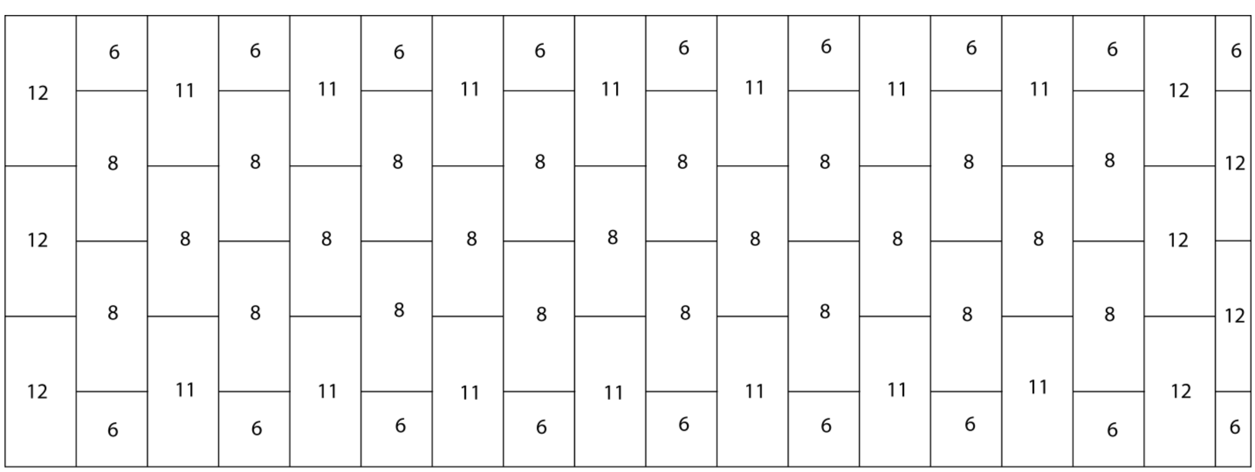

Figure 2.21 – Overall gypsum fastener layout

2.2.1.6. Rivets

Rivets were used as a repair means for the sidelap connectors for DIA7. Blind rivets of type G-bulb GSMD85SGB were installed in pre-drilled holes with two 1.2 mm thick and 18.21 mm diameter washers for each fastener. The washers were used to meet the minimum grip requirement of the rivets as specified by the manufacturer. The dimensions of the G-Bulb rivets and a picture of the rivet placement can be seen in Figure 2.22. The installation procedure is detailed in Table 2.9.

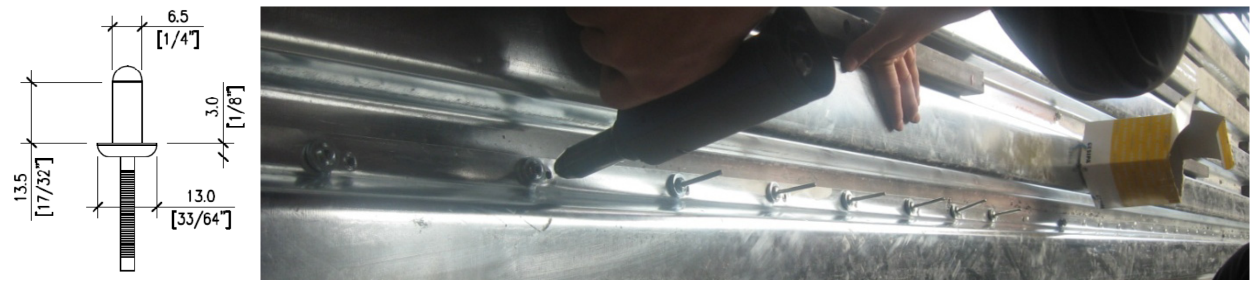

Figure 2.22 – G-Bulb rivet dimensions and placement

The strength of the rivet connection was evaluated using CSA-S136 (2007) for bearing failure. Clauses E3.3.1 and E3.3.2 specify the following Equations (2.1 and 2.2) to calculate the nominal resistance of the connection in bearing.

$$P_n = Cm_f dtF_u \tag{2-1}$$

Where:

C – is a bearing factor [Table E3.3.1-1 (CSA-S136, 2007)], 3.0 for d/t < 10

m_f – is a factor dependent on the number of shear planes [Table E3.3.1-2 (CSA-S136, 2007)], taken as 0.75 for a single shear plane

d – is the diameter of the connector, 6.5 mm is the nominal diameter of the g-bulb rivets

t – is the uncoated steel thickness of the connected sheets, 0.76 mm is the nominal uncoated thickness of the deck specimen

F_u – is the tensile strength of the steel, taken as the nominal strength of 310 MPa for the calculation of the nominal connection resistance and 363.4 MPa (Table 2.11) for the experimental resistance of the connection

$$P_n = (4.64\alpha t + 1.53)dtF_u \tag{2-2}$$

Where:

α – is a coefficient of conversion for the units used, 0.0394 for SI units

d, t, F_u – are as specified for Equation 2-1

All the results are summarized in Table 2.8 along with the resistance in shear provided by the manufacturer.

Table 2.8 – Bearing and shear resistance of sidelap rivet connection

Clause S136-07	**Resistance**
Cl. E3.3.1	P_n= 4.04 kN [with m_f = 0.75 & $F_{u,\ experimental}$ = 363.4 MPa] P_n= 3.45 kN [with m_f = 0.75 & $F_{u,\ standard}$ = 310.0 MPa]
Cl. E3.3.2	P_n= 3.00 kN [with $F_{u,\ experimental}$ = 363.4 MPa] P_n= 2.56 kN [with $F_{u,\ standard}$ = 310.0 MPa]
Manufacturer	11.0 kN [Shear resistance of rivet] (Gesipa – Fasteners USA Inc., 2007)

Table 2.9 – Rivet installation (Avdel, 2009)

Explanatory Figures	Installing Procedure
	1. Rivet is placed inside the breakstem system
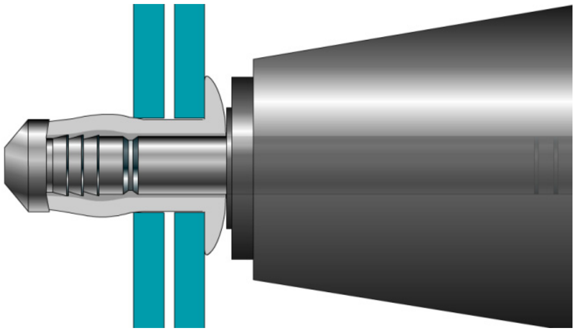	2. Place the rivet inside the holes which have already been predrilled
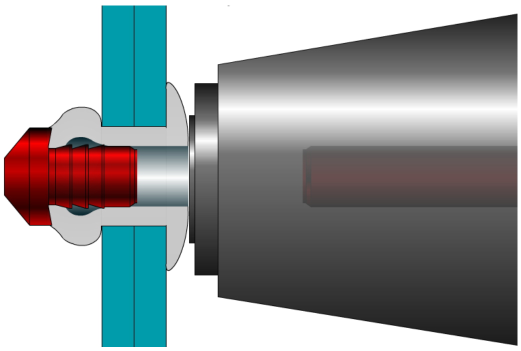	3. The breakstem system pulls on the rivet which forces the top of the rivet to buckle outwards and squeeze the steel sheets together. Once the desired load is reached, the system breaks off the stem and it is then collected in the back of the gun.
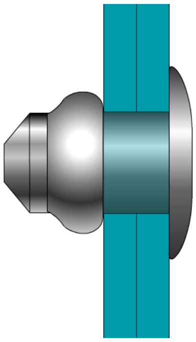	4. This is the final product of the rivet placement

2.3. Repair Procedure and Testing

After the inelastic seismic test, the diaphragm was repaired by replacing the connections that had failed and then adding connectors for strengthening. The purpose of this second experiment was to be able to evaluate whether the original stiffness and strength of the diaphragm could be recuperated. Different procedures (Table 2.10) were used to repair each of the specimens.

Table 2.10 – Repair methods

Test Specimen	Repair Methods
DIA1	Same pattern [36/4]
DIA3	Increase in Interior Frame Fastener Pattern to Match Fastener Pattern at Ends[36/4 to 36/7 with 152 mm]
DIA4	Increase in Frame Fastener Pattern [36/7 to 36/9 with 152 mm]
DIA5	Increase in Sidelap Pattern [152mm to 102mm with 36/9]
DIA6	Increase in Sidelap Pattern [152mm to 102mm with 36/11]
DIA7	Screws Replaced by Rivets with same Fastener Pattern [36/7 with 152 mm]
DIA8	Increase in Sidelap Pattern [152mm to 102mm with 36/9]
DIA9	Increase in Sidelap Pattern [152mm to 102mm with 36/11]
DIA10	Welds Replaced by Nails and Button-Punch Connections Replaced by Screwed 1.21mm plate

In the case of damaged frame fasteners, additional equivalent size nails were installed at the failed nail or weld location. Nails that experienced bearing damage in the surround sheet steel were not removed. For the welded specimen, DIA10, all welds were reinforced with nails. Figure 2.23 displays an example of a bearing damage and weld failure, with adjacent replacement nails.

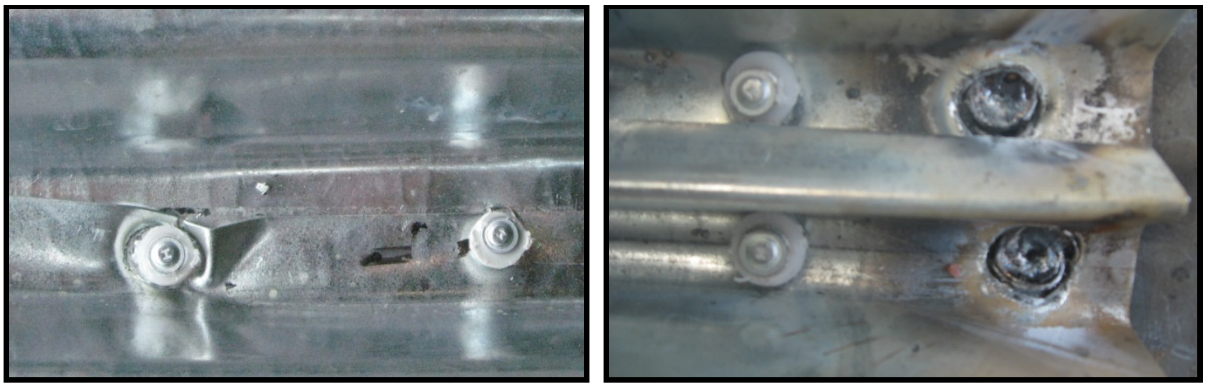

Figure 2.23 – Bearing damage (left) and fractured weld (right) replacement example

In the case of sidelap screw repairs, at all the locations where the deck had undergone bearing deformations, the screws were removed and replaced with new ones. For the button-punch connections, to improve the strength, 1.21 mm sheets were screwed with Hilti S-MD 12 screws from underneath on either side of the interlocking profile at all sidelap locations. Two screws were required at each connection as is shown in Figure 2.24. The sidelap rivet repair procedure was explained in Section 2.2.1.6.

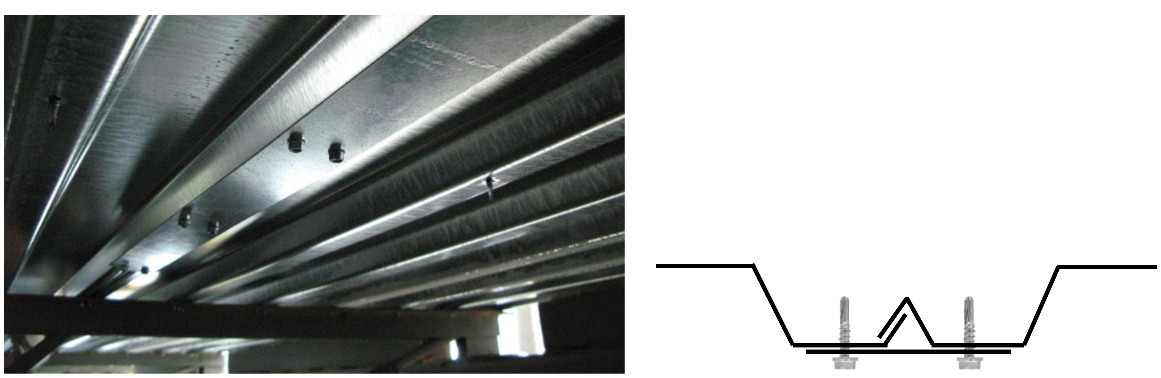

Figure 2.24 – Picture (left) and illustration (right) of the button punch sidelap repair scenario with screws and 1.21mm steel sheet

2.4. Material Properties

Material coupon tests were carried out to determine the thickness and material properties of each set of deck panels. Only one set of tests was performed for panels that originated from the same coil. All tests were performed according to ASTM A370. A crosshead rate of 0.6 mm/min was programmed for the coupon specimen's elastic range. This rate was then increased to 6 mm/min once the material was past its yield point. The test was paused three times to evaluate the difference between the static and non-zero strain rate characteristics of the steel. Three coupons were tested for each diaphragm set and average values were determined for evaluation (Table 2.11). To obtain the base metal uncoated thickness of the coupons, the specimens were placed in an acid solution to remove any galvanization.

The ratio of F_u/F_y exceeded the minimum limit of 1.2 as specified by CSA-S136 (2007) for all the specimens. In addition, the coupon elongation exceeded the minimum 10% limit required by the North American Specification for Cold-Formed Steel Members over the 50 mm gauge length. (CSA-S136, 2007).

Table 2.11 – Sheet steel material properties

Specimen	Nominal Thickness (mm)	Base Metal Thickness (mm)	Yield Stress F_y (MPa)	Ultimate Stress F_u (MPa)	F_u/F_y	% Elongation
DIA-1	0.76	0.80	339*	400*	1.18	33
DIA-2	0.76	0.80	335*	400*	1.20	36
DIA-3	0.76	0.76	252	363	1.44	28
DIA-4	0.76	0.77	322	403	1.25	29
DIA-5	0.76	0.76	318	414	1.30	29
DIA-6	0.76	0.75	300	411	1.37	32
DIA-7	0.91	0.90	314	420	1.34	31
DIA-8	0.91	0.90	291	401	1.38	29
DIA-9	0.91	0.92	310	394	1.27	28
DIA-10	0.76	0.77	296	376	1.27	35

*** These values correspond to non-zero strain rate characteristics of the coupons (ie. Crosshead was not paused during testing; strain rate of 0.6 mm/min for F_y and 6 mm/min for F_u)**

2.5. Dynamic Testing Protocols

Three types of dynamic tests were conducted sequentially on each diaphragm specimen to characterize and observe the behaviour under seismic loading. These tests included broadband excitation (white noise), single-frequency excitation and seismic excitation (Figure 2.25). Each of the experimental protocols is further explained in Section 2.5.1. to 2.5.4..

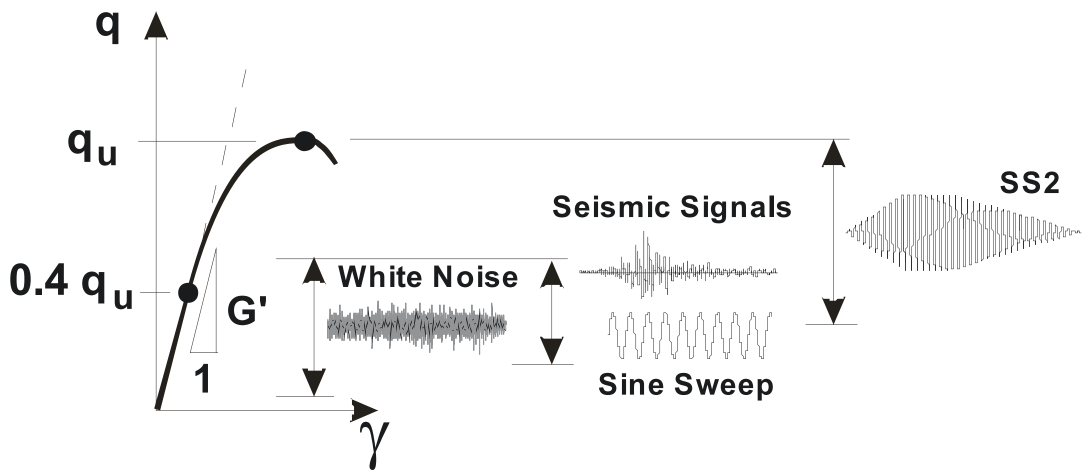

Figure 2.25 – Schematic representation of experimental testing protocols

2.5.1. Broadband Excitation

Broadband excitation is the process of applying a certain loading protocol to the test specimen which contains energy over a wide range of frequencies. Different signals can be used for broadband excitation but the most frequent are random, periodic random and impact signals (Braun *et al*., 2002). A purely random signal was generated by creating a white noise protocol which is characterized by a flat spectral density function that represents a uniform energy content at any frequency over a fixed bandwidth. The bandwidth is usually chosen to be equal to the acquisition frequency as that value is selected to cover the representative range of frequencies required for post-processing. The frequency bandwidth used in the context of the experimental program for the white noise acceleration record was from 0 to 25 Hz.

The output signal is of finite length; hence, Fourier analysis will produce spectra which are discrete instead of continuous. There will be a transfer of energy between adjacent spectral lines. This phenomenon is known as leakage and must be prevented by applying a window to each of the finite response signals (Braun *et al.*, 2002). The windowing process will be elaborated in Section 2.7.1.3.

The purpose of the broadband excitation was to determine the natural frequency of the diaphragm and by relation, to calculate its stiffness. Ambient vibration velocity data was first acquired from the specimen without any loading protocol. Thus, the fundamental frequency of the diaphragm at very low excitation amplitudes could be determined. The broadband signal was then applied, and systematically amplified until either the force reached 20% of the nominal predicted resistance or a root-mean-square (RMS) acceleration response of 0.2g was reached at the centre of the diaphragm. These amplifications at various intensities enabled the extraction of the change in fundamental frequency with different excitation amplitudes.

2.5.2. Single-Frequency Excitation

Single frequency excitation can be described as stepped-sine or swept-sine. The first is characterized by a protocol which has a single frequency while the second contains a sine signal whose amplitude varies continuously over its length. For the purpose of our experiments, the stepped sine excitation was used. The diaphragm was excited at a certain frequency and amplitude. It was allowed to settle under the applied motion to remove any transient effects and to obtain the steady-state response. Unlike the broadband excitation, this method has the advantage of controlling the frequency and the excitation amplitude and it is better suited to investigate non-linear effects. Single-frequency excitation was performed over a range of frequencies surrounding the first mode. Eight amplitudes were used for the acceleration and the acceleration was kept constant over the frequency range so that the input force would remain equal. Resonance curves, which show the shift in frequency, could then be obtained and damping could be derived from those same results. An upper limit of 20 % of the nominal predicted shear resistance of the diaphragm was used for these tests. Application of this loading protocol was only possible for specimens with natural periods of less than 7Hz because the actuator performance greatly decreased past this point.

2.5.3. Seismic Excitation

Seismic signals were applied to the diaphragm to observe its dynamic response under realistic earthquake excitation. The loading protocols for the seismic signals were tailored to attain different percentages of the diaphragm's ultimate resistance in the elastic range up to the 60% of the nominal SDI strength. The response along the length of the diaphragm allowed for the determination of the distribution of inertia forces and stiffness during an earthquake.

Two acceleration records with different response spectrum were selected for the tests. Seismic signal SS1 (Figure 2.26) is a 10 second acceleration record from the 1989 Loma Prieta earthquake (Stanford Univ. 360°) with a peak value of 0.29 g. A time scale factor of 1/3 was used to reflect the difference between the fundamental period of the test specimens and that of actual low-rise buildings. Seismic signal SS3 (Figure 2.27) was an acceleration record from the

Northridge Earthquake (Big Tujunga, 352°) with a peak value of 0.245 g and a duration of 12 seconds. A time factor of 1/2.5 was used for this acceleration record.

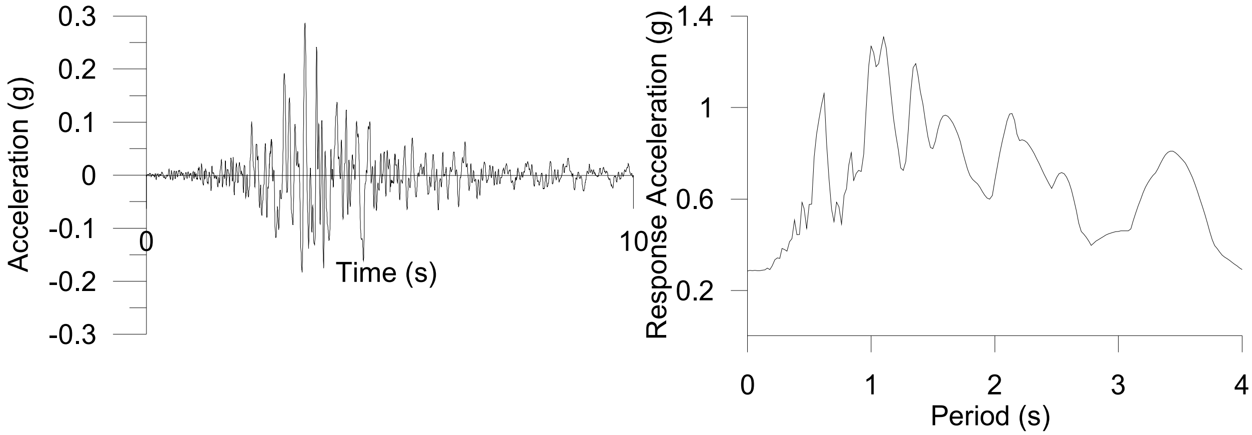

Figure 2.26 – Loma Prieta acceleration record and response spectrum for ξ = 2% [Time Scale 1/3]

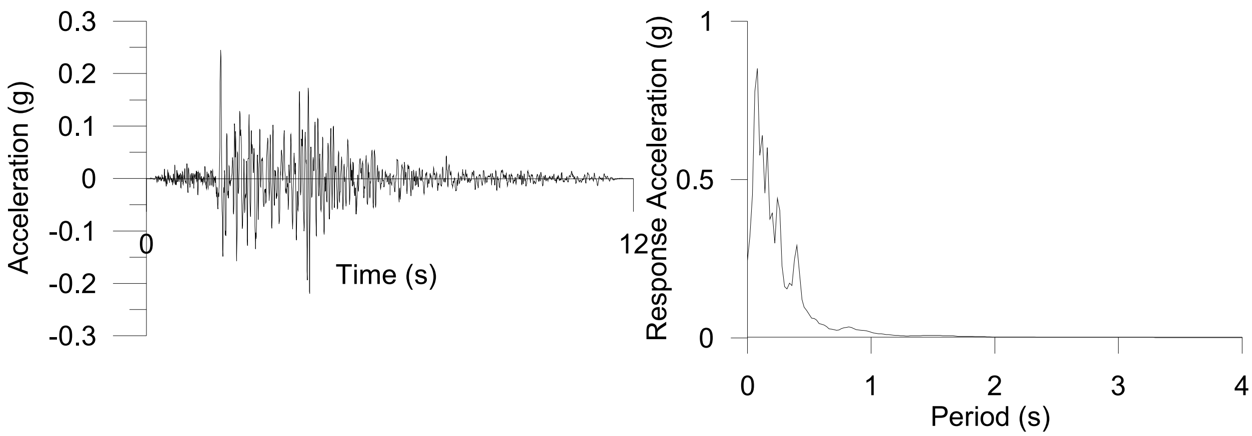

Figure 2.27 – Northridge acceleration record and response spectrum for ξ = 2% [Time Scale 1/2.5]

To determine the different amplifications in the elastic range of the diaphragm, the maximum load carried by the diaphragm was calculated using the Ruaumoko (Carr, 1994) model developed by Shrestha *et al.* (2009) when subjected to the ground motion. The percentages were then obtained using Equation 2-3 :

$$\%\ Amplification = \frac{Desired\ Edge\ Beam\ Shear\ Force}{Edge\ Beam\ Shear\ Force\ under\ 100\%\ Ground\ Motion} \qquad (2\text{-}3)$$

The 7m panel properties were used in the model along with 2% Rayleigh damping.

2.5.4. Excitation for Inelastic Response

The last test involved a loading protocol which forced the diaphragm into inelastic response; it was used to determine the ultimate shear force that could be carried by the diaphragm as well as the extent of inelastic deformations in the specimen. Cyclic loading at this intensity also allowed for the quantification of the diaphragm's ductility and hysteretic behaviour. The protocol consisted of a sine signal with a linearly-increasing amplitude and four peaks at the maximum amplitude which is displayed in Figure 2.28. To determine the maximum displacement required for inelastic behaviour to occur, a non-linear dynamic analysis was performed on Ruaumoko (Carr 1994) with the analysis model developed by Shrestha *et al.* (2009) prior to the test. The stiffness information obtained from the white noise excitation testing was used in this model to determine the amplification required to force the diaphragm into inelastic behaviour. The final tests in Phase I required a final signal at 4 Hz with an amplitude of 30mm while the tests completed in Phase II required a frequency of 5 Hz with amplitudes of 24 mm and 27.6 mm due to the considerable increase in strength obtained with closer fastener spacing. The acceleration record of Loma Prieta (SS3) with an amplification of 2000% was used for DIA3 and DIA3R but the lack of hysteresis curves in the response made it less adequate for the calibration of a numerical model. The lists of all the completed tests are included in Appendix E.

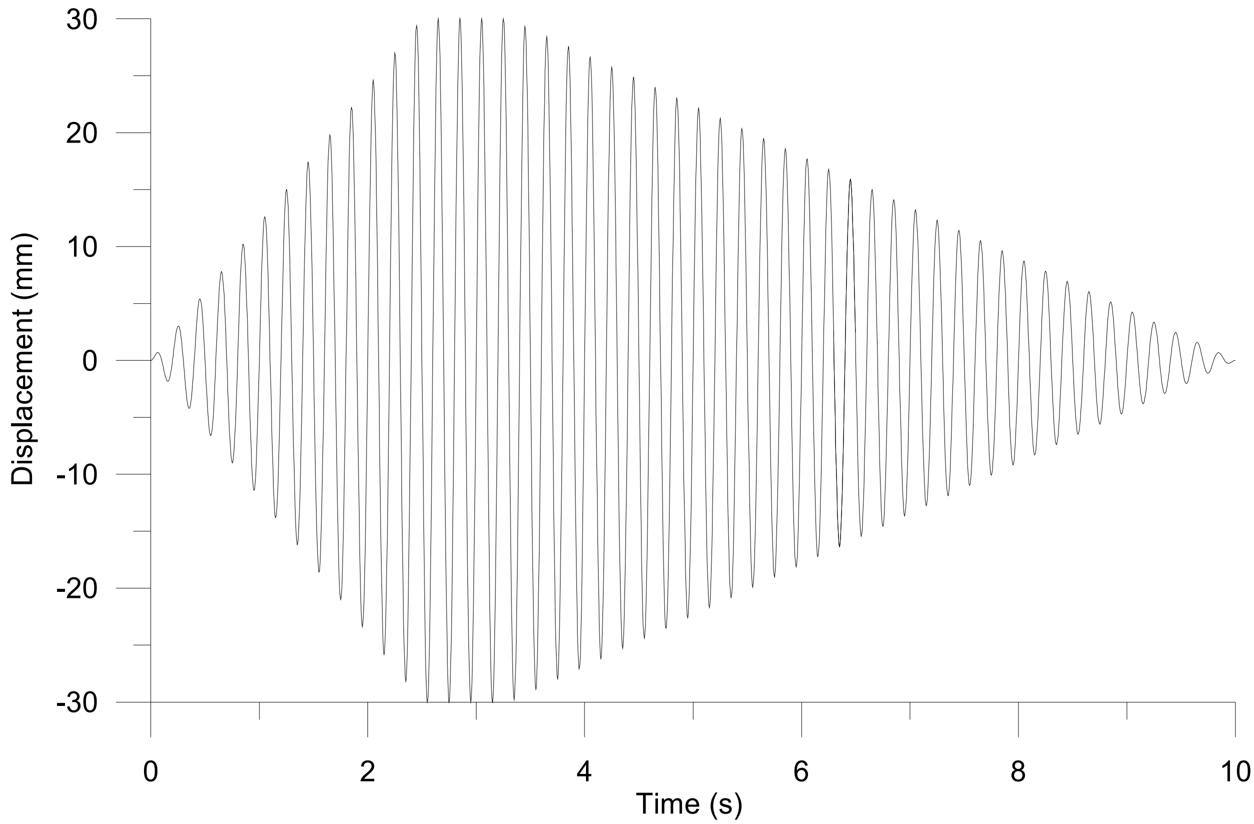

Figure 2.28 – SS2 - Signal for inelastic response [5Hz | 30 mm]

2.6. Instrumentation

The majority of the instrumentation (Figure 2.29) that was installed on each specimen was connected to a Hottinger Baldwin Messtechnik data acquisition system. All the tests were sampled at a rate of 100 Hz.

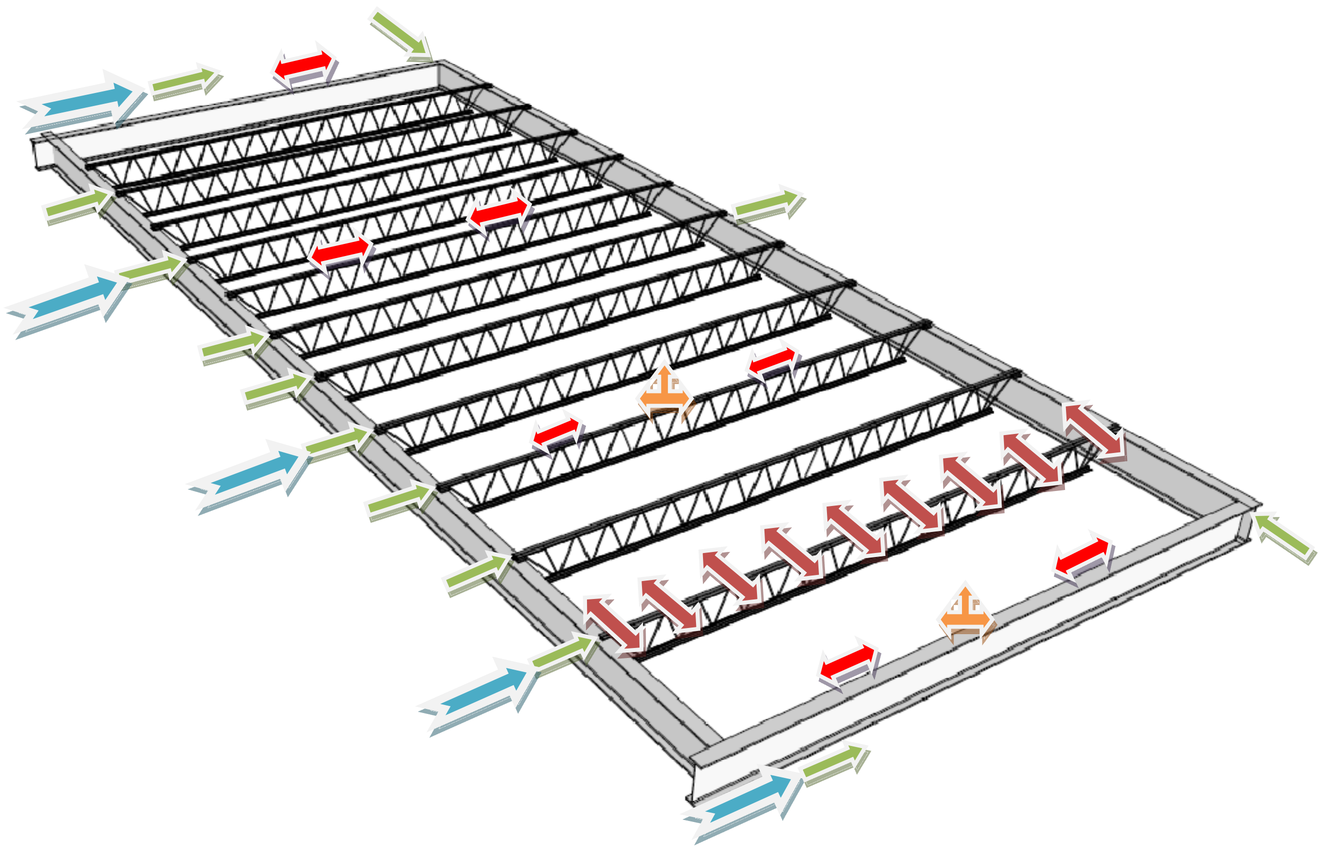

Figure 2.29 – Test setup instrumentation

 1. Accelerometers and string potentiometers measuring in the direction shown

 2. Uni-directional LVDTs which were used to measure the relative slip of two panels at sidelap locations

 3. 3-Dimensional LVDT measurement for warping at end panels [DIA1 and DIA2 only]

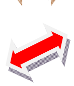 4. LVDTs which measured the longitudinal displacement of panel end joints

 5. Velocity transducers

Accelerometers and potentiometers were positioned at every joist to obtain representative acceleration and displacement readings over the width of the specimen. However, for the more sensitive tests, such as white noise, velocity transducers were used at five evenly spaced locations over the width of the deck specimen because the precision of the accelerometers and potentiometers was not adequate when displacement amplitudes were small. The velocity transducers were screwed onto the deck by means of a metal plate. The instrumentation installed at a typical joist is displayed in Figure 2.30.

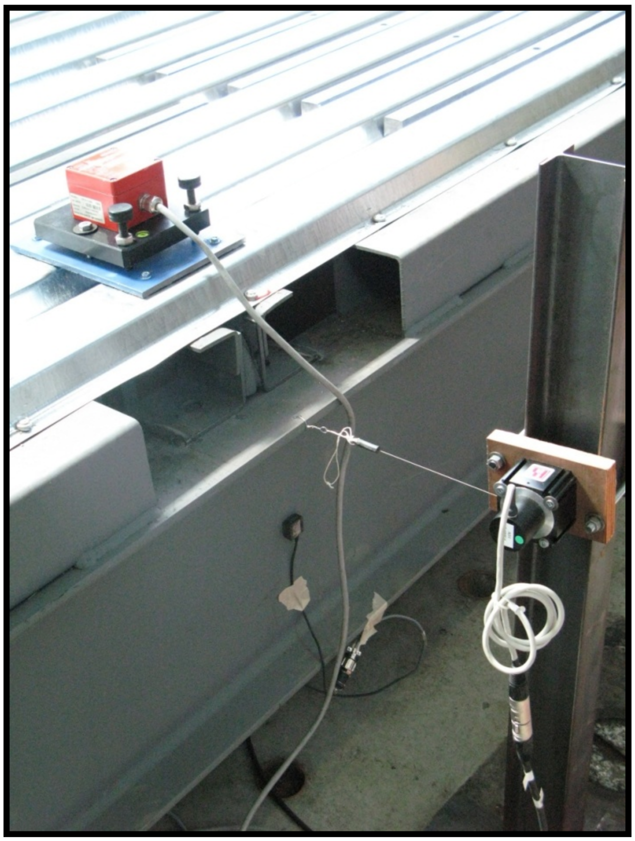

Figure 2.30 – External accelerometers, potentiometers and velocity transducers

The 3-dimensional LVDT setups were used to record the warping at a free end joint and an overlapped panel joint for comparison on specimen DIA1 and DIA2. These displacement transducers had a ± 5mm range. Similarly, LVDT displacement sensors were placed so as to record the lateral displacement of unrestrained and overlapped panel ends (Figure 2.31). This data could then be used to determine the amount of slip occurring in the specimen.

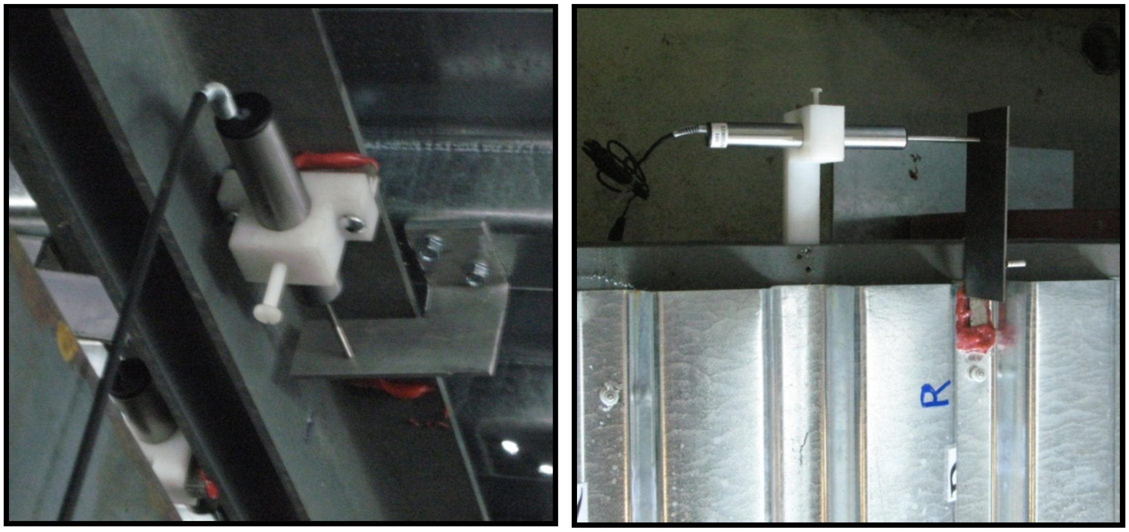

Figure 2.31 – Internal (Left) and External (Right) in-plane deck displacement recording LVDTs

LVDT displacement sensors measured the relative movement of two connected decks at sidelap locations (Figure 2.32). All the LVDT supports were made out of Teflon material and were either bolted, for the interior, or glued, for the exterior, to the frame of the diaphragm. Steel plates were then used as pressure points for the sensors.

Figure 2.32 – Slip recording LVDTs at sidelap locations

In addition to this instrumentation, force readings were obtained from the actuator load cell. The input displacement from the actuator interal displacement transducer and the external LVDTs were also controlled.

2.7. Analysis of Measured Test Data

The methods used in the analysis of the test data are described in this Section. Matlab (The Mathworks, Inc., 2009) was used as the mathematical interface for data processing from response measurements for both the broadband and single-frequency excitations to extract the dynamic characteristics of the diaphragms.

2.7.1. Natural Frequencies and Mode Shapes

The natural frequencies and mode shapes, f_i and u_i respectively, were determined using the Frequency Domain Decomposition (FDD) algorithm described by Brincker *et al.* (2001). This algorithm's specific purpose is to determine the natural frequencies from output-only systems subjected to broadband excitation. One of the main advantages of FDD over other classical techniques is its ability to identify closely-spaced modes using power spectral density (PSD) functions. Before describing the method to extract the dynamic characteristics of the system, some important signal processing fundamentals need to be defined.

2.7.1.1. Filtering

Filtering was used to eliminate a very low frequency drift which was present in the output signal of the SYSCOM MS2003+ velocity sensors. A second order highpass Butterworth filter with a frequency cut-off of 0.02 Hz was selected. A representative example of the magnitude response estimate of the filter can be seen in Figure 2.33 below.

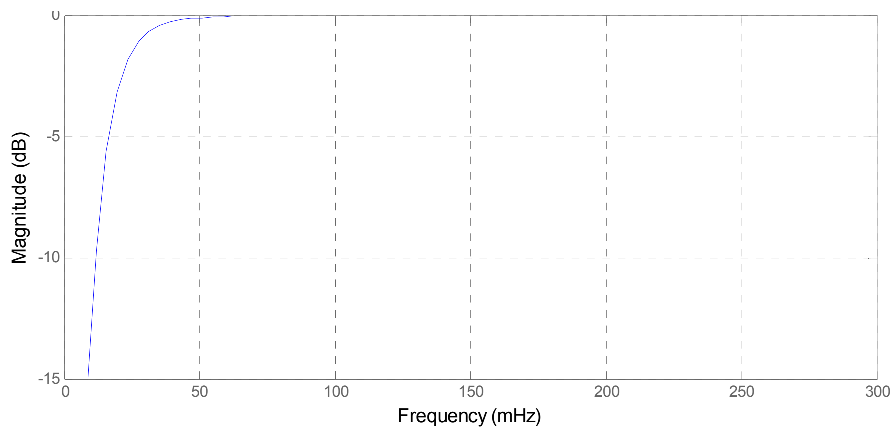

Figure 2.33 – Magnitude response function of filter

The filtering eliminated the parasitic low frequencies from the velocity transducers while keeping the rest of the frequency content unchanged. The main effect of the filtering was the slight decrease in the root-mean-squared values. Figure 2.34 displays the change in data due to the filtering.

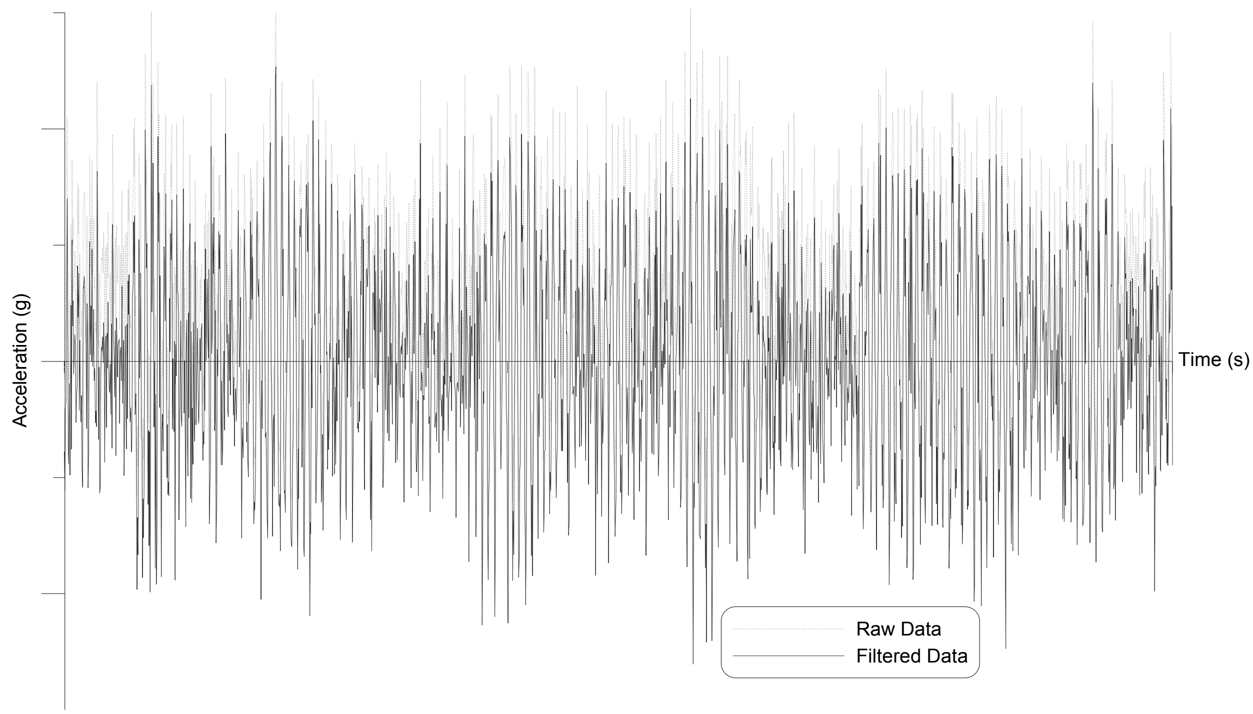

Figure 2.34 – Change in data due to filtering

2.7.1.2. Frequency Response Function

The frequency response function (FRF), or transfer function, of a physical system or structure, *H(jω)*, relates the discrete Fourier transform of the structure's output *Y* to the discrete Fourier transform of the input *X* as follows (Equation 2-4) (Brincker *et al.*, 2001):

$$Y_k(\omega) = H_{jk}(j\omega) * X_j(\omega) \tag{2-4}$$

For a multi degree-of-freedom (MDOF) system, the FRF is thus defined as the harmonic response at DOF *j* due to a unit harmonic excitation at DOF *k* at frequency *ω* (Braun *et al.*, 2002). The complete ***H****(jω)* matrix for all j and k combinations can then conveniently be related to a spatial or modal model (Equation 2-5) when expressed in the form of:

$$\boldsymbol{H}(j\omega) = (\boldsymbol{K} - \omega^2\boldsymbol{M})^{-1} = \boldsymbol{\Phi}[(\omega_r{}^2 - \omega^2)]^{\boldsymbol{-1}}\boldsymbol{\Phi}^{\mathrm{T}} \tag{2-5}$$

Where:

K – is the stiffness matrix of the spatial model

M – is the mass matrix of the spatial model

Φ – are the eigenvectors (mode-shapes) of the modal model

ω_r – are the eigenvalues (natural frequencies) of the modal model

2.7.1.3. Windowing

Spectral leakage is a process that occurs when periodicities are imposed on a certain finite portion of signal by performing a discrete Fourier transform which may result in the appearance of parasitic frequencies which are not present in the signal. To reduce the leakage that occurs during the manipulation of the response outputs, a process known as windowing was used. Applying a corrective window function (Figure 2.35) will diminish the weight of both the signal ends where the erroneous frequencies would come about.

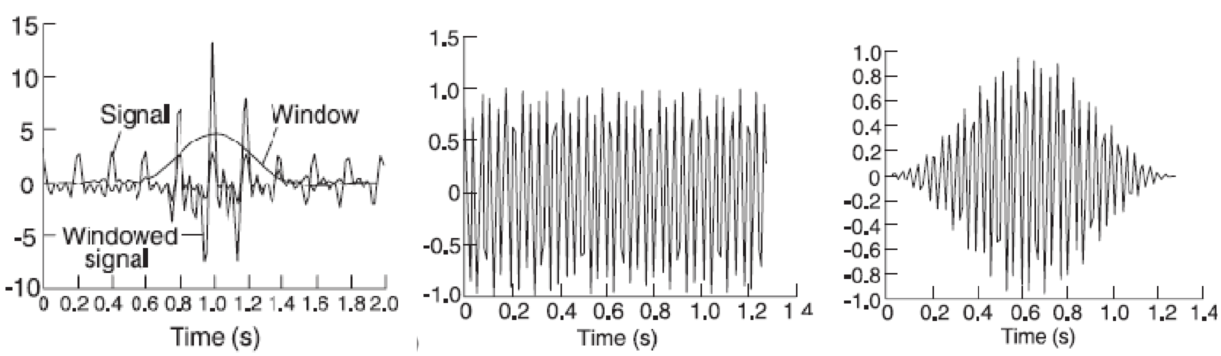

Figure 2.35 – Windowing effect of signal (left); Original signal (center); Windowed Signal (right) (Braun *et al.*, 2002)

A Hamming window (Hamming, 1977) was used to correct the different intervals. This particular window has the following correcting function (Equation 2-6) associated with it:

$$w_H(n) = 0.54 - 0.46\cos\left(2\pi\frac{n}{N}\right), 0 \leq n \leq N \tag{2-6}$$

The window length is equal to $N+1$ while symbol n represents any point along the corrective function. An overlap of fifty percent was specified and the intervals were taken to be 2000 points. This allowed for the consideration of the frequency content dimmed from the previous windowing action. Doing so made sure that the Fourier transform correctly represents the frequency content of the signal as a whole.

2.7.1.4. Power Spectral Density

The power spectral density (PSD) spectrum of a finite signal is a representation of the power that is present at each unit frequency. It is very similar to the Fourier transform of a signal as it indicates the prominence of certain frequencies but the units for the two spectra are different. In the case of power spectral densities, the values represent a quantity squared which is representative of the energy present at a certain frequency. For a complete derivation of the power spectral density function, see Bendat & Piersol (1986).

The PSD of an input (G_{xx}) can be related to the PSD of the output (G_{yy}) using the frequency response function as shown in Equation 2-7 (Braun *et al.,* 2002).

$$G_{yy}(j\omega) = \overline{\overline{H}}(j\omega)G_{xx}(j\omega)H(j\omega)^T \tag{2-7}$$

The overbar and superscript T refer to the complex conjugate and hermitian transpose respectively.

2.7.1.5. Modal Assurance Criterion

The modal assurance criterion (MAC) is a statistical indicator used for quality assurance purposes for experimental modal vectors that are determined from frequency response functions. This measure of consistency (degree of linearity) is obtained by determining the orthogonality between two singular vectors u_i and u_j. The criterion (Equation 2-8) can be computed as follows (Allemang, 2003; Allemang & Brown, 2005):

$$MAC = \frac{\left|{u_i}^H u_j\right|^2}{({u_i}^H u_i)({u_j}^H u_j)} \tag{2-8}$$

The MAC values will vary between zero and unity where zero would imply that both vectors are orthogonal and one that they are parallel. The criterion is used to produce two plots that are of interest. One can be referred to as a MAC bell curve where the solved mode-shape is compared to all the singular vectors in the range of frequency. In the case-of well defined modes, this would produce a distinct bell curve and a quantification of the level of consistency for the chosen mode-shape. The bell curve can be used to determine closely-shaped modes, as it would show a sudden drop towards lower values when the subsequent mode becomes dominant. The other curve, which is obtained by computing the MAC of each subsequent set of singular vectors, is very similar though it gives a better estimate of the frequency at which one mode becomes more prominent than the previous one. (Brincker *et al.,* 2004; Lamarche, 2005)

An advantage of the MAC bell plot is that it defines the range of frequencies over which that certain mode is dominant. Therefore, using a user-specified criterion, it is then possible to perform an inverse Fourier transform of the singular values, within that range of frequencies which satisfies the criterion, to obtain a signal in the time-domain that only contains the response of that particular mode. Hence, it is then possible to make a better estimate of the natural frequency and the damping using a logarithmic decrement of the signal (Figure 2.36).

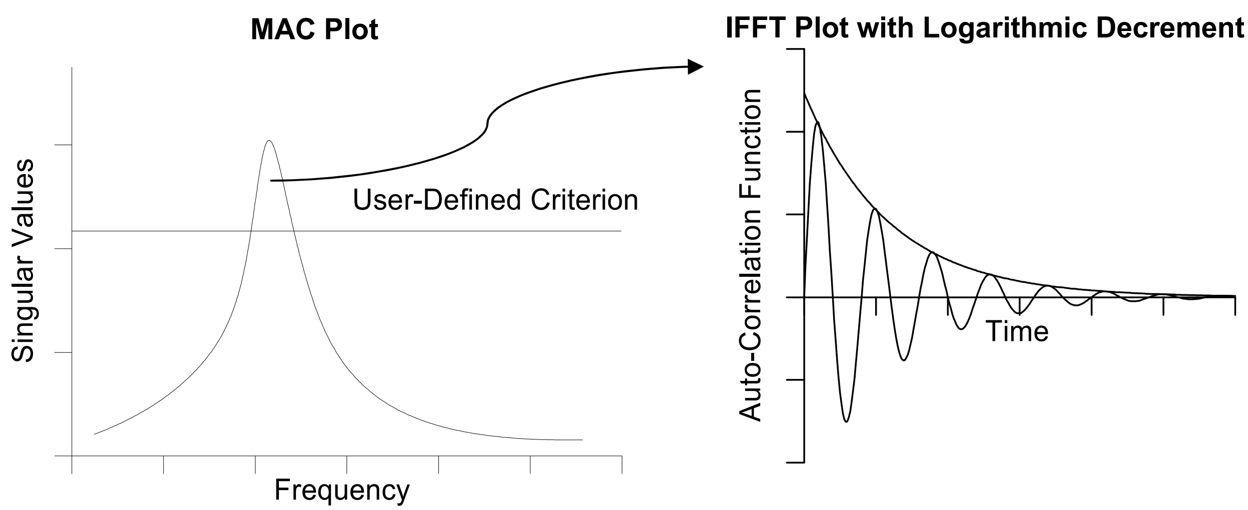

Figure 2.36 – Estimation of period and damping from MAC plot

2.7.1.6. Frequency Domain Decomposition

The FDD method, introduced by Brincker *et al.* (2001), was delevoped strictly for broadband white noise excitation as it assumes that the PSD of the input is constant. The modal parameters can therefore be directly extracted from the PSD of the ambient responses. The first step in the algorithm is to compute the power spectral density matrix by evaluating the cross-power spectral density (CPSD) function, $\bar{G}_{yy}(j\omega_i)$ at every discrete frequency of the system and forming a number $f_s/\Delta f$ of nxn matrices where f_s refers to the sampling frequency, Δf refers to the frequency spacing used for windowing. Thus, for every discrete frequency, a n by n matrix like the one in Equation 2-9 was formed, where n represents the number of response output signals.

$$\begin{bmatrix} \hat{G}_{11}(j\omega_i) & \hat{G}_{12}(j\omega_i) & \cdots & \hat{G}_{1n}(j\omega_i) \\ \hat{G}_{21}(j\omega_i) & \hat{G}_{22}(j\omega_i) & \cdots & \hat{G}_{2n}(j\omega_i) \\ \vdots & \vdots & \ddots & \vdots \\ \hat{G}_{n1}(j\omega_i) & \hat{G}_{n2}(j\omega_i) & \cdots & \hat{G}_{nn}(j\omega_i) \end{bmatrix} \tag{2-9}$$

The decomposition of the PSD matrix (Equation 2-10) using singular value decomposition (SVD) then yields the following scalar vectors from which the natural frequencies and mode shapes can be obtained.

$$\bar{G}_{yy}(j\omega_i) = U_i\, S_i\, U_i^H \tag{2-10}$$

S_i is a diagonal matrix which holds spectral values s_{jj}. It is by plotting those spectral values over the desired range of frequencies that the natural frequencies are determined using the standard peak-picking technique. Hence, spectral values at natural frequencies will dominate. The other matrix, U_i, is a unitary matrix which holds singular vectors u_{ij} for every frequency f_i. Thus, once a natural frequency is identified from the PSD plot, its corresponding mode shape can be obtained from matrix U_i at the frequency i and singular value j.

Usually, only the first singular values are required to depict the natural frequencies but the second singular values may be required in the case of closely-spaced modes. This is particularly useful when bringing the singular values back into the time domain as some of the frequency range determined using a user-defined MAC criterion for a certain mode may overlap with the next mode. The spectrum for each mode must then be identified using the second singular values similar to the method displayed in Figure 2.37.

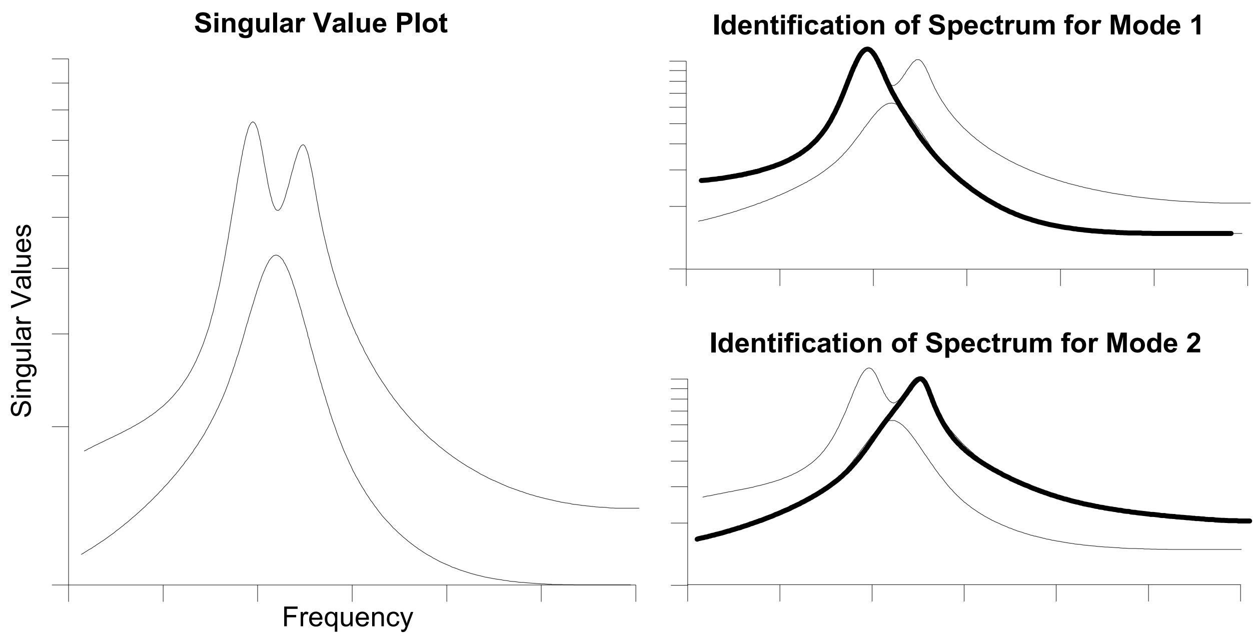

Figure 2.37 – Definition of spectrum for closely-shaped modes

2.7.2. Resonance

The results from the single-frequency excitation were used to obtain the values for the resonance plots. As was explained earlier in Section 2.5.2., each loading protocol contained a sine signal with eight different amplitudes at a single frequency. The velocity of the middle of each specimen was calculated relative to the average actuator velocity using Equation 2-11:

$$v_{relative} = v_{middle} - \frac{v_{north\ end} + v_{south\ end}}{2} \qquad (2\text{-}11)$$

The average of the actuator velocities was used as there is a possibility that the two actuators were not exactly in phase. The relative velocity was then plotted and the maximum amplitude of the forced response for each magnitude of excitation was determined. It was important to choose a representative steady-state portion of forced response output as there was always a significant transient response after every change in excitation amplitude. All the maximum values were then plotted on a single graph to come up with the curves that illustrate the range of frequencies over which the diaphragm would enter in resonance (Figure 2.38). Note that Figure 2.38 displays typical curves for DIA1, DIA1R and DIA2 while eight amplitudes were used for all other specimens.

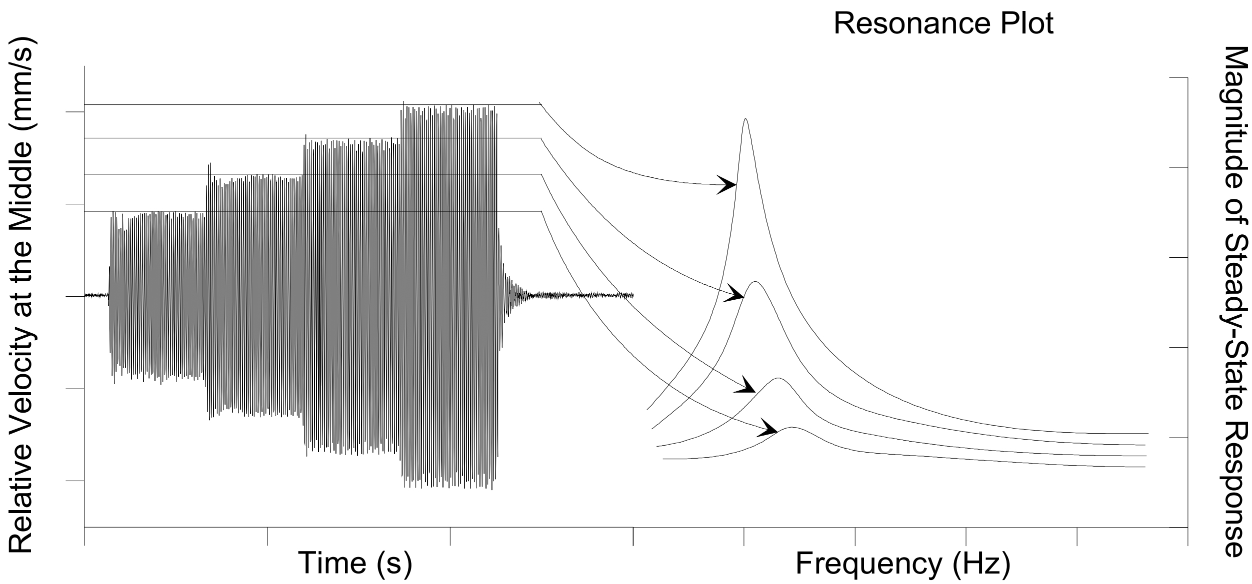

Figure 2.38 – Determination of resonance plots using sine-sweep data

2.7.3. Damping

The half-power bandwidth method was used in conjunction with the resonance data to determine the damping in the system. Damping was assumed to be constant for each excitation amplitude. This method has the advantage of determining the damping coefficient without knowing the applied force (Chopra, 2006). Figure 2.39 displays the values that are required to calculate the damping coefficient.

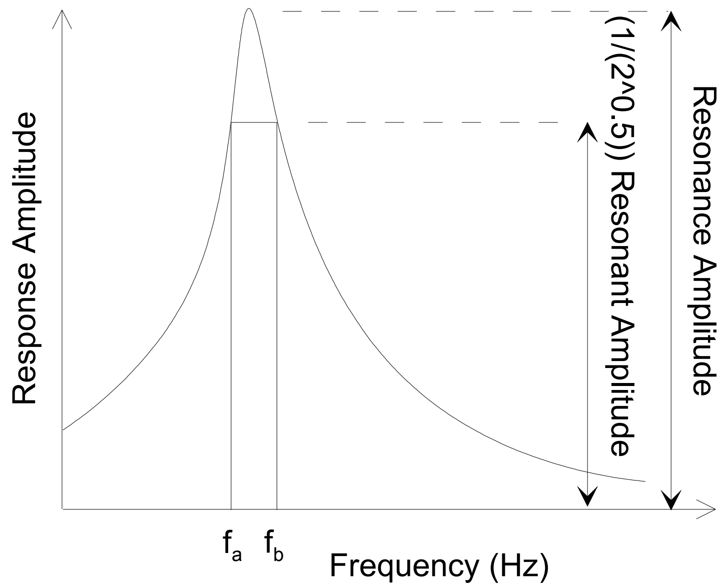

Figure 2.39 – Half-power bandwidth schematic representation

Using forcing frequencies f_a and f_b, which correspond to $1/\sqrt{2}$ times the resonant amplitude f_n, one can then calculate the damping using Equation 2-12:

$$\zeta = \frac{f_b - f_a}{2f_n} \tag{2-12}$$

The other method used to determine damping, when sinesweep data was not available, was to estimate the motion decay for viscous damping present at the first mode. This was done by defining a MAC criterion of 0.75 for the first fundamental frequency. The spectral values for that mode would then be brought back into the time domain by performing an inverse Fourier transform as is depicted in

Figure 2.36. From the exponential function which best fits the envelope of the response, the damping ratio is deduced. The damping ratio was found using Equation 2-11 and 2-12 (Chopra, 2006):

$$\delta = \frac{1}{n} \ln \left| \frac{x_1}{x_{n+1}} \right| \tag{2-13}$$

$$\zeta = \frac{\delta}{\sqrt{4\pi^2 + \delta^2}} \tag{2-14}$$

A damping coefficient average is presented for all of the specimens since the calculated damping differed slightly for different adjacent peaks in the auto-correlation function.

2.7.4. Resultant Shear Force

To determine the shear force carried by the diaphragm and the concurrent deformation, a time-history force balance was computed. With response acceleration measurements and with the mass known (Table 2.1 to Table 2.4) at all the joist lines, the inertia forces could be computed along the width of the diaphragm. The addition of all those horizontal forces would then be equal to the resultant shear force carried by the diaphragm. The latter was also compared with the force recorded by the actuator from which the inertia force of the swivel and end beam was removed to account for the force only present in the deck. Both methods coincided very well (Figure 2.40).

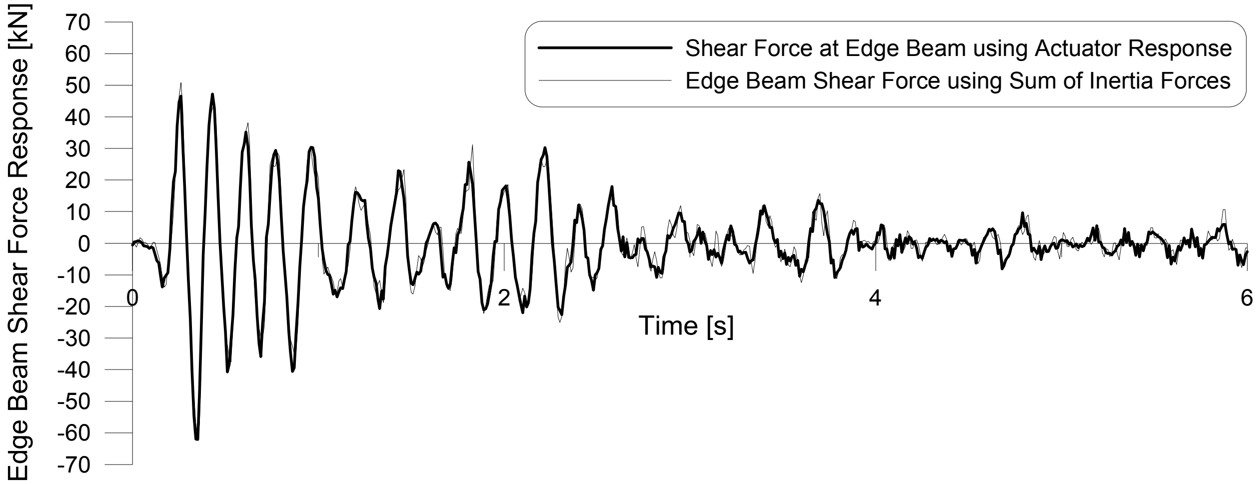

Figure 2.40 – Comparison of methods to determine edge beam shear force response

All the tributary inertia forces are shown schematically in Figure 2.41 where m_0 is the weight of the actuator load cell, swivel and the end beam; m_1 is the tributary mass of the end beam and m_2 is the tributary mass for any joist line. The tributary masses are listed in Table 2.1 to Table 2.4 for each of the specimens. The resultant shear force in the diaphragm was then calculated using Equation 2-15 and 2-16.

$$q * 7.31 = m_1 a_0 + \sum_{i=1}^{6} m_2 a_i \tag{2-15}$$

$$q * 7.31 = F - m_0 a_0 \tag{2-16}$$

Where:

q – is the shear force of the steel roof deck diaphragm in kN/m.

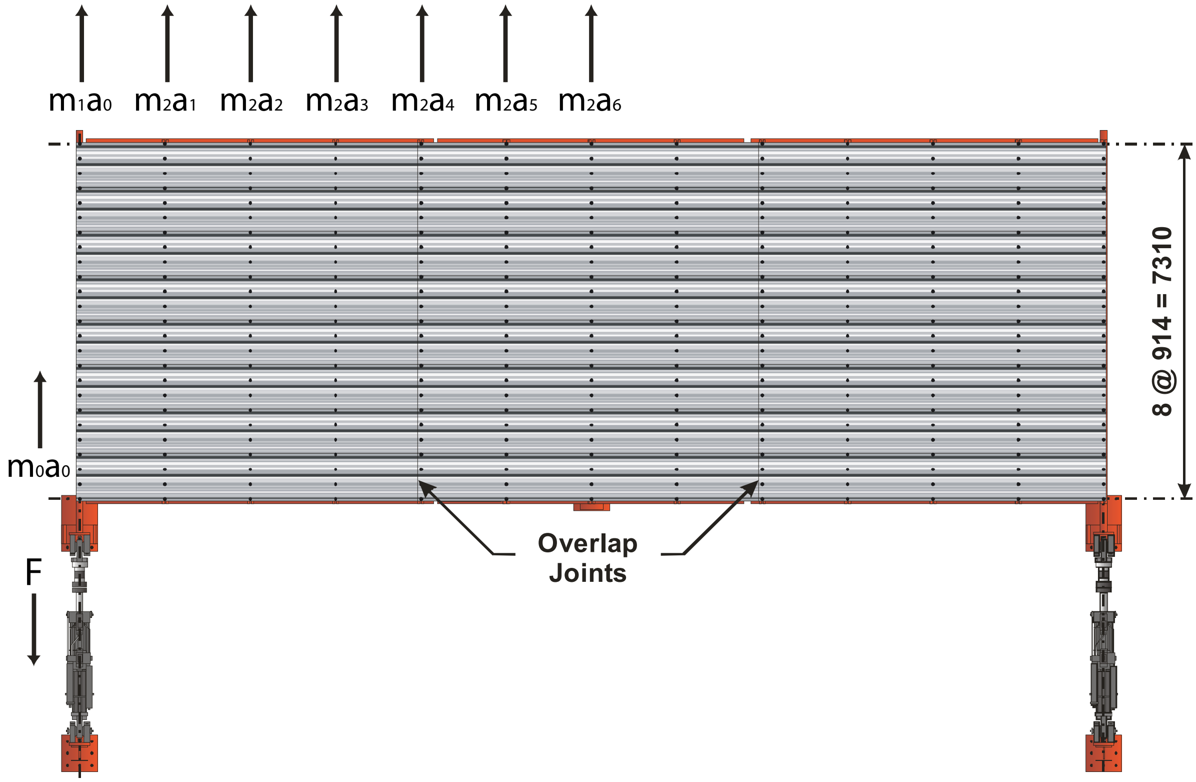

Figure 2.41 – Tributary masses for calculation of inertia forces

For Phase I test results, acceleration measurements were used to determine the inertia forces. During Phase II, multiple accelerometer reading problems made these values unusable for this calculation. Thus, potentiometer displacement values were used for all Phase II specimens to determine the acceleration. The derived acceleration measurements were then filtered using a lowpass second order Butterworth filter with a cutoff frequency of 25 Hz to eliminate high-frequency noise.

2.8. Test Result Summary

2.8.1. Natural Frequency of Diaphragm Specimens

It was possible to plot the change of the first mode period of the diaphragm specimen with varying forcing acceleration using the results of the white noise tests. The root-mean-square of the output acceleration at the middle of the specimen was chosen to represent the amplitude of the loading signal as it is well suited to represent the magnitude of a varying quantity. A typical plot is shown in Figure 2.42.

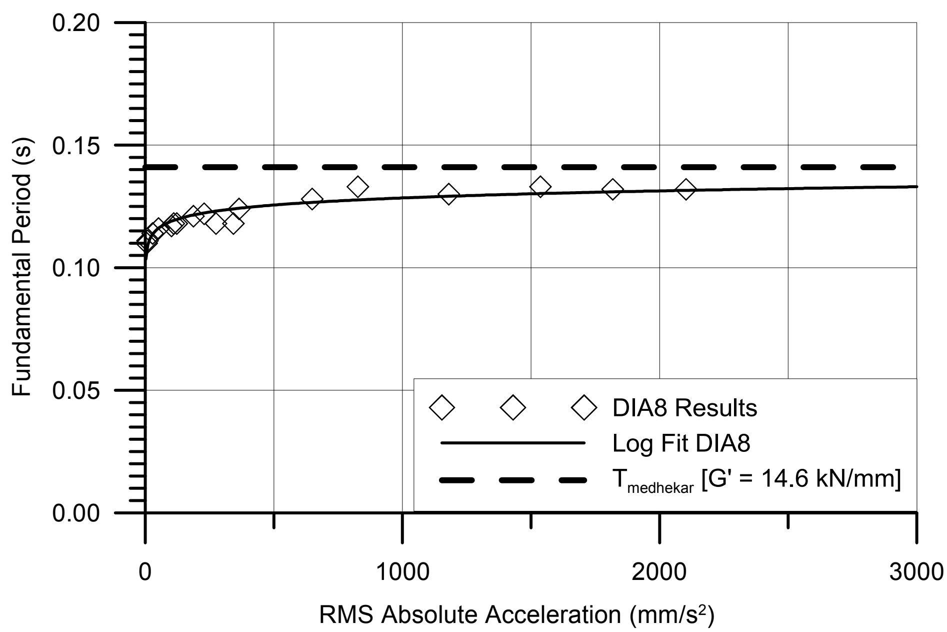

Figure 2.42 – Typical Fundamental Period vs. RMS Absolute Acceleration Plot [DIA8]

The dashed line corresponds to the natural period calculated using the equation proposed by Medhekar & Kennedy (1999a) using the G' value for which the longest measured fundamental period of the specimen matched the fundamental period of the Ruaumoko model developed by Shrestha *et al.* (2009). A plot is also presented, for each tested specimen, which compares the applied force and stiffness obtained from the white noise test results with the nominal capacity and shear stiffness obtained using the SDI (Luttrell, 2004) methodology for a single 7m panel length. The experimental stiffness, at each excitation amplitude, was obtained by solving Medhekar & Kennedy's equation (2009a) for G' (Equation 1-19). The plot in Figure 2.43 shows a general trend for one of the diaphragm specimens and includes a log fit as it best fit the data. The dashed line represents the limit where the experimental stiffness is equal to the stiffness predicted using the SDI methodology for a single panel length (Luttrell, 2004).

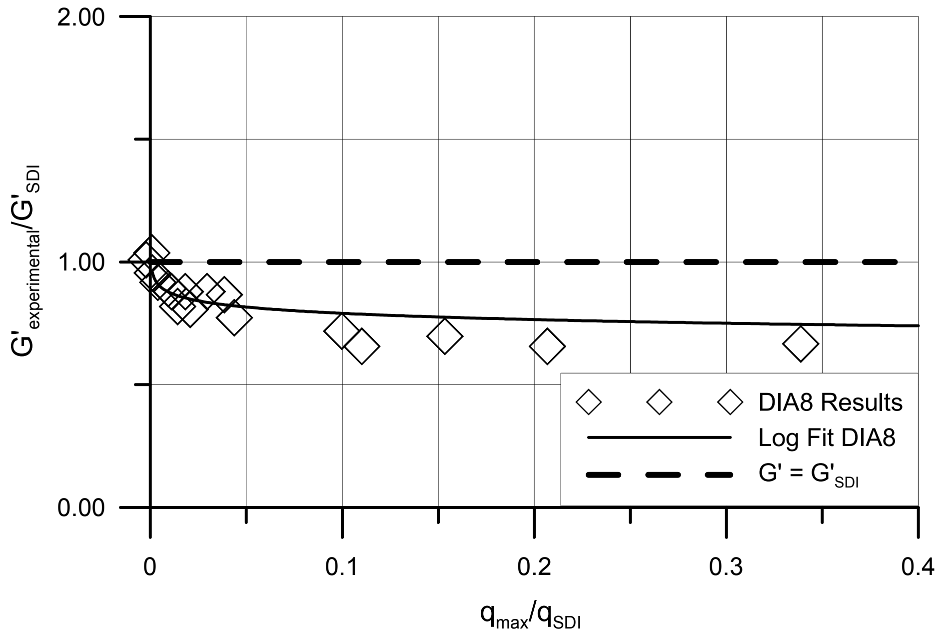

Figure 2.43 – Typical plot for the comparison of white noise experimental and SDI (Luttrell, 2004) stiffness [DIA8]

All of the plots have been compiled in Appendix B & C for review and further discussion is provided in Section 2.9.1.

2.8.2. *Resonance*

The magnitude of the steady-state relative velocity was determined and plotted at each frequency to observe the resonance for the diaphragm specimens with a natural frequency of 6Hz or less. Figure 2.44 displays the resonance curves from DIA1R over the selected frequency range. The decreasing shift towards lower frequencies with increasing excitation amplitude can be observed and compared with the results from the white noise test data.

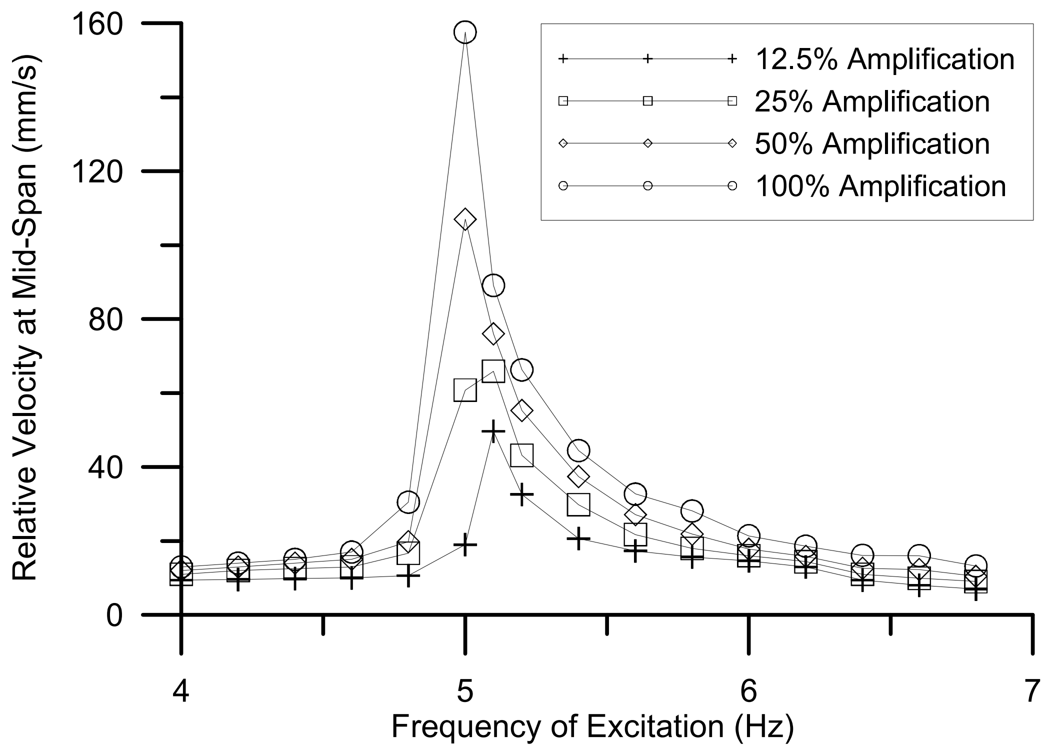

Figure 2.44 – Typical resonance curve for a diaphragm specimen.

The sinesweep plots for DIA1, DIA1R, DIA2, DIA3, DIA3G and DIA 10 have been compiled in Appendix D for review.

2.8.3. Damping

Using the methods explained in Section 2.7.3, damping ratios were determined for each of the new specimens. For the most flexible diaphragms, DIA1 to DIA3 and DIA10, displacement resonance plots were used to obtain the damping coefficients using the half-power bandwidth method. For all the other diaphragms, the spectral values for the largest amplified white noise test were used for the restitution of time response using an inverse Fourier transformation and the estimation of the damping ratio. The time-free decay and estimated damping envelopes are included in Appendix J for review.

2.8.4. Shear Force Profile and Deformation

Plots are presented for each diaphragm specimen which illustrate the calculated shear force profile and deformation of the specimen under seismic loading and during the inelastic loading protocol. For Phase I specimens, six graphs were created to show the shear force profile and deformation under the Loma Prieta earthquake record (SS1), for low and high amplification values, as well the inelastic loading protocol (SS2). In addition to those six graphs, for all the Phase II diaphragm assemblies, four additional plots were included to show the profile and deformation of the specimens under the Northridge earthquake record (SS3) in the diaphragm's elastic regime.

The shear force profiles are plotted over half the width of the specimens, and correspond to the instant in time at which a maximum shear flow is reached along a particular joist line or at the end beam. Hence, there can be up to seven profiles which would correspond to the profiles at which the maximum shear flow is obtained at each of the joists as well as at the end beam. The deformations plotted correspond to the concurrent deformed shapes that are recorded at the same instance in time as the calculated maximum shear force. The force time-history of the actuator, on the side where all the inertia measurements were calculated, was used for the calculation of the shear force carried by the diaphragm. Shown on the next page (Figure 2.45) is an example of the shear force profile and deformation of DIA8 under 80% of the SS1 signal. Only two shear force profiles are displayed as the maximum shear force at different joist lines occurred at the same instant in time.

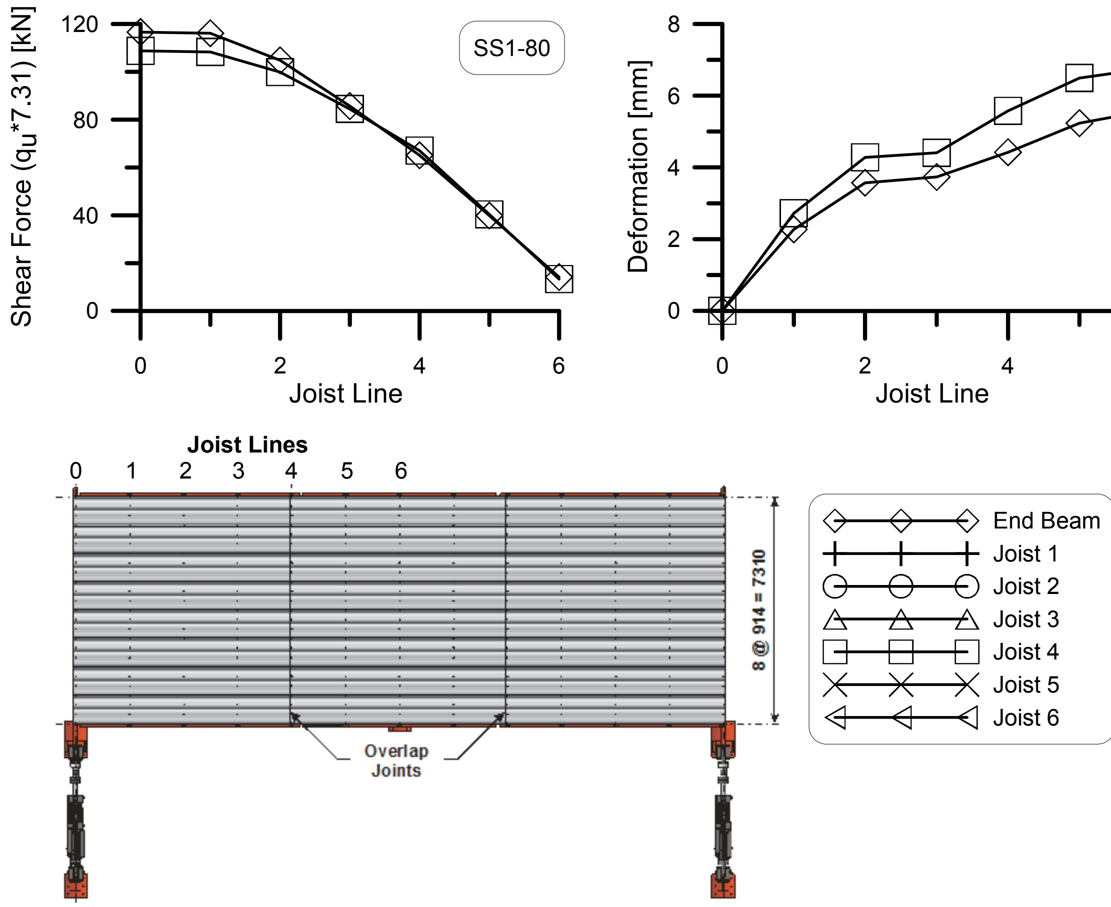

Figure 2.45 – Shear force profile and deformation example

All the graphs have been compiled into Appendix H (New specimens) & Appendix I (Repaired specimens).

2.9. Test Result Discussion

This section of the thesis includes comparisons and discussions for all the investigations conducted in the context of the large scale diaphragm testing program. Conclusions are presented at the end.

2.9.1. Natural Frequency of Diaphragm Specimens

The elongation of the natural period of the diaphragm with increasing excitation amplitude was recorded for all specimens. Though the white noise data was not sufficient for some specimens to determine the longest elastic fundamental period because of the lack of test data at higher amplifications, all the measured stiffnesses (Table 2.12), determined from the response of the specimens when subjected to the largest seismic signal, were lower than those determined as per SDI (Luttrell, 2004). Exceptions to the trend are DIA3 and DIA10. The periods in Table 2.12 correspond to the frequency with the highest energy content in the power spectral density function of the acceleration output at the centre of the diaphragm. The shear stiffnesses G' were calculated using Medhekar & Kennedy's equation (1999a), listed in Section 1.5.8., which relates the overall building period to the combined stiffness of the bracing and the diaphragm. Single panel properties were used in this calculation. The stiffness of the bracing was omitted such that only the period of the diaphragm assembly is considered. The stiffness for the welded and button-punch specimen, though slightly larger, coincides with the predicted value. The difference in values for DIA3 is explained in Section 0.

It was observed from the white noise results that once q_{max}/q_{SDI} is greater than 0.1 for a particular amplification of the white noise signal, all specimens exhibited a longer period, and therefore a lower stiffness, than the predicted SDI G' values for a single panel length. However, under ambient vibration and at low excitation amplitudes, the calculated stiffnesses were always higher than the predicted SDI G' values. The plots for all the specimens that illustrate the change in stiffness with respect to the RMS response acceleration at the middle can be found in Appendix B for the new specimens and Appendix C for the repaired specimens.

Table 2.12 – Fundamental period and stiffness determined for largest seismic excitations

Test No	SS3		SS1		Stiffness K_D for Longest Period	Medhekar & Kennedy Stiffness G' (kN/mm)	Difference with G'_{SDI} (%)
	Frequency (Hz)	Period (s)	Frequency (Hz)	Period (s)			
1	N/A	N/A	4.69	0.21	9.75	3.01	-28.5
1R	N/A	N/A	4.52	0.22	9.07	2.79	-33.8
2	N/A	N/A	3.59	0.28	5.71	1.72	-59.2
3	5.47	0.18	5.47	0.18	23.18	7.78	74.9
3G	5.86	0.17	5.86	0.17	28.95	10.10	127.0
3R	5.86	0.17	5.47	0.18	23.18	7.78	-54.2
4	5.86	0.17	5.47	0.18	23.18	7.78	-54.2
4R	6.64	0.15	5.86	0.17	26.61	9.14	-47.4
5	6.64	0.15	6.25	0.16	30.28	10.66	-38.7
5R	6.25	0.16	6.64	0.15	30.28	10.66	-41.8
6	6.25	0.16	5.86	0.17	26.61	9.14	-48.1
6R	6.25	0.16	6.25	0.16	30.28	10.66	-42.3
7	7.81	0.13	7.81	0.13	47.90	19.20	-12.1
7R	7.42	0.13	7.42	0.13	43.23	16.72	-25.4
8	7.42	0.13	7.42	0.13	43.23	16.72	-25.4
8R	7.81	0.13	7.42	0.13	43.23	16.72	-30.0
9	7.81	0.13	7.42	0.13	43.23	16.72	-26.6
9R	7.81	0.13	7.81	0.13	47.90	19.20	-20.4
10	3.91	0.26	3.91	0.26	11.83	3.69	3.9
10R	3.91	0.26	3.52	0.28	9.58	2.95	-30.1

2.9.2. Different End and Interior Connector Patterns

Specimen DIA3 exhibited a strength difference of 65.1 % between the experimental and predicted values (Table 2.14). A large underestimation of the stiffness by the SDI approach was also computed, even at large excitation amplitudes. A difference of 74.9% (Table 2.12) was calculated between the experimental and predicted stiffness which indicates that the warping is largely undervalued in the calculation of stiffness using the SDI method (Luttrell, 2004) for panels with different end and interior connector patterns if an alternate flute connection spacing is assumed. If every flute is assumed to be connected, the predicted stiffness is equal to 16.82 kN/mm. This compares to the value obtained from the ambient vibration measurements (G' 16.84 kN/mm) but it is much larger than the stiffness value of 7.78 kN/mm calculated from the seismic response (Table 2.12).

2.9.3. End Overlap

The effect of the end overlap was studied with specimens DIA1 and DIA2. Figure 2.16 illustrates the difference at deck ends with the 50 mm overlap included in DIA1. While strength values (Table 2.14) were comparable for the two diaphragm assemblies, there was a significant difference in stiffness (Table 2.12) between predicted and experimental values. This difference can be explained by the release of warping when sheets are not overlapped. However, ambient vibration results for DIA1 (0.10 sec) correspond closely to the period obtained with the equation developed by Medhekar & Kennedy (1999a) using the G' predicted using the SDI method (0.11 sec) (Tremblay & Rogers, 2008b).

Another effect of the end overlap was noticed in the deformation at maximum shear values (Figure 2.46). While DIA1 only displays a large deformation demand at the first span as it is the location of maximum shear, DIA2 exhibits an increased deformation on both sides of the non-overlapped region (fourth joist line) due to the augmented flexibility at that location.

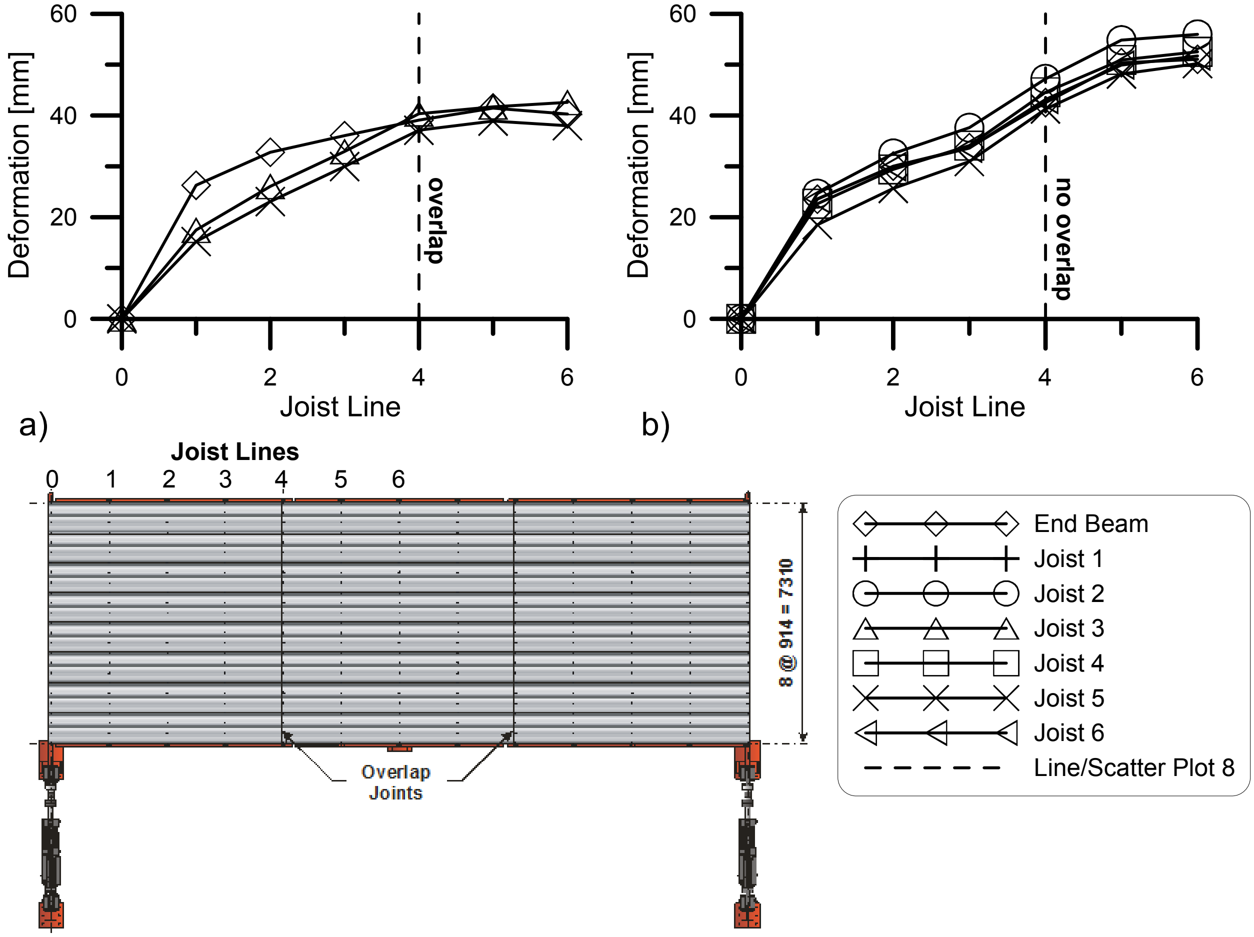

Figure 2.46 – Deformed shape of DIA1 (a) and DIA2 (b) under SS2 at times of maximum shear

2.9.4. Non-Structural Materials

The influence of non-structural materials, such as gypsum board, on the fundamental period consisted of a non-linear addition of stiffness. This stiffness increase varies also with the magnitude of the response acceleration of the diaphragm. Plotted in Figure 2.47 is the comparison between the change in stiffness of the bare diaphragm and the specimen with added gypsum (top) as well as the change in stiffness contribution with increasing response acceleration (bottom). This difference in the stiffness was estimated using the logarithmic fits for DIA3 and DIA3G by calculating the difference at intervals of 10 mm/s^2. The logarithmic fits were used as they were most representative prediction of the dynamic change in stiffness of the studied specimens. The plot shows an increase of 20.7% at the lowest amplitudes up to 27.6% at an RMS acceleration of 500 mm/s^2. This is considerably less than the stiffness contribution of 49% recorded by Yang (2003) and 46% recorded by Mastrogiuseppe *et al.* (2008). However, their calculation of G' consisted of computing the slope between 0 and 0.4 times the ultimate shear capacity of the load-to-deformation relationship from the static tests. This is different from the abovementioned method which was used for the data processing completed in the context of this testing program. The difference in derivation may explain the disparity between the results.

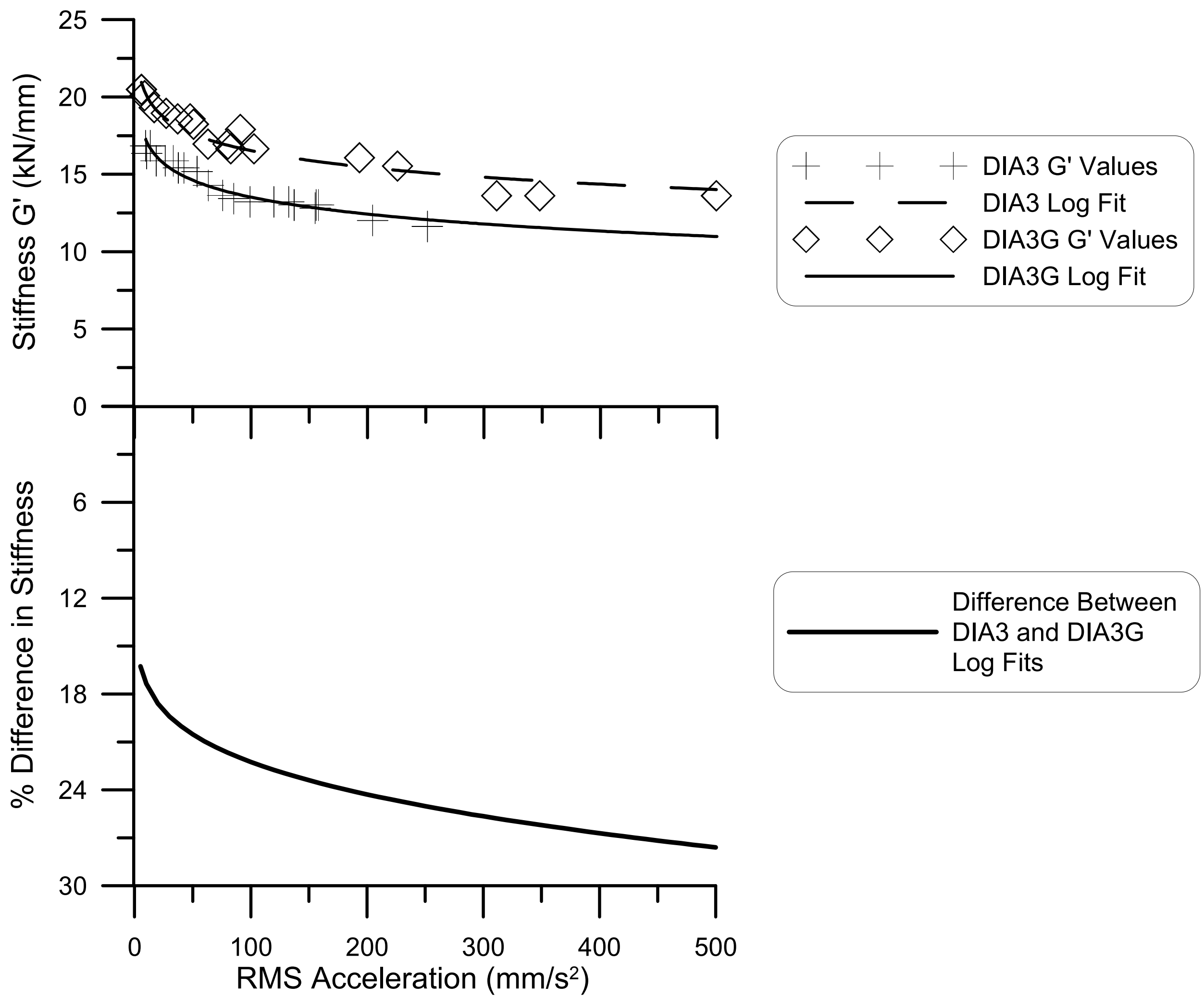

Figure 2.47 – Influence of gypsum on the stiffness of the diaphragm

During the seismic tests, the gypsum boards gradually fractured and only the stiffness of the bare steel deck diaphragm remained. Thus it can be concluded that at very high excitation amplitudes, the stiffness would be present at the beginning of the ground motion and would degrade during the large cycles of the seismic event. The difference was noticed up to RMS response accelerations of 500 mm/s^2 (0.05g); this signifies that the stiffness increase would be present during small amplitude ground motions. In addition, the gypsum caused an additional vertical acceleration component to develop which enlarged with increased excitation amplitude. This was likely due to the additional constriction of in-plane deformation.

2.9.5. Damping

The damping coefficients for the fundamental mode were calculated for each of the new specimens and are listed (Table 2.13). The values range from 1.45 to 3.3% for the nailed and screwed diaphragms. This is typical of steel structures. For the welded and button-punched specimen (DIA10), a value of 6.6% was obtained. Such a high value could be explained by the friction and sliding in the button-punch sidelap connections.

Table 2.13 – Damping coefficients for all the specimens

Specimen	Damping Coefficient ξ (%)	Method
DIA1	2.2	Half-Power Bandwidth
DIA1R	1.7	Half-Power Bandwidth
DIA2	2.2	Half-Power Bandwidth
DIA3G	2.0	Half-Power Bandwidth
DIA3	2.2 – 2.8	Half-Power Bandwidth
DIA4	3.3	Motion Decay
DIA5	1.3	Motion Decay
DIA6	1.4	Motion Decay
DIA7	1.5	Motion Decay
DIA8	1.3	Motion Decay
DIA9	1.9	Motion Decay
DIA10	6.6	Half-Power Bandwidth

2.9.6. Resultant Shear Force Profile and Deformation

The trends in shear force profile and deformation were consistent for almost all the specimens tested in Phase II of this research program. All the results can be consulted in Appendix H, for new diaphragms, and Appendix I, for the repaired diaphragms. The experiments show a deviation from the general theoretical assumption that the shear profile in the diaphragm is linear under uniform seismic loads. All diaphragms showed very little difference between the shear force attained at the first joist and that obtained by the edge beams. For some specimens, the results showed a slight increase of the maximum shear at joist 4 and 5 which does not occur at the same time as the maximum shear at the ends (Figure 2.48).

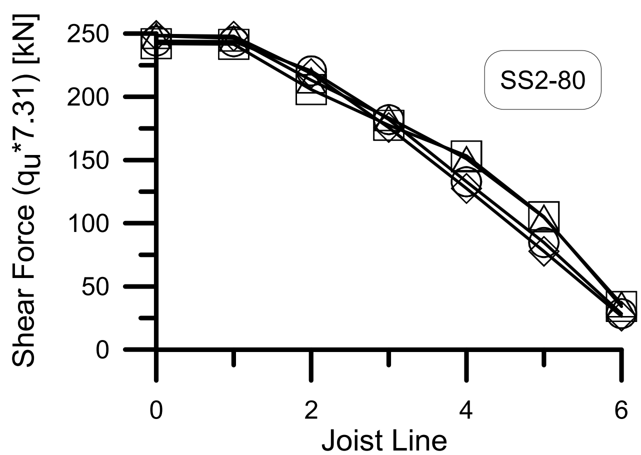

Figure 2.48 – Maximum shear force profile of DIA7 under 80% SS2

All the specimens in Phase II show a high deformation between the end beam and the first joist when subjected to the seismic signals at low amplifications. This effect, though diminished, is still visible at high amplifications of the seismic signal. Under the inelastic signal, the high deformation at the ends becomes even less visible as the deformed shape starts to resemble that of a parabola. Exceptions to this observation are specimens DIA8, DIA10 and DIA10R for which the deformation is still largely concentrated at the edge beams.

2.9.7. *Repair Schemes*

The repair scenarios were successful at restoring the original strength, stiffness and ductility. A discussion on each of the results of each repair scheme is elaborated in Sections 2.9.7.1 to 2.9.7.3.

2.9.7.1. *Nail and Screw Repair Scenarios*

DIA1 to DIA6 and DIA8 successfully regained the original strength. DIA9 suffered extensive damage during the SS2 signal including shear buckling of the steel deck sheets, large slotting at nail locations and pullout of screw sidelaps; this explains the difference between the strength prediction and the experimental results.

The stiffness recovery varied per specimen. DIA1R, DIA5R, DIA6R, DIA8R and DIA9R recaptured similar stiffnesses when compared to the new specimens after the addition and repair of the connectors. Specimen DIA3R exhibited a large decrease in fundamental period which is the result of applying the same connector pattern everywhere. Specimen DIA4R experienced a lengthening of its fundamental frequency, even after repair. This could be attributed to extensive damage during the first inelastic test. The fundamental periods calculated from the white noise response measurements for all the new and repaired nailed and screwed diaphragms are compared in Figure 2.49.

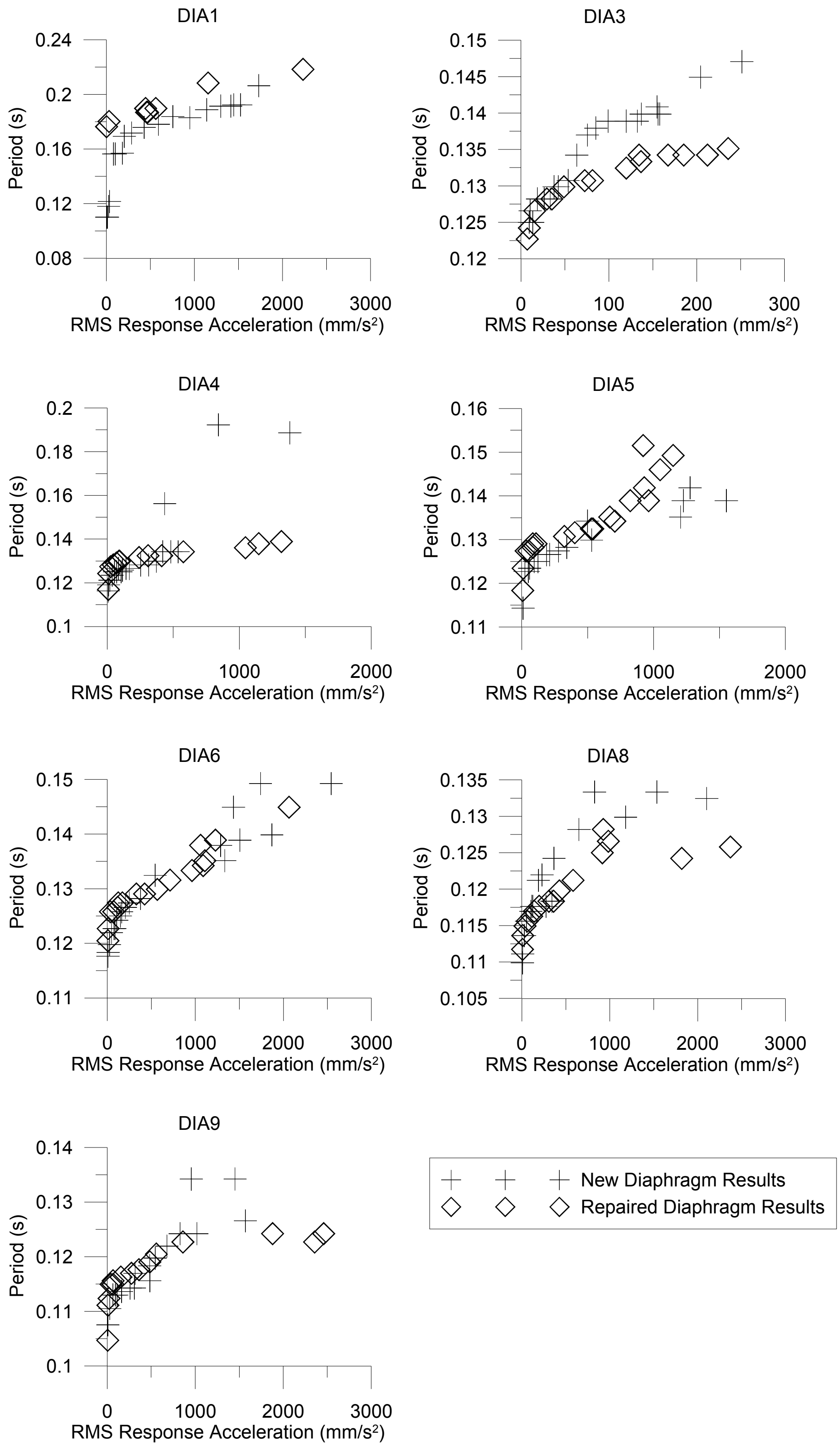

Figure 2.49 – Comparison of new and repaired diaphragm specimens fundamental periods with changing excitation amplitude

2.9.7.2. Nail and Rivet Repair Scenario

The nailed and rivet repair scenario used for specimen DIA7R was successful at recapturing the original strength and stiffness. An increase in strength of 33% was obtained and similar ductility and deformation capability was achieved (Figure 2.50).

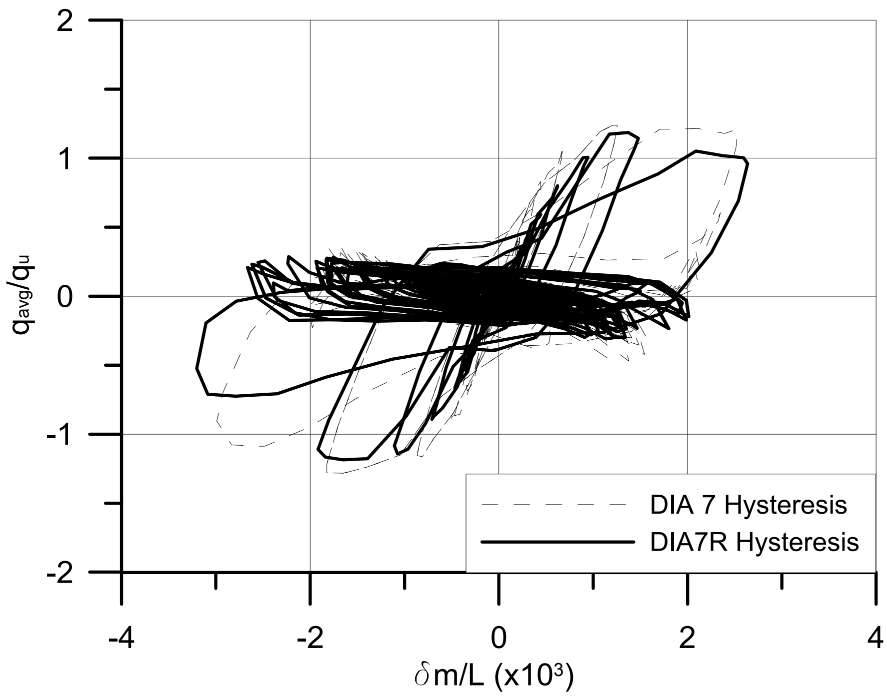

Figure 2.50 – Hysteresis comparison for repair scenario with rivets as sidelaps

The difference in strength and similar ductility can be explained by the increased rivet diameter which allows for bearing over a larger steel area. Figure 2.51 displays the difference in the bearing from that induced by a screw and that induced by a rivet. The loosening of the rivets due to bearing and the nail bearing resulted in pinched hysteretic behaviour of the specimen.

Figure 2.51 – Comparison between screw bearing; left hole; and rivet bearing; right hole

Another observation was the high variability in blind head diameter (Figure 2.52). This phenomenon was impossible to control and could influence the resistance of the rivets, especially when the pullout of a row of sidelap fasteners is considered. Perhaps the use of rivets specified for the steel sheet thickness alone could attenuate the effect.

Figure 2.52 – Variation in blind head diameter

2.9.7.3. Nail and Screw Plate Repair Scenario

The repair scheme devised for the diaphragm with button-punch sidelap connections and welded frame connections was very successful in terms of strength. An increase of 66% in the nominal strength was achieved. However, there was a significant loss in the ductility of the specimen. The repaired specimen was a lot more flexible and was not able to sustain as many cycles during the inelastic test. Instead of the weld fracture and button-punch separation failure noticed with DIA10, the failure for DIA10R was characterized by nail bearing and screw tilting causing detachment of the plate. The smaller loops in the hysteresis (Figure 2.53) indicate that less energy-dissipation has also occurred. This is an indication that the repaired scenario would likely not be suitable as the energy-dissipating element in the SFRS but, given the strength increase, would be very efficient if designed to remain elastic.

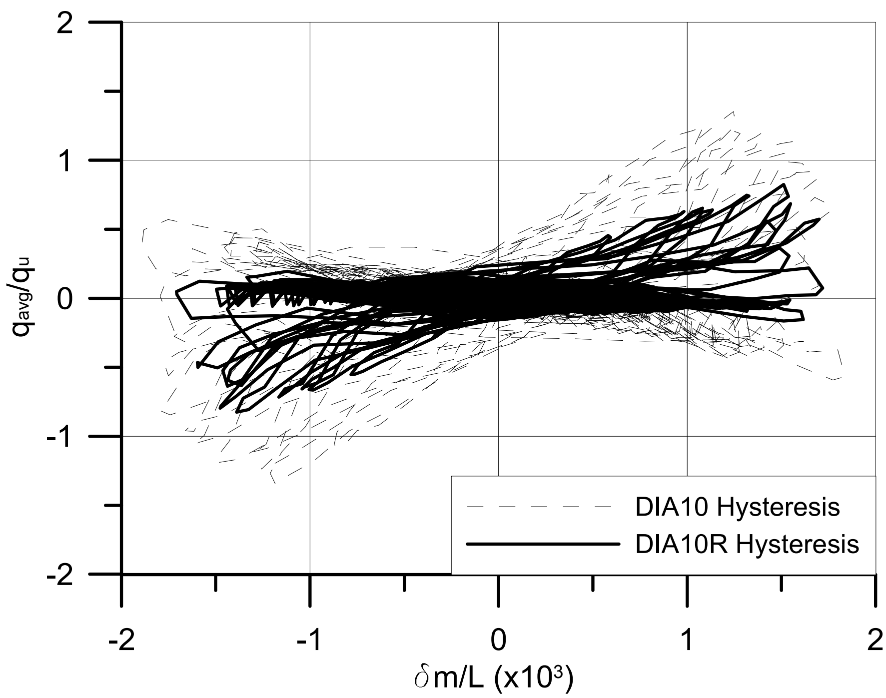

Figure 2.53 – DIA10 vs. DIA10R Hysteresis comparison for repair scenario with nails and screwed plate

The prediction of the shear strength of the specimen, which was computed using strength and stiffness values for a weld and a single screw, was a good estimation as the difference between the predicted and the experimental values was less than 1%. The stiffness of the weld was used as the majority of the welds were still intact and the welds are stiffer than the nail fasteners.

2.9.8. *Observed Inelastic Performance*

To take advantage of the inherent ductility, the desirable failure mode in the deck specimens would be characterized by bearing of the screws and nails where the shear demand exceeds the specimen's resistance followed by a re-distribution of the load further into the specimen such that additional energy dissipation can be achieved by subsequent bearing. This would either be followed by the excessive deformation demands at the sidelaps, causing the pullout of the whole row of screws, or excessive loading of frame fasteners causing large slotting. At this point, the load transferring-capability of the diaphragm would be lost.

Failure of the specimens from the inelastic loading protocol always propagated from the ends. This was to be expected as the diaphragms had been designed for a uniform resistance which would thus first be exceeded near the end beams (Figure 2.54).

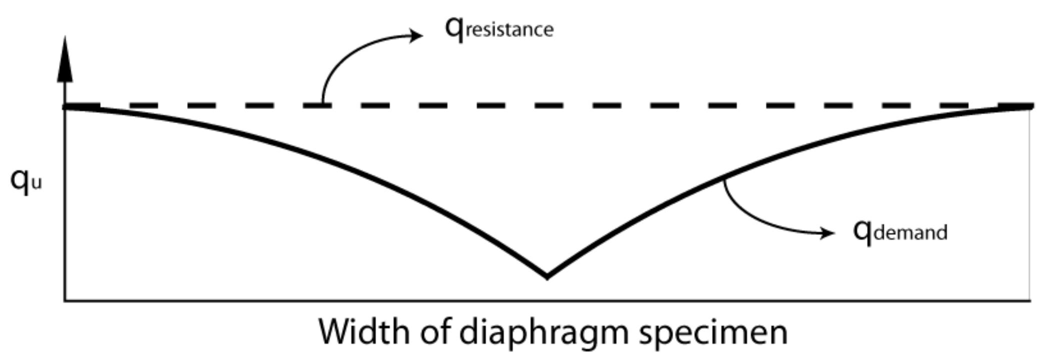

Figure 2.54 – Shear resistance and demand of diaphragm specimen

The various connection damage incurred during inelastic response are described in Table 2.15 and Table 2.16. Failure rarely occurred at eave beam sidelap connector locations because the sidelap connection solicitation occurs from large relative displacements between deck sheets which does not occur at the eave beams (Figure 2.55). In addition, all the connections at eave beams consist of frame fasteners which are much stronger than screw sidelaps.

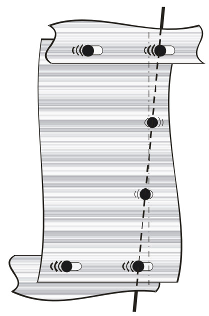

Figure 2.55 – Sidelap demand illustration

All connection failures have been recorded and included in Appendix E for review. More specific descriptions of the failure modes are detailed in Sections 2.9.8.1. to 2.9.8.3. The connectors denoted by an X refer to nails that either sheared off or experienced excessive slotting. In the case of screws, an X refers to a screw which pulled out of one of the connecting deck sheets. An O refers to either nails or screws that experienced bearing failure but are still capable to exhibit further resistance.

The difference in strength between the new diaphragm specimens and the predicted SDI (Luttrell, 2004) strength for a single panel response varied significantly. Differences from 1 to 65% were calculated. However, all the new diaphragm specimens achieved a nominal force greater than those determined with the SDI (Luttrell, 2004) methodology. Five of the nailed and screwed repaired diaphragms did not achieve their predicted strength. This is likely due to the residual damage (excessive slotting in deck at frame fastener locations, deck deformation) in the diaphragm from the previous inelastic test. The strength results have been tabulated for review (Table 2.14). All the hysteresis curves are also included in Appendix F & G of this thesis.

Table 2.14 – Comparison of experimental and theoretical strengths of specimens

Test No	SDI S_n (kN/m)	Experimental q_u (kN/m)	Ratio of SDI and Experimental (%)	Ratio of Experimental Repaired and SDI New (%)
1	13.03	15.46	1.19	
1R	13.03	20.02	1.54	1.54
2	13.03	14.74	1.13	
3	23.52	38.81	1.65	
3R	24.41	38.37	1.57	1.63
4	24.41	30.28	1.24	
4R	29.18	24.15	0.83	0.99
5	29.18	31.93	1.09	
5R	35.29	33.27	0.94	1.14
6	31.84	33.11	1.04	
6R	38.55	36.91	0.96	1.16
7	29.16	34.00	1.17	
7R	34.85	38.94	1.12	1.34
8	34.85	36.92	1.06	
8R	42.15	34.60	0.82	0.99
9	38.03	38.25	1.01	
9R	46.05	32.44	0.70	0.85
10	8.50	12.23	1.44	
10R	14.08	14.17	1.01	1.67

Table 2.15 – Connection damage type and illustration [Mechanical Fasteners]

Type of Connection Damage	Illustration
1. Sheet distortion at corner nails at the diaphragm ends	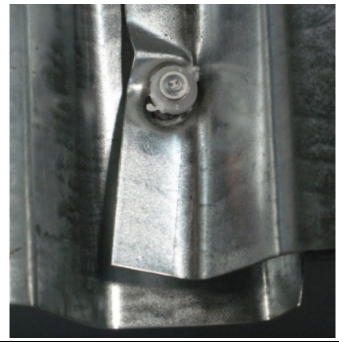
2. Bearing deformations against sidelap nails at intermediate joists	
3. Shear failure of frame fastener at intermediate joists	
4. Bearing failure of deck sheet at a screw side lap connection	

Table 2.16 – Connection damage type and illustration [Non-Mechanical Fasteners]

Type of Connection Damage	Illustration
1. Non-sidelap deck bearing failure followed by tearing of the deck sheet	
2. Non-sidelap weld perimeter fracture	
3. Sidelap weld perimeter fracture	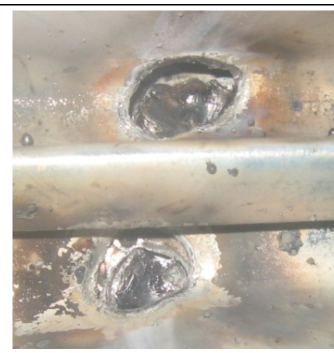
4. Button-Punch connection separation	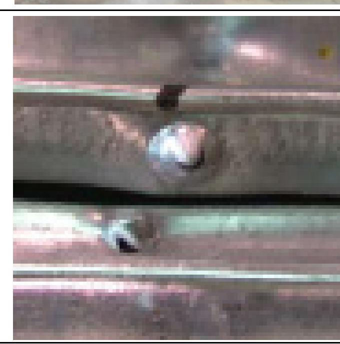

2.9.8.1. 22 Gauge Nailed and Screwed Specimen Performance

All the new specimens with 22 gauge (0.76 mm) deck were able to reach the load predicted using the SDI methodology. For the Phase II specimens, the difference between the predicted and experimental strength decreased as the fastener pattern increased. The diaphragms exhibited a pinched hysteretic response and strength degradation. The gradual pinching occurred from the loosening of the sidelap screw connections and the bearing of the deck around the frame fasteners. Figure 2.56 shows the end shear (q_1/q_u) *vs.* diaphragm mid-span deflection (δ_m/L) global hysteretic response of DIA4 under 0.8 times the SS2 signal. The two plots correspond to the load response from actuator 1 (left) and actuator 2 (right) respectively.

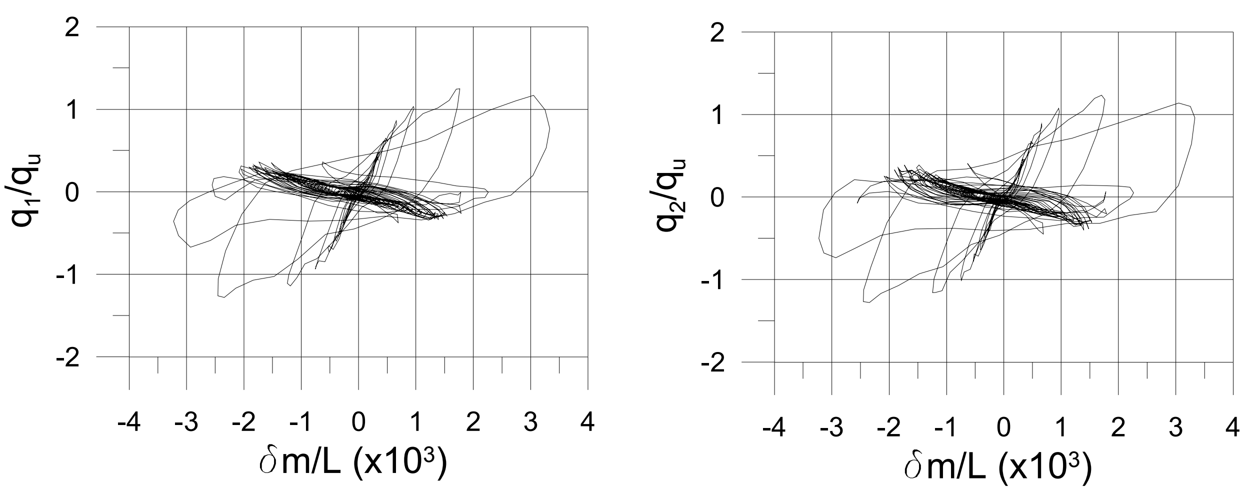

Figure 2.56 – Pinched hysteretic response of DIA4

Failure concentrated at the two extreme thirds for all the 0.76mm deck specimens with nailed and screwed connections; thus indicating that the majority of the connectors on the two extremities were solicited. Sidelap failure is consistent throughout all the 22 gauge specimens but variations in the frame fastener failure patterns were noticed. Figure 2.57 shows the percentage failure for all the frame fasteners along a beam or joist and all the sidelap connectors along the width of the specimen for a single span. The diagrams show the decrease in frame fastener failure for closer-spaced patterns while the sidelap failure remains consistent.

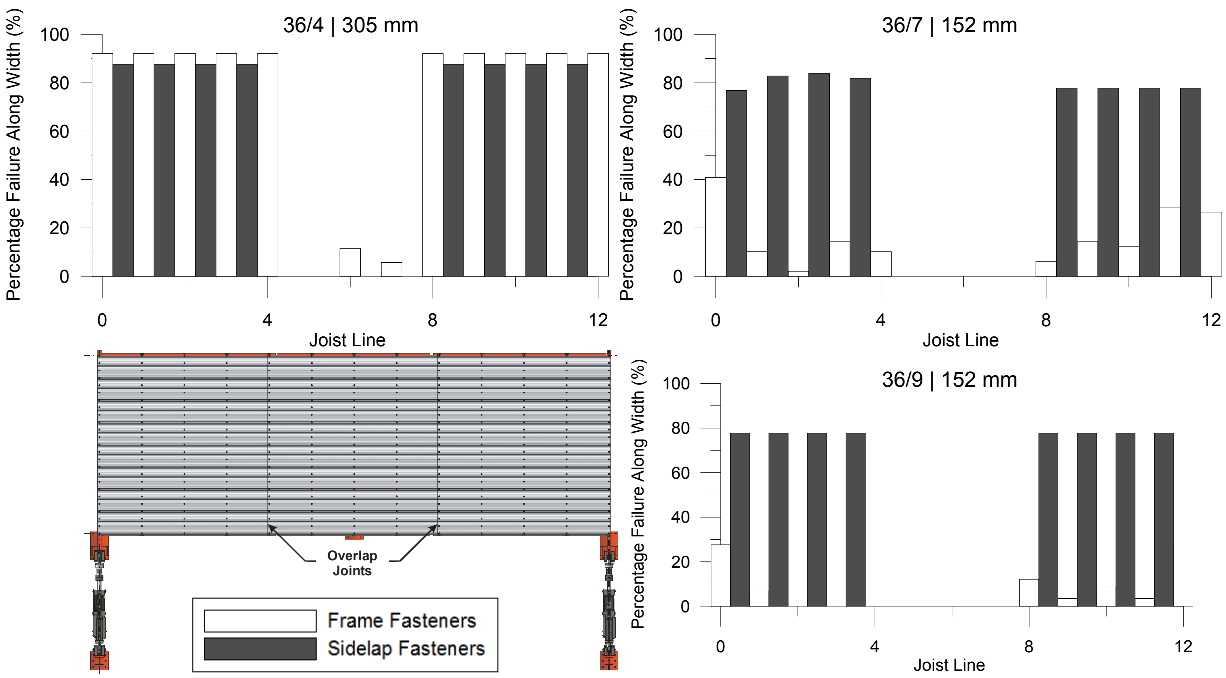

Figure 2.57 – Failure pattern comparison for DIA1 (top left), DIA4 (top right) and DIA5 (bottom)

2.9.8.2. 20 Gauge Deck Nailed and Screwed Specimen Performance

With the stiffer 20 gauge (0.91mm) diaphragm specimens, differences in failure patterns on either side of the specimen were noticed. This was either due to slight differences in the actuator displacements, thus causing an eccentricity in the loading, or a difference in stiffness on one side of the diaphragm assembly. This localization of failure could mean that the diaphragms are very susceptible to slight differences in the loading amplitude or local stiffness dissimilarities. This was prominently noticed for specimens DIA7, DIA8, DIA9 and DIA9R.

Pinched hysteretic response and degradation was again achieved though the maximum deformation recorded at the centre of the 20 gauge specimens was less than for the 22 gauge diaphragms with the same fastener pattern. The only exception was that of DIA9, with a pattern of 36/11, which exhibited a larger deformation than DIA6 while sustaining a large shear force. Figure 2.58 shows the end shear (q/q_u) *vs* diaphragm mid-span deflection (δ_m/L) global hysteretic response of DIA8 under 0.8 times the SS2 signal. The two plots correspond to the load response from actuator 1 (left) and actuator 2 (right) respectively. The difference in the hysteretic behaviour can be explained by the loss of capacity on one side (left) of the specimen while the other side still retained significant strength (right).

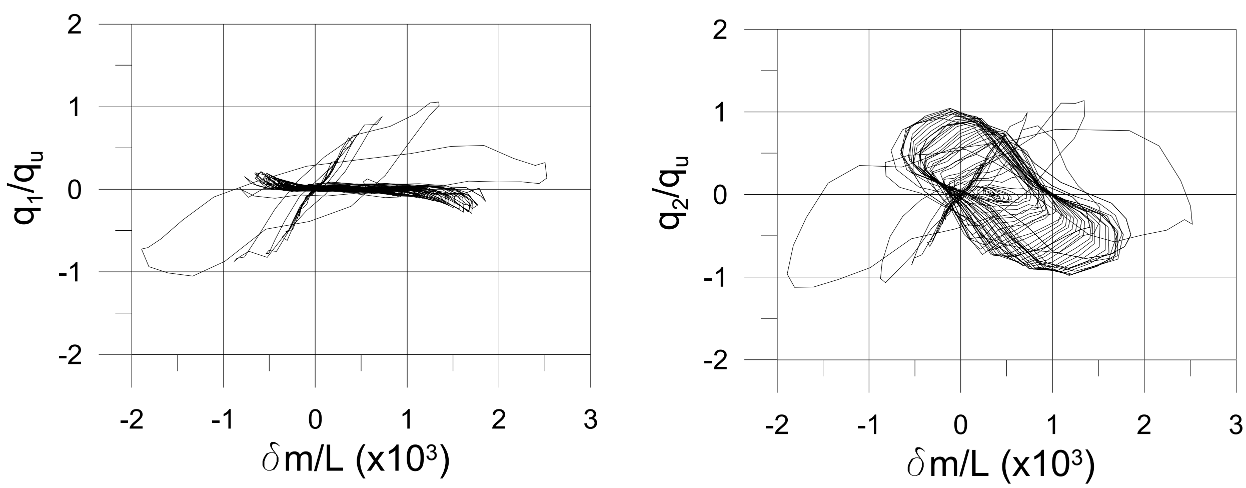

Figure 2.58 – Pinched hysteretic response of DIA8

Failure concentrated again on the two outer panels though the failure did not extend to the deck sheet overlap. Only DIA9 experienced extensive failure all the way to the overlap. A consistency in all the 20 gauge specimens was the failure of frame fasteners around the sidelap locations. This is consistent with the solicitation illustrated in Figure 2.55 which indicates that frame fasteners closer to the sidelap will be heavily solicited due to inter-deck relative displacements.

2.9.8.3. 22 Guage Deck Welded and Button-Punched Specimen Performance

The button-punched diaphragm specimen (DIA10) was able to reach the maximum load as determined by SDI and sustain it for at least six cycles before experiencing any significant loss in capacity. Figure 2.59 shows the end shear (q_1/q_u) *vs.* diaphragm mid-span deflection (δ_m/L) global hysteretic response of DIA8 under 0.8 times the SS2 signal. A frequency multiplier of 80% was used for the inelastic loading protocol to account for the increased flexibility of the specimen. The two plots correspond to the load response from actuator 1 (left) and actuator 2 (right) respectively. The oval response along the x-axis displayed by actuator 2 is due to a second increase in load subsequent to the loss of capacity experienced on the side of actuator 1.

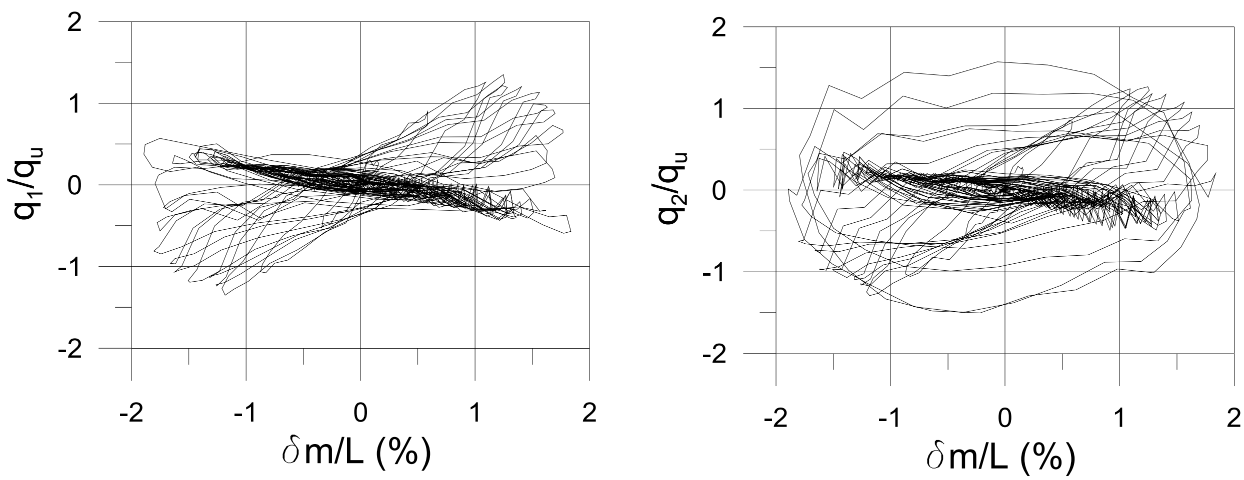

Figure 2.59 – Pinched hysteretic response of DIA10

Failure concentrated at the outer panel as the deformation at the end was greater than 50% of the total deformation. The majority of the welds connecting the deck to the outer beams failed along with the button punched-sidelaps for the first panel. A significant concentration of weld failures at sidelap locations were also recorded for the first three joists.

CHAPTER 3

3.0 BUILDING DESIGN

3.1. Introduction

The calculation of the seismic load acting on a structure is directly related to the fundamental period of vibration of the building. Current design codes (NRCC, 2006; CSA-S16, 2005) oblige structural engineers to detail diaphragms, if used as a load-transferring means in the SFRS, for the actual capacity of the bracing system. The in-plane deformations of the diaphragm must also be accounted for in design. Different single-storey design methodologies were compared in previous studies (Tremblay & Rogers, 2005) to assess possible cost savings that would result from alternate design methods such as attenuating the period limit or using the diaphragm as the energy-dissipating element in the SFRS. The advantage of incorporating the diaphragm flexibility in the calculation of the overall building period, in order to lower the design seismic forces, was also stressed in this study.

A comparative study was carried out to complement the abovementioned investigation where only the following concentric braced frames (CBF) categories were considered as per the NBCC: Moderately ductile (Type MD, R_d = 3.0), Limited-Ductility (Type LD, R_d = 2.0) and Conventional Construction (Type CC, R_d = 1.5). In the context of this comparison, eccentric braced frames (EBF) were considered with a ductility-related factor (R_d) equal to 4.0 and an overstrength factor (R_o) equal to 1.5.EBFs are beneficial as they combine the advantage of a CBF, by providing high elastic stiffness, and a moment resisting frame, by exhibiting a stable inelastic response (Mazzolani, 2008).

3.2. Description and Design of Building Studied

3.2.1. Canadian Seismic Design Provisions

Single-storey buildings of regular geometry are typically designed using the equivalent static force procedure as defined in the 2005 edition of the NBCC (NRCC, 2006). The procedure consists of obtaining an elastic base shear, V (Equation 3-1), which depends mainly on the fundamental period of the structure (T_a), the type of bracing system, the ductility (R_d) and overstrength (R_o) of the fuse element and the seismic weight (W). Upper and lower bound limits are also provided by the code. In the context of this study, the building considered is of normal importance, I_E = 1.0.

$$V = \frac{S(T_a)M_v I_E W}{R_d R_o} \leq \frac{(\frac{2}{3})S(0.2)I_E W}{R_d R_o} \tag{3-1}$$

The code provides location specific Uniform Hazard Spectra (UHS) from which spectral response accelerations $S_a(T_a)$ for periods T = 0.2, 0.5, 1.0 & 2.0 can be obtained. Intermediate UHS ordinates are to be linearly interpolated between the presented values. These values are to be multiplied by acceleration and velocity-based coefficients, F_a and F_v respectively, that take into account the local soil effects on the ground acceleration, in order to obtain the design spectral response acceleration used in Equation 3-1.

The NBCC also specifies that accidental torsion be taken into account in the seismic load scenarios. Two load cases (Equation 3-2 and 3-3) are to be added onto the existing elastic base shear to account for the possible eccentricity in the lateral load.

$$T_x = F_X(e_x + 0.10D_{nx}) \tag{3-2}$$

$$T_x = F_X(e_x - 0.10D_{nx}) \tag{3-3}$$

Where:

T_x – is the force to be applied which takes into account accidential torsion

F_x – is the seismic force acting at the considered floor

e_x – is the existent eccentricity between the centre of mass and the centre of rigidity

D_{nx} – is the in-plan dimension of the building in the direction considered

In the case of braced frames, an empirical approximation as to the period of the structure (T_a), based solely on its height, is given as 0.025 h_n (NRCC, 2005; CSA-S16, 2005), where h_n is the height of the building. This period may be substituted by a first mode period of the building, obtained through methods of mechanics, so long as it doesn't exceed twice that calculated with the empirical formula. Formulas that take the diaphragm flexibility into account in the calculation of the overall building period are proposed in FEMA-356 (2000) and Medhekar & Kennedy (1999a) ; Medhakar's equation (Equation 3-4) was used for the purpose of this building study.

$$T = 2\pi \sqrt{\frac{(K_B + K_D)}{K_B K_D} \frac{W}{g}} \tag{3-4}$$

Where

$$K_D = \frac{\pi^2}{\frac{L^3}{\pi^2 EI} + \frac{L}{G'b}} \tag{3-5}$$

K_B, K_D – stand for the brace and diaphragm stiffness correspondingly

L, b – represents the length and width of the diaphragm, respectively, in the direction considered

W – is the seismic weight of the single-storey building

G', EI – is the shear stiffness and the flexural stiffness of the diaphragm respectively

(Medhekar and Kennedy, 1999a)

The NBCC 2005 also specifies a limit for the inelastic inter-storey drift of 0.025 times the inter-storey height. These anticipated drifts must be calculated whilst taking into account the ductility and the inelastic behaviour of the SFRS. As such, drifts computed elastically using the equivalent static base shear are to be multiplied by R_dR_o/I_E to obtain the expected inelastic deformation of the building. The total drift included the deformation of the braced frame, obtained through matrix analysis, as well as the shear and bending deformation of the diaphragm assembly.

All the structural steel members were designed using CSA-S16 (2005) and the corrugated steel decking using CSA-S136 (2007) for gravity loads. The bracing members in the EBF were designed such that the slenderness limit, $kL/r \leq 200$, and cross-section width-to-thickness ratios, for class 2 minimum, are satisfied. Hollow structural sections (ASTM A500 F_y = 345 MPa) and W beams (ASTM A992 F_y = 345 MPa) were used for the design of the braces. All the elements that were not part of the fuse, namely the beams, columns, diaphragm, connections and the braces, were designed to remain elastic under the full capacity of the link such that the energy-dissipation would be maintained in the event of an earthquake. This implies that the factored resistance of these elements must be greater than the actual shear capacity of the link; that capacity must be calculated with the probable yield strength of the steel, $R_yF_y \geq 385$ MPa, where R_y is equal to 1.1 and accounts for the reserve in strength subsequent to yielding.

The braced frames were assumed to be located at mid-length along the perimeter walls such that the axial load remains negligible in the design of the link sections. Gravity loads were accounted for in the design of the bracing members, beams and columns.

The design was performed for Vancouver. Site Class C, or firm ground, was assumed for all cases and corresponds to acceleration and velocity-based coefficients of $F_v = F_a = 1.0$. A roof dead load of 1.0 kPa was assumed along with a cladding dead load of 0.2 kPa on the perimeter. The design comprised one braced frame per perimeter wall. The load combination used for the calculation of the seismic weight was 100% of the dead load, 25% of the snow load, and 50% of the cladding around the perimeter.

The decking used for the design of the roof was typical 914 mm wide and 38 mm deep corrugated steel panels (Figure 2.11). The nominal properties for galvanized steel complying with ASTM A653, $F_y = 230$ MPa, $F_u = 310$ MPa, and $E = 203000$ MPa, were used to calculate the nominal strengths. Only powder-actuated nailed and self-tapping screwed diaphragms were considered for this study as previous studies by Rogers & Tremblay (2003a; 2003b) had shown the satisfactory response of these fasteners under seismic loading. The types of nails and their respective properties are included in Table 3.1. The SDI methodology (Luttrell, 2004) was used to obtain the nominal strength and the shear stiffness of the diaphragm. Factored strengths were attained by multiplying the nominal shear strength by $\Phi = 0.6$ as specified by CSA-S136 (2007) for nailed and screwed diaphragms.

Table 3.1 – Nails and screw properties used in comparative analysis

Nail Type	Strength [kN]	Stiffness [mm/kN]
Hilti ENP2-21-L15	12.37	0.0292
#12 Screws	6.46	0.0700

3.2.2. Design Strategies

In total, five seismic design strategies were considered for this study. All of the scenarios are listed in Table 3.2.

Table 3.2 – Design scenarios for comparative analysis

Design	Capacity Design	Selected Ductile Element	Maximum Load for Diaphragm Design	Diaphragm Stiffness Assumption for T_a	T_a Limit
0	Yes	Link	V	Rigid	$0.05\ h_n$
1A	Yes	Link	R_dV	Rigid	$0.05\ h_n$
1B	Yes	Link	R_dV	Actual	None
2A	Yes	Link	$R_dV/1.95$	Rigid	$0.05\ h_n$
2B	Yes	Link	$R_dV/1.95$	Actual	None

The design procedure was automated and commences the initial design with an equivalent static force obtained with the empirical period. An iterative design process then occurs, until the building period reaches the 2 T_a limit or did not elongate anymore if no limit was specified. Should drift limits not be satisfied by the end of the process, the diaphragm stiffness would be increased by adding more connectors and/or increasing the deck thickness to satisfy code drift requirements. The lateral resisting system is designed in both directions while the diaphragm is designed for the maximum shear demand in either direction.

3.2.3. Link Length Design Method

This section explains the method used to define the link length, e, for the eccentric braced system. The method enforces a shear critical link once a beam satisfies the required shear area (CSA-S16, 2005). Equation 3-6 is used to define the link length once the iterative process finds the most economical Class 1 beam that satisfies the minimum shear area condition defined by Equation 3-7 (CSA-S16, 2005). That link length remains the same throughout the iterative process.

$$e = 1.6\frac{M_p}{V_p} \tag{3-6}$$

Where:

M_p – is the plastic moment of the link section = Z_xF_y

V_p – is the plastic shear capacity of the link section

$$dw \geq \frac{V_{f,link}}{\emptyset 0.55 F_y} \tag{3-7}$$

Where:

d – is the depth of the W-section

w – is the web thickness of the W-Section

$V_{f,\,link}$ – is the factored shear force in the link due to the lateral seismic loads

Φ – is the resistance factor which is equal to 0.9 and;

F_y – is the yield strength of the W-Section (345 MPa)

3.2.4. Design 1

Design 1 is based on the current capacity-based design methodology sanctioned by the NBCC 2005 (NRCC, 2006) and CSA-S16 (2005) for the earthquake-resistant design of structures. The link is used as the means of energy dissipation in the eccentric braced frame and the lateral seismic forces are calculated using the equivalent static force procedure and the prescribed seismic force modification factors for an EBF system ($R_d = 4.0$; $R_o = 1.5$). Accidental torsion is taken into account. The period is first calculated with the empirical formula and then modified using Medhekar & Kennedy's approximation (Equation 3-4) of the period of a single-storey structure with a flexible diaphragm (Medhekar & Kennedy, 1999a). Design 1A sets an upper limit of $0.05h_n$ ($2T_a$) for the maximum period used in the calculation of seismic forces while Design 1B allows the period to elongate without any restrictions.

The diaphragm is designed as per the plastic shear capacity of the link. Using the braced frame geometry, Equation 3-8 describes the seismic demand on the diaphragm.

$$q_f = 2 * \frac{V_{link}}{\tan(\theta)} \left(\frac{L}{L-e}\right) \frac{1}{b} \tag{3-8}$$

Where:

q_f – is the seismic demand on the diaphragm

V_{link} – is equal to $1.3R_yV_P$ where: $R_y = 1.1$ and V_p is the plastic shear capacity of the link

θ – is the angle, from the horizontal, produced by the braces

L – is the length of braced frame

e – is the length of the link

b – is the width of the diaphragm

3.2.5. Design 0

Design 0 is identical to the method used in Design 1 except that capacity design considerations are not applied to the diaphragm. The EBF system is therefore detailed as per capacity design principles while the diaphragm is strictly designed to carry the equivalent static force calculated using Equation 3-9. The diaphragm is therefore not protected against inelastic response during a seismic event. The period limit of $0.05h_n$ was applied and the diaphragm flexibility was not taken into account for period calculations.

$$q_f = \frac{1}{2b}\frac{V_e}{R_d R_o} \tag{3-9}$$

Where:

V_e – is the elastic base shear

b – is the width of the diaphragm

R_d, R_o – Ductility and overstrength seismic force modification factors respectively

3.2.6. Design 2

Design 2 involves capacity design principles but diaphragm forces are limited to those corresponding to $R_dR_o = 1.95$ (Equation 3-10). This implies that the diaphragm possesses minimum ductility, and therefore does not need to be designed for the full probable capacity of the bracing system. This force limitation is currently already endorsed by the NBCC 2005 (NRCC, 2006) for conventional construction (Type CC) framing systems. Note that the other components of the SFRS are still designed for the probable capacity of the link in this case. Design 2 was applied as an alternative design method to evaluate possible cost savings. Design 2A again applies the period limit of $0.05h_n$ while Design 2B does not apply any restrictions on the period but incorporates the flexibility of the diaphragm.

$$q_f = 2 * \frac{V_{p,link}}{\tan(\theta)}\left(\frac{L}{L-e}\right)\frac{1}{b} \leq \frac{S(T_a)M_vI_EW}{(1.95)(2)} \tag{3-10}$$

Where all the variables are the same as those described for Equation 3-1 and 3-9.

3.2.7. Evaluation of SFRS Costs

The main comparison in this section of the thesis is that of the structural characteristics of the different design outcomes. However, given the main objective to try to lower building costs, an evaluation of the SFRS cost was also completed for to offer another basis of comparison. The cost includes the braces and columns located in the EBF, the perimeter beams and the roof diaphragm including the steel deck and its fasteners. The unit costs, for each structural component, incorporate the material, fabrication, shipping and erection; they are the same as the ones used in Tremblay & Rogers (2005). A cost of $6500/tonne was used for the braces in the EBF. All the beams, including the link beam were valued at a cost of $4100/tonne. Different costs were associated with each of the deck thicknesses. Unit prices of $17, $20, $27 and $31 per meter squared of roof covering were used for thicknesses of 0.76mm, 0.91mm, 1.21mm and 1.52mm respectively. In addition, unit costs of $4.00 per nail frame fastener and $1.10 per screw sidelap fastener were used for the comparison. Those unit costs include the price of installation of the fasteners.

The cost presented consists of the sum of all the costs of the different SFRS components which was divided by building area. This value was then compared with the costs of the different design outcomes. Additional costs of $90-100/m^2 in Montreal and $70-80/m^2 in Vancouver for the rest of the gravity load resisting structure could also be added. The difference lies in the values are due to the prevalent higher snow loads in Quebec.

3.3. Comparative Building Study

In order to illustrate the effect of the different design strategies, the design of a 60 m wide by 30m long and 6.6m high building situated in Vancouver will be elaborated on in this section. The same building was considered in the CBF comparative study by Tremblay and Rogers (2005). Figure 3.1 shows an illustration of the building considered and lists the dead and snow loads as well as the seismic weight of the building.

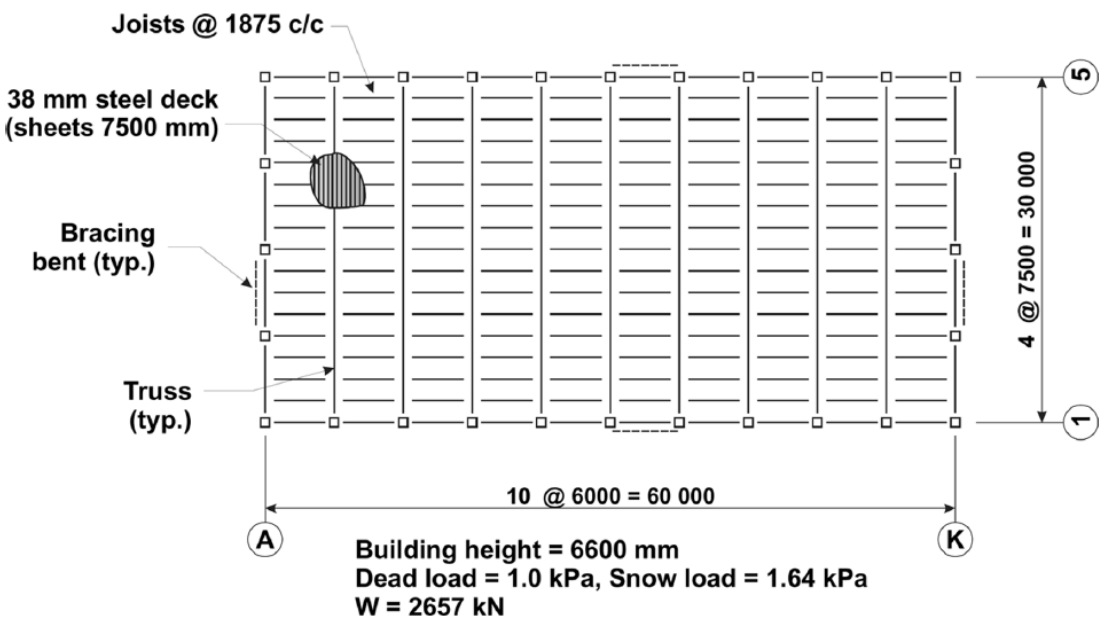

Figure 3.1 – Building example for comparative study (Tremblay & Rogers, 2005)

Only the design of the walls in the short direction was computed, including torsional effects, as they represent the most critical load case for the seismic demand on the roof diaphragm. The bracing system stiffness was calculated using matrix methods for the entire braced frame. It thus considers the brace and column stiffness as well as the flexibility of the link. All the results are included in Table 3.3 and Table 3.4.

In the instance of Design 0, capacity-based design was only applied to the bracing system and the link; the diaphragm was designed to carry the elastic base shear without any consideration for the actual resistance of the link. Prior to the implementation of the NBCC 2005, this was the method utilized by design engineers. Design 0 yields the largest building deformation since the design force of the diaphragm is small, resulting in very few connectors and shear stiffness. The cost of this design solution was more economical than all the other methods.

Table 3.3 – Building design – EBF Frame

System	Design No.				
	0	1A	1B	2A	2B
	Vancouver				
R_d/R_o	4.0/1.5	4.0/1.5	4.0/1.5	4.0/1.5	4.0/1.5
T_a (s)	0.165	0.165	0.165	0.165	0.165
T_{design} (s)	0.33	0.33	0.87	0.33	0.87
$T_{medhekar}$ NS (s)	0.90	0.80	0.87	0.80	0.87
V/W (%)	10.6	10.6	7.0	10.6	7.0
Link					
Link Shape	W310x38.7	W310x38.7	W250x32.7	W310x38.7	W250x32.7
e_{link} (mm)	635	635	635	635	635
A_{link} (mm^2)	4930	4930	4180	4930	4180
V_f (kN)	299	299	198	299	198
V'_p (kN)	341	341	299	341	299
Bracing Bent					
C_{Brace} (kN)	607	607	532	607	532
Brace Shape	HSS203.2x7.9	HSS203.2x7.9	HSS177.8x7.9	HSS203.2x7.9	HSS177.8x7.9
A_{Brace} (mm^2)	5650	5650	4900	5650	4900
C_{Column} (kN)	84.8	84.8	76.1	84.8	76.1
Column Shape	HSS114.3x3.2	HSS114.3x3.2	HSS114.3x3.2	HSS114.3x3.2	HSS114.3x3.2
A_{Column} (mm^2)	1290	1290	1290	1290	1290
K_B (mm^2)	38.1	38.1	27.9	38.1	27.9

Table 3.4 – Building design – Diaphragm

System	Design No.				
	0	1A	1B	2A	2B
	Vancouver				
R_d/R_o	4.0/1.5	4.0/1.5	4.0/1.5	4.0/1.5	4.0/1.5
V/W (%)	10.6	10.6	7.0	10.6	7.0
Roof Diaphragm					
q_f (kN/mm)	9.4	18.5	16.2	18.5	16.2
t_d	0.76	0.91	0.76	0.91	0.76
Frame Fastener	4/7	5/7	5/7	5/7	5/7
s_s (mm)	170	82	104	82	104
G' (kN/mm)	4.6	7.1	7.0	7.1	7.0
q_u (kN/m)	15.8	30.9	24.3	30.9	24.3
Δ_r/h_s (%)	0.019	0.014	0.010	0.014	0.010
Cost ($\$/m^3$)	55.80	68.84	63.96	68.84	63.96

Design 1A, which follows current building code (NRCC, 2006) and material standards (CSA-S16, 2005) was designed for seismic loads determined with a maximum period of 0.05 times the height (0.33s). This empirical value is much shorter than the period obtained using Medhekar & Kennedy's estimation (0.80s). This signifies that easing the period limitation would lower seismic loads. Design 1A yielded the highest cost due the high demand on both the braces of the diaphragm.

Design 1B, which incorporates the diaphragm flexibility, is designed for a period of 0.87s which is more than 3 times higher than the empirical estimation given by the NBCC (NRCC, 2006). It results in a significant cost reduction as the seismic force is reduced from 10.6 % to 7% of the seismic weight of the building. The decrease caused the downsizing of both the bracing system and the diaphragm and yielded a much more economical solution, though not as low as Design 0. Design 2A and 2B produced the exact same solutions as Design 1A and 1B. This was due to the fact that the diaphragm design was governed by the capacity of the beam link and not the upper seismic force limit of V/1.95. In addition, none of the designs were governed by drift.

3.4. Comparative Building Design Conclusions

In this building study, a typical 30 by 60m single-storey structure was considered and designed for earthquake resistance as per previous (Design 0) and current (Design 1A) building codes and steel design standards. Other design methodologies, where the period limitation is relaxed or where the force is limited to the elastic base shear calculated with $R_dR_o = 1.95$, were also considered.

The results show that period limitations do cause an increase in the cost of a typical structure. Allowing the period to elongate can yield significant cost savings. The design obtained using past practice did produce a cost-effective design but inelastic behaviour will likely be expected in the diaphragm. Design 1B and 2B, which had no period limitation, proved to be the most advantageous. This study highlights the importance of incorporating the diaphragm flexibility in the evaluation of the overall building period as well as utilizing the appropriate diaphragm characteristics in design.

CHAPTER 4

4.0 CONCLUSIONS AND RECOMMENDATIONS

4.1. General Discussion

In the context of this testing program, ten 21m long by 7.31m wide roof deck diaphragm specimens were tested under dynamic loading. This permitted the dynamic characterization of their properties along with the evaluation of their ductility demand and seismic performance. The test specimens had been specifically chosen to cover the most common frame fastener configurations for nails in the North American construction industry, as well as one welded button-punched diaphragm.

4.2. Conclusions

The main conclusions from the experimental program are the following:

1. The period of diaphragms does elongate, and the stiffness consequently lowers, with increasing excitation amplitude. The frequency of buildings obtained from in-situ ambient vibration acceleration measurements (Tremblay *et al.*, 2008; Lamarche *et al.*, 2009) would not be representative of the diaphragm characteristics during ground motion shaking.
2. The SDI method overestimates the stiffness of diaphragms under dynamic loading conditions except for diaphragms with different end and interior frame fastener patterns if an alternate fastener spacing is assumed in the stiffness prediction.

3. All the 22 gauge nailed and screwed specimens showed strength degradation after the peak load but could withstand and dissipate energy during several cycles. All exhibited a pinched hysteretic behaviour resulting from bearing of the deck around nails and screws.
4. All the 20 gauge nailed and screwed specimens showed strength degradation after the peak load but only some exhibited energy dissipation for several cycles. Sensitivity to slight differences in stiffness and/or slight differences in actuator displacements was also seen with the thicker decks and resulted in one-sided failure of the specimens.
5. The welded and button-punch diaphragm was able to sustain the peak load during several cycles but exhibited very little dissipation of energy during the inelastic cycles; it would therefore not be a viable option when considering the diaphragm as the energy-dissipating element in the SFRS.
6. The overlap at sheet ends constricts the warping, increases the stiffness of the diaphragm and should be considered in the in-plane flexibility of the diaphragm.
7. The diaphragm with gypsum experienced a maximum increase of 28% in its stiffness. This increase is not negligible if computing the in-plane flexibility of the diaphragm but may not be critical in terms of overall building performance as was shown by Mastrogiuseppe *et al.* (2008).
8. Rivets can be used successfully as sidelap connectors and will achieve similar strength and ductility when compared to screwed diaphragms because of their larger diameter.

4.3. Design Recommendations

1. The experimental program and building study showed that accounting for the in-plane flexibility for the diaphragm will lower seismic forces and result in a more cost-efficient design.
2. Nailed and Screwed diaphragms with a thickness of 0.76mm exhibit satisfactory ductile inelastic behaviour in order to be used as the energy-dissipating element in the SFRS. Thicker decks did not consistently fail in a ductile manner; caution should thus be exercised before detailing 0.91mm gauge deck diaphragms as the fuse element in the SFRS.

4.4. Recommendations for Future Studies

1. It is recommended that a numerical model be created that successfully predicts the inelastic behaviour of all the nailed and screwed diaphragms
2. Other similar dynamic tests should be performed to investigate other fastener patterns and types, deck thicknesses and the influence of the deck orientation
3. Model or equations for the prediction of G' and S_n should be proposed for the modelling of diaphragms as the fuse and in the elastic range.
4. Full building models should be run to evaluate the viability of diaphragms as the energy-dissipating element while incorporating the dynamic characteristics determined in this study and;
5. Ductility-related and overstrength-related seismic force modification factors should be established for the use of diaphragms as the energy-dissipating element in the SFRS.

BIBLIOGRAPHY

Allemang, R. J. (2003). The modal assurance criterion – twenty years of use and abuse. *Sound and Vibration*, 37(8):14–21.

Allemang, R. J. & Brown, D. L. (1982). A Correlation Coefficient for Modal Vector Analysis. Proceedings of the International Modal Analysis Conference, 110-116.

American Institute of Steel Construction. (1963). Design manual for orthotropic steel plate deck bridges. New York : American Institute of Steel Construction.

ASAP 3S Roofing Fasteners (2009). OMG, Inc. from http://www.olyfast.com/

American Society for Testing and Materials (2009). ASTM A500/A500M - Standard Specification for Cold-Formed Welded and Seamless Carbon Steel Structural Tubing in Rounds and Shapes. West Conshohocken, PA, USA.

American Society for Testing and Materials (2009). ASTM A653 / A653M - Standard Specification for Steel Sheet, Zinc-Coated (Galvanized) or Zinc-Iron Alloy-Coated (Galvannealed) by the Hot-Dip Process. West Conshohocken, PA, USA.

American Society for Testing and Materials (2006). ASTM A992 /A992M - Standard Specification for Structural Steel Shapes. West Conshohocken, PA, USA.

Avdel. (2009). Avdel Global. from http://www.avdel-global.com/

Basu, D., & Jain, S. K. (2004). Seismic analysis of asymmetric buildings with flexible floor diaphragms. *Journal of Structural Engineering, 130*(8), 1169-1176.

Bendat, J. S. & Piersol, A. G. (1986). Random Data, Analysis and Measurement Procedures. New York: Wiley.

Braun, S., Ewins, D. J., Rao, S. S., & Knovel. (2002). Encyclopedia of vibration. San Diego: Academic Press.

Brincker, R., Zhang, L., & Andersen, P. (2001). Modal identification of output-only systems using frequency domain decomposition. *Smart Materials and Structures*, 10(3), 441-445.

Bryan, E. R. (1973). The stressed skin design of steel buildings. New York: Wiley.

Canadian Commission on Building and Fire Codes, National Research Council Canada, & Institute for Research in Construction. (2006). User's guide--NBC 2005 : structural commentaries (Part 4 of division B). Ottawa: National Research Council of Canada.

Canadian Institute of Steel Construction. (2006). Handbook of steel construction. Willowdale, ON, Canada: Canadian Institute of Steel Construction.

Canadian Sheet Steel Building Institute, (2006). CSSBI B13-06 - Design of Steel Deck Diaphragms - 3rd Edition, Cambridge, ON, Canada.

Canadian Standards Association S16 (2005). Limit States Design of Steel Structures, Mississauga, ON, Canada.

Canadian Standards Association S16 – 2009 Draft (2008). Limit States Design of Steel Structures, Mississauga, ON, Canada.

Canadian Standards Association S136 (2007) North American Specification for the Design of Cold-Formed Steel Structural Members, Mississauga, ON, Canada.

Canadian Roofing Contractors' Association. (1993). Fastening of Gypsum Boards to Steel Roof Deck. *Technical Bulletin, 37*.

CANAM. (2007). Steel Deck Diaphragm. *Technical Bulletin.*

Carr, A.J. 2004. Ruaumoko, Inelastic Dynamic Analysis Program. Department of civil engineering. University of Canterbury, NZ.

CertainTeed Corporation (2009). Gypsum - ProRoc® Sheathing Treated Core. from http://www.certaineed.com/products/gypsum/

Chopra, A. K. (2006). Dynamics of Structures - Theory and Applications to Earthquake Engineering (3rd ed.). Upper Saddle River, New Jersey: Prentice Hall.

Cohen, G. L., Klingner, R. E., Hayes, J. J. R., & Sweeney, S. C. (2006). Seismic Evaluation of Low-Rise Reinforced Masonry Buildings with Flexible Diaphragms: III. Synthesis and Application. *Earthquake Spectra, 22*(2), 329-347.

Davies, J. M., & Bryan, E. R. (1982). Manual of stressed skin diaphragm design. New York: Wiley.

Davies, J. M. (1986a). General Solution for the Shear Flexibility of Profiled Sheets I: Development and Verification of the Method. *Thin-Walled Structures, 4*(1), 41-68.

Davies, J. M. (1986b). General Solution for the Shear Flexibility of Profiled Sheets II: Application of the Method. *Thin-Walled Structures, 4*(2), 151-161.

Davies, J.M. (2006). Developments in stressed skin design. *Thin-Walled Structures, 44*(12), 1250-1260.

De Matteis, G., & Landolfo, R. (1999). Mechanical fasteners for cladding sandwich panels: Interpretative models for shear behaviour. *Thin-Walled Structures, 35*(1), 61-79.

Dolce, M., Lorusso, V. D., & Masi, A. (1994). Seismic response of building structures with flexible inelastic diaphragm. *The Structural Design of Tall Buildings, 3*(2), 87-106.

Essa, H. S., Tremblay, R., & Rogers, C. A. (2001). Inelastic Seismic Behaviour of Steel Deck Roof Diaphragms Under Quasi-Static Cyclic Loading: *Report No. EPM/CGS – 2001 – 11*. Ecole Polytechnique de Montreal, Montreal, QC, Canada.

Federal Emergency Management Agency. (1997). FEMA 273 - NEHRP Guidelines for the Seismic Rehabilitationg of Buildings. Washington.

Federal Emergency Management Agency. (1997). FEMA 274 - NEHRP Commentary on the Guidelines for the Seismic Rehabilitationg of Buildings. Washington.

Federal Emergency Management Agency. (2000). FEMA 356 – Prestandard and Commentary for the Seismic Rehabilitation of Buildings. Washington.

Gesipa - Fasteners USA Inc. (2007). Blind Rivets: G-Bulb - G-Bulb Steel. from http://www.gesipausa.com

Hamming, R. W. (1977). Digital filters. Englewood Cliffs, N.J.: Prentice-Hall.

Humar, J. (2007). Seismic Provisions of NBCC 2005. Ottawa.

Jain, S. K. (1984). Seismic Response of Buildings with Flexible Floors. *Journal of Engineering Mechanics, 110*(1), 125-129.

Ju, S. H., & Lin, M. C. (1999). Comparison of building analyses assuming rigid or flexible floors. *Journal of structural engineering New York, N.Y., 125*(1), 25-31.

Kennedy, D. J. L., & Medhekar, M. S. (1999). Proposed strategy for seismic design of steel buildings. *Canadian Journal of Civil Engineering*, 26(5), 564-571.

Kim, S.-C., & White, D. W. Three-Dimensional NonLinear Time-History Analysis of Low-Rise Shear Wall Buildings with Flexible Diaphragm*s*. Paper presented at the 7th US National Conference on Earthquake Engineering (7NCEE).

Kim, S.-C., & White, D. W. (2004). Nonlinear analysis of a one-story low-rise masonry building with a flexible diaphragm subjected to seismic excitation. *Engineering Structures, 26*(14), 2053-2067.

Lamarche, C.-P. (2005). Etude Expérimentale du Comportement Dynamique des Bâtiments de Faible Hauteur en Acier. M.A.Sc. thesis. Université de Sherbrooke, Montreal, QC, Canada.

Lamarche, C.-P., Proulx, J., Paultre, P., Turek, M., Ventura, C. E., Le, T. P., et al. (2009). Toward a better understanding of the dynamic characteristics of single-storey braced steel frame buildings in Canada. *Canadian Journal of Civil Engineering, 36*(6), 969-979.

Luttrell, L. D. (1981). Diaphragm design manual (1st ed.). Fox River Grove, Ill.: Steel Deck Institute.

Luttrell, L. D. (1995). Diaphragm design manual (2nd ed.). Fox River Grove, Ill.: Steel Deck Institute.

Luttrell, L. D. (2004). Diaphragm design manual (3rd ed.). Fox River Grove, Ill.: Steel Deck Institute.

Maia, N. M. M., & Montalvão e Silva, J. M. (1997). Theoretical and experimental modal analysis. Taunton, Somerset, England: New York : Research Studies Press ; Wiley.

Martin, E. (2002). Inelastic Response of Steel Roof Deck Diaphragms Under Simulated Dynamically Applied Seismic Loading. M.A.Sc. thesis. Ecole Polytechnique de Montreal, Montreal, QC, Canada.

Masi, A., Dolce, M., & Caterina, F. (1997). Seismic response of irregular multi-storey buildings with flexible inelastic diaphragms. *The Structural Design of Tall Buildings, 6*(2), 99-124.

Mastrogiuseppe, S. (2006). Numerical Linear Elastic Investigation of Steel Roof Deck Diaphragm Behaviour Accounting for the Contribution of Nonstructural Components. M. Eng. thesis. McGill University, Montreal, QC, Canada.

Mastrogiuseppe, S., Rogers, C. A., Tremblay, R., & Nedisan, C. D. (2008). Influence of nonstructural components on roof diaphragm stiffness and fundamental periods of single-storey steel buildings. *Journal of Constructional Steel Research, 64*(2), 214-227.

Mazzolani F.M. (2008). Steel against Earthquake. University of Naples "Federico II", Naples, Italy. *Technical Bulletin.*

Medhekar, M. S., & Kennedy, D. J. L. (1999a). Seismic evaluation of single-storey steel buildings. *Canadian Journal of Civil Engineering*, 26(4), 379-394.

Medhekar, M. S., & Kennedy, D. J. L. (1999b). Seismic response of two-storey buildings with concentrically braced steel frames. *Canadian Journal of Civil Engineering*, 26(4), 497-509.

Moanda, E. (2000). Étude Numérique de L'Influence de la Flexibilité du Diaphragme de Toit sur le Comportement d'un Bâtiment d'un Étage. Report. École Polytechnique de Montréal, Montreal, QC, Canada.

Naman, S. K., & Goodno, B. J. (1986). Seismic evaluation of a low rise steel building. *Engineering Structures, 8*(1), 9-16.

Nedisan, C. D. (2002). Comportement Sismique de Batiments d'un Seul Etage en Acier Avec Diapragme de Toit Flexible. M.A.Sc. thesis. Ecole Polytechnique de Montreal, Montreal, QC, Canada.

Prakash, V. and Powell, G.H. (1993). DRAIN-2DX, DRAIN-3DX and DRAIN-BUILDING: Base Program Design Documentation, *Report UCB/SEMM-93/16*, Dept. of Civil Eng., Univ. Of California, Berkeley, CA.

Rogers, C. A., & Tremblay, R. (2003a). Inelastic seismic response of frame fasteners for steel roof deck diaphragms. *Journal of Structural Engineering*, 129(12), 1647-1657.

Rogers, C. A., & Tremblay, R. (2003b). Inelastic seismic response of side lap fasteners for steel roof deck diaphragms. *Journal of Structural Engineering*, 129(12), 1637-1646.

Rogers, C.A., Tremblay, R., (2010), "Impact of diaphragm behavior on the seismic design of low-rise steel buildings", *AISC Engineering Journal*. (In press)

Steel Deck Institute, (1987). Diaphragm design manual, 2nd Edition, Steel Deck Institute, Canton, OH, US.

Shrestha, K., Franquet, J., Rogers, C., & Tremblay, R. (2009). OpenSees Modeling of the Inelastic Seismic Response of Steel Roof Deck Diaphragms. Paper presented at the 6th International Conference - Behaviour of Steel Structures in Seismic Areas (STESSA), Philadelphia

Tena-Colunga, A., & Abrams, D. P. (1996). Seismic Behavior of Structures with Flexible Diaphragms. *Journal of Structural Engineering, 122*(4), 439-445.

The Mathworks, Inc. (2009). Matlab. Natick, MA.

Tremblay, R., Berair, T., & Filiatrault, A. (2000). Experimental Behaviour of Low-Rise Steel Buildings with Flexible Roof Diaphragms. Paper presented at the 12th World Conference on Earthquake Engineering, Auckland, New Zealand.

Tremblay, R., Martin, E., Yang, W., & Rogers, C. A. (2004). Analysis, Testing and Design of Steel Roof Deck Diaphragms for Ductile Earthquake Resistance. *Journal of Earthquake Engineering, 8*(5), 775 - 816.

Tremblay, R., Nedisan, C., Lamarche, C.-P., & Rogers, C. (2008a). Periods of Vibration of a Low-Rise Building with a Flexible Steel Roof Deck Diaphragm. Paper presented at the Fifth International Conference on Thin-Walled Structures.

Tremblay, R., & Rogers, C. (2005). Influence of Seismic Design Requirements and Building Period on the Design of Low-Rise Steel Buildings. Paper presented at the 4th International Conference on Advances in Steel Structures, Shanghai, China.

Tremblay, R., Rogers, C., Lamarche, C.-P., Nedisan, C., Franquet, J., & Massarelli, R. (2008b). Dynamic Seismic Testing of Large Size Steel Deck Diaphragm for Low-Rise Building Applications. Paper presented at the 14th World Conference on Earthquake Engineering.

Tremblay, R., Rogers, C.A., Nedisan, C. (2003). Seismic Torsional Response of Single-Storey Steel Structures With Flexible Roof Diaphragms. *Advances in Structures, Vols 1 and 2,* 1299-1305.

Tremblay, R., Rogers, C., and Nedisan, C. (2002). Use of Uniform Hazard Spectrum and Computed Period in the Seismic Design of Single-Storey Steel Structures. *Proc. 7th U.S. Nat. Conf. on Earthquake Eng.*, Boston, MA, Paper No. 195.

Tremblay, R., & Stiemer, S. F. (1996). Seismic behavior of single-storey steel structures with a flexible roof diaphragm. *Canadian Journal of Civil Engineering, 23*(1), 49-62.

Turek, M., and Ventura, C.E. 2005. Ambient vibration testing of low-rise buildings with flexible diaphragms. Paper presented at the 23rd International Modal Analysis Conference, Orlando, Florida, 31 Jan. – 3 Feb. 2005. Paper no. 304.

Wright, B. W., & Manbeck, H. B. (1992). Theoretical prediction models for diaphragm panel behavior-a review. *Transactions of the American Society of Agricultural Engineers, 35*(1), 287-295.

Yang, W. (2003). Inelastic Seismic Response of Steel Roof Deck Diaphragms Including Effects of Non-Structural Components and End Laps. M.A.Sc. thesis. Ecole Polytechnique de Montreal, Montreal, QC, Canada.

APPENDIX A: SHEAR STRENGTH AND STIFFNESS PREDICTION WITH SDI METHOD

Calculation of the diaphragm resistance and rigidity according to the "SDI Diaphragm Design Manual 3rd edition"
Connection resistance values are provided in the data sheet (according to the value of t specified)
The values of I_X and x_e are also provided in the adjacent section

	I_X (mm^4/m)		CSSBI Diaphragm Manual Values (3rd Edition)		
t (mm)	P3615	P2436	36" x 1.5"	24" x 3" (6" spacing)	24" x 3" (8" spacing)
0.76	228227	1001000	234000	1310000	1070000
0.91	272365	1189000	280000	1570000	1280000
1.22	364468	1718000	375000	2100000	1720000
1.52	452803	2213000	466000	2610000	2140000

Deck-to-frame Connections		Q_f (kN)	S_f (mm/kN)	
Welds	13 mm	6.19	0.0380	
	16 mm	7.84	0.0380	
	19 mm	9.49	0.0380	
	Washers. 1.52 x 9.5 mm - 410XX	13.68	0.0380	Note : 9.5 mm = 3/8" hole diameter
	Washers 1.52 x 9.5 mm - 480XX	14.87	0.0380	Note : 9.5 mm = 3/8" hole diameter
Screws	#12 et #14	4.63	0.0429	
Nails	Hilti ENP2-21-L15	7.16	0.0413	Note : 2nd edition of SDI manual
	Hilti ENP3-21-L15	7.16	0.0413	Note : 2nd edition of SDI manual
	Hilti ENKK	6.30	0.0515	Note : 2nd edition of SDI manual
	Ramset 26SD	7.07	0.0825	Note : 2nd edition of SDI manual
	Buildex BX14	7.07	0.0825	Note : 3rd edition of SDI manual
	Buildex BX12	6.68	0.0825	Note : 3rd edition of SDI manual
	Hilti ENP2 & ENPH2	7.16	0.0413	Note : 3rd edition of SDI manual
	Hilti ENP2K, X-EDN19 & X-EDNK22	6.71	0.0413	Note : 3rd edition of SDI manual

Sidelap Connections		Q_s (kN)	S_s (mm/kN)	
Weld	13 mm	4.64	0.0413	Note : 0.75 of Q_f from above welds
Button Punch		0.96	0.9903	
Screw	#8	2.50	0.0990	
	#10	2.86	0.0990	
	#12	3.23	0.0990	
	#14	3.79	0.0990	

Deck Connection Patterns	$\Sigma(x_e/w)$	$\Sigma(x_e/w)^2$	Npas	
P3615 - 3/7 (914/3)	1.000	0.500	3	Note: All from Appendix
P3615 - 4/7 (914/4)	1.333	0.556	2	IV of SDI manual
P3615 - 5/7 (914/5)	1.667	0.722	2	
P3615 - 7/7 (914/7)	2.000	0.778	1	
P3615 - 9/7 (914/9)	3.000	1.278	1	
P3615 - 11/7 (914/11)	3.667	1.500	1	

Figure A.1 – SDI manual data sheet for 22 gauge deck diaphragms (Lutrell, 2004)

	I_X (mm^4/m)		CSSBI Diaphragm Manual Values (3rd Edition)		
t (mm)	P3615	P2436	36" x 1.5"	24" x 3" (6" spacing)	24" x 3" (8" spacing)
0.76	228227	1001000	234000	1310000	1070000
0.91	272365	1189000	280000	1570000	1280000
1.22	364468	1718000	375000	2100000	1720000
1.52	452803	2213000	466000	2610000	2140000

Deck-to-frame Connections		Q_f (kN)	S_f (mm/kN)	
Welds	13 mm	7.32	0.0347	
	16 mm	9.29	0.0347	
	19 mm	11.27	0.0347	
	Washers. 1.52 x 9.5 mm - 410XX	18.06	0.0347	Note : 9.5 mm = 3/8" hole diameter
	Washers 1.52 x 9.5 mm - 480XX	19.76	0.0347	Note : 9.5 mm = 3/8" hole diameter
Screws	#12 et #14	5.54	0.0392	
Nails	Hilti ENP2-21-L15	8.34	0.0377	Note : 2nd edition of SDI manual
	Hilti ENP3-21-L15	8.34	0.0377	Note : 2nd edition of SDI manual
	Hilti ENKK	7.40	0.0471	Note : 2nd edition of SDI manual
	Ramset 26SD	8.18	0.0754	Note : 2nd edition of SDI manual
	Buildex BX14	8.18	0.0754	Note : 3rd edition of SDI manual
	Buildex BX12	7.72	0.0754	Note : 3rd edition of SDI manual
	Hilti ENP2 & ENPH2	8.34	0.0377	Note : 3rd edition of SDI manual
	Hilti ENP2K, X-EDN19 & X-EDNK22	7.99	0.0377	Note : 3rd edition of SDI manual

Sidelap Connections		Q_s (kN)	S_s (mm/kN)	
Weld	13 mm	5.49	0.0377	Note : 0.75 of Q_f from above welds
Button Punch		1.37	0.9050	
Screw	#8	3.00	0.0905	
	#10	3.42	0.0905	
	#12	3.87	0.0905	
	#14	4.54	0.0905	

Deck Connection Patterns	$\Sigma(x_e/w)$	$\Sigma(x_e/w)^2$	Npas	
P3615 - 3/7 (914/3)	1.000	0.500	3	Note: All from Appendix
P3615 - 4/7 (914/4)	1.333	0.556	2	IV of SDI manual
P3615 - 5/7 (914/5)	1.667	0.722	2	
P3615 - 7/7 (914/7)	2.000	0.778	1	
P3615 - 9/7 (914/9)	3.000	1.278	1	
P3615 - 11/7 (914/11)	3.667	1.500	1	
P2436 - 3/5 (610/3)	1.000	0.500	2	
P2436 - 5/5 (610/5)	1.500	0.625	1	

Figure A.2 – SDI manual data sheet for 20 gauge deck diaphragms (Lutrell, 2004)

Steel			
Steel thickness	**tt**	**0.76**	**mm**
Steel yield strength (for the calculation of Qf of screws according to the SDI method)	Fy	230	**MPa**
Steel ultimate tensile strength (for the calculation of Q_f of welds according to the SDI method)	Fu	310	**MPa**
Young's modulus	E	203000	**MPa**
Deck			
Depth of deck	hh	38	**mm**
Length of web (measured over the inclined distance)	ww	40.16	**mm**
Pitch (o/c spacing of flutes)	dd	152	**mm**
Half-length of the lower flange	ee	19.05	**mm**
Length of the upper flange	ff	88.9	**mm**
Horizontal projection of the web	gg	12.7	**mm**
Developed length of steel per flute	ss	207.32	mm
Overall deck width	w_f	914	**mm**
Overall deck length	**LL**	**7006.67**	**mm**
Number of intermediate joists	**np**	**3**	
Joist spacing (o/c)	Lv	1751.67	mm
Gross Moment of inertia of the deck (see adjcaent)	Ix	228227	**mm^4/m**
Connections			
Resistance of the frame connectors (see adjacent)	**Q_f**	**6.71**	**kN**
Flexibility of the frame connectors (see adjacent)	**S_f**	**0.0413**	**mm/kN**
Resistance of the sidelap connectors (see adjacent)	**Q_s**	**3.23**	**kN**
Flexibilty of the sidelap connectors (see adjacent)	**S_s**	**0.099**	**mm/kN**
Valley spacing (each = 1, alternate = 2, third = 3, fourth = 4) (is every flute connected or not?) (see data sheet)	**n_pas**	**2**	
$S(x_e/w)$ on the end joists (over w, including the edge connectors) (see data sheet)	α_1	**1.333**	
$S(x_p/w)$ on the intermediate joists (over w, including the edge connectors) (see data sheet)	α_2	**1.333**	
$S(x_e/w)^2$ on the end joists (over w, including the edge connectors) (see data sheet)	**$\Sigma(x_e/w)^2$**	**0.556**	
$S(x_p/w)^2$ on the intermediate joists (over w, including the edge connectors) (see data sheet)	**$\Sigma(x_p/w)^2$**	**0.556**	
Number of end connectors (total over width w including those on the edge	**n_v**	**4**	
Number of frame connectors on the side of the deck (total over length LL excluding those on the joists)	**n_e**	**20**	
Number of sidelap connectors (total over length LL excluding those on the joists)	**n_s**	**20**	
Resistance			
Corner factor	λ	0.793	
Factor B	B	15.187	
Resistance based on the panel end	Sn	25.54	kN/m
Resistance based on the interior panel	Sn	14.15	kN/m
Resistance based on the corner connection	Sn	13.03	kN/m
Resistance based on the overall shear buckling of the deck (Lower bound 2 span case where coeff = 3.25)	S_{cr}	24.99	kN/m
Nominal shear resistance	**min S_n**	**13.03**	**kN/m**
See latest CSA S136 for phi factors			
Flexibility and Rigidity			
Flexibility due to the deformation of a flat steel sheet in shear	Fs	0.0230	mm/kN
Flexibility due to warping of the deck (parameter Dn)	Fn	0.1876	mm/kN
Flexibility due to deformation at the connections (parameter C)	Fslip	0.0271	mm/kN
Flexibility	**F**	0.2377	**mm/kN**
Rigidity	**G'**	4.207	**kN/mm**

Figure A.3 – Calculation of DIA1, DIA1R and DIA2 strength for one panel length

Steel			
Steel thickness	**tt**	**0.76**	**mm**
Steel yield strength (for the calculation of Qf of screws according to the SDI method)	Fy	230	**MPa**
Steel ultimate tensile strength (for the calculation of Q_f of welds according to the SDI method)	Fu	310	**MPa**
Young's modulus	E	203000	**MPa**
Deck			
Depth of deck	hh	38	**mm**
Length of web (measured over the inclined distance)	ww	40.16	**mm**
Pitch (o/c spacing of flutes)	dd	152	**mm**
Half-length of the lower flange	ee	19.05	**mm**
Length of the upper flange	ff	88.9	**mm**
Horizontal projection of the web	gg	12.7	**mm**
Developed length of steel per flute	ss	207.32	mm
Overall deck width	w_f	914	**mm**
Overall deck length	**LL**	**21020.0**	**mm**
Number of intermediate joists	**np**	**11**	
Joist spacing (o/c)	Lv	1751.67	mm
Gross Moment of inertia of the deck (see adjcaent)	Ix	228227	**mm^4/m**
Connections			
Resistance of the frame connectors (see adjacent)	**Q_f**	**6.71**	**kN**
Flexibility of the frame connectors (see adjacent)	**S_f**	**0.0413**	**mm/kN**
Resistance of the sidelap connectors (see adjacent)	**Q_s**	**3.23**	**kN**
Flexibilty of the sidelap connectors (see adjacent)	**S_s**	**0.099**	**mm/kN**
Valley spacing (each = 1, alternate = 2, third = 3, fourth = 4) (is every flute connected or not?) (see data sheet)	**n_pas**	**2**	
$S(x_e/w)$ on the end joists (over w, including the edge connectors) (see data sheet)	α_1	**1.333**	
$S(x_p/w)$ on the intermediate joists (over w, including the edge connectors) (see data sheet)	α_2	**1.333**	
$S(x_e/w)^2$ on the end joists (over w, including the edge connectors) (see data sheet)	**$\Sigma(x_e/w)^2$**	**0.556**	
$S(x_p/w)^2$ on the intermediate joists (over w, including the edge connectors) (see data sheet)	**$\Sigma(x_p/w)^2$**	**0.556**	
Number of end connectors (total over width w including those on the edge	**n_v**	**4**	
Number of frame connectors on the side of the deck (total over length LL excluding those on the joists)	**n_e**	**60**	
Number of sidelap connectors (total over length LL excluding those on the joists)	**n_s**	**60**	
Resistance			
Corner factor	λ	0.793	
Factor B	B	43.338	
Resistance based on the panel end	Sn	24.68	kN/m
Resistance based on the interior panel	Sn	13.70	kN/m
Resistance based on the corner connection	Sn	12.52	kN/m
Resistance based on the overall shear buckling of the deck (Lower bound 2 span case where coeff = 3.25)	S_{cr}	24.99	kN/m
Nominal shear resistance	**min S_n**	**12.52**	**kN/m**
See latest CSA S136 for phi factors			
Flexibility and Rigidity			
Flexibility due to the deformation of a flat steel sheet in shear	Fs	0.0230	mm/kN
Flexibility due to warping of the deck (parameter Dn)	Fn	0.0259	mm/kN
Flexibility due to deformation at the connections (parameter C)	Fslip	0.0282	mm/kN
Flexibility	**F**	0.0770	**mm/kN**
Rigidity	**G'**	12.980	**kN/mm**

Figure A.4 – Calculation of DIA1, DIA1R and DIA2 strength for three panel length

Steel			
Steel thickness	**tt**	**0.76**	**mm**
Steel yield strength (for the calculation of Qf of screws according to the SDI method)	Fy	230	**MPa**
Steel ultimate tensile strength (for the calculation of Q_f of welds according to the SDI method)	Fu	310	**MPa**
Young's modulus	E	203000	**MPa**
Deck			
Depth of deck	hh	38	**mm**
Length of web (measured over the inclined distance)	ww	40.16	**mm**
Pitch (o/c spacing of flutes)	dd	152	**mm**
Half-length of the lower flange	ee	19.05	**mm**
Length of the upper flange	ff	88.9	**mm**
Horizontal projection of the web	gg	12.7	**mm**
Developed length of steel per flute	ss	207.32	mm
Overall deck width	w_f	914	**mm**
Overall deck length	**LL**	7006.67	**mm**
Number of intermediate joists	**np**	**3**	
Joist spacing (o/c)	Lv	1751.67	mm
Gross Moment of inertia of the deck (see adjcaent)	Ix	228227	**mm^4/m**
Connections			
Resistance of the frame connectors (see adjacent)	**Q_f**	**6.71**	**kN**
Flexibility of the frame connectors (see adjacent)	**S_f**	**0.0413**	**mm/kN**
Resistance of the sidelap connectors (see adjacent)	**Q_s**	**3.23**	**kN**
Flexibilty of the sidelap connectors (see adjacent)	**S_s**	**0.099**	**mm/kN**
Valley spacing (each = 1, alternate = 2, third = 3, fourth = 4) (is every flute connected or not?) (see data sheet)	**n_pas**	**2**	
S(x_e/w) on the end joists (over w, including the edge connectors) (see data sheet)	α_1	**2**	
S(x_p/w) on the intermediate joists (over w, including the edge connectors) (see data sheet)	α_2	**1.333**	
S$(x_e/w)^2$ on the end joists (over w, including the edge connectors) (see data sheet)	**$\Sigma(x_e/w)^2$**	**0.778**	
S$(x_p/w)^2$ on the intermediate joists (over w, including the edge connectors) (see data sheet)	**$\Sigma(x_p/w)^2$**	**0.556**	
Number of end connectors (total over width w including those on the edge	**n_v**	**7**	
Number of frame connectors on the side of the deck (total over length LL excluding those on the joists)	**n_e**	**44**	
Number of sidelap connectors (total over length LL excluding those on the joists)	**n_s**	**44**	
Resistance			
Corner factor	λ	0.793	
Factor B	B	27.628	
Resistance based on the panel end	Sn	49.80	kN/m
Resistance based on the interior panel	Sn	26.06	kN/m
Resistance based on the corner connection	Sn	23.52	kN/m
Resistance based on the overall shear buckling of the deck (Lower bound 2 span case where coeff = 3.25)	S_{cr}	24.99	kN/m
Nominal shear resistance	**min S_n**	**23.52**	**kN/m**
See latest CSA S136 for phi factors			
Flexibility and Rigidity			
Flexibility due to the deformation of a flat steel sheet in shear	Fs	0.0230	mm/kN
Flexibility due to warping of the deck (parameter Dn)	Fn	0.1876	mm/kN
Flexibility due to deformation at the connections (parameter C)	Fslip	0.0142	mm/kN
Flexibility	**F**	0.2248	**mm/kN**
Rigidity	**G'**	4.449	**kN/mm**

Figure A.5 – Calculation of DIA3 strength for one panel length

Steel			
Steel thickness	**tt**	**0.76**	**mm**
Steel yield strength (for the calculation of Qf of screws according to the SDI method)	Fy	230	**MPa**
Steel ultimate tensile strength (for the calculation of Q_f of welds according to the SDI method)	Fu	310	**MPa**
Young's modulus	E	203000	**MPa**
Deck			
Depth of deck	hh	38	**mm**
Length of web (measured over the inclined distance)	ww	40.16	**mm**
Pitch (o/c spacing of flutes)	dd	152	**mm**
Half-length of the lower flange	ee	19.05	**mm**
Length of the upper flange	ff	88.9	**mm**
Horizontal projection of the web	gg	12.7	**mm**
Developed length of steel per flute	ss	207.32	mm
Overall deck width	w_f	914	**mm**
Overall deck length	**LL**	**21020**	**mm**
Number of intermediate joists	**np**	**11**	
Joist spacing (o/c)	Lv	1751.67	mm
Gross Moment of inertia of the deck (see adjcaent)	Ix	228227	**mm^4/m**
Connections			
Resistance of the frame connectors (see adjacent)	**Q_f**	**6.71**	**kN**
Flexibility of the frame connectors (see adjacent)	**S_f**	**0.0413**	**mm/kN**
Resistance of the sidelap connectors (see adjacent)	**Q_s**	**3.23**	**kN**
Flexibilty of the sidelap connectors (see adjacent)	**S_s**	**0.099**	**mm/kN**
Valley spacing (each = 1, alternate = 2, third = 3, fourth = 4) (is every flute connected or not?) (see data sheet)	**n_pas**	**2**	
$S(x_e/w)$ on the end joists (over w, including the edge connectors) (see data sheet)	α_1	**2**	
$S(x_p/w)$ on the intermediate joists (over w, including the edge connectors) (see data sheet)	α_2	**1.333**	
$S(x_e/w)^2$ on the end joists (over w, including the edge connectors) (see data sheet)	**$\Sigma(x_e/w)^2$**	**0.778**	
$S(x_p/w)^2$ on the intermediate joists (over w, including the edge connectors) (see data sheet)	**$\Sigma(x_p/w)^2$**	**0.556**	
Number of end connectors (total over width w including those on the edge	**n_v**	**7**	
Number of frame connectors on the side of the deck (total over length LL excluding those on the joists)	**n_e**	**132**	
Number of sidelap connectors (total over length LL excluding those on the joists)	**n_s**	**132**	
Resistance			
Corner factor	λ	0.793	
Factor B	B	78.885	
Resistance based on the panel end	Sn	48.09	kN/m
Resistance based on the interior panel	Sn	25.05	kN/m
Resistance based on the corner connection	Sn	22.61	kN/m
Resistance based on the overall shear buckling of the deck (Lower bound 2 span case where coeff = 3.25)	S_{cr}	24.99	kN/m
Nominal shear resistance	**min S_n**	**22.61**	**kN/m**
See latest CSA S136 for phi factors			
Flexibility and Rigidity			
Flexibility due to the deformation of a flat steel sheet in shear	Fs	0.0230	mm/kN
Flexibility due to warping of the deck (parameter Dn)	Fn	0.0259	mm/kN
Flexibility due to deformation at the connections (parameter C)	Fslip	0.0147	mm/kN
Flexibility	**F**	0.0636	**mm/kN**
Rigidity	**G'**	15.723	**kN/mm**

Figure A.6 – Calculation of DIA3 strength for three panel length

Steel			
Steel thickness	**tt**	**0.76**	**mm**
Steel yield strength (for the calculation of Qf of screws according to the SDI method)	Fy	230	**MPa**
Steel ultimate tensile strength (for the calculation of Q_f of welds according to the SDI method)	Fu	310	**MPa**
Young's modulus	E	203000	**MPa**
Deck			
Depth of deck	hh	38	**mm**
Length of web (measured over the inclined distance)	ww	40.16	**mm**
Pitch (o/c spacing of flutes)	dd	152	**mm**
Half-length of the lower flange	ee	19.05	**mm**
Length of the upper flange	ff	88.9	**mm**
Horizontal projection of the web	gg	12.7	**mm**
Developed length of steel per flute	ss	207.32	mm
Overall deck width	w_f	914	**mm**
Overall deck length	**LL**	**7006.67**	**mm**
Number of intermediate joists	**np**	**3**	
Joist spacing (o/c)	Lv	1751.67	mm
Gross Moment of inertia of the deck (see adjcaent)	Ix	228227	**mm^4/m**
Connections			
Resistance of the frame connectors (see adjacent)	**Q_f**	**6.71**	**kN**
Flexibility of the frame connectors (see adjacent)	**S_f**	**0.0413**	**mm/kN**
Resistance of the sidelap connectors (see adjacent)	**Q_s**	**3.23**	**kN**
Flexibilty of the sidelap connectors (see adjacent)	**S_s**	**0.099**	**mm/kN**
Valley spacing (each = 1, alternate = 2, third = 3, fourth = 4) (is every flute connected or not?) (see data sheet)	**n_pas**	**1**	
$S(x_e/w)$ on the end joists (over w, including the edge connectors) (see data sheet)	α_1	**2**	
$S(x_p/w)$ on the intermediate joists (over w, including the edge connectors) (see data sheet)	α_2	**2**	
$S(x_e/w)^2$ on the end joists (over w, including the edge connectors) (see data sheet)	**$\Sigma(x_e/w)^2$**	**0.778**	
$S(x_p/w)^2$ on the intermediate joists (over w, including the edge connectors) (see data sheet)	**$\Sigma(x_p/w)^2$**	**0.778**	
Number of end connectors (total over width w including those on the edge	**n_v**	**7**	
Number of frame connectors on the side of the deck (total over length LL excluding those on the joists)	**n_e**	**44**	
Number of sidelap connectors (total over length LL excluding those on the joists)	**n_s**	**44**	
Resistance			
Corner factor	λ	0.793	
Factor B	B	28.960	
Resistance based on the panel end	Sn	51.71	kN/m
Resistance based on the interior panel	Sn	27.34	kN/m
Resistance based on the corner connection	Sn	24.41	kN/m
Resistance based on the overall shear buckling of the deck (Lower bound 2 span case where coeff = 3.25)	S_{cr}	24.99	kN/m
Nominal shear resistance	**min S_n**	**24.41**	**kN/m**
See latest CSA S136 for phi factors			
Flexibility and Rigidity			
Flexibility due to the deformation of a flat steel sheet in shear	Fs	0.0230	mm/kN
Flexibility due to warping of the deck (parameter Dn)	Fn	0.0223	mm/kN
Flexibility due to deformation at the connections (parameter C)	Fslip	0.0136	mm/kN
Flexibility	**F**	0.0588	**mm/kN**
Rigidity	**G'**	16.993	**kN/mm**

Figure A.7 – Calculation of DIA3R and DIA4 strength for one panel length

Steel			
Steel thickness	**tt**	**0.76**	**mm**
Steel yield strength (for the calculation of Qf of screws according to the SDI method)	Fy	230	**MPa**
Steel ultimate tensile strength (for the calculation of Q_f of welds according to the SDI method)	Fu	310	**MPa**
Young's modulus	E	203000	**MPa**
Deck			
Depth of deck	hh	38	**mm**
Length of web (measured over the inclined distance)	ww	40.16	**mm**
Pitch (o/c spacing of flutes)	dd	152	**mm**
Half-length of the lower flange	ee	19.05	**mm**
Length of the upper flange	ff	88.9	**mm**
Horizontal projection of the web	gg	12.7	**mm**
Developed length of steel per flute	ss	207.32	mm
Overall deck width	w_f	914	**mm**
Overall deck length	**LL**	**21020**	**mm**
Number of intermediate joists	**np**	**11**	
Joist spacing (o/c)	Lv	1751.67	mm
Gross Moment of inertia of the deck (see adjcaent)	Ix	228227	**mm^4/m**
Connections			
Resistance of the frame connectors (see adjacent)	**Q_f**	**6.71**	**kN**
Flexibility of the frame connectors (see adjacent)	**S_f**	**0.0413**	**mm/kN**
Resistance of the sidelap connectors (see adjacent)	**Q_s**	**3.23**	**kN**
Flexibilty of the sidelap connectors (see adjacent)	**S_s**	**0.099**	**mm/kN**
Valley spacing (each = 1, alternate = 2, third = 3, fourth = 4) (is every flute connected or not?) (see data sheet)	**n_pas**	**1**	
$S(x_e/w)$ on the end joists (over w, including the edge connectors) (see data sheet)	α_1	**2**	
$S(x_p/w)$ on the intermediate joists (over w, including the edge connectors) (see data sheet)	α_2	**2**	
$S(x_e/w)^2$ on the end joists (over w, including the edge connectors) (see data sheet)	**$\Sigma(x_e/w)^2$**	**0.778**	
$S(x_p/w)^2$ on the intermediate joists (over w, including the edge connectors) (see data sheet)	**$\Sigma(x_p/w)^2$**	**0.778**	
Number of end connectors (total over width w including those on the edge	**n_v**	**7**	
Number of frame connectors on the side of the deck (total over length LL excluding those on the joists)	**n_e**	**132**	
Number of sidelap connectors (total over length LL excluding those on the joists)	**n_s**	**132**	
Resistance			
Corner factor	λ	0.793	
Factor B	B	83.769	
Resistance based on the panel end	Sn	50.44	kN/m
Resistance based on the interior panel	Sn	26.61	kN/m
Resistance based on the corner connection	Sn	23.72	kN/m
Resistance based on the overall shear buckling of the deck (Lower bound 2 span case where coeff = 3.25)	S_{cr}	24.99	kN/m
Nominal shear resistance	**min S_n**	**23.72**	**kN/m**
See latest CSA S136 for phi factors			
Flexibility and Rigidity			
Flexibility due to the deformation of a flat steel sheet in shear	Fs	0.0230	mm/kN
Flexibility due to warping of the deck (parameter Dn)	Fn	0.0031	mm/kN
Flexibility due to deformation at the connections (parameter C)	Fslip	0.0140	mm/kN
Flexibility	**F**	0.0400	**mm/kN**
Rigidity	**G'**	24.990	**kN/mm**

Figure A.8 – Calculation of DIA3R and DIA4 strength for three panel length

Steel			
Steel thickness	**tt**	**0.76**	**mm**
Steel yield strength (for the calculation of Qf of screws according to the SDI method)	Fy	230	**MPa**
Steel ultimate tensile strength (for the calculation of Q_f of welds according to the SDI method)	Fu	310	**MPa**
Young's modulus	E	203000	**MPa**
Deck			
Depth of deck	hh	38	**mm**
Length of web (measured over the inclined distance)	ww	40.16	**mm**
Pitch (o/c spacing of flutes)	dd	152	**mm**
Half-length of the lower flange	ee	19.05	**mm**
Length of the upper flange	ff	88.9	**mm**
Horizontal projection of the web	gg	12.7	**mm**
Developed length of steel per flute	ss	207.32	mm
Overall deck width	w_f	914	**mm**
Overall deck length	**LL**	**7006.67**	**mm**
Number of intermediate joists	**np**	**3**	
Joist spacing (o/c)	Lv	1751.67	mm
Gross Moment of inertia of the deck (see adjcaent)	Ix	228227	**mm^4/m**
Connections			
Resistance of the frame connectors (see adjacent)	**Q_f**	**6.71**	**kN**
Flexibility of the frame connectors (see adjacent)	**S_f**	**0.0413**	**mm/kN**
Resistance of the sidelap connectors (see adjacent)	**Q_s**	**3.23**	**kN**
Flexibilty of the sidelap connectors (see adjacent)	**S_s**	**0.099**	**mm/kN**
Valley spacing (each = 1, alternate = 2, third = 3, fourth = 4) (is every flute connected or not?) (see data sheet)	**n_pas**	**1**	
$S(x_e/w)$ on the end joists (over w, including the edge connectors) (see data sheet)	α_1	**3**	
$S(x_p/w)$ on the intermediate joists (over w, including the edge connectors) (see data sheet)	α_2	**3**	
$S(x_e/w)^2$ on the end joists (over w, including the edge connectors) (see data sheet)	**$\Sigma(x_e/w)^2$**	**1.278**	
$S(x_p/w)^2$ on the intermediate joists (over w, including the edge connectors) (see data sheet)	**$\Sigma(x_p/w)^2$**	**1.278**	
Number of end connectors (total over width w including those on the edge	**n_v**	**9**	
Number of frame connectors on the side of the deck (total over length LL excluding those on the joists)	**n_e**	**44**	
Number of sidelap connectors (total over length LL excluding those on the joists)	**n_s**	**44**	
Resistance			
Corner factor	λ	0.793	
Factor B	B	33.960	
Resistance based on the panel end	Sn	56.50	kN/m
Resistance based on the interior panel	Sn	32.13	kN/m
Resistance based on the corner connection	Sn	29.18	kN/m
Resistance based on the overall shear buckling of the deck (Lower bound 2 span case where coeff = 3.25)	S_{cr}	24.99	kN/m
Nominal shear resistance	**min S_n**	**24.99**	**kN/m**
See latest CSA S136 for phi factors			
Flexibility and Rigidity			
Flexibility due to the deformation of a flat steel sheet in shear	Fs	0.0230	mm/kN
Flexibility due to warping of the deck (parameter Dn)	Fn	0.0223	mm/kN
Flexibility due to deformation at the connections (parameter C)	Fslip	0.0122	mm/kN
Flexibility	**F**	0.0575	**mm/kN**
Rigidity	**G'**	17.380	**kN/mm**

Figure A.9 – Calculation of DIA4R and DIA5 strength for one panel length

Steel			
Steel thickness	**tt**	**0.76**	**mm**
Steel yield strength (for the calculation of Qf of screws according to the SDI method)	Fy	230	**MPa**
Steel ultimate tensile strength (for the calculation of Q_f of welds according to the SDI method)	Fu	310	**MPa**
Young's modulus	E	203000	**MPa**
Deck			
Depth of deck	hh	38	**mm**
Length of web (measured over the inclined distance)	ww	40.16	**mm**
Pitch (o/c spacing of flutes)	dd	152	**mm**
Half-length of the lower flange	ee	19.05	**mm**
Length of the upper flange	ff	88.9	**mm**
Horizontal projection of the web	gg	12.7	**mm**
Developed length of steel per flute	ss	207.32	mm
Overall deck width	w_f	914	**mm**
Overall deck length	**LL**	**21020**	**mm**
Number of intermediate joists	**np**	**11**	
Joist spacing (o/c)	Lv	1751.67	mm
Gross Moment of inertia of the deck (see adjcaent)	Ix	228227	**mm^4/m**
Connections			
Resistance of the frame connectors (see adjacent)	**Q_f**	**6.71**	**kN**
Flexibility of the frame connectors (see adjacent)	**S_f**	**0.0413**	**mm/kN**
Resistance of the sidelap connectors (see adjacent)	**Q_s**	**3.23**	**kN**
Flexibilty of the sidelap connectors (see adjacent)	**S_s**	**0.099**	**mm/kN**
Valley spacing (each = 1, alternate = 2, third = 3, fourth = 4) (is every flute connected or not?) (see data sheet)	**n_pas**	**1**	
$S(x_e/w)$ on the end joists (over w, including the edge connectors) (see data sheet)	α_1	**3**	
$S(x_p/w)$ on the intermediate joists (over w, including the edge connectors) (see data sheet)	α_2	**3**	
$S(x_e/w)^2$ on the end joists (over w, including the edge connectors) (see data sheet)	$\Sigma(x_e/w)^2$	**1.278**	
$S(x_p/w)^2$ on the intermediate joists (over w, including the edge connectors) (see data sheet)	$\Sigma(x_p/w)^2$	**1.278**	
Number of end connectors (total over width w including those on the edge	**n_v**	**9**	
Number of frame connectors on the side of the deck (total over length LL excluding those on the joists)	**n_e**	**132**	
Number of sidelap connectors (total over length LL excluding those on the joists)	**n_s**	**132**	
Resistance			
Corner factor	λ	0.793	
Factor B	B	96.769	
Resistance based on the panel end	Sn	54.59	kN/m
Resistance based on the interior panel	Sn	30.76	kN/m
Resistance based on the corner connection	Sn	27.98	kN/m
Resistance based on the overall shear buckling of the deck (Lower bound 2 span case where coeff = 3.25)	S_{cr}	24.99	kN/m
Nominal shear resistance	**min S_n**	**24.99**	**kN/m**
See latest CSA S136 for phi factors			
Flexibility and Rigidity			
Flexibility due to the deformation of a flat steel sheet in shear	Fs	0.0230	mm/kN
Flexibility due to warping of the deck (parameter Dn)	Fn	0.0031	mm/kN
Flexibility due to deformation at the connections (parameter C)	Fslip	0.0127	mm/kN
Flexibility	**F**	0.0388	**mm/kN**
Rigidity	**G'**	25.774	**kN/mm**

Figure A.10 – Calculation of DIA4R and DIA5 strength for three panel length

Steel			
Steel thickness	**tt**	**0.76**	**mm**
Steel yield strength (for the calculation of Qf of screws according to the SDI method)	Fy	230	**MPa**
Steel ultimate tensile strength (for the calculation of Q_f of welds according to the SDI method)	Fu	310	**MPa**
Young's modulus	E	203000	**MPa**
Deck			
Depth of deck	hh	38	**mm**
Length of web (measured over the inclined distance)	ww	40.16	**mm**
Pitch (o/c spacing of flutes)	dd	152	**mm**
Half-length of the lower flange	ee	19.05	**mm**
Length of the upper flange	ff	88.9	**mm**
Horizontal projection of the web	gg	12.7	**mm**
Developed length of steel per flute	ss	207.32	mm
Overall deck width	w_f	914	**mm**
Overall deck length	**LL**	**7006.67**	**mm**
Number of intermediate joists	**np**	**3**	
Joist spacing (o/c)	Lv	1751.67	mm
Gross Moment of inertia of the deck (see adjcaent)	Ix	228227	**mm^4/m**
Connections			
Resistance of the frame connectors (see adjacent)	**Q_f**	**6.71**	**kN**
Flexibility of the frame connectors (see adjacent)	**S_f**	**0.0413**	**mm/kN**
Resistance of the sidelap connectors (see adjacent)	**Q_s**	**3.23**	**kN**
Flexibilty of the sidelap connectors (see adjacent)	**S_s**	**0.099**	**mm/kN**
Valley spacing (each = 1, alternate = 2, third = 3, fourth = 4) (is every flute connected or not?) (see data sheet)	**n_pas**	**1**	
$S(x_e/w)$ on the end joists (over w, including the edge connectors) (see data sheet)	α_1	**3**	
$S(x_p/w)$ on the intermediate joists (over w, including the edge connectors) (see data sheet)	α_2	**3**	
$S(x_e/w)^2$ on the end joists (over w, including the edge connectors) (see data sheet)	**$\Sigma(x_e/w)^2$**	**1.278**	
$S(x_p/w)^2$ on the intermediate joists (over w, including the edge connectors) (see data sheet)	**$\Sigma(x_p/w)^2$**	**1.278**	
Number of end connectors (total over width w including those on the edge	**n_v**	**9**	
Number of frame connectors on the side of the deck (total over length LL excluding those on the joists)	**n_e**	**64**	
Number of sidelap connectors (total over length LL excluding those on the joists)	**n_s**	**64**	
Resistance			
Corner factor	λ	0.793	
Factor B	B	43.588	
Resistance based on the panel end	Sn	75.66	kN/m
Resistance based on the interior panel	Sn	41.35	kN/m
Resistance based on the corner connection	Sn	35.29	kN/m
Resistance based on the overall shear buckling of the deck (Lower bound 2 span case where coeff = 3.25)	S_{cr}	24.99	kN/m
Nominal shear resistance	**min S_n**	**24.99**	**kN/m**
See latest CSA S136 for phi factors			
Flexibility and Rigidity			
Flexibility due to the deformation of a flat steel sheet in shear	Fs	0.0230	mm/kN
Flexibility due to warping of the deck (parameter Dn)	Fn	0.0223	mm/kN
Flexibility due to deformation at the connections (parameter C)	Fslip	0.0093	mm/kN
Flexibility	**F**	0.0545	**mm/kN**
Rigidity	**G'**	18.332	**kN/mm**

Figure A.11 – Calculation of DIA5R strength for one panel length

Steel			
Steel thickness	**tt**	**0.76**	**mm**
Steel yield strength (for the calculation of Qf of screws according to the SDI method)	Fy	230	**MPa**
Steel ultimate tensile strength (for the calculation of Q_f of welds according to the SDI method)	Fu	310	**MPa**
Young's modulus	E	203000	**MPa**
Deck			
Depth of deck	hh	38	**mm**
Length of web (measured over the inclined distance)	ww	40.16	**mm**
Pitch (o/c spacing of flutes)	dd	152	**mm**
Half-length of the lower flange	ee	19.05	**mm**
Length of the upper flange	ff	88.9	**mm**
Horizontal projection of the web	gg	12.7	**mm**
Developed length of steel per flute	ss	207.32	mm
Overall deck width	w_f	914	**mm**
Overall deck length	**LL**	**21020**	**mm**
Number of intermediate joists	**np**	**11**	
Joist spacing (o/c)	Lv	1751.67	mm
Gross Moment of inertia of the deck (see adjcaent)	Ix	228227	**mm^4/m**
Connections			
Resistance of the frame connectors (see adjacent)	**Q_f**	**6.71**	**kN**
Flexibility of the frame connectors (see adjacent)	**S_f**	**0.0413**	**mm/kN**
Resistance of the sidelap connectors (see adjacent)	**Q_s**	**3.23**	**kN**
Flexibilty of the sidelap connectors (see adjacent)	**S_s**	**0.099**	**mm/kN**
Valley spacing (each = 1, alternate = 2, third = 3, fourth = 4) (is every flute connected or not?) (see data sheet)	**n_pas**	**1**	
$S(x_e/w)$ on the end joists (over w, including the edge connectors) (see data sheet)	α_1	**3**	
$S(x_p/w)$ on the intermediate joists (over w, including the edge connectors) (see data sheet)	α_2	**3**	
$S(x_e/w)^2$ on the end joists (over w, including the edge connectors) (see data sheet)	$\Sigma(x_e/w)^2$	**1.278**	
$S(x_p/w)^2$ on the intermediate joists (over w, including the edge connectors) (see data sheet)	$\Sigma(x_p/w)^2$	**1.278**	
Number of end connectors (total over width w including those on the edge	**n_v**	**9**	
Number of frame connectors on the side of the deck (total over length LL excluding those on the joists)	**n_e**	**192**	
Number of sidelap connectors (total over length LL excluding those on the joists)	**n_s**	**192**	
Resistance			
Corner factor	λ	0.793	
Factor B	B	125.651	
Resistance based on the panel end	Sn	73.74	kN/m
Resistance based on the interior panel	Sn	39.98	kN/m
Resistance based on the corner connection	Sn	34.29	kN/m
Resistance based on the overall shear buckling of the deck (Lower bound 2 span case where coeff = 3.25)	S_{cr}	24.99	kN/m
Nominal shear resistance	**min S_n**	**24.99**	**kN/m**
See latest CSA S136 for phi factors			
Flexibility and Rigidity			
Flexibility due to the deformation of a flat steel sheet in shear	Fs	0.0230	mm/kN
Flexibility due to warping of the deck (parameter Dn)	Fn	0.0031	mm/kN
Flexibility due to deformation at the connections (parameter C)	Fslip	0.0095	mm/kN
Flexibility	**F**	0.0356	**mm/kN**
Rigidity	**G'**	28.092	**kN/mm**

Figure A.12 – Calculation of DIA5R strength for three panel length

Steel			
Steel thickness	**tt**	**0.76**	**mm**
Steel yield strength (for the calculation of Qf of screws according to the SDI method)	Fy	230	**MPa**
Steel ultimate tensile strength (for the calculation of Q_f of welds according to the SDI method)	Fu	310	**MPa**
Young's modulus	E	203000	**MPa**
Deck			
Depth of deck	hh	38	**mm**
Length of web (measured over the inclined distance)	ww	40.16	**mm**
Pitch (o/c spacing of flutes)	dd	152	**mm**
Half-length of the lower flange	ee	19.05	**mm**
Length of the upper flange	ff	88.9	**mm**
Horizontal projection of the web	gg	12.7	**mm**
Developed length of steel per flute	ss	207.32	mm
Overall deck width	w_f	914	**mm**
Overall deck length	**LL**	**7006.67**	**mm**
Number of intermediate joists	**np**	**3**	
Joist spacing (o/c)	Lv	1751.67	mm
Gross Moment of inertia of the deck (see adjcaent)	Ix	228227	**mm^4/m**
Connections			
Resistance of the frame connectors (see adjacent)	**Q_f**	**6.71**	**kN**
Flexibility of the frame connectors (see adjacent)	**S_f**	**0.0413**	**mm/kN**
Resistance of the sidelap connectors (see adjacent)	**Q_s**	**3.23**	**kN**
Flexibilty of the sidelap connectors (see adjacent)	**S_s**	**0.099**	**mm/kN**
Valley spacing (each = 1, alternate = 2, third = 3, fourth = 4) (is every flute connected or not?) (see data sheet)	**n_pas**	**1**	
$S(x_e/w)$ on the end joists (over w, including the edge connectors) (see data sheet)	α_1	**3.667**	
$S(x_p/w)$ on the intermediate joists (over w, including the edge connectors) (see data sheet)	α_2	**3.667**	
$S(x_e/w)^2$ on the end joists (over w, including the edge connectors) (see data sheet)	**$\Sigma(x_e/w)^2$**	**1.5**	
$S(x_p/w)^2$ on the intermediate joists (over w, including the edge connectors) (see data sheet)	**$\Sigma(x_p/w)^2$**	**1.5**	
Number of end connectors (total over width w including those on the edge	**n_v**	**11**	
Number of frame connectors on the side of the deck (total over length LL excluding those on the joists)	**n_e**	**44**	
Number of sidelap connectors (total over length LL excluding those on the joists)	**n_s**	**44**	
Resistance			
Corner factor	λ	0.793	
Factor B	B	36.180	
Resistance based on the panel end	Sn	59.70	kN/m
Resistance based on the interior panel	Sn	34.25	kN/m
Resistance based on the corner connection	Sn	31.84	kN/m
Resistance based on the overall shear buckling of the deck (Lower bound 2 span case where coeff = 3.25)	S_{cr}	24.99	kN/m
Nominal shear resistance	**min S_n**	**24.99**	**kN/m**
See latest CSA S136 for phi factors			
Flexibility and Rigidity			
Flexibility due to the deformation of a flat steel sheet in shear	Fs	0.0230	mm/kN
Flexibility due to warping of the deck (parameter Dn)	Fn	0.0223	mm/kN
Flexibility due to deformation at the connections (parameter C)	Fslip	0.0115	mm/kN
Flexibility	**F**	0.0568	**mm/kN**
Rigidity	**G'**	17.607	**kN/mm**

Figure A.13 – Calculation of DIA6 strength for one panel length

Steel			
Steel thickness	**tt**	**0.76**	**mm**
Steel yield strength (for the calculation of Qf of screws according to the SDI method)	Fy	230	**MPa**
Steel ultimate tensile strength (for the calculation of Q_f of welds according to the SDI method)	Fu	310	**MPa**
Young's modulus	E	203000	**MPa**
Deck			
Depth of deck	hh	38	**mm**
Length of web (measured over the inclined distance)	ww	40.16	**mm**
Pitch (o/c spacing of flutes)	dd	152	**mm**
Half-length of the lower flange	ee	19.05	**mm**
Length of the upper flange	ff	88.9	**mm**
Horizontal projection of the web	gg	12.7	**mm**
Developed length of steel per flute	ss	207.32	mm
Overall deck width	w_f	914	**mm**
Overall deck length	**LL**	**21020**	**mm**
Number of intermediate joists	**np**	**11**	
Joist spacing (o/c)	Lv	1751.67	mm
Gross Moment of inertia of the deck (see adjcaent)	Ix	228227	**mm^4/m**
Connections			
Resistance of the frame connectors (see adjacent)	**Q_f**	**6.71**	**kN**
Flexibility of the frame connectors (see adjacent)	**S_f**	**0.0413**	**mm/kN**
Resistance of the sidelap connectors (see adjacent)	**Q_s**	**3.23**	**kN**
Flexibilty of the sidelap connectors (see adjacent)	**S_s**	**0.099**	**mm/kN**
Valley spacing (each = 1, alternate = 2, third = 3, fourth = 4) (is every flute connected or not?) (see data sheet)	**n_pas**	**1**	
$S(x_e/w)$ on the end joists (over w, including the edge connectors) (see data sheet)	α_1	**3.667**	
$S(x_p/w)$ on the intermediate joists (over w, including the edge connectors) (see data sheet)	α_2	**3.667**	
$S(x_e/w)^2$ on the end joists (over w, including the edge connectors) (see data sheet)	**$\Sigma(x_e/w)^2$**	**1.5**	
$S(x_p/w)^2$ on the intermediate joists (over w, including the edge connectors) (see data sheet)	**$\Sigma(x_p/w)^2$**	**1.5**	
Number of end connectors (total over width w including those on the edge	**n_v**	**11**	
Number of frame connectors on the side of the deck (total over length LL excluding those on the joists)	**n_e**	**132**	
Number of sidelap connectors (total over length LL excluding those on the joists)	**n_s**	**132**	
Resistance			
Corner factor	λ	0.793	
Factor B	B	102.541	
Resistance based on the panel end	Sn	57.35	kN/m
Resistance based on the interior panel	Sn	32.60	kN/m
Resistance based on the corner connection	Sn	30.34	kN/m
Resistance based on the overall shear buckling of the deck (Lower bound 2 span case where coeff = 3.25)	S_{cr}	24.99	kN/m
Nominal shear resistance	**min S_n**	**24.99**	**kN/m**
See latest CSA S136 for phi factors			
Flexibility and Rigidity			
Flexibility due to the deformation of a flat steel sheet in shear	Fs	0.0230	mm/kN
Flexibility due to warping of the deck (parameter Dn)	Fn	0.0031	mm/kN
Flexibility due to deformation at the connections (parameter C)	Fslip	0.0120	mm/kN
Flexibility	**F**	0.0381	**mm/kN**
Rigidity	**G'**	26.247	**kN/mm**

Figure A.14 – Calculation of DIA6 strength for three panel length

Steel			
Steel thickness	**tt**	**0.76**	**mm**
Steel yield strength (for the calculation of Qf of screws according to the SDI method)	Fy	230	**MPa**
Steel ultimate tensile strength (for the calculation of Q_f of welds according to the SDI method)	Fu	310	**MPa**
Young's modulus	E	203000	**MPa**
Deck			
Depth of deck	hh	38	**mm**
Length of web (measured over the inclined distance)	ww	40.16	**mm**
Pitch (o/c spacing of flutes)	dd	152	**mm**
Half-length of the lower flange	ee	19.05	**mm**
Length of the upper flange	ff	88.9	**mm**
Horizontal projection of the web	gg	12.7	**mm**
Developed length of steel per flute	ss	207.32	mm
Overall deck width	w_f	914	**mm**
Overall deck length	**LL**	**7006.67**	**mm**
Number of intermediate joists	**np**	**3**	
Joist spacing (o/c)	Lv	1751.67	mm
Gross Moment of inertia of the deck (see adjcaent)	Ix	228227	**mm^4/m**
Connections			
Resistance of the frame connectors (see adjacent)	**Q_f**	**6.71**	**kN**
Flexibility of the frame connectors (see adjacent)	**S_f**	**0.0413**	**mm/kN**
Resistance of the sidelap connectors (see adjacent)	**Q_s**	**3.23**	**kN**
Flexibilty of the sidelap connectors (see adjacent)	**S_s**	**0.099**	**mm/kN**
Valley spacing (each = 1, alternate = 2, third = 3, fourth = 4) (is every flute connected or not?) (see data sheet)	**n_pas**	**1**	
$S(x_e/w)$ on the end joists (over w, including the edge connectors) (see data sheet)	α_1	**3.667**	
$S(x_p/w)$ on the intermediate joists (over w, including the edge connectors) (see data sheet)	α_2	**3.667**	
$S(x_e/w)^2$ on the end joists (over w, including the edge connectors) (see data sheet)	**$\Sigma(x_e/w)^2$**	**1.5**	
$S(x_p/w)^2$ on the intermediate joists (over w, including the edge connectors) (see data sheet)	**$\Sigma(x_p/w)^2$**	**1.5**	
Number of end connectors (total over width w including those on the edge	**n_v**	**11**	
Number of frame connectors on the side of the deck (total over length LL excluding those on the joists)	**n_e**	**64**	
Number of sidelap connectors (total over length LL excluding those on the joists)	**n_s**	**64**	
Resistance			
Corner factor	λ	0.793	
Factor B	B	45.808	
Resistance based on the panel end	Sn	78.85	kN/m
Resistance based on the interior panel	Sn	43.47	kN/m
Resistance based on the corner connection	Sn	38.55	kN/m
Resistance based on the overall shear buckling of the deck (Lower bound 2 span case where coeff = 3.25)	S_{cr}	24.99	kN/m
Nominal shear resistance	**min S_n**	**24.99**	**kN/m**
See latest CSA S136 for phi factors			
Flexibility and Rigidity			
Flexibility due to the deformation of a flat steel sheet in shear	Fs	0.0230	mm/kN
Flexibility due to warping of the deck (parameter Dn)	Fn	0.0223	mm/kN
Flexibility due to deformation at the connections (parameter C)	Fslip	0.0088	mm/kN
Flexibility	**F**	0.0541	**mm/kN**
Rigidity	**G'**	18.478	**kN/mm**

Figure A.15 – Calculation of DIA6R strength for one panel length

Steel			
Steel thickness	**tt**	**0.76**	**mm**
Steel yield strength (for the calculation of Qf of screws according to the SDI method)	Fy	230	**MPa**
Steel ultimate tensile strength (for the calculation of Q_f of welds according to the SDI method)	Fu	310	**MPa**
Young's modulus	E	203000	**MPa**
Deck			
Depth of deck	hh	38	**mm**
Length of web (measured over the inclined distance)	ww	40.16	**mm**
Pitch (o/c spacing of flutes)	dd	152	**mm**
Half-length of the lower flange	ee	19.05	**mm**
Length of the upper flange	ff	88.9	**mm**
Horizontal projection of the web	gg	12.7	**mm**
Developed length of steel per flute	ss	207.32	mm
Overall deck width	w_f	914	**mm**
Overall deck length	**LL**	**21020**	**mm**
Number of intermediate joists	**np**	**11**	
Joist spacing (o/c)	Lv	1751.6667	mm
Gross Moment of inertia of the deck (see adjcaent)	Ix	228227	**mm^4/m**
Connections			
Resistance of the frame connectors (see adjacent)	**Q_f**	**6.71**	**kN**
Flexibility of the frame connectors (see adjacent)	**S_f**	**0.0413**	**mm/kN**
Resistance of the sidelap connectors (see adjacent)	**Q_s**	**3.23**	**kN**
Flexibilty of the sidelap connectors (see adjacent)	**S_s**	**0.099**	**mm/kN**
Valley spacing (each = 1, alternate = 2, third = 3, fourth = 4) (is every flute connected or not?) (see data sheet)	**n_pas**	**1**	
$S(x_e/w)$ on the end joists (over w, including the edge connectors) (see data sheet)	α_1	**3.667**	
$S(x_p/w)$ on the intermediate joists (over w, including the edge connectors) (see data sheet)	α_2	**3.667**	
$S(x_e/w)^2$ on the end joists (over w, including the edge connectors) (see data sheet)	**$\Sigma(x_e/w)^2$**	**1.5**	
$S(x_p/w)^2$ on the intermediate joists (over w, including the edge connectors) (see data sheet)	**$\Sigma(x_p/w)^2$**	**1.5**	
Number of end connectors (total over width w including those on the edge	**n_v**	**11**	
Number of frame connectors on the side of the deck (total over length LL excluding those on the joists)	**n_e**	**192**	
Number of sidelap connectors (total over length LL excluding those on the joists)	**n_s**	**192**	
Resistance			
Corner factor	λ	0.793	
Factor B	B	131.423	
Resistance based on the panel end	Sn	76.51	kN/m
Resistance based on the interior panel	Sn	41.82	kN/m
Resistance based on the corner connection	Sn	37.23	kN/m
Resistance based on the overall shear buckling of the deck (Lower bound 2 span case where coeff = 3.25)	S_{cr}	24.99	kN/m
Nominal shear resistance	**min S_n**	**24.99**	**kN/m**
See latest CSA S136 for phi factors			
Flexibility and Rigidity			
Flexibility due to the deformation of a flat steel sheet in shear	Fs	0.0230	mm/kN
Flexibility due to warping of the deck (parameter Dn)	Fn	0.0031	mm/kN
Flexibility due to deformation at the connections (parameter C)	Fslip	0.0091	mm/kN
Flexibility	**F**	0.0352	**mm/kN**
Rigidity	**G'**	28.409	**kN/mm**

Figure A.16 – Calculation of DIA6R strength for three panel length

Steel			
Steel thickness	**tt**	**0.91**	**mm**
Steel yield strength (for the calculation of Qf of screws according to the SDI method)	Fy	230	**MPa**
Steel ultimate tensile strength (for the calculation of Q_f of welds according to the SDI method)	Fu	310	**MPa**
Young's modulus	E	203000	**MPa**
Deck			
Depth of deck	hh	38	**mm**
Length of web (measured over the inclined distance)	ww	40.16	**mm**
Pitch (o/c spacing of flutes)	dd	152	**mm**
Half-length of the lower flange	ee	19.05	**mm**
Length of the upper flange	ff	88.9	**mm**
Horizontal projection of the web	gg	12.7	**mm**
Developed length of steel per flute	ss	207.32	mm
Overall deck width	w_f	914	**mm**
Overall deck length	**LL**	**7006.67**	**mm**
Number of intermediate joists	**np**	**3**	
Joist spacing (o/c)	Lv	1751.67	mm
Gross Moment of inertia of the deck (see adjcaent)	**Ix**	**272365**	**mm^4/m**
Connections			
Resistance of the frame connectors (see adjacent)	**Q_f**	**7.99**	**kN**
Flexibility of the frame connectors (see adjacent)	**S_f**	**0.0377**	**mm/kN**
Resistance of the sidelap connectors (see adjacent)	**Q_s**	**3.87**	**kN**
Flexibilty of the sidelap connectors (see adjacent)	**S_s**	**0.0905**	**mm/kN**
Valley spacing (each = 1, alternate = 2, third = 3, fourth = 4) (is every flute connected or not?) (see data sheet)	**n_pas**	**1**	
$S(x_e/w)$ on the end joists (over w, including the edge connectors) (see data sheet)	α_1	**2**	
$S(x_p/w)$ on the intermediate joists (over w, including the edge connectors) (see data sheet)	α_2	**2**	
$S(x_e/w)^2$ on the end joists (over w, including the edge connectors) (see data sheet)	**$\Sigma(x_e/w)^2$**	**0.778**	
$S(x_p/w)^2$ on the intermediate joists (over w, including the edge connectors) (see data sheet)	**$\Sigma(x_p/w)^2$**	**0.778**	
Number of end connectors (total over width w including those on the edge	**n_v**	**7**	
Number of frame connectors on the side of the deck (total over length LL excluding those on the joists)	**n_e**	**44**	
Number of sidelap connectors (total over length LL excluding those on the joists)	**n_s**	**44**	
Resistance			
Corner factor	λ	0.811	
Factor B	B	29.092	
Resistance based on the panel end	Sn	61.58	kN/m
Resistance based on the interior panel	Sn	32.74	kN/m
Resistance based on the corner connection	Sn	29.16	kN/m
Resistance based on the overall shear buckling of the deck (Lower bound 2 span case where coeff = 3.25)	S_{cr}	32.66	kN/m
Nominal shear resistance	**min S_n**	**29.16**	**kN/m**
See latest CSA S136 for phi factors			
Flexibility and Rigidity			
Flexibility due to the deformation of a flat steel sheet in shear	Fs	0.0192	mm/kN
Flexibility due to warping of the deck (parameter Dn)	Fn	0.0142	mm/kN
Flexibility due to deformation at the connections (parameter C)	Fslip	0.0124	mm/kN
Flexibility	**F**	0.0458	**mm/kN**
Rigidity	**G'**	21.832	**kN/mm**

Figure A.17 – Calculation of DIA7 strength for one panel length

Steel			
Steel thickness	**tt**	**0.91**	**mm**
Steel yield strength (for the calculation of Qf of screws according to the SDI method)	Fy	230	**MPa**
Steel ultimate tensile strength (for the calculation of Q_f of welds according to the SDI method)	Fu	310	**MPa**
Young's modulus	E	203000	**MPa**
Deck			
Depth of deck	hh	38	**mm**
Length of web (measured over the inclined distance)	ww	40.16	**mm**
Pitch (o/c spacing of flutes)	dd	152	**mm**
Half-length of the lower flange	ee	19.05	**mm**
Length of the upper flange	ff	88.9	**mm**
Horizontal projection of the web	gg	12.7	**mm**
Developed length of steel per flute	ss	207.32	mm
Overall deck width	w_f	914	**mm**
Overall deck length	**LL**	**21020**	**mm**
Number of intermediate joists	**np**	**11**	
Joist spacing (o/c)	Lv	1751.67	mm
Gross Moment of inertia of the deck (see adjcaent)	**Ix**	**272365**	**mm^4/m**
Connections			
Resistance of the frame connectors (see adjacent)	**Q_f**	**7.99**	**kN**
Flexibility of the frame connectors (see adjacent)	**S_f**	**0.0377**	**mm/kN**
Resistance of the sidelap connectors (see adjacent)	**Q_s**	**3.87**	**kN**
Flexibilty of the sidelap connectors (see adjacent)	**S_s**	**0.0905**	**mm/kN**
Valley spacing (each = 1, alternate = 2, third = 3, fourth = 4) (is every flute connected or not?) (see data sheet)	**n_pas**	**1**	
$S(x_e/w)$ on the end joists (over w, including the edge connectors) (see data sheet)	α_1	**2**	
$S(x_p/w)$ on the intermediate joists (over w, including the edge connectors) (see data sheet)	α_2	**2**	
$S(x_e/w)^2$ on the end joists (over w, including the edge connectors) (see data sheet)	**$\Sigma(x_e/w)^2$**	**0.778**	
$S(x_p/w)^2$ on the intermediate joists (over w, including the edge connectors) (see data sheet)	**$\Sigma(x_p/w)^2$**	**0.778**	
Number of end connectors (total over width w including those on the edge	**n_v**	**7**	
Number of frame connectors on the side of the deck (total over length LL excluding those on the joists)	**n_e**	**132**	
Number of sidelap connectors (total over length LL excluding those on the joists)	**n_s**	**132**	
Resistance			
Corner factor	λ	0.811	
Factor B	B	84.163	
Resistance based on the panel end	Sn	60.06	kN/m
Resistance based on the interior panel	Sn	31.85	kN/m
Resistance based on the corner connection	Sn	28.35	kN/m
Resistance based on the overall shear buckling of the deck (Lower bound 2 span case where coeff = 3.25)	S_{cr}	32.66	kN/m
Nominal shear resistance	**min S_n**	**28.35**	**kN/m**
See latest CSA S136 for phi factors			
Flexibility and Rigidity			
Flexibility due to the deformation of a flat steel sheet in shear	Fs	0.0192	mm/kN
Flexibility due to warping of the deck (parameter Dn)	Fn	0.0020	mm/kN
Flexibility due to deformation at the connections (parameter C)	Fslip	0.0128	mm/kN
Flexibility	**F**	0.0339	**mm/kN**
Rigidity	**G'**	29.490	**kN/mm**

Figure A.18 – Calculation of DIA7 strength for three panel length

Steel			
Steel thickness	**tt**	**0.91**	**mm**
Steel yield strength (for the calculation of Qf of screws according to the SDI method)	Fy	230	**MPa**
Steel ultimate tensile strength (for the calculation of Q_f of welds according to the SDI method)	Fu	310	**MPa**
Young's modulus	E	203000	**MPa**
Deck			
Depth of deck	hh	38	**mm**
Length of web (measured over the inclined distance)	ww	40.16	**mm**
Pitch (o/c spacing of flutes)	dd	152	**mm**
Half-length of the lower flange	ee	19.05	**mm**
Length of the upper flange	ff	88.9	**mm**
Horizontal projection of the web	gg	12.7	**mm**
Developed length of steel per flute	ss	207.32	mm
Overall deck width	w_f	914	**mm**
Overall deck length	**LL**	**7006.67**	**mm**
Number of intermediate joists	**np**	**3**	
Joist spacing (o/c)	Lv	1751.67	mm
Gross Moment of inertia of the deck (see adjcaent)	**Ix**	**272365**	**mm^4/m**
Connections			
Resistance of the frame connectors (see adjacent)	$\mathbf{Q_f}$	**7.99**	**kN**
Flexibility of the frame connectors (see adjacent)	$\mathbf{S_f}$	**0.0377**	**mm/kN**
Resistance of the sidelap connectors (see adjacent)	$\mathbf{Q_s}$	**3.87**	**kN**
Flexibilty of the sidelap connectors (see adjacent)	$\mathbf{S_s}$	**0.0905**	**mm/kN**
Valley spacing (each = 1, alternate = 2, third = 3, fourth = 4) (is every flute connected or not?) (see data sheet)	**n_pas**	**1**	
$S(x_e/w)$ on the end joists (over w, including the edge connectors) (see data sheet)	α_1	**3**	
$S(x_p/w)$ on the intermediate joists (over w, including the edge connectors) (see data sheet)	α_2	**3**	
$S(x_e/w)^2$ on the end joists (over w, including the edge connectors) (see data sheet)	$\Sigma(\mathbf{x_e/w})^2$	**1.278**	
$S(x_p/w)^2$ on the intermediate joists (over w, including the edge connectors) (see data sheet)	$\Sigma(\mathbf{x_p/w})^2$	**1.278**	
Number of end connectors (total over width w including those on the edge	$\mathbf{n_v}$	**9**	
Number of frame connectors on the side of the deck (total over length LL excluding those on the joists)	$\mathbf{n_e}$	**44**	
Number of sidelap connectors (total over length LL excluding those on the joists)	$\mathbf{n_s}$	**44**	
Resistance			
Corner factor	λ	0.811	
Factor B	B	34.092	
Resistance based on the panel end	Sn	67.28	kN/m
Resistance based on the interior panel	Sn	38.44	kN/m
Resistance based on the corner connection	Sn	34.85	kN/m
Resistance based on the overall shear buckling of the deck (Lower bound 2 span case where coeff = 3.25)	S_{cr}	32.66	kN/m
Nominal shear resistance	**min $\mathbf{S_n}$**	**32.66**	**kN/m**
See latest CSA S136 for phi factors			
Flexibility and Rigidity			
Flexibility due to the deformation of a flat steel sheet in shear	Fs	0.0192	mm/kN
Flexibility due to warping of the deck (parameter Dn)	Fn	0.0142	mm/kN
Flexibility due to deformation at the connections (parameter C)	Fslip	0.0112	mm/kN
Flexibility	**F**	0.0446	**mm/kN**
Rigidity	**G'**	22.419	**kN/mm**

Figure A.19 – Calculation of DIA8 strength for one panel length

Steel			
Steel thickness	**tt**	**0.91**	**mm**
Steel yield strength (for the calculation of Qf of screws according to the SDI method)	Fy	230	**MPa**
Steel ultimate tensile strength (for the calculation of Q_f of welds according to the SDI method)	Fu	310	**MPa**
Young's modulus	E	203000	**MPa**
Deck			
Depth of deck	hh	38	**mm**
Length of web (measured over the inclined distance)	ww	40.16	**mm**
Pitch (o/c spacing of flutes)	dd	152	**mm**
Half-length of the lower flange	ee	19.05	**mm**
Length of the upper flange	ff	88.9	**mm**
Horizontal projection of the web	gg	12.7	**mm**
Developed length of steel per flute	ss	207.32	mm
Overall deck width	w_f	914	**mm**
Overall deck length	**LL**	**21020**	**mm**
Number of intermediate joists	**np**	**11**	
Joist spacing (o/c)	Lv	1751.67	mm
Gross Moment of inertia of the deck (see adjcaent)	**Ix**	**272365**	**mm^4/m**
Connections			
Resistance of the frame connectors (see adjacent)	Q_f	**7.99**	**kN**
Flexibility of the frame connectors (see adjacent)	S_f	**0.0377**	**mm/kN**
Resistance of the sidelap connectors (see adjacent)	Q_s	**3.87**	**kN**
Flexibilty of the sidelap connectors (see adjacent)	S_s	**0.0905**	**mm/kN**
Valley spacing (each = 1, alternate = 2, third = 3, fourth = 4) (is every flute connected or not?) (see data sheet)	**n_pas**	**1**	
$S(x_e/w)$ on the end joists (over w, including the edge connectors) (see data sheet)	α_1	**3**	
$S(x_p/w)$ on the intermediate joists (over w, including the edge connectors) (see data sheet)	α_2	**3**	
$S(x_e/w)^2$ on the end joists (over w, including the edge connectors) (see data sheet)	$\Sigma(x_e/w)^2$	**1.278**	
$S(x_p/w)^2$ on the intermediate joists (over w, including the edge connectors) (see data sheet)	$\Sigma(x_p/w)^2$	**1.278**	
Number of end connectors (total over width w including those on the edge	n_v	**9**	
Number of frame connectors on the side of the deck (total over length LL excluding those on the joists)	n_e	**132**	
Number of sidelap connectors (total over length LL excluding those on the joists)	n_s	**132**	
Resistance			
Corner factor	λ	0.811	
Factor B	B	97.163	
Resistance based on the panel end	Sn	65.00	kN/m
Resistance based on the interior panel	Sn	36.79	kN/m
Resistance based on the corner connection	Sn	33.43	kN/m
Resistance based on the overall shear buckling of the deck (Lower bound 2 span case where coeff = 3.25)	S_{cr}	32.66	kN/m
Nominal shear resistance	**min S_n**	**32.66**	**kN/m**
See latest CSA S136 for phi factors			
Flexibility and Rigidity			
Flexibility due to the deformation of a flat steel sheet in shear	Fs	0.0192	mm/kN
Flexibility due to warping of the deck (parameter Dn)	Fn	0.0020	mm/kN
Flexibility due to deformation at the connections (parameter C)	Fslip	0.0116	mm/kN
Flexibility	**F**	0.0328	**mm/kN**
Rigidity	**G'**	30.491	**kN/mm**

Figure A.20 – Calculation of DIA8 strength for three panel length

Steel			
Steel thickness	**tt**	**0.91**	**mm**
Steel yield strength (for the calculation of Qf of screws according to the SDI method)	Fy	230	**MPa**
Steel ultimate tensile strength (for the calculation of Q_f of welds according to the SDI method)	Fu	310	**MPa**
Young's modulus	E	203000	**MPa**
Deck			
Depth of deck	hh	38	**mm**
Length of web (measured over the inclined distance)	ww	40.16	**mm**
Pitch (o/c spacing of flutes)	dd	152	**mm**
Half-length of the lower flange	ee	19.05	**mm**
Length of the upper flange	ff	88.9	**mm**
Horizontal projection of the web	gg	12.7	**mm**
Developed length of steel per flute	ss	207.32	mm
Overall deck width	w_f	914	**mm**
Overall deck length	**LL**	**7006.67**	**mm**
Number of intermediate joists	**np**	**3**	
Joist spacing (o/c)	Lv	1751.67	mm
Gross Moment of inertia of the deck (see adjcaent)	**Ix**	**272365**	**mm^4/m**
Connections			
Resistance of the frame connectors (see adjacent)	$\mathbf{Q_f}$	**7.99**	**kN**
Flexibility of the frame connectors (see adjacent)	$\mathbf{S_f}$	**0.0377**	**mm/kN**
Resistance of the sidelap connectors (see adjacent)	$\mathbf{Q_s}$	**3.87**	**kN**
Flexibilty of the sidelap connectors (see adjacent)	$\mathbf{S_s}$	**0.0905**	**mm/kN**
Valley spacing (each = 1, alternate = 2, third = 3, fourth = 4) (is every flute connected or not?) (see data sheet)	**n_pas**	**1**	
$S(x_e/w)$ on the end joists (over w, including the edge connectors) (see data sheet)	α_1	**3**	
$S(x_p/w)$ on the intermediate joists (over w, including the edge connectors) (see data sheet)	α_2	**3**	
$S(x_e/w)^2$ on the end joists (over w, including the edge connectors) (see data sheet)	$\mathbf{\Sigma(x_e/w)^2}$	**1.278**	
$S(x_p/w)^2$ on the intermediate joists (over w, including the edge connectors) (see data sheet)	$\mathbf{\Sigma(x_p/w)^2}$	**1.278**	
Number of end connectors (total over width w including those on the edge	$\mathbf{n_v}$	**9**	
Number of frame connectors on the side of the deck (total over length LL excluding those on the joists)	$\mathbf{n_e}$	**64**	
Number of sidelap connectors (total over length LL excluding those on the joists)	$\mathbf{n_s}$	**64**	
Resistance			
Corner factor	λ	0.811	
Factor B	B	43.779	
Resistance based on the panel end	Sn	90.09	kN/m
Resistance based on the interior panel	Sn	49.49	kN/m
Resistance based on the corner connection	Sn	42.15	kN/m
Resistance based on the overall shear buckling of the deck (Lower bound 2 span case where coeff = 3.25)	S_{cr}	32.66	kN/m
Nominal shear resistance	**min $\mathbf{S_n}$**	**32.66**	**kN/m**
See latest CSA S136 for phi factors			
Flexibility and Rigidity			
Flexibility due to the deformation of a flat steel sheet in shear	Fs	0.0192	mm/kN
Flexibility due to warping of the deck (parameter Dn)	Fn	0.0142	mm/kN
Flexibility due to deformation at the connections (parameter C)	Fslip	0.0085	mm/kN
Flexibility	**F**	0.0419	**mm/kN**
Rigidity	**G'**	23.880	**kN/mm**

Figure A.21 – Calculation of DIA8R strength for one panel length

Steel			
Steel thickness	**tt**	**0.91**	**mm**
Steel yield strength (for the calculation of Qf of screws according to the SDI method)	Fy	230	**MPa**
Steel ultimate tensile strength (for the calculation of Q_f of welds according to the SDI method)	Fu	310	**MPa**
Young's modulus	E	203000	**MPa**
Deck			
Depth of deck	hh	38	**mm**
Length of web (measured over the inclined distance)	ww	40.16	**mm**
Pitch (o/c spacing of flutes)	dd	152	**mm**
Half-length of the lower flange	ee	19.05	**mm**
Length of the upper flange	ff	88.9	**mm**
Horizontal projection of the web	gg	12.7	**mm**
Developed length of steel per flute	ss	207.32	mm
Overall deck width	w_f	914	**mm**
Overall deck length	**LL**	**21020**	**mm**
Number of intermediate joists	**np**	**11**	
Joist spacing (o/c)	Lv	1751.6667	mm
Gross Moment of inertia of the deck (see adjcaent)	**Ix**	**258000**	**mm^4/m**
Connections			
Resistance of the frame connectors (see adjacent)	**Q_f**	**7.99**	**kN**
Flexibility of the frame connectors (see adjacent)	**S_f**	**0.0377**	**mm/kN**
Resistance of the sidelap connectors (see adjacent)	**Q_s**	**3.87**	**kN**
Flexibilty of the sidelap connectors (see adjacent)	**S_s**	**0.0905**	**mm/kN**
Valley spacing (each = 1, alternate = 2, third = 3, fourth = 4) (is every flute connected or not?) (see data sheet)	**n_pas**	**1**	
$S(x_e/w)$ on the end joists (over w, including the edge connectors) (see data sheet)	α_1	**3**	
$S(x_p/w)$ on the intermediate joists (over w, including the edge connectors) (see data sheet)	α_2	**3**	
$S(x_e/w)^2$ on the end joists (over w, including the edge connectors) (see data sheet)	**$\Sigma(x_e/w)^2$**	**1.278**	
$S(x_p/w)^2$ on the intermediate joists (over w, including the edge connectors) (see data sheet)	**$\Sigma(x_p/w)^2$**	**1.278**	
Number of end connectors (total over width w including those on the edge	**n_v**	**9**	
Number of frame connectors on the side of the deck (total over length LL excluding those on the joists)	**n_e**	**192**	
Number of sidelap connectors (total over length LL excluding those on the joists)	**n_s**	**192**	
Resistance			
Corner factor	λ	0.811	
Factor B	B	126.224	
Resistance based on the panel end	Sn	87.81	kN/m
Resistance based on the interior panel	Sn	47.84	kN/m
Resistance based on the corner connection	Sn	40.96	kN/m
Resistance based on the overall shear buckling of the deck (Lower bound 2 span case where coeff = 3.25)	S_{cr}	31.36	kN/m
Nominal shear resistance	**min S_n**	**31.36**	**kN/m**
See latest CSA S136 for phi factors			
Flexibility and Rigidity			
Flexibility due to the deformation of a flat steel sheet in shear	Fs	0.0192	mm/kN
Flexibility due to warping of the deck (parameter Dn)	Fn	0.0020	mm/kN
Flexibility due to deformation at the connections (parameter C)	Fslip	0.0087	mm/kN
Flexibility	**F**	0.0299	**mm/kN**
Rigidity	**G'**	33.475	**kN/mm**

Figure A.22 – Calculation of DIA8R strength for three panel length

Steel			
Steel thickness	**tt**	**0.91**	**mm**
Steel yield strength (for the calculation of Qf of screws according to the SDI method)	Fy	230	**MPa**
Steel ultimate tensile strength (for the calculation of Q_f of welds according to the SDI method)	Fu	310	**MPa**
Young's modulus	E	203000	**MPa**
Deck			
Depth of deck	hh	38	**mm**
Length of web (measured over the inclined distance)	ww	40.16	**mm**
Pitch (o/c spacing of flutes)	dd	152	**mm**
Half-length of the lower flange	ee	19.05	**mm**
Length of the upper flange	ff	88.9	**mm**
Horizontal projection of the web	gg	12.7	**mm**
Developed length of steel per flute	ss	207.32	mm
Overall deck width	w_f	914	**mm**
Overall deck length	**LL**	**7006.67**	**mm**
Number of intermediate joists	**np**	**3**	
Joist spacing (o/c)	Lv	1751.67	mm
Gross Moment of inertia of the deck (see adjcaent)	**Ix**	**272365**	**mm^4/m**
Connections			
Resistance of the frame connectors (see adjacent)	**Q_f**	**7.99**	**kN**
Flexibility of the frame connectors (see adjacent)	**S_f**	**0.0377**	**mm/kN**
Resistance of the sidelap connectors (see adjacent)	**Q_s**	**3.87**	**kN**
Flexibilty of the sidelap connectors (see adjacent)	**S_s**	**0.0905**	**mm/kN**
Valley spacing (each = 1, alternate = 2, third = 3, fourth = 4) (is every flute connected or not?) (see data sheet)	**n_pas**	**1**	
$S(x_e/w)$ on the end joists (over w, including the edge connectors) (see data sheet)	α_1	**3.667**	
$S(x_p/w)$ on the intermediate joists (over w, including the edge connectors) (see data sheet)	α_2	**3.667**	
$S(x_e/w)^2$ on the end joists (over w, including the edge connectors) (see data sheet)	**$\Sigma(x_e/w)^2$**	**1.5**	
$S(x_p/w)^2$ on the intermediate joists (over w, including the edge connectors) (see data sheet)	**$\Sigma(x_p/w)^2$**	**1.5**	
Number of end connectors (total over width w including those on the edge	**n_v**	**11**	
Number of frame connectors on the side of the deck (total over length LL excluding those on the joists)	**n_e**	**44**	
Number of sidelap connectors (total over length LL excluding those on the joists)	**n_s**	**44**	
Resistance			
Corner factor	λ	0.811	
Factor B	B	36.312	
Resistance based on the panel end	Sn	71.08	kN/m
Resistance based on the interior panel	Sn	40.98	kN/m
Resistance based on the corner connection	Sn	38.03	kN/m
Resistance based on the overall shear buckling of the deck (Lower bound 2 span case where coeff = 3.25)	S_{cr}	32.66	kN/m
Nominal shear resistance	**min S_n**	**32.66**	**kN/m**
See latest CSA S136 for phi factors			
Flexibility and Rigidity			
Flexibility due to the deformation of a flat steel sheet in shear	Fs	0.0192	mm/kN
Flexibility due to warping of the deck (parameter Dn)	Fn	0.0142	mm/kN
Flexibility due to deformation at the connections (parameter C)	Fslip	0.0105	mm/kN
Flexibility	**F**	0.0439	**mm/kN**
Rigidity	**G'**	22.766	**kN/mm**

Figure A.23 – Calculation of DIA9 strength for one panel length

Steel			
Steel thickness	**tt**	**0.91**	**mm**
Steel yield strength (for the calculation of Qf of screws according to the SDI method)	Fy	230	**MPa**
Steel ultimate tensile strength (for the calculation of Q_f of welds according to the SDI method)	Fu	310	**MPa**
Young's modulus	E	203000	**MPa**
Deck			
Depth of deck	hh	38	**mm**
Length of web (measured over the inclined distance)	ww	40.16	**mm**
Pitch (o/c spacing of flutes)	dd	152	**mm**
Half-length of the lower flange	ee	19.05	**mm**
Length of the upper flange	ff	88.9	**mm**
Horizontal projection of the web	gg	12.7	**mm**
Developed length of steel per flute	ss	207.32	mm
Overall deck width	w_f	914	**mm**
Overall deck length	**LL**	**21020**	**mm**
Number of intermediate joists	**np**	**11**	
Joist spacing (o/c)	Lv	1751.67	mm
Gross Moment of inertia of the deck (see adjcaent)	**Ix**	**272365**	**mm^4/m**
Connections			
Resistance of the frame connectors (see adjacent)	**Q_f**	**7.99**	**kN**
Flexibility of the frame connectors (see adjacent)	**S_f**	**0.0377**	**mm/kN**
Resistance of the sidelap connectors (see adjacent)	**Q_s**	**3.87**	**kN**
Flexibilty of the sidelap connectors (see adjacent)	**S_s**	**0.0905**	**mm/kN**
Valley spacing (each = 1, alternate = 2, third = 3, fourth = 4) (is every flute connected or not?) (see data sheet)	**n_pas**	**1**	
$S(x_e/w)$ on the end joists (over w, including the edge connectors) (see data sheet)	α_1	**3.667**	
$S(x_p/w)$ on the intermediate joists (over w, including the edge connectors) (see data sheet)	α_2	**3.667**	
$S(x_e/w)^2$ on the end joists (over w, including the edge connectors) (see data sheet)	**$\Sigma(x_e/w)^2$**	**1.5**	
$S(x_p/w)^2$ on the intermediate joists (over w, including the edge connectors) (see data sheet)	**$\Sigma(x_p/w)^2$**	**1.5**	
Number of end connectors (total over width w including those on the edge	**n_v**	**11**	
Number of frame connectors on the side of the deck (total over length LL excluding those on the joists)	**n_e**	**132**	
Number of sidelap connectors (total over length LL excluding those on the joists)	**n_s**	**132**	
Resistance			
Corner factor	λ	0.811	
Factor B	B	102.935	
Resistance based on the panel end	Sn	68.30	kN/m
Resistance based on the interior panel	Sn	38.98	kN/m
Resistance based on the corner connection	Sn	36.24	kN/m
Resistance based on the overall shear buckling of the deck (Lower bound 2 span case where coeff = 3.25)	S_{cr}	32.66	kN/m
Nominal shear resistance	**min S_n**	**32.66**	**kN/m**
See latest CSA S136 for phi factors			
Flexibility and Rigidity			
Flexibility due to the deformation of a flat steel sheet in shear	Fs	0.0192	mm/kN
Flexibility due to warping of the deck (parameter Dn)	Fn	0.0020	mm/kN
Flexibility due to deformation at the connections (parameter C)	Fslip	0.0110	mm/kN
Flexibillty	**F**	0.0322	**mm/kN**
Rigidity	**G'**	31.098	**kN/mm**

Figure A.24 – Calculation of DIA9 strength for three panel length

Steel			
Steel thickness	**tt**	**0.91**	**mm**
Steel yield strength (for the calculation of Qf of screws according to the SDI method)	Fy	230	**MPa**
Steel ultimate tensile strength (for the calculation of Q_f of welds according to the SDI method)	Fu	310	**MPa**
Young's modulus	E	203000	**MPa**
Deck			
Depth of deck	hh	38	**mm**
Length of web (measured over the inclined distance)	ww	40.16	**mm**
Pitch (o/c spacing of flutes)	dd	152	**mm**
Half-length of the lower flange	ee	19.05	**mm**
Length of the upper flange	ff	88.9	**mm**
Horizontal projection of the web	gg	12.7	**mm**
Developed length of steel per flute	ss	207.32	mm
Overall deck width	w_f	914	**mm**
Overall deck length	**LL**	**7006.67**	**mm**
Number of intermediate joists	**np**	**3**	
Joist spacing (o/c)	Lv	1751.67	mm
Gross Moment of inertia of the deck (see adjcaent)	**Ix**	**272365**	**mm^4/m**
Connections			
Resistance of the frame connectors (see adjacent)	**Q_f**	**7.99**	**kN**
Flexibility of the frame connectors (see adjacent)	**S_f**	**0.0377**	**mm/kN**
Resistance of the sidelap connectors (see adjacent)	**Q_s**	**3.87**	**kN**
Flexibilty of the sidelap connectors (see adjacent)	**S_s**	**0.0905**	**mm/kN**
Valley spacing (each = 1, alternate = 2, third = 3, fourth = 4) (is every flute connected or not?) (see data sheet)	**n_pas**	**1**	
$S(x_e/w)$ on the end joists (over w, including the edge connectors) (see data sheet)	α_1	**3.667**	
$S(x_p/w)$ on the intermediate joists (over w, including the edge connectors) (see data sheet)	α_2	**3.667**	
$S(x_e/w)^2$ on the end joists (over w, including the edge connectors) (see data sheet)	**$\Sigma(x_e/w)^2$**	**1.5**	
$S(x_p/w)^2$ on the intermediate joists (over w, including the edge connectors) (see data sheet)	**$\Sigma(x_p/w)^2$**	**1.5**	
Number of end connectors (total over width w including those on the edge	**n_v**	**11**	
Number of frame connectors on the side of the deck (total over length LL excluding those on the joists)	**n_e**	**64**	
Number of sidelap connectors (total over length LL excluding those on the joists)	**n_s**	**64**	
Resistance			
Corner factor	λ	0.811	
Factor B	B	45.999	
Resistance based on the panel end	Sn	93.89	kN/m
Resistance based on the interior panel	Sn	52.02	kN/m
Resistance based on the corner connection	Sn	46.05	kN/m
Resistance based on the overall shear buckling of the deck (Lower bound 2 span case where coeff = 3.25)	S_{cr}	32.66	kN/m
Nominal shear resistance	**min S_n**	**32.66**	**kN/m**
See latest CSA S136 for phi factors			
Flexibility and Rigidity			
Flexibility due to the deformation of a flat steel sheet in shear	Fs	0.0192	mm/kN
Flexibility due to warping of the deck (parameter Dn)	Fn	0.0142	mm/kN
Flexibility due to deformation at the connections (parameter C)	Fslip	0.0081	mm/kN
Flexibillty	**F**	0.0415	**mm/kN**
Rigidity	**G'**	24.107	**kN/mm**

Figure A.25 – Calculation of DIA9R strength for one panel length

Steel			
Steel thickness	**tt**	**0.91**	**mm**
Steel yield strength (for the calculation of Qf of screws according to the SDI method)	Fy	230	**MPa**
Steel ultimate tensile strength (for the calculation of Q_f of welds according to the SDI method)	Fu	310	**MPa**
Young's modulus	E	203000	**MPa**
Deck			
Depth of deck	hh	38	**mm**
Length of web (measured over the inclined distance)	ww	40.16	**mm**
Pitch (o/c spacing of flutes)	dd	152	**mm**
Half-length of the lower flange	ee	19.05	**mm**
Length of the upper flange	ff	88.9	**mm**
Horizontal projection of the web	gg	12.7	**mm**
Developed length of steel per flute	ss	207.32	mm
Overall deck width	w_f	914	**mm**
Overall deck length	**LL**	**21020**	**mm**
Number of intermediate joists	**np**	**11**	
Joist spacing (o/c)	Lv	1751.67	mm
Gross Moment of inertia of the deck (see adjcaent)	**Ix**	**272365**	**mm^4/m**
Connections			
Resistance of the frame connectors (see adjacent)	**Q_f**	**7.99**	**kN**
Flexibility of the frame connectors (see adjacent)	**S_f**	**0.0377**	**mm/kN**
Resistance of the sidelap connectors (see adjacent)	**Q_s**	**3.87**	**kN**
Flexibilty of the sidelap connectors (see adjacent)	**S_s**	**0.0905**	**mm/kN**
Valley spacing (each = 1, alternate = 2, third = 3, fourth = 4) (is every flute connected or not?) (see data sheet)	**n_pas**	**1**	
$S(x_e/w)$ on the end joists (over w, including the edge connectors) (see data sheet)	α_1	**3.667**	
$S(x_p/w)$ on the intermediate joists (over w, including the edge connectors) (see data sheet)	α_2	**3.667**	
$S(x_e/w)^2$ on the end joists (over w, including the edge connectors) (see data sheet)	**$\Sigma(x_e/w)^2$**	**1.5**	
$S(x_p/w)^2$ on the intermediate joists (over w, including the edge connectors) (see data sheet)	**$\Sigma(x_p/w)^2$**	**1.5**	
Number of end connectors (total over width w including those on the edge	**n_v**	**11**	
Number of frame connectors on the side of the deck (total over length LL excluding those on the joists)	**n_e**	**192**	
Number of sidelap connectors (total over length LL excluding those on the joists)	**n_s**	**192**	
Resistance			
Corner factor	λ	0.811	
Factor B	B	131.996	
Resistance based on the panel end	Sn	91.10	kN/m
Resistance based on the interior panel	Sn	50.03	kN/m
Resistance based on the corner connection	Sn	44.48	kN/m
Resistance based on the overall shear buckling of the deck (Lower bound 2 span case where coeff = 3.25)	S_{cr}	32.66	kN/m
Nominal shear resistance	**min S_n**	**32.66**	**kN/m**
See latest CSA S136 for phi factors			
Flexibility and Rigidity			
Flexibility due to the deformation of a flat steel sheet in shear	Fs	0.0192	mm/kN
Flexibility due to warping of the deck (parameter Dn)	Fn	0.0020	mm/kN
Flexibility due to deformation at the connections (parameter C)	Fslip	0.0084	mm/kN
Flexibillty	**F**	0.0295	**mm/kN**
Rigidity	**G'**	33.888	**kN/mm**

Figure A.26 – Calculation of DIA9R strength for one panel length

Steel			
Steel thickness	**tt**	**0.76**	**mm**
Steel yield strength (for the calculation of Qf of screws according to the SDI method)	Fy	230	**MPa**
Steel ultimate tensile strength (for the calculation of Q_f of welds according to the SDI method)	Fu	310	**MPa**
Young's modulus	E	203000	**MPa**
Deck			
Depth of deck	hh	38	**mm**
Length of web (measured over the inclined distance)	ww	40.16	**mm**
Pitch (o/c spacing of flutes)	dd	152	**mm**
Half-length of the lower flange	ee	19.05	**mm**
Length of the upper flange	ff	88.9	**mm**
Horizontal projection of the web	gg	12.7	**mm**
Developed length of steel per flute	ss	207.32	mm
Overall deck width	w_f	914	**mm**
Overall deck length	**LL**	**7006.67**	**mm**
Number of intermediate joists	**np**	**3**	
Joist spacing (o/c)	Lv	1751.67	mm
Gross Moment of inertia of the deck (see adjcaent)	**Ix**	**228227**	**mm^4/m**
Connections			
Resistance of the frame connectors (see adjacent)	**Q_f**	**7.84**	**kN**
Flexibility of the frame connectors (see adjacent)	**S_f**	**0.038**	**mm/kN**
Resistance of the sidelap connectors (see adjacent)	**Q_s**	**0.96**	**kN**
Flexibilty of the sidelap connectors (see adjacent)	**S_s**	**0.9903**	**mm/kN**
Valley spacing (each = 1, alternate = 2, third = 3, fourth = 4) (is every flute connected or not?) (see data sheet)	**n_pas**	**2**	
$S(x_e/w)$ on the end joists (over w, including the edge connectors) (see data sheet)	α_1	**1.333**	
$S(x_p/w)$ on the intermediate joists (over w, including the edge connectors) (see data sheet)	α_2	**1.333**	
$S(x_e/w)^2$ on the end joists (over w, including the edge connectors) (see data sheet)	**$\Sigma(x_e/w)^2$**	**0.556**	
$S(x_p/w)^2$ on the intermediate joists (over w, including the edge connectors) (see data sheet)	**$\Sigma(x_p/w)^2$**	**0.556**	
Number of end connectors (total over width w including those on the edge	**n_v**	**4**	
Number of frame connectors on the side of the deck (total over length LL excluding those on the joists)	**n_e**	**20**	
Number of sidelap connectors (total over length LL excluding those on the joists)	**n_s**	**20**	
Resistance			
Corner factor	λ	0.793	
Factor B	B	8.009	
Resistance based on the panel end	Sn	29.84	kN/m
Resistance based on the interior panel	Sn	8.50	kN/m
Resistance based on the corner connection	Sn	8.67	kN/m
Resistance based on the overall shear buckling of the deck (Lower bound 2 span case where coeff = 3.25)	S_{cr}	24.99	kN/m
Nominal shear resistance	**min S_n**	**8.50**	**kN/m**
See latest CSA S136 for phi factors			
Flexibility and Rigidity			
Flexibility due to the deformation of a flat steel sheet in shear	Fs	0.0230	mm/kN
Flexibility due to warping of the deck (parameter Dn)	Fn	0.1876	mm/kN
Flexibility due to deformation at the connections (parameter C)	Fslip	0.0711	mm/kN
Flexibility	**F**	0.2816	**mm/kN**
Rigidity	**G'**	3.551	**kN/mm**

Figure A.27 – Calculation of DIA10 strength for one panel length

Steel			
Steel thickness	**tt**	**0.76**	**mm**
Steel yield strength (for the calculation of Qf of screws according to the SDI method)	Fy	230	**MPa**
Steel ultimate tensile strength (for the calculation of Q_f of welds according to the SDI method)	Fu	310	**MPa**
Young's modulus	E	203000	**MPa**
Deck			
Depth of deck	hh	38	**mm**
Length of web (measured over the inclined distance)	ww	40.16	**mm**
Pitch (o/c spacing of flutes)	dd	152	**mm**
Half-length of the lower flange	ee	19.05	**mm**
Length of the upper flange	ff	88.9	**mm**
Horizontal projection of the web	gg	12.7	**mm**
Developed length of steel per flute	ss	207.32	mm
Overall deck width	w_f	914	**mm**
Overall deck length	**LL**	**21020**	**mm**
Number of intermediate joists	**np**	**11**	
Joist spacing (o/c)	Lv	1751.67	mm
Gross Moment of inertia of the deck (see adjcaent)	**Ix**	**228227**	**mm^4/m**
Connections			
Resistance of the frame connectors (see adjacent)	**Q_f**	**7.84**	**kN**
Flexibility of the frame connectors (see adjacent)	**S_f**	**0.038**	**mm/kN**
Resistance of the sidelap connectors (see adjacent)	**Q_s**	**0.96**	**kN**
Flexibilty of the sidelap connectors (see adjacent)	**S_s**	**0.9903**	**mm/kN**
Valley spacing (each = 1, alternate = 2, third = 3, fourth = 4) (is every flute connected or not?) (see data sheet)	**n_pas**	**2**	
$S(x_e/w)$ on the end joists (over w, including the edge connectors) (see data sheet)	α_1	**1.333**	
$S(x_p/w)$ on the intermediate joists (over w, including the edge connectors) (see data sheet)	α_2	**1.333**	
$S(x_e/w)^2$ on the end joists (over w, including the edge connectors) (see data sheet)	**$\Sigma(x_e/w)^2$**	**0.556**	
$S(x_p/w)^2$ on the intermediate joists (over w, including the edge connectors) (see data sheet)	**$\Sigma(x_p/w)^2$**	**0.556**	
Number of end connectors (total over width w including those on the edge	**n_v**	**4**	
Number of frame connectors on the side of the deck (total over length LL excluding those on the joists)	**n_e**	**60**	
Number of sidelap connectors (total over length LL excluding those on the joists)	**n_s**	**60**	
Resistance			
Corner factor	λ	0.793	
Factor B	B	21.803	
Resistance based on the panel end	Sn	28.84	kN/m
Resistance based on the interior panel	Sn	7.98	kN/m
Resistance based on the corner connection	Sn	7.91	kN/m
Resistance based on the overall shear buckling of the deck (Lower bound 2 span case where coeff = 3.25)	S_{cr}	24.99	kN/m
Nominal shear resistance	**min S_n**	**7.91**	**kN/m**
See latest CSA S136 for phi factors			
Flexibility and Rigidity			
Flexibility due to the deformation of a flat steel sheet in shear	Fs	0.0230	mm/kN
Flexibility due to warping of the deck (parameter Dn)	Fn	0.0259	mm/kN
Flexibility due to deformation at the connections (parameter C)	Fslip	0.0797	mm/kN
Flexibility	**F**	0.1285	**mm/kN**
Rigidity	**G'**	7.780	**kN/mm**

Figure A.28 – Calculation of DIA10 strength for one panel length

APPENDIX B: PHASE I & II – FREQUENCY RESULTS FOR NEW DIAPHRAGMS

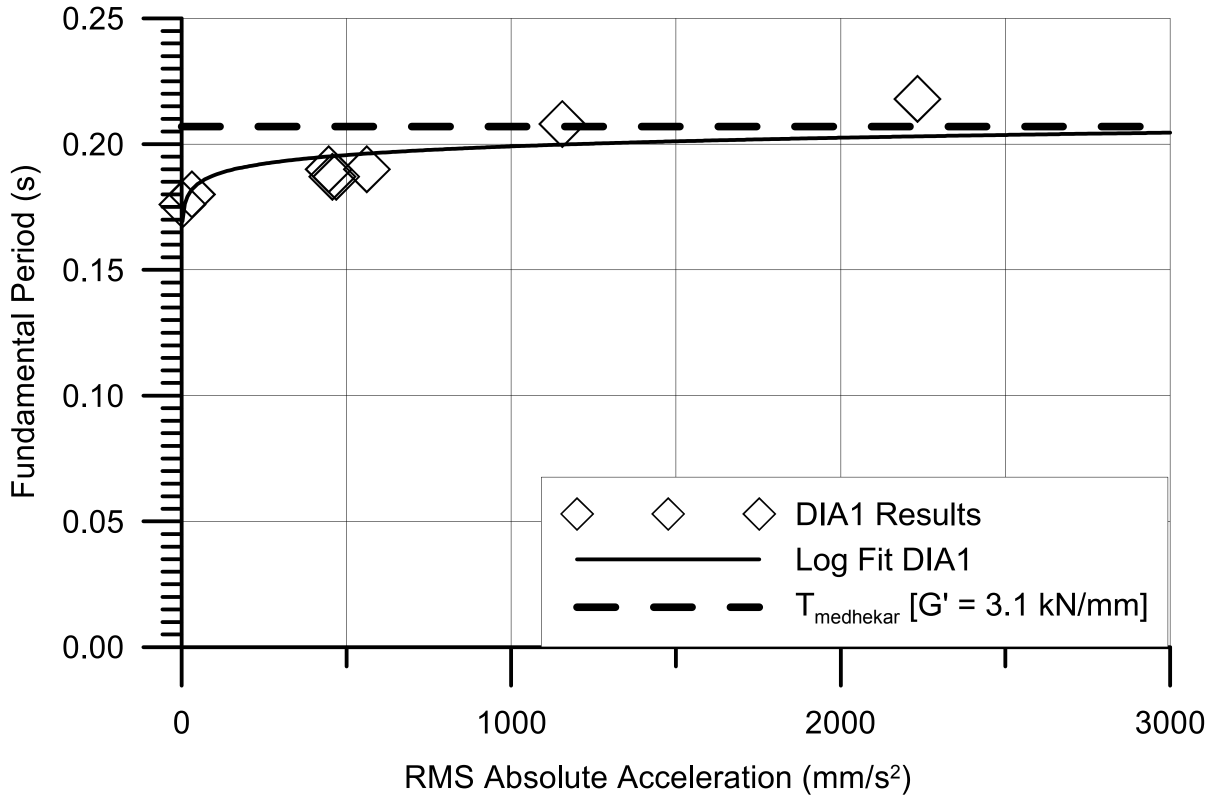

Figure B.1 – Fundamental period vs. RMS response acceleration for DIA1

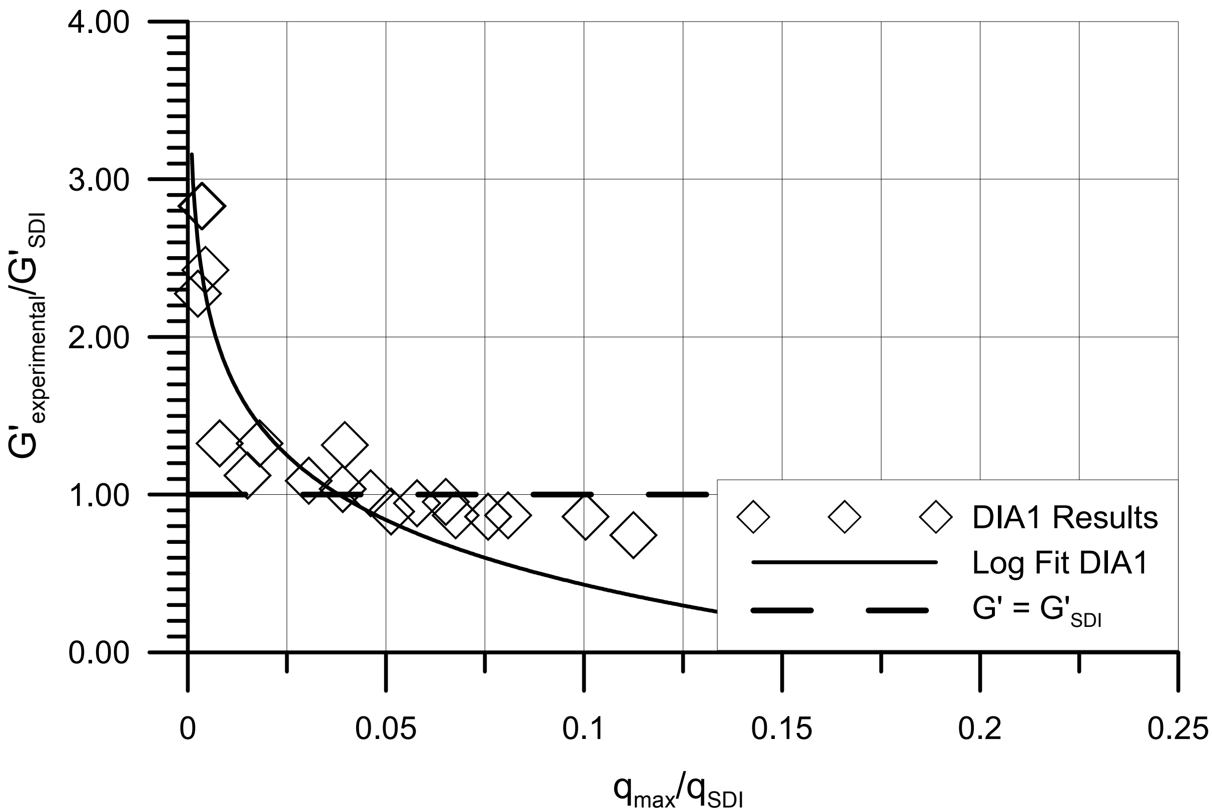

Figure B.2 – Comparison of experimental and theoretical strengths and stiffness's for DIA1

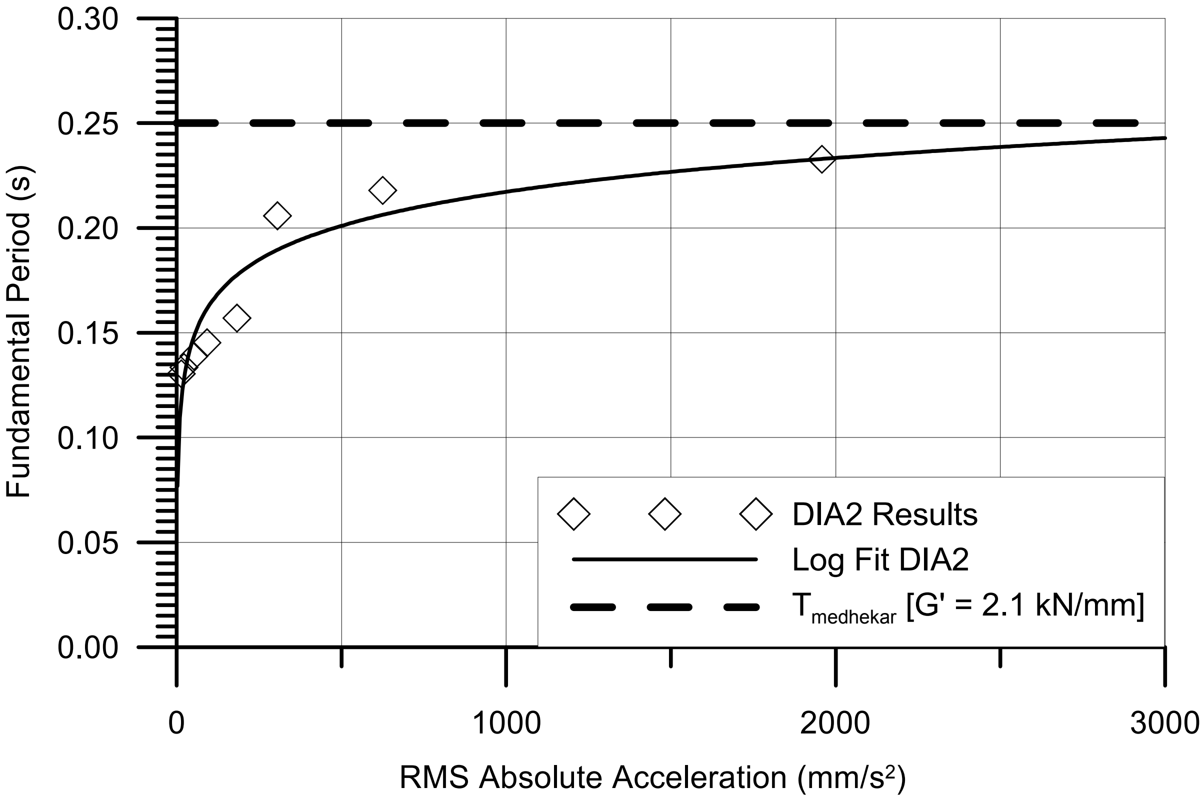

Figure B.3 – Fundamental period vs. RMS response acceleration for DIA2

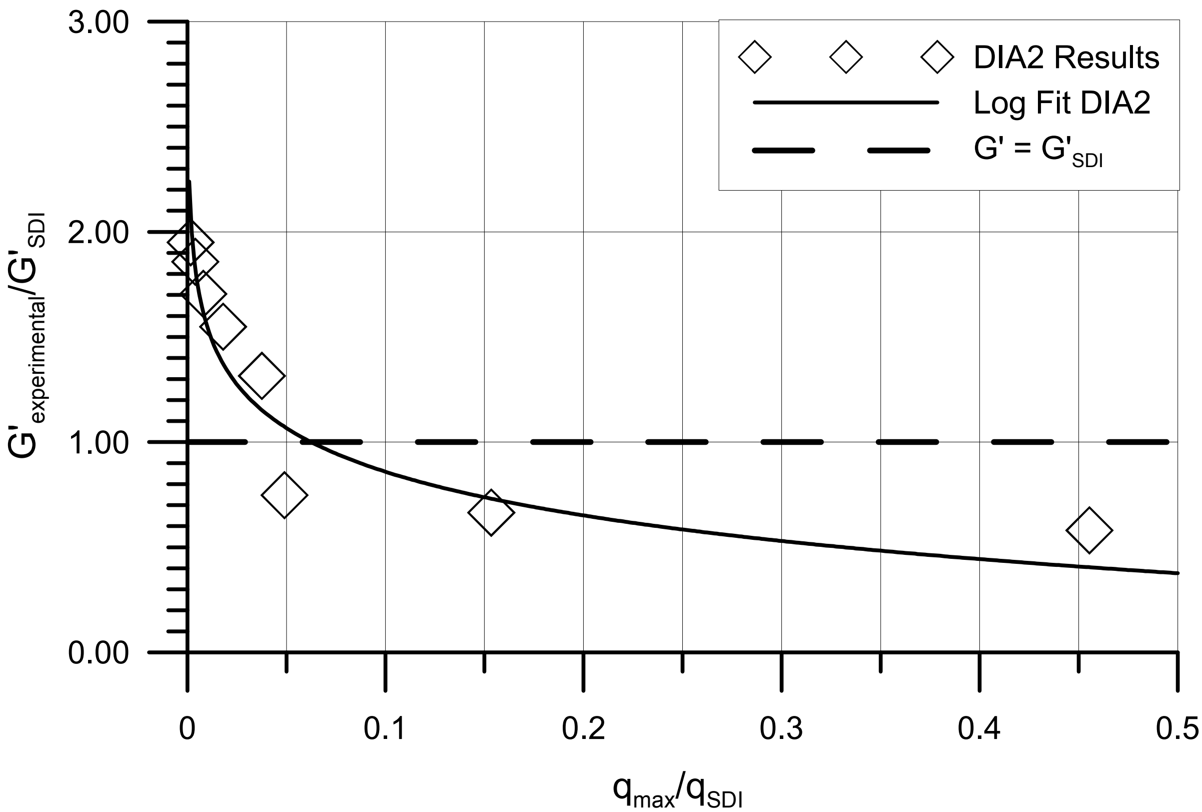

Figure B.4 – Comparison of experimental and theoretical strengths and stiffness's for DIA2

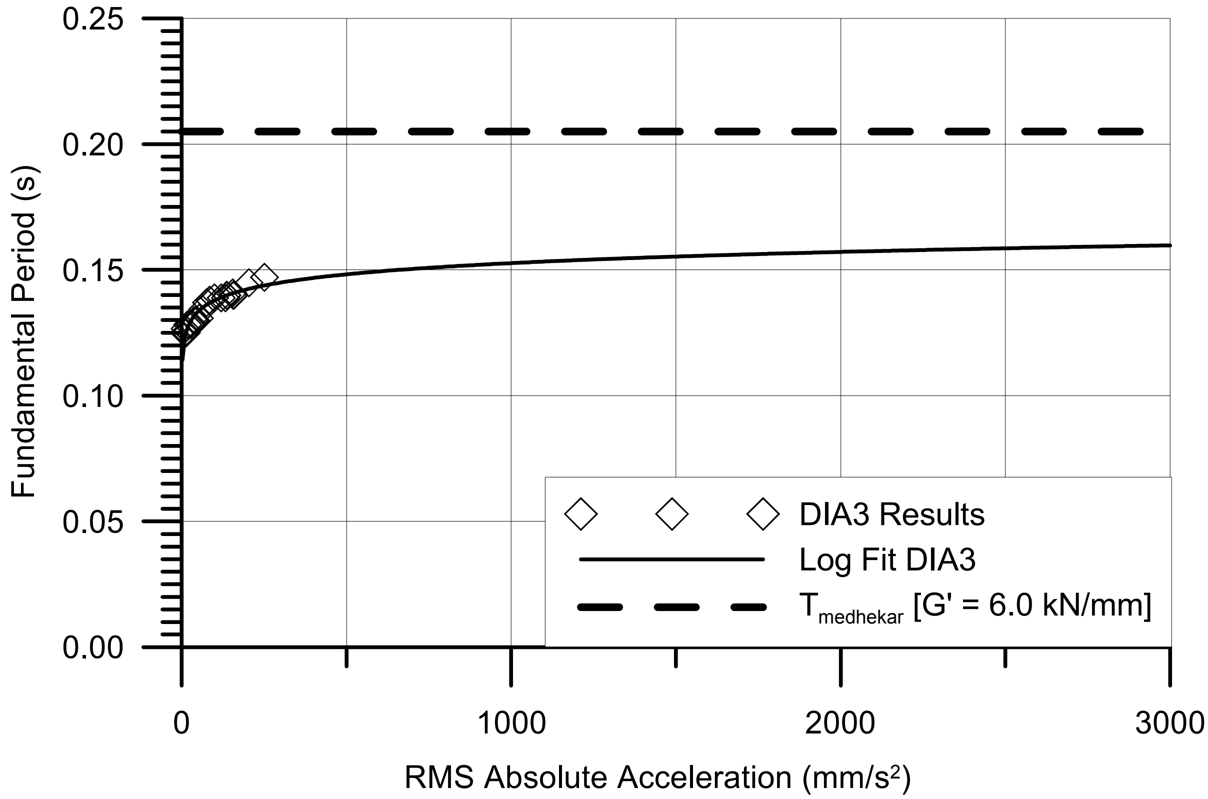

Figure B.5 – Fundamental period vs. RMS response acceleration for DIA3

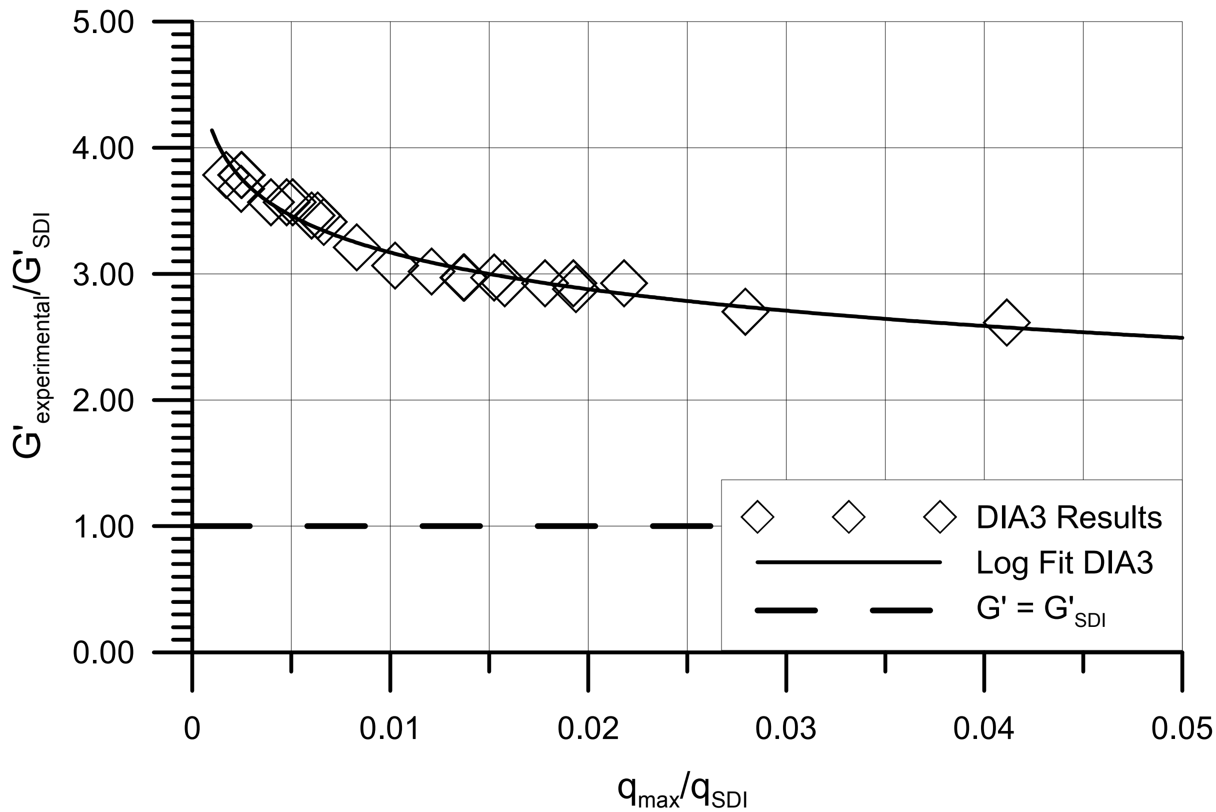

Figure B.6 – Comparison of experimental and theoretical strengths and stiffness's for DIA3

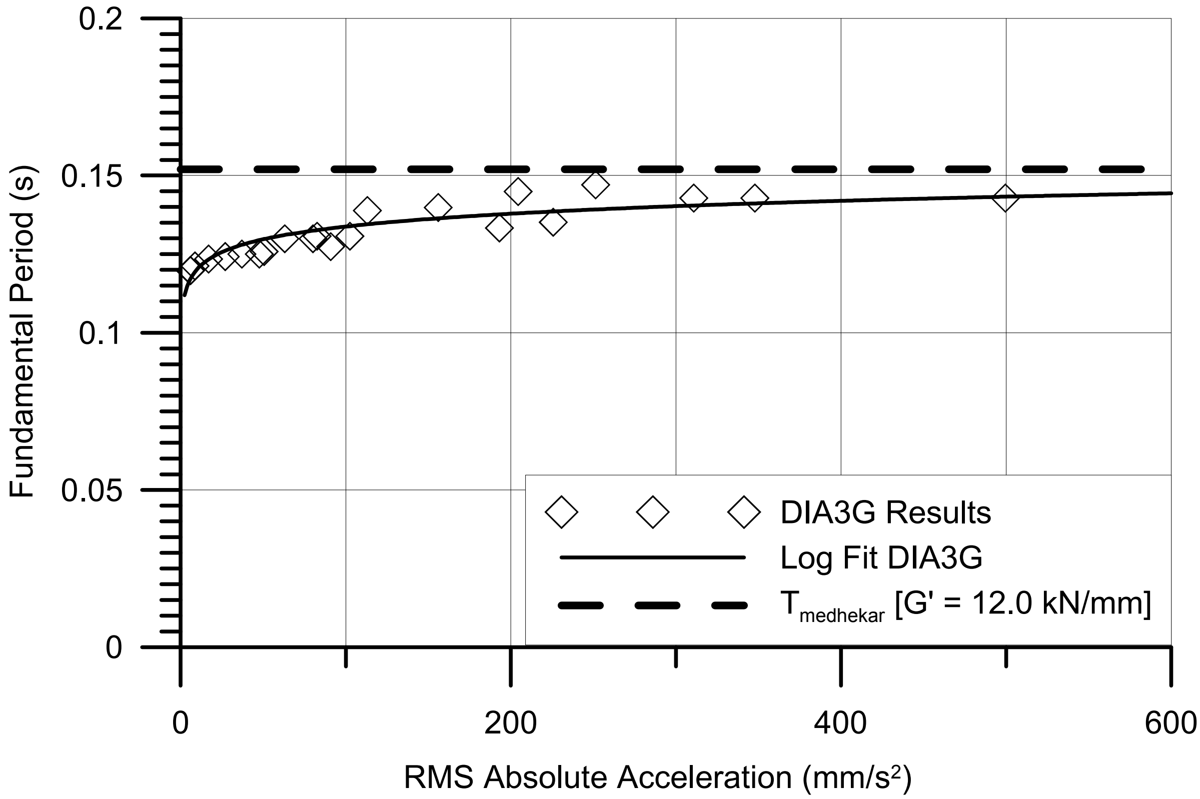

Figure B.7 – Fundamental period vs. RMS response acceleration for DIA3G

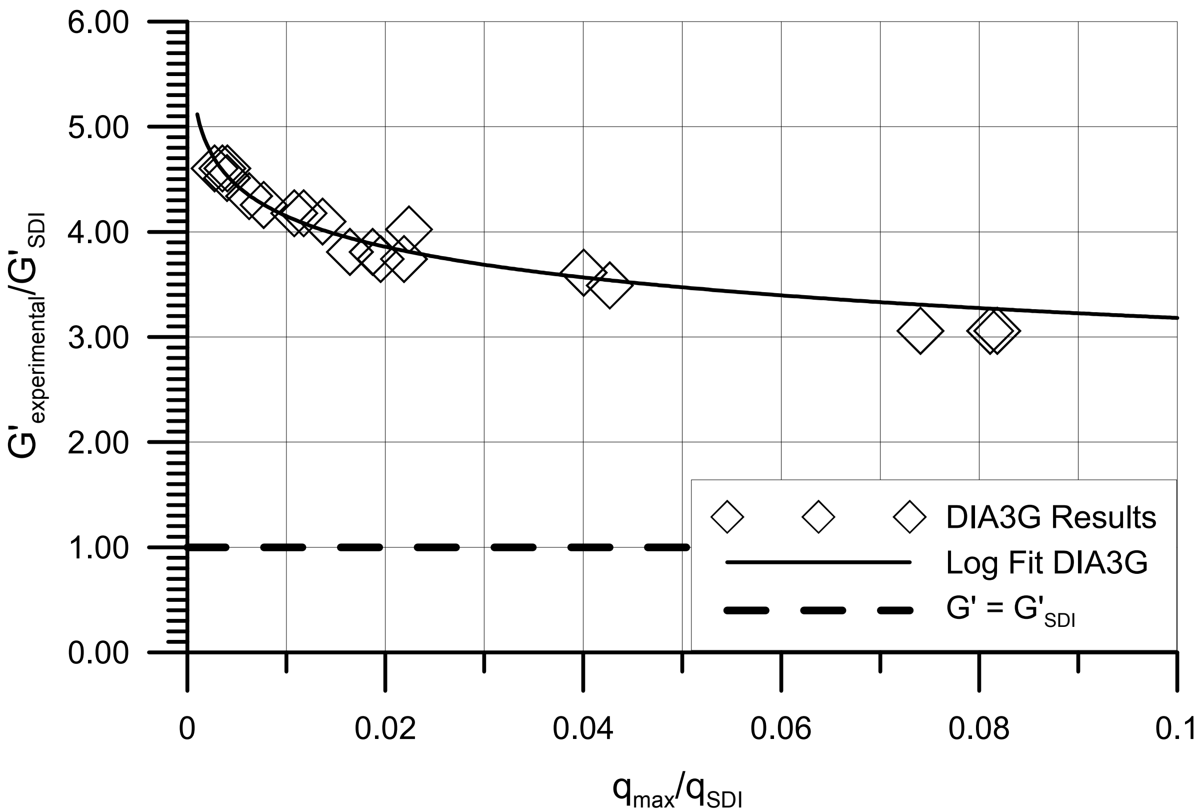

Figure B.8 – Comparison of experimental and theoretical strengths and stiffness's for DIA3G

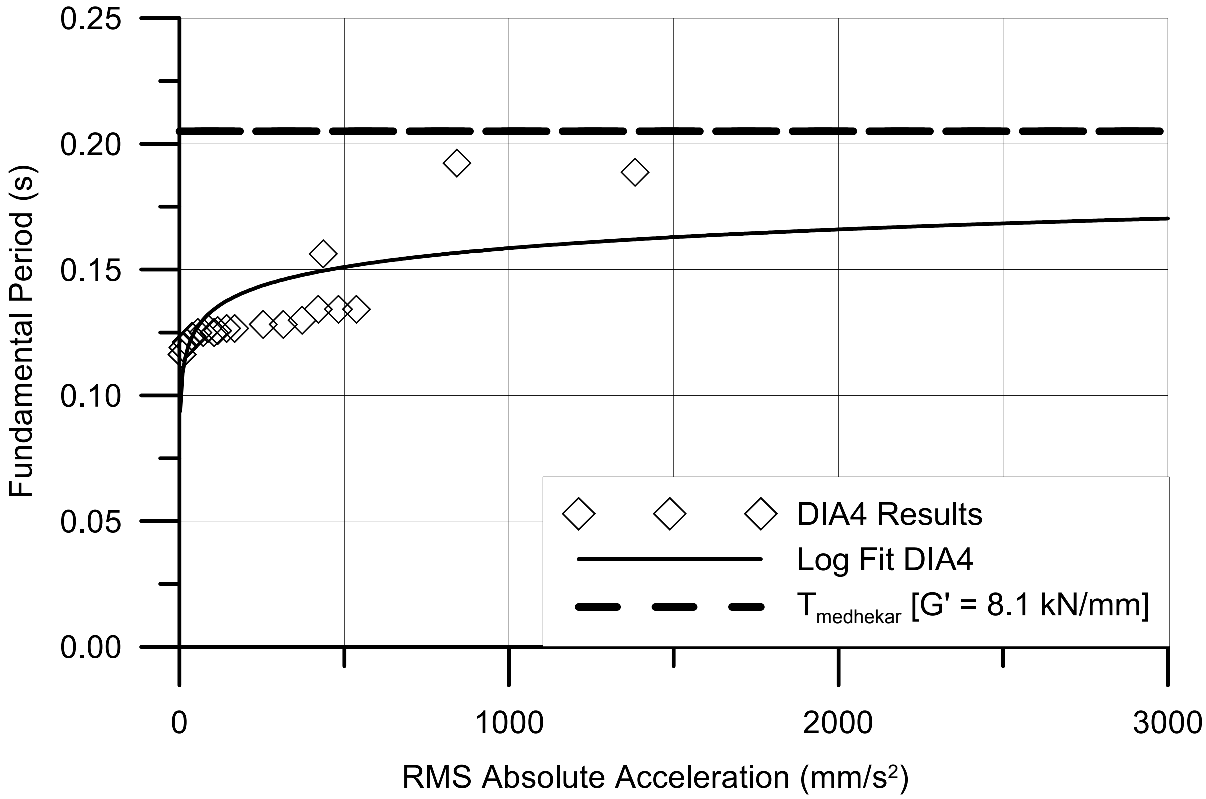

Figure B.9 – Fundamental period vs. RMS response acceleration for DIA4

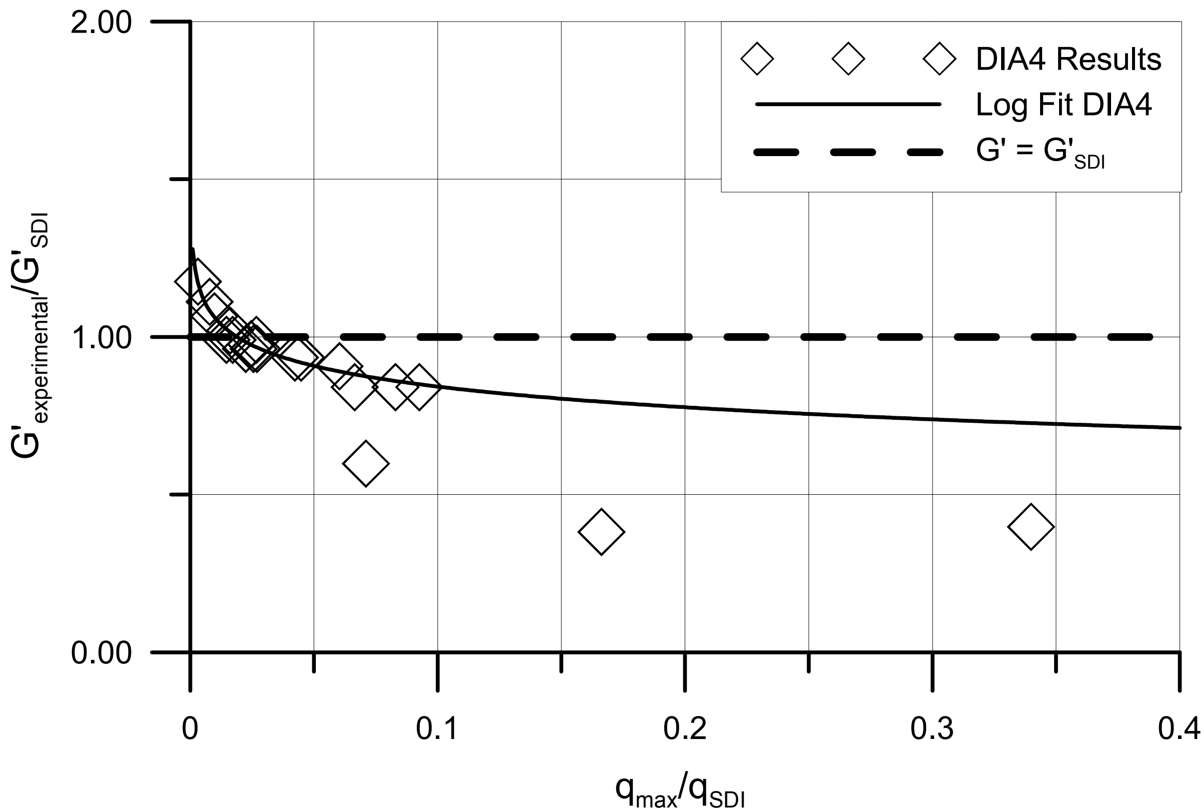

Figure B.10 – Comparison of experimental and theoretical strengths and stiffness's for DIA4

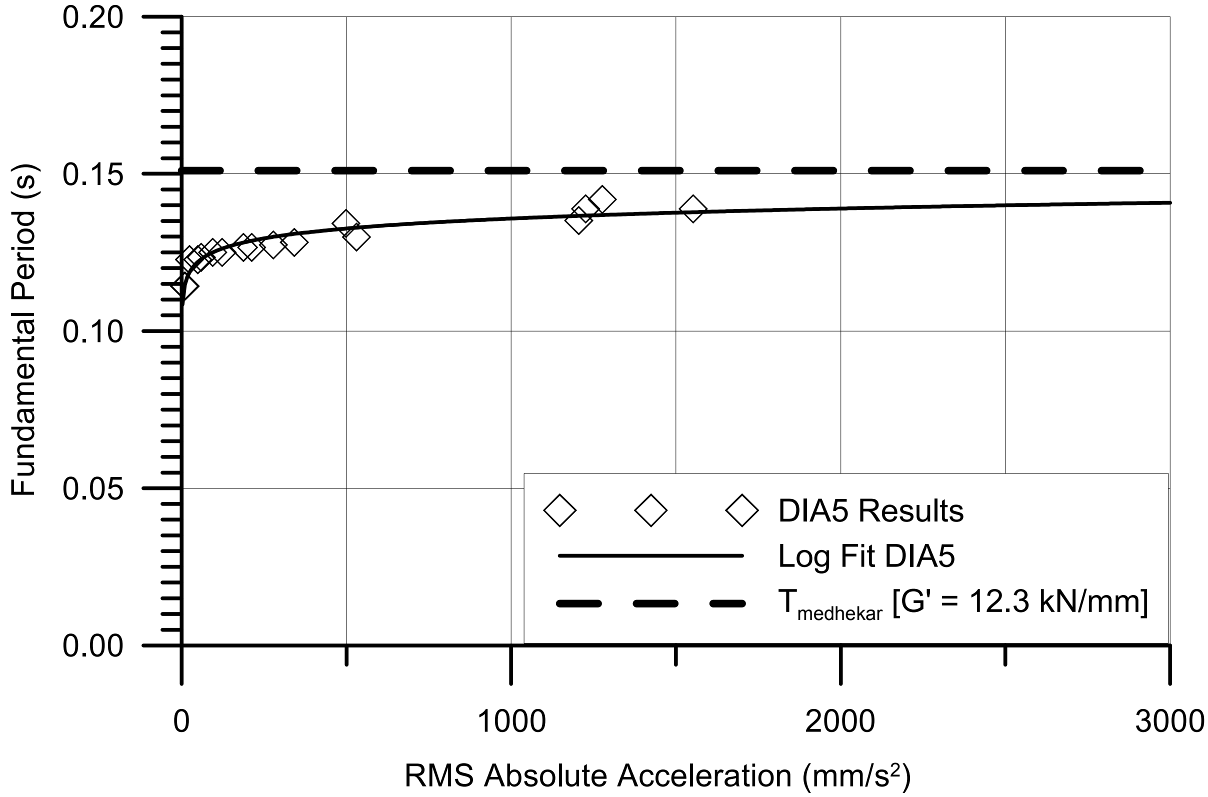

Figure B.11 – Fundamental period vs. RMS response acceleration for DIA5

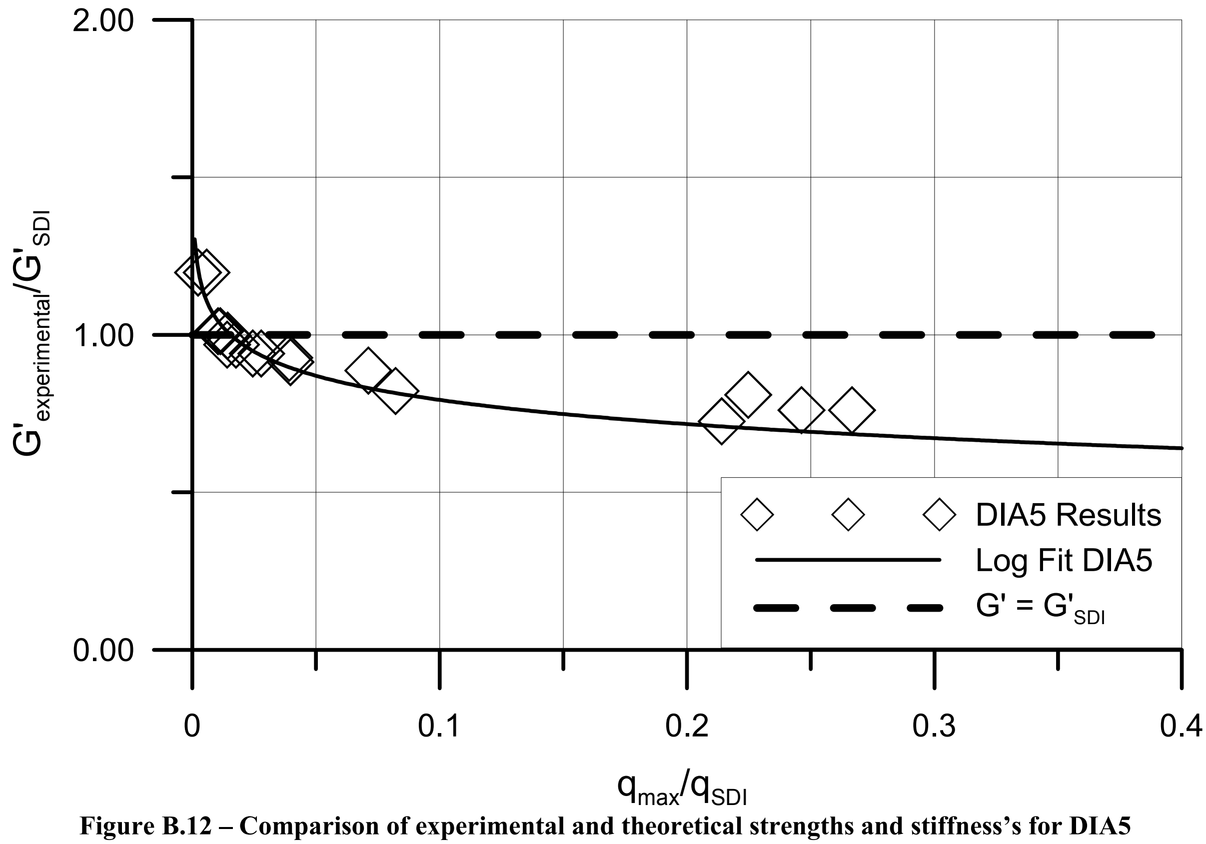

Figure B.12 – Comparison of experimental and theoretical strengths and stiffness's for DIA5

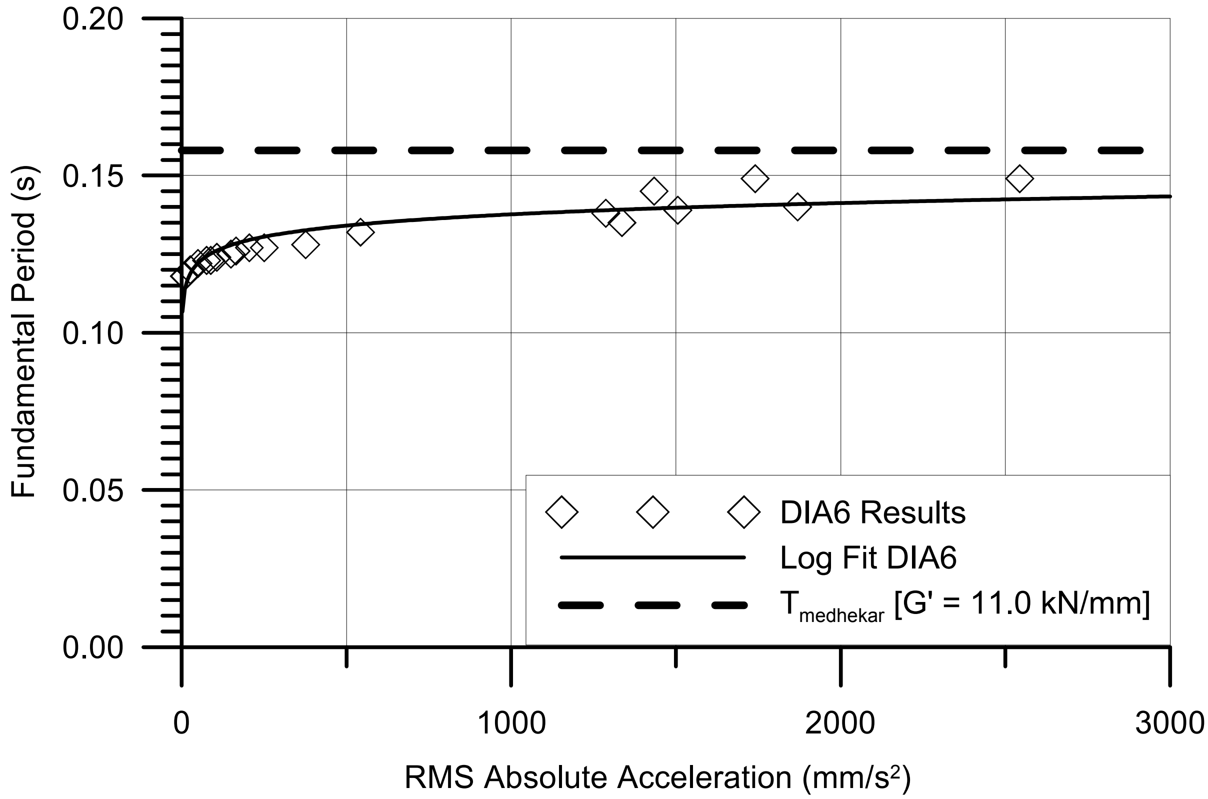

Figure B.13 – Fundamental period vs. RMS response acceleration for DIA6

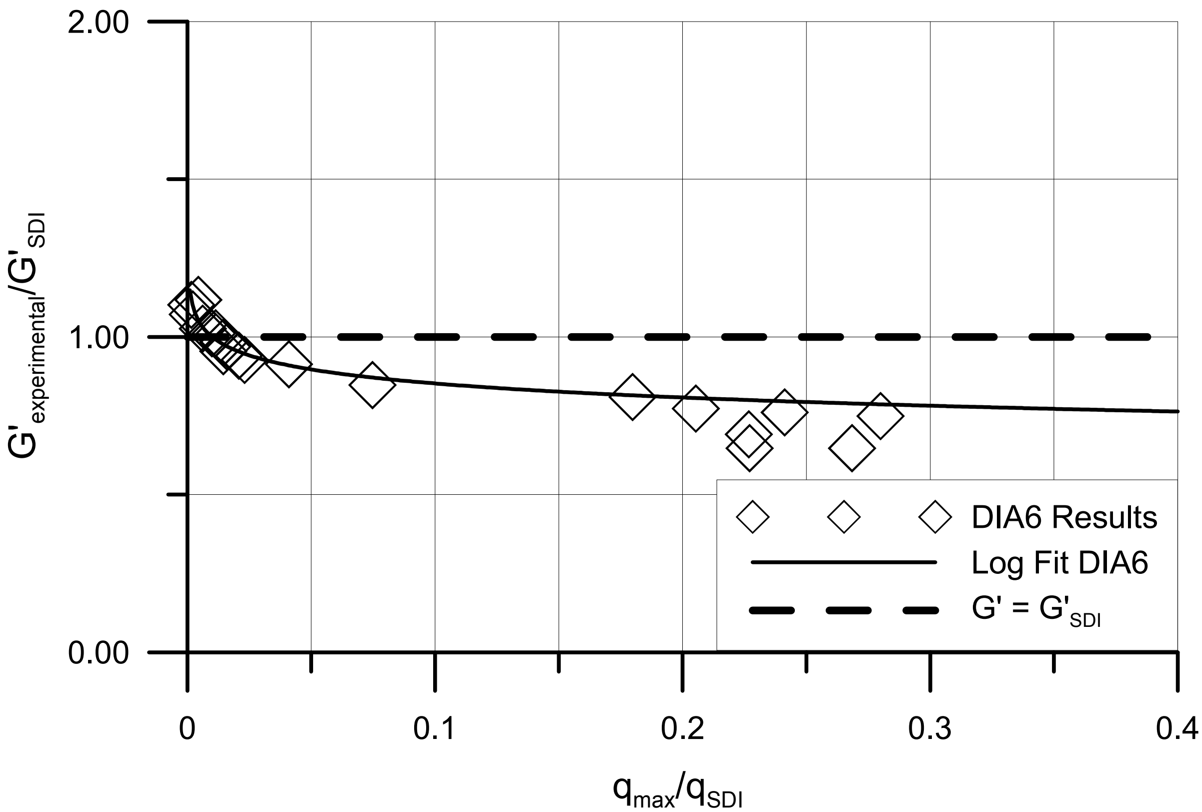

Figure B.14 – Comparison of experimental and theoretical strengths and stiffness's for DIA12

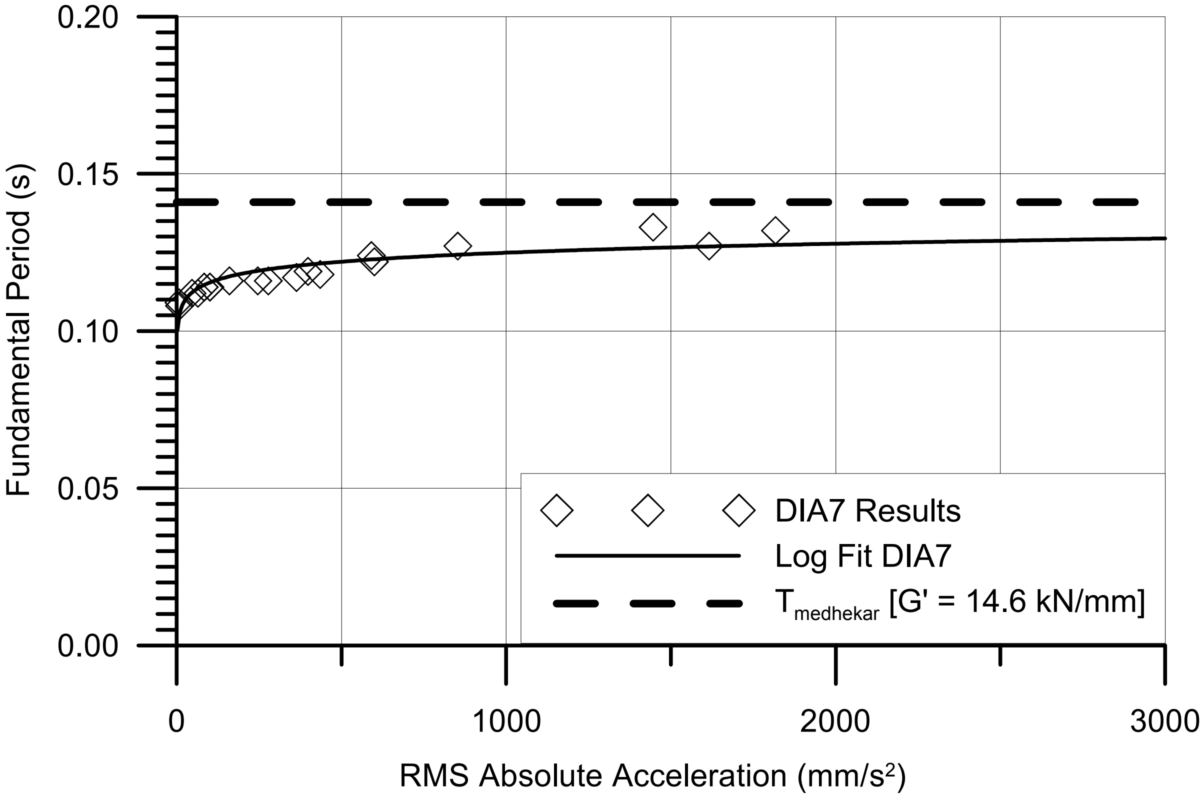

Figure B.15 – Fundamental period vs. RMS response acceleration for DIA7

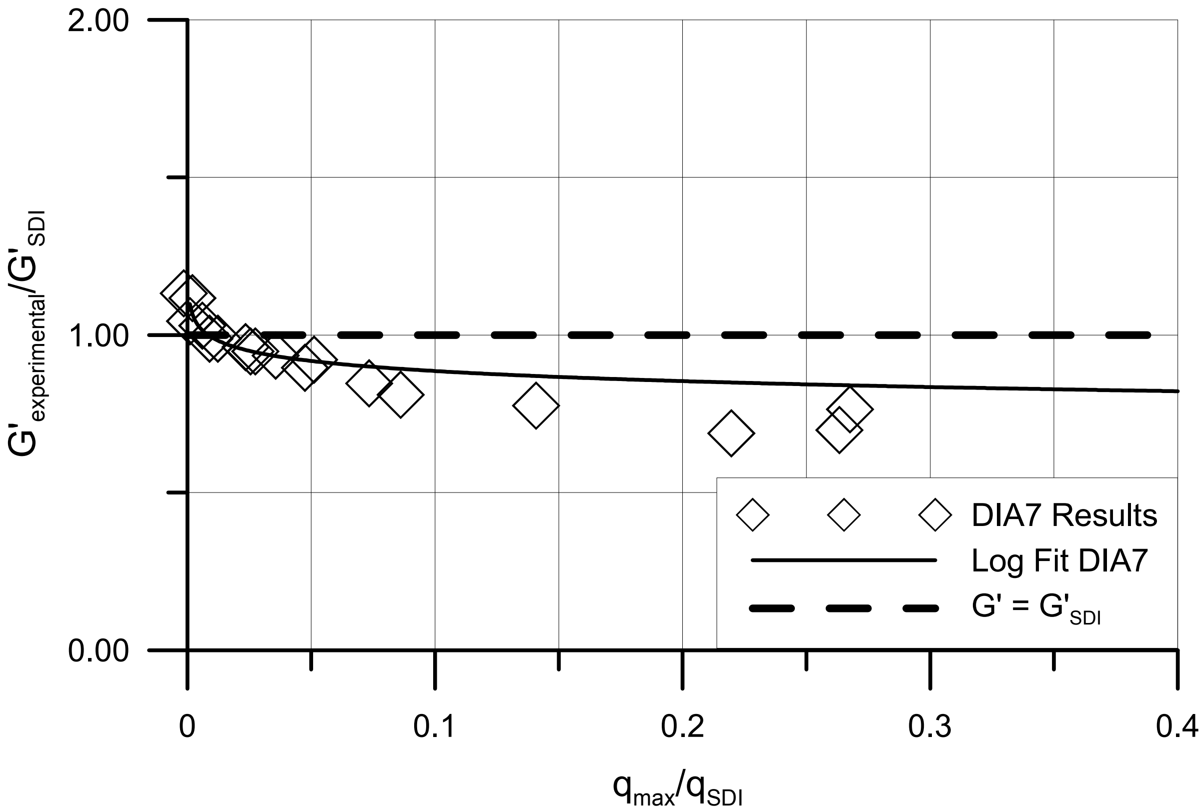

Figure B.16 – Comparison of experimental and theoretical strengths and stiffness's for DIA7

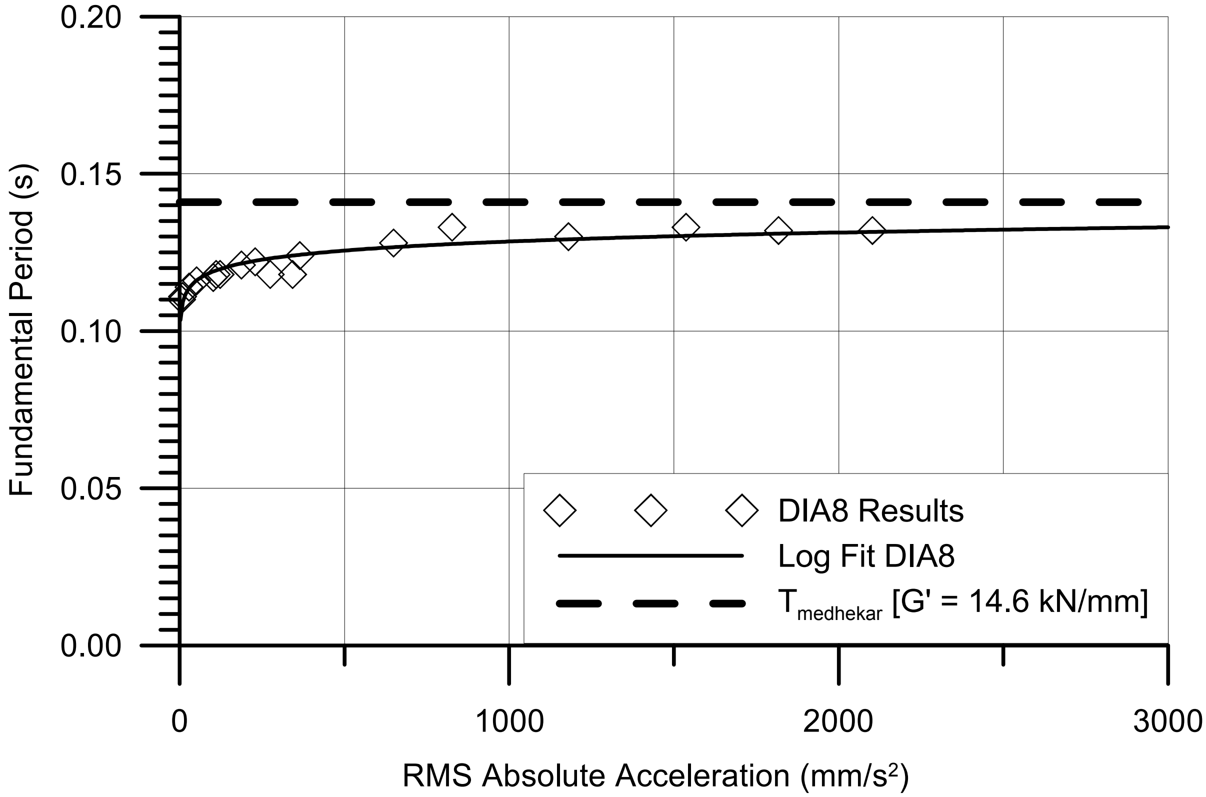

Figure B.17 – Fundamental period vs. RMS response acceleration for DIA8

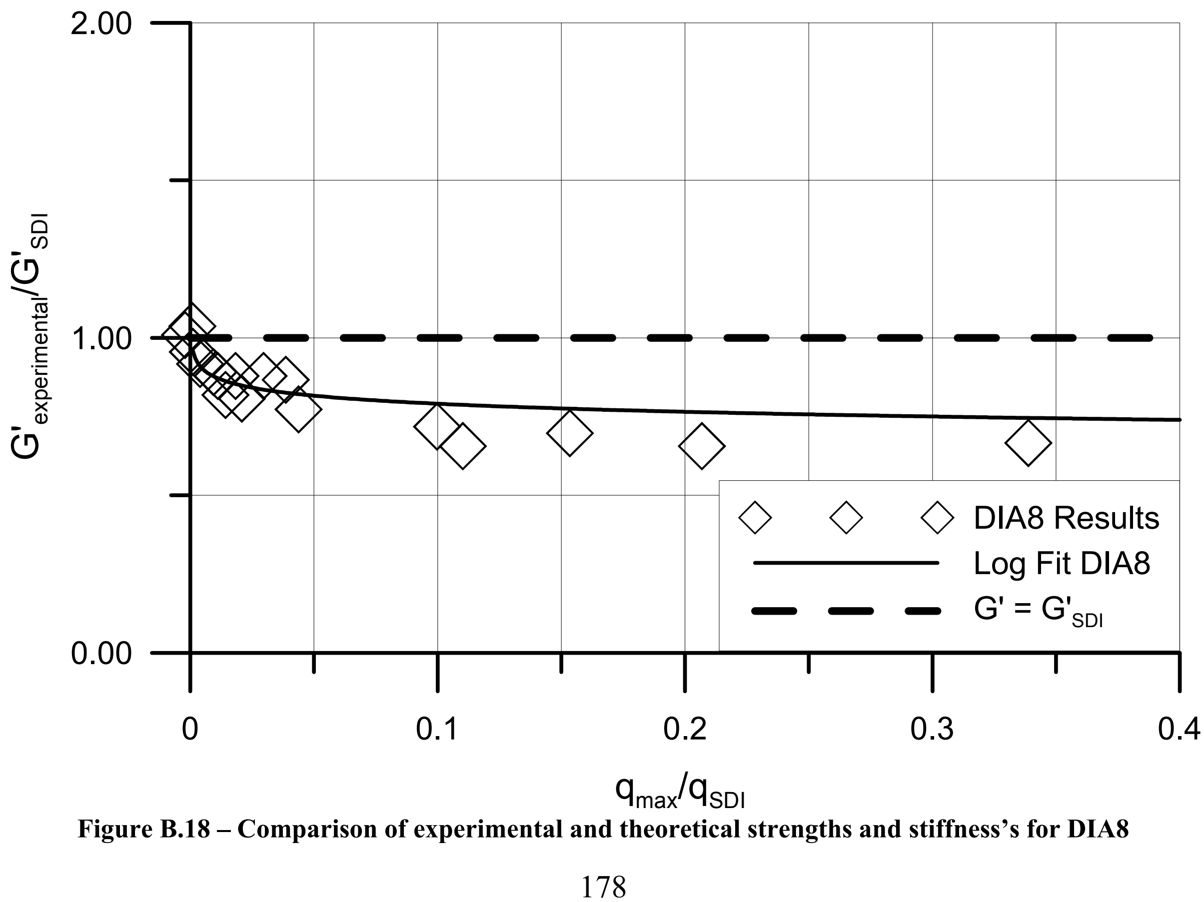

Figure B.18 – Comparison of experimental and theoretical strengths and stiffness's for DIA8

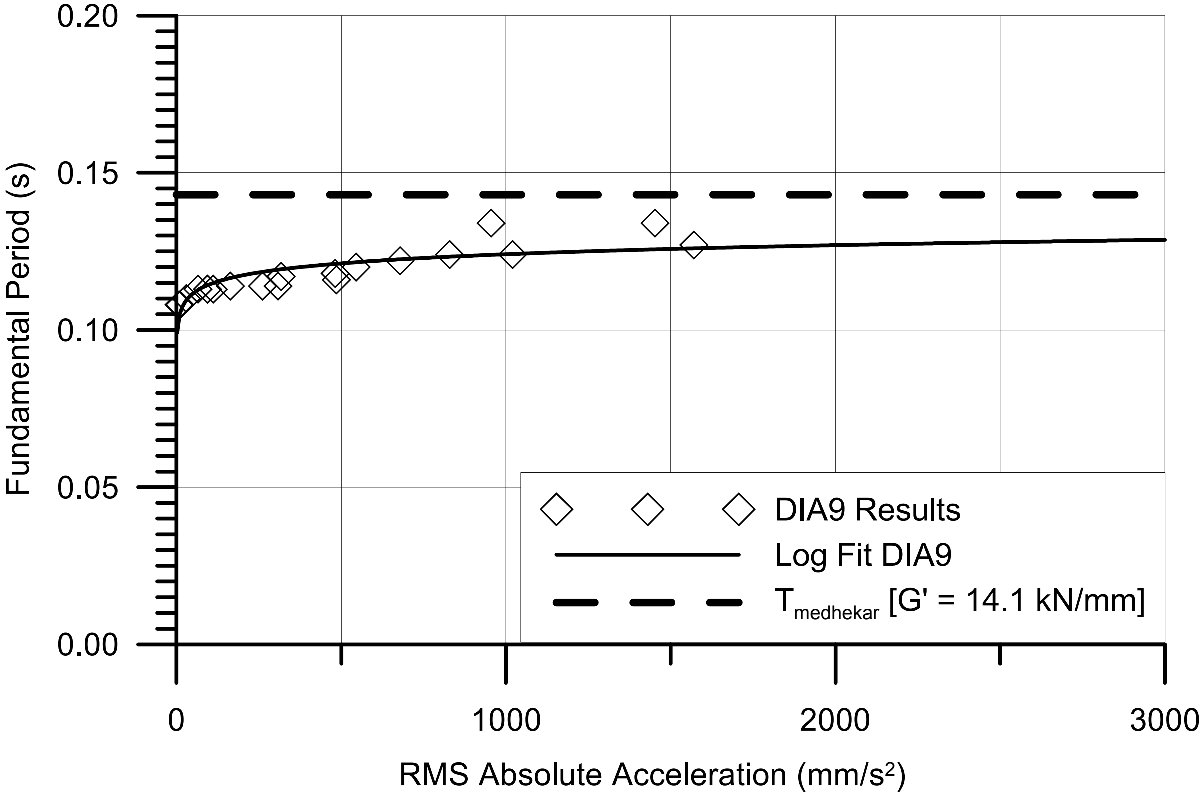

Figure B.19 – Fundamental period vs. RMS response acceleration for DIA9

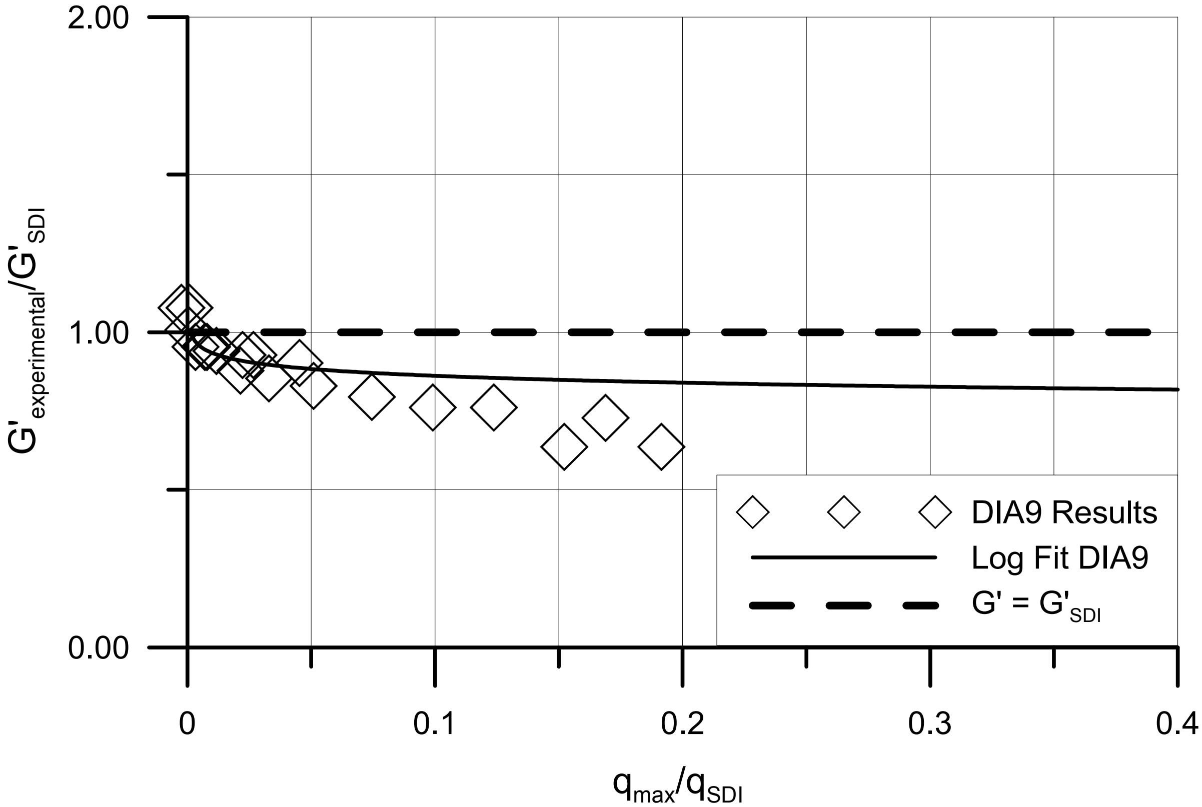

Figure B.20 – Comparison of experimental and theoretical strengths and stiffness's for DIA9

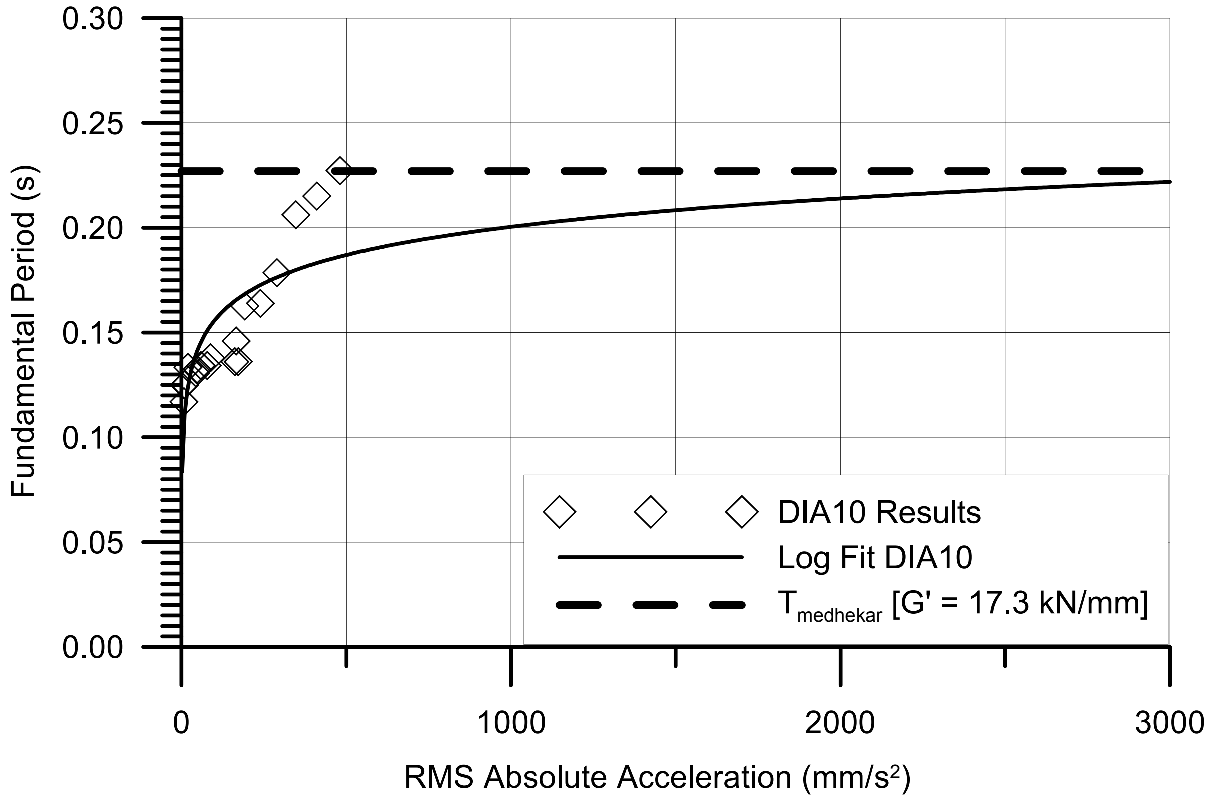

Figure B.21 – Fundamental period vs. RMS response acceleration for DIA10

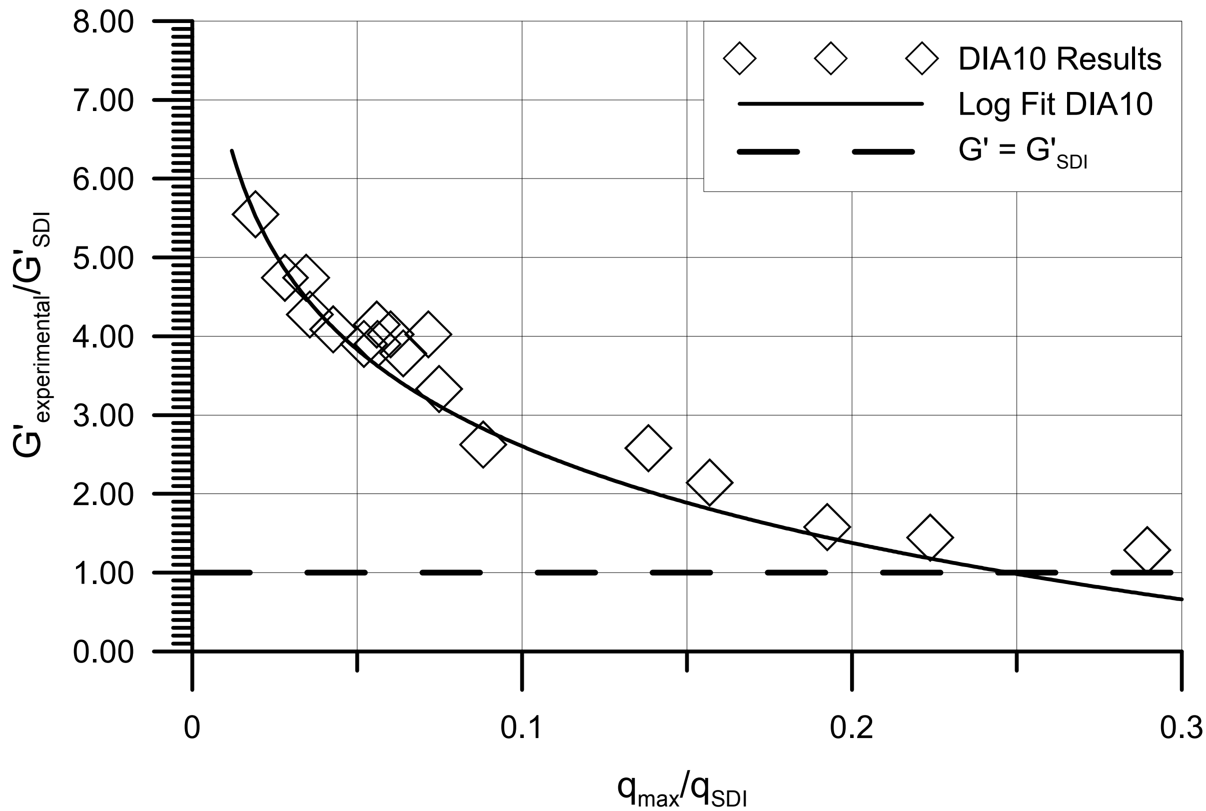

Figure B.22 – Comparison of experimental and theoretical strengths and stiffness's for DIA10

APPENDIX C: PHASE I & II – FREQUENCY RESULTS FOR REPAIRED DIAPHRAGMS

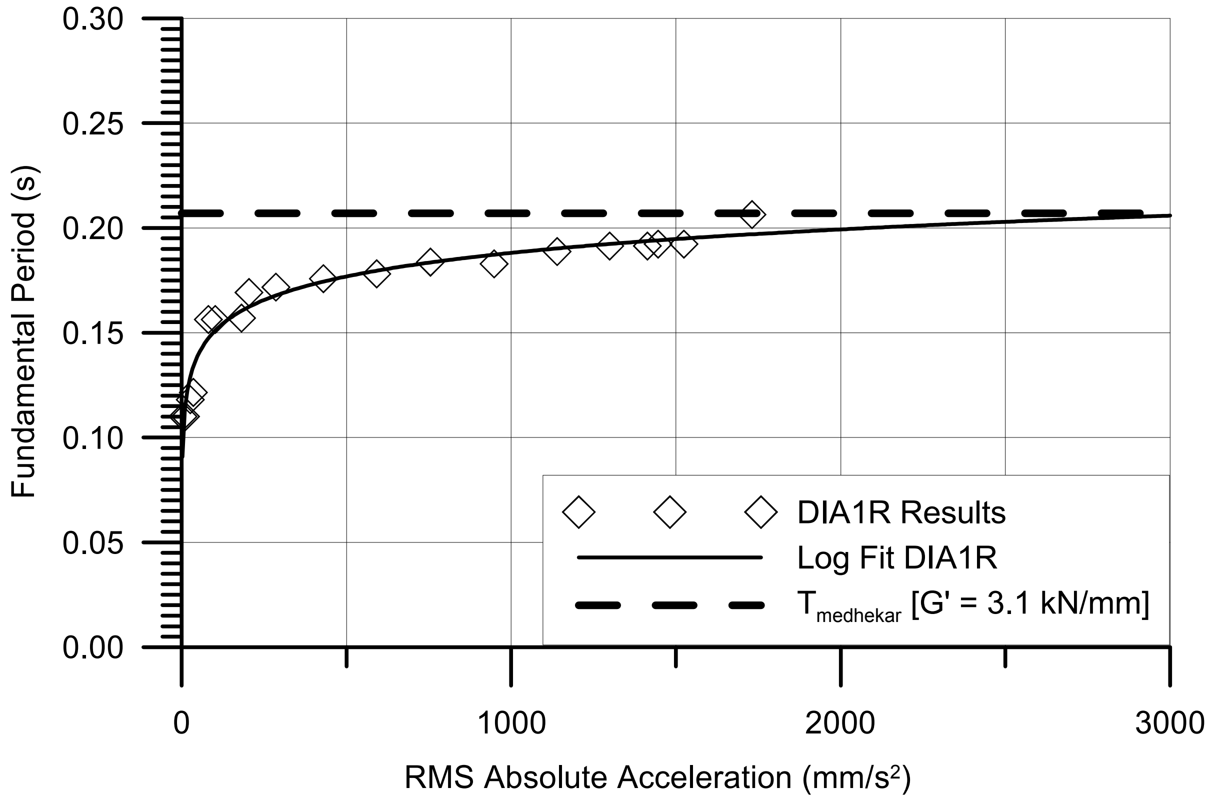

Figure C.1 – Fundamental period vs. RMS response acceleration for DIA1R

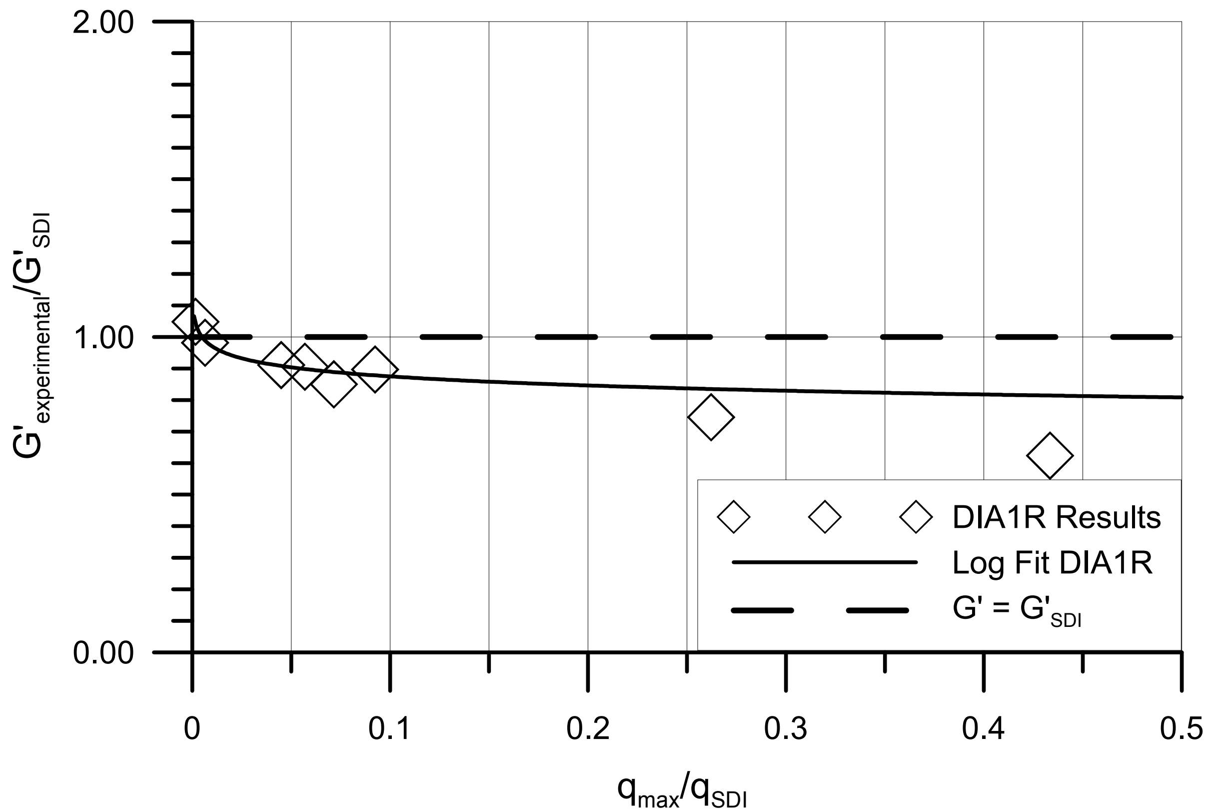

Figure C.2 – Comparison of experimental and theoretical strengths and stiffness's for DIA1R

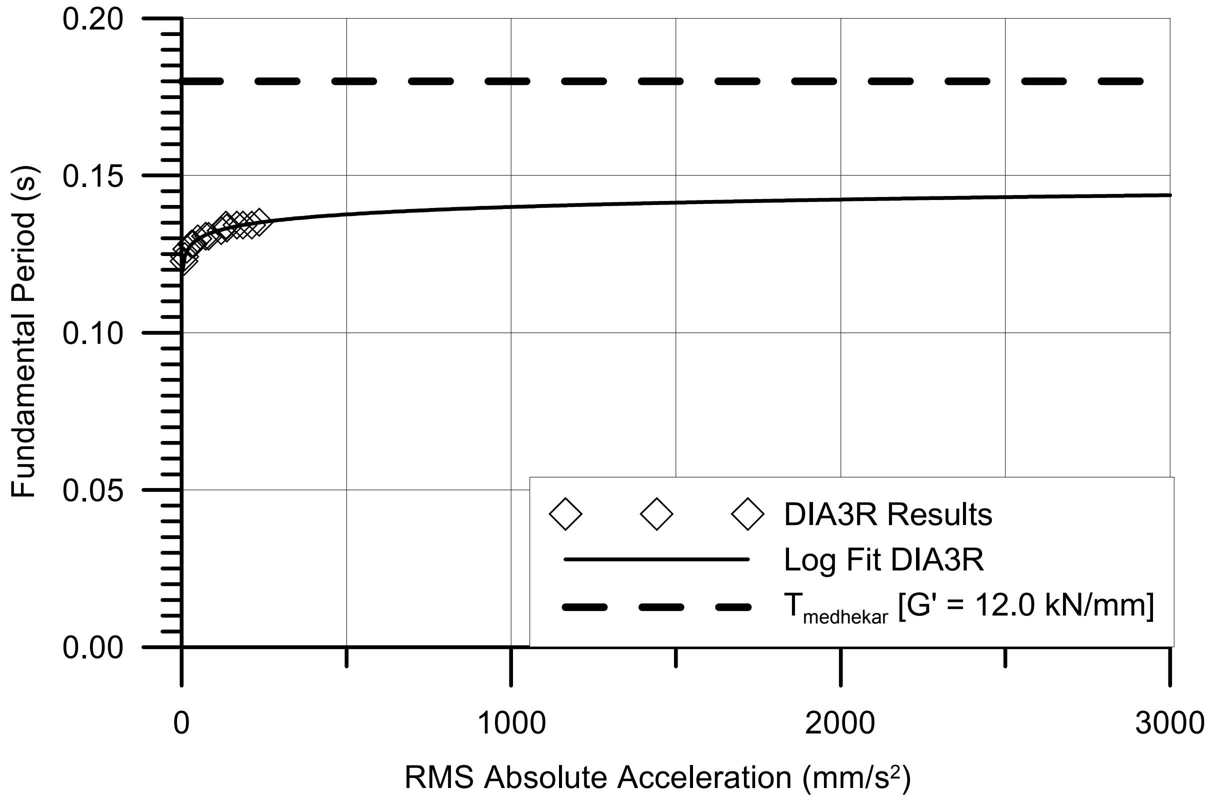

Figure C.3 – Fundamental period vs. RMS response acceleration for DIA3R

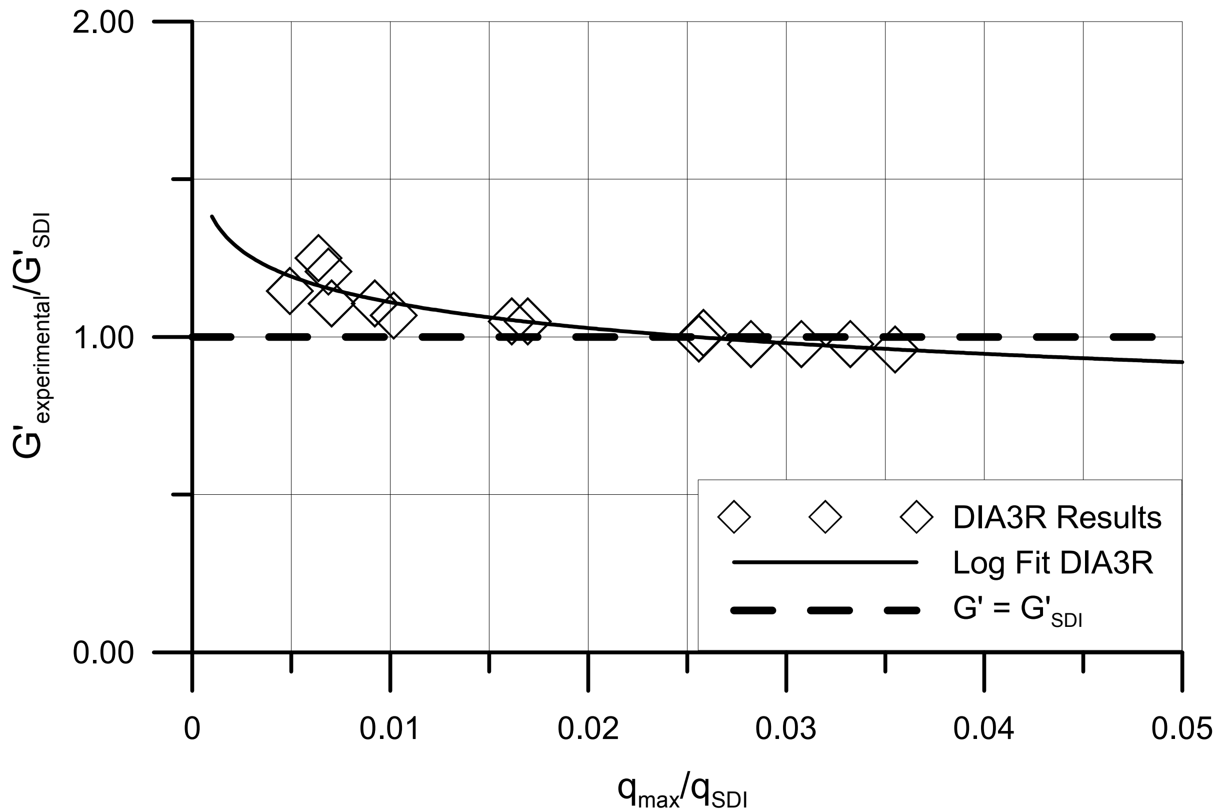

Figure C.4 – Comparison of experimental and theoretical strengths and stiffness's for DIA3R

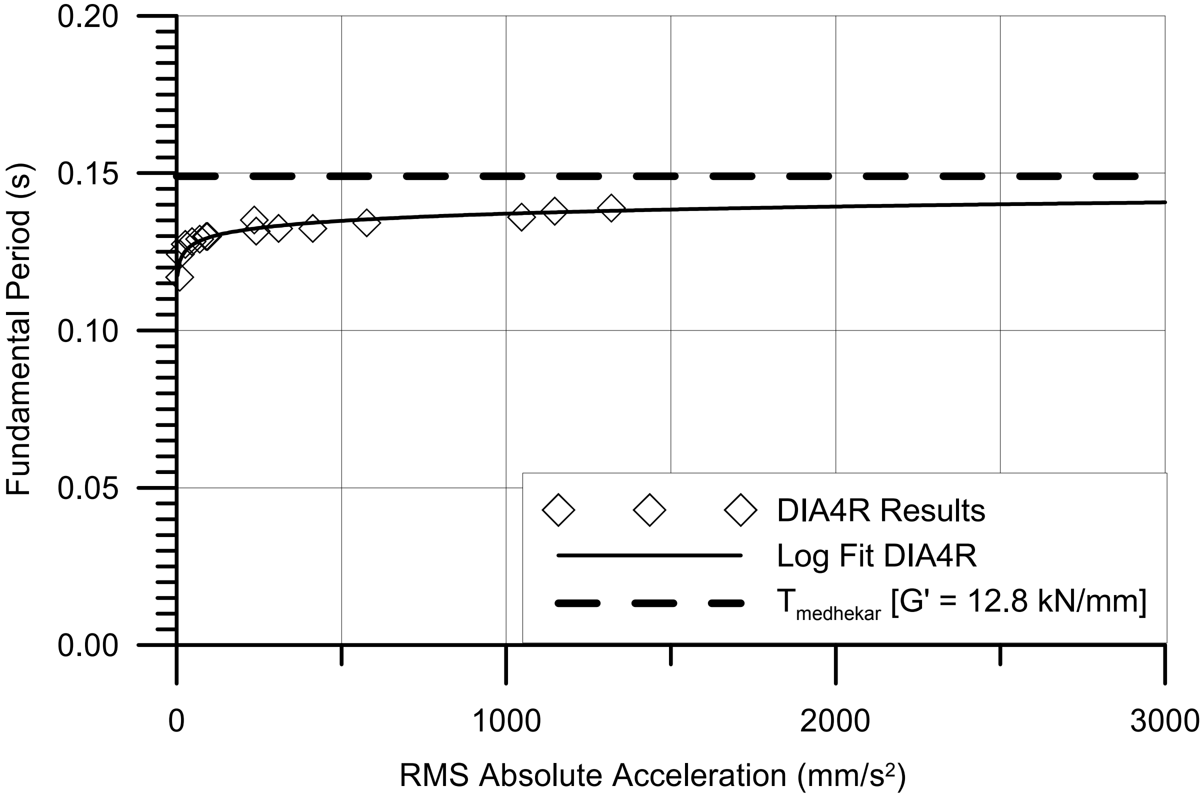

Figure C.5 – Fundamental period vs. RMS response acceleration for DIA4R

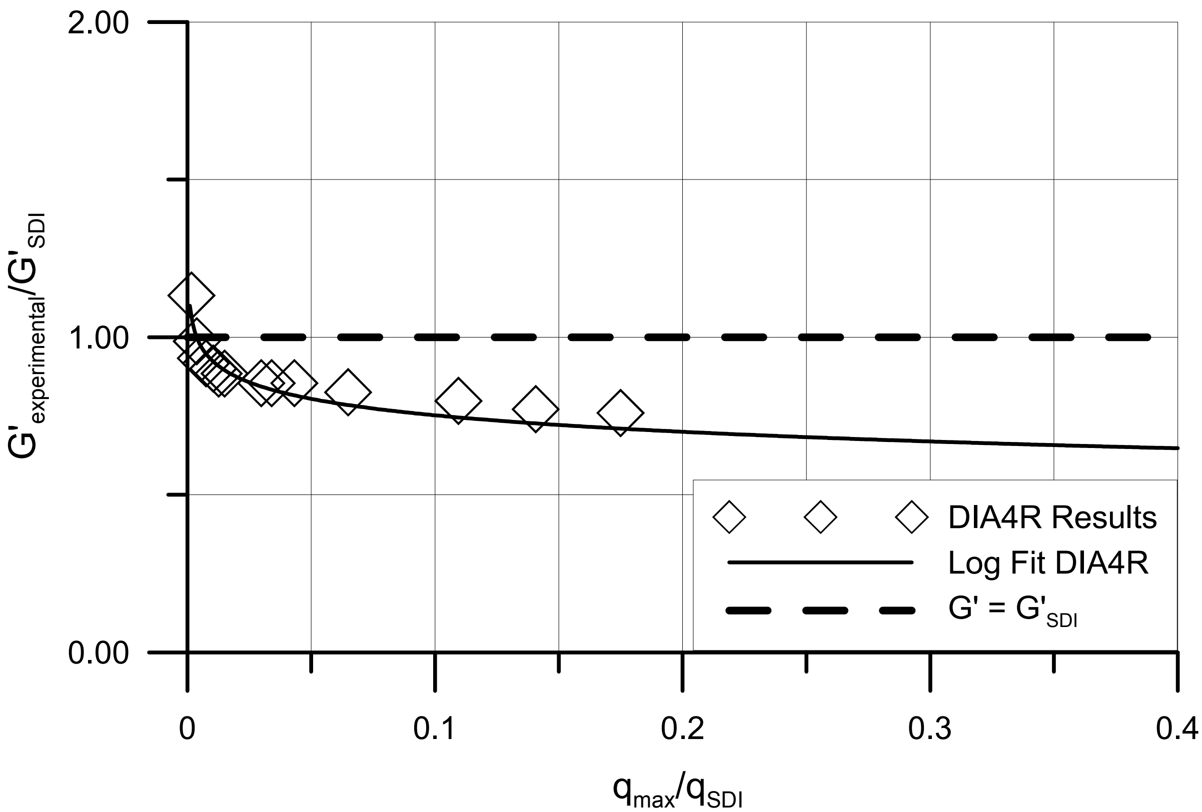

Figure C.6 – Comparison of experimental and theoretical strengths and stiffness's for DIA4R

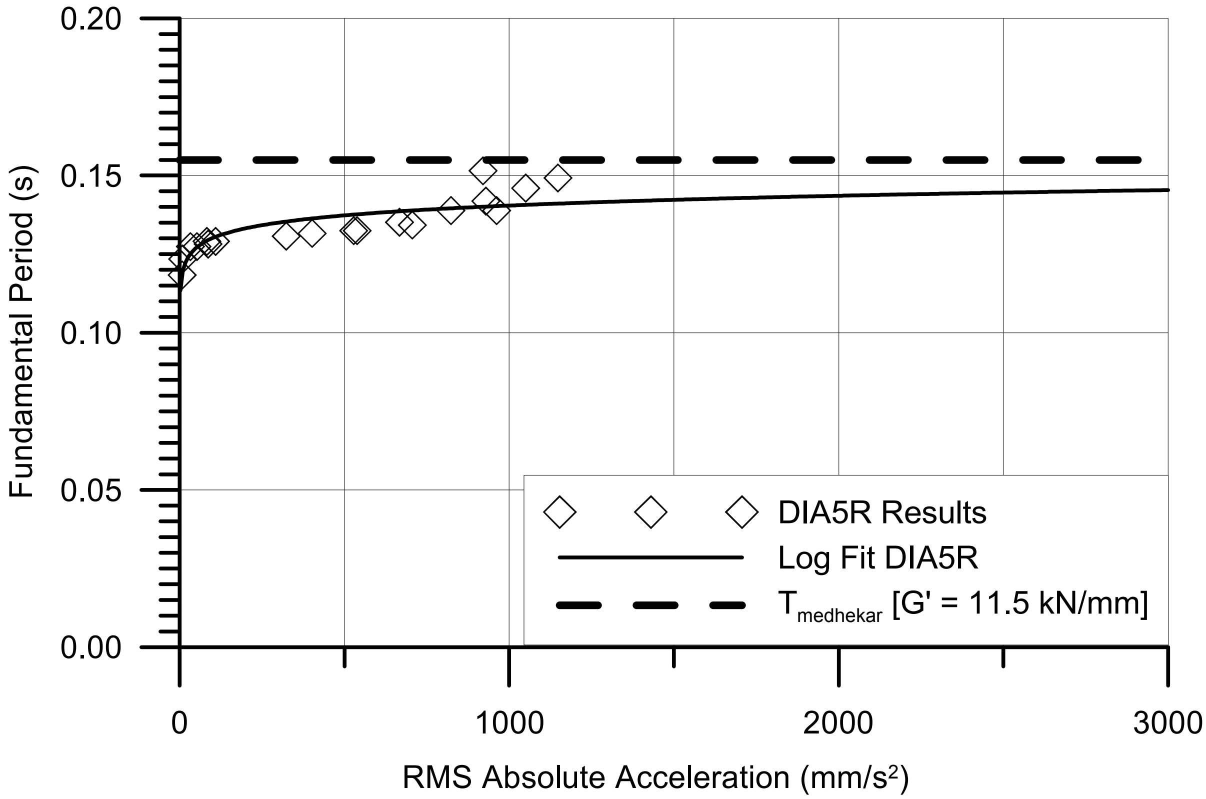

Figure C.7 – Fundamental period vs. RMS response acceleration for DIA5R

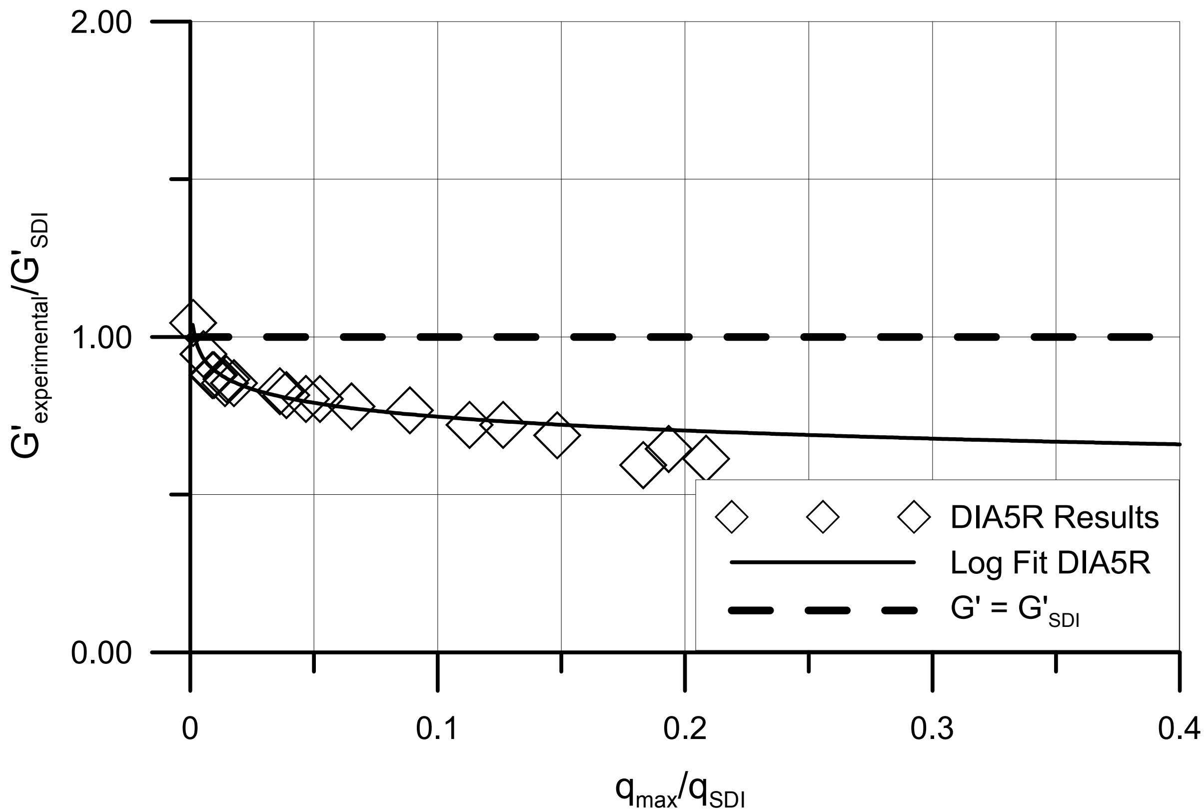

Figure C.8 – Comparison of experimental and theoretical strengths and stiffness's for DIA5R

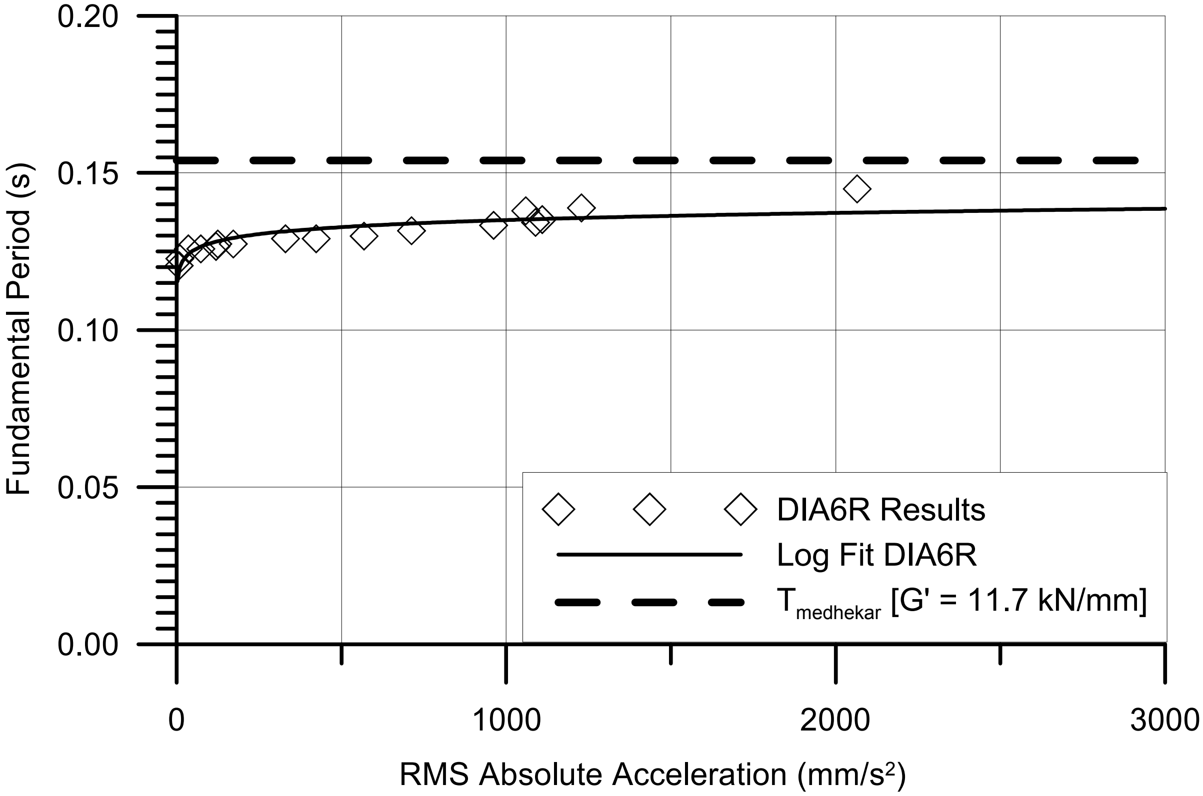

Figure C.9 – Fundamental period vs. RMS response acceleration for DIA6R

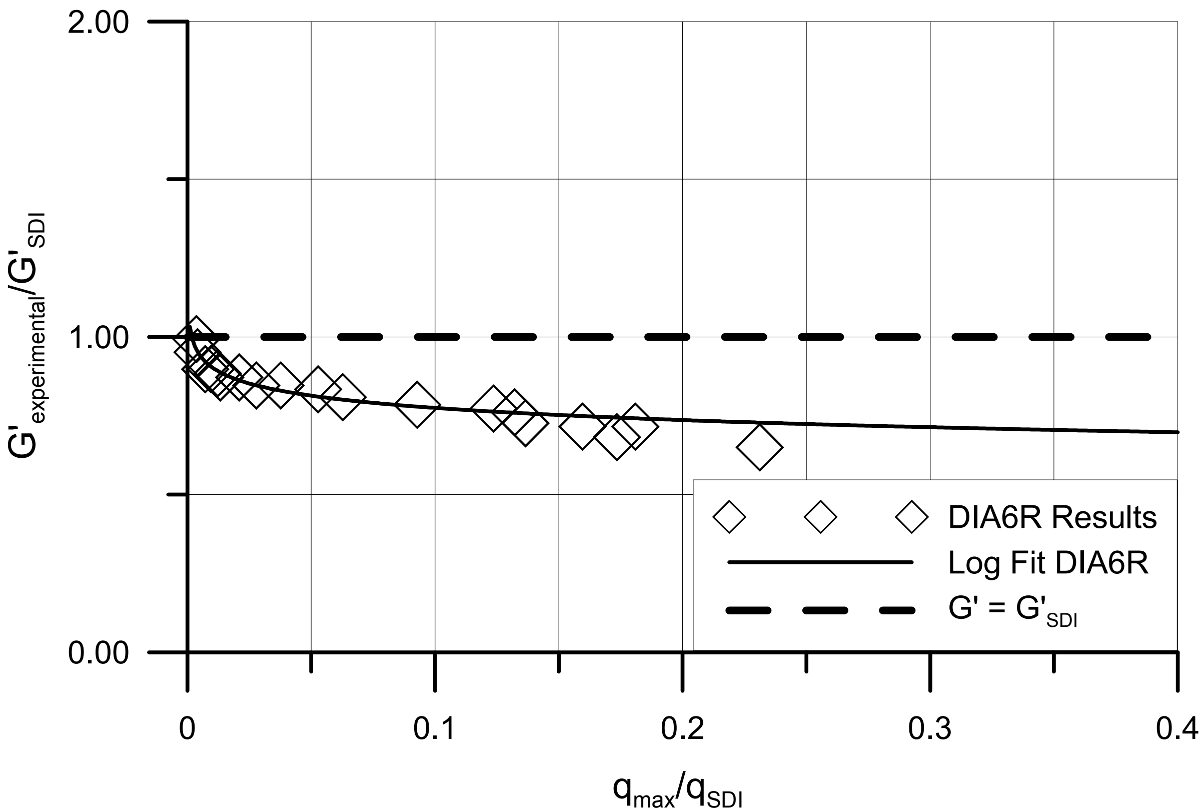

Figure C.10 – Comparison of experimental and theoretical strengths and stiffness's for DIA6R

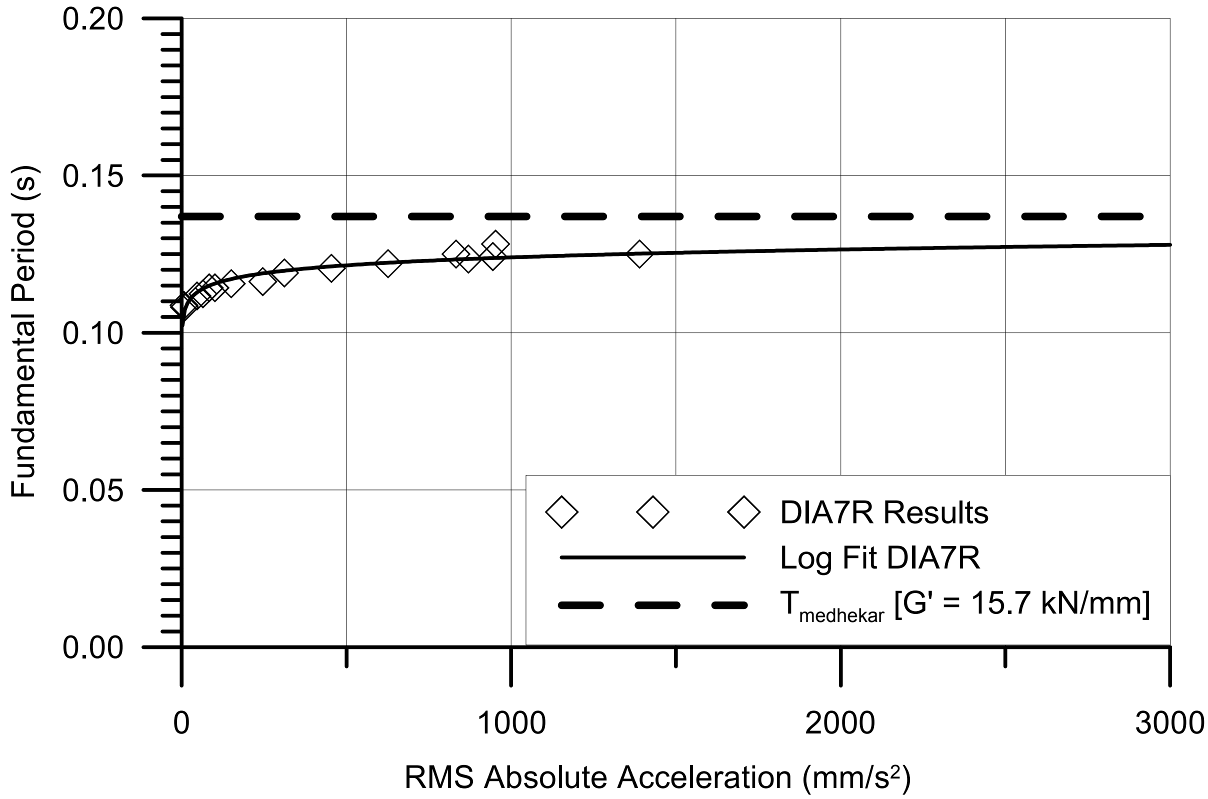

Figure C.11 – Fundamental period vs. RMS response acceleration for DIA7R

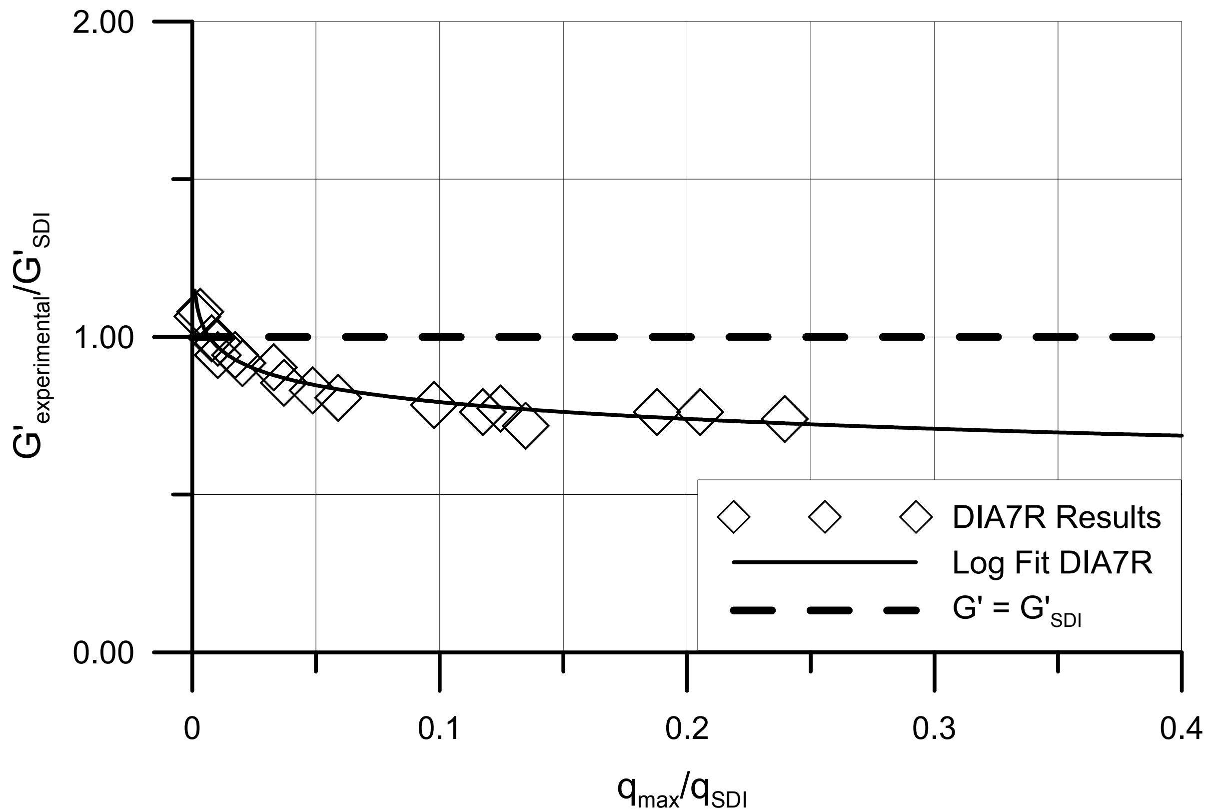

Figure C.12 – Comparison of experimental and theoretical strengths and stiffness's for DIA7R

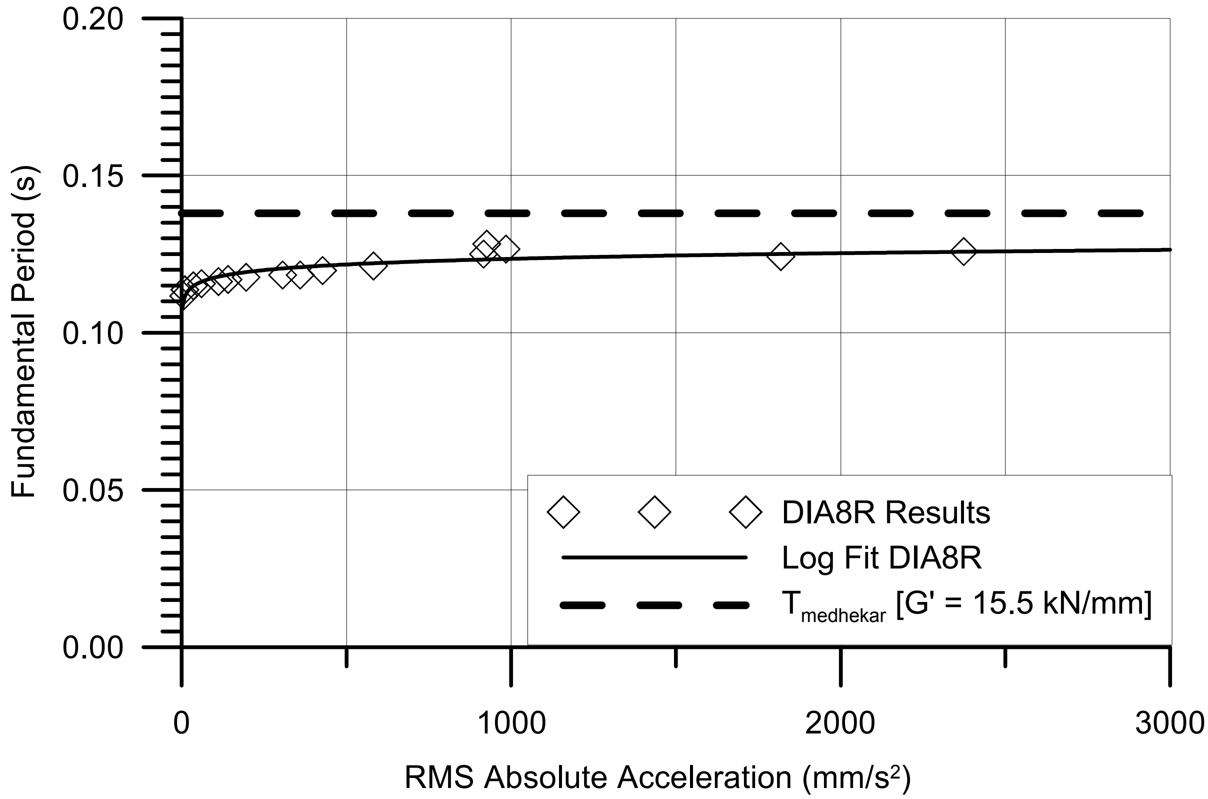

Figure C.13 – Fundamental period vs. RMS response acceleration for DIA8R

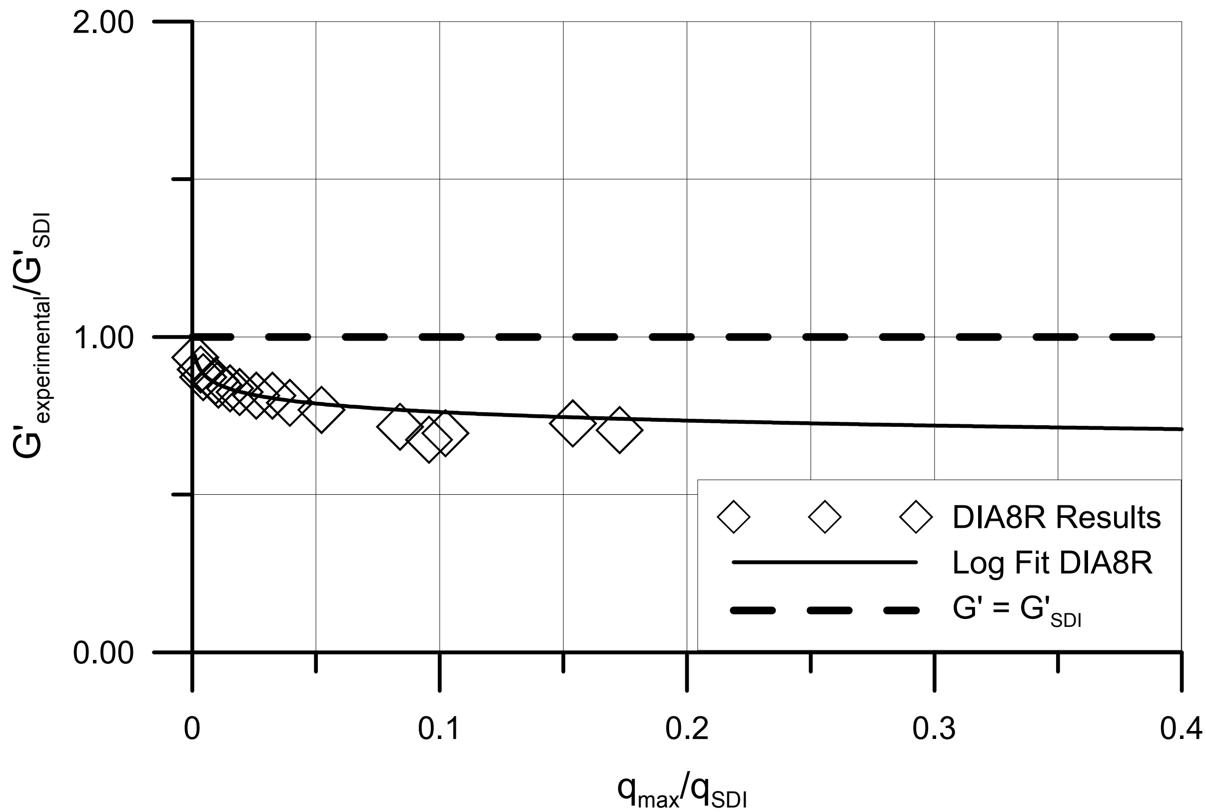

Figure C.14 – Comparison of experimental and theoretical strengths and stiffness's for DIA7R

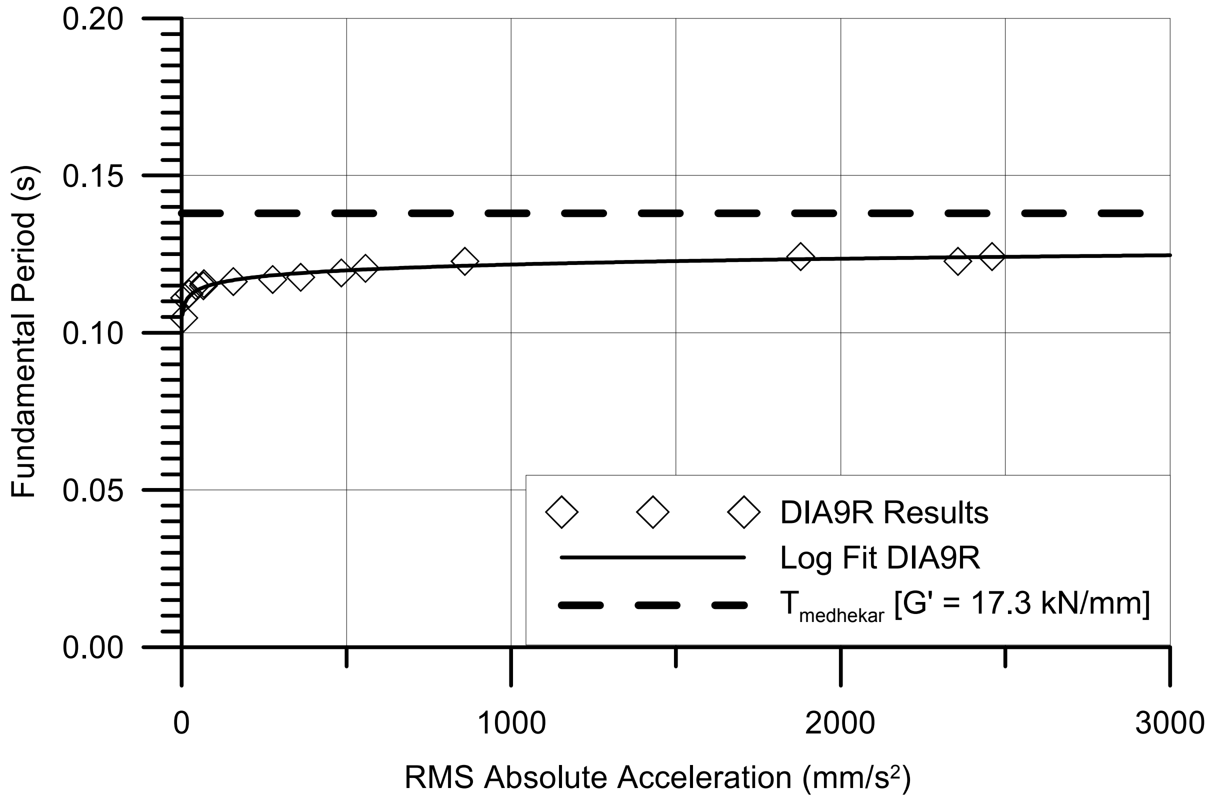

Figure C.15 – Fundamental period vs. RMS response acceleration for DIA9R

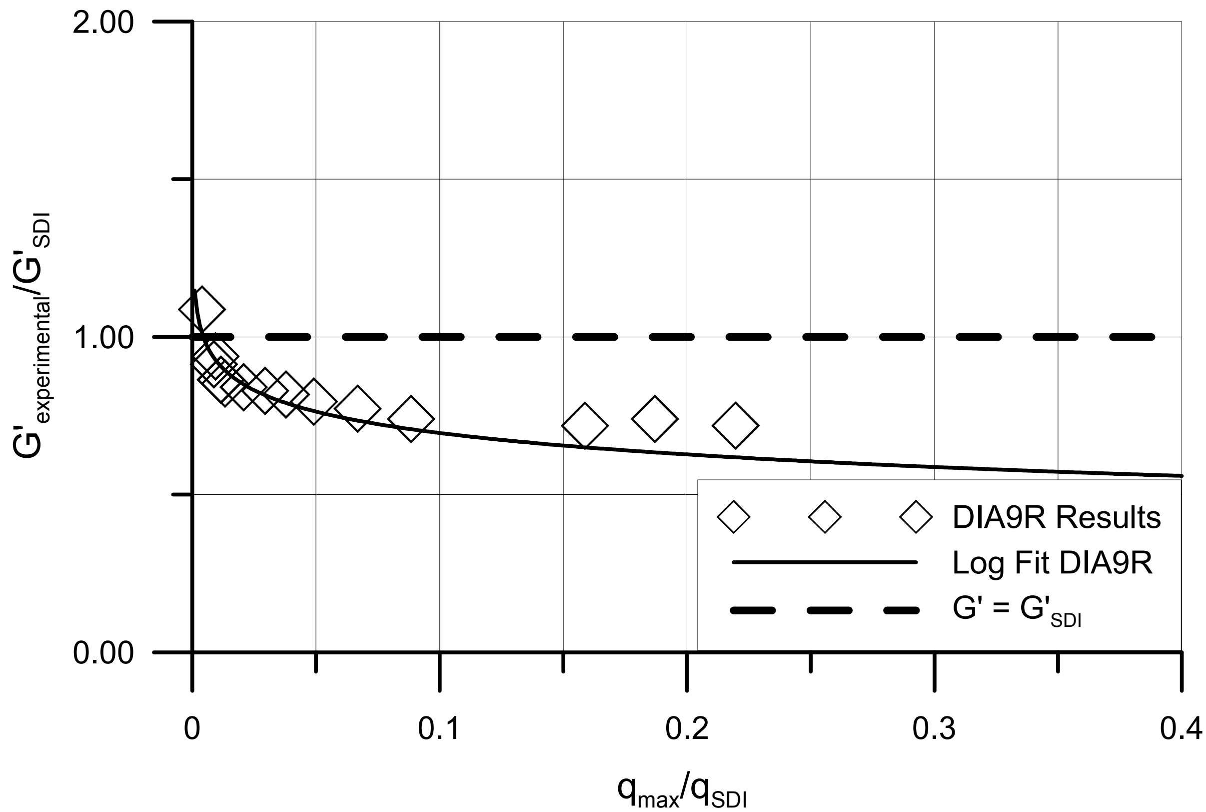

Figure C.16 – Comparison of experimental and theoretical strengths and stiffness's for DIA9R

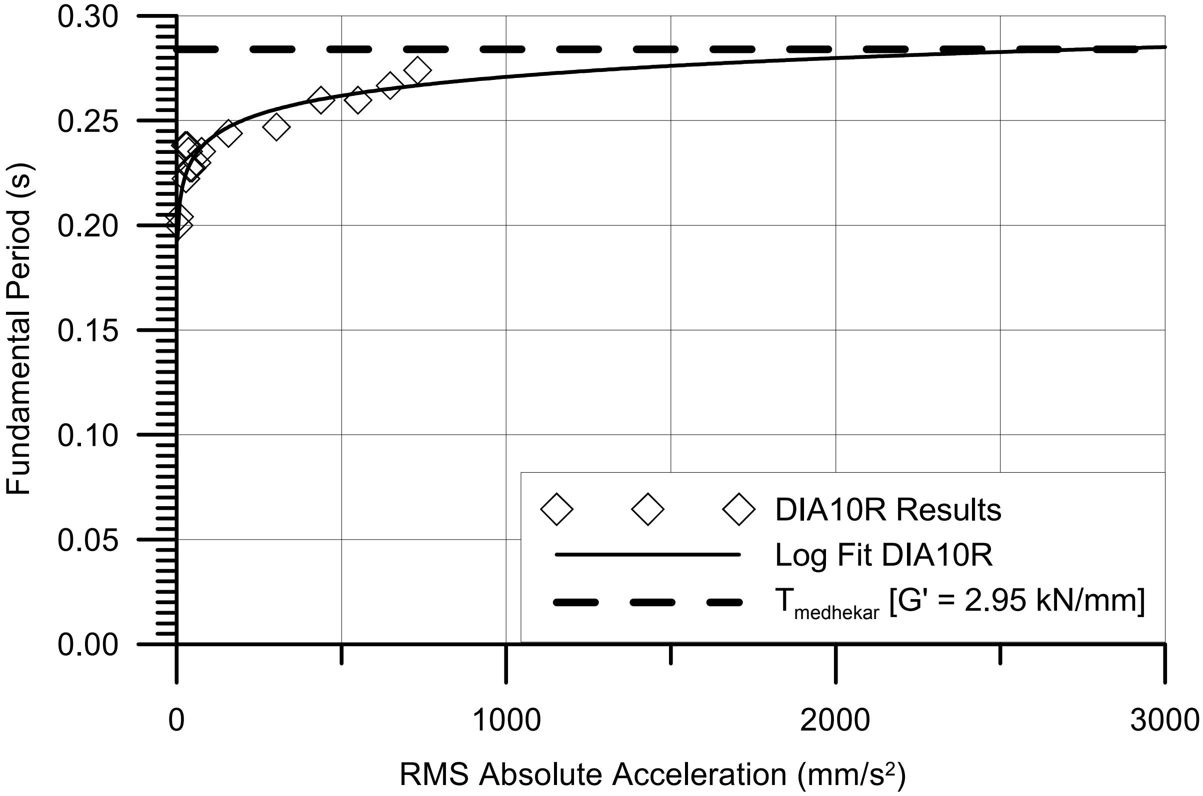

Figure C.17 – Fundamental period vs. RMS response acceleration for DIA10R

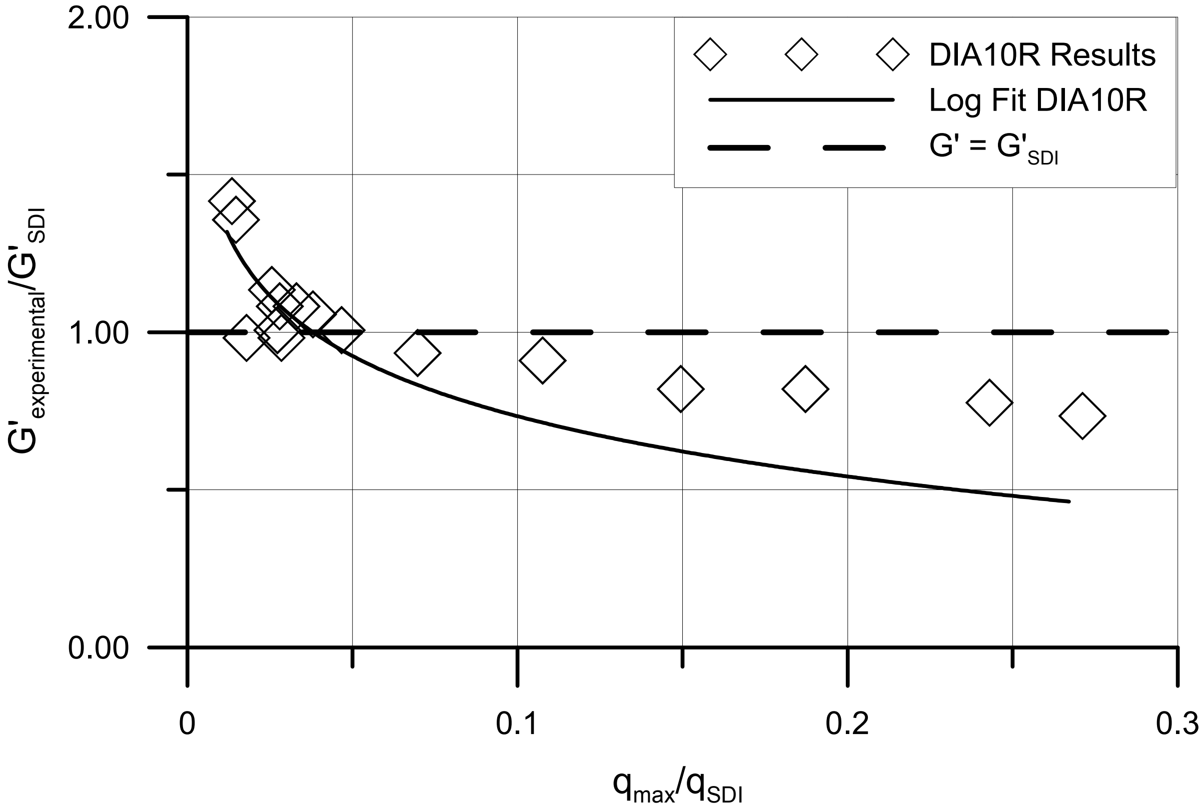

Figure C.18 – Comparison of experimental and theoretical strengths and stiffness's for DIA10R

APPENDIX D: PHASE I & II – SINESWEEP RESULTS

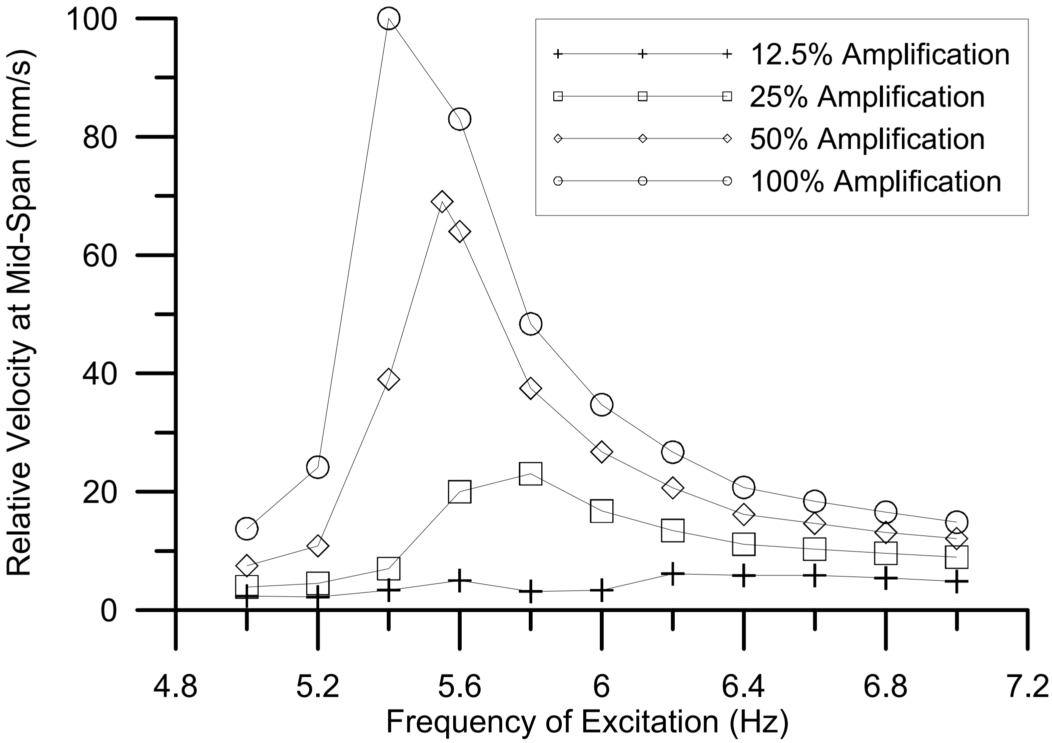

Figure D.1 – Sinesweep results for DIA1

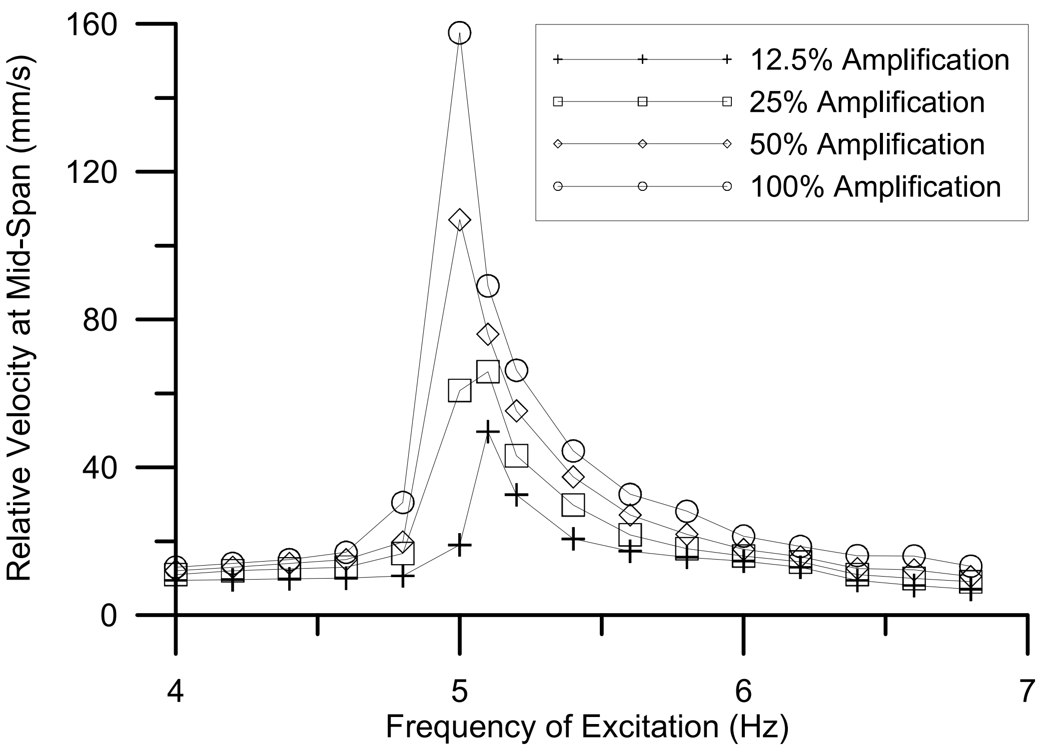

Figure D.2 – Sinesweep results for DIA1R

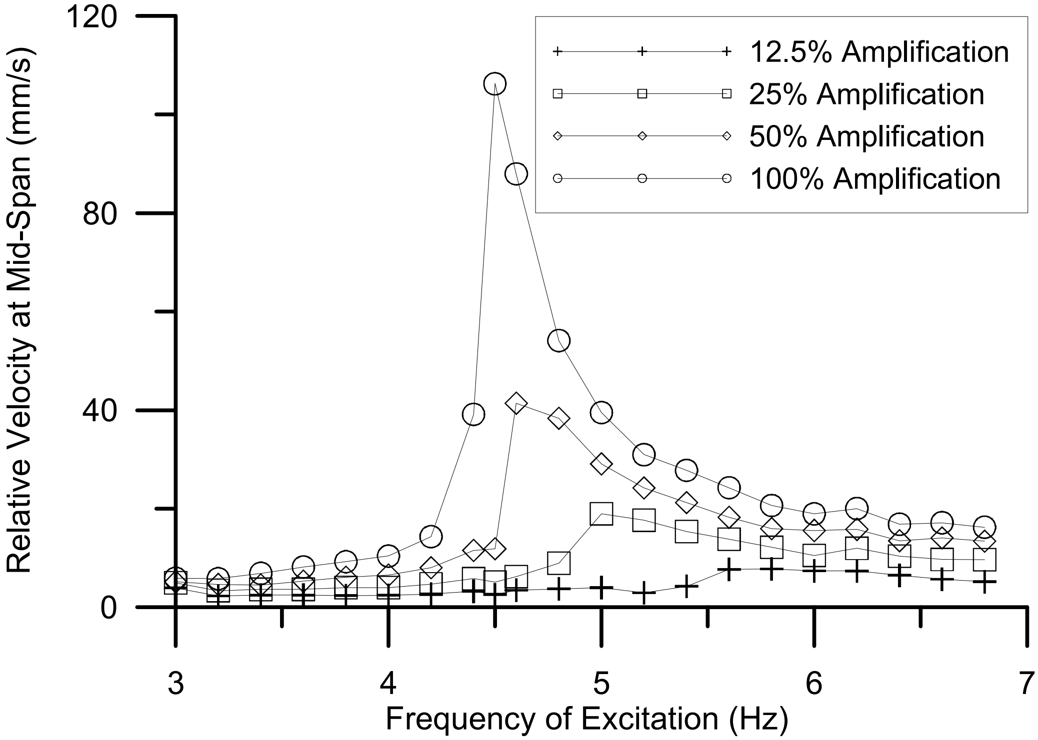

Figure D.3 – Sinesweep results for DIA2

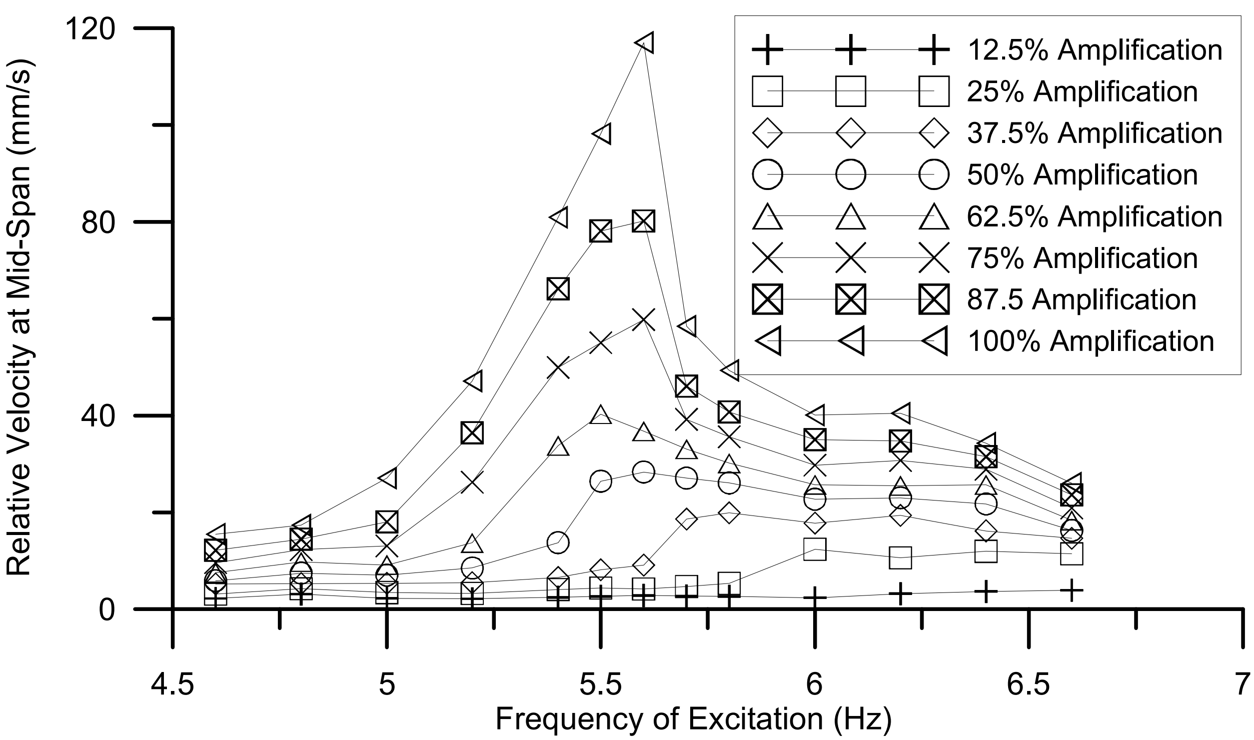

Figure D.4 – Sinesweep results for DIA3

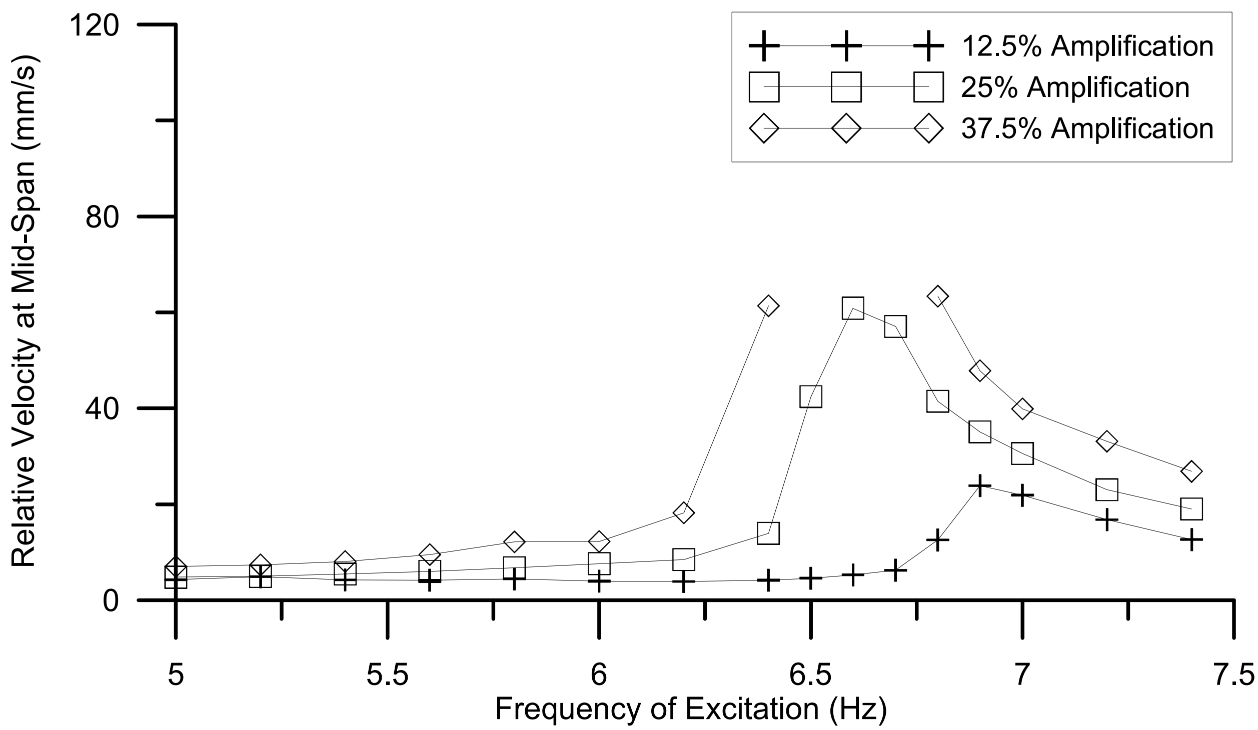

Figure D.5 – Sinesweep results for DIA3G

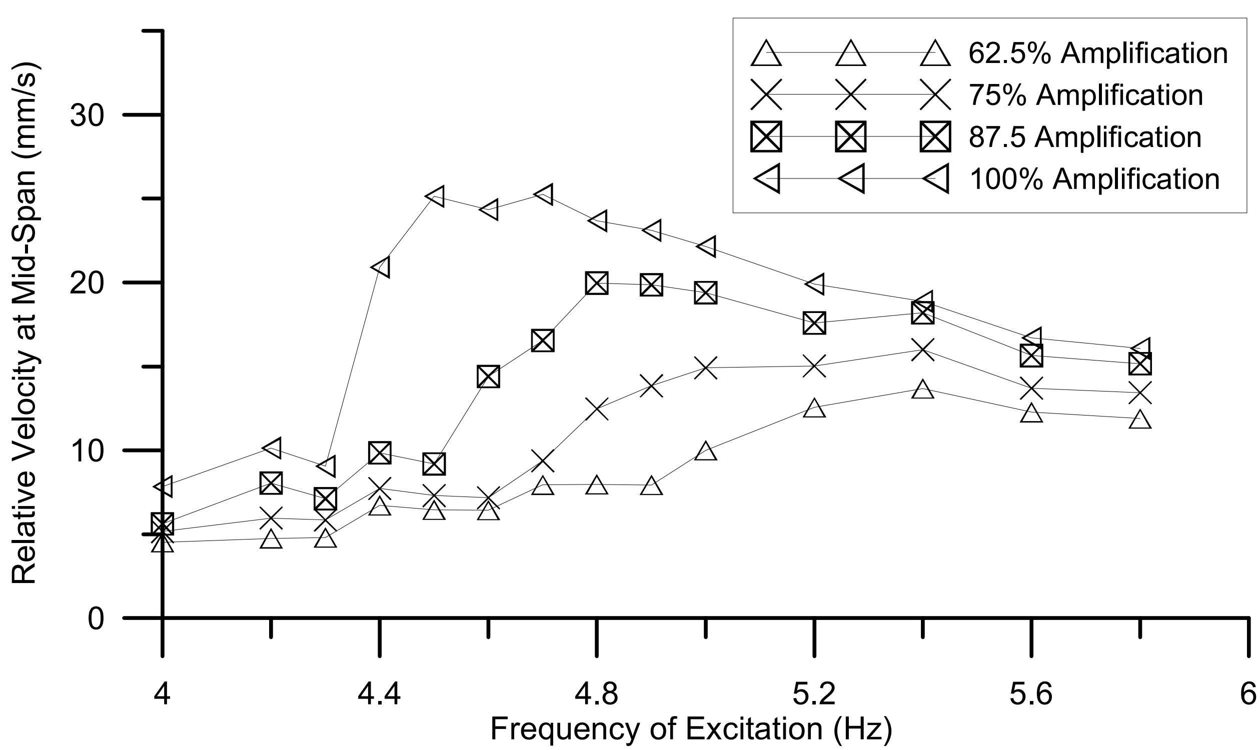

Figure D.6 – Sinesweep results for DIA10

APPENDIX E: TEST DATA

Table E.1 – DIA1 – list of testing protocols

BB		BF		SS1		SS2	
0	☑	5	☑	25	☑	5	☑
5	☑	5.2	☑	30	☑	7	☑
25	☑	5.4	☑	40	☑	10	☑
125	☑	5.6	☑	50	☑	100	☑
250	☑	5.8	☑	60	☑		
375	☑	6	☑	70	☑		
500	☑	6.2	☑	80	☑		
625	☑	6.4	☑	100	☑		
750	☑	6.6	☑	110	☑		
1000	☑	6.8	☑	120	☑		
1250	☑	7	☑	130	☑		
1500	☑	7.2	☑	140	☑		
1750	☑	7.4	☑	150	☑		
2000	☑	7.6	☑	160	☑		
2250	☑	7.8	☑				
2500	☑	8	☑				
2750	☑	8.2	☑				
3000	☑	8.4	☑				
3125	☑	8.6	☑				
		8.8	☑				
		9	☑				

Notes

- A frequency multiplier of 80% was used for SS2-80

	1	2	3	4	5	6	7	8	9	10	11	12	13	14	15	16	17	18	19	20	21	22	23	24	25
A																									
B	X						X						X						X						
C	X						X						X						X						
D	X	X	X	X	X	X	X	X	X	X	X	X	X	X	X	X	X	X	X	X	X	X	X	X	
E	X						X						X						X						
F	X						X						X						X						
G	X	X	X	X	X	X	X	X	X	X	X	X	X	X	X	X	X	X	X	X	X	X	X	X	
H	X						X						X						X						
I	X						X						X						X						
J	X	X	X	X	X	X	X	X	X	X	X	X	X	X	X	X	X	X	X	X	X	X	X	X	
K	X						X						X						X						
L	X						X						X						X						
M	X	X	X	X	X	X	X	X	X	X	X	X	X	X	X	X	X	X	X	X	X	X	X	X	
N	X						X						X						X						
O	X						X						X						X						
P	X	X	X	X	X	X	X	X	X	X	X	X	X	X	X	X	X	X	X	X	X	X	X	X	
Q	X						X						X						X						
R	X						X						X						X						
S	X	X	X	X	X	X	X	X	X	X	X	X	X	X	X	X	X	X	X	X	X	X	X	X	
T	X						X						X						X						
U	X						X						X						X						
V	X	X	X	X	X	X	X	X	X	X	X	X	X	X	X	X	X	X	X	X	X	X	X	X	
W	X						X						X						X						
X	X						X						X						X						
Y																									

O All nails X have bearing / slotting deformations

All screws X have bearing / slotting / tilting deformations

Nails in line 25 probably created bearing deformations in sheet below

Figure E.1 – DIA1 – record of fastener failure during inelastic test (1/3)

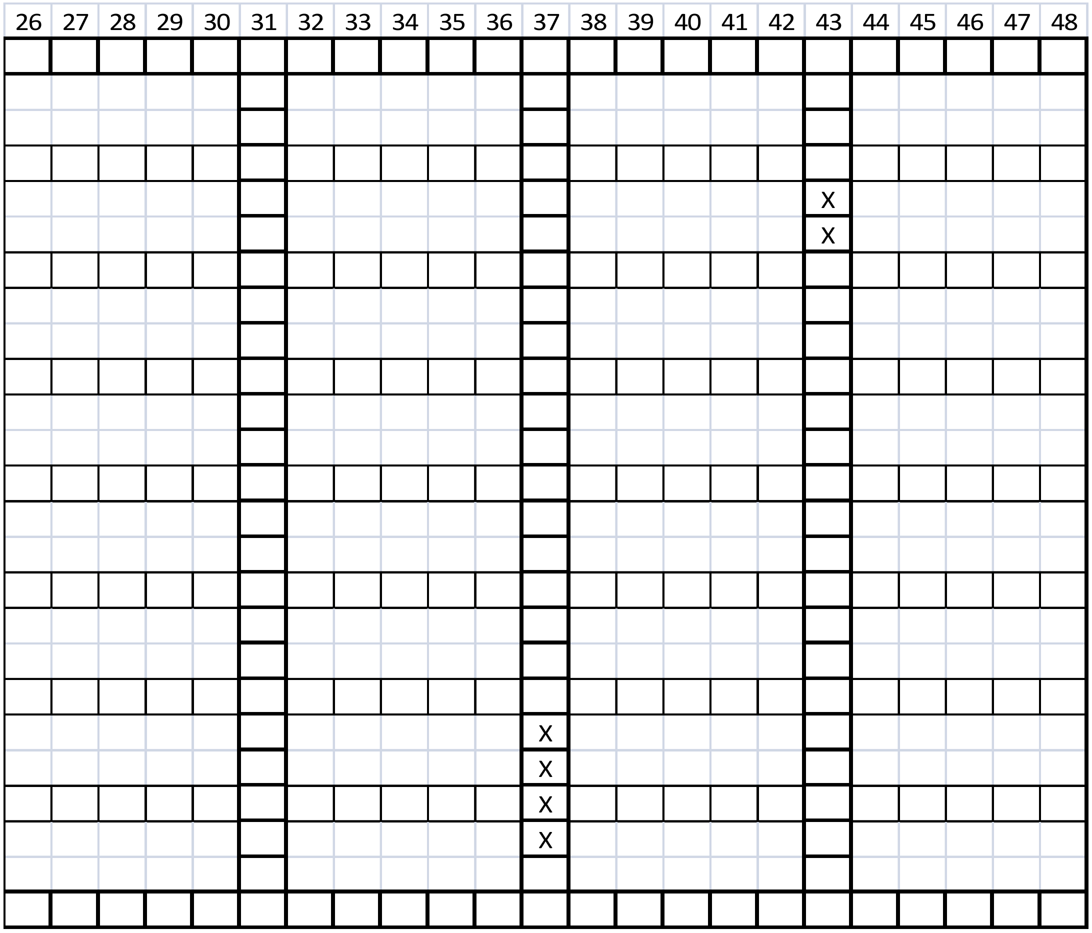

Figure E.2 – DIA1 – record of fastener failure during inelastic test (2/3)

49	50	51	52	53	54	55	56	57	58	59	60	61	62	63	64	65	66	67	68	69	70	71	72	73
X						X						X						X						X
X						X						X						X						X
X	X	X	X	X	X	X	X	X	X	X	X	X	X	X	X	X		X	X	X	X	X	X	X
X						X						X						X						X
X						X						O						X						X
X	X	X	X	X	X	X	X	X	X	X	X	X	X	X	X	X	X	X	X	X	X	X	X	X
X						X						X						X						X
X						X						X						X						X
X	X	X	X	X	X	X	X	X	X	X	X	X	X	X	X	X	X	X	X	X	X	X	X	X
X						X						X						X						X
						X						X						X						X
	X	X	X	X	X	X	X	X	X	X		X	X	X	X	X	X	X	X	X	X	X	X	X
X						X						X						X						X
X						X						X						X						X
X	X	X	X	X	X	X	X	X	X	X		X	X	X	X	X	X	X	X	X	X	X	X	X
						X						X						X						X
						X						X						X						X
X	X	X	X	X	X	X	X	X	X	X	X	X	X	X	X	X	X	X		X	X	X		X
						X						X						X						X
						X						X						X						X
X	X	X	X	X	X	X		X	X			X	X	X	X	X		X	X	X	X	X	X	X
						X						X						X						X
						X						X						X						X

Figure E.3 – DIA1 – record of fastener failure during inelastic test (3/3)

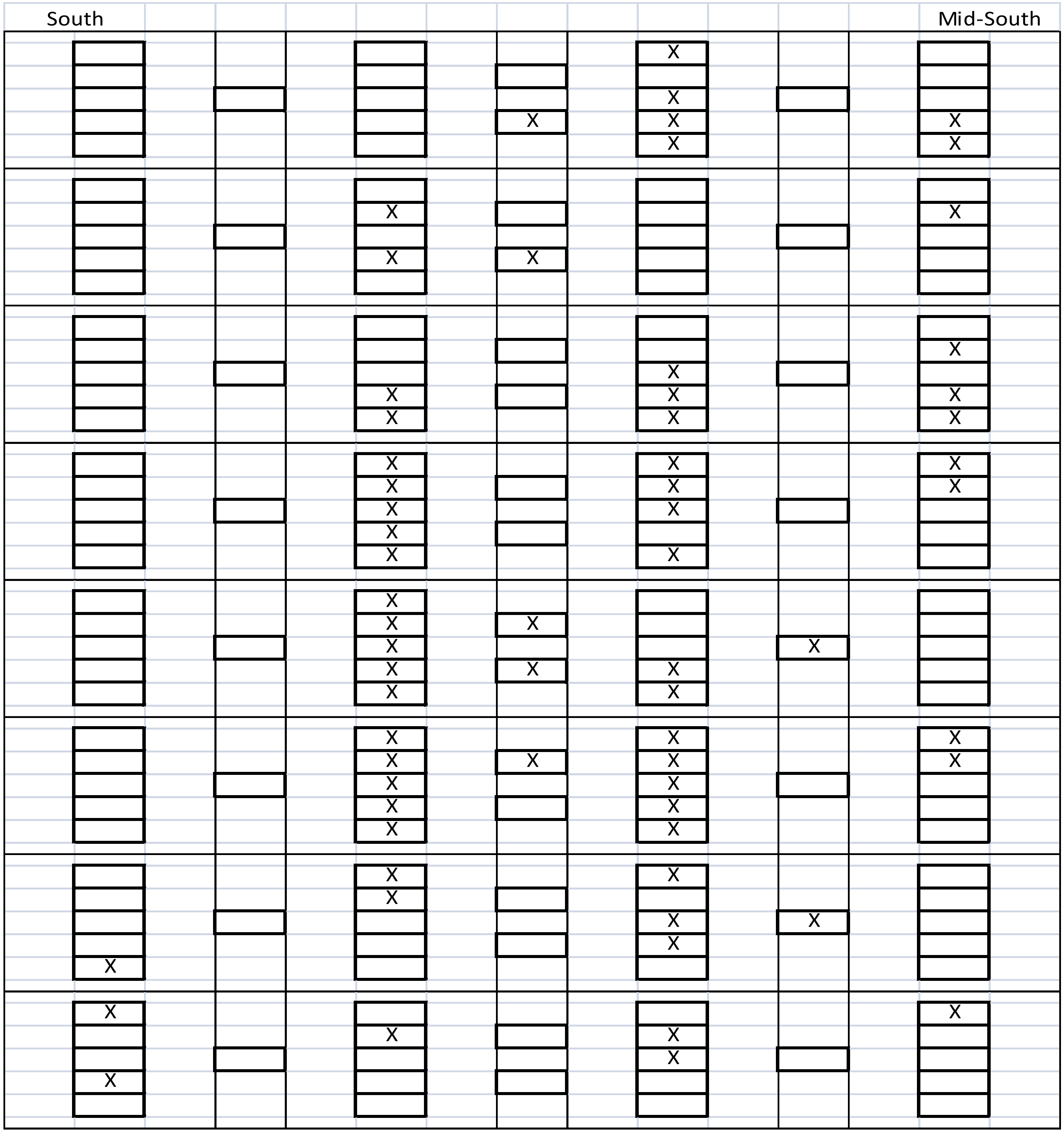

Figure E.4 – DIA1 – steel mass loss during inelastic test (1/3)

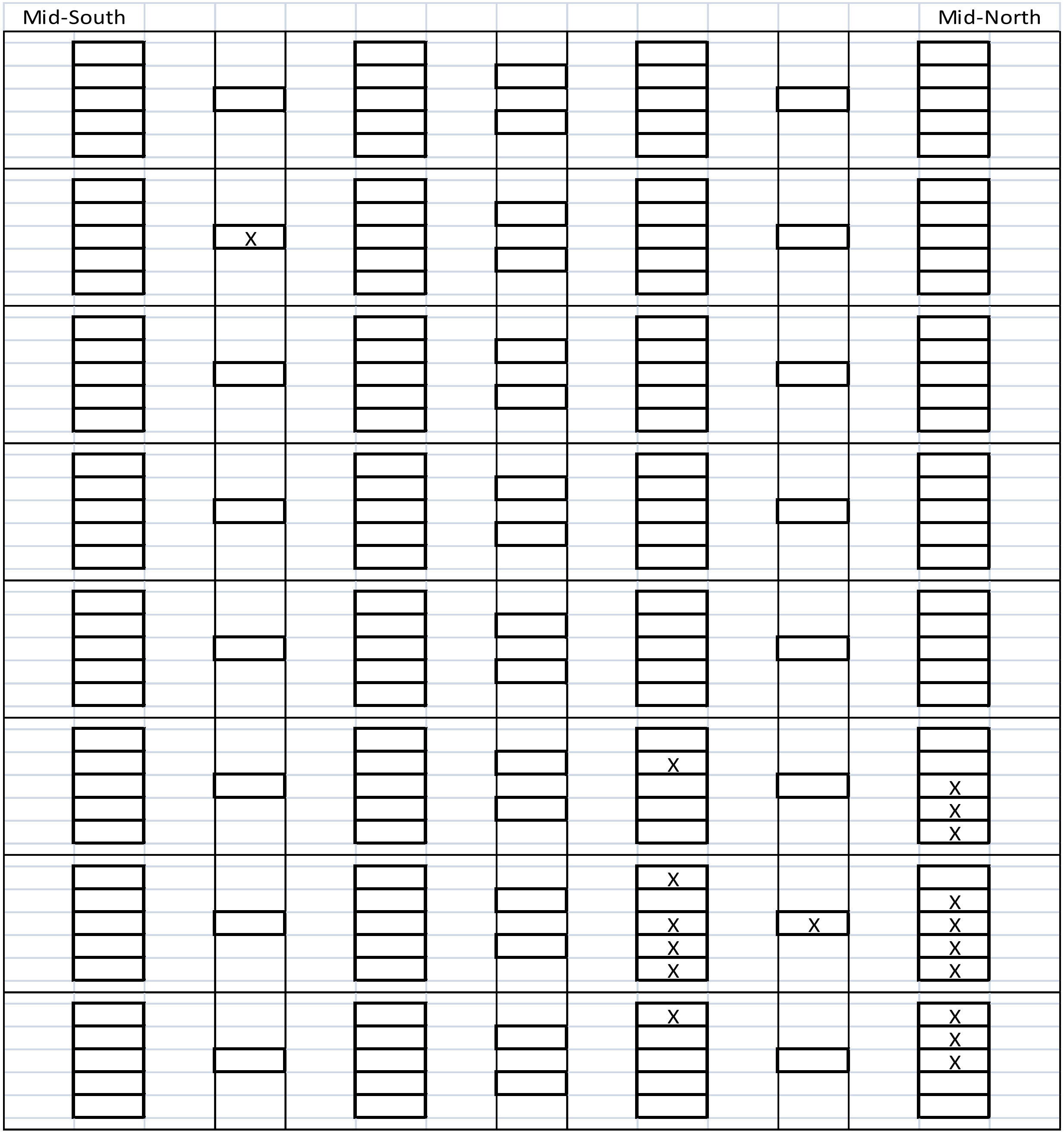

Figure E.5 – DIA1 – steel mass loss during inelastic test (2/3)

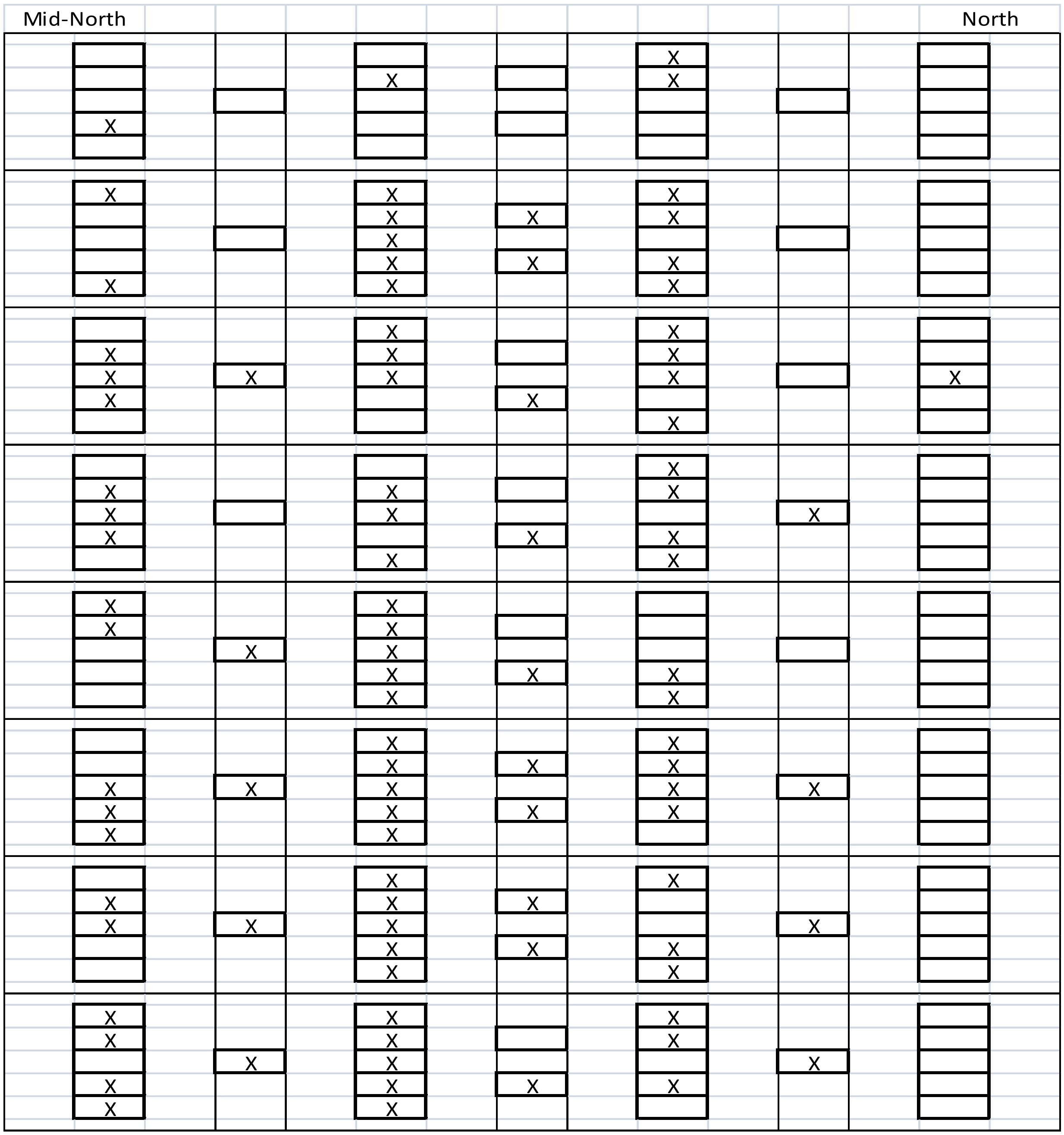

Figure E.6 – DIA1 – steel mass loss during inelastic test (3/3)

Table E.2 – DIA1R – list of testing protocols

BB		BF		SS1		SS2	
0	☑	3	☑	25	☑	5	☑
5	☑	3.2	☑	40	☑	80	☑
25	☑	3.4	☑	80	☑		
125	☑	3.6	☑	120	☑		
375	☑	3.8	☑	140	☑		
625	☑	4	☑	160	☑		
1500	☑	4.2	☑				
3125	☑	4.4	☑				
		4.6	☑				
		4.8	☑				
		4.9	☑				
		5	☑				
		5.1	☑				
		5.2	☑				
		5.4	☑				
		5.6	☑				
		5.8	☑				
		6	☑				
		6.2	☑				
		6.4	☑				
		6.6	☑				
		6.8	☑				

Notes

- A frequency multiplier of 80% was used for SS2-80

Table E.3 – DIA2 – list of testing protocols

BB	
0	☑
5	☑
25	☑
125	☑
375	☑
625	☑
1500	☑
3125	☑

BF	
2	☑
2.2	☑
2.4	☑
2.6	☑
2.8	☑
3	☑
3.2	☑
3.4	☑
3.6	☑
3.8	☑
4	☑
4.2	☑
4.4	☑
4.6	☑
4.8	☑
5	☑
5.2	☑
5.4	☑
5.6	☑
5.8	☑
6	☑
6.2	☑
6.4	☑
6.6	☑
6.8	☑
7	☑

SS1	
25	☑
40	☑
80	☑
120	☑
140	☑
160	☑

SS3	
5	☑
80	☑

Notes

- A frequency multiplier of 80% was used for SS2-80

	1	2	3	4	5	6	7	8	9	10	11	12	13	14	15	16	17	18	19	20	21	22	23	24	25
A																									
B	X						X						X						X						
C	X						X						X						X						
D	X			X	X	X	X	X	X	X	X		X	X	X	X	X	X	X	X	X	X	X	X	
E	X						X						X						X						
F	X						X						X						X						
G	X	X	X	X	X	X	X	X	X	X	X	X		X	X	X	X	X		X	X	X	X	X	
H	X						X						X						X						
I	X						X						X						X						
J	O	X	X	X	X	X	X	X	X	X	X	X	X	X	X	X	X	X	X	X	X	X	X	X	
K	X						X						X						X						
L	X						X						X						X						
M	O	X	X	X	X	X	X	X	X	X	X	X	X	X	X	X	X	X	X	X	X	X	X	X	
N	X						X						X						X						
O	X						X						X						X						
P	X	X	X	X	X	X	X	X	X	X	X	X	X	X	X	X	X	X	X	X	X	X	X	X	
Q	X						X						X						X						
R	X						X						X						X						
S	O	X	X	X	X	X	X	X	X	X	X	X	X	X	X	X	X	X	X	X	X	X	X	X	
T	X						X						X						X						
U	X						X						X						X						
V	X		X	X	X	X	X	X	X	X	X	X	X	X	X	X	X	X	X	X	X	X	X	X	
W	X						X						X						X						
X	X						X						X						X						
Y																									

O Nail shear or pullout

Bearing damage in sheet most pronounced at sidelap locations.

Between sidelaps bearing damage was much less

Towards centre of specimen, bearing damage decreased

Figure E.7 – DIA2 – record of fastener failure during inelastic test (1/3)

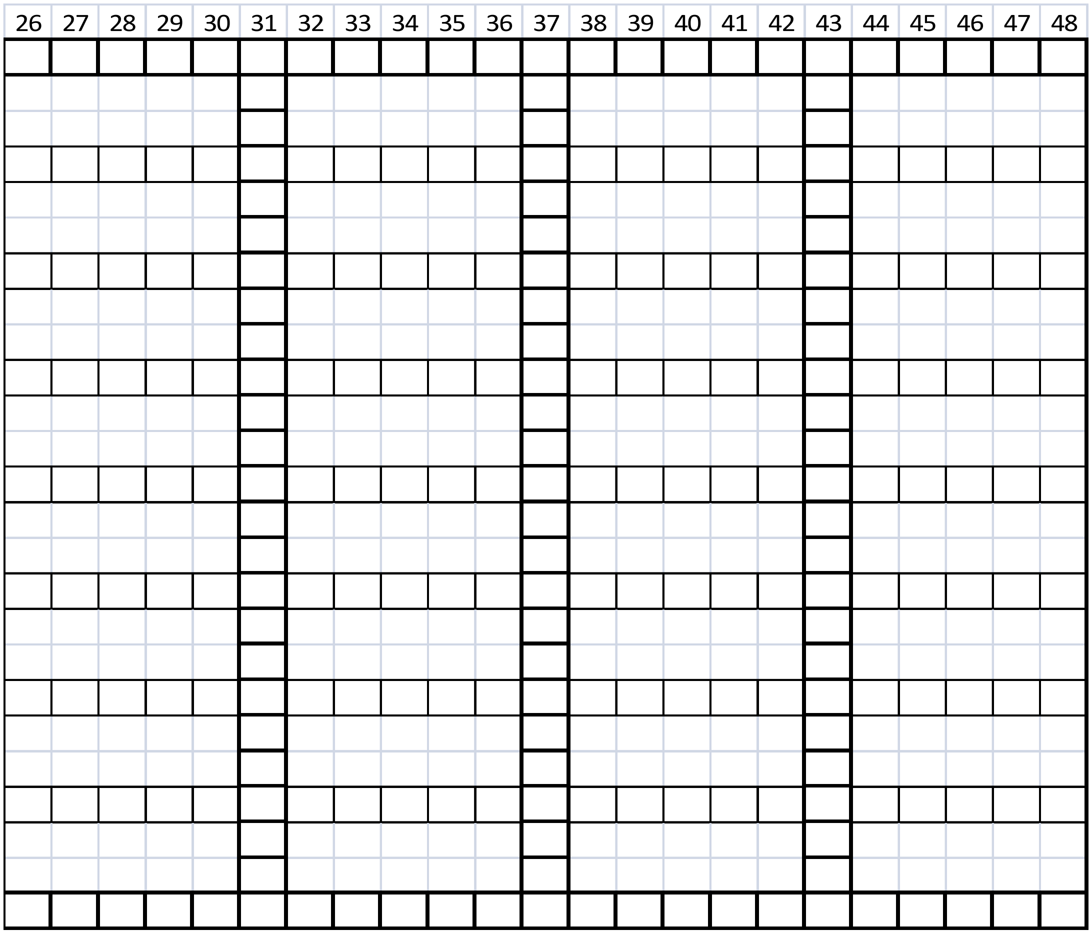

Figure E.8 – DIA2 – record of fastener failure during inelastic test (2/3)

49	50	51	52	53	54	55	56	57	58	59	60	61	62	63	64	65	66	67	68	69	70	71	72	73
X						X						X						X						X
X						X						X						X						X
X	X	X	X	X	X	X	X	X	X	X	X	X	X	X	X	X		X	X	X	X	X	X	X
X						X						X						X						X
X						X						O						X						X
X	X	X	X	X	X	X	X	X	X	X	X	X	X	X	X	X	X	X	X	X	X	X	X	X
X						X						X						X						X
X						X						X						X						X
X	X	X	X	X	X	X	X	X	X	X	X	X	X	X	X	X	X	X	X	X	X	X	X	X
X						X						X						X						X
X						X						X						X						X
X	X	X	X	X	X	X	X	X	X	X	X	X	X	X	X	X	X	X	X	X	X	X	X	X
X						X						X						X						X
X						X						X						X						X
X	X	X	X	X	X	X	X	X	X	X	X	X	X	X	X	X	X	X	X	X	X	X	X	X
X						X						X						X						X
X						X						X						X						X
X	X	X	X	X	X	X	X	X	X	X	X	X	X	X	X	X	X	X	X	X	X	X	X	X
X						X						X						X						X
X						X						X						X						X
X	X	X	X	X	X	X	X	X	X	X	X	X	X	X	X	X	X	X	X	X	X	X	X	X
X						X						X						X						X
X						X						X						X						X

Figure E.9 – DIA2 – record of fastener failure during inelastic test (3/3)

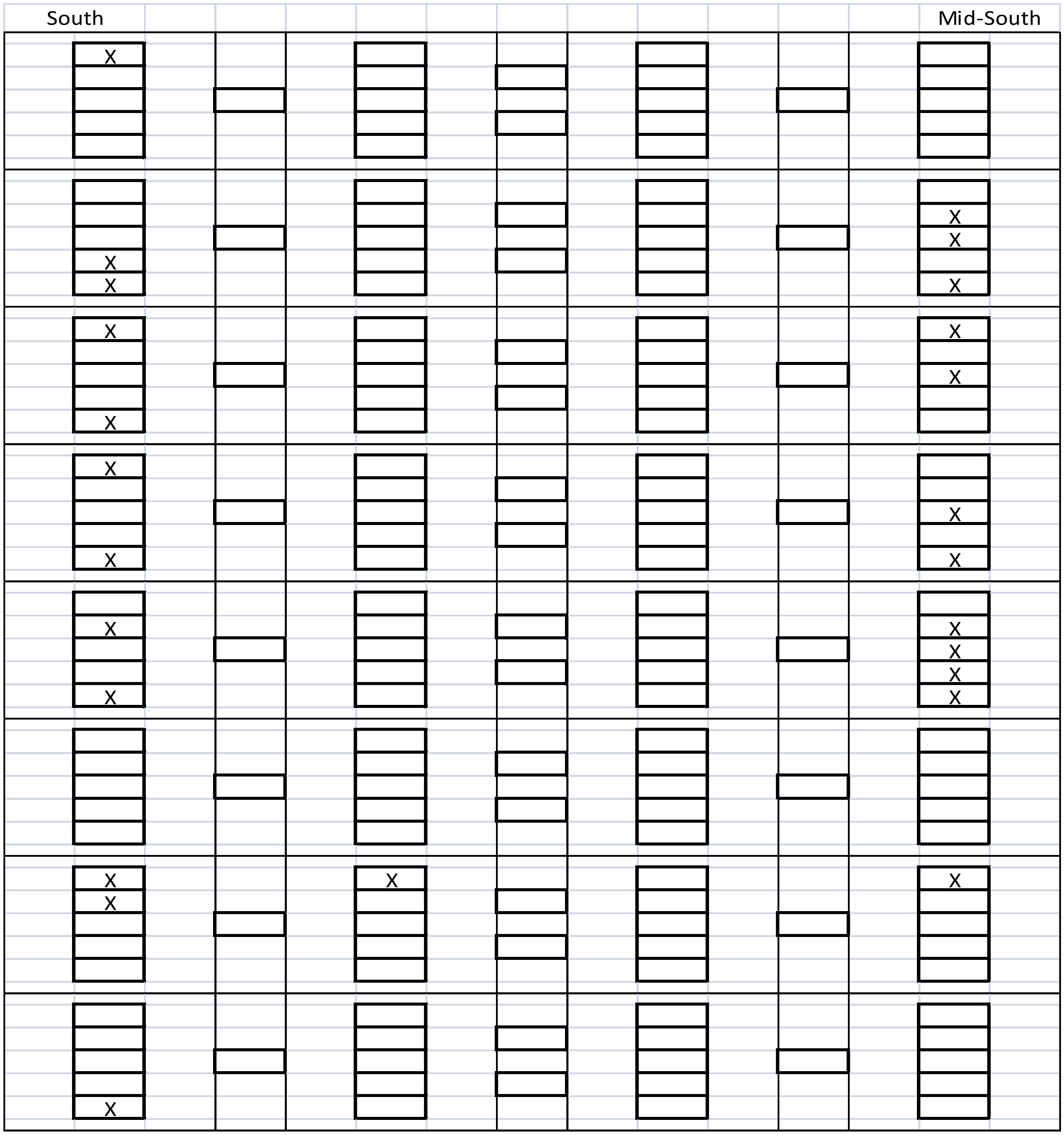

Figure E.10 – DIA2 – steel mass loss during inelastic test (1/3)

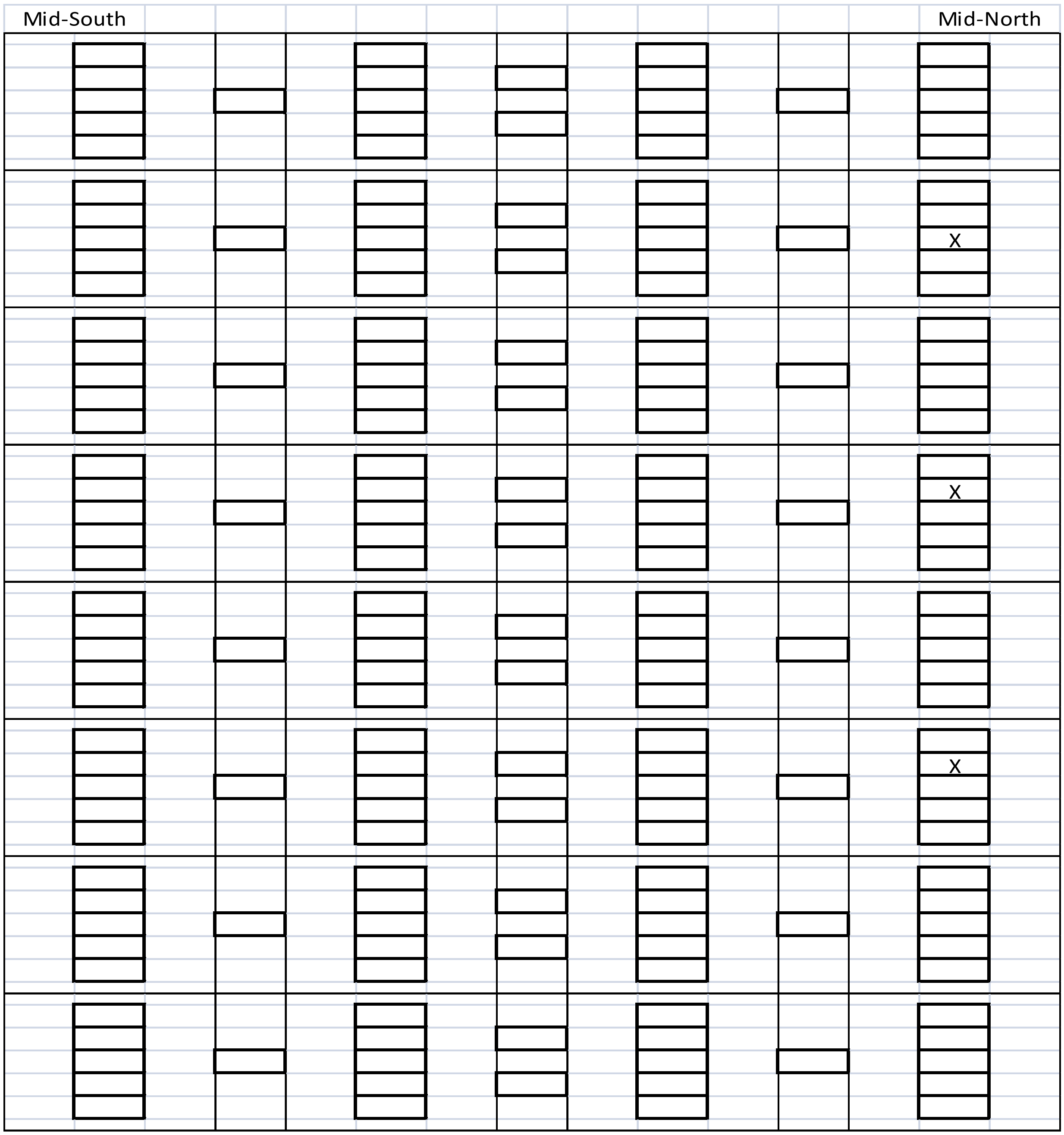

Figure E.11 – DIA2 – steel mass loss during inelastic test (2/3)

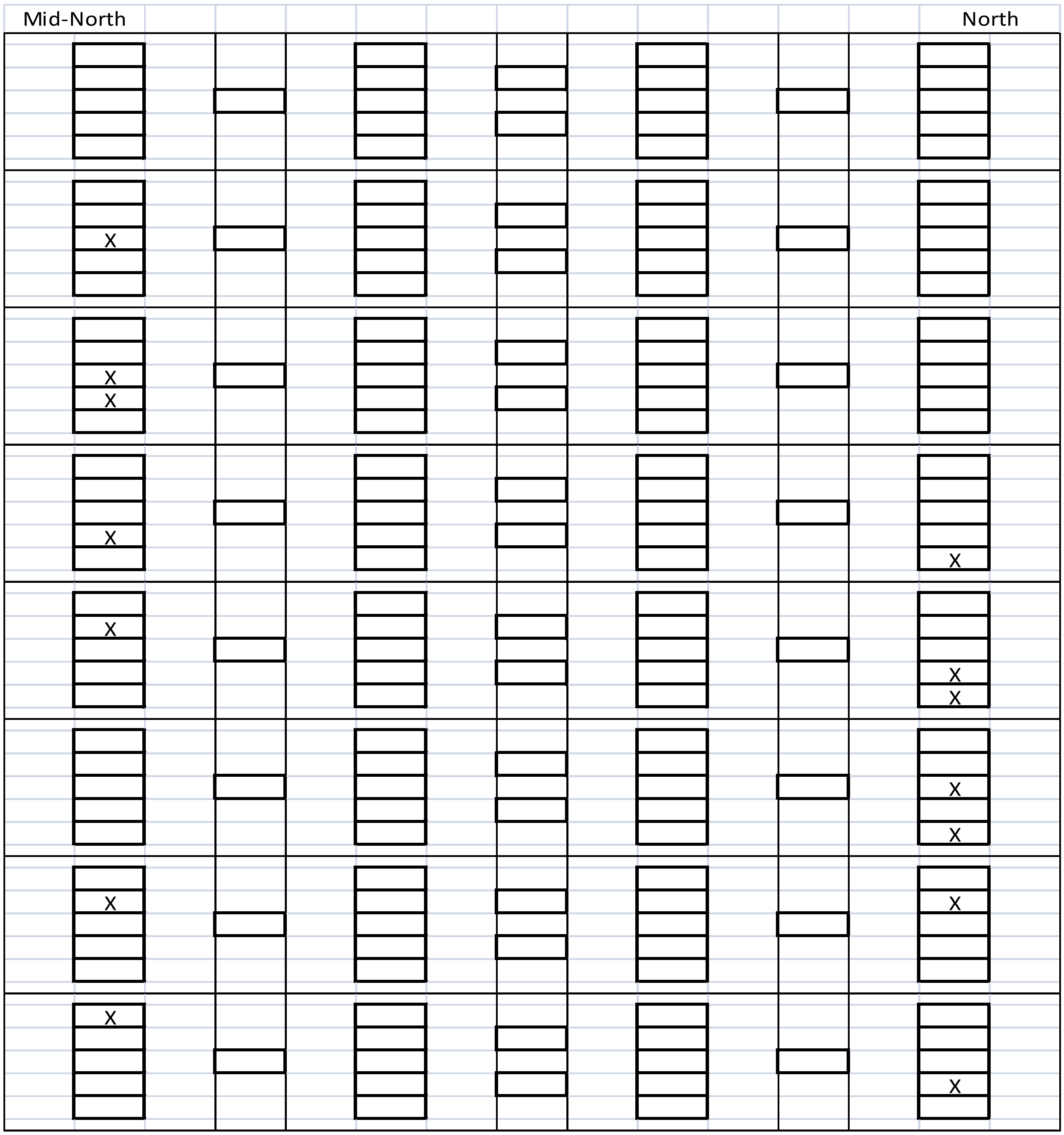

Figure E.12 – DIA2 – steel mass loss during inelastic test (3/3)

Table E.4 – DIA3 – list of testing protocols

BB		BF		SS3		SS1		SS3	
0	☑	4.6	☑	50	☑	50	☑	5	☑
10	☑	4.8	☑	60	☑	60	☑	10	☑
50	☑	5	☑	70	☑	70	☑	2000	☑
225	☑	5.2	☑	80	☑	80	☑		
450	☑	5.4	☑	90	☑	90	☑		
650	☑	5.5	☑	100	☑				
875	☑	5.6	☑	110	☑				
1100	☑	5.7	☑	120	☑				
1325	☑	5.8	☑	130	☑				
1750	☑	5.9	☑	140	☑				
2200	☑	6	☑	150	☑				
2625	☑	6.2	☑	160	☑				
3075	☑	6.4	☑	170	☑				
3500	☑	6.6	☑	180	☑				
4825	☑			190	☑				
5275	☑			200	☑				
5475	☑								
7000	☑								
8000	☑								
9000	☑								
10000	☑								
20000	☑								
30000	☑								

<u>Notes</u>

- Big actuator valves used for SS1-200 and SS1-80 and all larger amplitudes for those two loading protocols
- Maximum acceleration used for the sinesweep protocol (BF) is 358.267 mm/s^2

	1	2	3	4	5	6	7	8	9	10	11	12	13	14	15	16	17	18	19	20	21	22	23	24	25	26	27	28	29	30	31	32	33	34	35	36	37
A																																					
B																																					
C													X												X												
D	O																																				
E	O												O												O												
F	O																																				
G	X	X	X	X	X	X	X	X	X	X	X	X	O	X	X	X	X	X	X	X	X	X	X	X	O	X	X	X	X	X	X	X	X	X	X	X	
H																																					
I																																					
J																																					
K																																					O
L																																					
M	O	O	O	O	O	O	O	O	O	O	O	O	O	O	O	O	O	O	O	O	O	X	O	O		O	O	O	O	O	O	O	O	O	O	O	
N																																					
O													O																								O
P																																					
Q																									X												
R																																					
S	O	O	O	O	O	O	O	O	O	O	O	O	X	O	O	O	O	O	O	O	O	O	O	O	O	O											
T	O																																				
U	O												O												O												O
V	O																																				
W	O												O												X												O
X	O																																				
Y	O	X	X	X	X	X	X	X	X	X	X	X	O	X	X	X	X	X	X	X	X	X	X	X	X	X	X	X	X	X	X	X	X	X	X	X	O
Z	O																																				
AA	O												O												X												O
AB	O																																				
AC																																					O
AD																																					
AE	O	O	O	O	O	O	O	O	O	O	O	O	O	O	O	O	O	O	O	O	O	O	O	O	O	O	O	O	O	O	O	O	O	O	O	O	X
AF																																					
AG																																					
AH																																					
AI																																					
AJ																																					
AK	O	O	O	O	O	O	O	O	O	O	O	O	O	O	O	O	O	O	O	O	O	O	O	O	O	O	O	O	O	O	O	O	O	O	O	O	
AL																																					
AM																									O												
AN																																					
AO	O												O												O												
AP	O																																				
AQ	O	X	X	X	X	X	X	X	X	X	X	X	O	X	X	X	X	X	X	X	X	X	X	X	O	X	X	X	X	X	X	X	X	X	X	X	O
AR	O																																				
AS	O																																				
AT	O																																				
AU																																					
AV	X																																				
AW	O																																				

Figure E.13 – DIA3 – record of fastener failure during inelastic test (1/4)

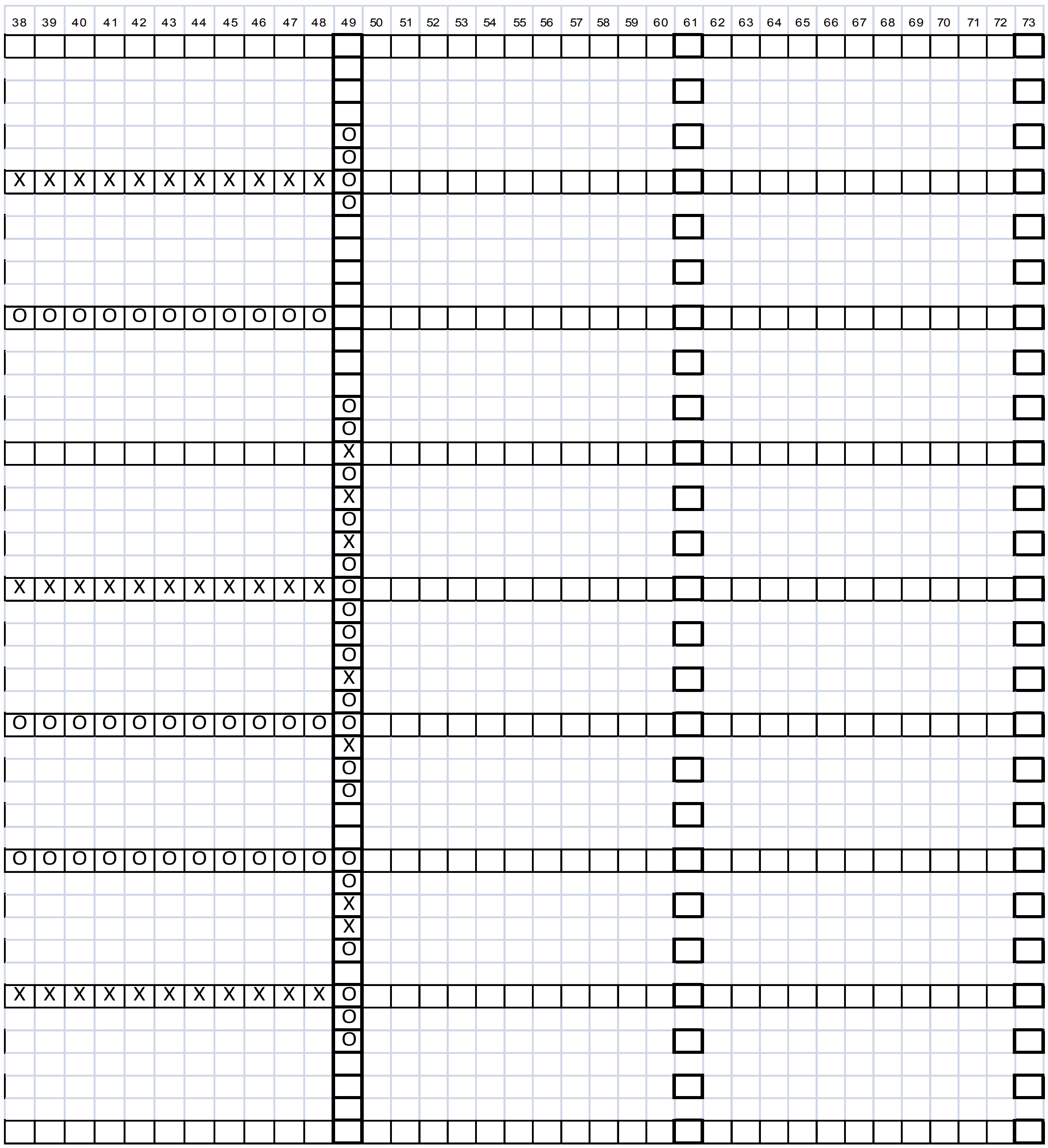

Figure E.14 – DIA3 – record of fastener failure during inelastic test (2/4)

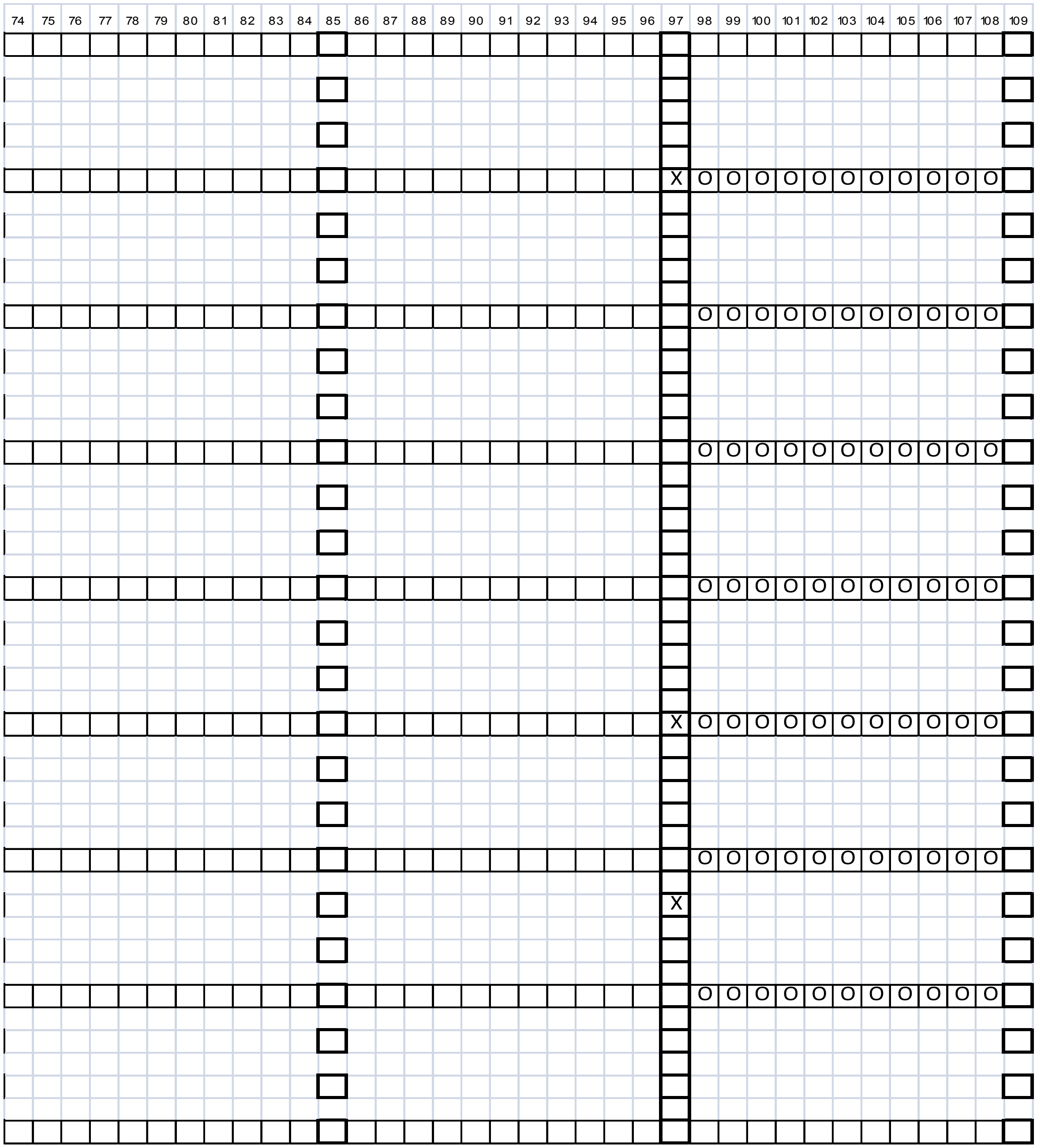

Figure E.15 – DIA3 – record of fastener failure during inelastic test (3/4)

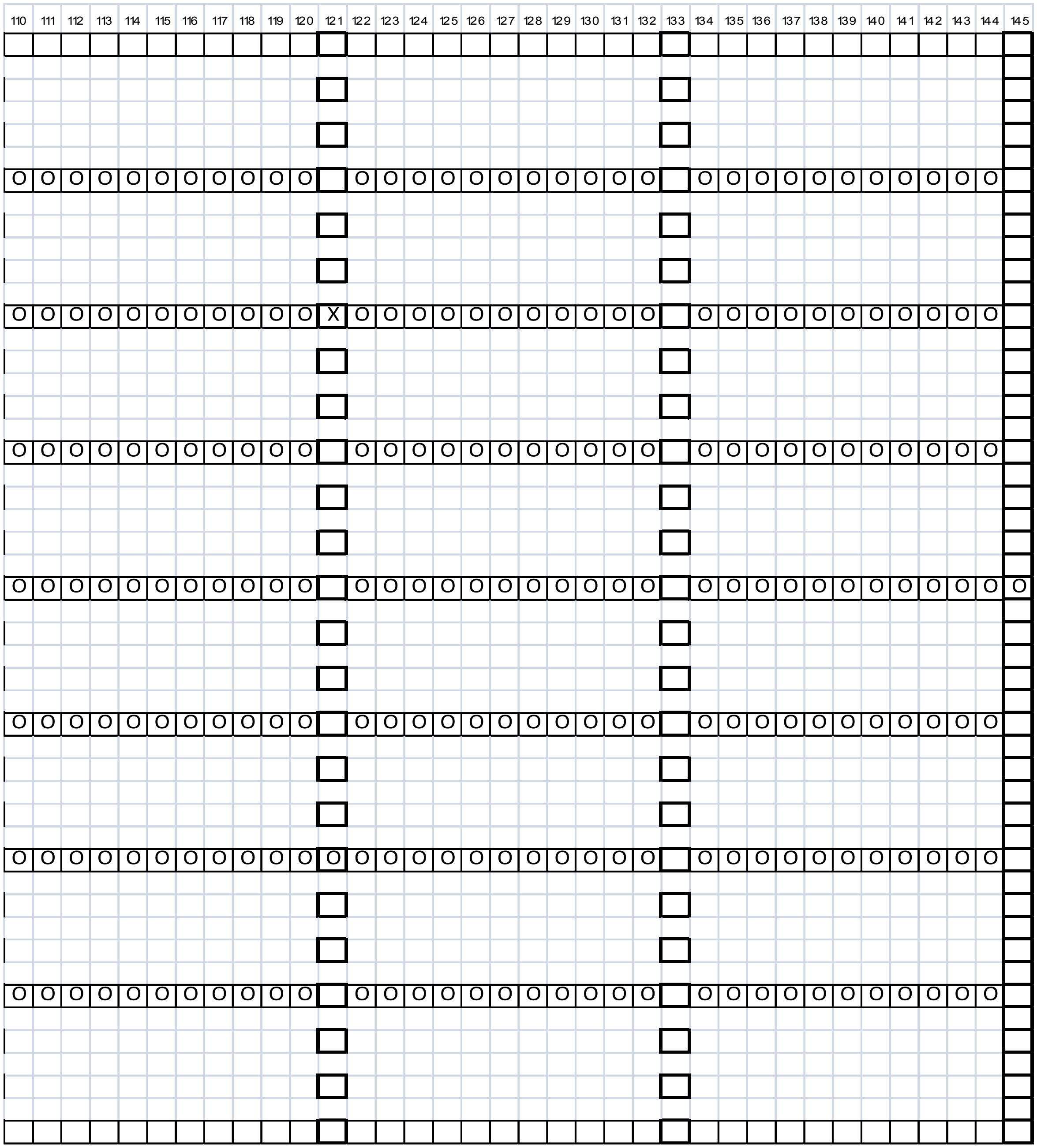

Figure E.16 – DIA3 – record of fastener failure during inelastic test (4/4)

Table E.5 – DIA3G – list of testing protocols

BB		BF		SS3		SS1	
0	☑	4	☑	50	☑	50	☑
10	☑	4.2	☑	60	☑	60	☑
50	☑	4.4	☑	70	☑	70	☑
225	☑	4.6	☑	80	☑	80	☑
450	☑	4.8	☑	90	☑	90	☑
650	☑	5	☑	100	☑	100	☑
875	☑	5.1	☑	110	☑	110	☑
1100	☑	5.2	☑	120	☑	120	☑
1325	☑	5.3	☑	130	☑	130	☑
1750	☑	5.4	☑	140	☑		
2200	☑	5.5	☑	150	☑		
2625	☑	5.6	☑	160	☑		
3075	☑	5.7	☑	170	☑		
3500	☑	5.8	☑	180	☑		
4825	☑	5.9	☑	190	☑		
5275	☑	6	☑	200	☑		
5475	☑	6.2	☑	210	☑		
6000	☑	6.4	☑	220	☑		
6500	☑	6.6	☑	230	☑		
		6.8	☑	240	☑		
		7	☑				

<u>Notes</u>

- Big actuator valves used for SS1-200 and SS1-80 and all larger amplitudes for those two loading protocols
- Maximum acceleration used for the sinesweep protocol (BF) is 716 mm/s^2

Table E.6 – DIA3R – list of testing protocols

BB	
0	☑
225	☑
475	☑
675	☑
900	☑
1375	☑
2275	☑
3200	☑
5025	☑
5475	☑
6000	☑
7000	☑
8000	☑
9000	☑
10000	☑

BF	
6	☑
6.2	☑
6.4	☑
6.6	☑
6.8	☑
7	☑

SS3	
50	☑
60	☑
70	☑
80	☑
90	☑
100	☑
110	☑
120	☑
130	☑
140	☑
150	☑
160	☑
170	☑
180	☑
190	☑
200	☑
210	☑

SS1	
50	☑
60	☑
70	☑
80	☑
90	☑
100	☑

SS3	
5	☑
10	☑
2000	☑

<u>Notes</u>

- Big actuator valves used for SS1-200 and SS1-80 and all larger amplitudes for those two loading protocols
- Maximum acceleration used for the sinesweep protocol (BF) is 289.988 mm/s^2

	1	2	3	4	5	6	7	8	9	10	11	12	13	14	15	16	17	18	19	20	21	22	23	24	25
A																									
B																									
C	O																								
D	O																								
E	O												O												O
F	O												O												O
G	O	X	X	X	X	X	X	X	X	X	X	X	O	X	X	X	X	X	X	X	X	X	X	X	O
H	O												O												
I	O												O												
J	O																								
K																									
L													O												
M	O	O	O	O	O	O	O	O	O	O	O	O		O	O	O	O	O	O	O	O	O	O	O	
N													O												
O																									
P																									
Q																									O
R													O												O
S	O	O	O	O	O	O	O	O	O	O	O	O	O	O	O	O	O	O	O	O	O	O	O	O	O
T	O												O												
U	O																								
V	O																								X
W	O												O												O
X	O												O												O
Y	O	X	X	X	X	X	X	X	X	X	X	X	O	X	X	X	X	X	X	X	X	X	X	X	O
Z	O												O												O
AA	O												O												
AB																									
AC																									
AD																									
AE				O	O	O	O	O	O	O	O	O	O	O	O	O	O	O	O	O	O	O	O	O	O
AF																									
AG																									
AH																									
AI	O																								
AJ																									O
AK	O	O	O	O	O	O	O	O	O	O	O	O	O	O	O	O	O	O	O		O	O	O	O	O
AL																									
AM																									
AN	O																								
AO	O												O												O
AP	O												O												O
AQ	O	X	X	X	X	X	X	X	X	X	X	X	O	X	X	X	X	X	X	X	X	X	X	X	O
AR	O												O												O
AS	O																								
AT	O																								
AU	O																								
AV	O																								
AW	O																								

Figure E.17 – DIA3R – record of fastener failure during inelastic test (1/5)

26	27	28	29	30	31	32	33	34	35	36	37	38	39	40	41	42	43	44	45	46	47	48	49
											O												
											O												O
X	X	X	X	X	X	X	X	X	X	X	O	X	X	X	X	X	X	X	X	X	X	X	O
											O												O
											O												O
																							O
											O												
O	O	O	O	O	O	O	O	O	O	O	O	O	O	O			O	O	O	O	O	O	
											O												
																							O
																							O
O	O		O	O	O	O	O	O	O	O		O	O	O	O	X	X	X	X	X	X	X	X
											O												
											O												
																							O
																							O
											O												O
X	X	X	X	X	X	X	X	X	X	X	O	X	X	X	X	X	X	X	X	X	X	X	O
											O												O
											O												O
																							O
																							X
											O												O
O	O	O	O	O	O	O	O	O	O	O		O	O		O	O	O		O	O	O	O	O
																							X
																							O
																							O
O			O	O					O		O	O	O	O	O				O	O	O	O	O
																							O
																							X
																							X
																							O
																							O
X	X	X	X	X	X	X	X	X	X	X	O	X	X	X	X	X	X	X	X	X	X	X	O
											O												O
																							O

Figure E.18 – DIA3R – record of fastener failure during inelastic test (2/5)

50	51	52	53	54	55	56	57	58	59	60	61	62	63	64	65	66	67	68	69	70	71	72	73

Figure E.19 – DIA3R – record of fastener failure during inelastic test (3/5)

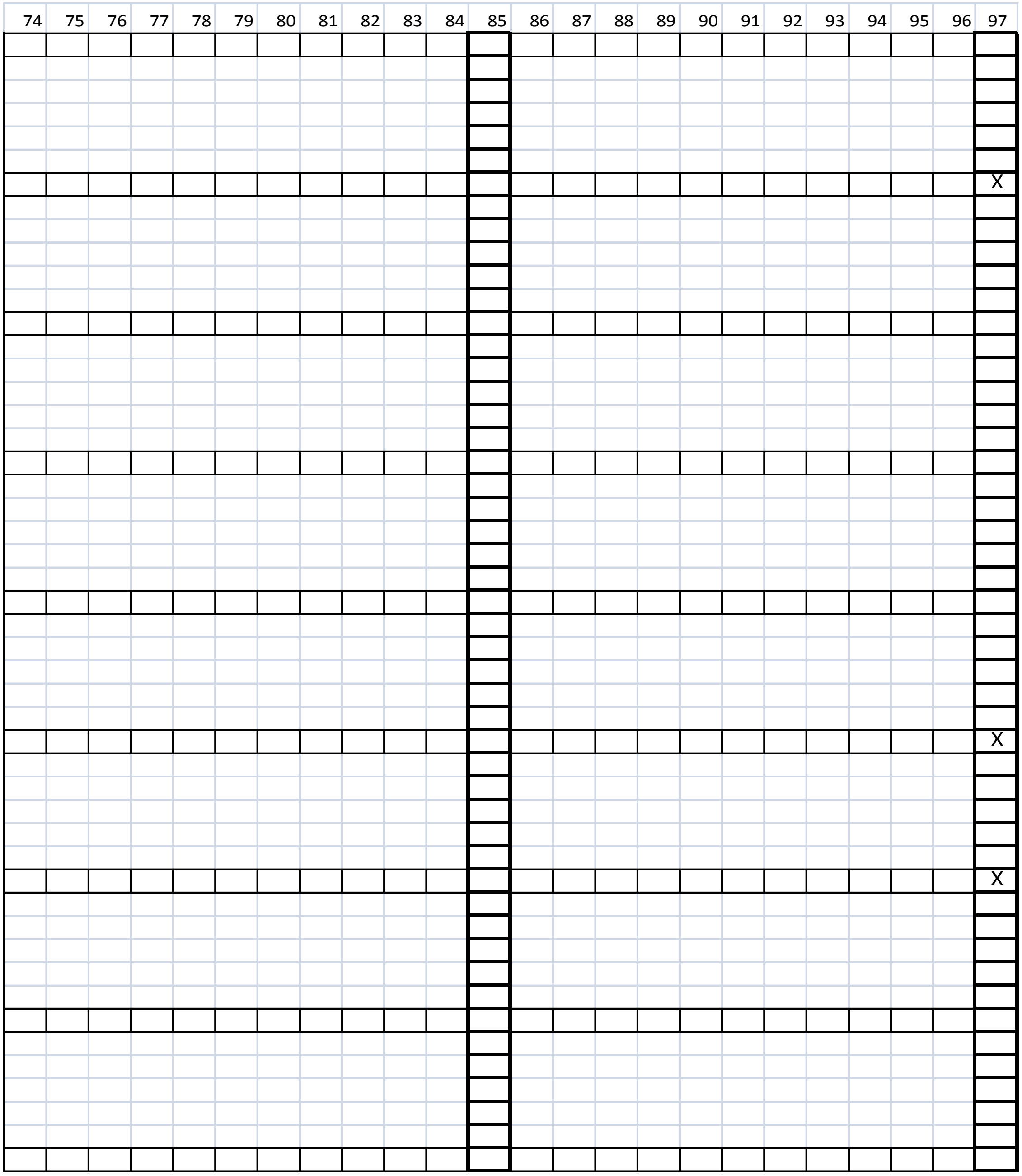

Figure E.20 – DIA3R – record of fastener failure during inelastic test (4/5)

98	99	100	101	102	103	104	105	106	107	108	109	110	111	112	113	114	115	116	117	118	119	120	121
X																							
																O	O	O	O	O	O	O	
			O															O	O	O	O	O	
														O	O	O	O	O	O	O	O	O	
															O	O	O	O	O	O	O	O	
																	O	O	O	O	O	O	O
															O	O	O	O	O	O	O	O	

Figure E.21 – DIA3R – record of fastener failure during inelastic test (5/5)

Table E.7 – DIA4 – list of testing protocols

BB		BF		SS3		SS1		SS2	
0	☑	5.6	☑	50	☑	50	☑	5	☑
225	☑	5.8	☑	60	☑	60	☑	10	☑
475	☑	6	☑	70	☑	70	☑	80	☑
675	☑	6.2	☑	80	☑	80	☑		
900	☑	6.4	☑	90	☑	90	☑		
1375	☑	6.6	☑	100	☑	100	☑		
2275	☑	6.7	☑	110	☑				
3200	☑	6.8	☑	120	☑				
5025	☑	6.9	☑	130	☑				
5475	☑	7	☑	140	☑				
6000	☑	7.2	☑	150	☑				
7000	☑	7.4	☑	160	☑				
8000	☑			170	☑				
9000	☑			180	☑				
10000	☑			190	☑				
20000	☑			200	☑				
30000	☑			210	☑				
40000	☑								
50000	☑								
60000	☑								
70000	☑								
100000	☑								
200000	☑								
300000	☑								

Notes

- Big actuator valves used for SS1-190 and SS1-80 and all larger amplitudes for those two loading protocols
- Maximum acceleration used for the sinesweep protocol (BF) is 289.988 mm/s^2

	1	2	3	4	5	6	7	8	9	10	11	12	13	14	15	16	17	18	19	20	21	22	23	24	25
A																									
B																									X
C																									
D																									
E	O																								
F	O																								
G	O	X	X	X	X	X	X	X	X	X	X	X		O	O	O	O	O	O	O	O	O	O	O	
H	O																								
I	O																								
J																									
K																									
L																									
M	O	O	O	O	O	O	O	O		O	O	O		O	O	O	O	O	O	O	O		O	O	
N																									
O																									
P																									
Q	O																								
R	O																								
S	O	X	X	X	X	X	X	X	X	X	X	X		X	X	X	X	X	X	O	O	O	O	O	
T																									
U																									
V																									
W	O																								
X	O																								
Y	O	O	O	O	O	O	O	O	O	O	O	O	X	O	O	O	O				O		O	O	O
Z																									
AA																									
AB																									
AC																									
AD																									
AE	O	O	O	O	O	O	O	O	O	O	O	O	X	O	O	O	O	O	O	O	O	O	O	O	
AF	O																								
AG																									
AH																									
AI																									
AJ													O												
AK	O	O	O	O	O	O	O	O	O	O	O	O		O	O	O	O	O	O	O	O	O	O	O	
AL	O																								
AM													O												
AN																									
AO																									
AP	O																								
AQ	X	X	X	X	X	X	X	X	X	X	X	X	O	O	O	O	O	O	O	O	O	O	O	O	
AR	O																								
AS	O																								
AT																									
AU																									
AV																									
AW																									

Figure E.22 – DIA4 – record of fastener failure during inelastic test (1/6)

26	27	28	29	30	31	32	33	34	35	36	37	38	39	40	41	42	43	44	45	46	47	48	49
											O												
X	O	O	O	O	O	O	O	O	O	O		X	O	O	X	O	O	O	O	O	O	O	O
											X												
											O												
O	O	O	O			O	O	O	O	O	O				O	O	O	O	O	O	O	O	
											O												
											O												
																							X
O	O		O	O	O	O	O	O	O	O		O	O	O	O	O	O	O	O	O	O	O	
											O												
	O	O	O	O	O	O	O	O	O	O		O	O	O	O	O	O	O	O	O	O	O	
O	O	O	O	O	O	O	O	O	O	O		O	O	O	O	O	O	O	O	O	O	O	
O	O	O	O	O	O	O	O	O	O	O			O	O	O	O	O	O	O	O	O		X
																							X
																							X
X	O	O	X	O	O	O	O	O	O	O		X	X	O	O	O		O	O	O	O	O	

Figure E.23 – DIA4 – record of fastener failure during inelastic test (2/6)

50	51	52	53	54	55	56	57	58	59	60	61	62	63	64	65	66	67	68	69	70	71	72	73

Figure E.24 – DIA4 – record of fastener failure during inelastic test (3/6)

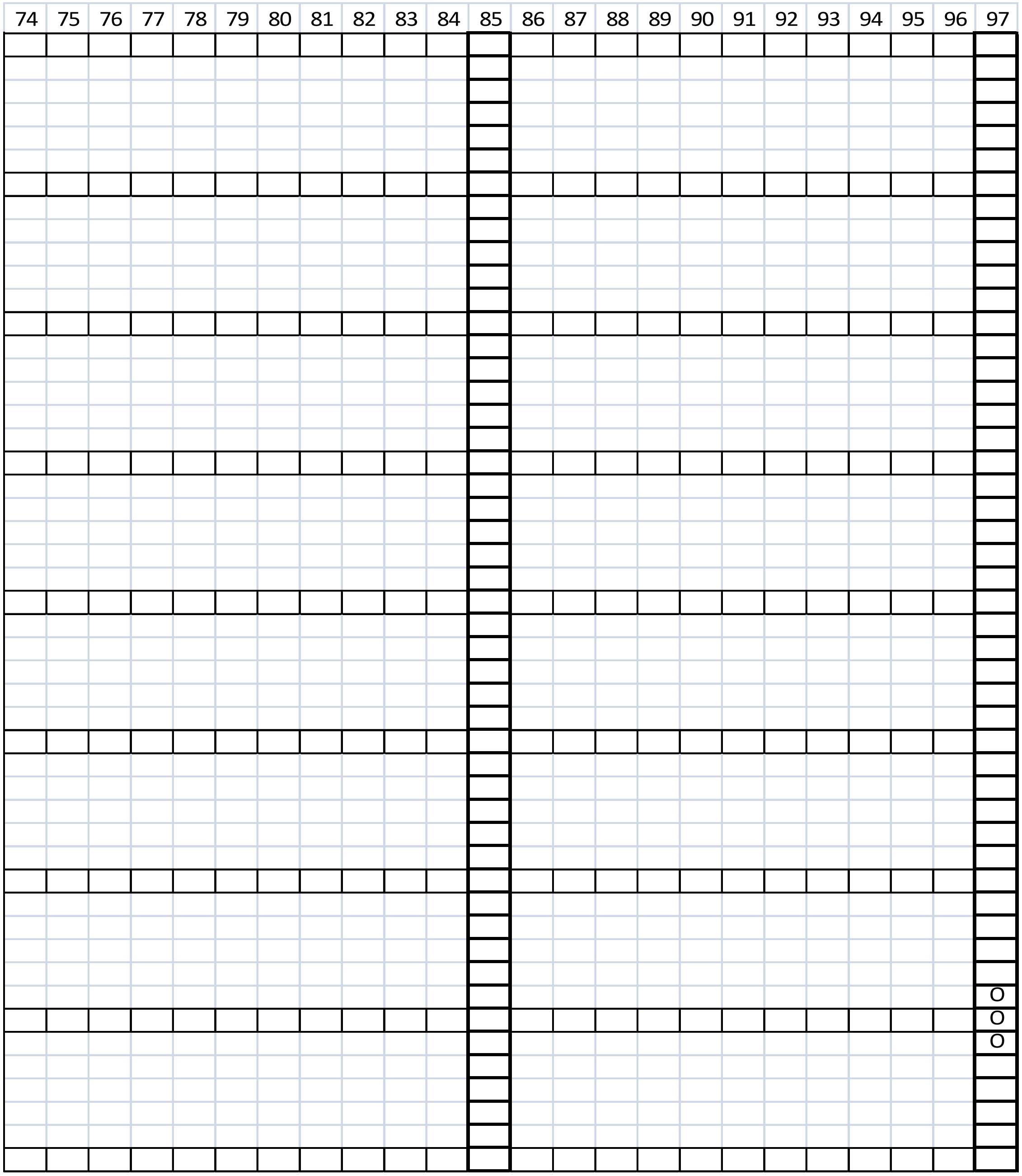

Figure E.25 – DIA4 – record of fastener failure during inelastic test (4/6)

98	99	100	101	102	103	104	105	106	107	108	109	110	111	112	113	114	115	116	117	118	119	120	121
																							O
O	O	O	O	X	X	X	O	O	O	O	O	O	O	O	O	O	O	O	O	O	O	O	O
											O												O
											O												
O	O	O	O	O	O	O	O	O	O	O		O	O	O	O	O	O	O	O	O	O	O	
O	O	O	O	O	O	O	O	O	O	O		O	O	O	O	O	O	O	O	O	O	O	
O	O	O	O	O	O	O	O	O	O	O		O	O	O	O	O	O	O	O	O	O	O	
											X												
O	O	O	O	O	O	O	O	O	O	O		O	O	O	O	O	O	O	O	O	O	O	
O	O	O	O	O	O	O	O	O	O	O		O	O	O	O	O	O	O	O	O	O	O	
											O												O
O	O	O	O	O	X	O	X	O	O	O	O	O	O	O	O	O	O	O	X	O	O	O	O
											O												O

Figure E.26 – DIA4 – record of fastener failure during inelastic test (5/6)

122	123	124	125	126	127	128	129	130	131	132	133	134	135	136	137	138	139	140	141	142	143	144	145
																							O
											O												O
											O												O
											O												O
O	X	O	X	X	X	X	O	X	X	O	O	O	O	O	O	O	X	X	X	X	O	O	O
											O												O
											O												O
																							O
O	O	O	O	O	O	O	O	O	O	O		O	O	O	O	O	O	O	O	O	O	O	O
																							O
O	O	O	O	O	O	O	O	O	O	O		O	O	O	O	O	O	O	O	O	O	O	O
											O												
											O												O
O	O	O	O	O	O	O	O	O	O	O	X	O	O	X	O	O	O	O	O	X	O	O	O
O	O	O	O	O	O	O	O	O	O	O	X	O	O	O	O	O	O	O	O	O	O	O	
											O												
O	O	O	O	O	O	O	O	O	O	O		O	O	O	O	O	O	O	O	O	O	O	
											O												
O	O	O	O	O	O	O	O	O	O	O	O	O	O	O	X	O	O	O	O	O	X	O	
											O												

Figure E.27 – DIA4 – record of fastener failure during inelastic test (6/6)

Table E.8 – DIA4R – list of testing protocols

BB		SS3		SS1		SS2	
0	☑	50	☑	50	☑	5	☑
225	☑	60	☑	60	☑	10	☑
475	☑	70	☑	70	☑	80	☑
675	☑	80	☑	80	☑		
900	☑	90	☑	90	☑		
1375	☑	100	☑	100	☑		
2275	☑	110	☑	110	☑		
3200	☑	120	☑	120	☑		
5025	☑	130	☑				
5475	☑	140	☑				
6000	☑	150	☑				
7000	☑	160	☑				
8000	☑	170	☑				
9000	☑	180	☑				
10000	☑						
20000	☑						
30000	☑						
40000	☑						
50000	☑						
60000	☑						
80000	☑						

<u>Notes</u>

- Big actuator valves used for SS1-80 and all larger amplitudes for this loading protocol

	1	2	3	4	5	6	7	8	9	10	11	12	13	14	15	16	17	18	19	20	21	22	23	24	25
A																									
B																									
C																									
D																									
E																									
F	O																								
G	O O	X	X	X	X	X	X	X	X	X	X	X	X	O	O	O	O	O	O	O	O	O	O	O	O
H	O																								
I	O																								
J																									
K																									
L	O																								
M	O O	O	O	O	O	O	O	O	O	O	O	O	O	O	O	O	O	O	O	O	O	O	O	O	
N																									
O																									
P																									
Q																									
R	O																								
S	O O	X	X	X	X	X	X	X	X	X	X	X	X X	X	X	X	X	X	X	X	X	X	X	X	
T																									
U																									
V																									
W																									
X	O																								
Y	O O	O	O	O	O	O	O	O	O	O	O	O	O	O	O	O	O	O	O	O	O	O	O	O	
Z																									
AA																									
AB																									
AC																									
AD	O																								
AE	O O	X	X	X	X	X	X	X	X	X	X	X	X X	X	X	X	X	X	X	X	X	X	O	O	
AF																									
AG																									
AH																									
AI																									
AJ	O												O												
AK	O O	X	X	X	X	X	O	O	O	O	O	O		O	O	O	O	O	O	O	O	O	O	O	
AL																									
AM																									
AN																									
AO																									
AP																									
AQ	O O				X	X	X	X	X	X	X		O O		O	O	O	O	O	O	O	O	O	O	
AR	O																								
AS																									
AT																									
AU																									
AV																									
AW																									

Figure E.28 – DIA4R – record of fastener failure during inelastic test (1/6)

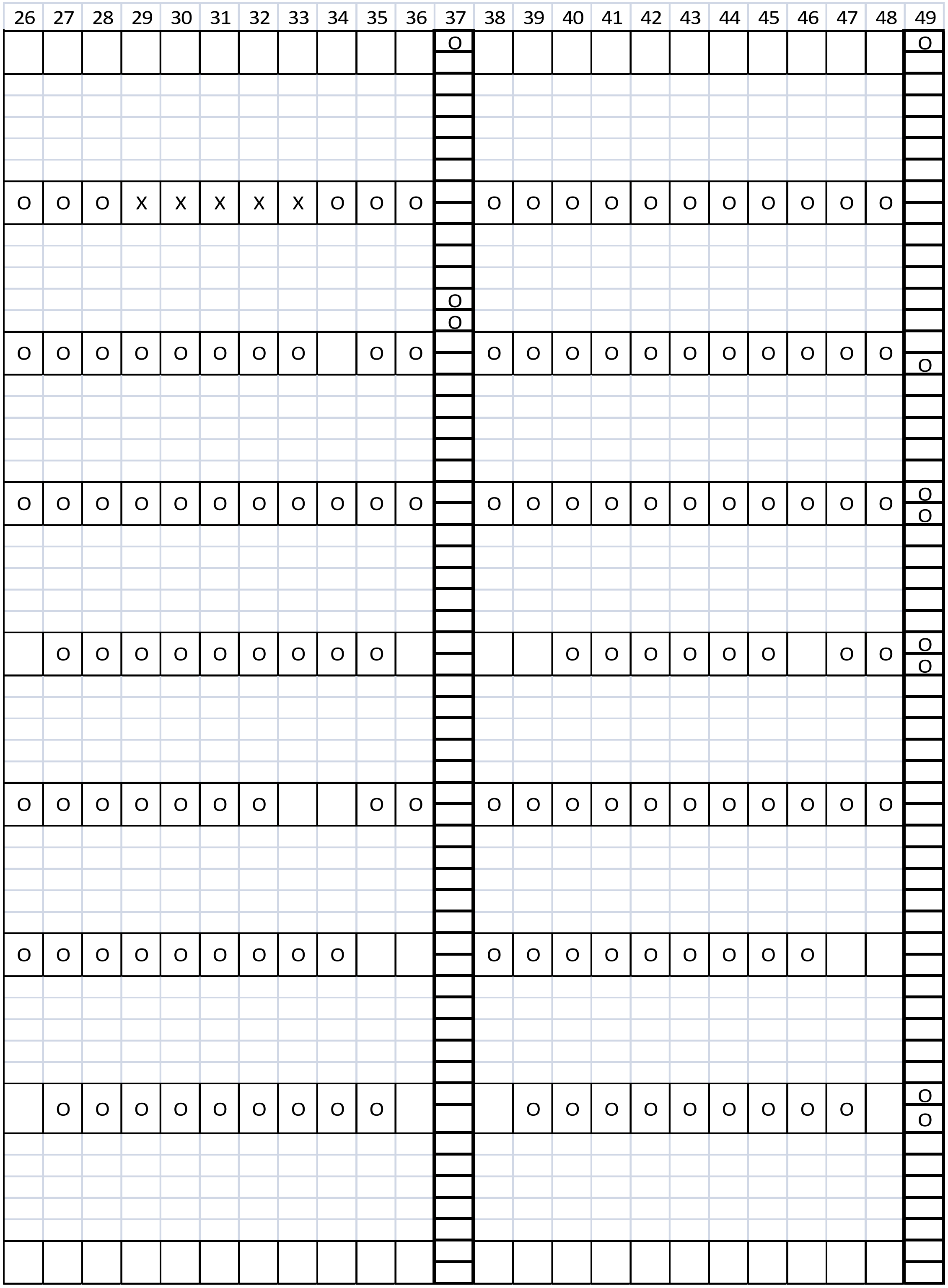

Figure E.29 – DIA4R – record of fastener failure during inelastic test (2/6)

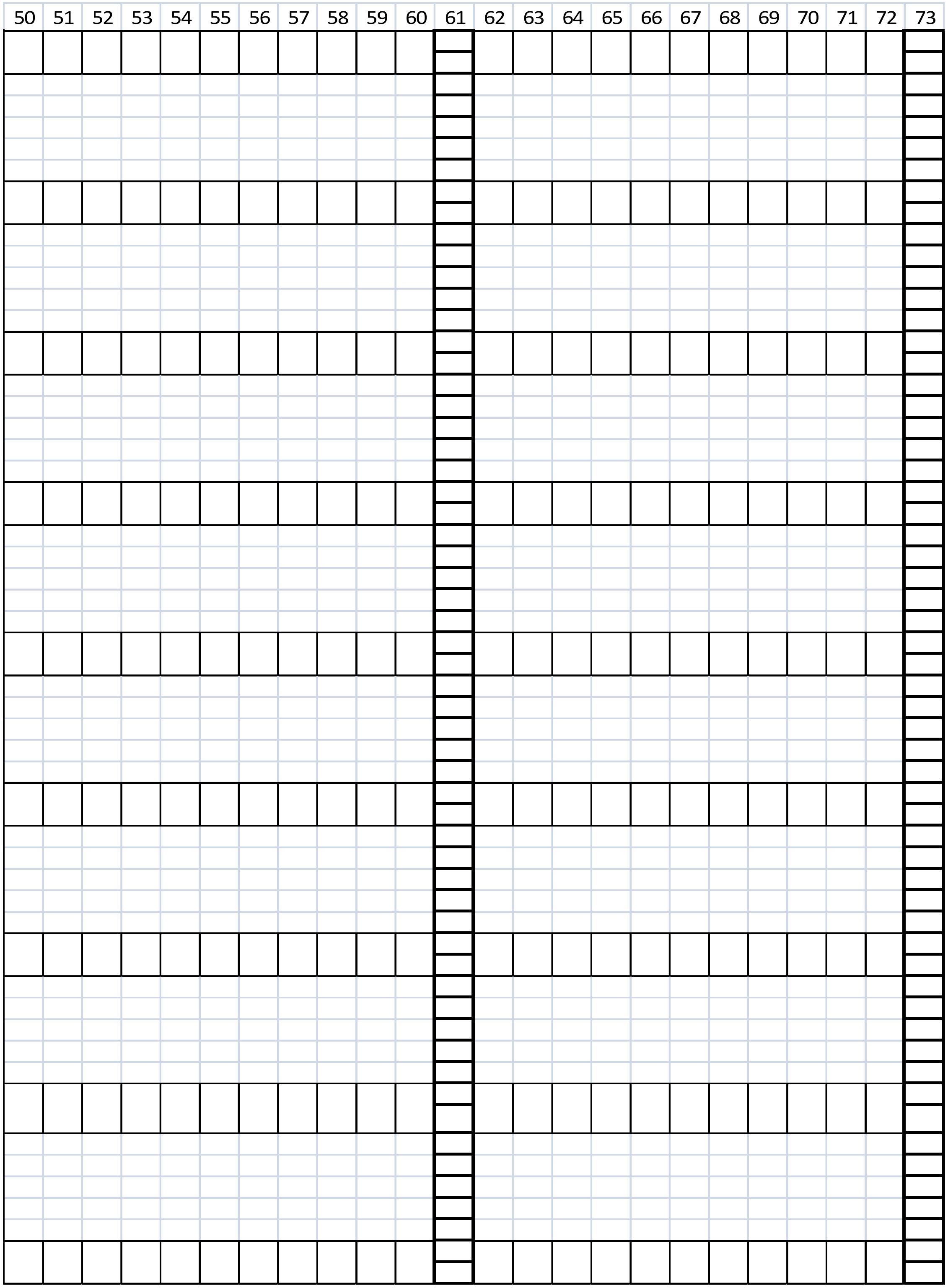

Figure E.30 – DIA4R – record of fastener failure during inelastic test (3/6)

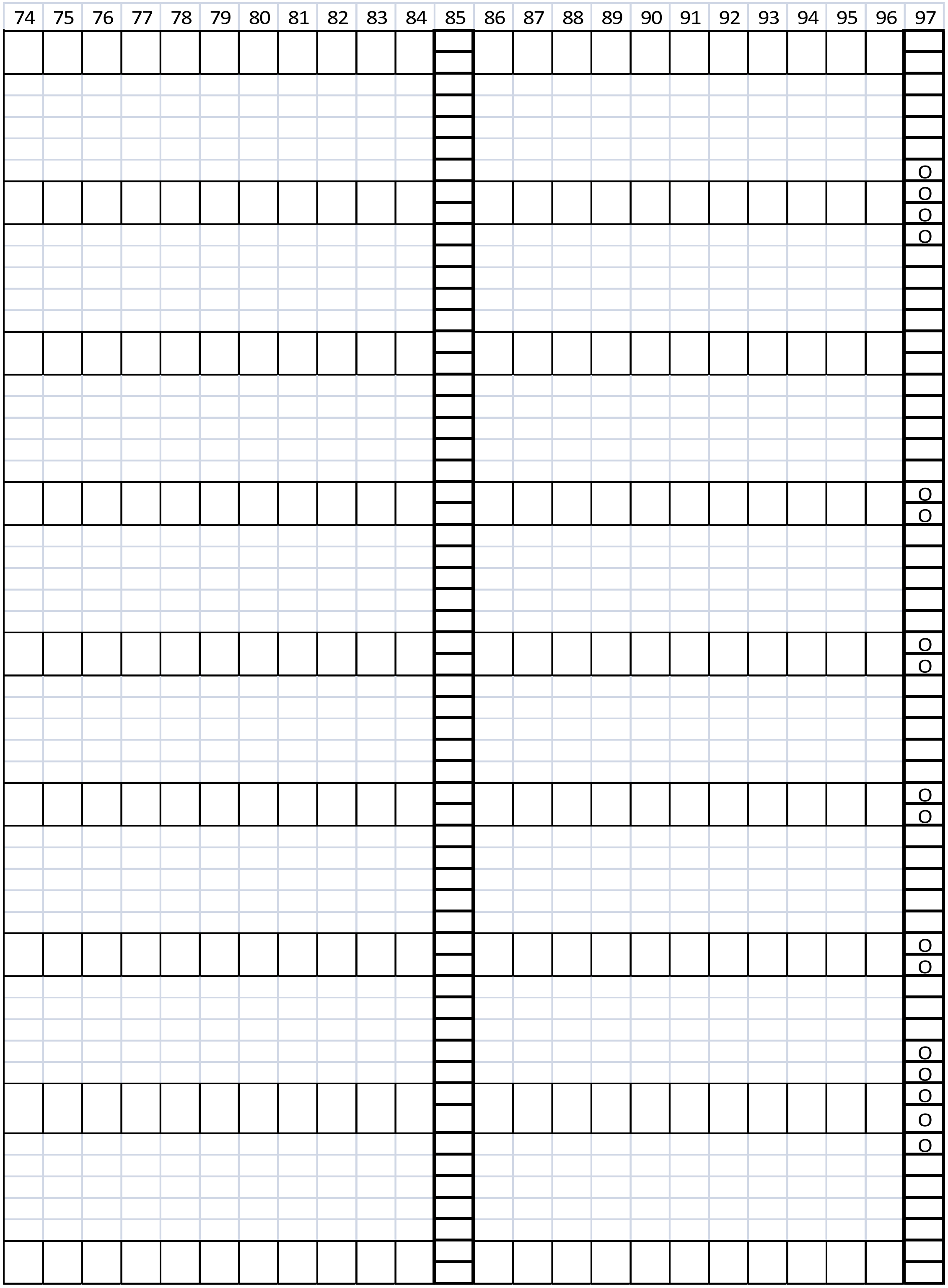

Figure E.31 – DIA4R – record of fastener failure during inelastic test (4/6)

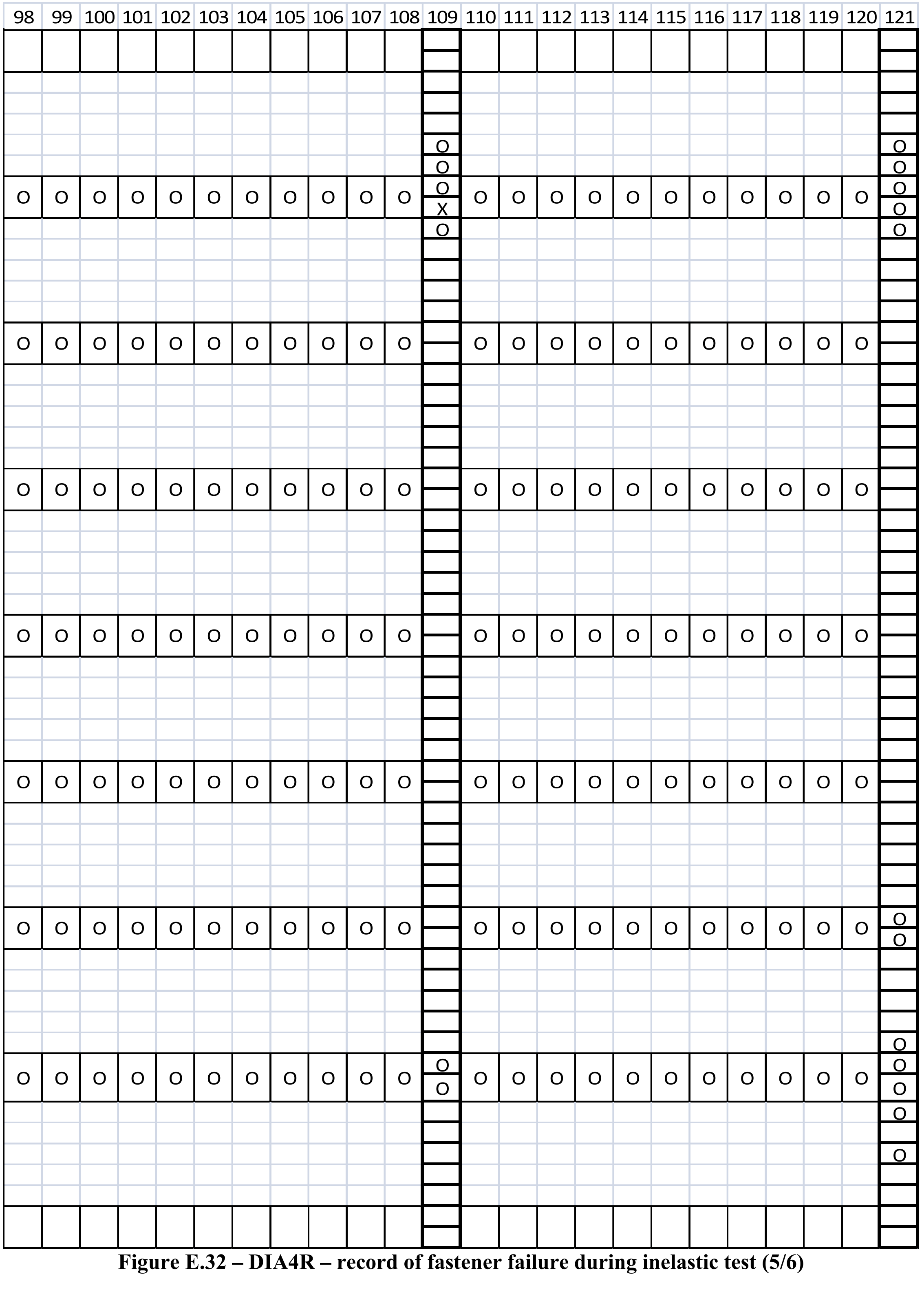

Figure E.32 – DIA4R – record of fastener failure during inelastic test (5/6)

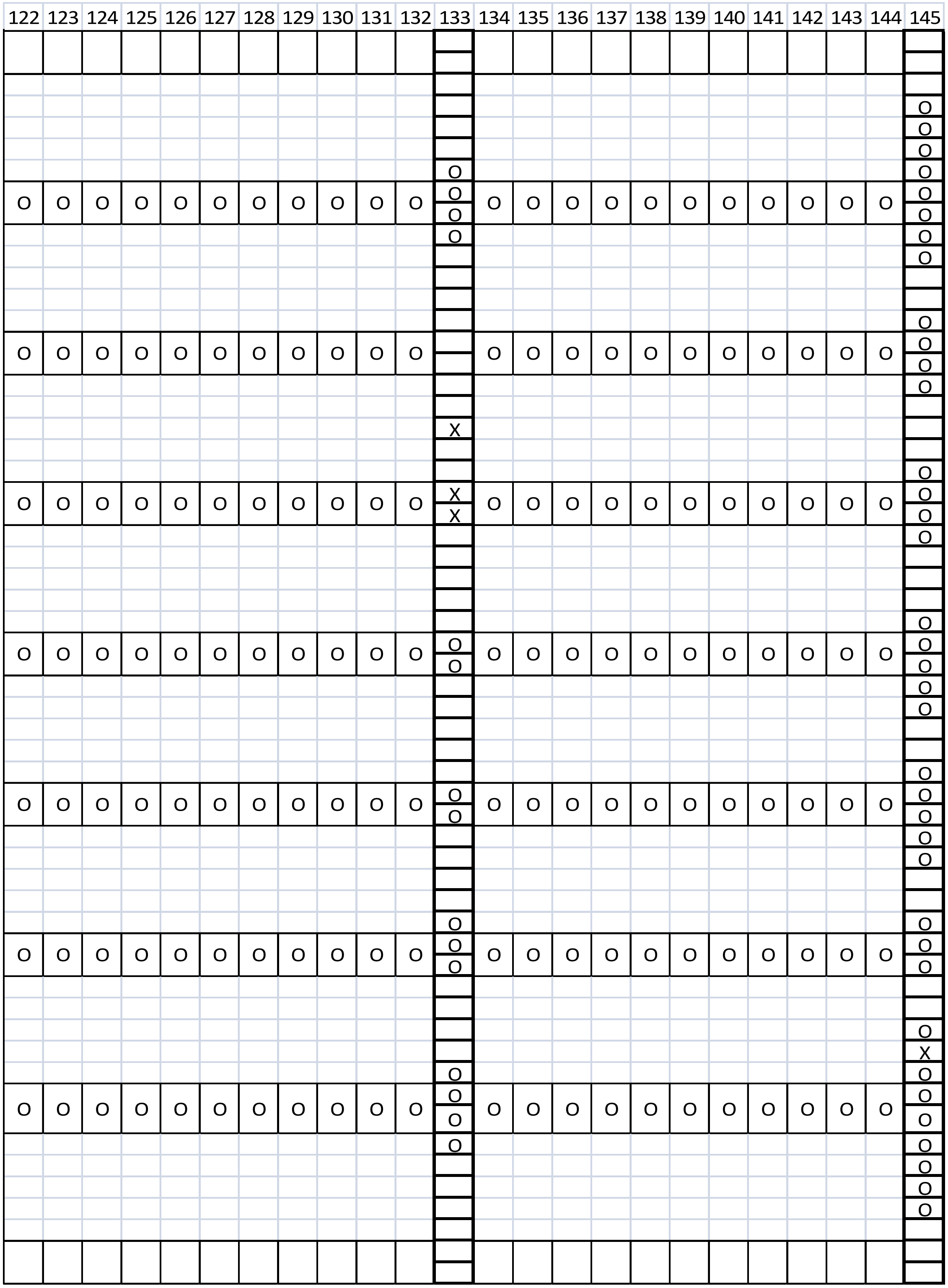

Figure E.33 – DIA4R – record of fastener failure during inelastic test (6/6)

Table E.9 – DIA5 – list of testing protocols

BB		SS3		SS1		SS2	
0	☑	50	☑	50	☑	5	☑
225	☑	60	☑	60	☑	10	☑
675	☑	70	☑	70	☑	80	☑
1150	☑	80	☑	80	☑		
1825	☑	90	☑	90	☑		
2275	☑	100	☑	100	☑		
3200	☑	110	☑	110	☑		
5050	☑	120	☑	120	☑		
6000	☑	130	☑				
8000	☑	140	☑				
10000	☑	150	☑				
20000	☑	160	☑				
30000	☑	170	☑				
40000	☑	180	☑				
60000	☑						
80000	☑						
100000	☑						
120000	☑						

Notes

- Big actuator valves used for SS1-80 and all larger amplitudes for this loading protocol

	1	2	3	4	5	6	7	8	9	10	11	12	13	14	15	16	17	18	19	20	21	22	23	24	25
A																									
B																									
C																									
D																									
E																									
F																									
G	O O	O	O	O	O	O	O	O	O	O	O	O	O	O	O	O	O	O	O	O	O	O	O	O	
H																									
I																									
J																									
K																									
L																									
M	O O	O	O	O	O	O	O	O	O	O	O	O		O	O	O	O	O	O	O	O	O	O	O	
N																									
O																									
P																									
Q																									
R																									
S	O O	O	O	O	O	O	O	O	O	O	O	O		O	O	O	O	O	O	O	O	O	O	O	
T																									
U																									
V																									
W																									
X																									
Y	O O	O	O	O	O	O	O	O	O	O	O	O	X X	O	O	O	O	O	O	O	O	O	O	O	
Z																									
AA																									
AB																									
AC																									
AD																									
AE	O O	O	O	O	O	O	O	O	O	O	O	O		O	O	O	O	O	O	O	O	O	O	O	
AF																									
AG																									
AH																									
AI																									
AJ																									
AK	O O	O	O	O	O	O	O	O	O	O	O	O		O	O	O	O	O	O	O	O	O	O	O	
AL																									
AM																									
AN																									
AO																									
AP																									
AQ	O O	O	O	O	O	O	O	O	O	O	O	O		O	O	O	O	O	O	O	O	O	O	O	
AR																									
AS																									
AT																									
AU													X												
AV																									
AW	O O																								

Figure E.34 – DIA5 – record of fastener failure during inelastic test (1/6)

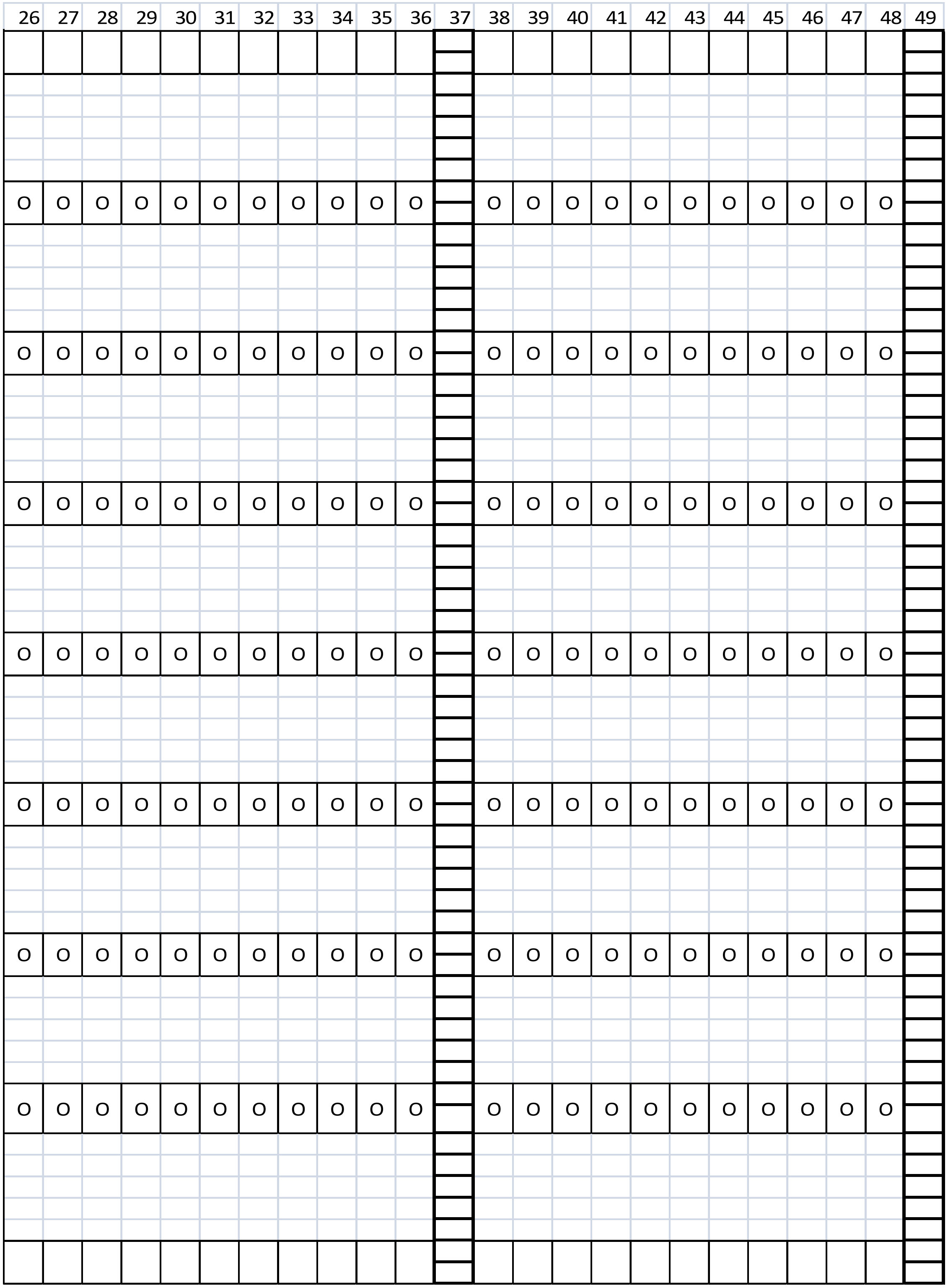

Figure E.35 – DIA5 – record of fastener failure during inelastic test (2/6)

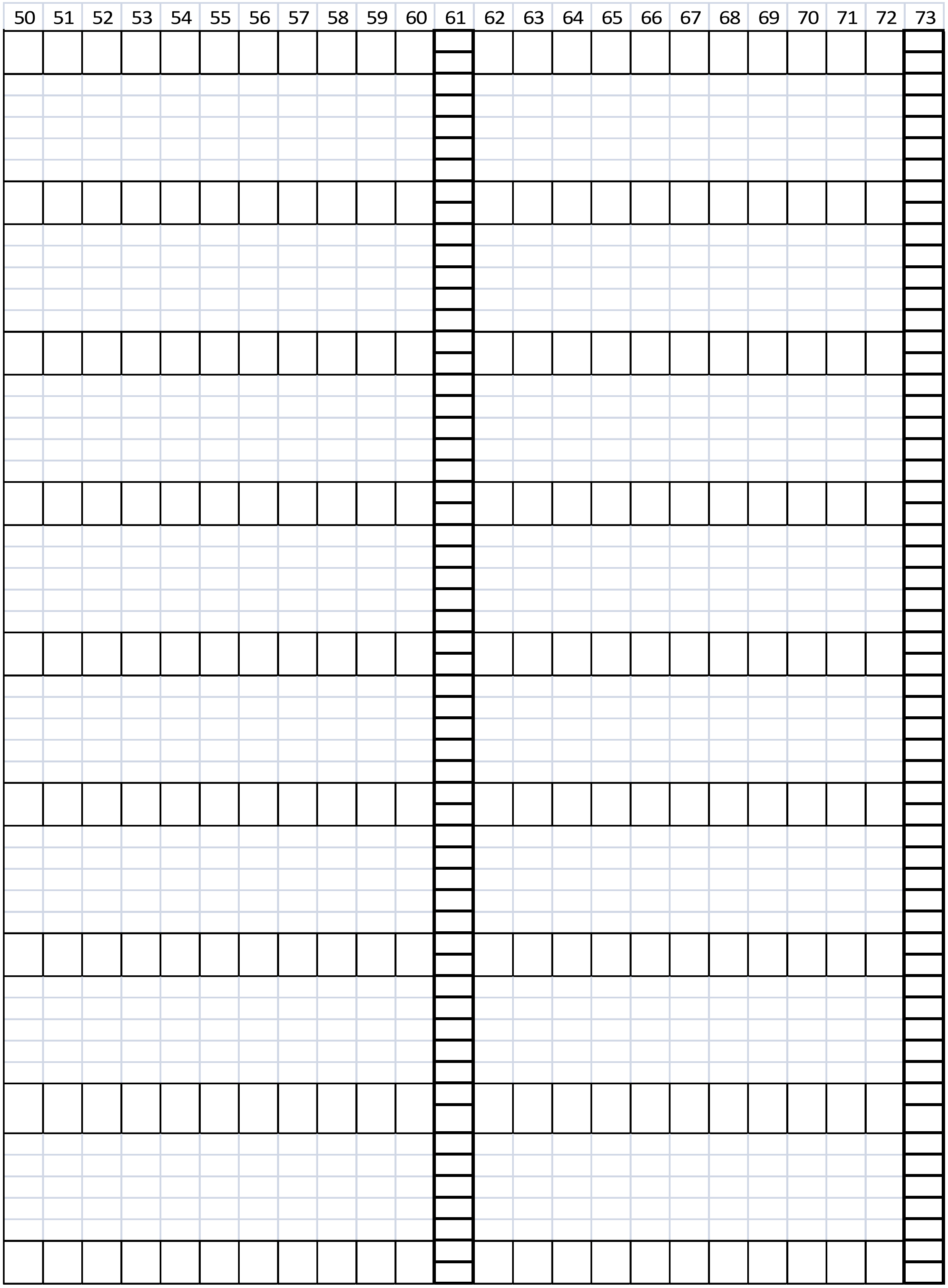

Figure E.36 – DIA5 – record of fastener failure during inelastic test (3/6)

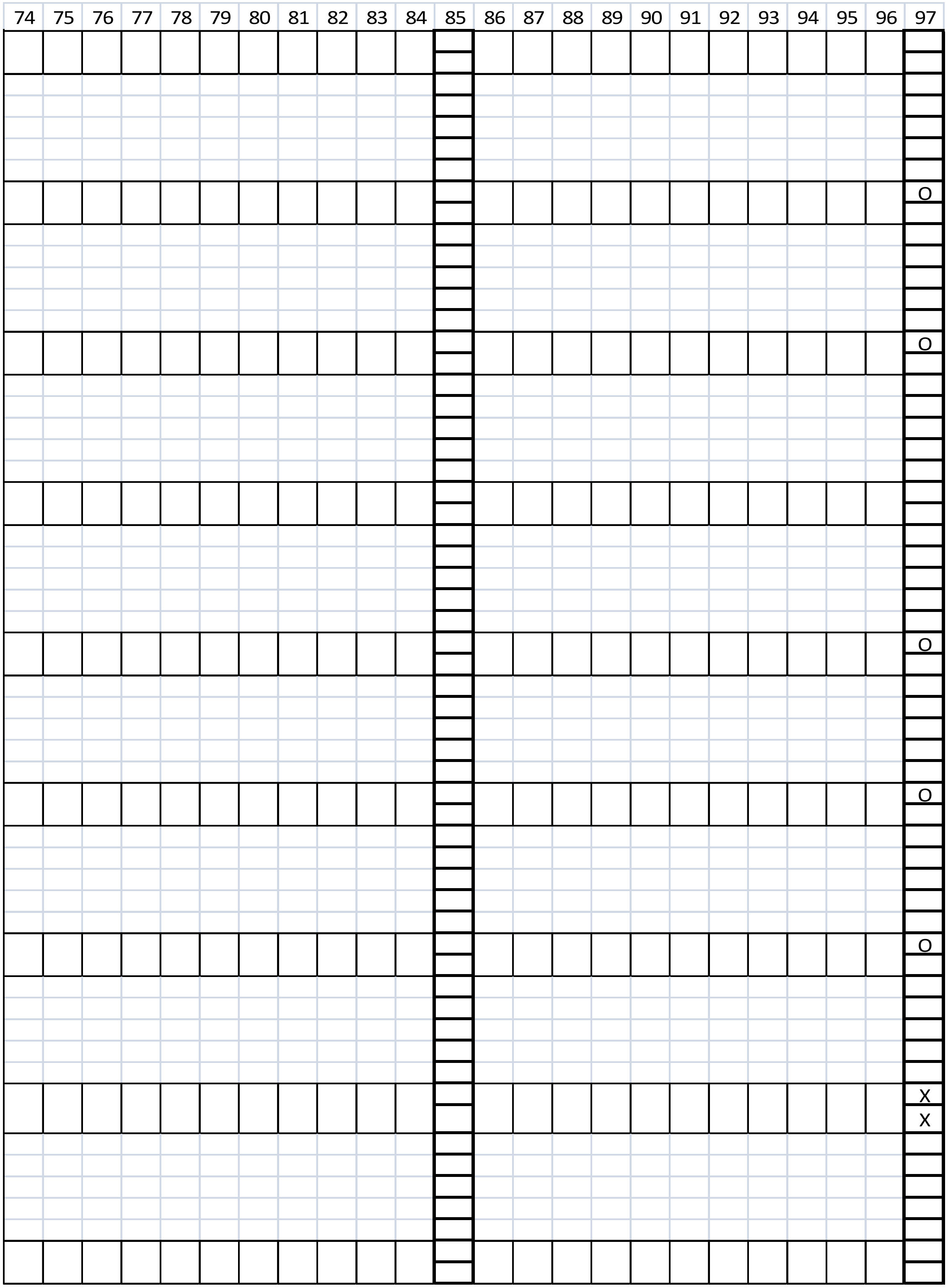

Figure E.37 – DIA5 – record of fastener failure during inelastic test (4/6)

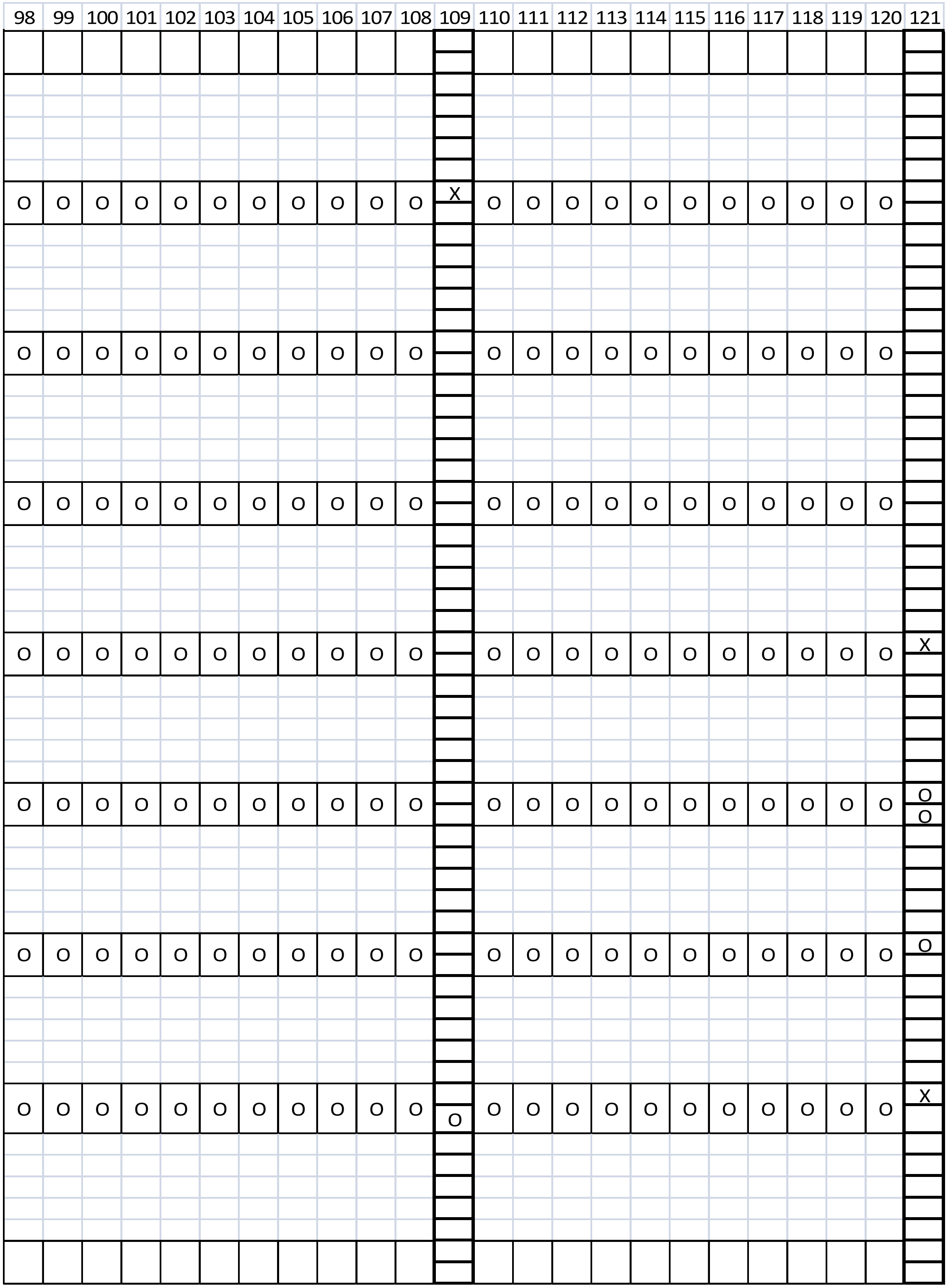

Figure E.38 – DIA5 – record of fastener failure during inelastic test (5/6)

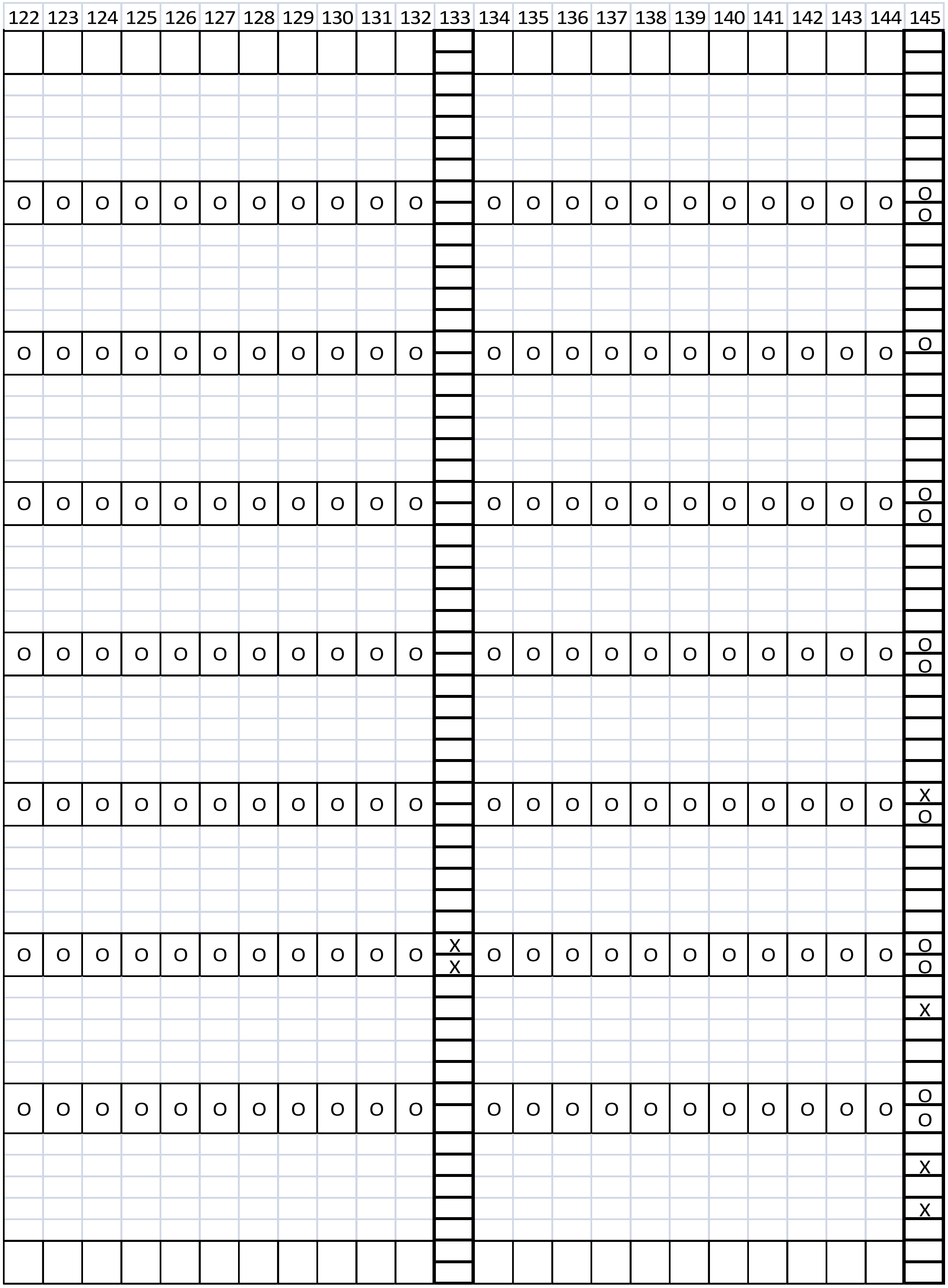

Figure E.39 – DIA5 – record of fastener failure during inelastic test (6/6)

Table E.10 – DIA5R – list of testing protocols

BB		SS3		SS1		SS2	
0	☑	50	☑	50	☑	5	☑
225	☑	60	☑	60	☑	10	☑
675	☑	80	☑	70	☑	92	☑
1150	☑	100	☑	80	☑		
1825	☑	120	☑	90	☑		
2275	☑	140	☑	100	☑		
3200	☑	160	☑	110	☑		
5050	☑	180	☑	120	☑		
6000	☑	200	☑				
8000	☑	220	☑				
10000	☑	240	☑				
20000	☑	260	☑				
30000	☑	280	☑				
40000	☑						
60000	☑						
80000	☑						
100000	☑						
120000	☑						
140000	☑						
160000	☑						

Notes

- Big actuator valves used for SS1-200 and SS1-80 and all larger amplitudes for those two loading protocols

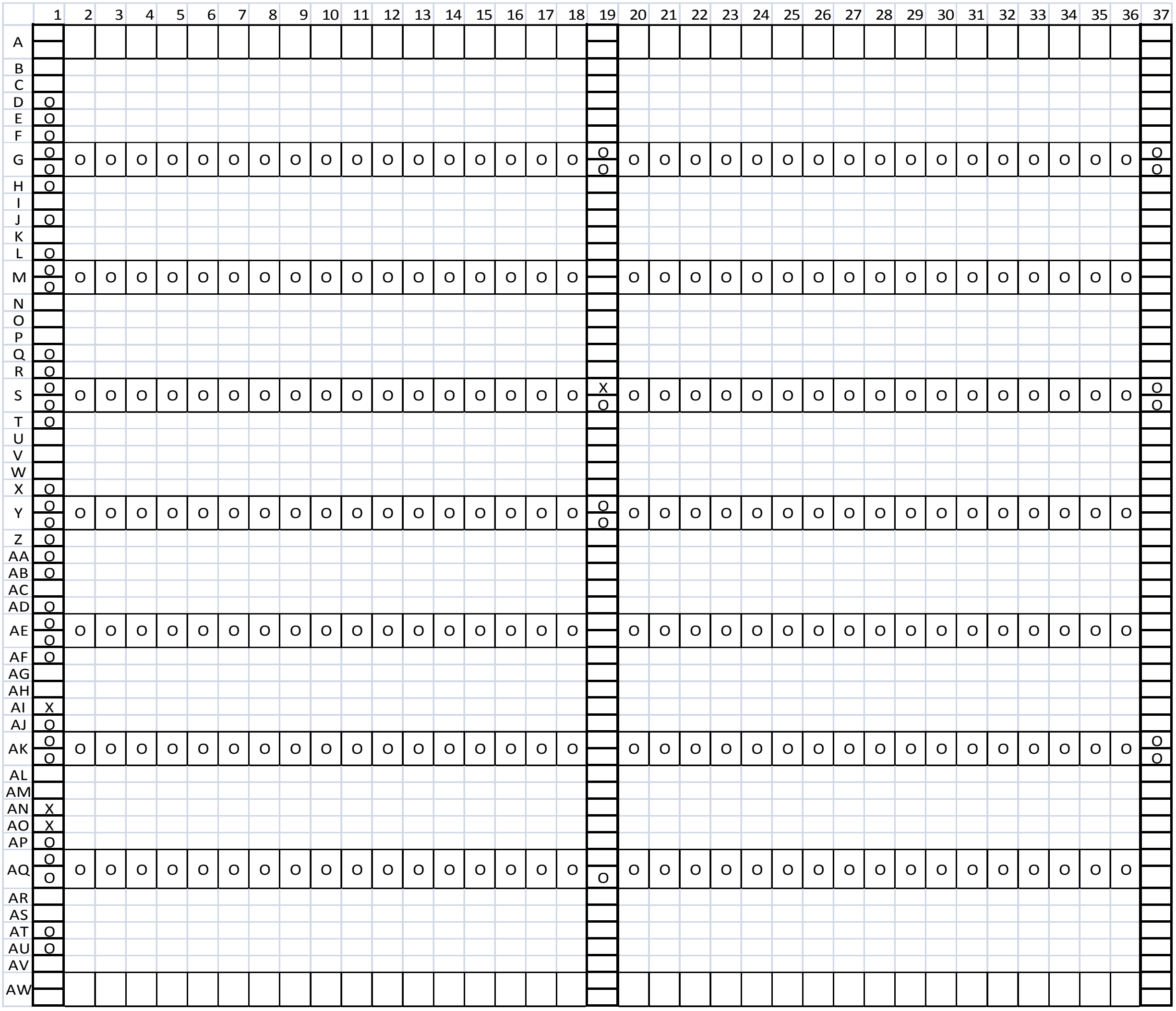

Figure E.40 – DIA5R – record of fastener failure during inelastic test (1/6)

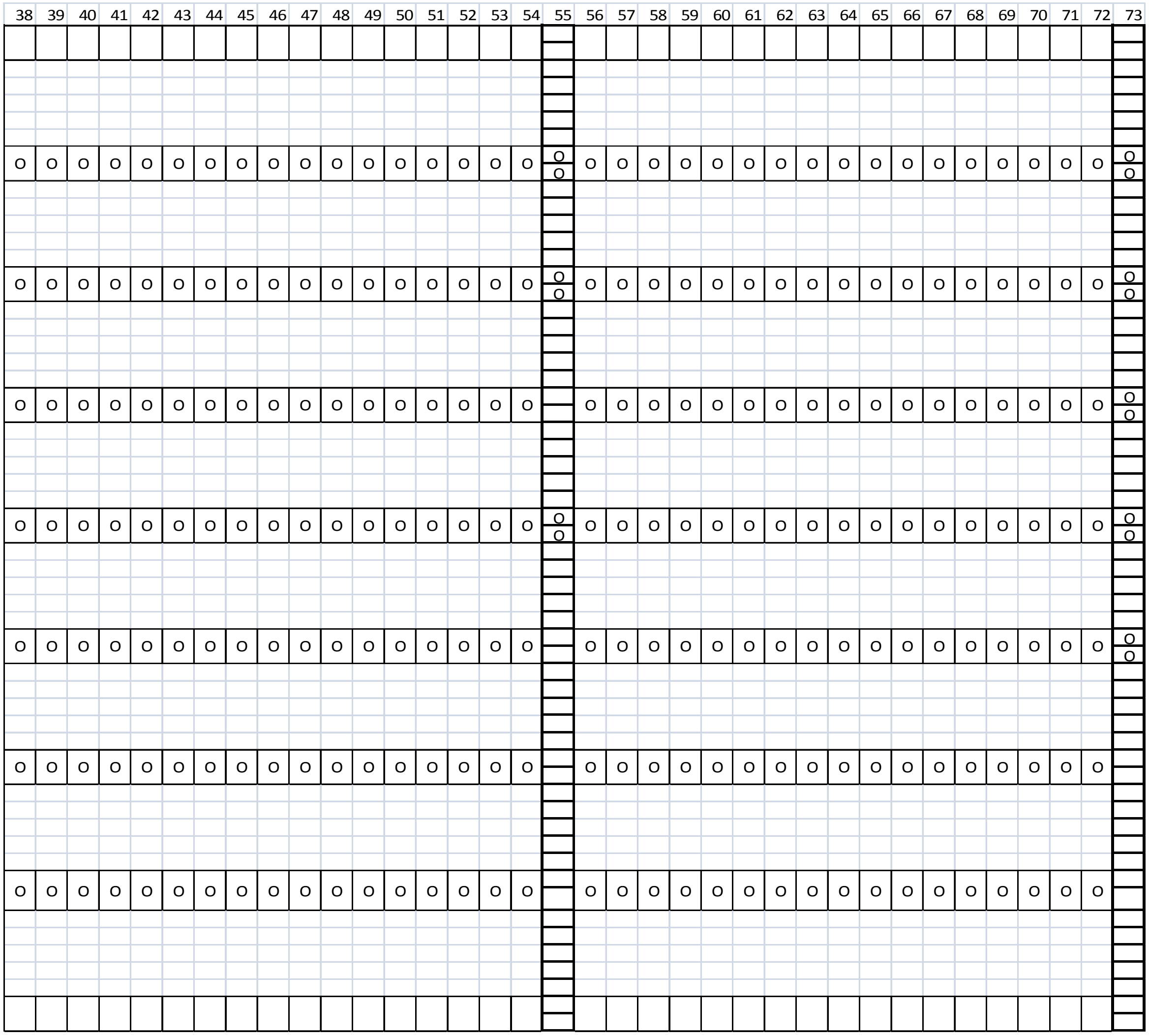

Figure E.41 – DIA5R – record of fastener failure during inelastic test (2/6)

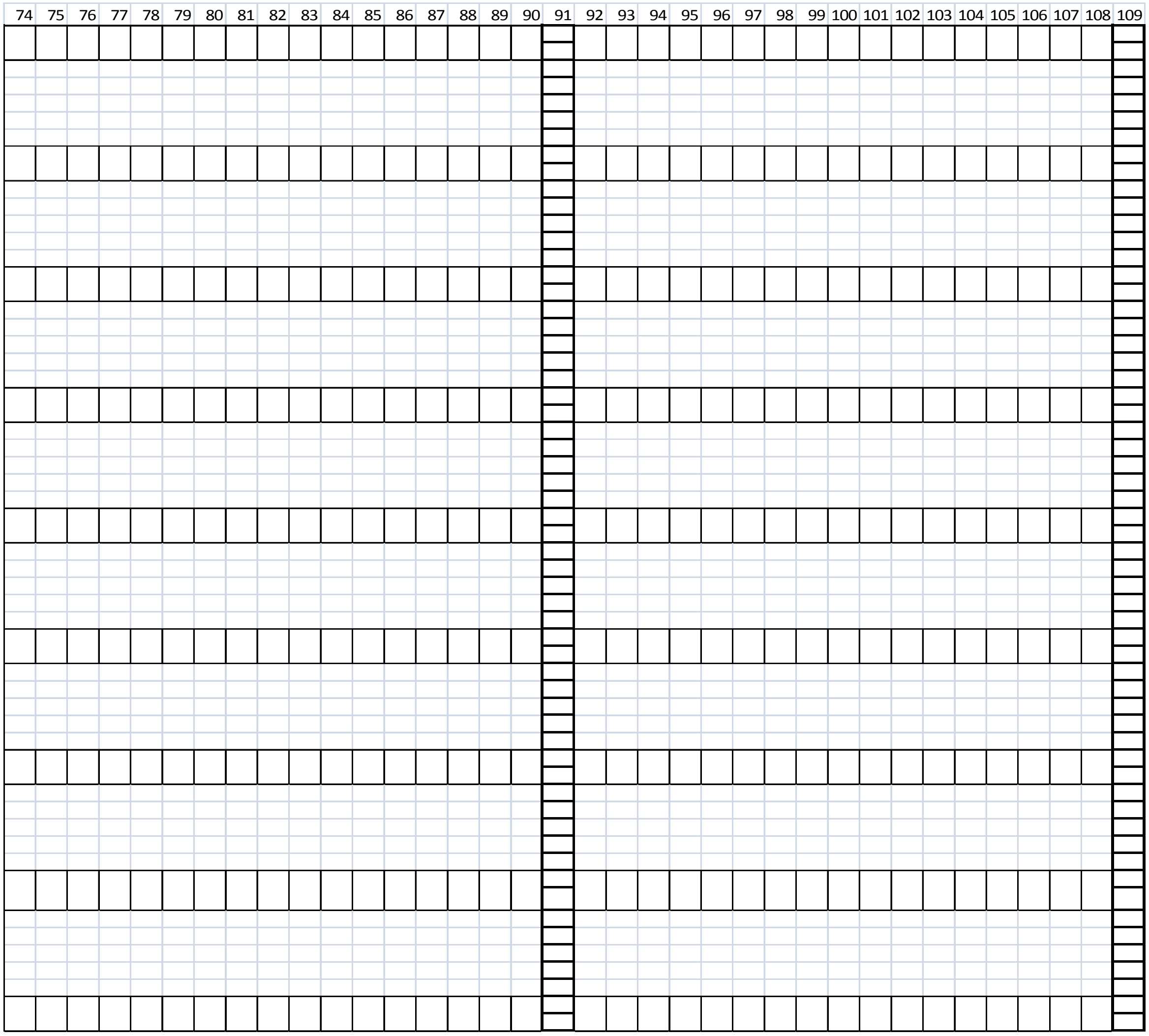

Figure E.42 – DIA5R – record of fastener failure during inelastic test (3/6)

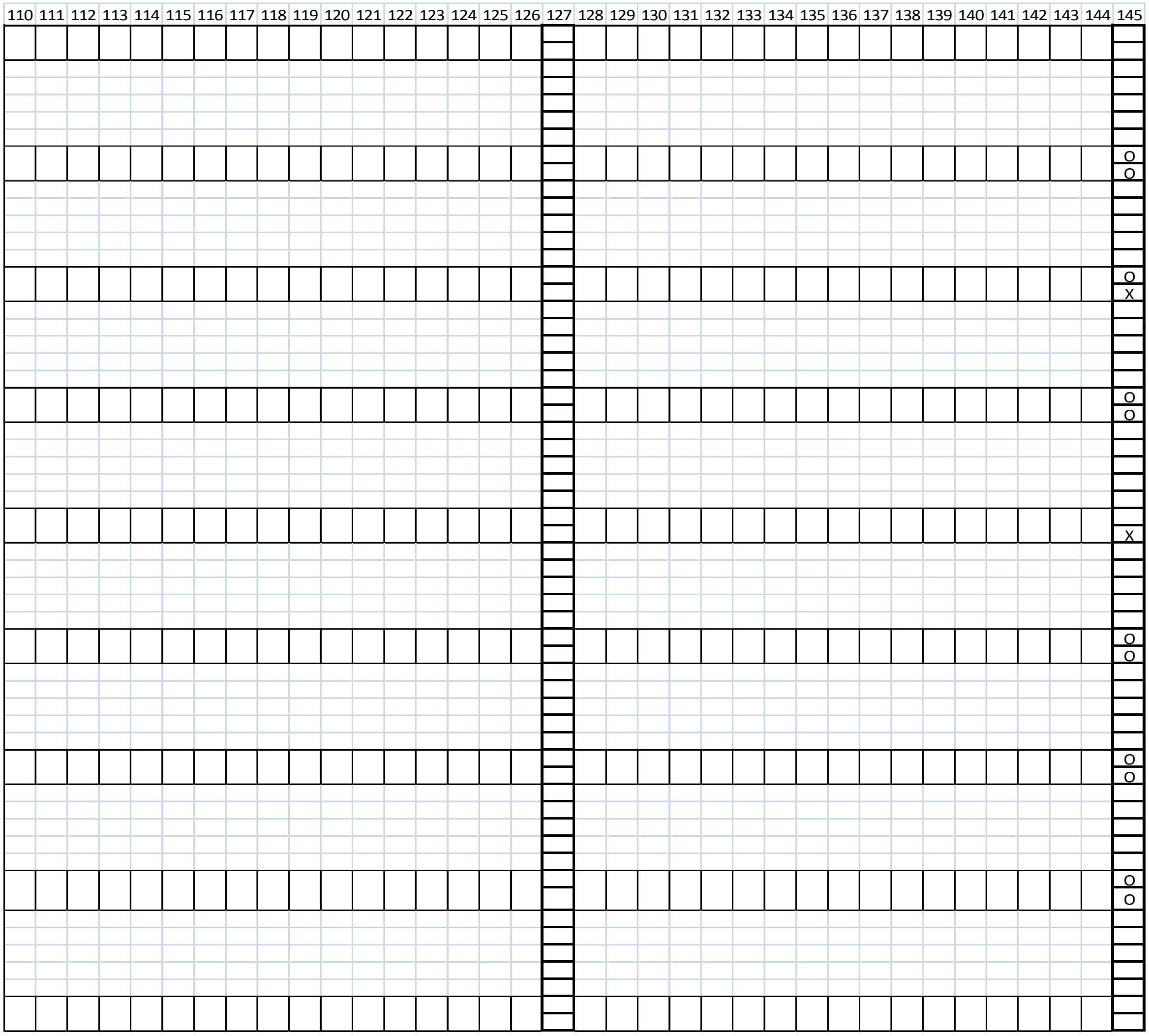

Figure E.43 – DIA5R – record of fastener failure during inelastic test (4/6)

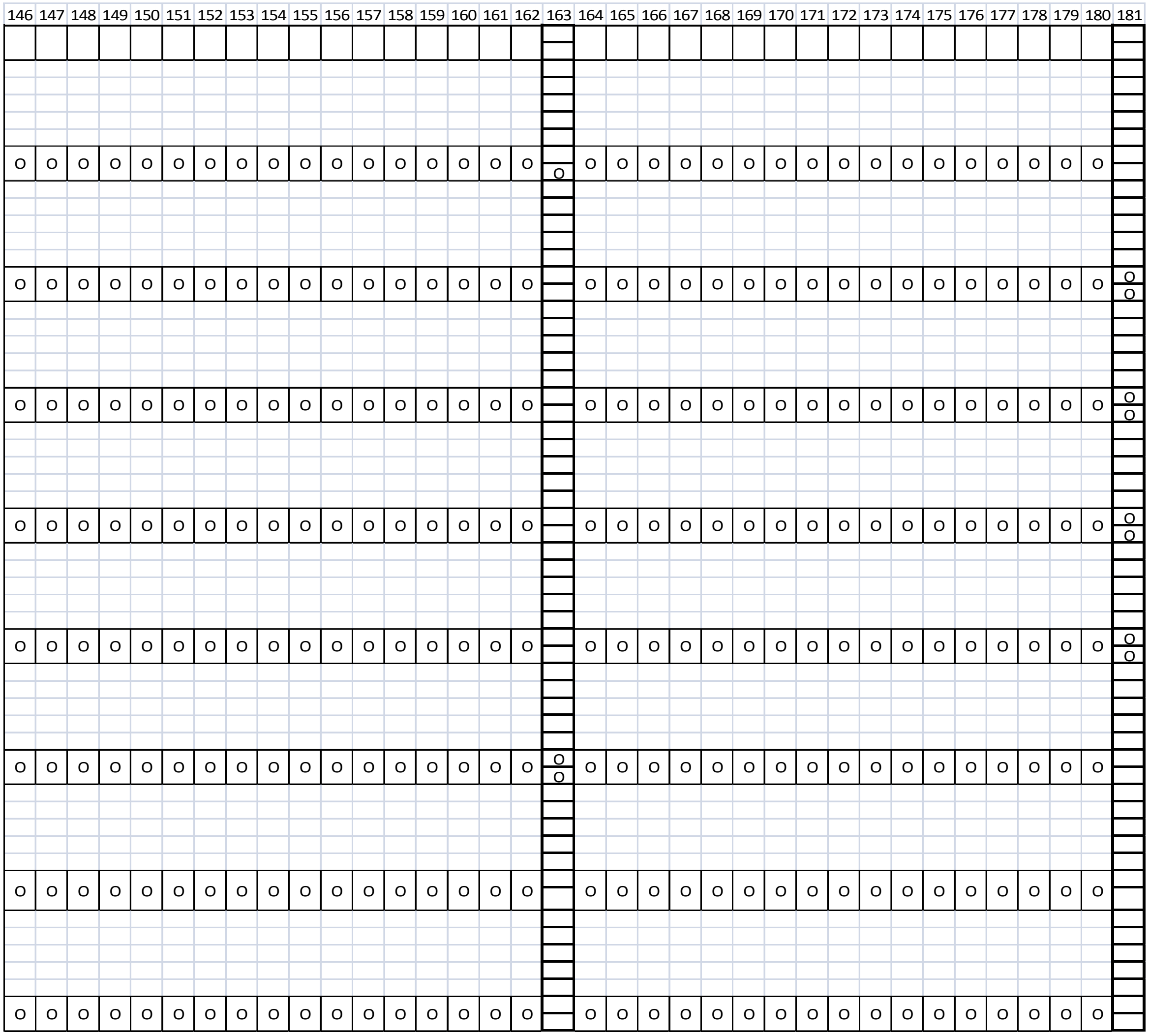

Figure E.44 – DIA5R – record of fastener failure during inelastic test (5/6)

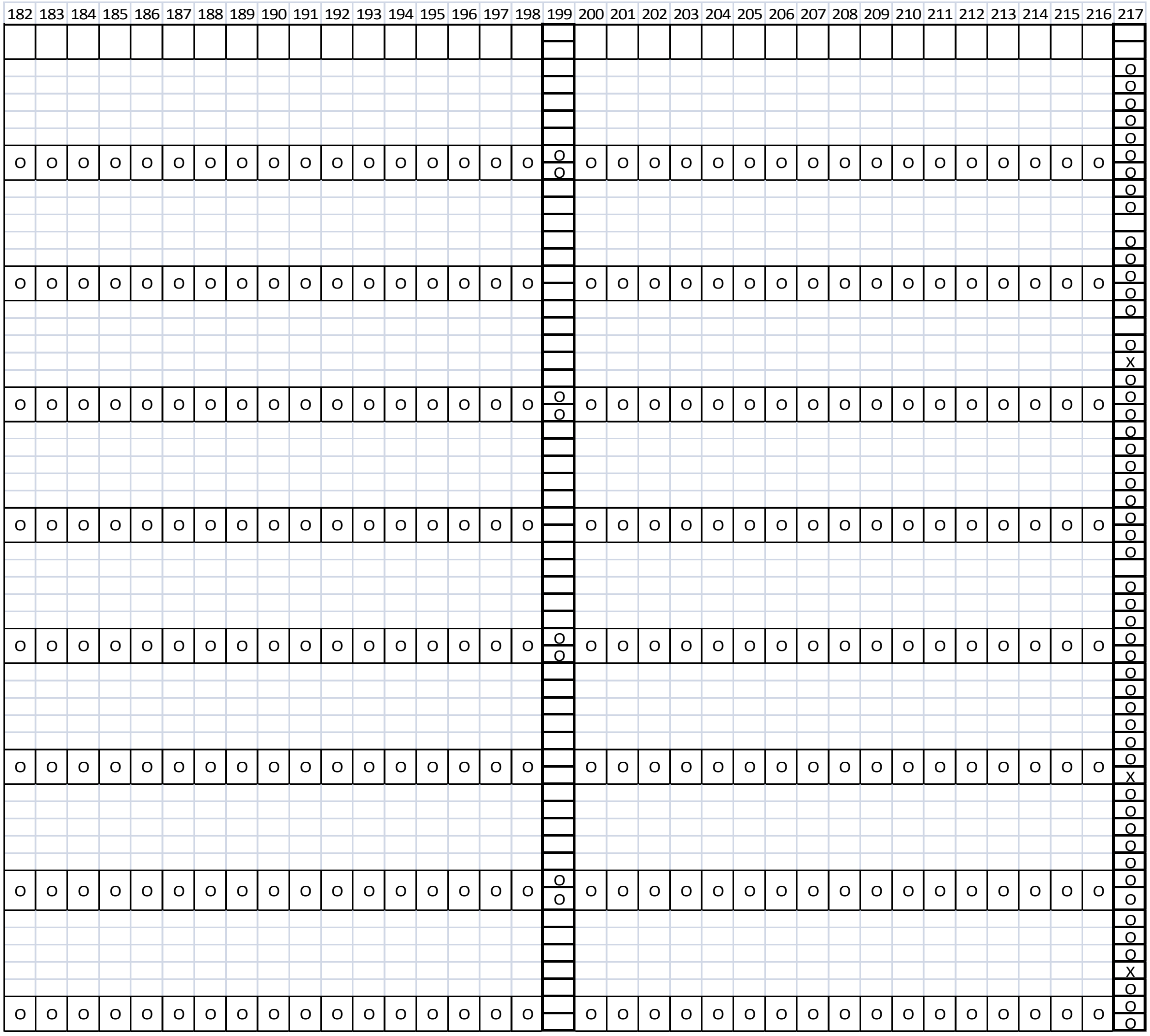

Figure E.45 – DIA5R – record of fastener failure during inelastic test (6/6)

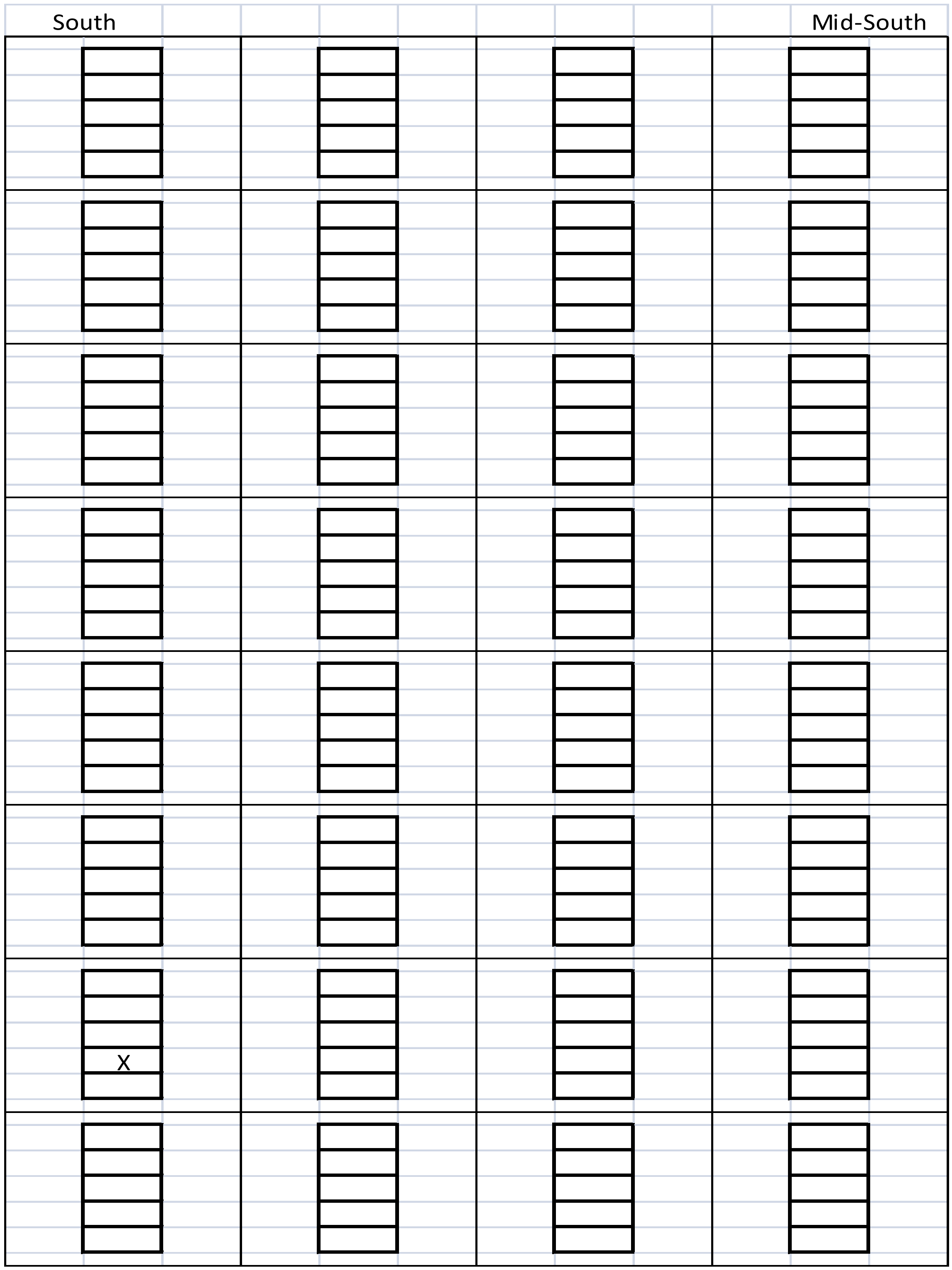

Figure E.46 – DIA5R – steel mass loss during inelastic test (1/3)

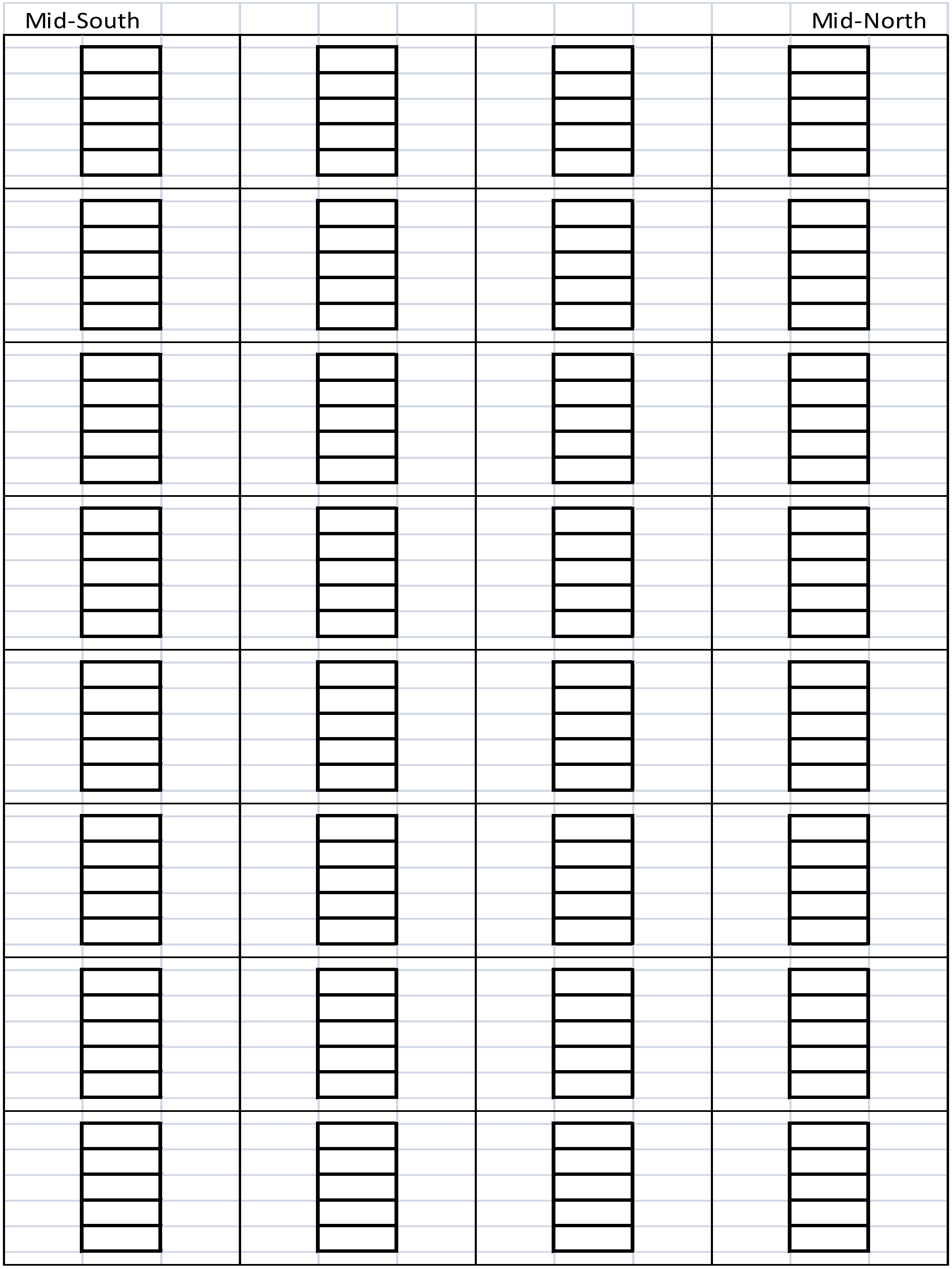

Figure E.47 – DIA5R – steel mass loss during inelastic test (2/3)

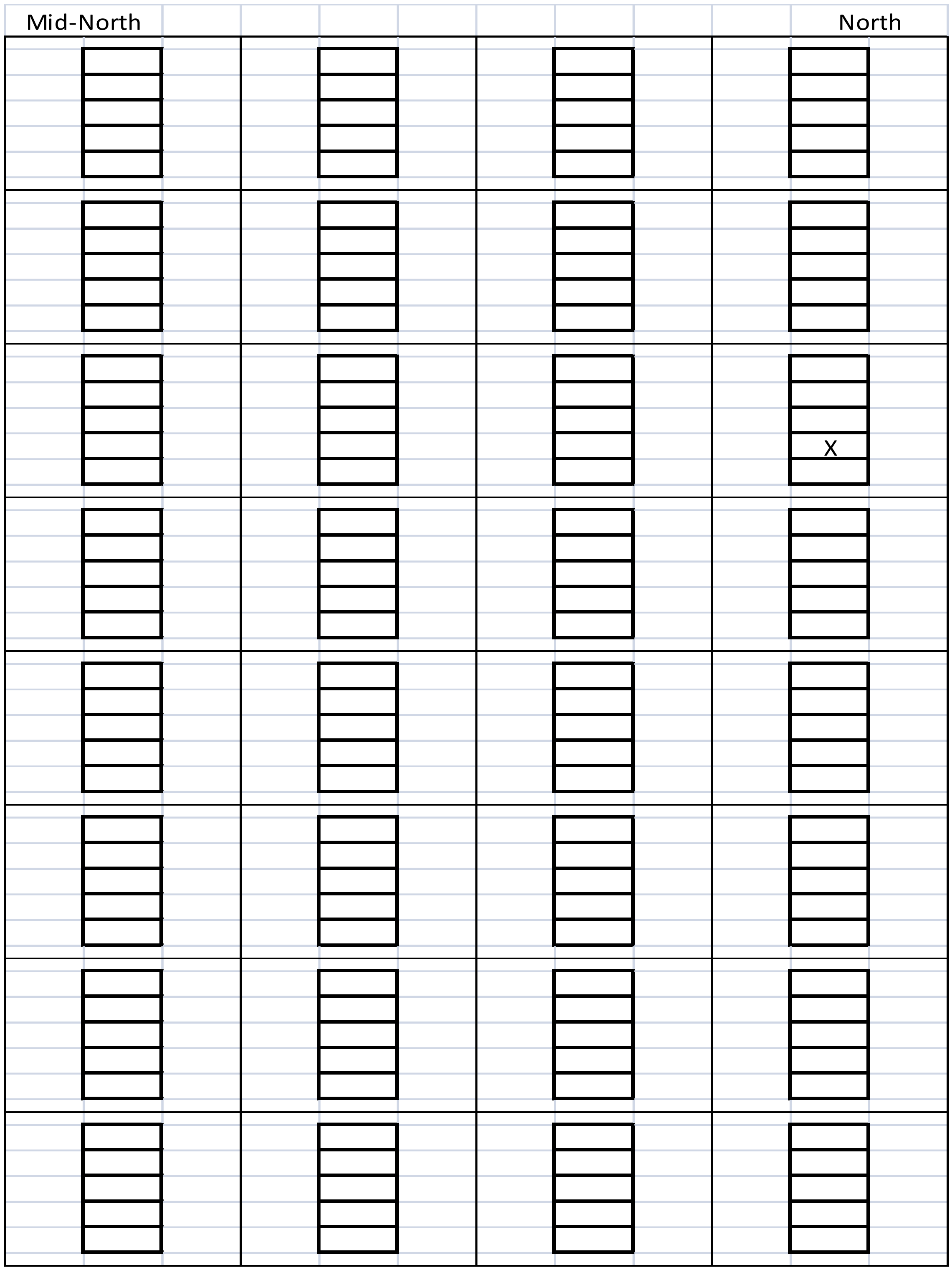

Figure E.48 – DIA5R – steel mass loss during inelastic test (3/3)

Table E.11 – DIA6 – list of testing protocols

BB		SS3		SS1		SS2	
0	☑	50	☑	50	☑	5	☑
225	☑	60	☑	60	☑	10	☑
675	☑	80	☑	70	☑	92	☑
1150	☑	100	☑	80	☑		
1825	☑	120	☑	90	☑		
2275	☑	140	☑	100	☑		
3200	☑	160	☑	110	☑		
5050	☑	180	☑	120	☑		
6000	☑	200	☑	130	☑		
8000	☑	220	☑				
10000	☑	240	☑				
20000	☑	260	☑				
30000	☑	280	☑				
40000	☑						
60000	☑						
80000	☑						
100000	☑						
120000	☑						
140000	☑						
160000	☑						
180000	☑						

<u>Notes</u>

- Big actuator valves used for SS1-200 and SS1-80 and all larger amplitudes for those two loading protocols

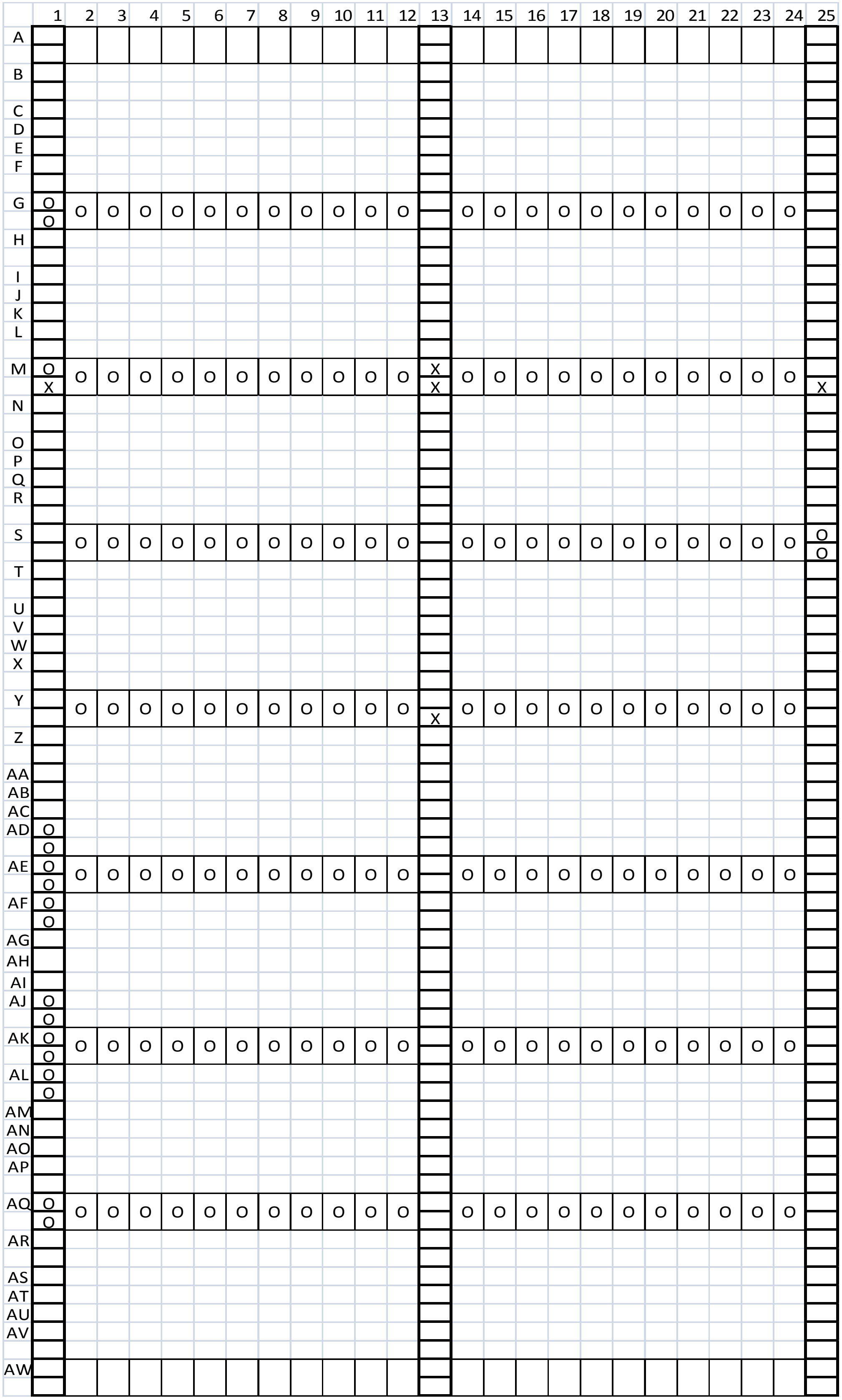

Figure E.49 – DIA6 – record of fastener failure during inelastic test (1/6)

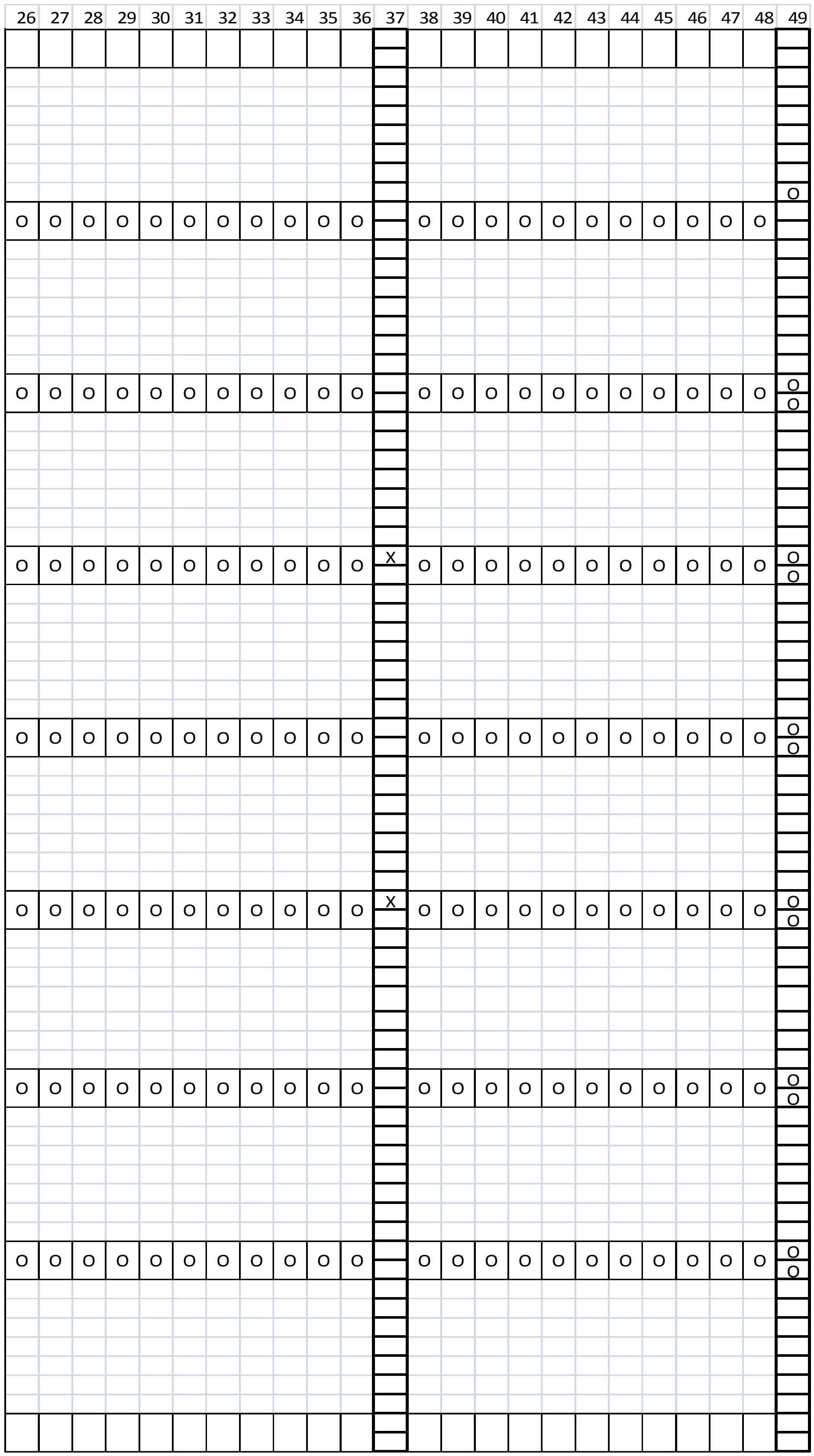

Figure E.50 – DIA6 – record of fastener failure during inelastic test (2/6)

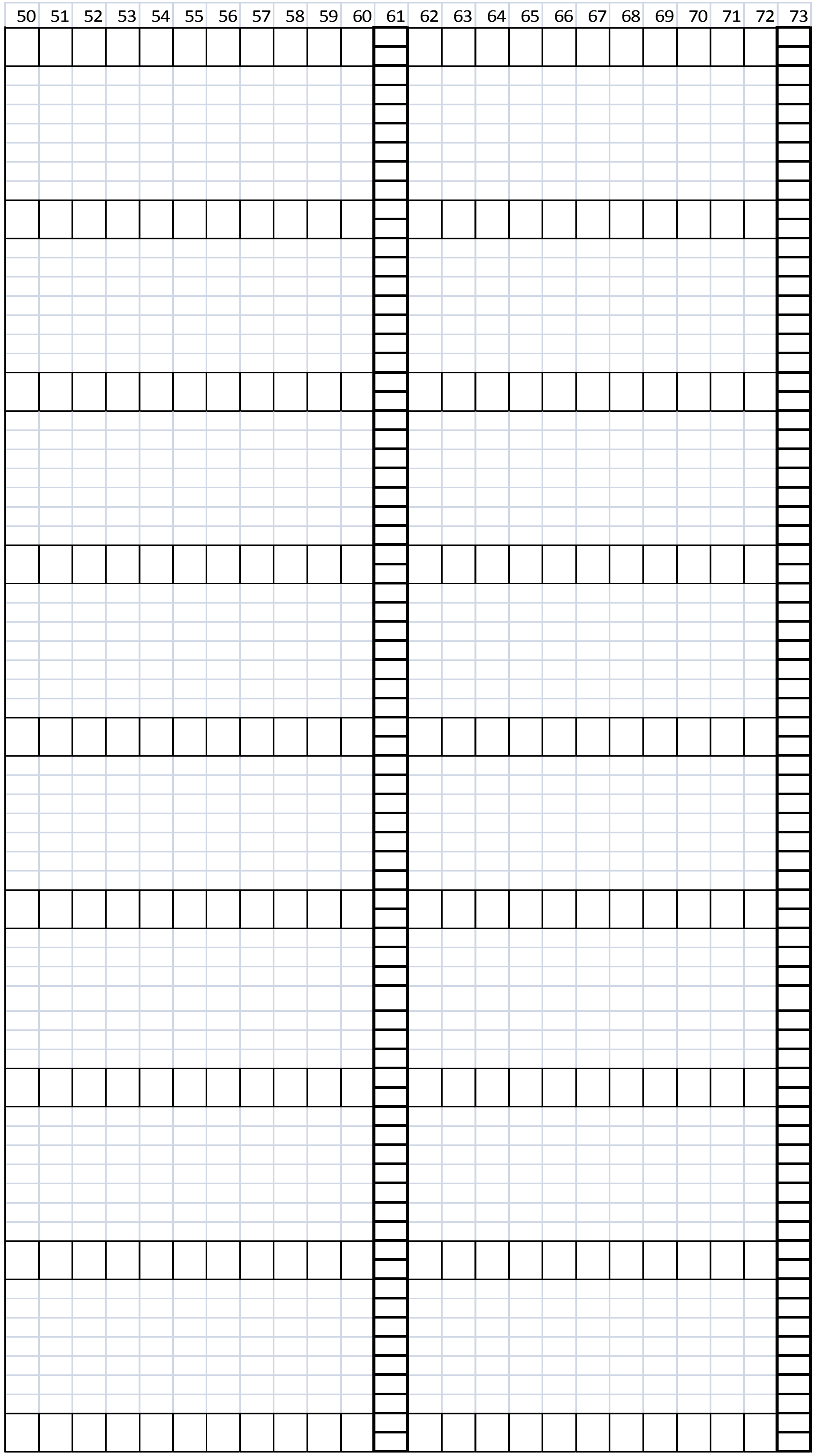

Figure E.51 – DIA6 – record of fastener failure during inelastic test (3/6)

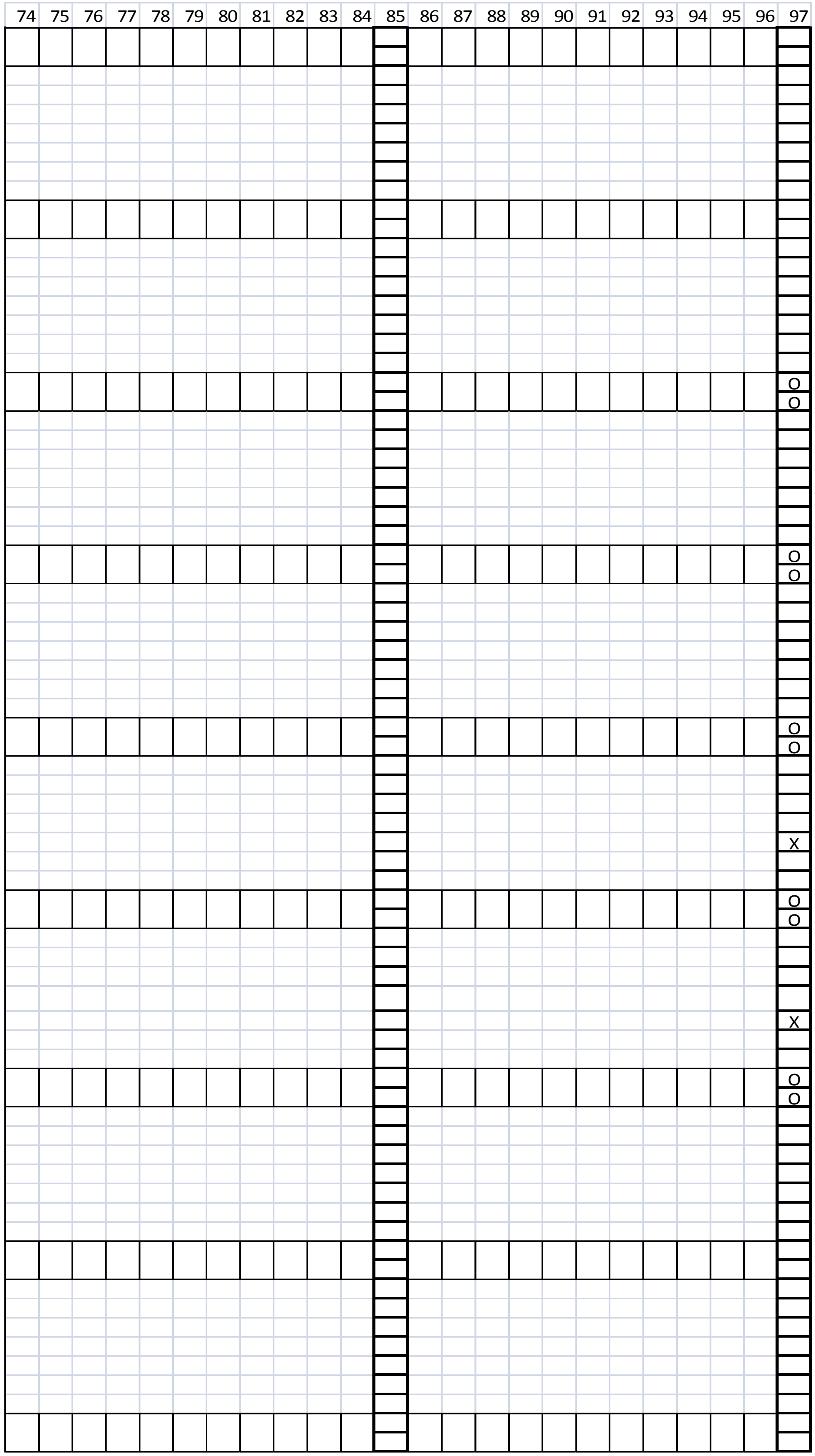

Figure E.52 – DIA6 – record of fastener failure during inelastic test (4/6)

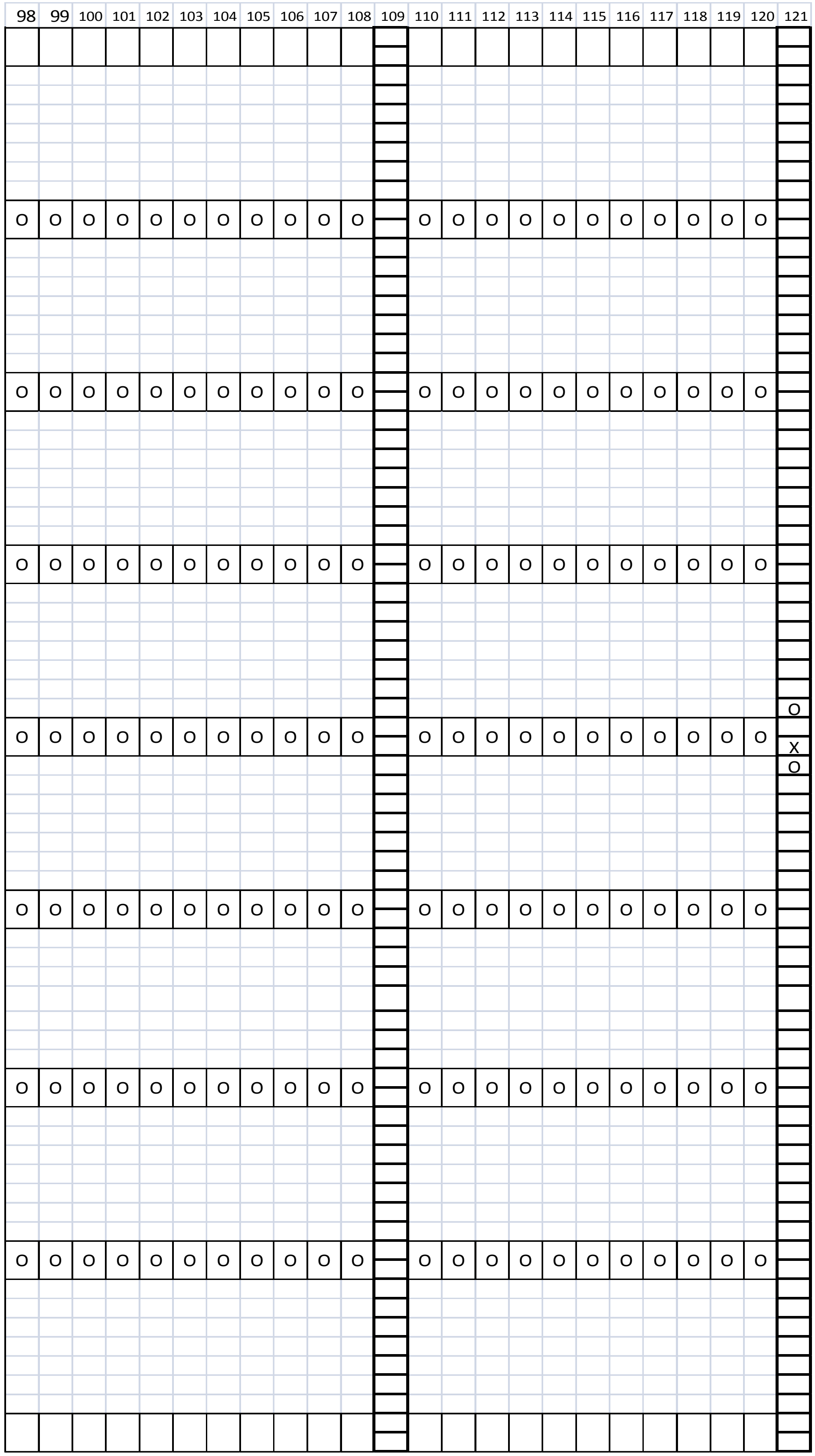

Figure E.53 – DIA6 – record of fastener failure during inelastic test (5/6)

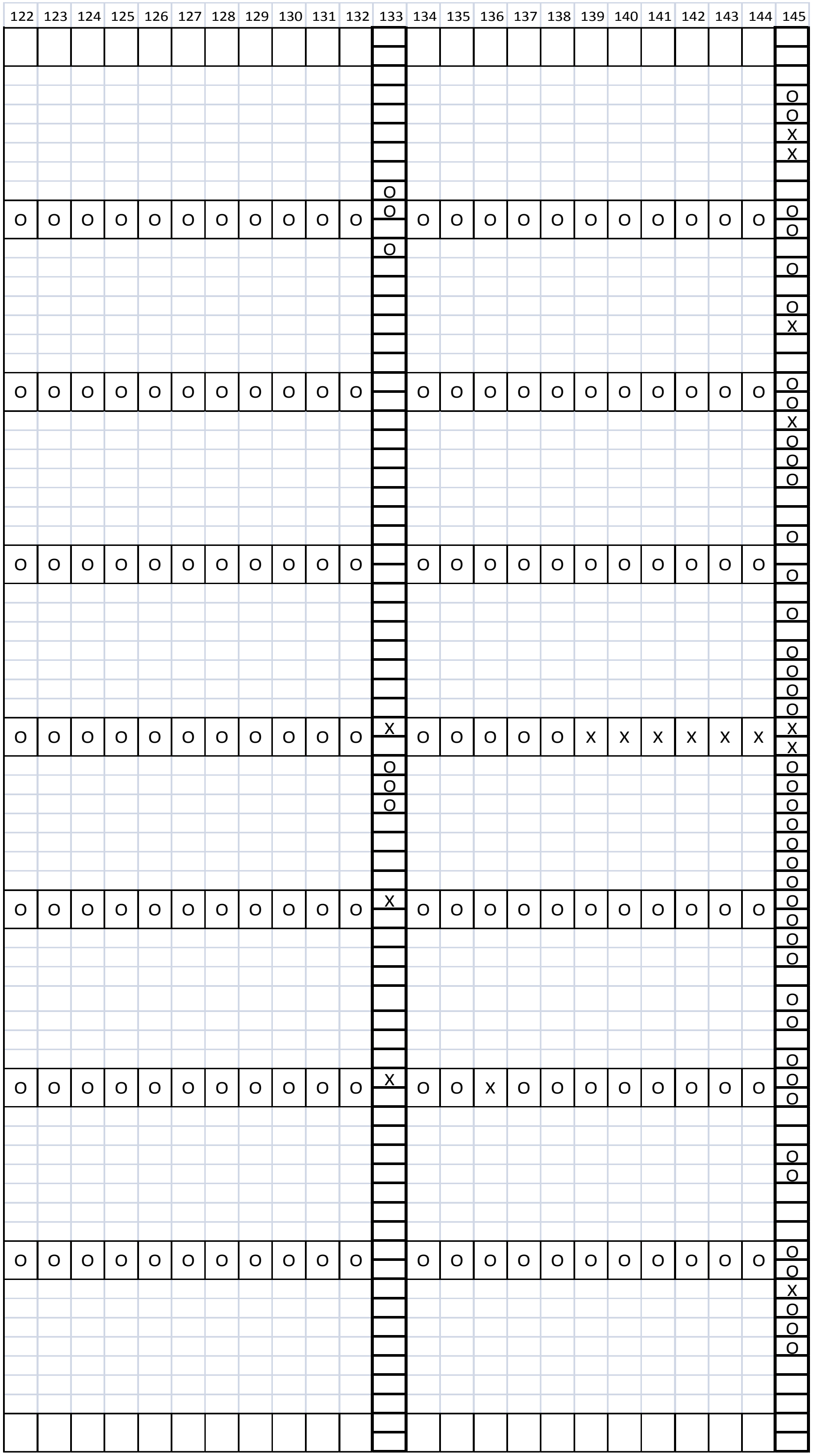

Figure E.54 – DIA6 – record of fastener failure during inelastic test (6/6)

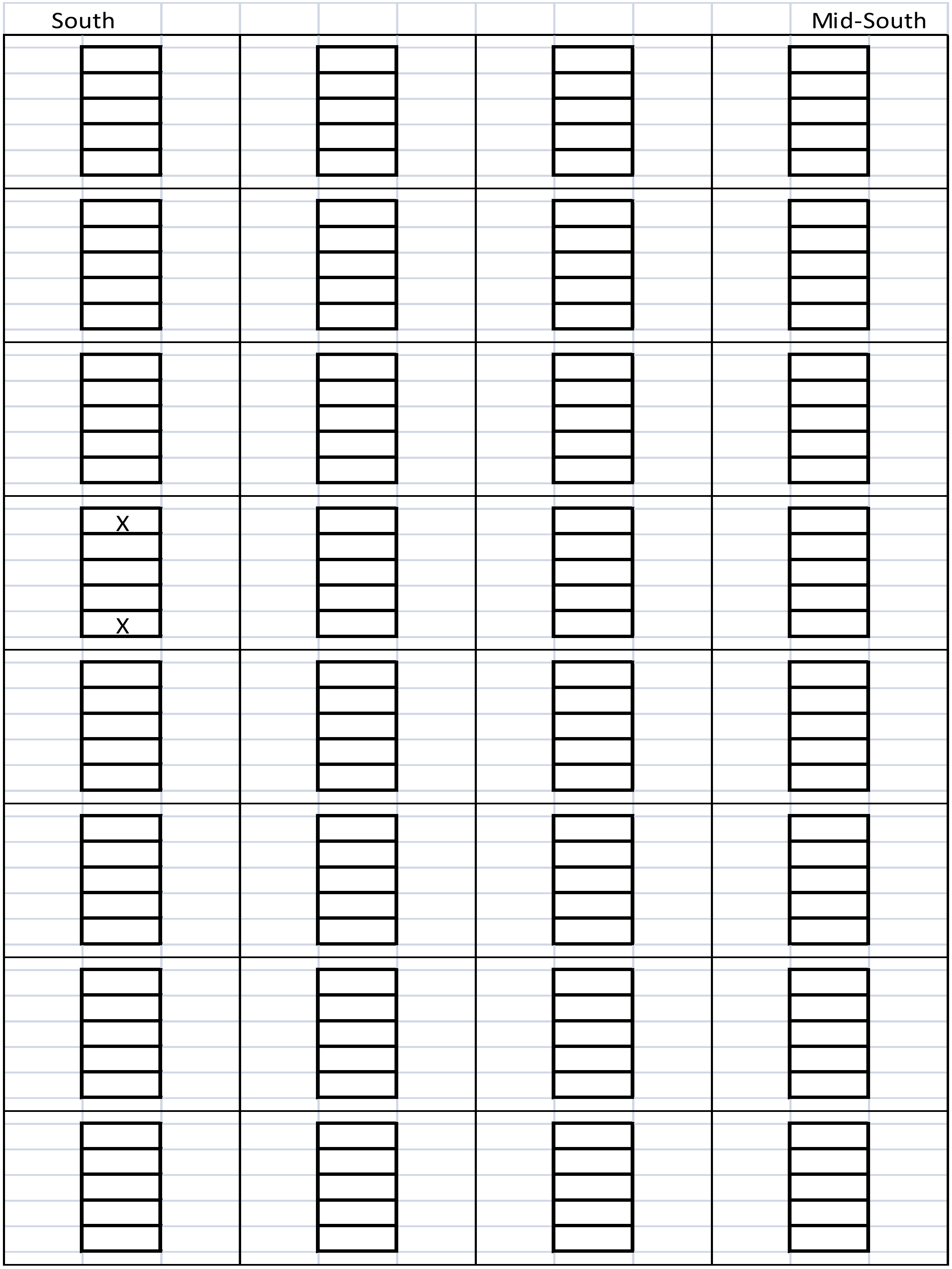

Figure E.55 – DIA6 – steel mass loss during inelastic test (1/3)

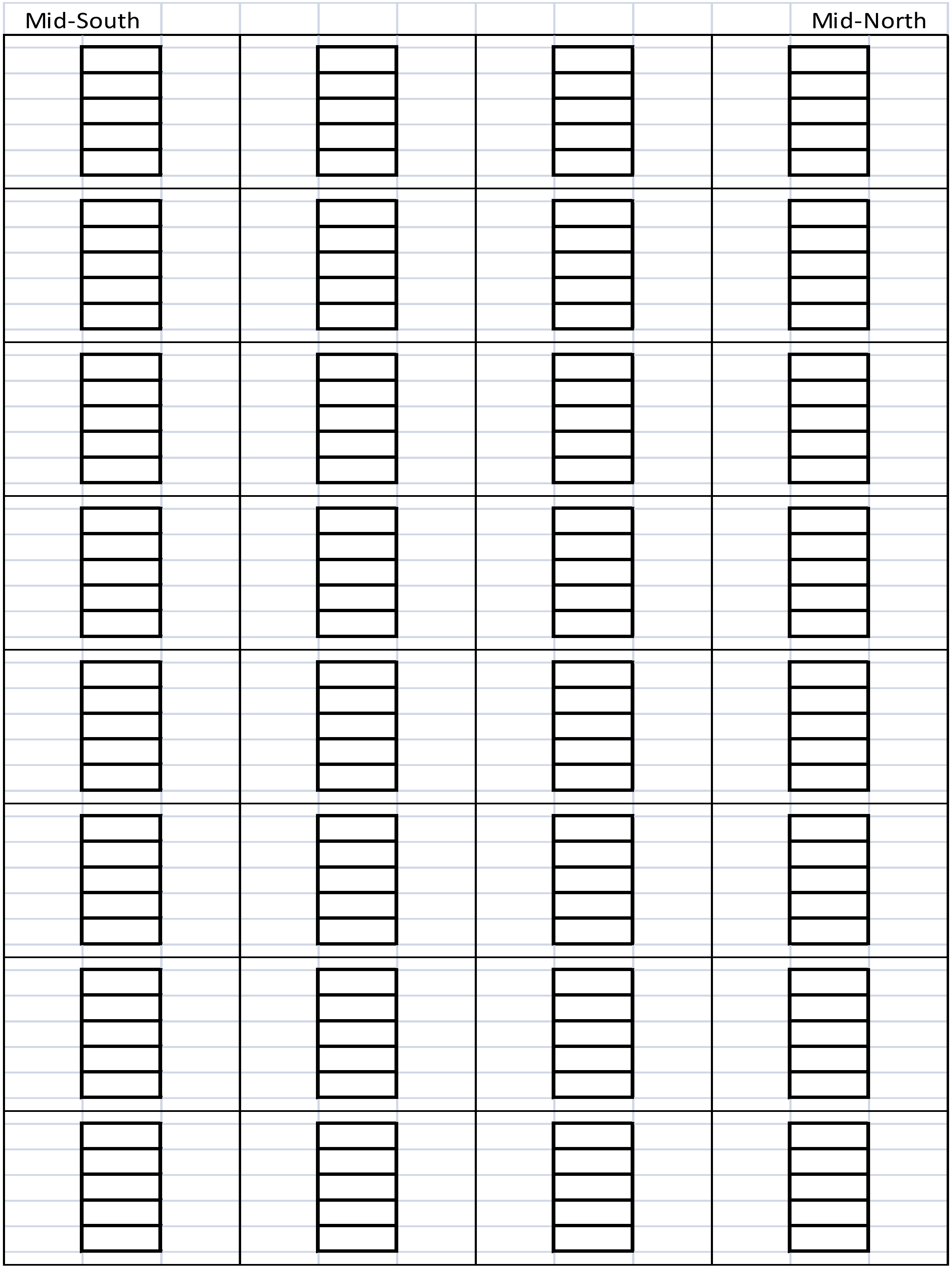

Figure E.56 – DIA6 – steel mass loss during inelastic test (2/3)

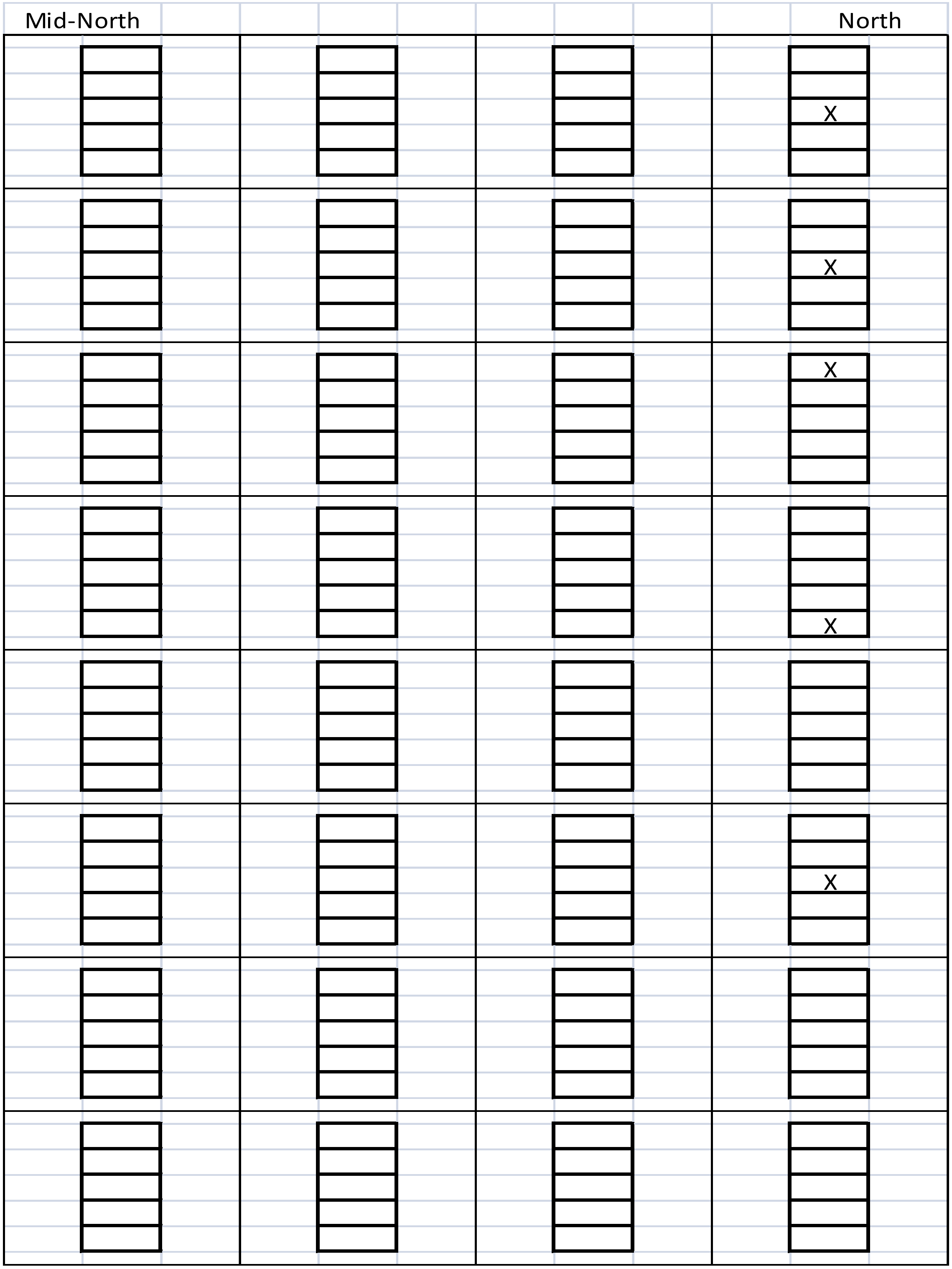

Figure E.57 – DIA6 – steel mass loss during inelastic test (3/3)

Table E.12 – DIA6R – list of testing protocols

BB		SS3		SS1		SS2	
0	☑	50	☑	50	☑	5	☑
225	☑	60	☑	60	☑	10	☑
675	☑	80	☑	70	☑	92	☑
1150	☑	100	☑	80	☑		
1825	☑	120	☑	90	☑		
2275	☑	140	☑	100	☑		
3200	☑	160	☑	110	☑		
5050	☑	180	☑	120	☑		
6000	☑	200	☑	130	☑		
8000	☑	220	☑	140	☑		
10000	☑	240	☑	150	☑		
20000	☑	260	☑				
30000	☑	280	☑				
40000	☑	300	☑				
60000	☑						
80000	☑						
100000	☑						
120000	☑						
140000	☑						
160000	☑						

<u>Notes</u>

- Big actuator valves used for SS1-200 and SS1-80 and all larger amplitudes for those two loading protocols

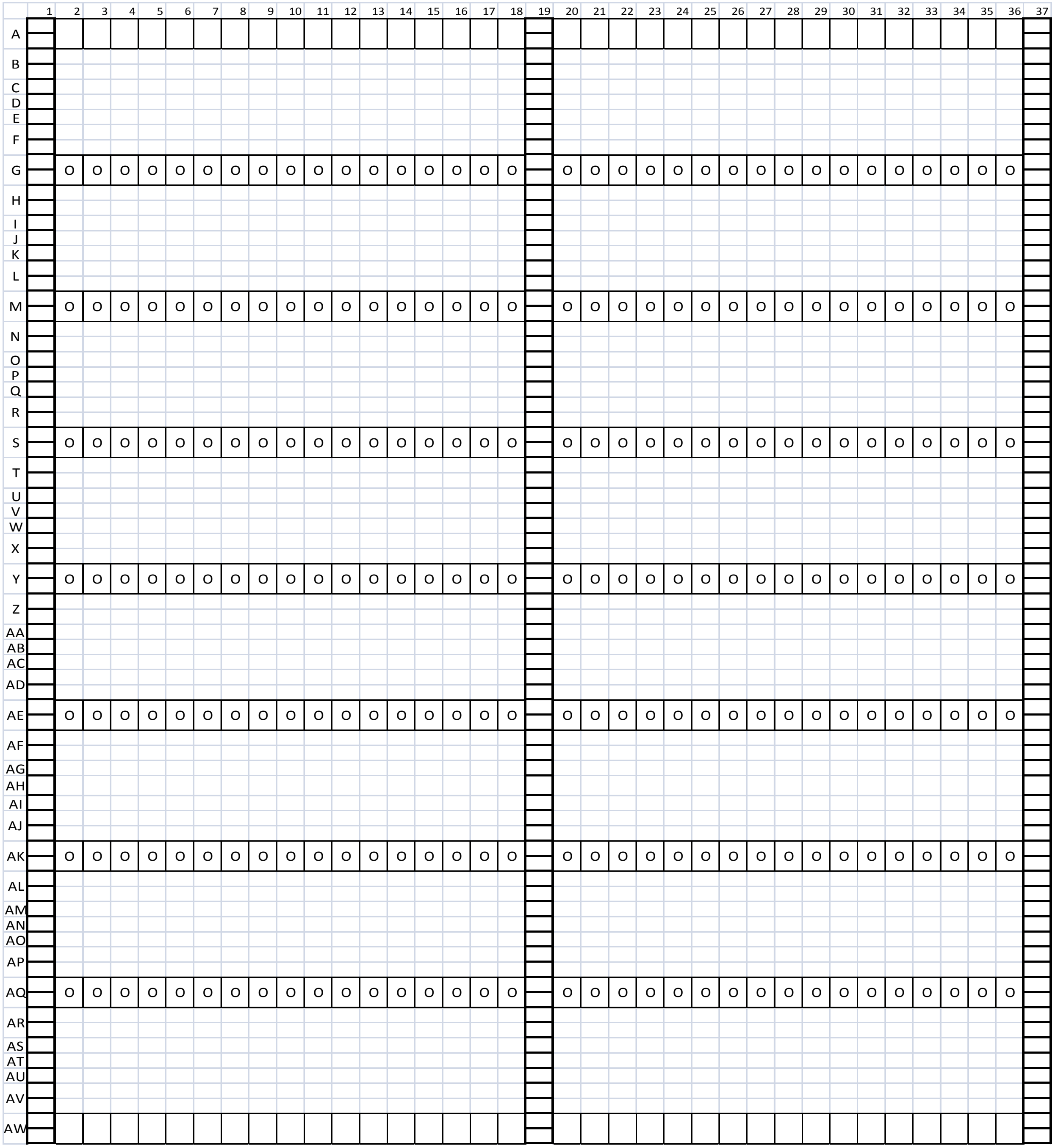

Figure E.58 – DIA6R – record of fastener failure during inelastic test (1/6)

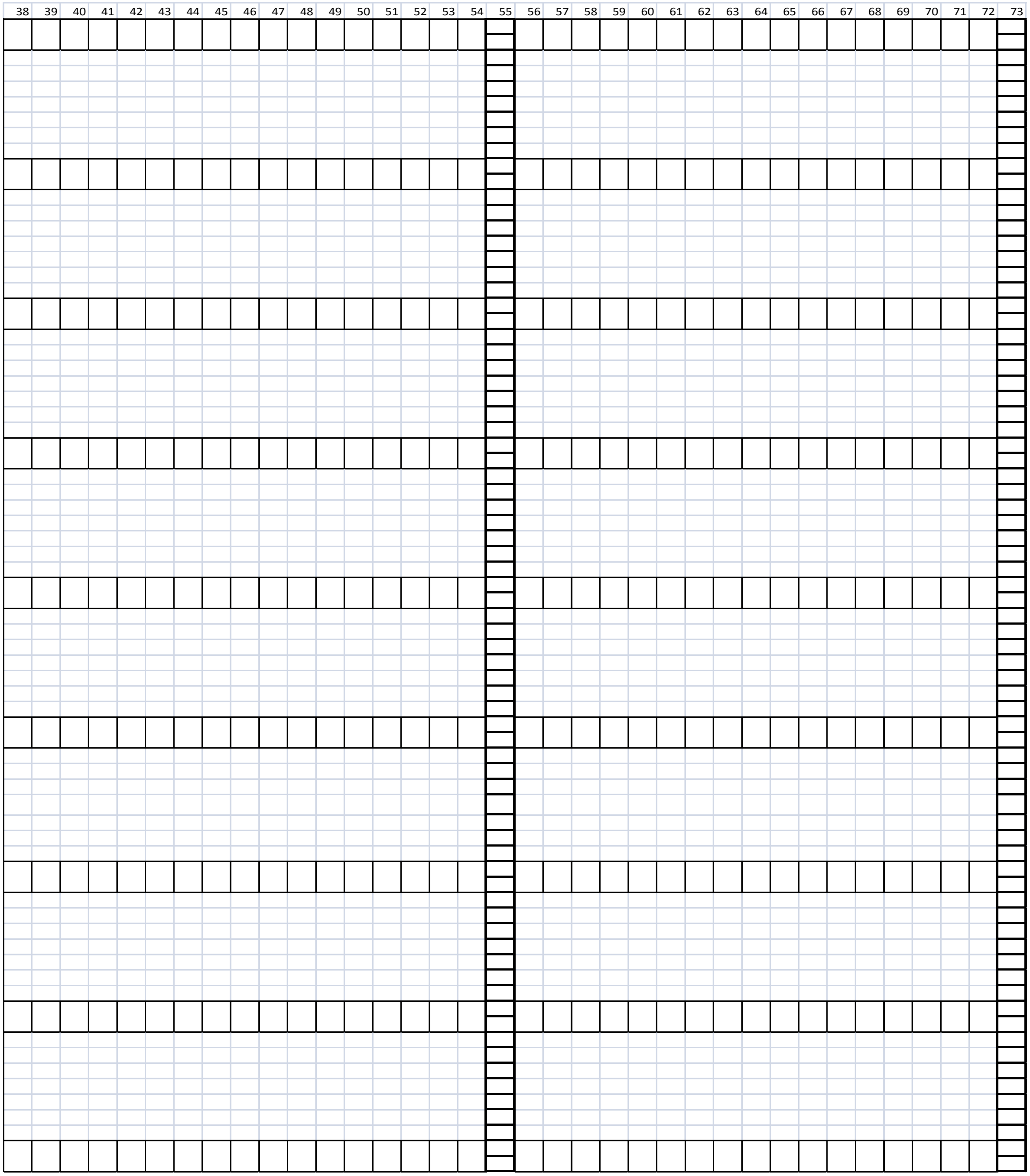

Figure E.59 – DIA6R – record of fastener failure during inelastic test (2/6)

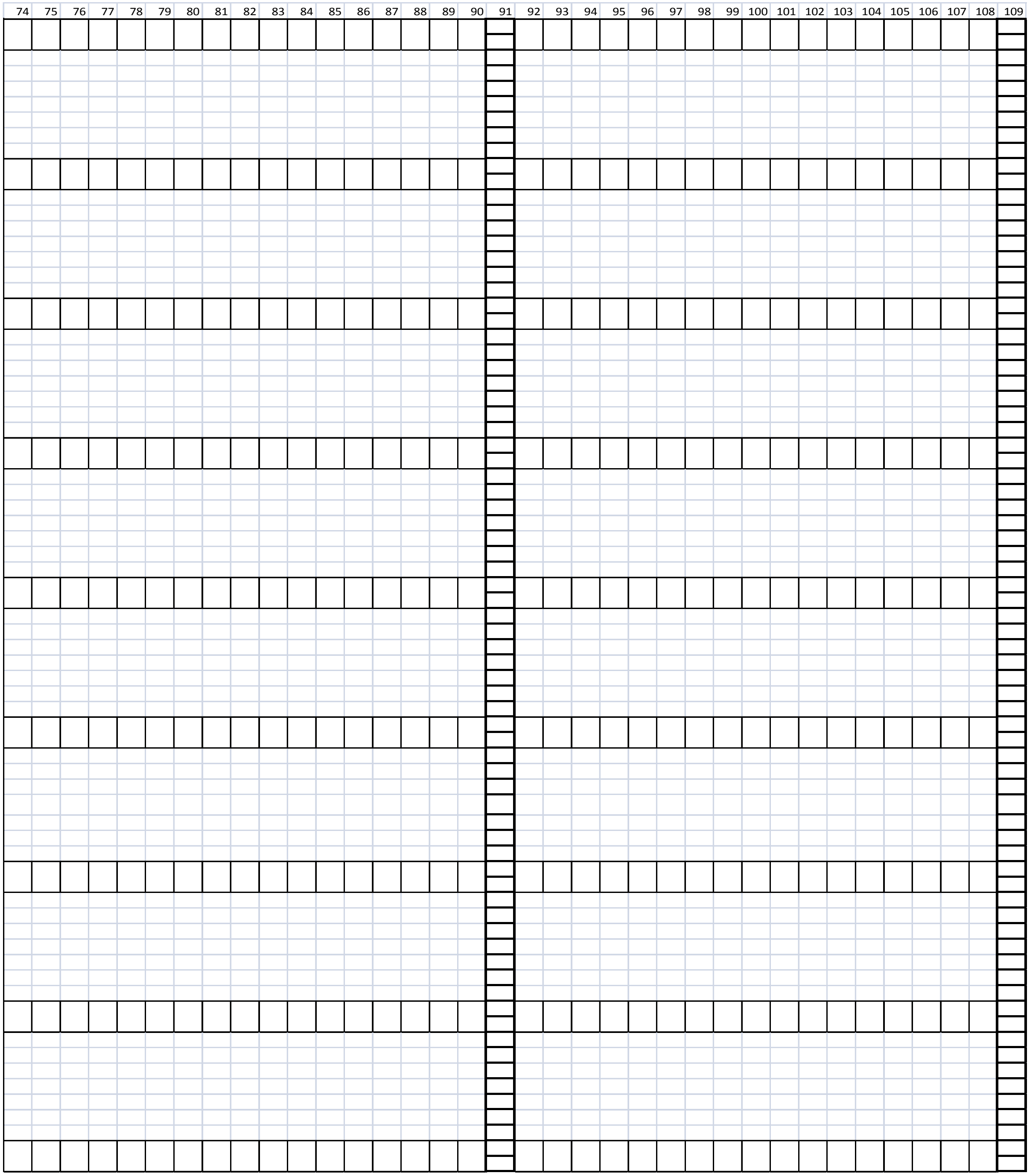

Figure E.60 – DIA6R – record of fastener failure during inelastic test (3/6)

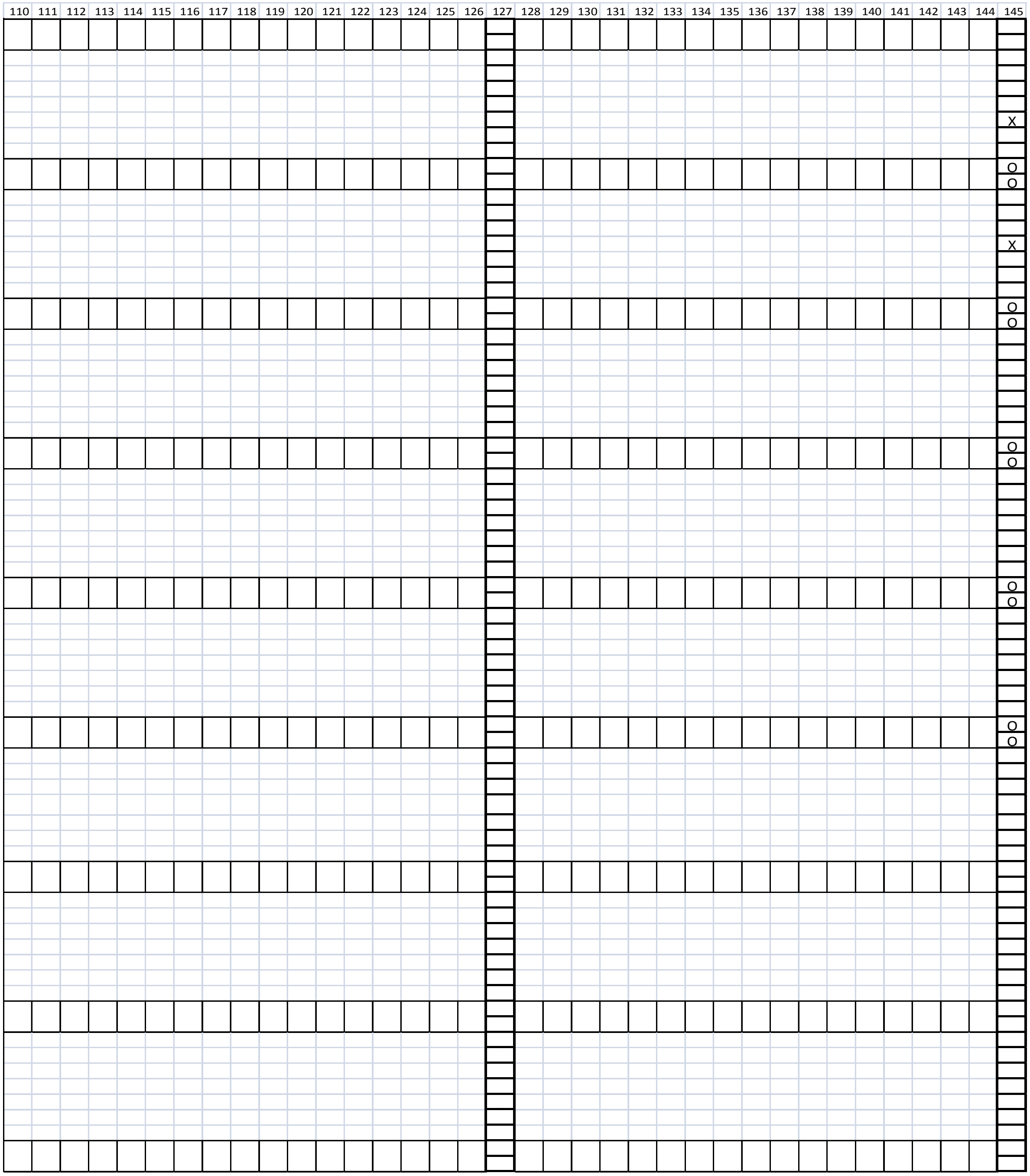

Figure E.61 – DIA6R – record of fastener failure during inelastic test (4/6)

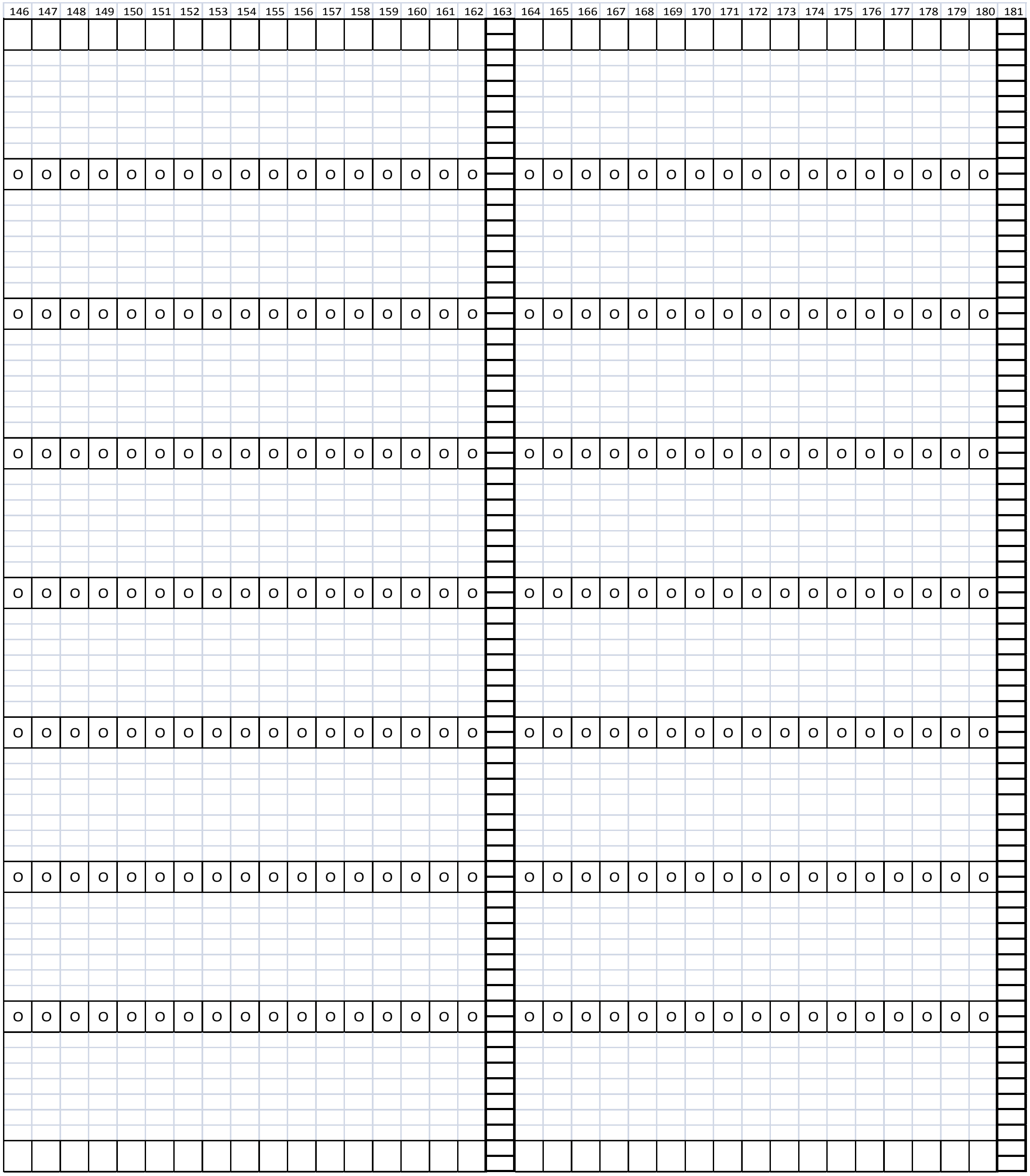

Figure E.62 – DIA6R – record of fastener failure during inelastic test (5/6)

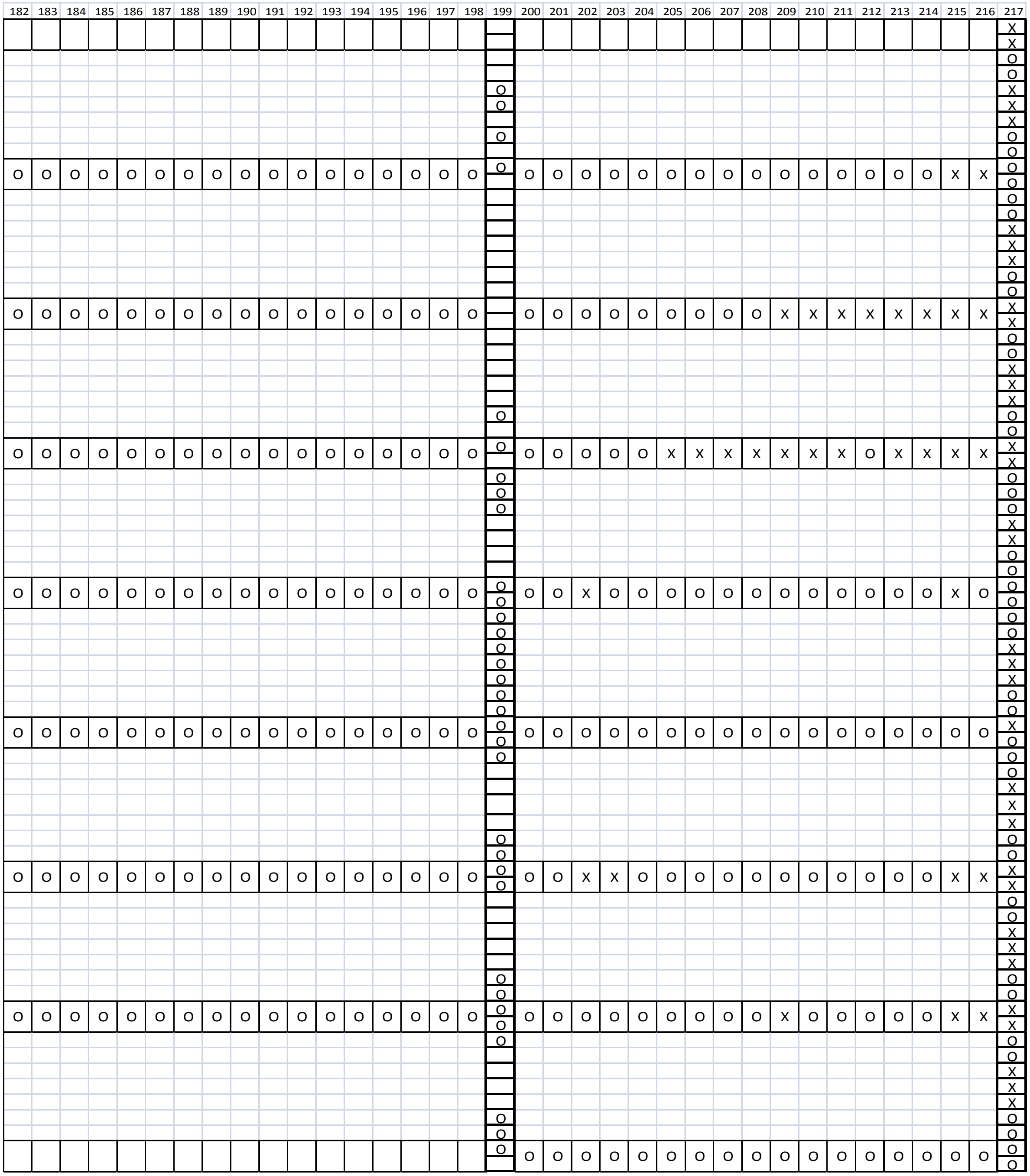

Figure E.63 – DIA6R – record of fastener failure during inelastic test (6/6)

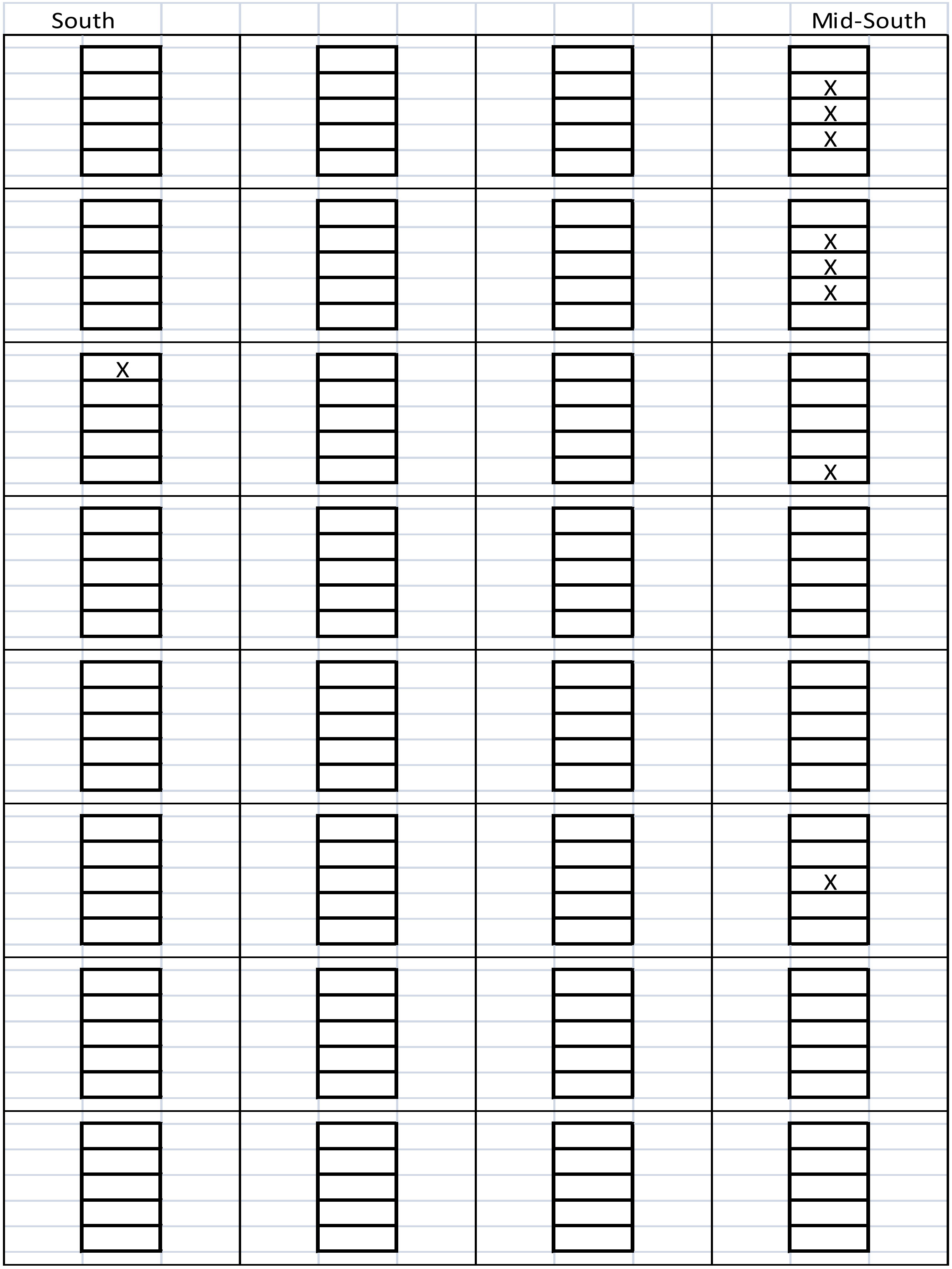

Figure E.64 – DIA6R – steel mass loss during inelastic test (1/3)

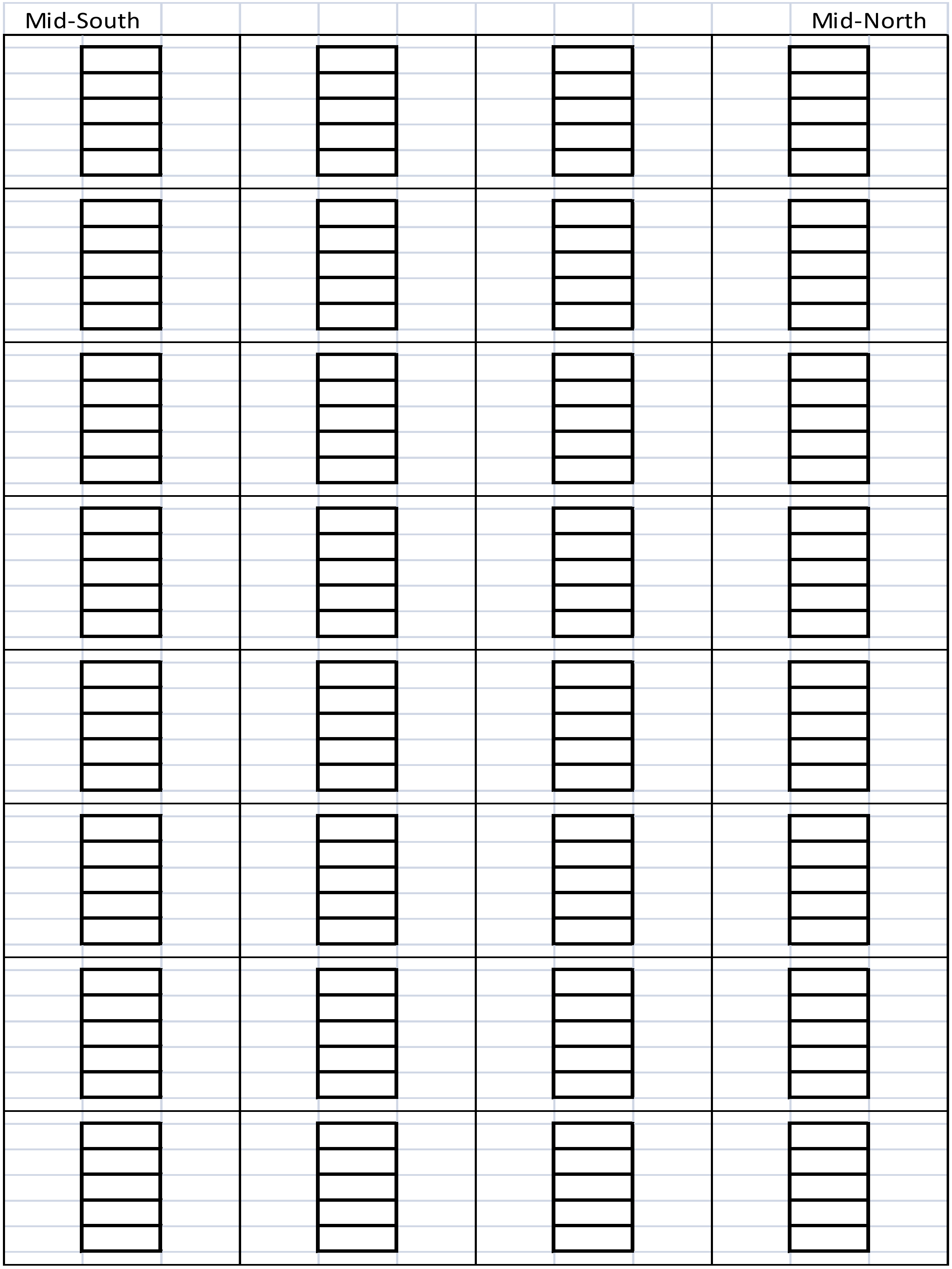

Figure E.65 – DIA6R – steel mass loss during inelastic test (2/3)

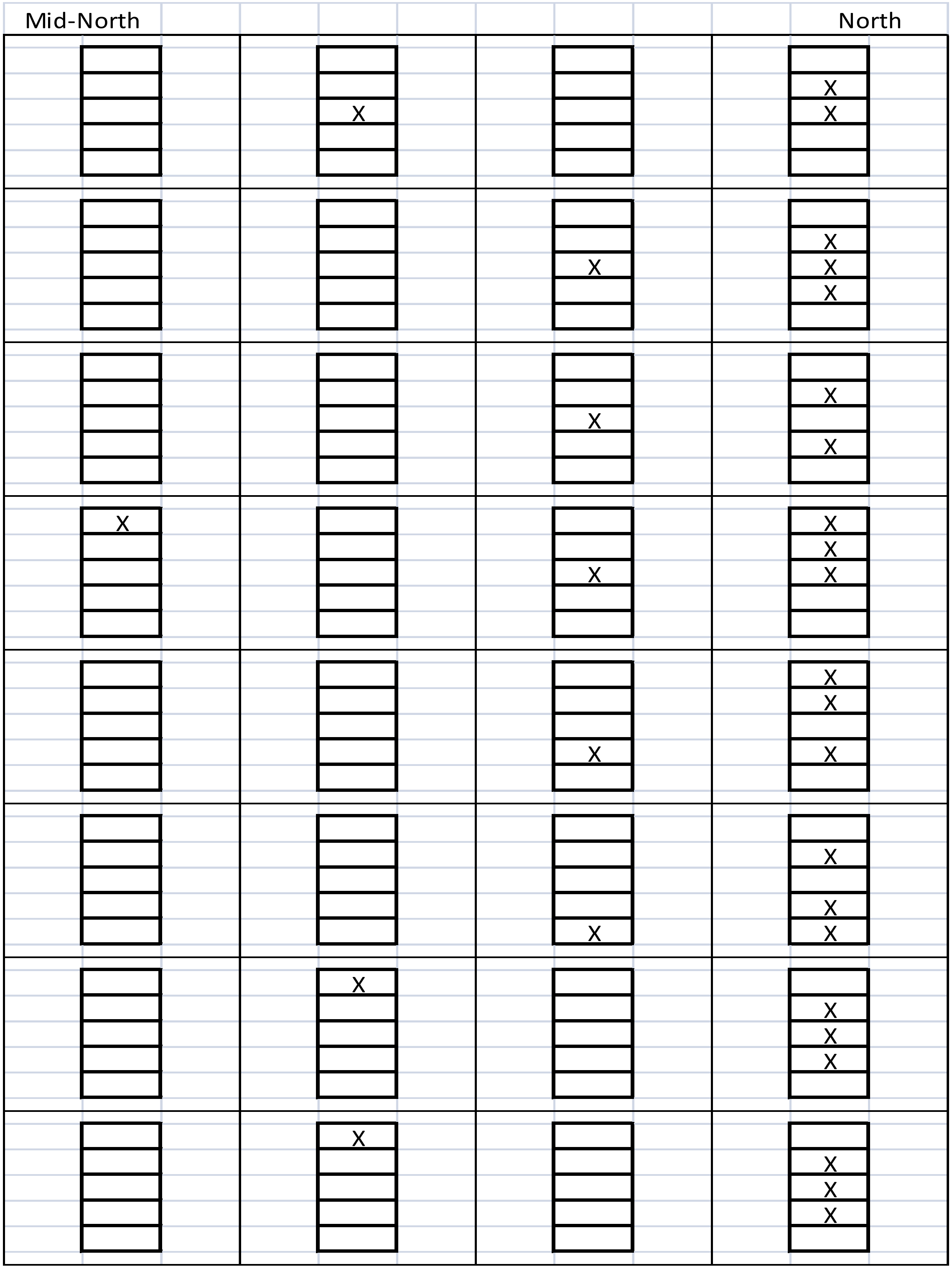

Figure E.66 – DIA6R – steel mass loss during inelastic test (3/3)

Table E.13 – DIA7 – list of testing protocols

BB		SS3		SS1		SS2	
0	☑	50	☑	50	☑	5	☑
225	☑	60	☑	60	☑	10	☑
675	☑	80	☑	70	☑	80	☑
1150	☑	100	☑	80	☑		
1825	☑	120	☑				
2275	☑	140	☑				
3200	☑	160	☑				
5050	☑	180	☑				
6000	☑	200	☑				
8000	☑	220	☑				
10000	☑						
20000	☑						
30000	☑						
40000	☑						
60000	☑						
80000	☑						
100000	☑						
120000	☑						
140000	☑						
160000	☑						

Notes

- Big actuator valves used for SS1-200 and SS1-80 and all larger amplitudes for those two loading protocols

	1	2	3	4	5	6	7	8	9	10	11	12	13	14	15	16	17	18	19	20	21	22	23	24	25	26	27	28	29	30	31	32	33	34	35	36	37
A																																					
B																																					
C	O																																				
D																																					
E																																					
F																																					
G		O	O	O	O	O	O	O	O	O	O	O	O												O												
H																																					
I																																					
J																																					
K																																					
L																																					
M		O	O	O	O	O	O	O	O	O	O	O	O												O												
N																																					
O																																					
P																																					
Q																																					
R																																					
S	X												O												O												
T																																					
U																																					
V																																					
W																																					
X																																					
Y	X												O												O												
Z																																					
AA																																					
AB																																					
AC																																					
AD																																					
AE													O												O												
AF																																					
AG																																					
AH																																					
AI																																					
AJ																																					
AK													O												O												
AL																																					
AM																																					
AN																																					
AO																																					
AP																																					
AQ													O																								
AR																																					
AS																																					
AT																																					
AU																																					
AV																																					
AW																																					

Figure E.67 – DIA7 – record of fastener failure during inelastic test (1/4)

38	39	40	41	42	43	44	45	46	47	48	49	50	51	52	53	54	55	56	57	58	59	60	61	62	63	64	65	66	67	68	69	70	71	72	73

Figure E.68 – DIA7 – record of fastener failure during inelastic test (2/4)

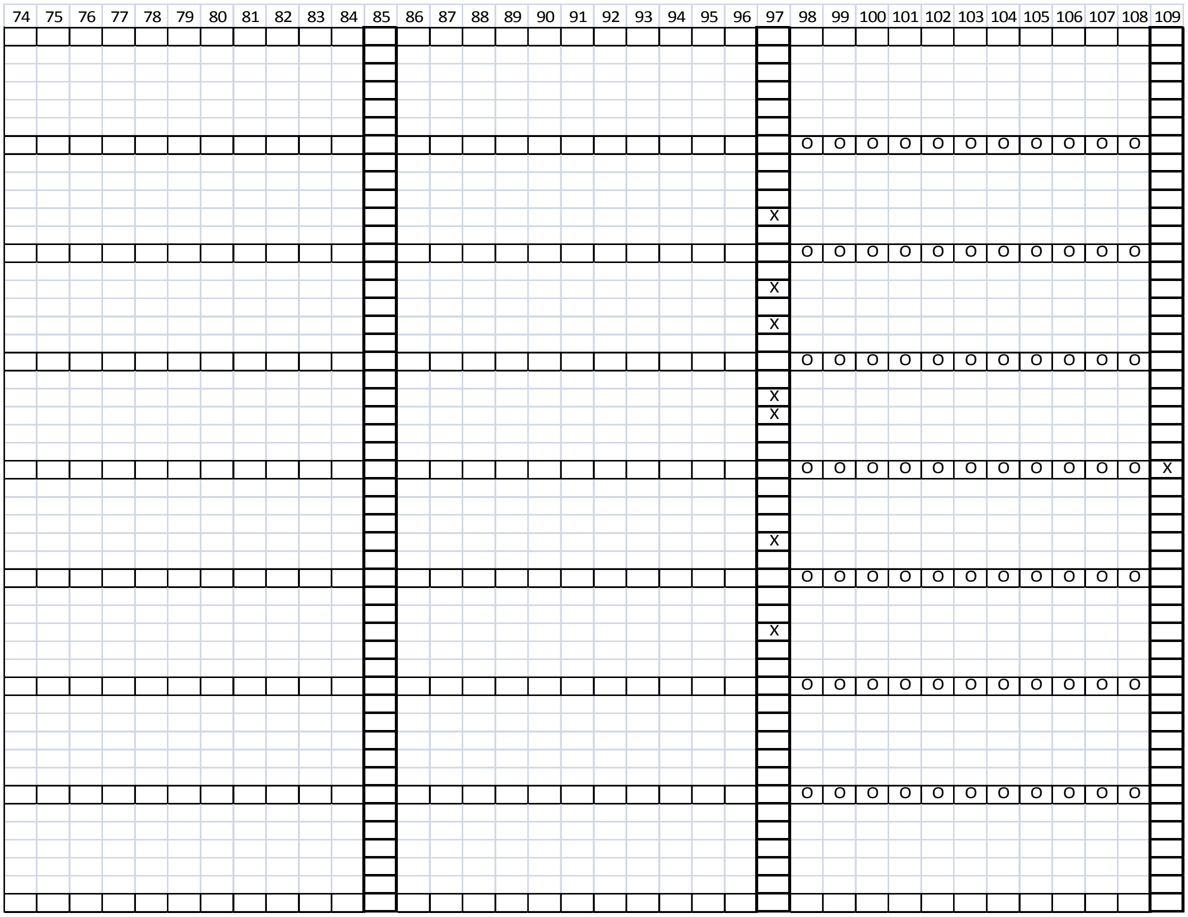

Figure E.69 – DIA7 – record of fastener failure during inelastic test (3/4)

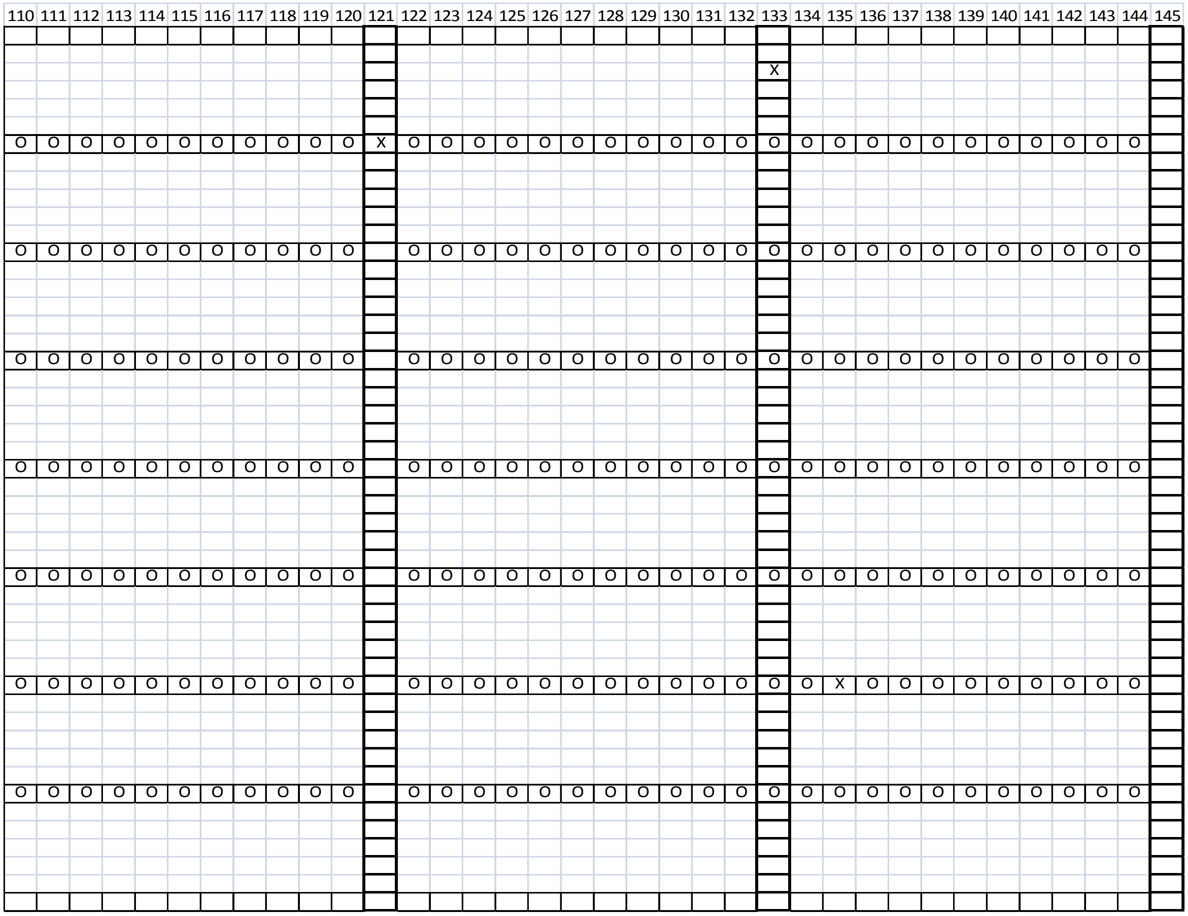

Figure E.70 – DIA7 – record of fastener failure during inelastic test (4/4)

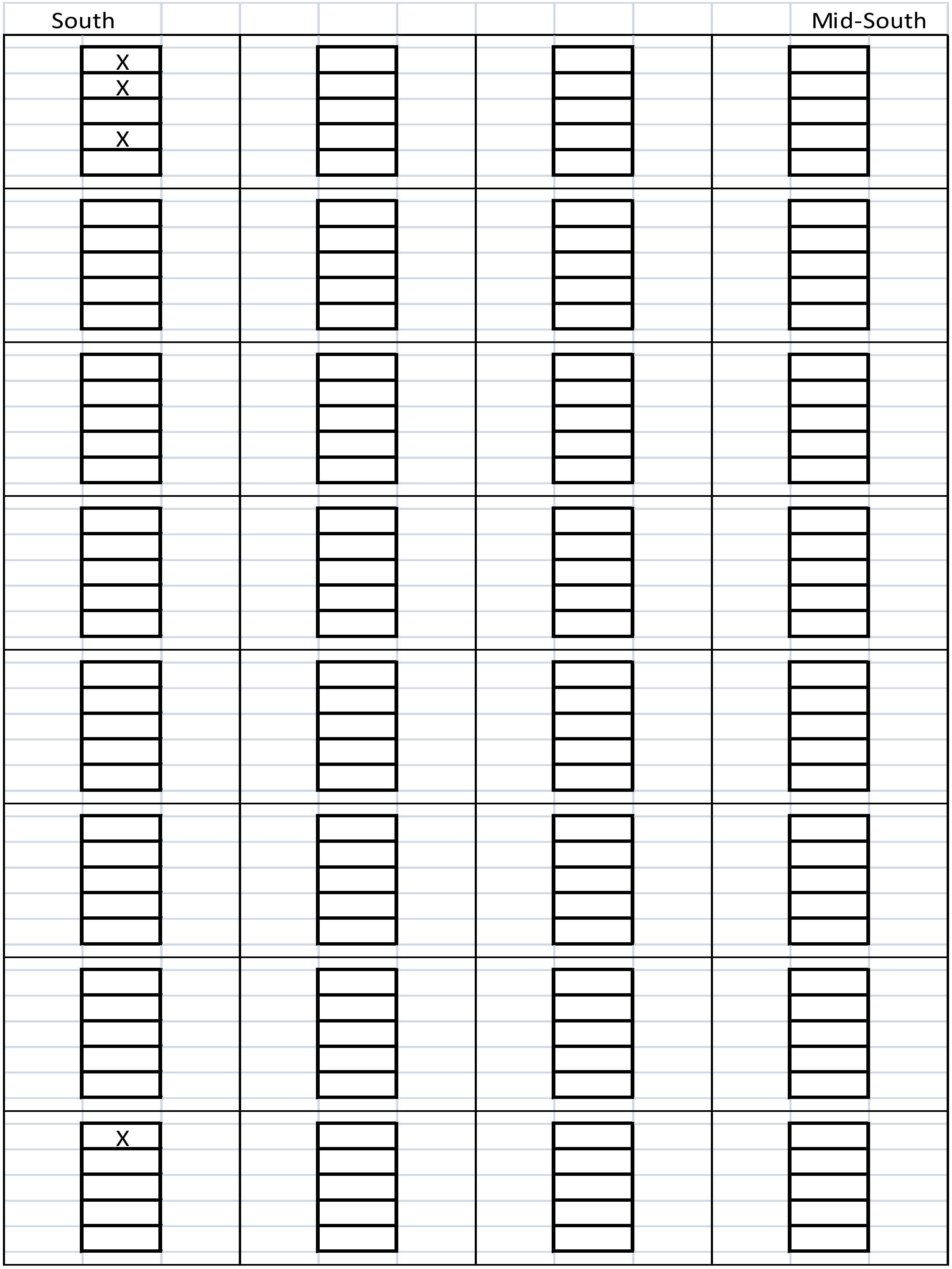

Figure E.71 – DIA7 – steel mass loss during inelastic test (1/3)

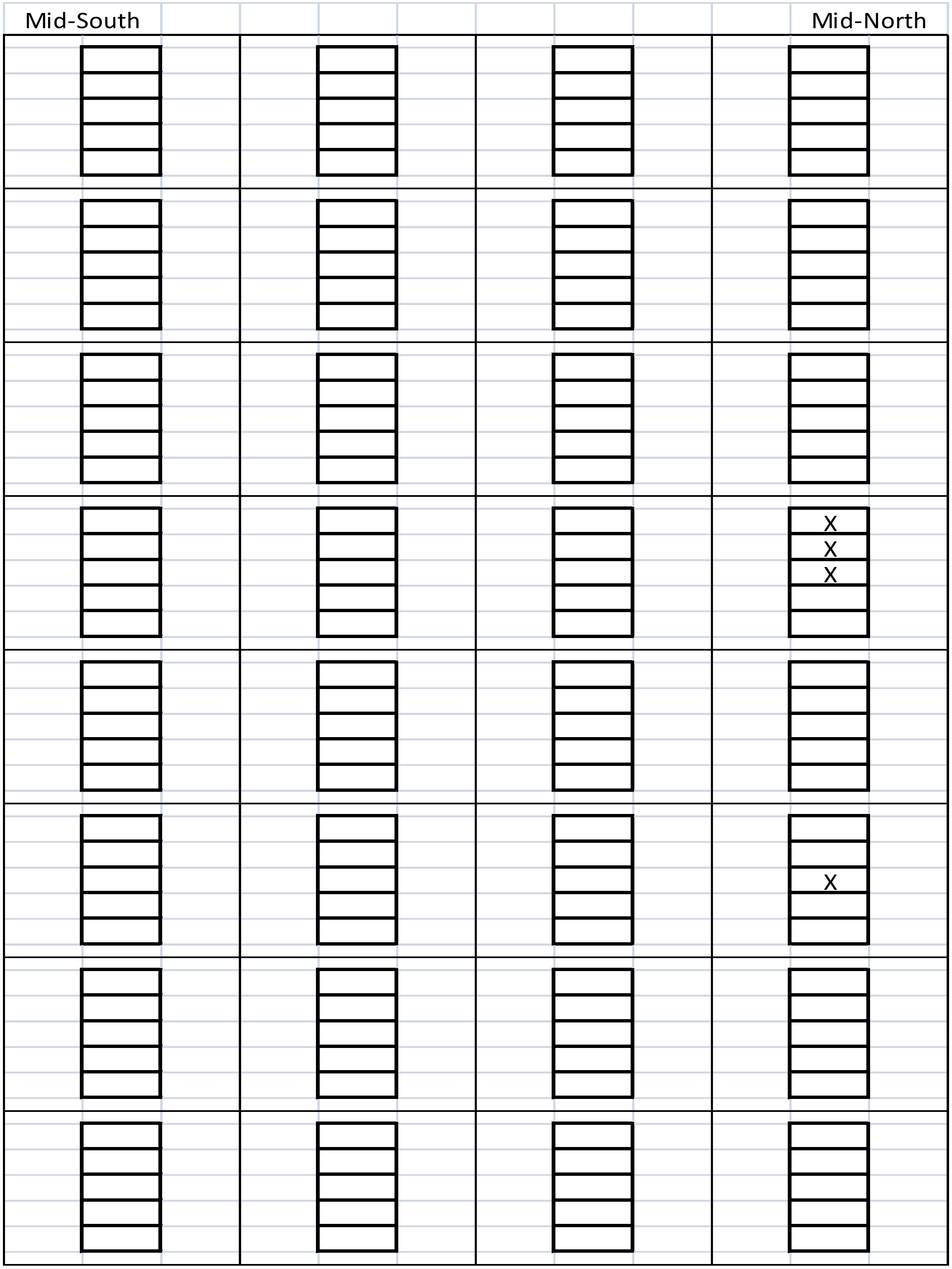

Figure E.72 – DIA7 – steel mass loss during inelastic test (2/3)

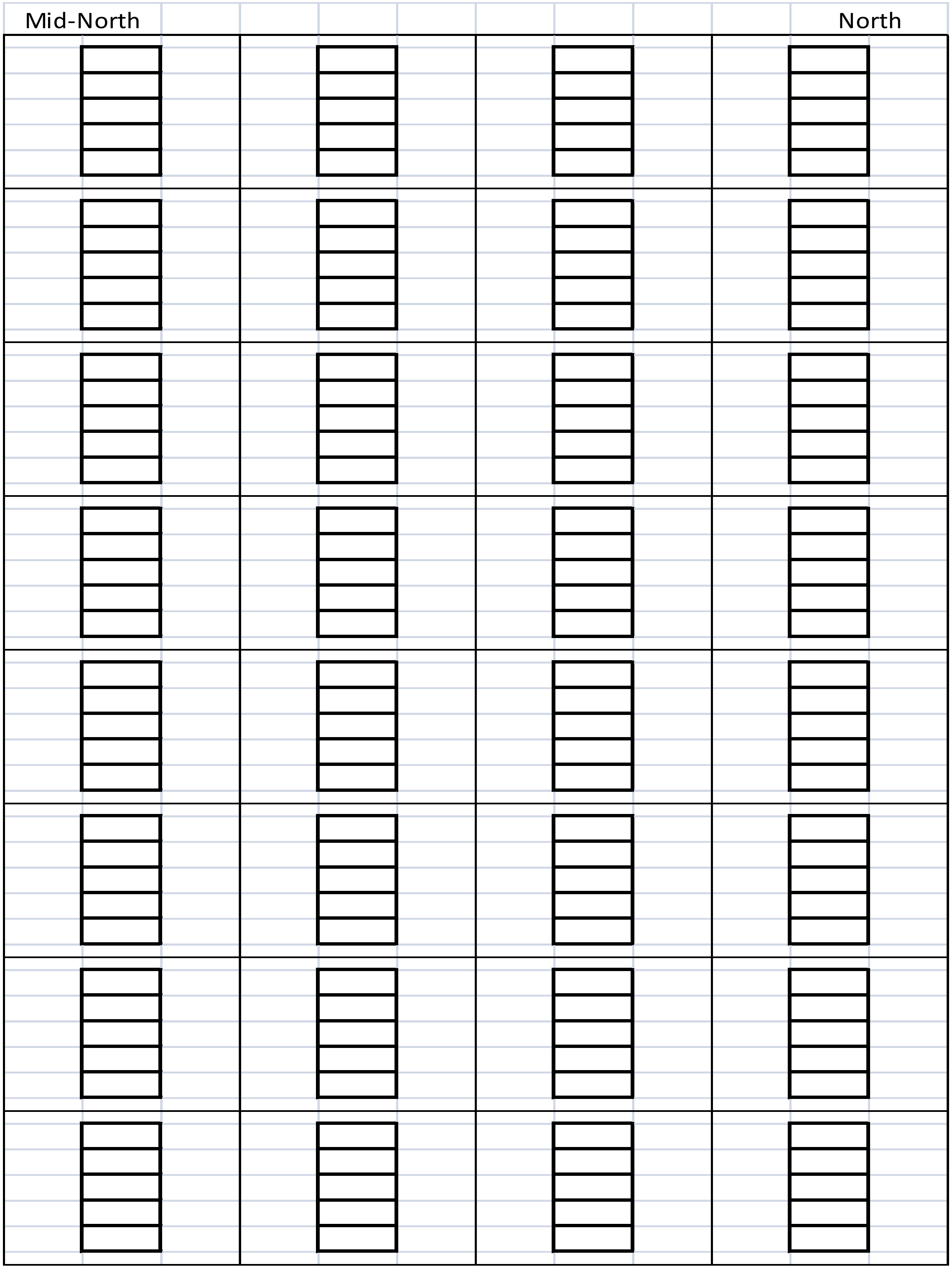

Figure E.73 – DIA7 – steel mass loss during inelastic test (3/3)

Table E.14 – DIA7R – list of testing protocols

BB		SS3		SS1		SS2	
0	☑	50	☑	50	☑	5	☑
225	☑	60	☑	60	☑	10	☑
675	☑	80	☑	70	☑	80	☑
1150	☑	100	☑	80	☑		
1825	☑	120	☑	90	☑		
2275	☑	140	☑	100	☑		
3200	☑	160	☑	110	☑		
5050	☑	180	☑				
6000	☑	200	☑				
8000	☑	220	☑				
10000	☑	240	☑				
20000	☑						
30000	☑						
40000	☑						
60000	☑						
80000	☑						
100000	☑						
120000	☑						
140000	☑						

<u>Notes</u>

- Big actuator valves used for SS1-200 and SS1-80 and all larger amplitudes for those two loading protocols

	1	2	3	4	5	6	7	8	9	10	11	12	13	14	15	16	17	18	19	20	21	22	23	24	25	26	27	28	29	30	31	32	33	34	35	36	37
A																																					
B	O																																				
C	O																																				
D	O																																				
E																																					
F	O																																				
G	O	O	O	O	O	O	O	O	O	O	O	O	O	O	O	O	O	O	O	O	O	O	O	O													
H	O																																				
I																																					
J																																					
K	X																																				
L	O												O																								
M	X										X	O	O	O	O	O	O	O	O	O	O	O	O	O	O	O	O	O	O	O	O	O	O	X			
N	O												O																								
O																									O												
P	X																																				
Q																																					
R	O																																				
S	X	O	O	O	O	O	O	O	O	O	O	O	O	O	O	O	O	O	O	O	O	O	O	O		O	O	O	O	O	O						
T																																					
U	O																																				
V																																					
W	O																																				
X	O																																				
Y	X	O	O	O	O	O	O	O	O	O	O	O	X	O	O	O	O	O	O	O	O	O	X	O		O	O	O	O	O	X	O	X	O	O	O	
Z	O																																				
AA																																					
AB	O																																				
AC																																					
AD	O																																				O
AE	O	O	O	O	O	O	O	O	O	O	O	O		O	O	O	O	O	O	O	O	O	O	O		O	O										
AF	O																																				
AG	O																																				
AH																																					
AI	O																																				
AJ	O																																				
AK	O	O	O	O	O	O	O	O	O	O	O	O	O	O	O	O	O	O	O	O	O	O	O	O		O	O	O									
AL	X																																				
AM																																					
AN	O																																				
AO	O																																				
AP	O																																				
AQ	O	O	O	O	X	O	X	O	O	O	O	O	O	O	O	O	O	O	O	O	O	O	O	O		O	O	O	O	O	O	O	O	O	X	X	
AR	O												O																								
AS	O																																				
AT	O																																				
AU	O																																				
AV																																					
AW	O																								O												

Figure E.74 – DIA7R – record of fastener failure during inelastic test (1/4)

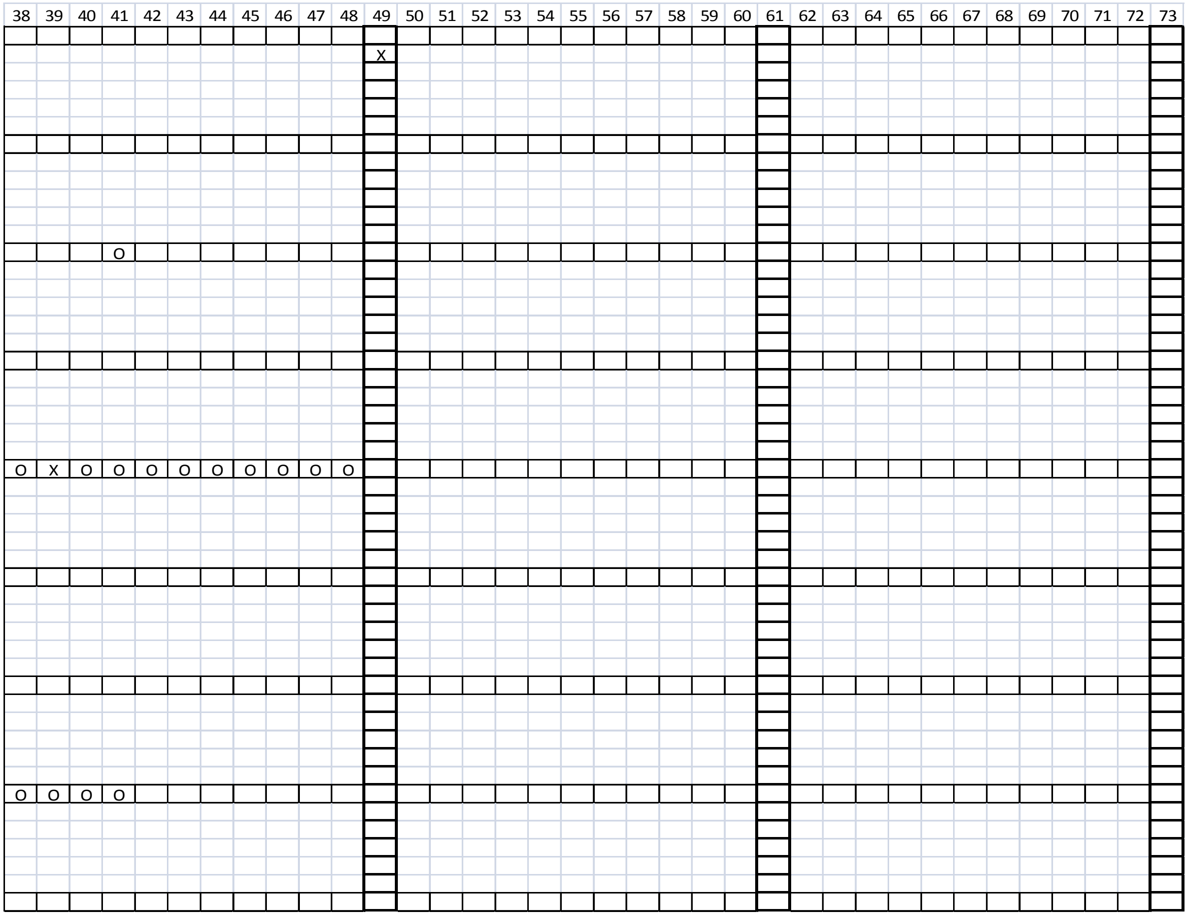

Figure E.75 – DIA7R – record of fastener failure during inelastic test (2/4)

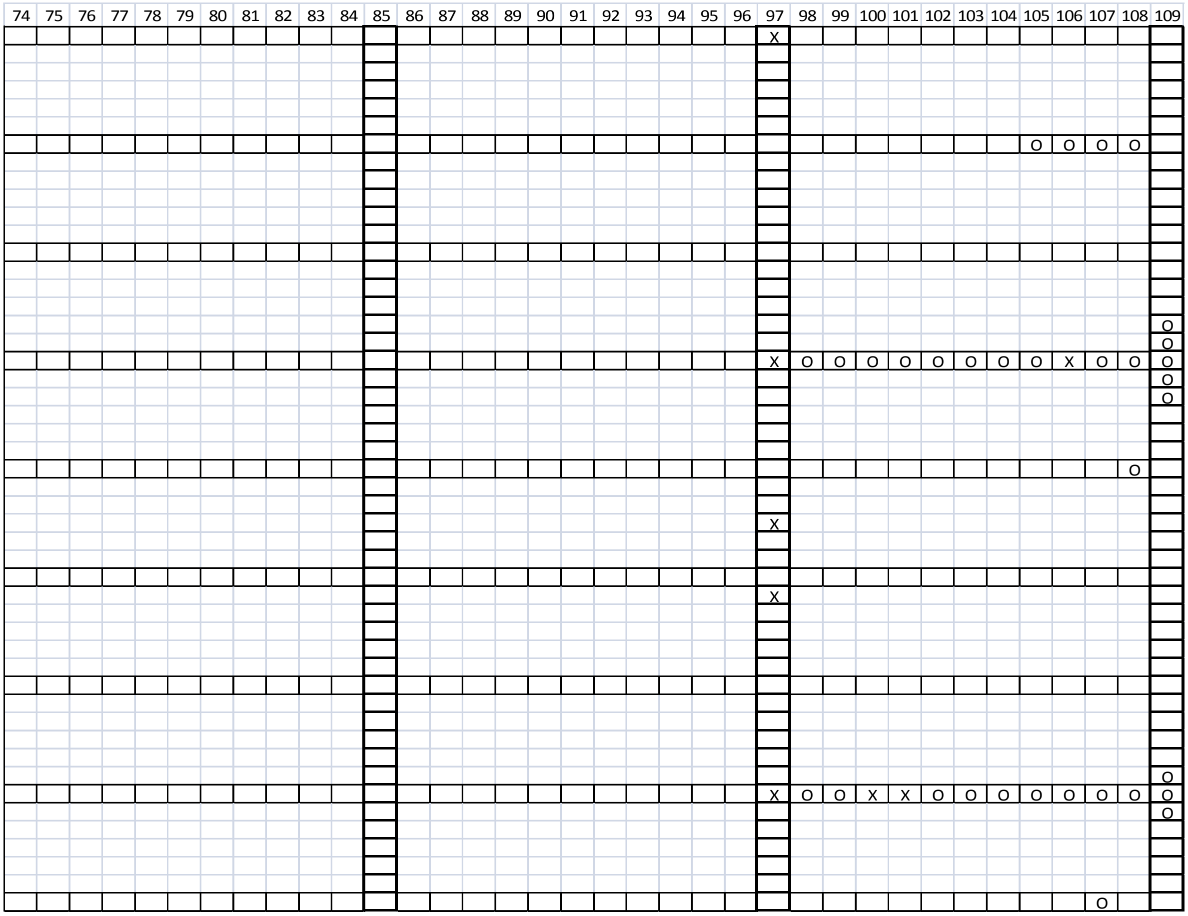

Figure E.76 – DIA7R – record of fastener failure during inelastic test (3/4)

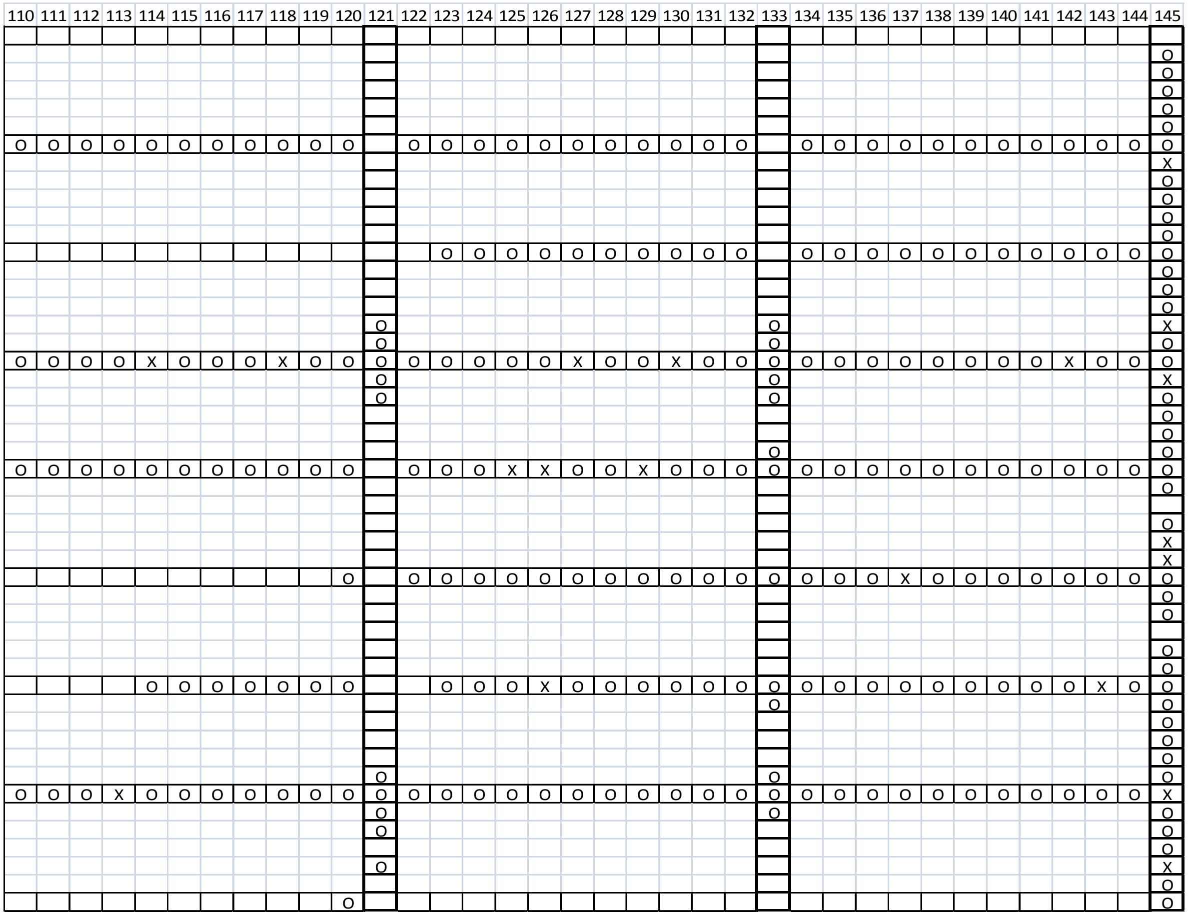

Figure E.77 – DIA7R – record of fastener failure during inelastic test (4/4)

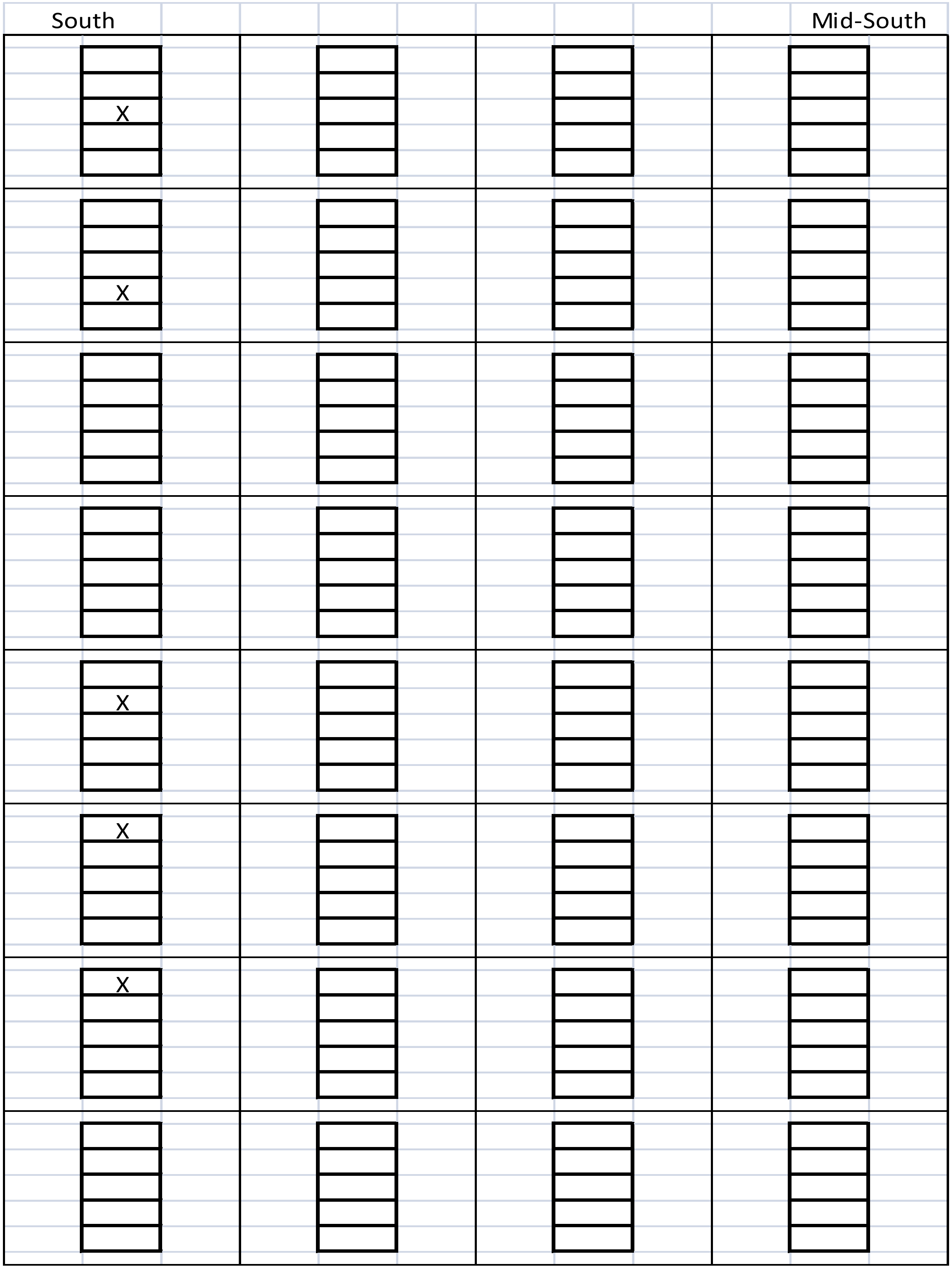

Figure E.78 – DIA7R – steel mass loss during inelastic test (1/3)

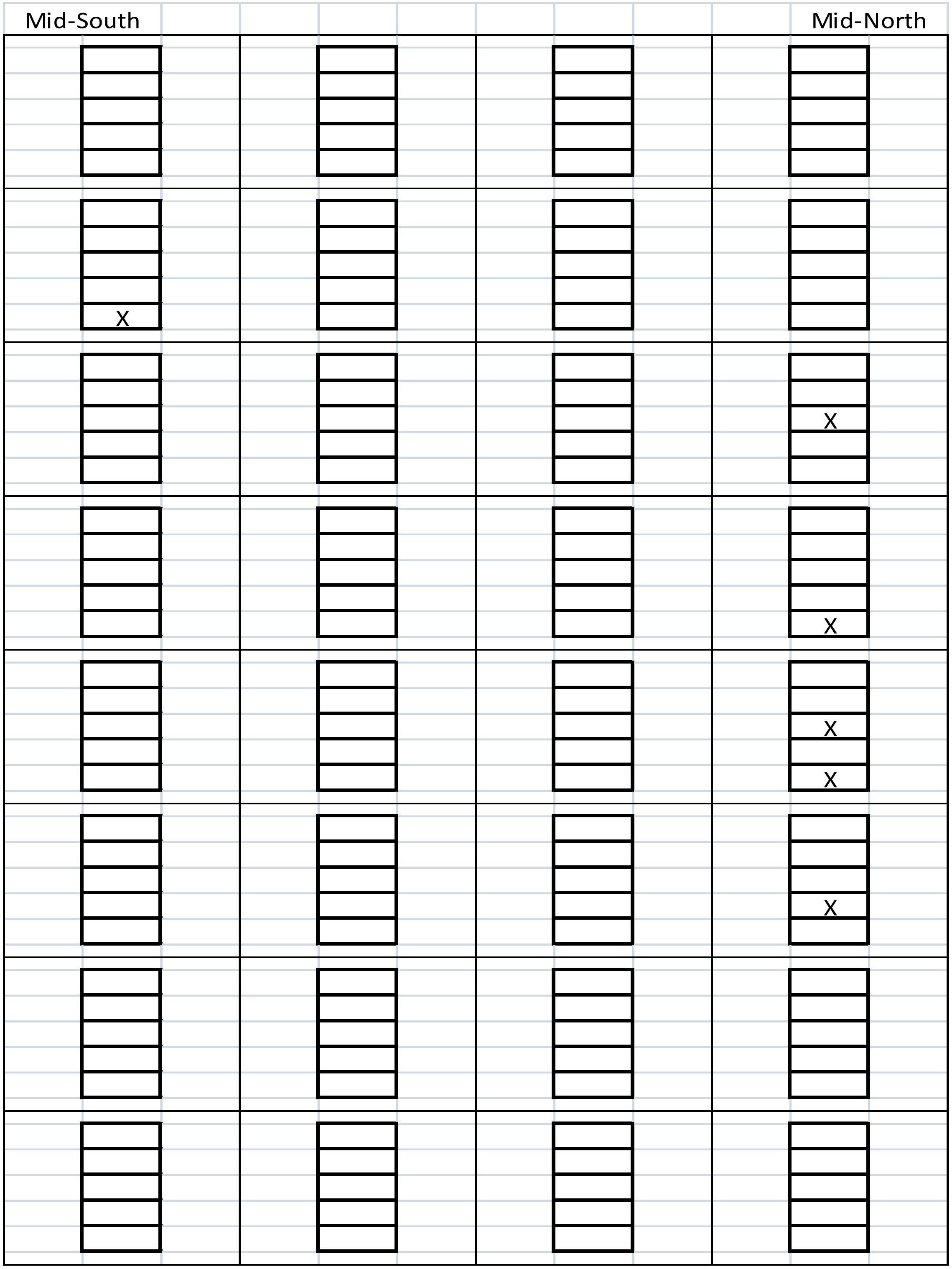

Figure E.79 – DIA7R – steel mass loss during inelastic test (2/3)

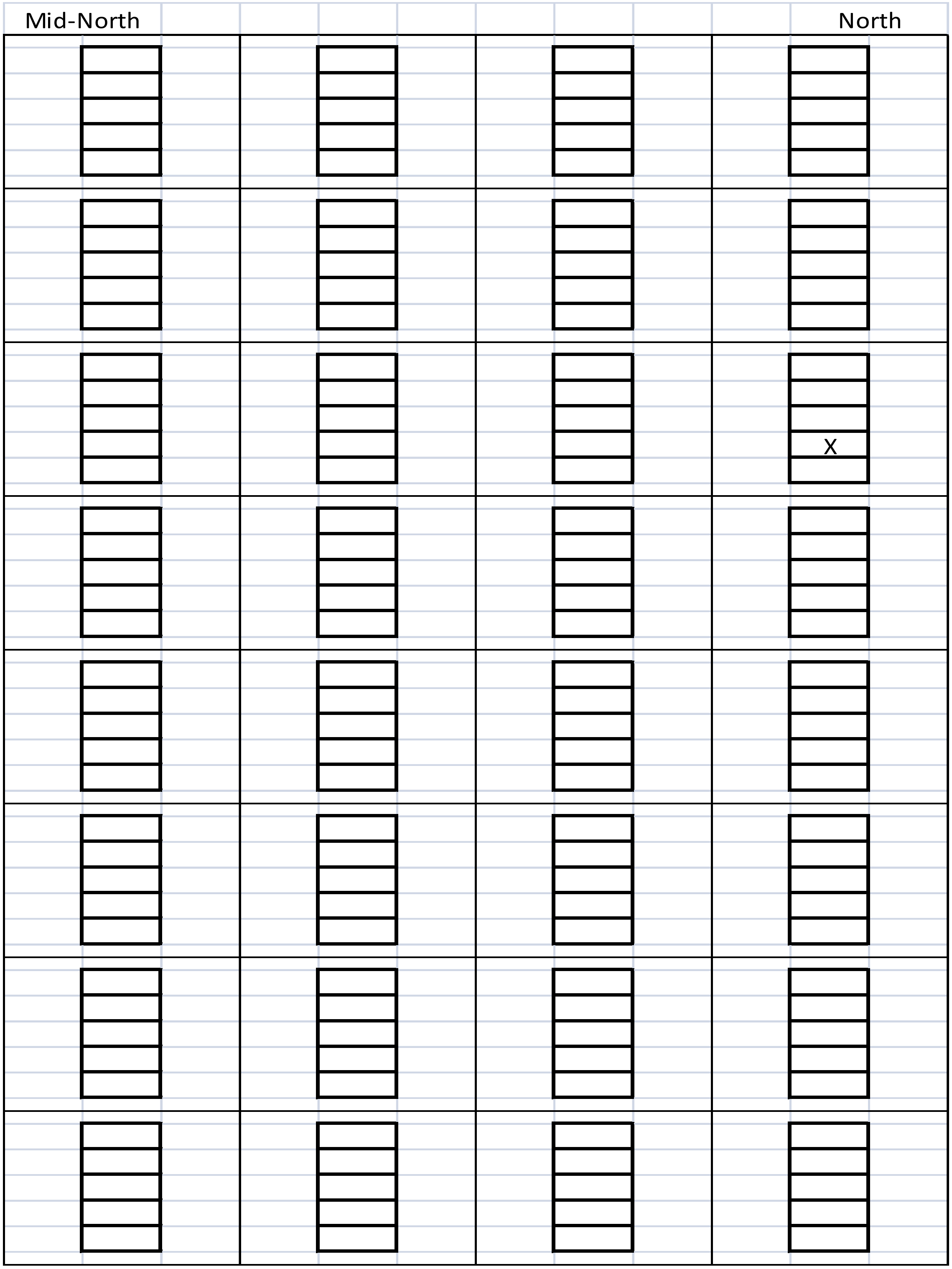

Figure E.80 – DIA7R – steel mass loss during inelastic test (3/3)

Table E.15 – DIA8 – list of testing protocols

BB		SS3		SS1		SS2	
0	☑	50	☑	50	☑	5	☑
225	☑	60	☑	60	☑	10	☑
675	☑	80	☑	70	☑	80	☑
1150	☑	100	☑	80	☑		
1825	☑	120	☑	90	☑		
2275	☑	140	☑				
3200	☑	160	☑				
5050	☑	180	☑				
6000	☑	200	☑				
8000	☑	220	☑				
10000	☑						
20000	☑						
30000	☑						
40000	☑						
60000	☑						
80000	☑						
100000	☑						
120000	☑						

Notes

- Big actuator valves used for SS1-200 and SS1-80 and all larger amplitudes for those two loading protocols

	1	2	3	4	5	6	7	8	9	10	11	12	13	14	15	16	17	18	19	20	21	22	23	24	25
A																									
B	X																								
C																									
D																									
E	O																								
F																									
G	X / X	O	O	O	O	O	O	O	O	O	O	O		O	O	O	O	O	O	O	O	O	O	O	
H	O																								
I	O																								
J	O																								
K	O																								
L	O																								
M	O / O	O	O	O	O	O	O	O	O	O	O	O		O	O	O	O	O	O	O	O	O	O	O	
N																									
O																									
P	X																								
Q	O																								
R	O																								
S	O / X	O	O	O	O	O	O	O	O	O	O	O		O	O	O	O	O	O	O	O	O	O	O	
T	O																								
U	O																								
V	O																								
W	O																								
X	O																								
Y	O / O	O	O	O	O	O	O	O	O	O	O	O	O	O	O	O	O	O	O	O	O	O	O	O	
Z	O																								O
AA	O																								O
AB	O																								
AC	O																								X
AD	O																								
AE	O / O	O	O	O	O	O	O	O	O	O	O	O		O	O	O	O	O	O	O	O	O	O	O	
AF	O																								
AG	O																								
AH	O																								
AI	O																								
AJ	O																								
AK	O / O	O	O	O	O	O	O	O	O	O	O	O		O	O	O	O	O	O	O	O	O	O	O	
AL	O																								
AM	O																								
AN	O																								
AO	O																								
AP	O																								
AQ	O / O	O	O	O	O	O	O	O	O	O	O	O		O	O	O	O	O	O	O	O	O	O	O	
AR													O												
AS																									
AT																									O
AU	O																								O
AV	O																								
AW	O / O																								

Figure E.81 – DIA8 – record of fastener failure during inelastic test (1/6)

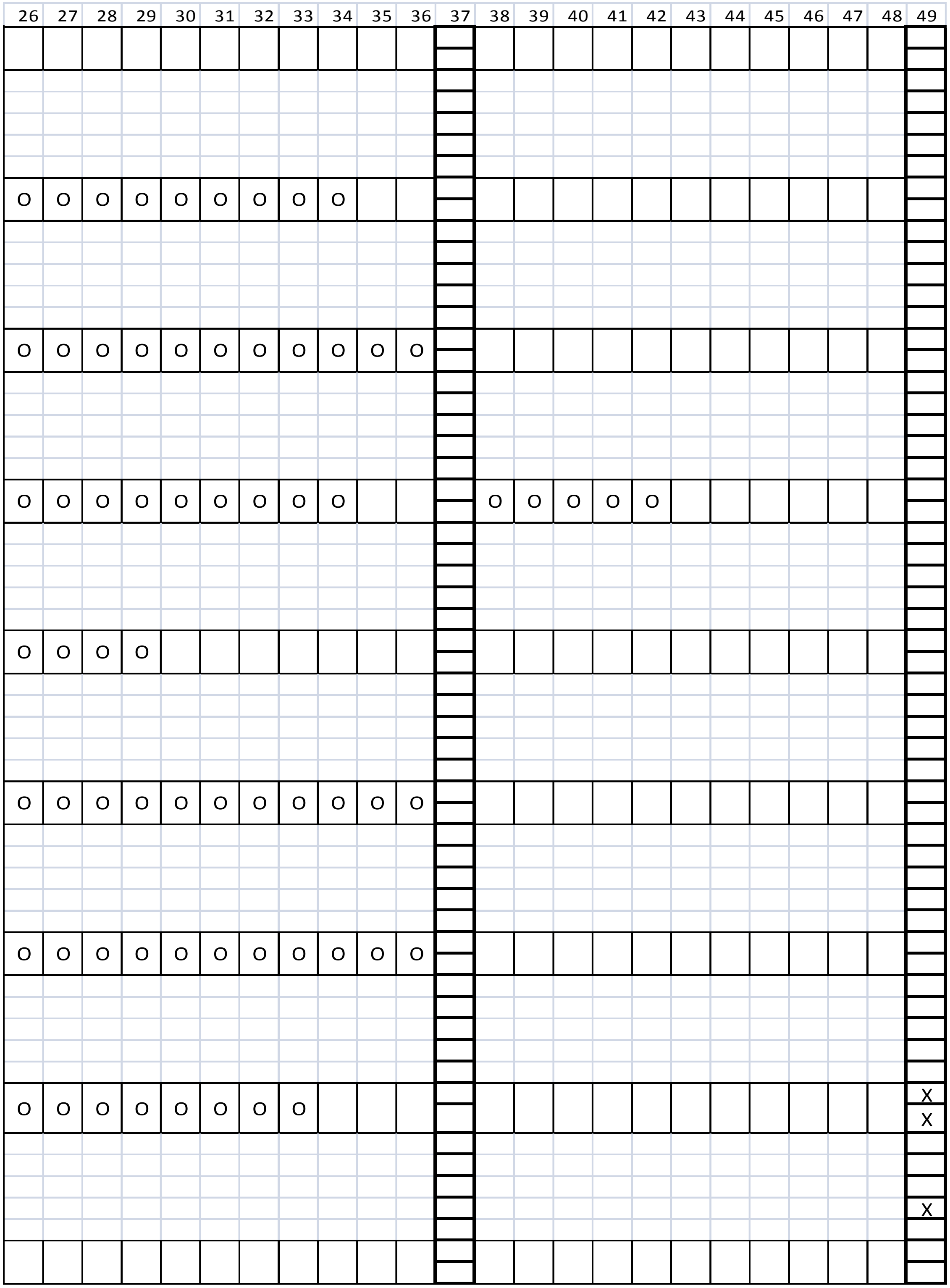

Figure E.82 – DIA8 – record of fastener failure during inelastic test (2/6)

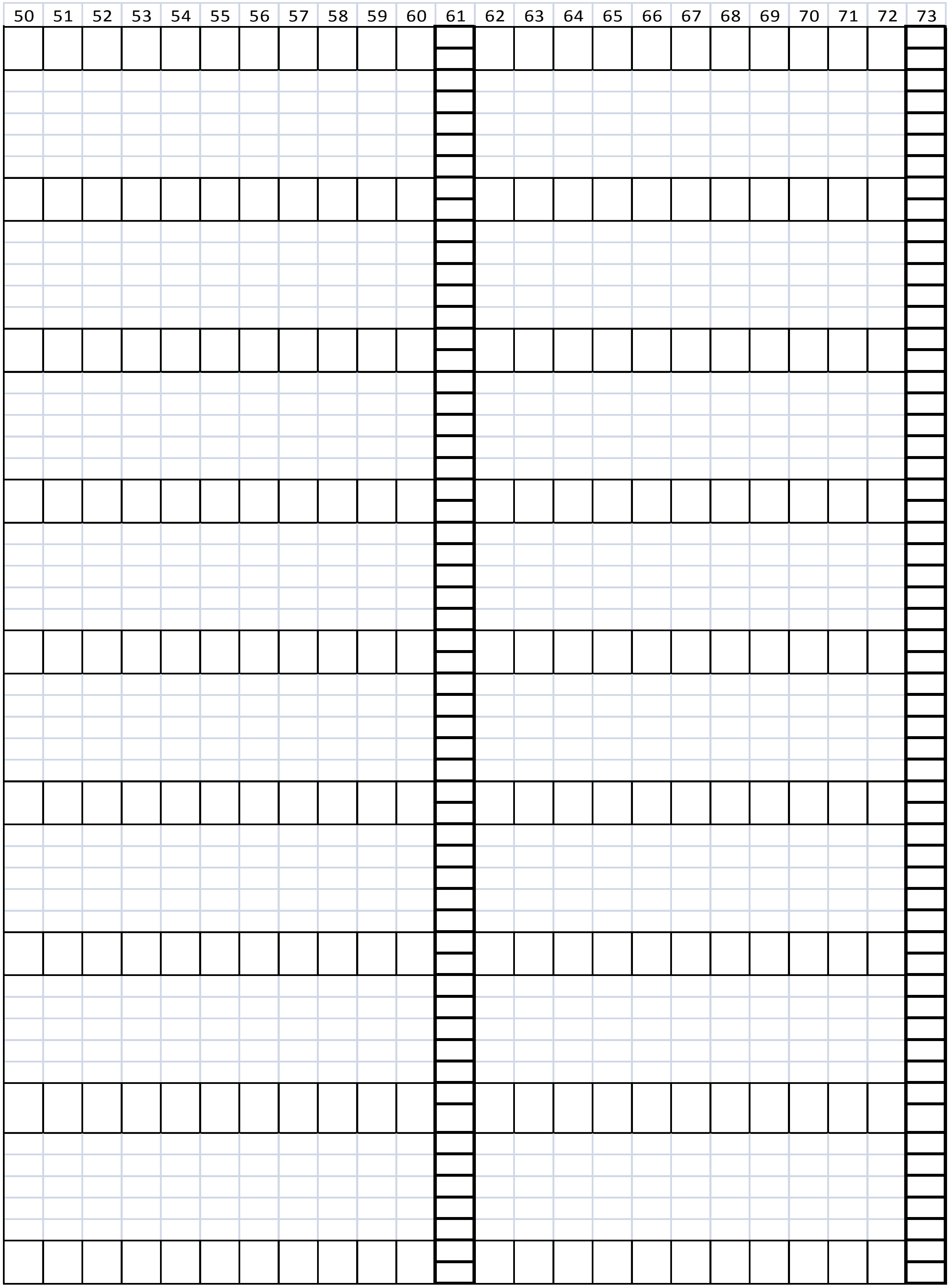

Figure E.83 – DIA8 – record of fastener failure during inelastic test (3/6)

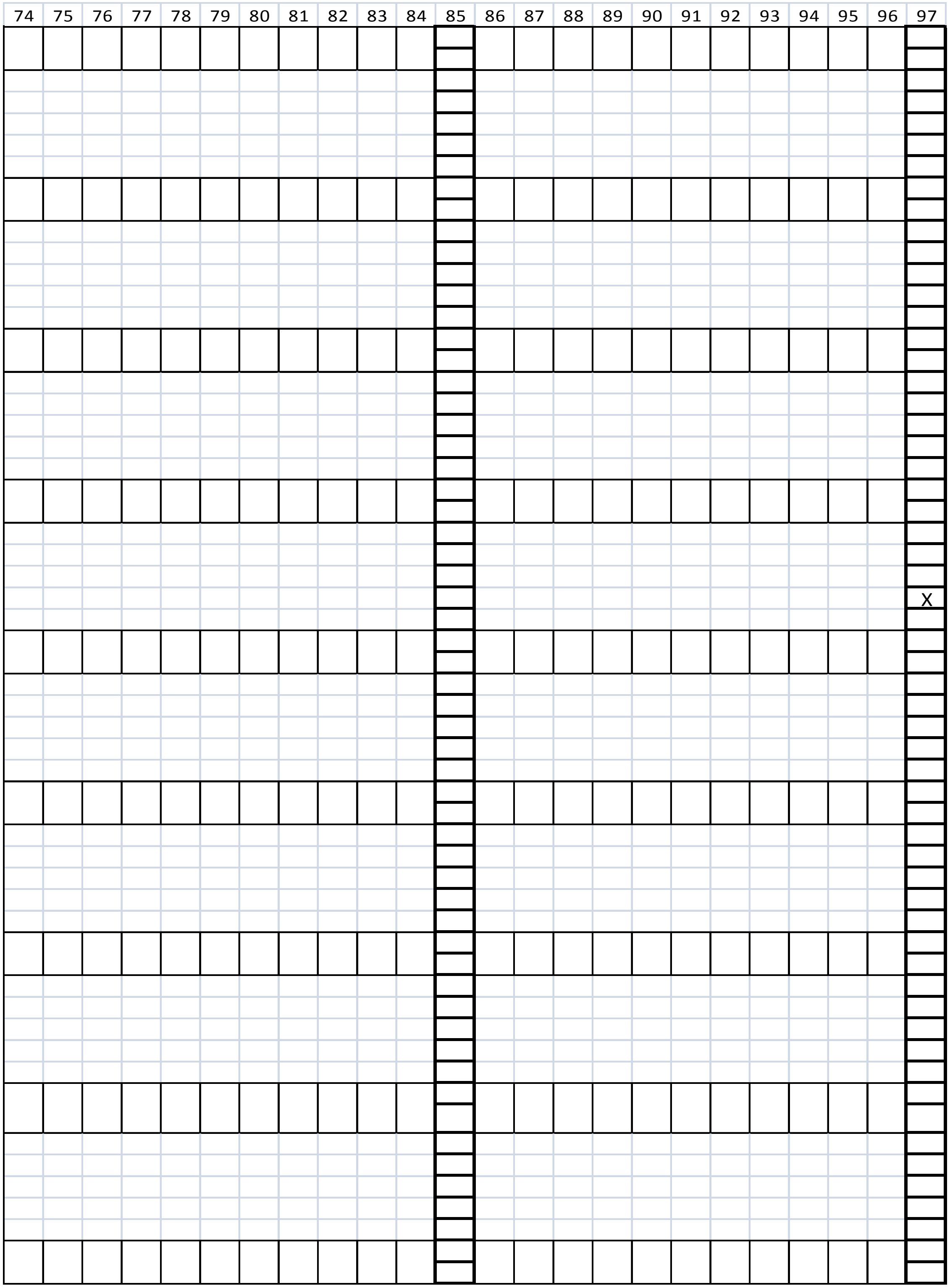

Figure E.84 – DIA8 – record of fastener failure during inelastic test (4/6)

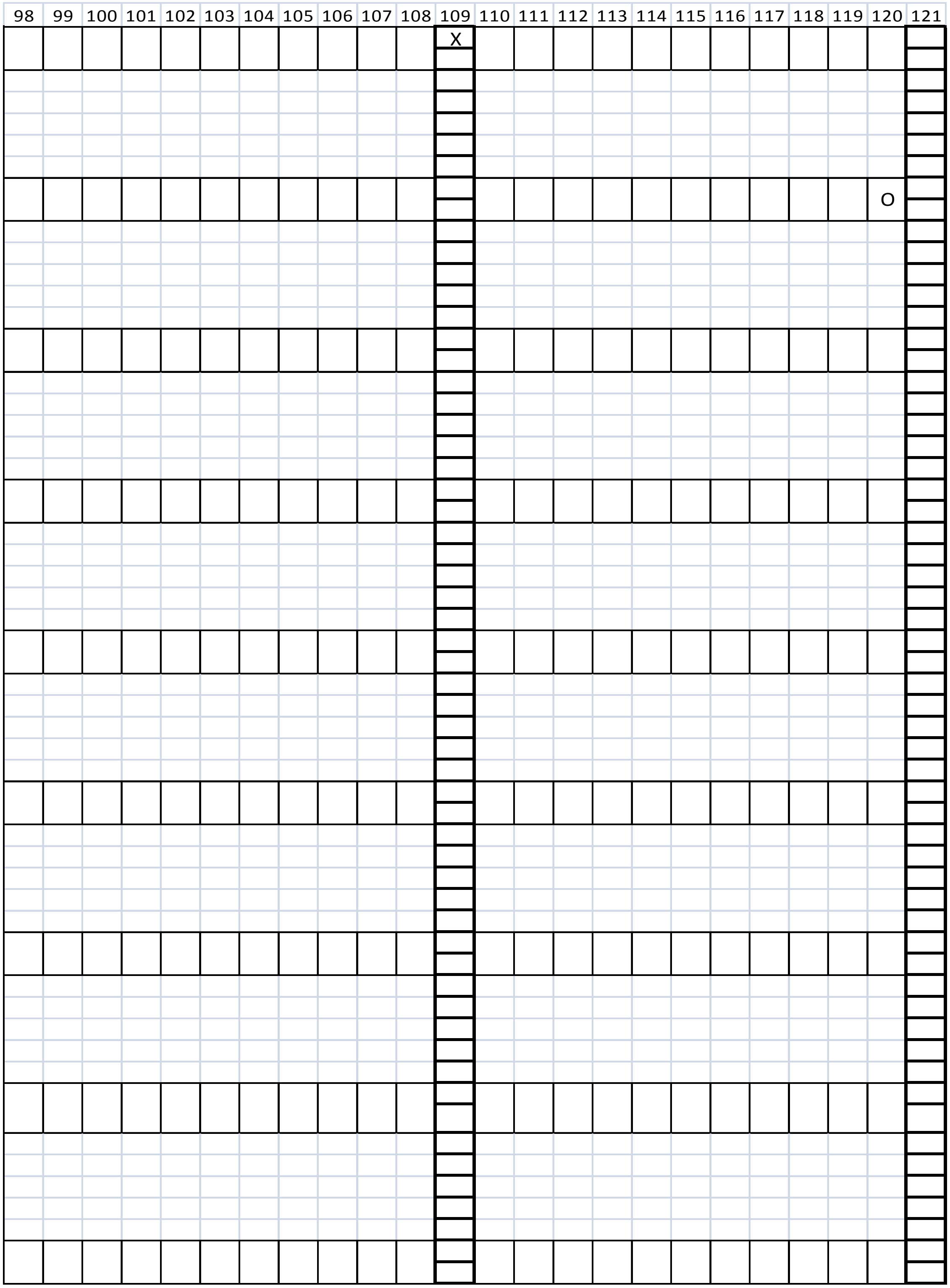

Figure E.85 – DIA8 – record of fastener failure during inelastic test (5/6)

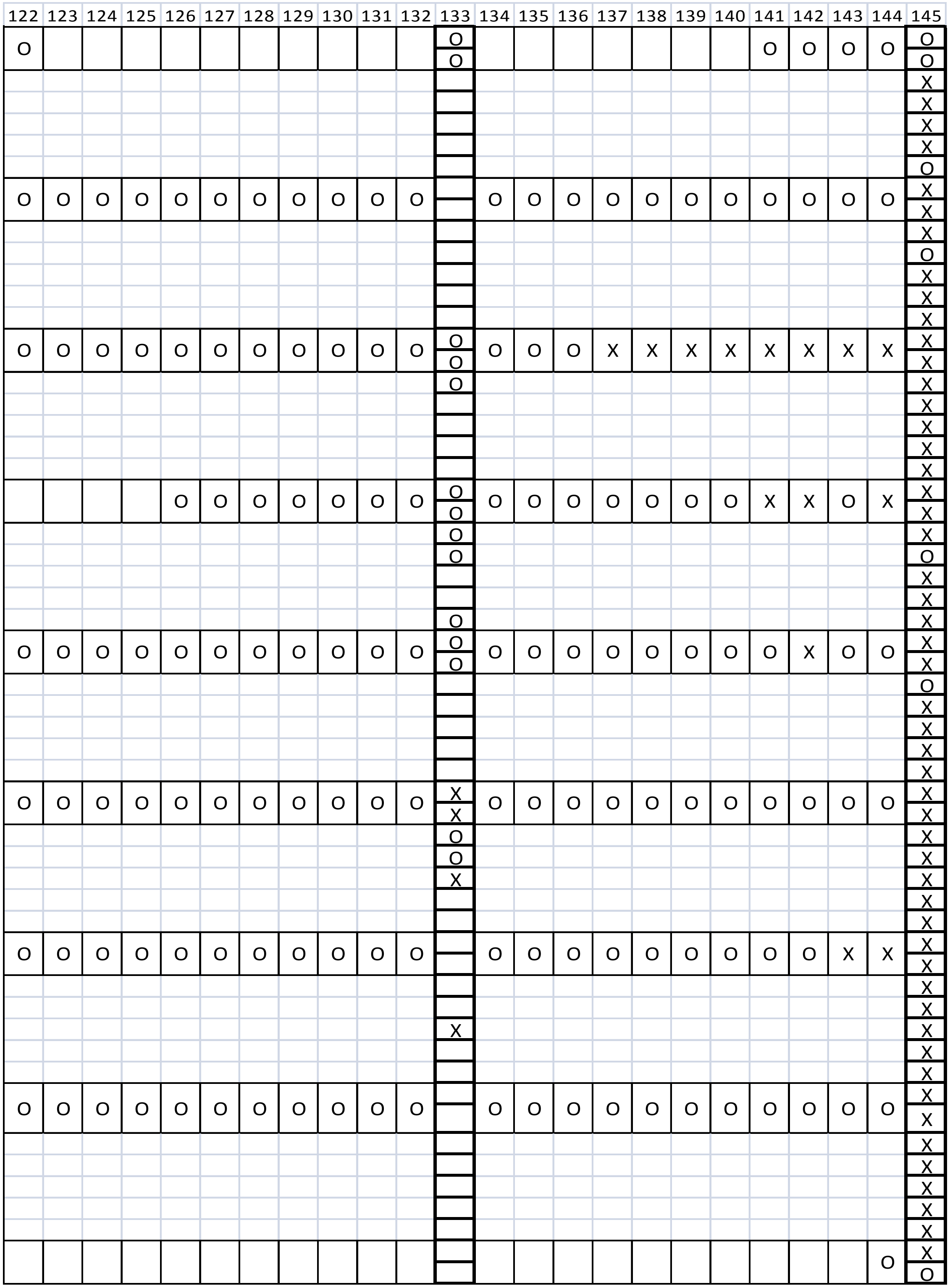

Figure E.86 – DIA8 – record of fastener failure during inelastic test (6/6)

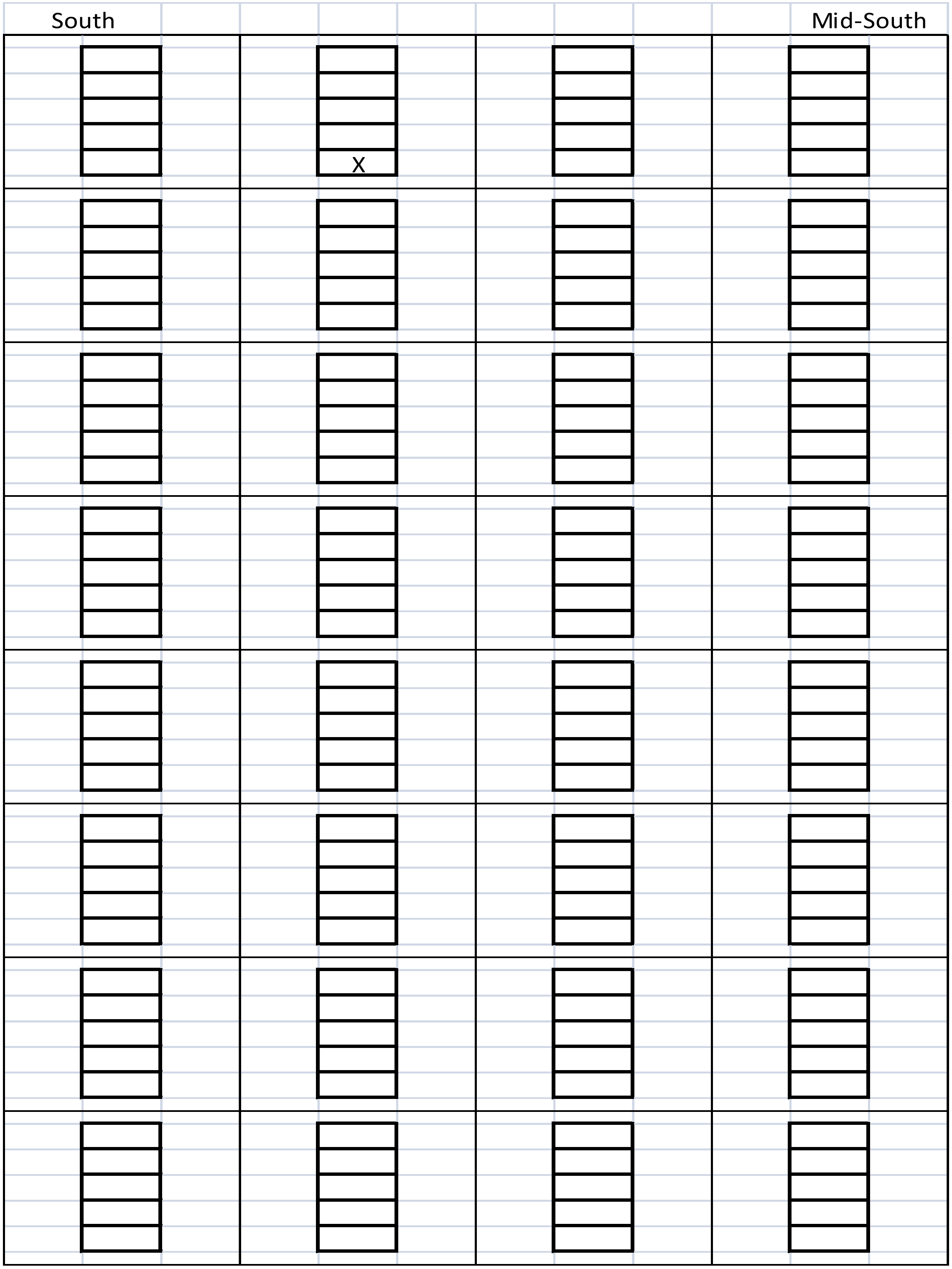

Figure E.87 – DIA8 – steel mass loss during inelastic test (1/3)

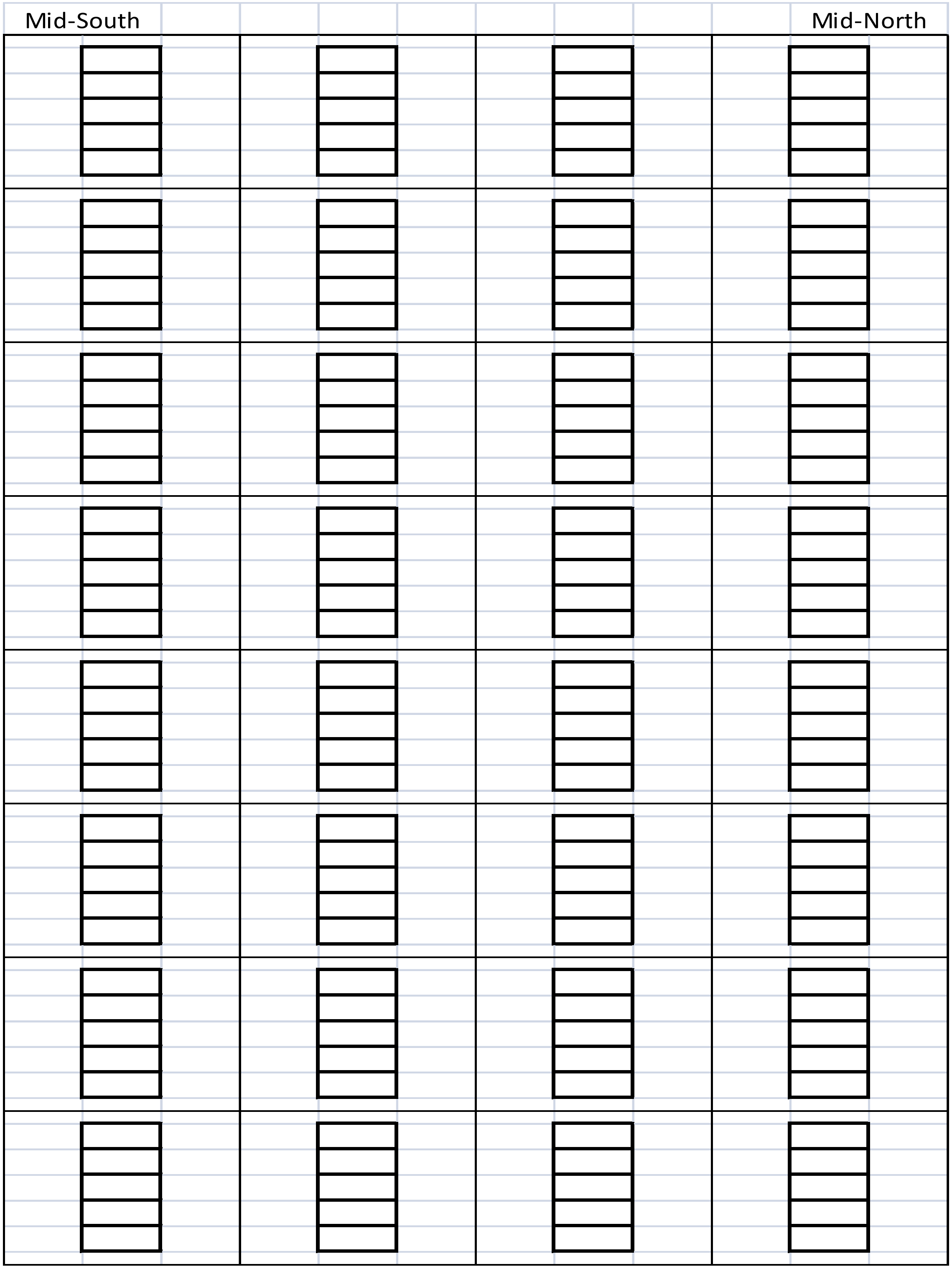

Figure E.88 – DIA8 – steel mass loss during inelastic test (2/3)

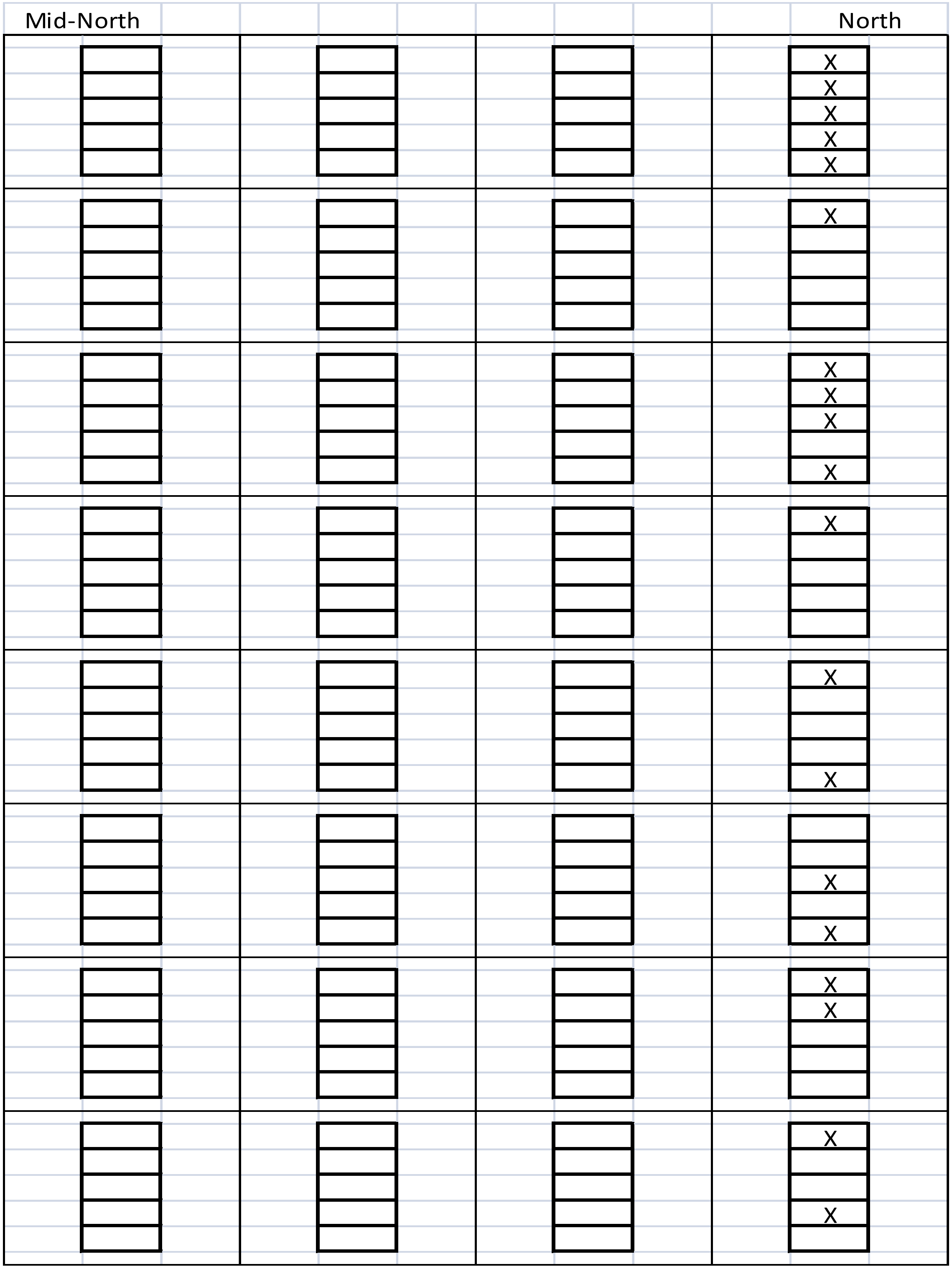

Figure E.89 – DIA8 – steel mass loss during inelastic test (3/3)

Table E.16 – DIA8R – list of testing protocols

BB		SS3		SS1		SS2	
0	☑	50	☑	50	☑	5	☑
225	☑	60	☑	60	☑	10	☑
675	☑	80	☑	70	☑	80	☑
1150	☑	100	☑	80	☑		
1825	☑	120	☑	90	☑		
2275	☑	140	☑				
3200	☑	160	☑				
5050	☑	180	☑				
6000	☑	200	☑				
8000	☑	220	☑				
10000	☑						
20000	☑						
40000	☑						
60000	☑						
80000	☑						
100000	☑						
120000	☑						

<u>Notes</u>

- Big actuator valves used for SS1-200 and SS1-80 and all larger amplitudes for those two loading protocols

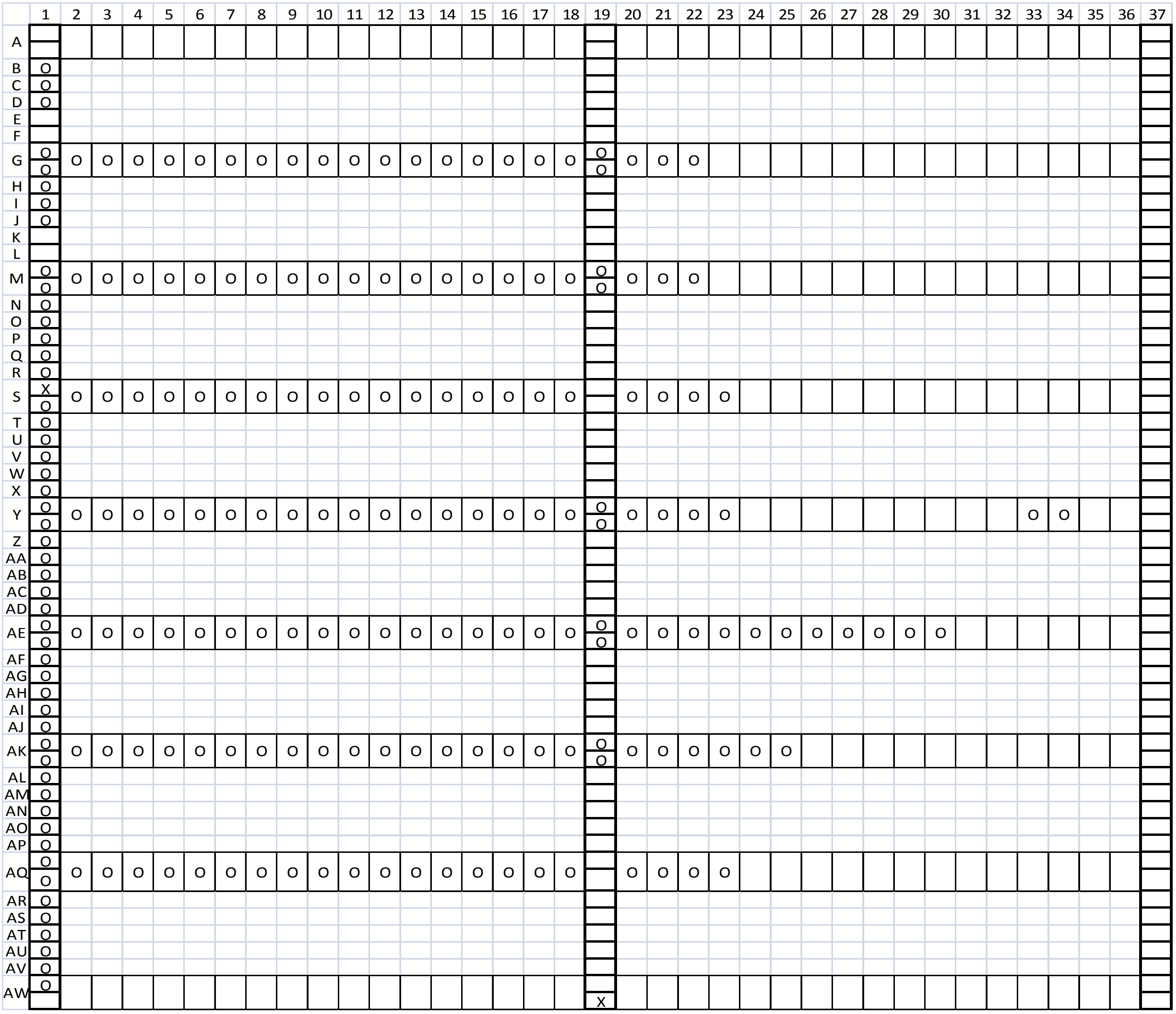

Figure E.90 – DIA8R – record of fastener failure during inelastic test (1/6)

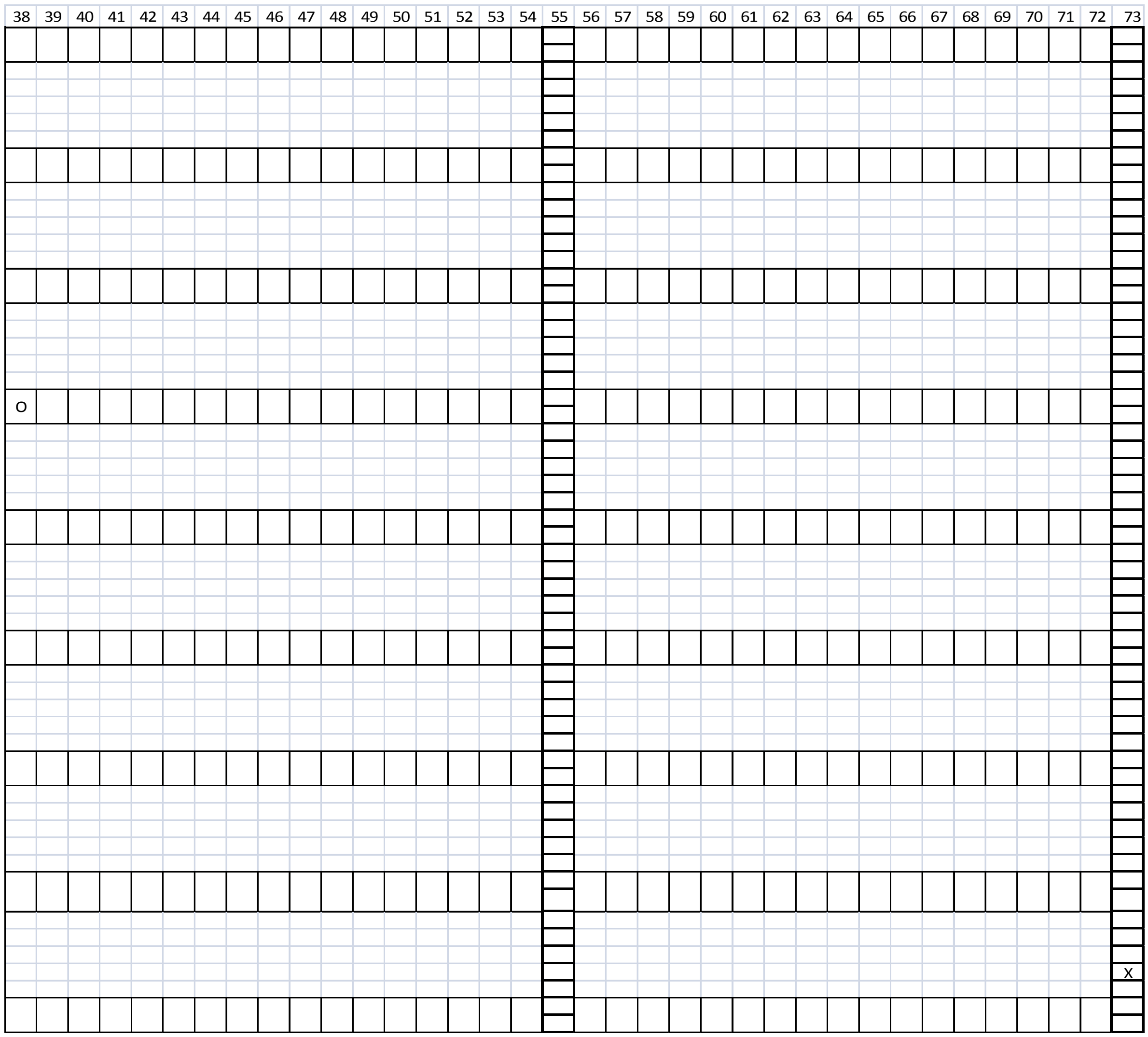

Figure E.91 – DIA8R – record of fastener failure during inelastic test (2/6)

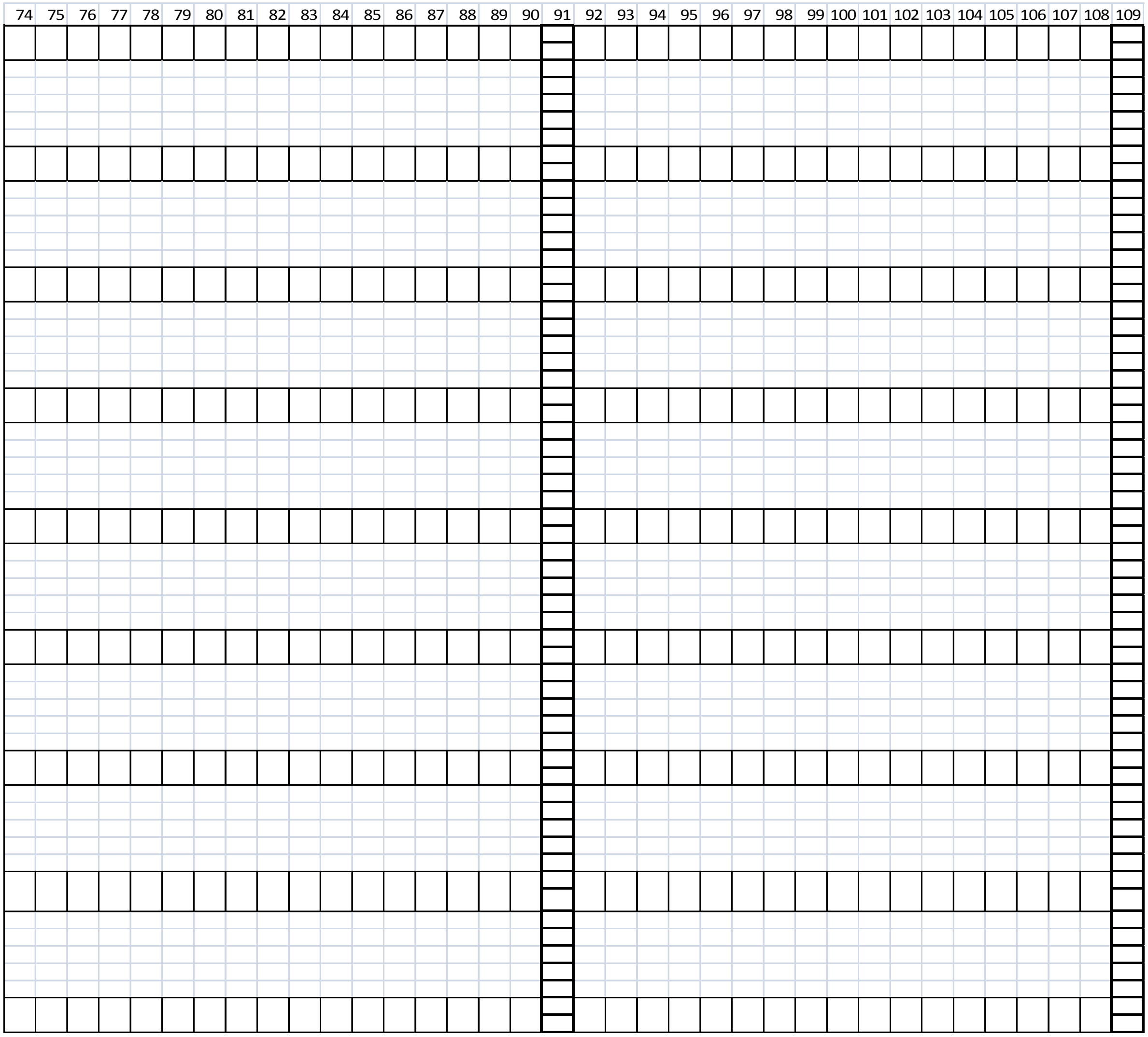

Figure E.92 – DIA8R – record of fastener failure during inelastic test (3/6)

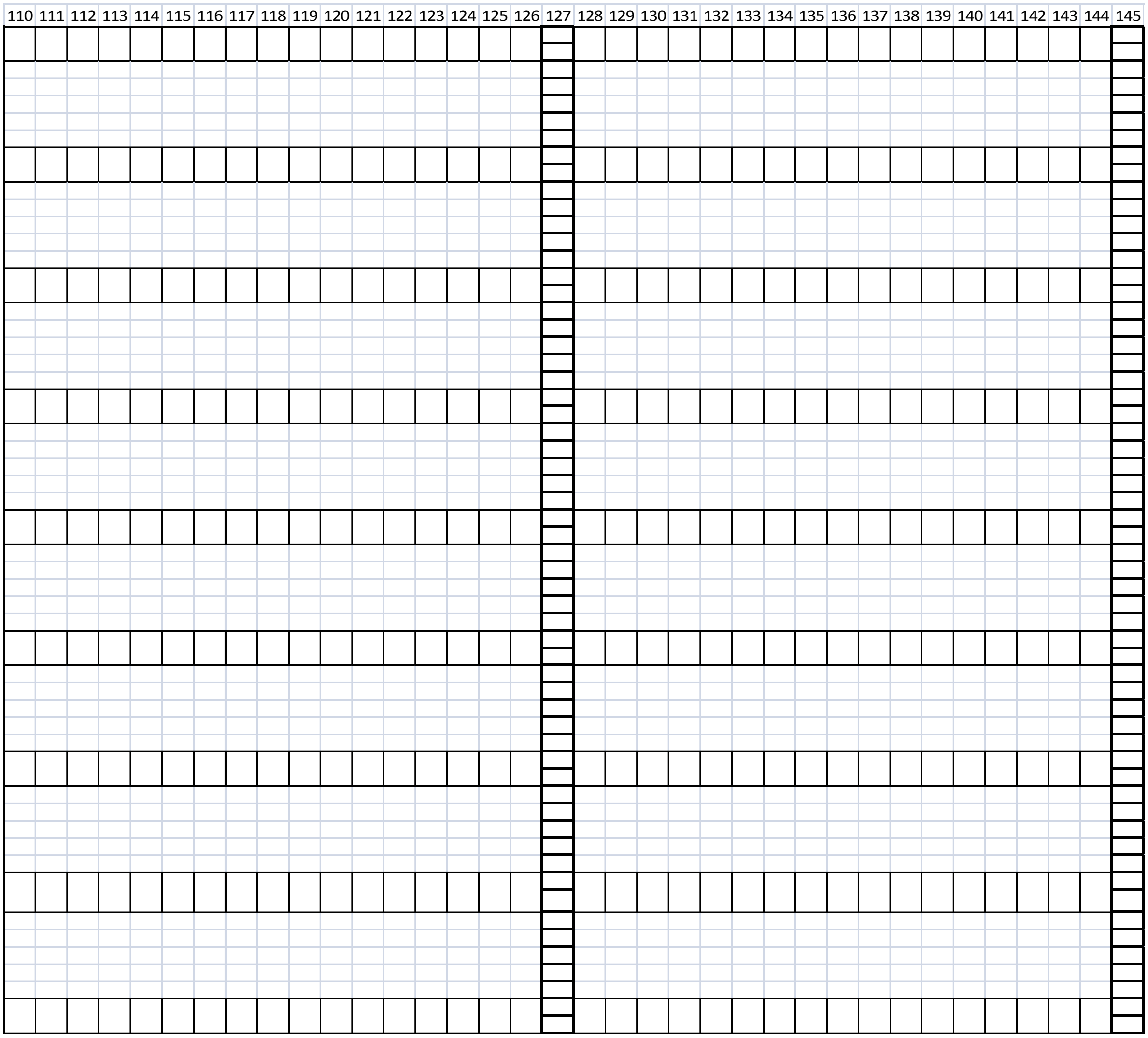

Figure E.93 – DIA8R – record of fastener failure during inelastic test (4/6)

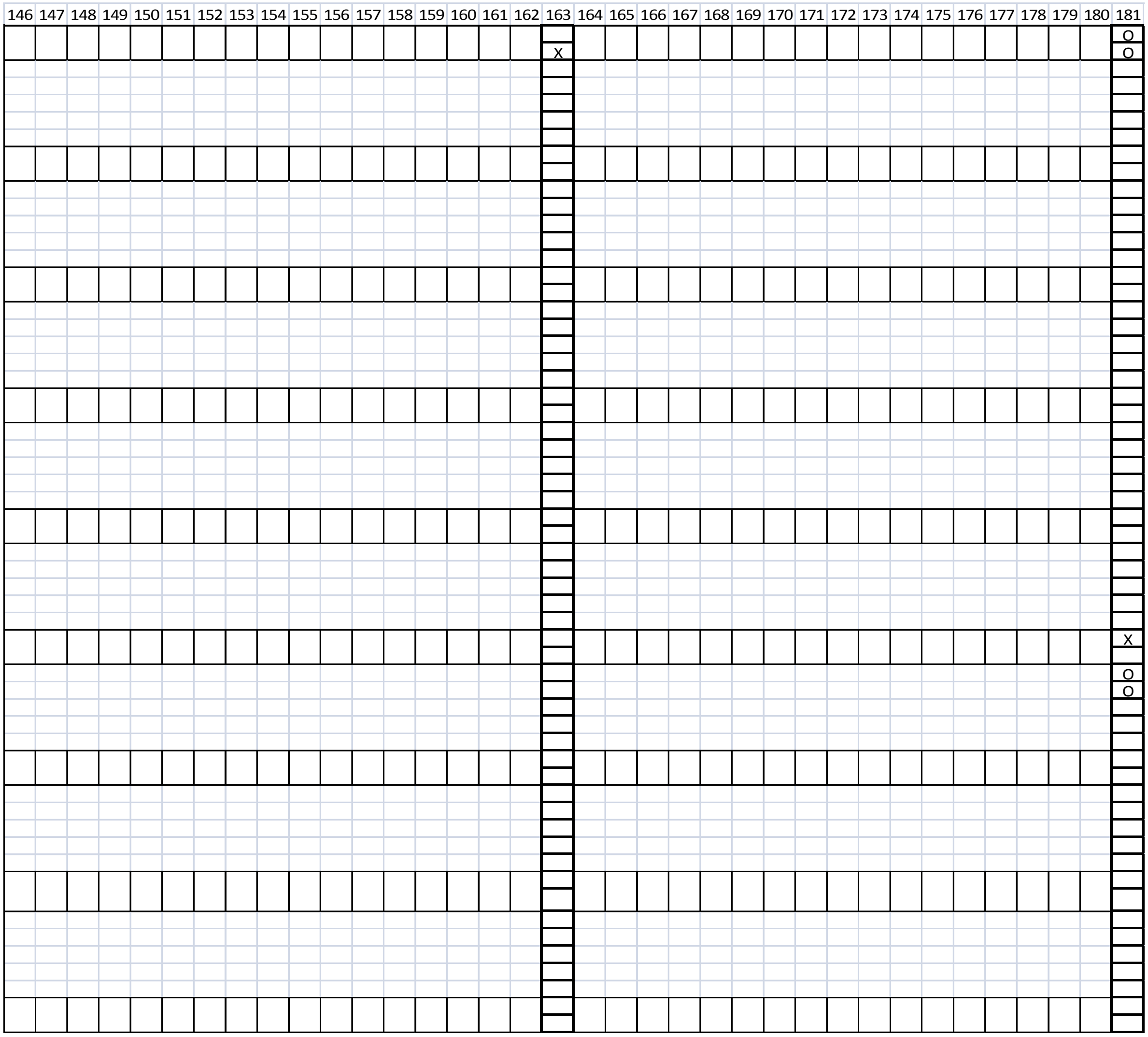

Figure E.94 – DIA8R – record of fastener failure during inelastic test (5/6)

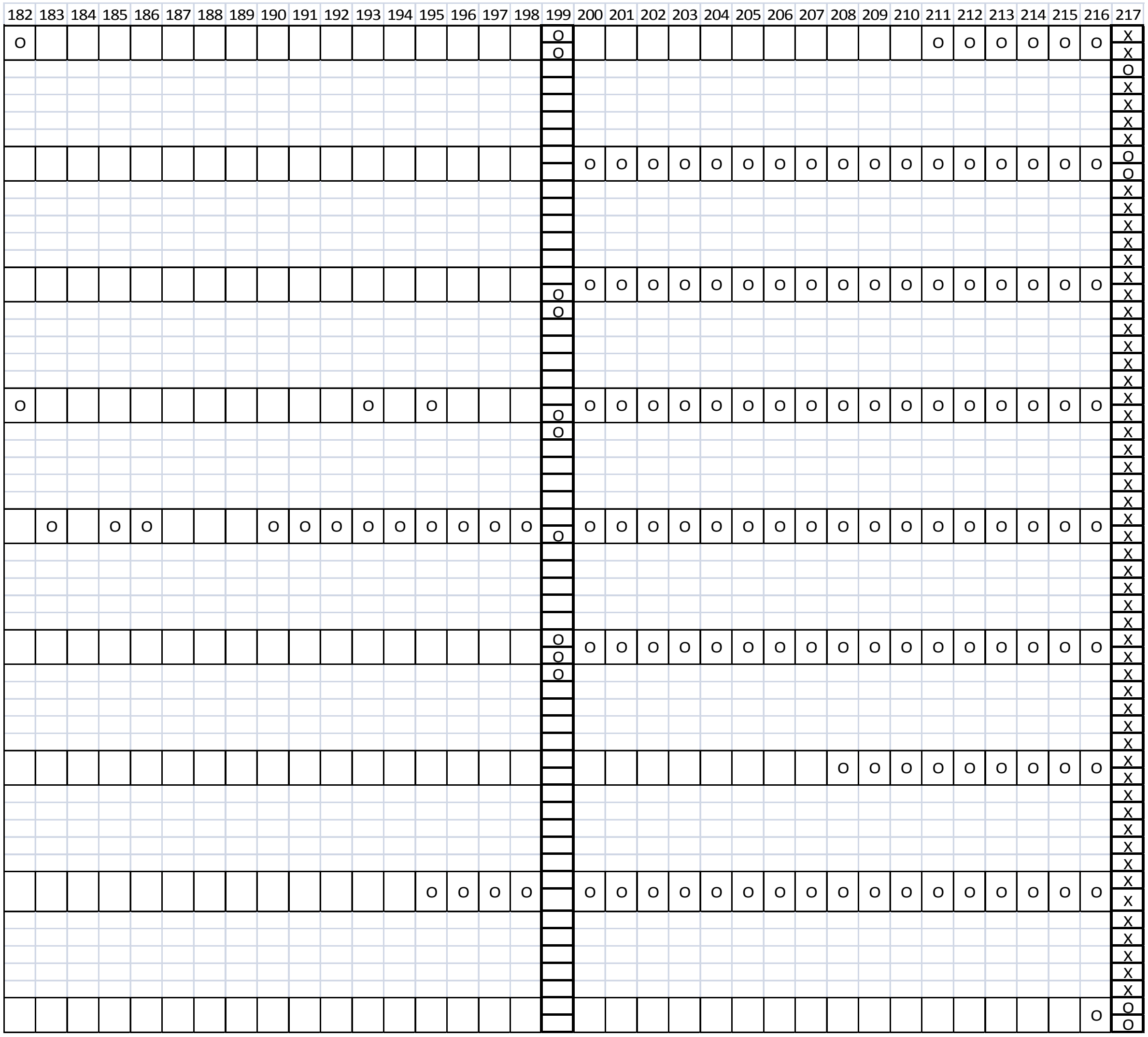

Figure E.95 – DIA8R – record of fastener failure during inelastic test (6/6)

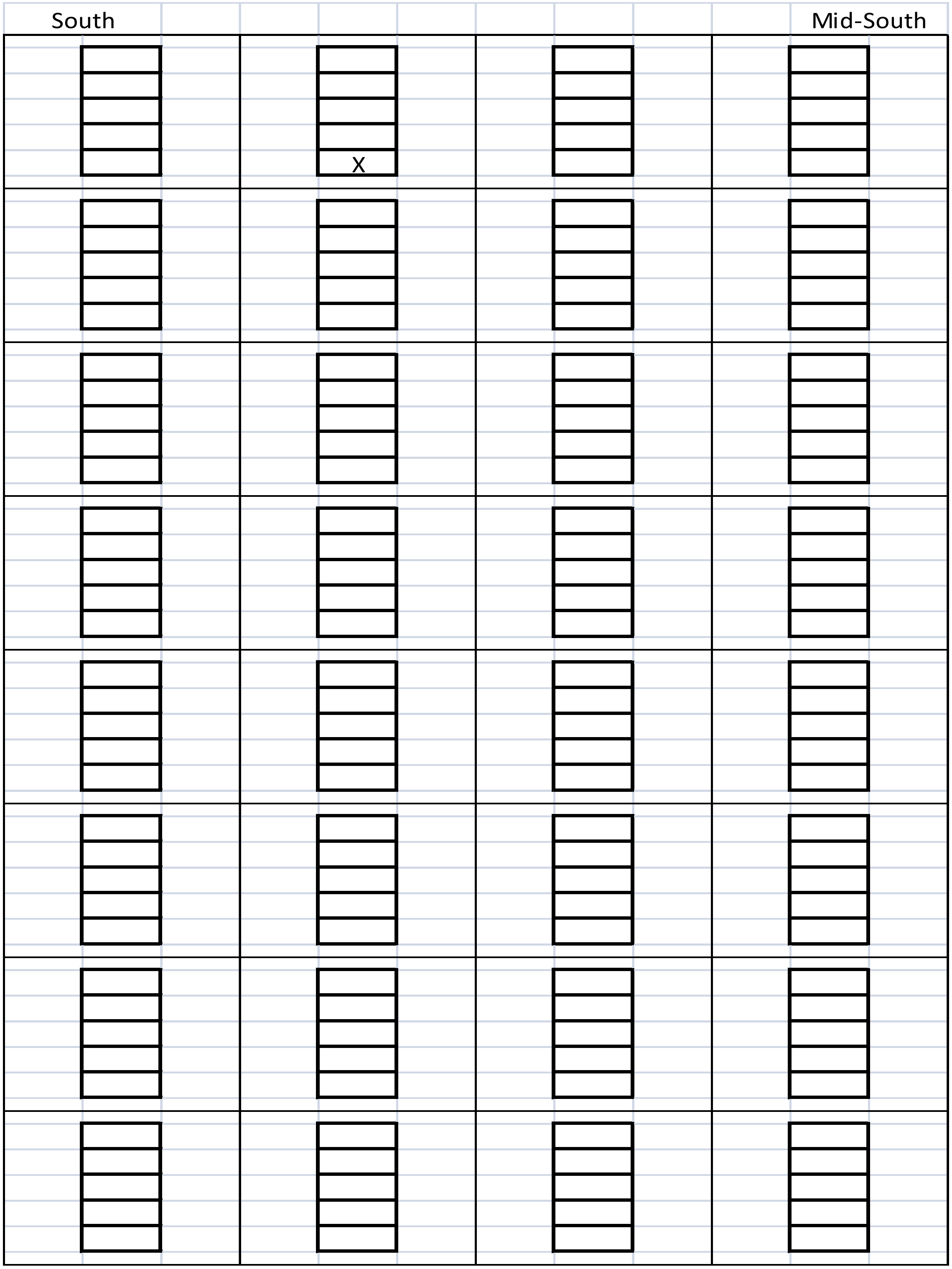

Figure E.96 – DIA8R – steel mass loss during inelastic test (1/3)

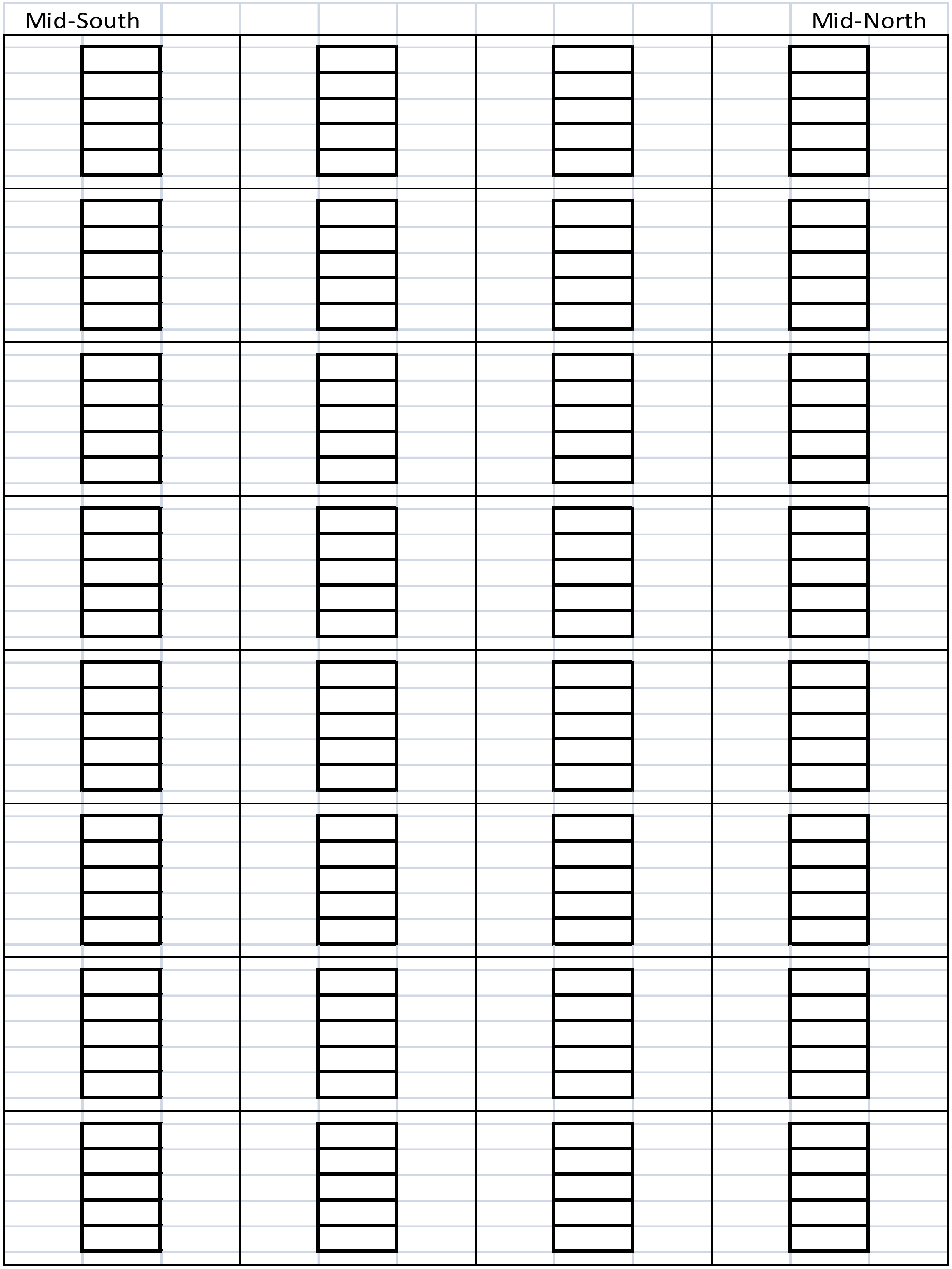

Figure E.97 – DIA8R – steel mass loss during inelastic test (2/3)

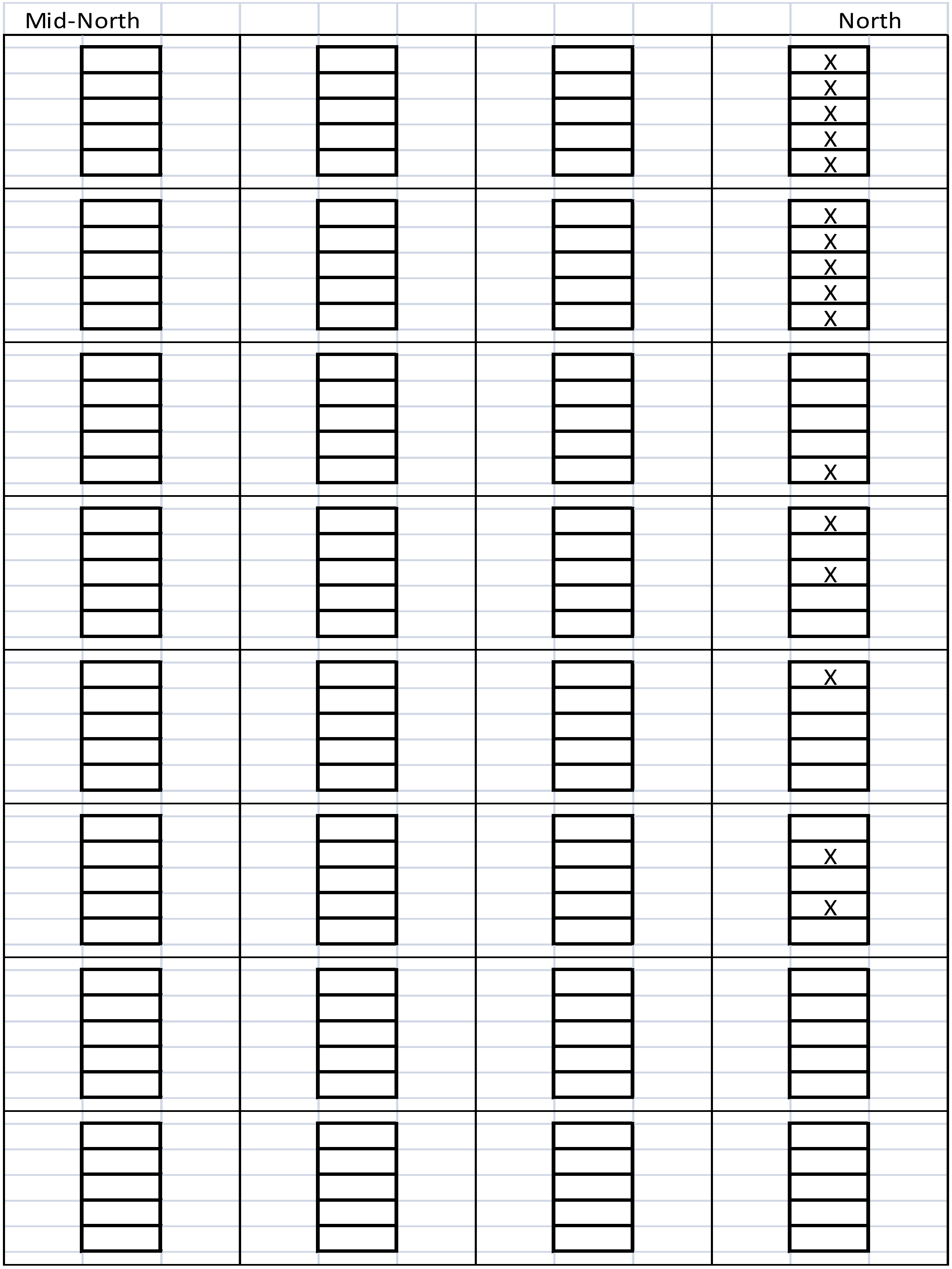

Figure E.98 – DIA8R – steel mass loss during inelastic test (3/3)

Table E.17 – DIA9 – list of testing protocols

BB		SS3		SS1		SS2	
0	☑	50	☑	50	☑	5	☑
225	☑	60	☑	60	☑	10	☑
675	☑	80	☑	70	☑	80	☑
1150	☑	100	☑	80	☑		
1825	☑	120	☑	90	☑		
2275	☑	140	☑				
3200	☑	160	☑				
5050	☑	180	☑				
6000	☑	200	☑				
8000	☑	220	☑				
10000	☑						
20000	☑						
40000	☑						
60000	☑						
80000	☑						
100000	☑						
120000	☑						
140000	☑						
160000	☑						

Notes

- Big actuator valves used for SS1-200 and SS1-80 and all larger amplitudes for those two loading protocols

	1	2	3	4	5	6	7	8	9	10	11	12	13	14	15	16	17	18	19	20	21	22	23	24	25
A	O																								
	O																								X
B																									
C	O																								
D	O																								
E	X																								
F	O																								
	X																								
G	O	O	O	O	O	O	O	O	O	O	O	O	O	O	O	O	O	O	O	O	O	O	O	O	
	O												O												
H	O																								
	O																								
I	O																								
J	O																								
K	X																								
L	O																								
	O																								
M	X	X	O	O	X	O	X	X	O	O	O	O	O	O	O	O	O	O	O	O	O	O	O	O	
	O												O												X
N	O																								
	O												X												
O	X																								
P	O																								
Q	O																								
R	O																								
	X																								
S	O	O	X	O	O	O	O	O	O	O	O	O	O	O	O	O	O	O	O	O	O	O	O	O	X
	O												O												
T	O																								
	O												X												
U	O																								
V	O																								
W	O																								
X	O																								
	O																								
Y	O	O	O	O	O	O	O	O	O	O	O	O	O	O	O	O	O	O	O	O	O	O	O	O	
	O												O												
Z	O																								
	O																								
AA	X																								
AB	X																								
AC	O																								
AD													O												
AE	O	O	O	O	O	O	O	X	X	O	O	O	O												
	O												O												
AF	O												O												
	O												X												
AG	O																								
AH	O																								
AI	O																								
AJ	O																								
	O																								
AK	O	O	O	O	X	O	X	O	O	O	O	X	O	O	O	O	O	O	O	O	O	O	O	O	
	O												O												
AL	O																								
	O																								
AM	O																								
AN	O																								
AO	O																								
AP	O																								
	O																								
AQ	O	O	O	X	O	X	O	O	X	O	O	O													
	O																								
AR	O																								
	O																								
AS	O																								
AT	O																								
AU	O																								
AV	O																								
	O																								
AW	O	O																							
	O																								X

Figure E.99 – DIA9 – record of fastener failure during inelastic test (1/6)

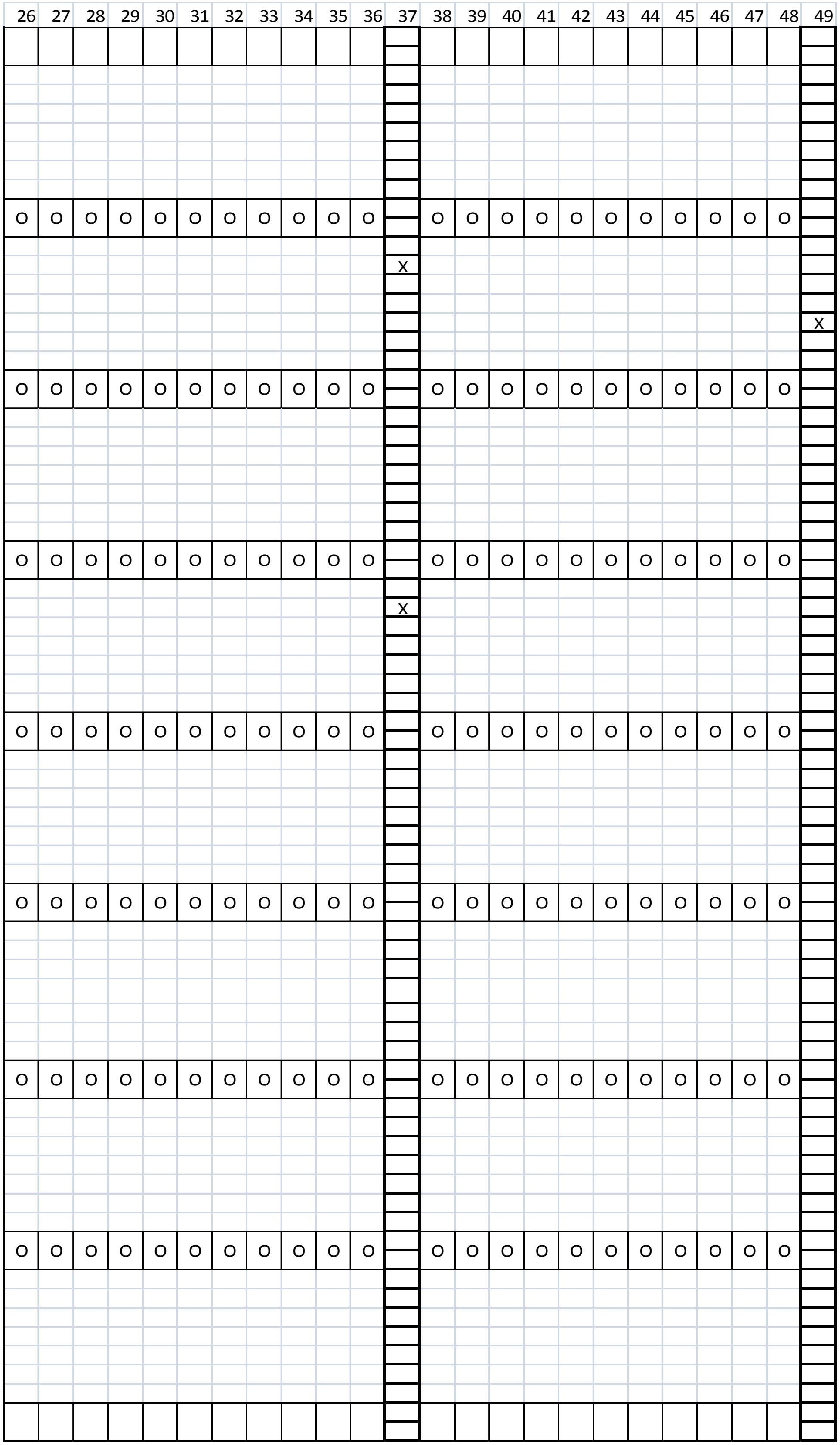

Figure E.100 – DIA9 – record of fastener failure during inelastic test (2/6)

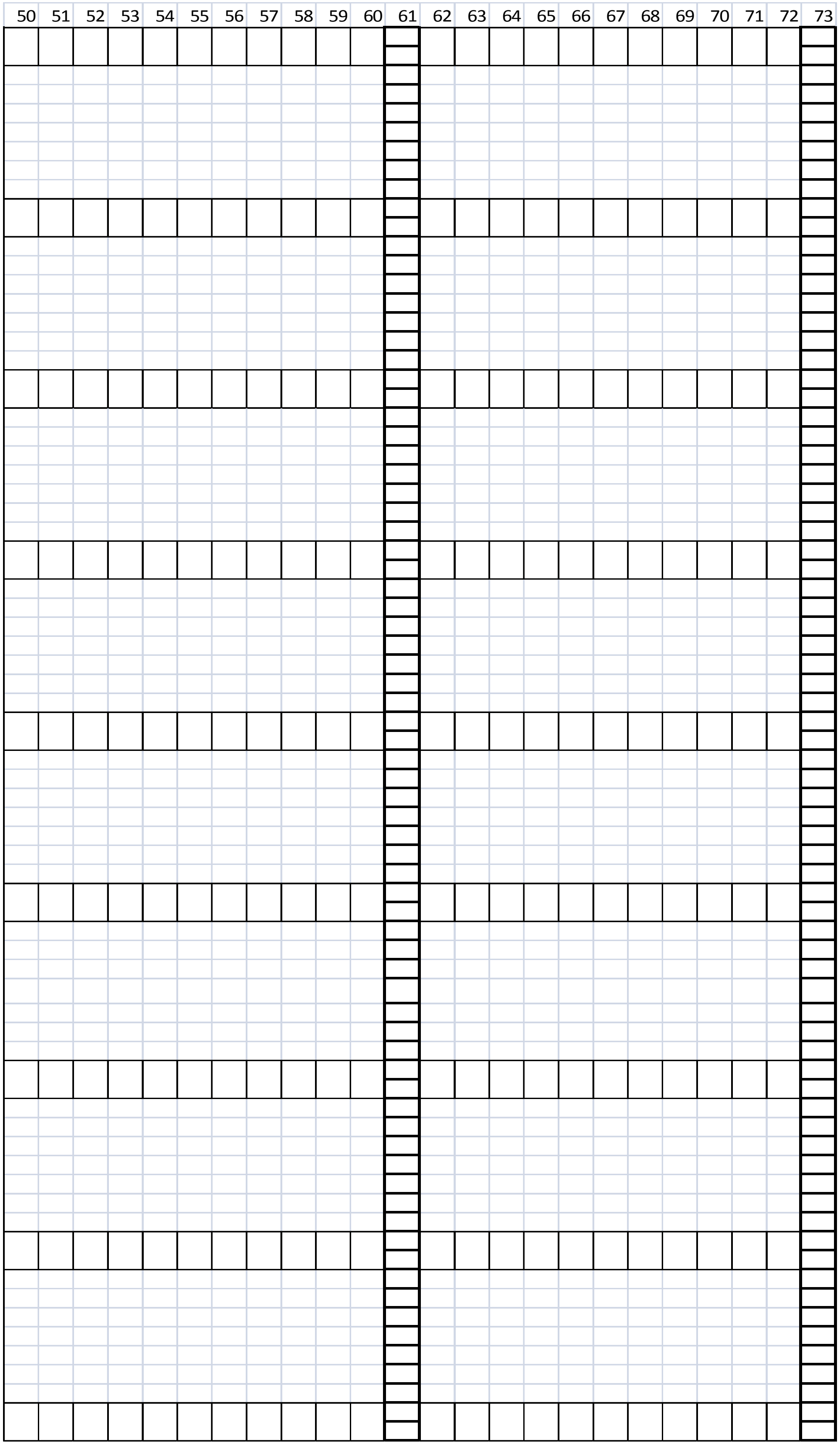

Figure E.101 – DIA9 – record of fastener failure during inelastic test (3/6)

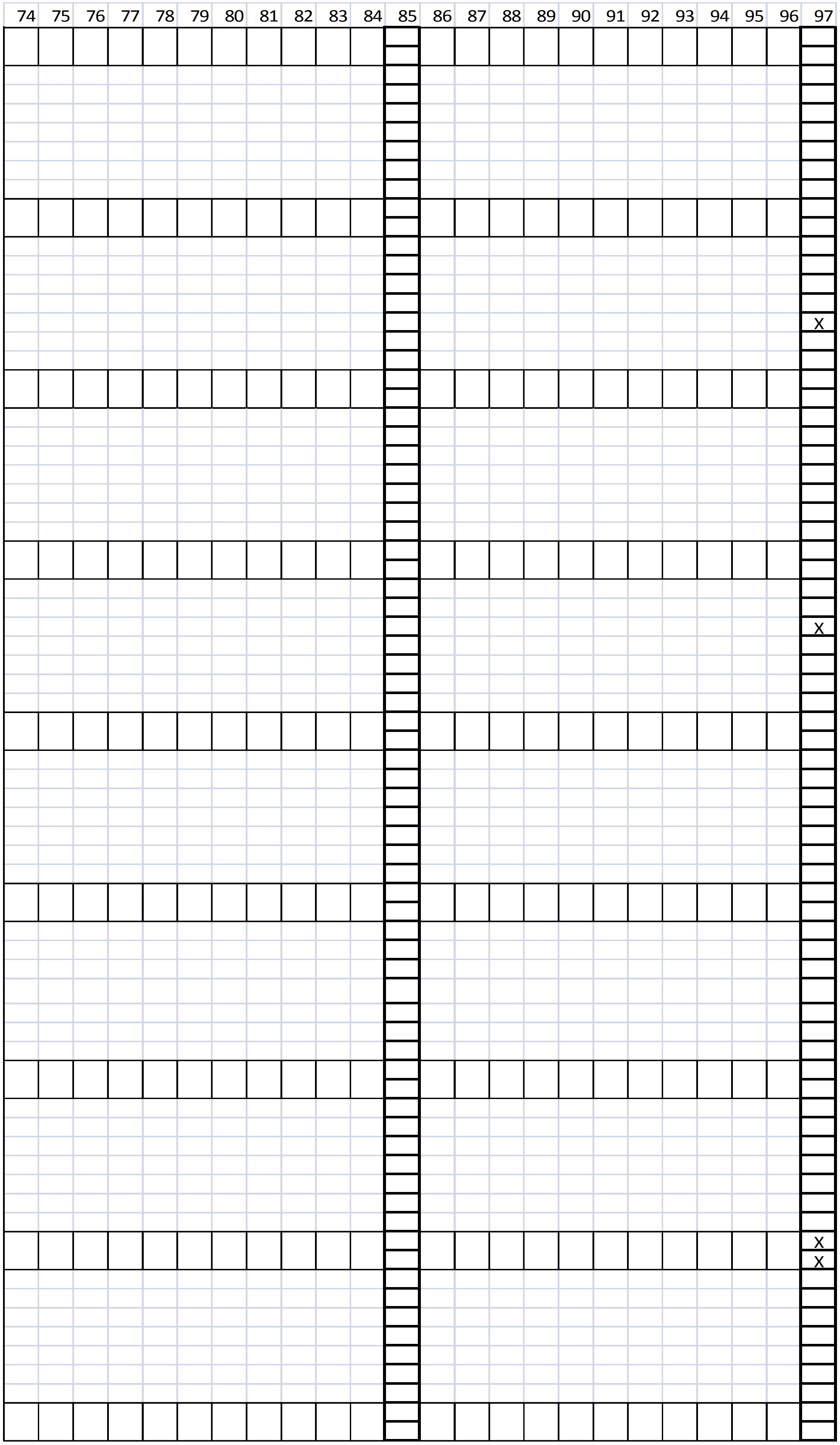

Figure E.102 – DIA9 – record of fastener failure during inelastic test (4/6)

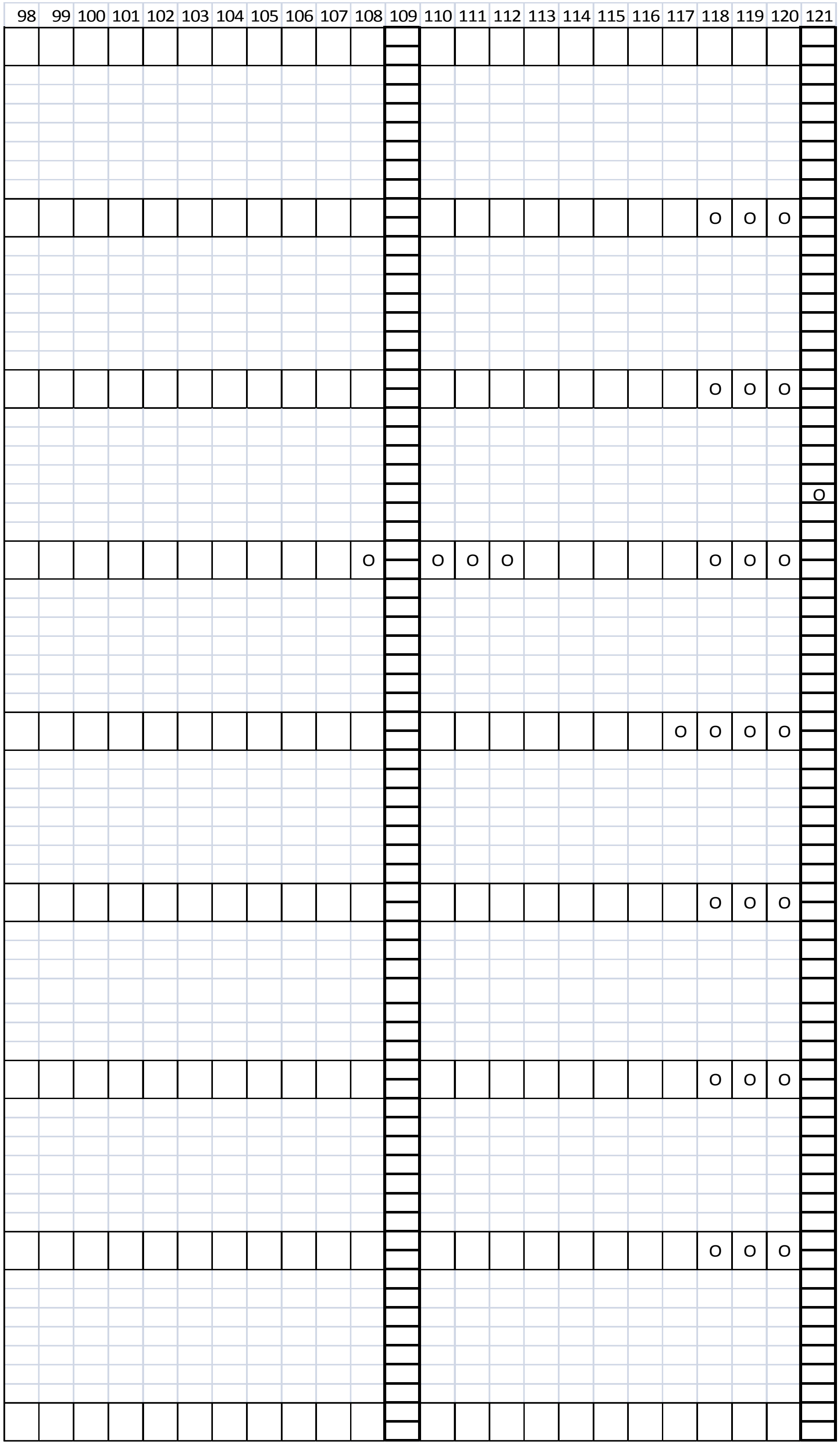

Figure E.103 – DIA9 – record of fastener failure during inelastic test (5/6)

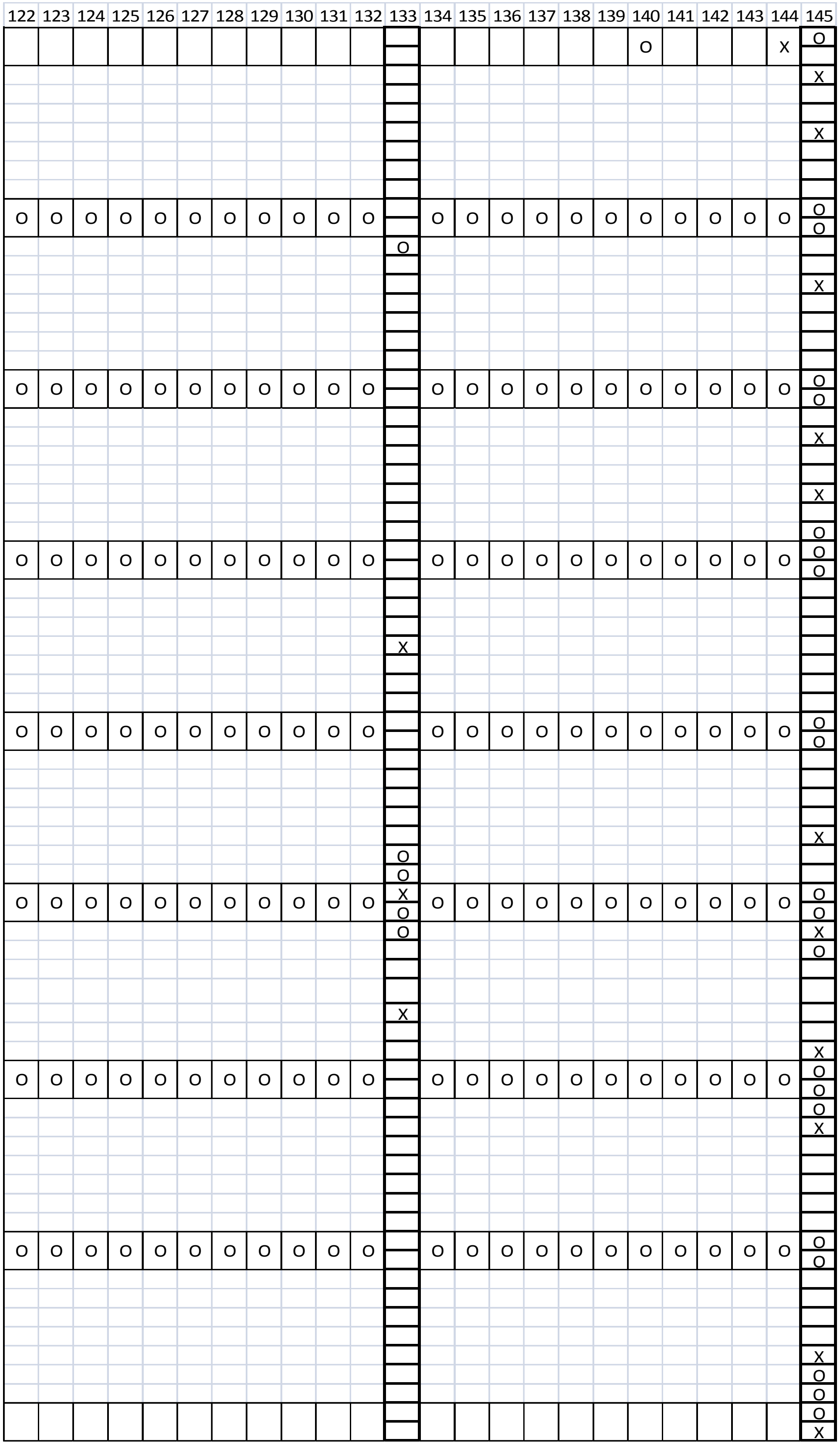

Figure E.104 – DIA9 – record of fastener failure during inelastic test (6/6)

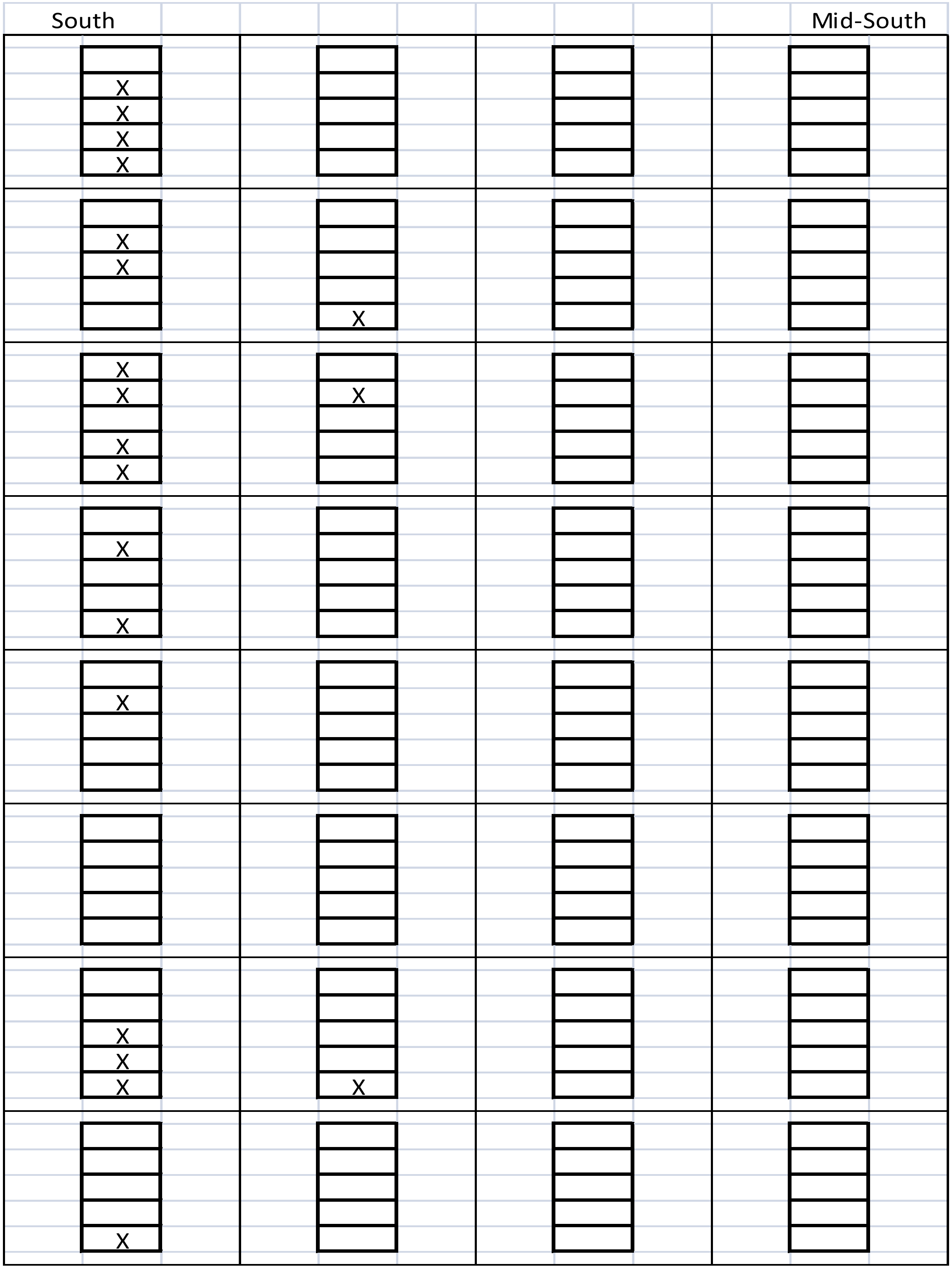

Figure E.105 – DIA9 – steel mass loss during inelastic test (1/3)

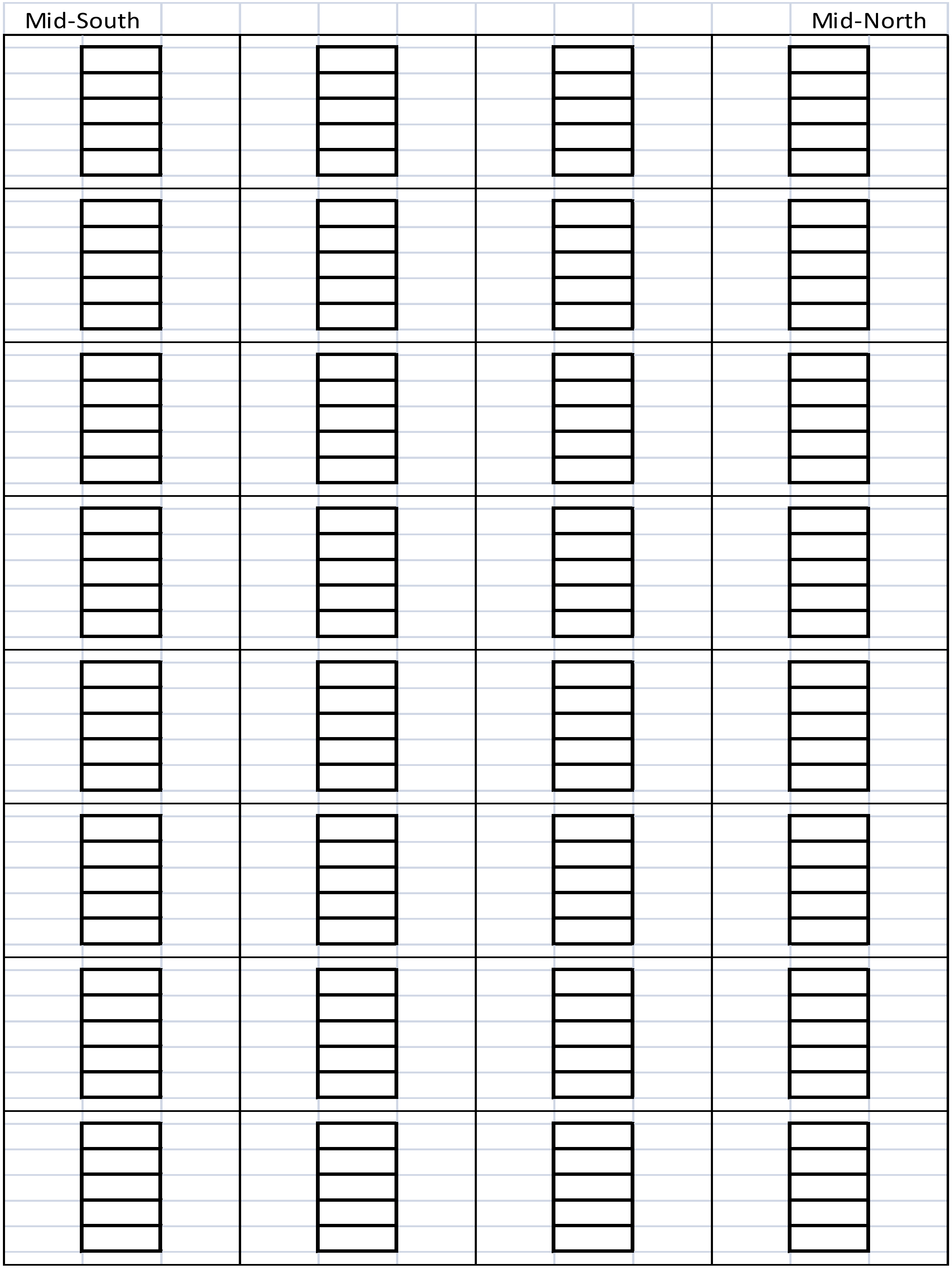

Figure E.106 – DIA9 – steel mass loss during inelastic test (2/3)

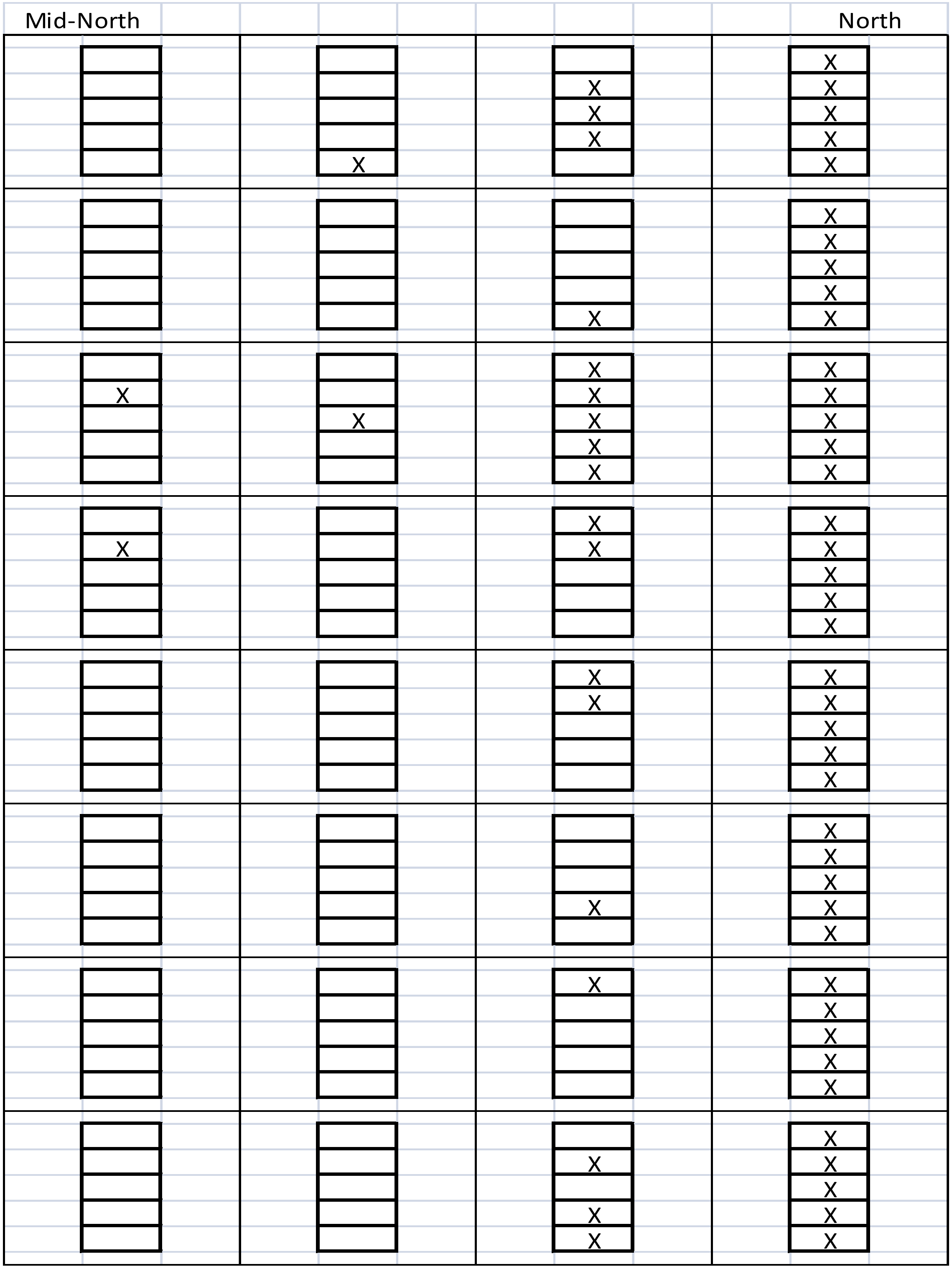

Figure E.107 – DIA9 – steel mass loss during inelastic test (3/3)

Table E.18 – DIA9R – list of testing protocols

BB		SS3		SS1		SS2	
0	☑	50	☑	50	☑	5	☑
225	☑	60	☑	60	☑	10	☑
675	☑	80	☑	70	☑	80	☑
1150	☑	100	☑	80	☑		
1825	☑	120	☑	90	☑		
2275	☑	140	☑	100	☑		
3200	☑	160	☑				
5050	☑	180	☑				
6000	☑	200	☑				
8000	☑						
10000	☑						
20000	☑						
40000	☑						
60000	☑						
80000	☑						

Notes

- Big actuator valves used for SS1-200 and SS1-80 and all larger amplitudes for those two loading protocols

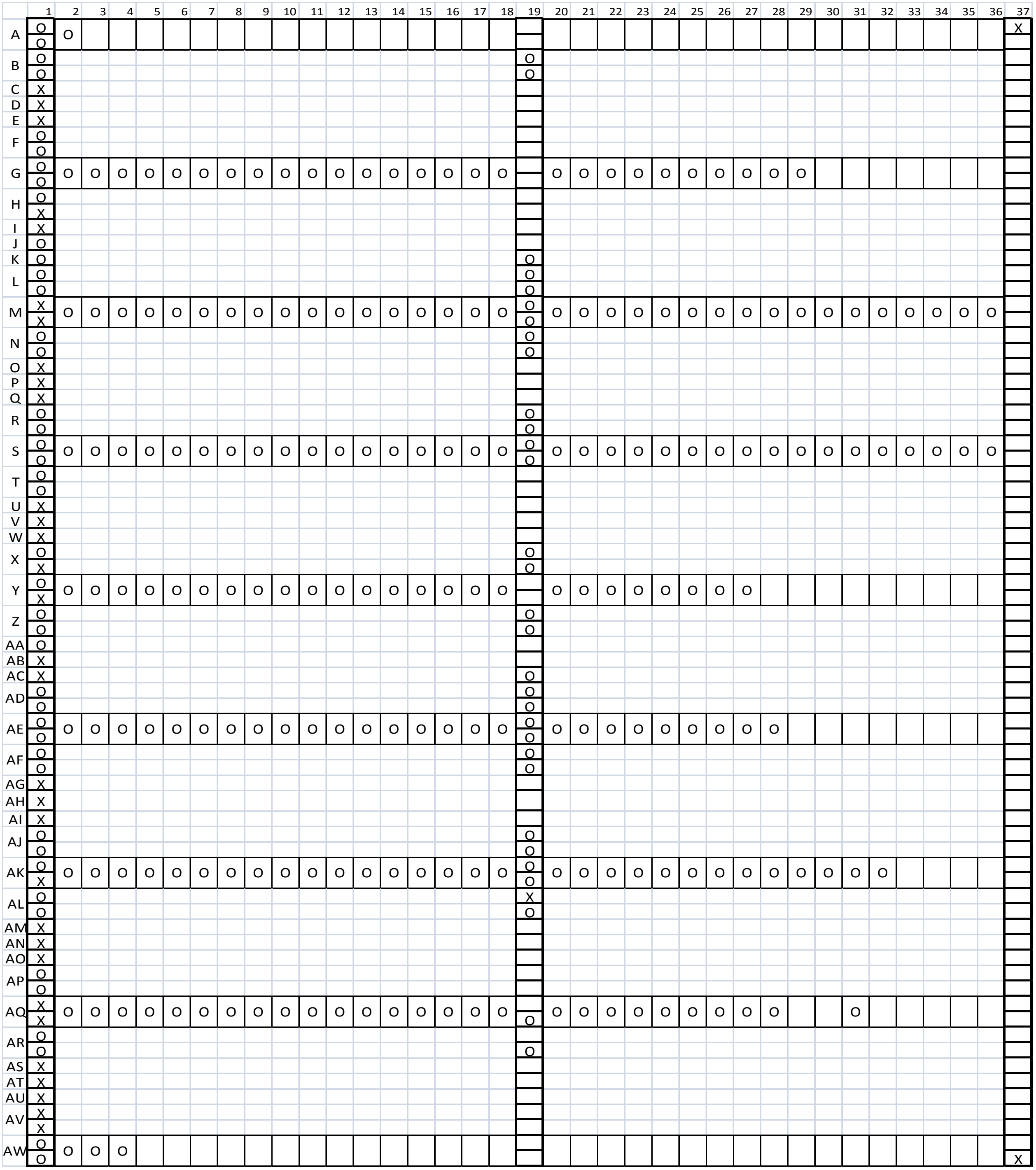

Figure E.108 – DIA9R – record of fastener failure during inelastic test (1/6)

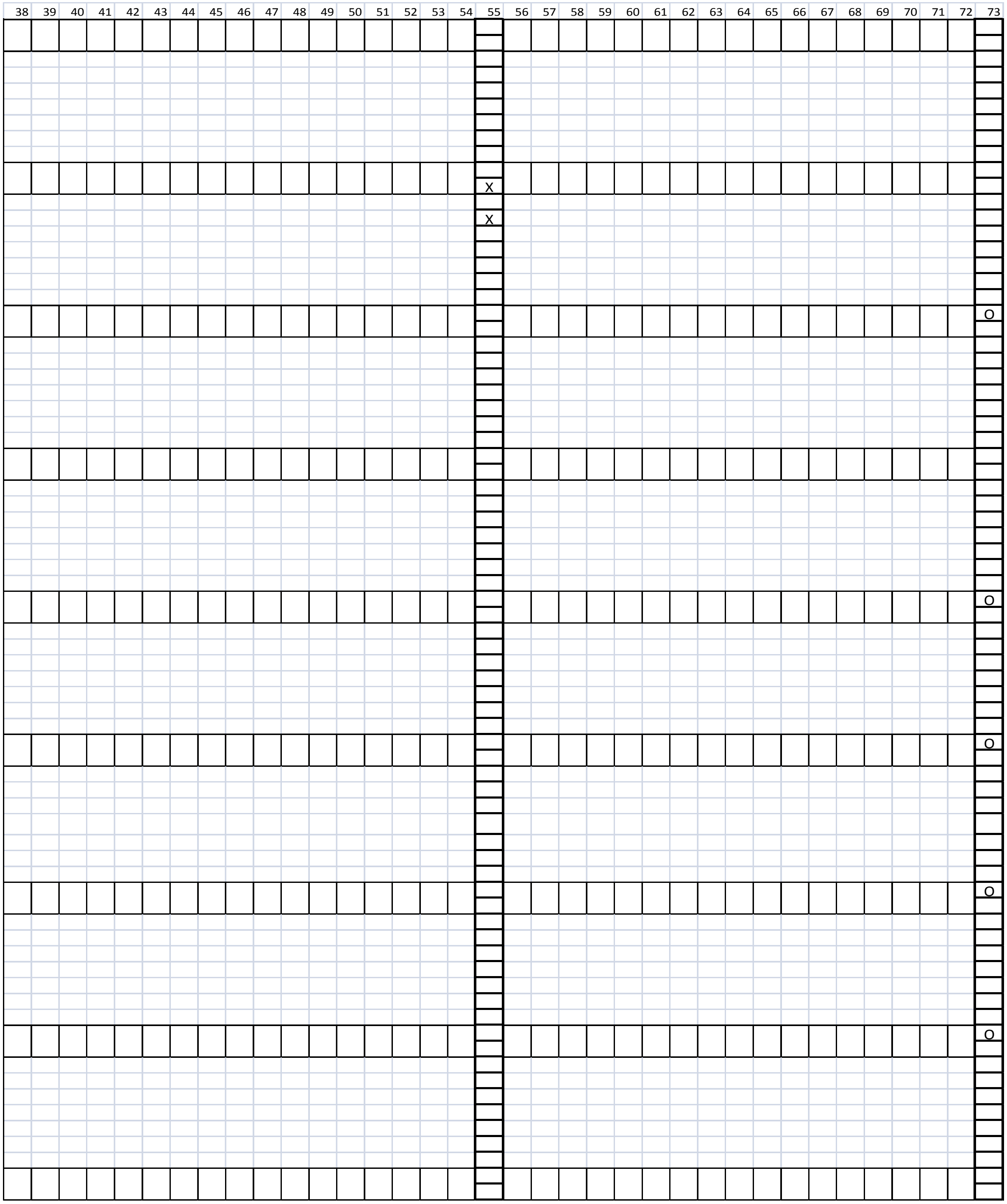

Figure E.109 – DIA9R – record of fastener failure during inelastic test (2/6)

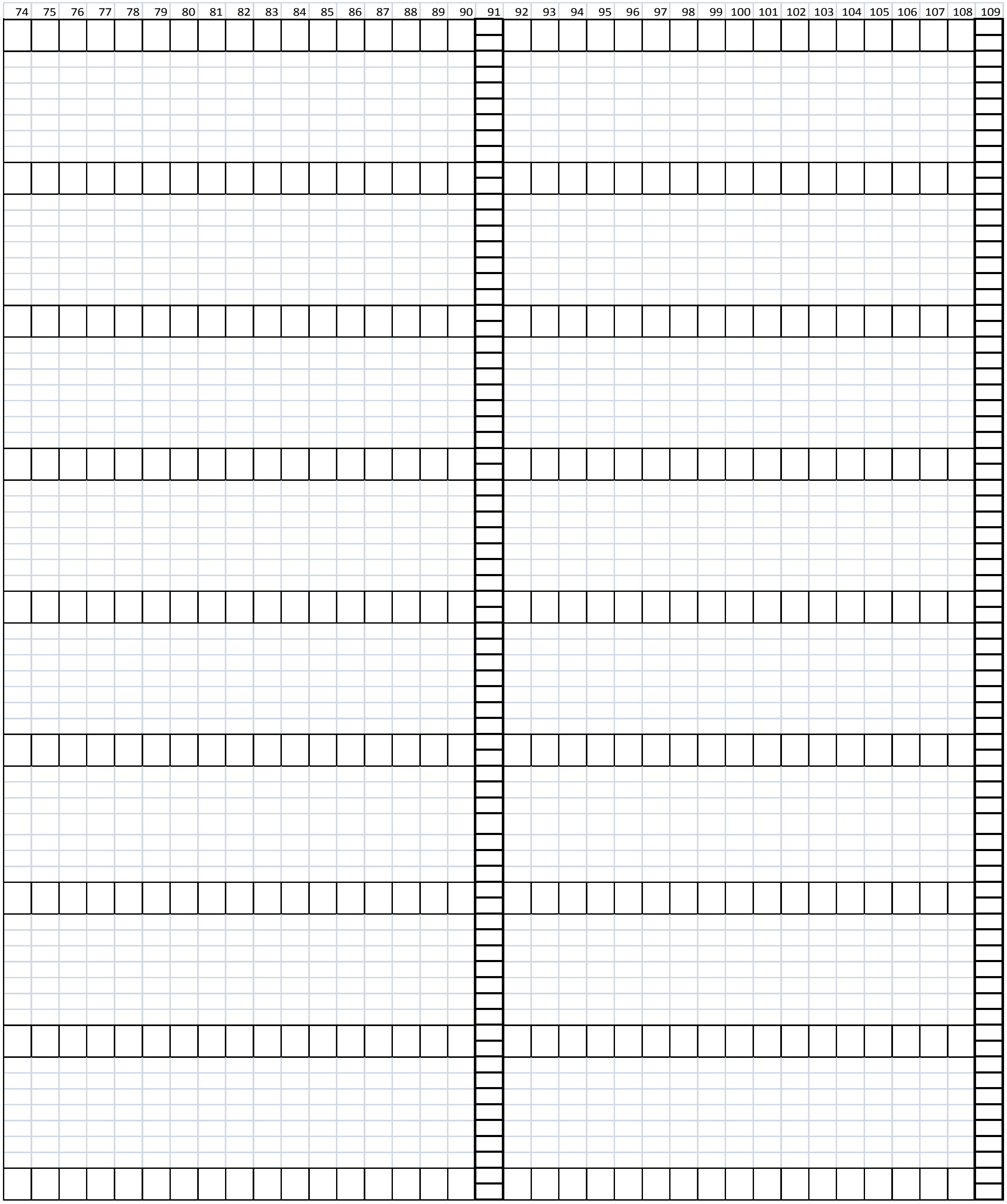

Figure E.110 – DIA9R – record of fastener failure during inelastic test (3/6)

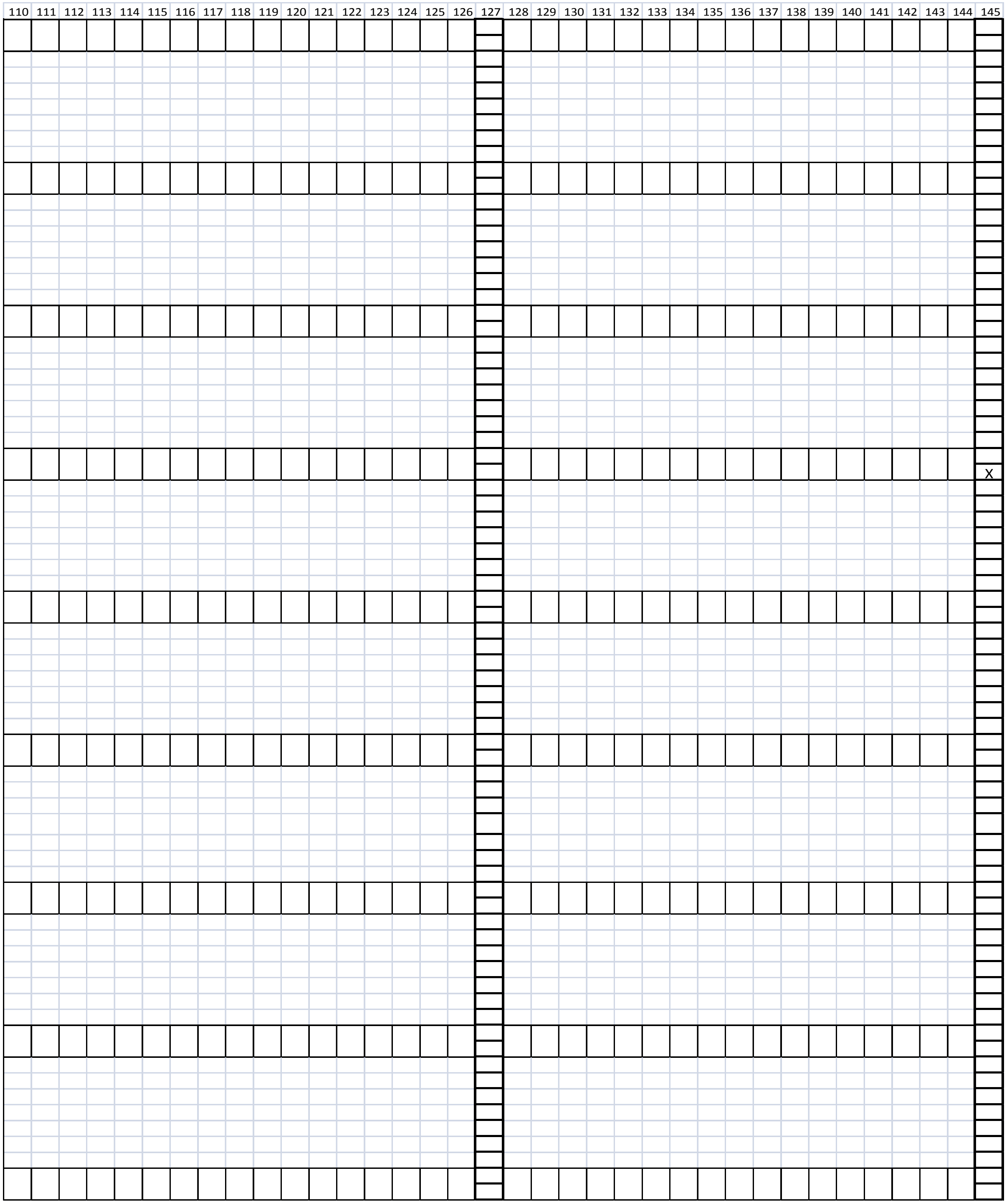

Figure E.111 – DIA9R – record of fastener failure during inelastic test (4/6)

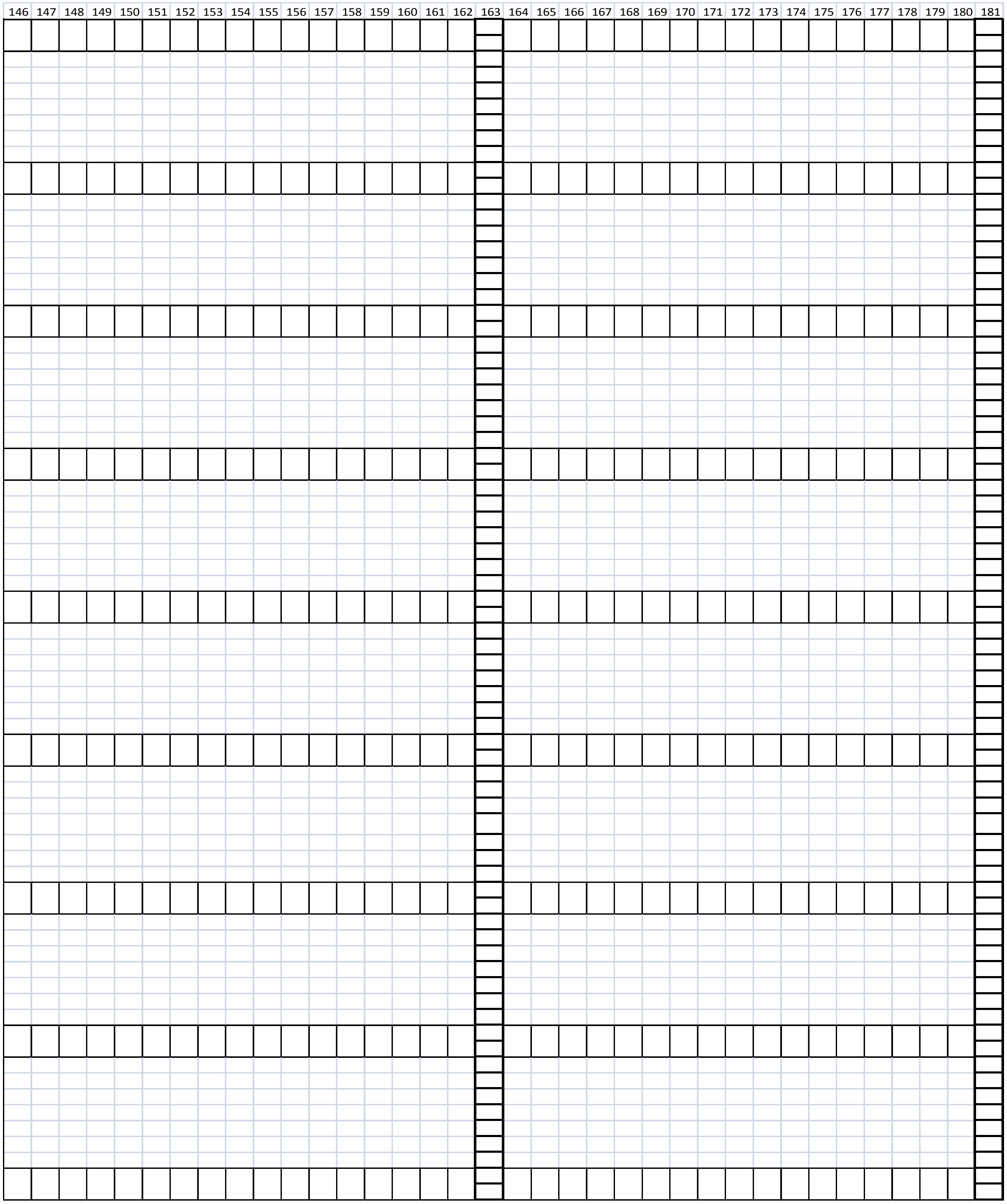

Figure E.112 – DIA9R – record of fastener failure during inelastic test (5/6)

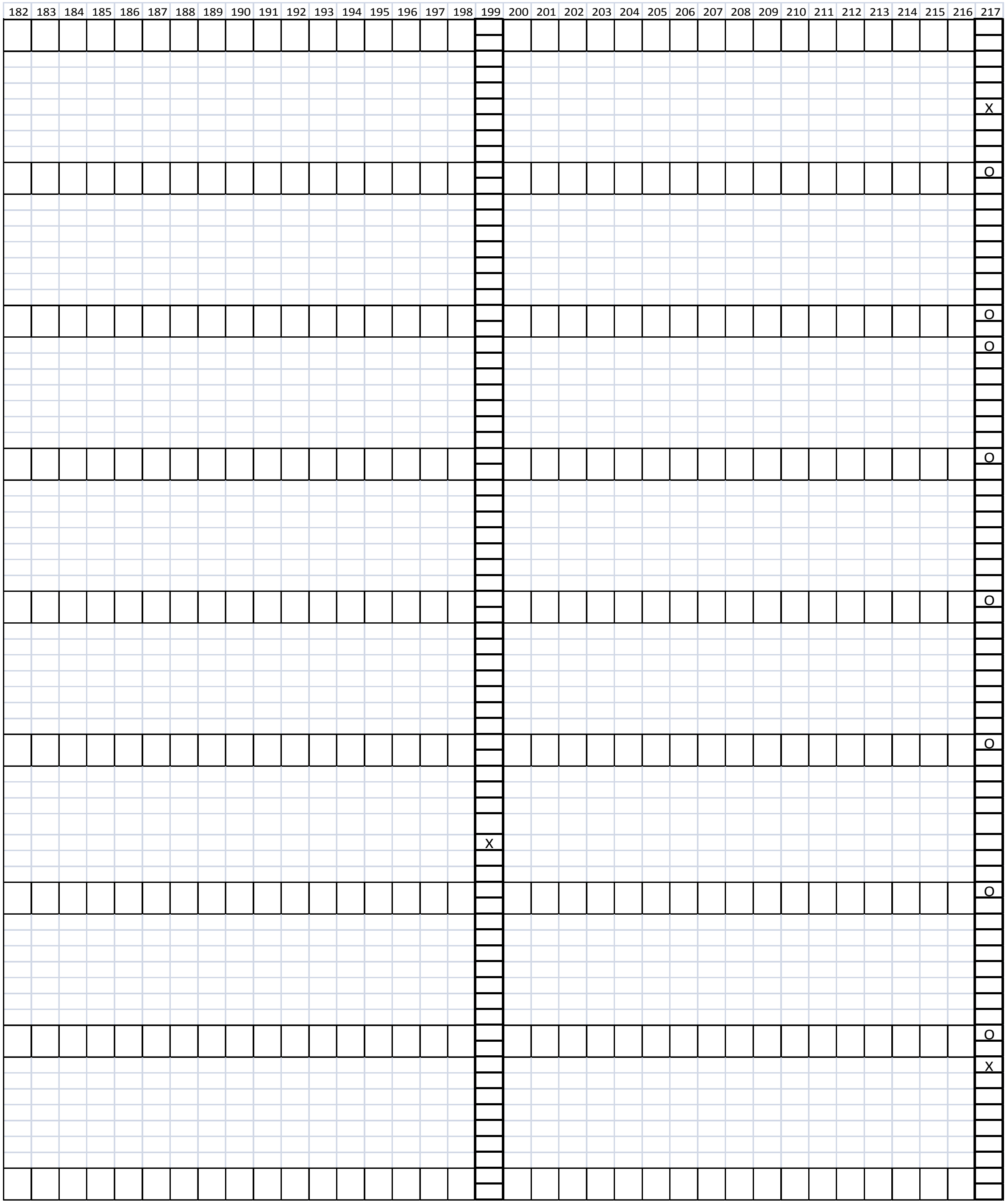

Figure E.113 – DIA9R – record of fastener failure during inelastic test (6/6)

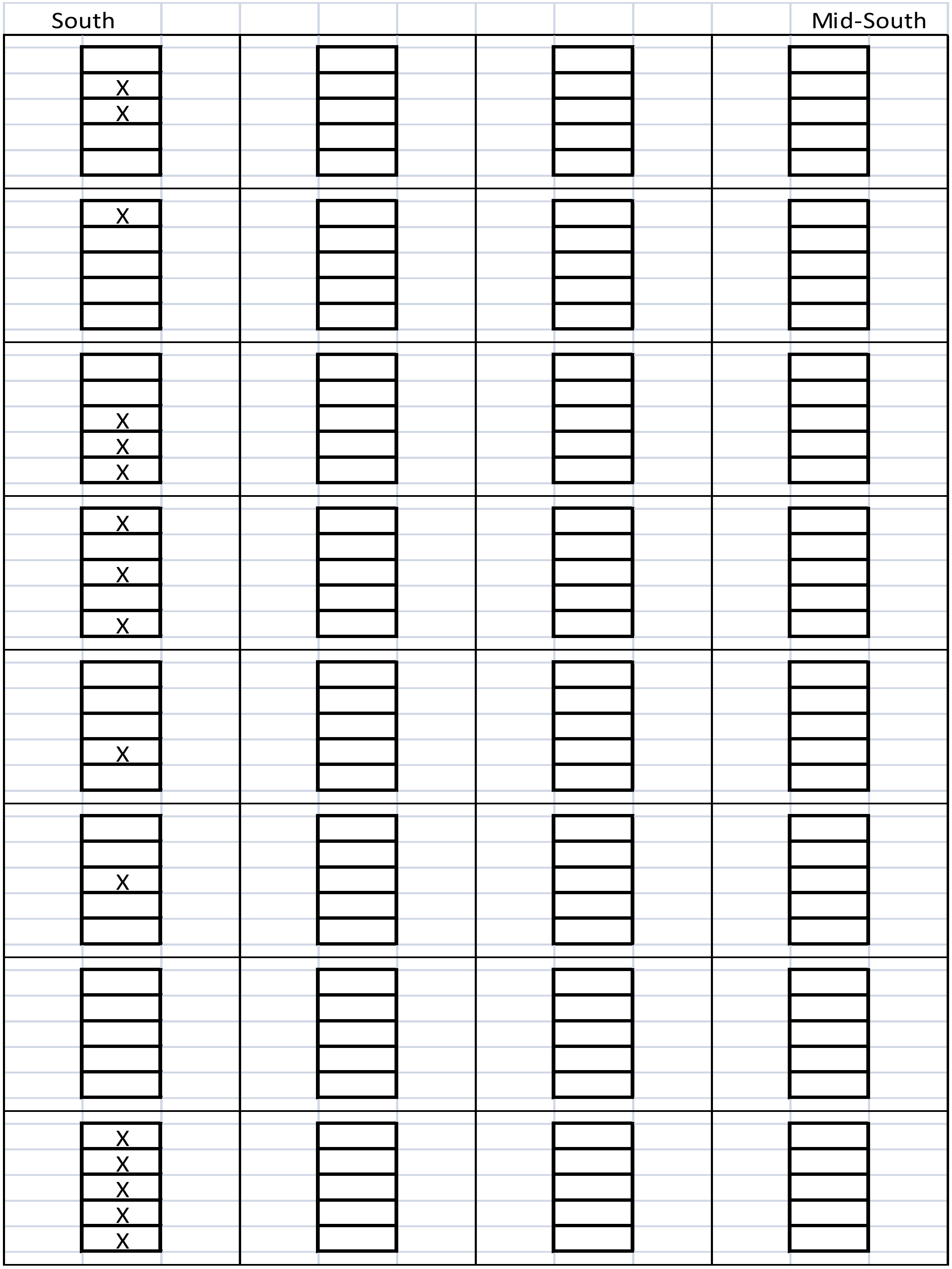

Figure E.114 – DIA9R – steel mass loss during inelastic test (1/3)

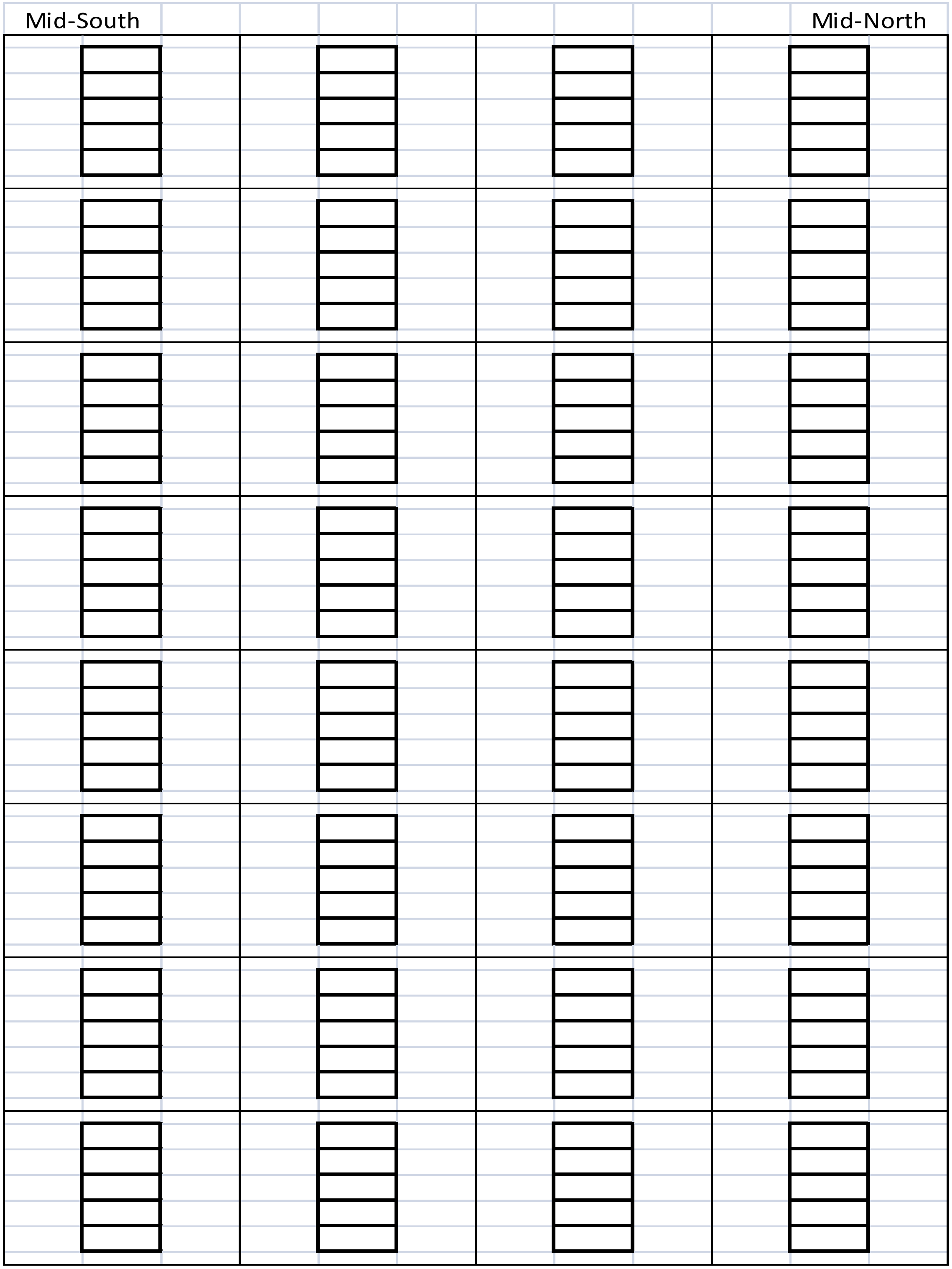

Figure E.115 – DIA9R – steel mass loss during inelastic test (2/3)

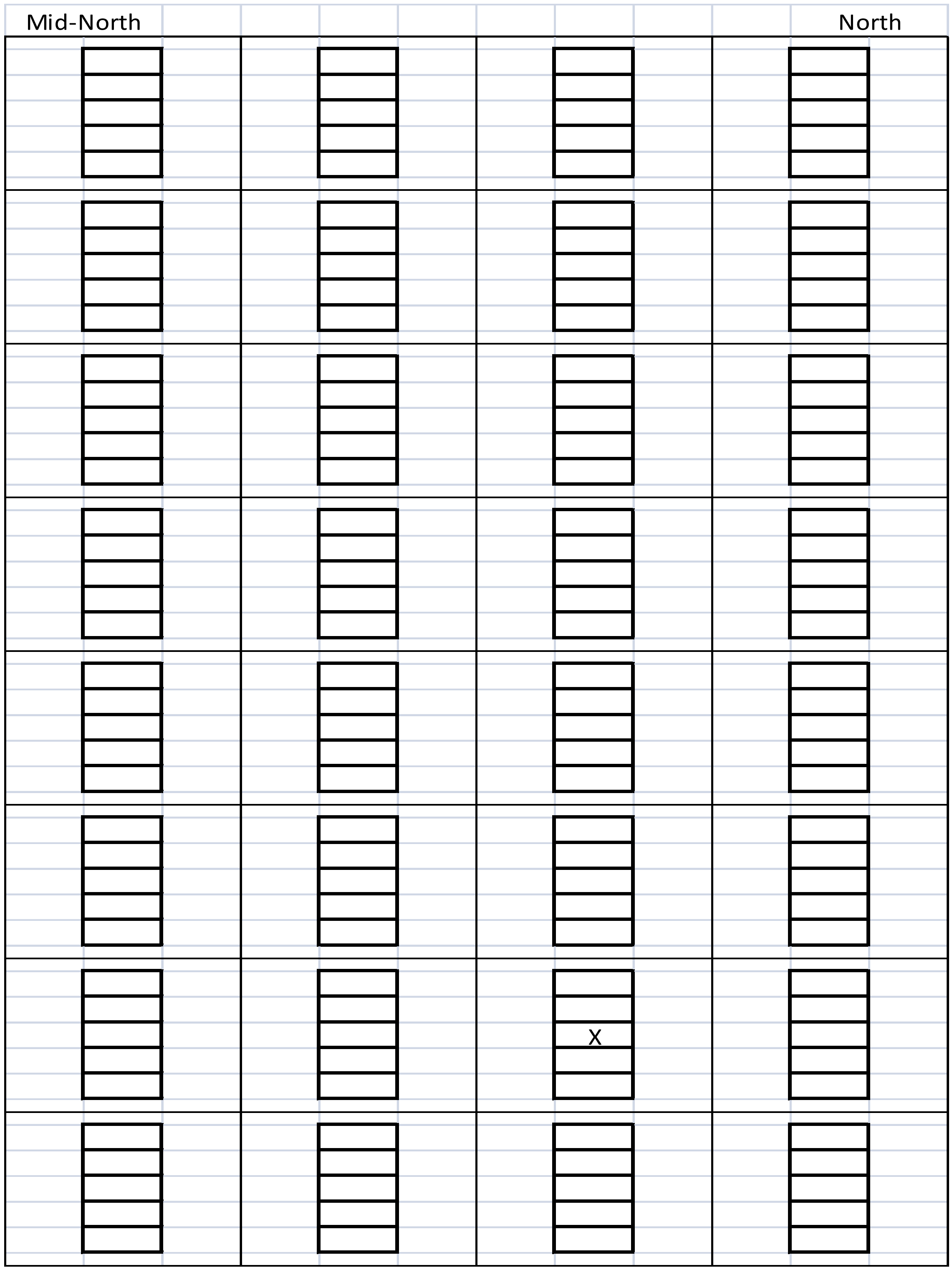

Figure E.116 – DIA9R – steel mass loss during inelastic test (3/3)

Table E.19 – DIA10 – list of loading protocols

BB		BF		SS3		SS1		SS2	
0	☑	4	☑	10	☑	10	☑	5	☑
150	☑	4.2	☑	20	☑	20	☑	10	☑
225	☑	4.3	☑	40	☑	30	☑	100	☑
925	☑	4.4	☑	60	☑	40	☑		
1725	☑	4.5	☑	80	☑	50	☑		
2500	☑	4.6	☑	100	☑	60	☑		
3200	☑	4.7	☑	120	☑	70	☑		
5050	☑	4.8	☑						
8000	☑	4.9	☑						
10000	☑	5	☑						
15000	☑	5.2	☑						
20000	☑	5.4	☑						
40000	☑	5.6	☑						
60000	☑	5.8	☑						
80000	☑	6	☑						
120000	☑		☑						
140000	☑		☑						
160000	☑		☑						
			☑						

<u>Notes</u>

- Big actuator valves used for SS1-200 and SS1-80 and all larger amplitudes for those two loading protocols
- A frequency multiplier of 80% was used for SS2-80

	1	2	3	4	5	6	7	8	9	10	11	12	13	14	15	16	17	18	19	20	21	22	23	24	25
A																									
B	X																								
C	X																								
D	X	X	X										X												
	X																								
E	X																								
F	X																								
G	X	X	X				X						X												X
	X																								
H																									
I	X																								
J	X	X					X																		
																									X
K																									
L	X																								
M	X	X	X	X									X						X						X
	X																								
N	X																								
O	X																								
P	X	X	X	X	X		X						X												
	X																								
Q	X																								
R	X																								
S	X	X	X				X																		
	X																								
T	X																								
U	X																								
V	X	X	X	X			X						X												
	X																								
W	X																								
X	X																								

Figure E.117 – DIA10 – record of fastener failure during inelastic test (1/3)

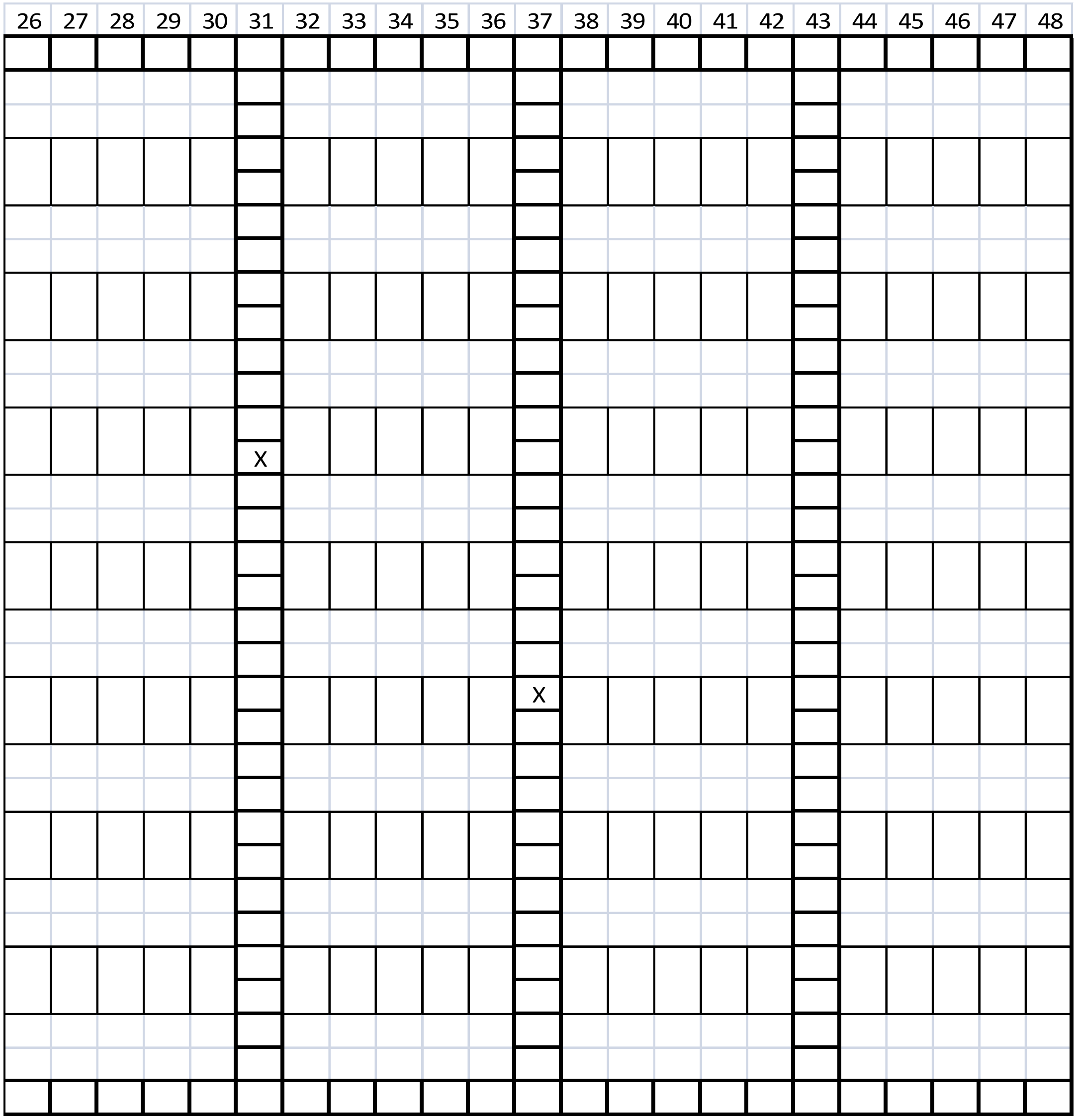

Figure E.118 – DIA10 – record of fastener failure during inelastic test (2/3)

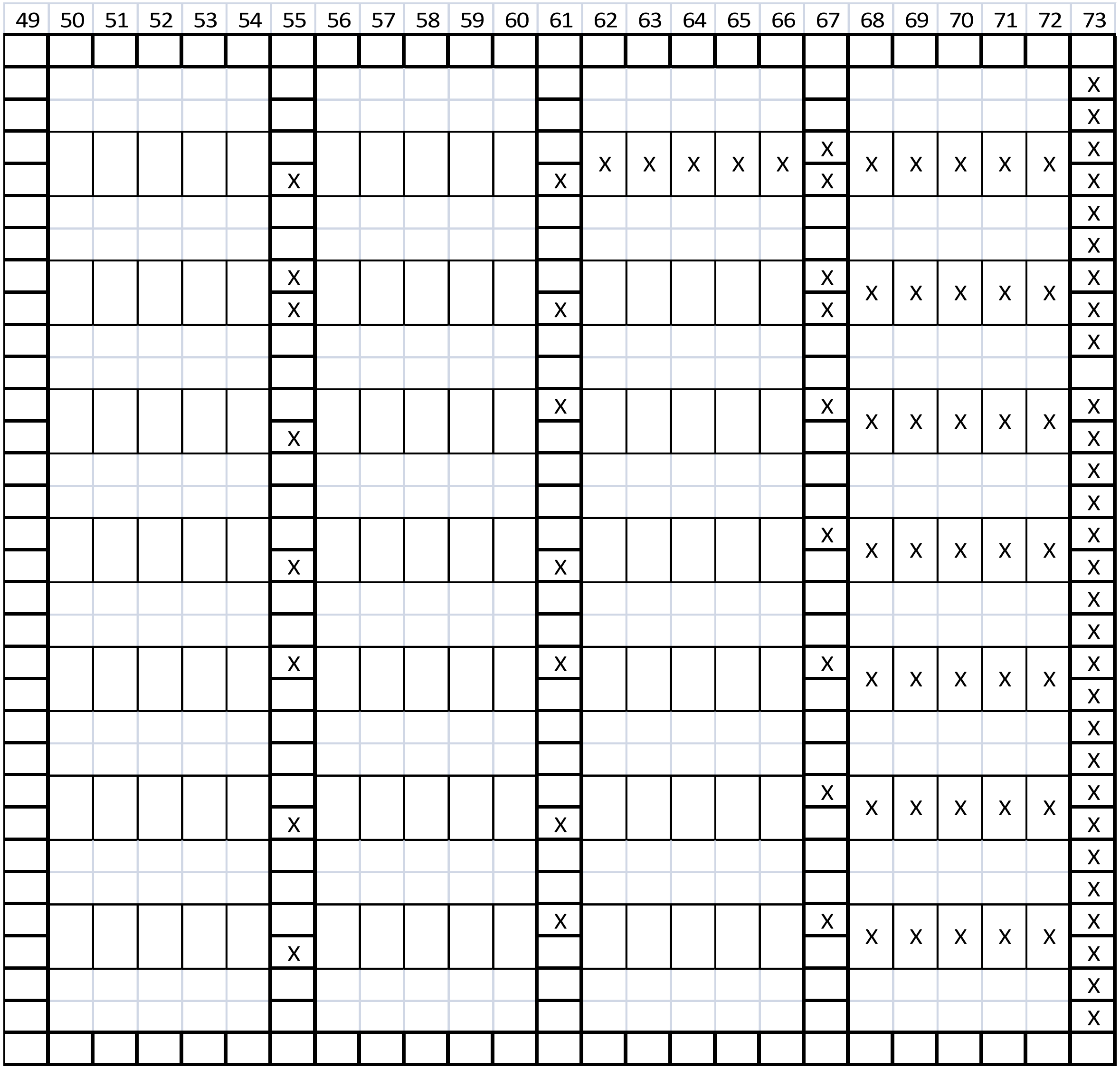

Figure E.119 – DIA10 – record of fastener failure during inelastic test (3/3)

	1	2	3	4	5	6	7	8	9	10	11	12	13	14	15	16	17	18	19	20	21	22	23	24	25
A	8.6	4.3	4.5	4.3	3.1	3	12	5.7	5.5	4.8	5.3	5.4	8	3.4	4.6	3.8	5	3.8	8	6.9	4.2	4.9	4.8	5	13
B	7.2						6.4						8.1						7.7						14
C	8.1						8.4						10						7.1						11
D	7.7						7						8.7						8.1						11
E	6.5						8.5						9.9						9.9						14
F	12						7.9						6.3						6.3						9.7
G	9.2						6.5						6.5						5.8						12
H	10						7.3						8						7.2						11
I	6.1						12						7.9						6.3						11
J	5.6						6.3						6.3						5.9						9.5
K	9.1						5.6						5.7						7.6						9.7
L	9.2						7.6						7.6						12						8.8
M	9.5						10						15						9.2						9.9
N	8.1						8.4						8						8.2						15
O	5.9						6.1						7.4						7.9						9.5
P	5.6						6.8						7.8						6.3						11
Q	8.1						10						11						5.2						8.7
R	11						9.2						7.7						7.2						13
S	9.4						8.5						8						8.4						8.8
T	6.6						10						9						8						7.8
U	7.2						6.5						7						6.6						17
V	11						7.7						5.5						8.2						13
W	9.3						10						5.9						9.3						11
X	8.7						9						7.3						8.6						11
Y	15	6.4	6.9	5.7	5.9	6.3	9.7	4.7	5.2	6.4	9.1	5.2	8.7	6.7	4.8	6.7	7.3	7.3	7.3	7.2	7.4	5.9	3.7	4.1	15

Start	6:50am	
End	9:47am	
Total Welds	64	mins
Total	177	mins

Figure E.120 – DIA10 – time record for arc-spot welding (1/3)

26	27	28	29	30	31	32	33	34	35	36	37	38	39	40	41	42	43	44	45	46	47	48
4.6	7.2	5.3	6.1	5.2	7.2	7.8	3.3	5.8	6.3	6.2	4.9	3.8	4.2	4.6	9	3.9	5.9	3.1	2.9	4.5	3	4.7
					12						9.1						4.9					
					5.6						8.6						10					
					7.5						7.4						7.2					
					7.9						5.8						6.6					
					9.3						3.6						8.1					
					5.1						8.5						7.7					
					5.2						8.4						5.3					
					6.3						7.2						8.4					
					13						7.8						5.8					
					9.3						7						6.3					
					12						7.5						7.4					
					14						6.8						4.8					
					10						7.2						6.2					
					7.5						5.3						5.1					
					8.3						8.6						6.7					
					8.8						7.4						6.2					
					7.1						11						8.3					
					6.5						6.8						8.7					
					8.8						6.4						11					
					7.5						7.4						7					
					9.6						4.5						11					
					6.8						8						5.3					
					6.9						6.5						7					
7.1	5.1	5.8	5.2	6.3	9.6	3.2	4.8	4.7	4.2	4.1	5.8	6	6	5.9	4.7	5.4	7.6	8.2	7.6	5.7	7.8	5.7

Figure E.121 – DIA10 – time record for arc-spot welding (2/3)

49	50	51	52	53	54	55	56	57	58	59	60	61	62	63	64	65	66	67	68	69	70	71	72	73
8.9	4.9	5	4.6	5.8	5.4	7.8	4	3.6	5.6	3.7	3.9	6.2	5.3	4	5	6.5	4	9.3	4.3	3.6	4.7	5.1	6	8.2
7.5						8.3						7.6						5.2						4.9
9.4						4.3						6.1						6.2						5.7
10						6.3						6.1						8.2						4.9
9.4						8.1						5.9						5.1						8.4
9.1						8.4						9.7						6.2						8.8
7						6.5						9.1						9.2						7.7
7.4						9.8						6.4						11						11
8.8						8.5						4.8						5.2						8.8
7.9						7.9						7.9						4.4						9
9.8						7.5						7.2						6.7						5.9
21						5						8.6						5.3						5.2
8.7						9.3						14						4.8						5.8
10						7.4						5.3						6.1						7.8
13						8.7						8.7						5.9						8
14						6.5						6.8						6.7						8.4
13						7.6						7.5						4.2						6.8
15						8.9						9.6						10						4.5
6.8						8.1						7.8						5.5						7.7
5.5						6.5						10						8.7						7.6
11						7.6						5.6						7.4						6.4
11						6						11						11						8
4.6						5.8						8.6						11						11
9.4						9.1						5.7						6.5						6.3
7.1	3.9	3.7	9.3	6.9	7.5	7.5	6.6	5.4	3.8	4	5.3	6.7	4.3	6.2	4.2	5.8	3.1	5.5	4.6	3.9	5.1	5.8	4.3	8.6

Figure E.122 – DIA10 – time record for arc-spot welding (3/3)

	1	2	3	4	5	6	7	8	9	10	11	12	13	14	15	16	17	18	19	20	21	22	23	24	25
A	17	18	16	17	16	15	15	15	16	17	17	15	11	14	15	15	17	15	15	19	18	17	16	16	15
B	19						16						18						17						20
C	21						17						16						19						17
D	16						16						18						15						17
E	18						18						19						19						17
F	17						18						17						18						17
G	14						18						16						16						15
H	18						17						16						19						17
I	17						17						17						18						15
J	19						18						17						17						16
K	17						17						17						17						18
L	21						17						18						17						17
M	14						18						14						16						15
N	16						16						17						17						16
O	17						17						17						16						15
P	23						16						18						16						15
Q	21						17						17						19						20
R	19						19						20						19						19
S	19						13						16						18						17
T	18						18						17						20						18
U	19						18						16						19						18
V	19						15						14						19						16
W	18						17						16						16						17
X	15						16						17						18						19
Y	12	17	17	18	18	16	16	16	16	16	17	16	16	15	16	17	18	16	16	17	18	17	16	18	14

Average Diameter for Frame Weld	16	mm
Average Diameter for Joist Weld	17	mm
Average Diameter for 2-Sheet Weld	17	mm
Average Diameter for 4-Sheet Weld	17	mm

Figure E.123 – DIA10 – record of weld diameter (1/3)

26	27	28	29	30	31	32	33	34	35	36	37	38	39	40	41	42	43	44	45	46	47	48
17	15	15	16	16	15	14	14	15	14	14	18	18	17	17	18	13	16	15	15	13	14	14
					20						20						18					
					19						19						18					
					17						19						18					
					17						18						18					
					18						18						16					
					16						17						14					
					16						20						15					
					15						17						20					
					16						18						19					
					16						18						16					
					17						18						16					
					17						18						18					
					17						18						18					
					18						17						18					
					17						18						17					
					17						19						16					
					17						19						18					
					18						18						17					
					19						16						18					
					19						18						18					
					16						17						17					
					17						17						17					
					18						16						18					
16	18	19	17	15	16	18	17	17	17	17	18	19	17	17	17	19	14	19	15	14	14	16

Figure E.124 – DIA10 – record of weld diameter (2/3)

49	50	51	52	53	54	55	56	57	58	59	60	61	62	63	64	65	66	67	68	69	70	71	72	73
13	16	13	16	14	16	18	17	17	17	15	12	16	16	15	16	13	15	19	17	15	14	15	18	14
16						19						15						15						19
16						18						18						16						18
19						18						16						14						17
18						20						14						18						16
16						16						17						17						19
21						17						17						16						17
17						16						16						17						15
17						19						18						16						14
15						13						16						18						16
19						17						20						16						15
17						19						16						15						16
18						18						17						13						15
19						18						15						16						17
20						18						20						17						18
18						16						15						17						17
18						16						16						19						16
20						15						17						17						17
17						15						18						16						16
17						17						17						17						16
17						16						17						17						16
16						18						16						17						16
23						17						19						17						17
17						15						17						16						15
15	14	15	17	17	14	20	15	15	16	16	16	12	18	14	15	14	20	17	16	12	14	16	16	14

Figure E.125 – DIA10 – record of weld diameter (3/3)

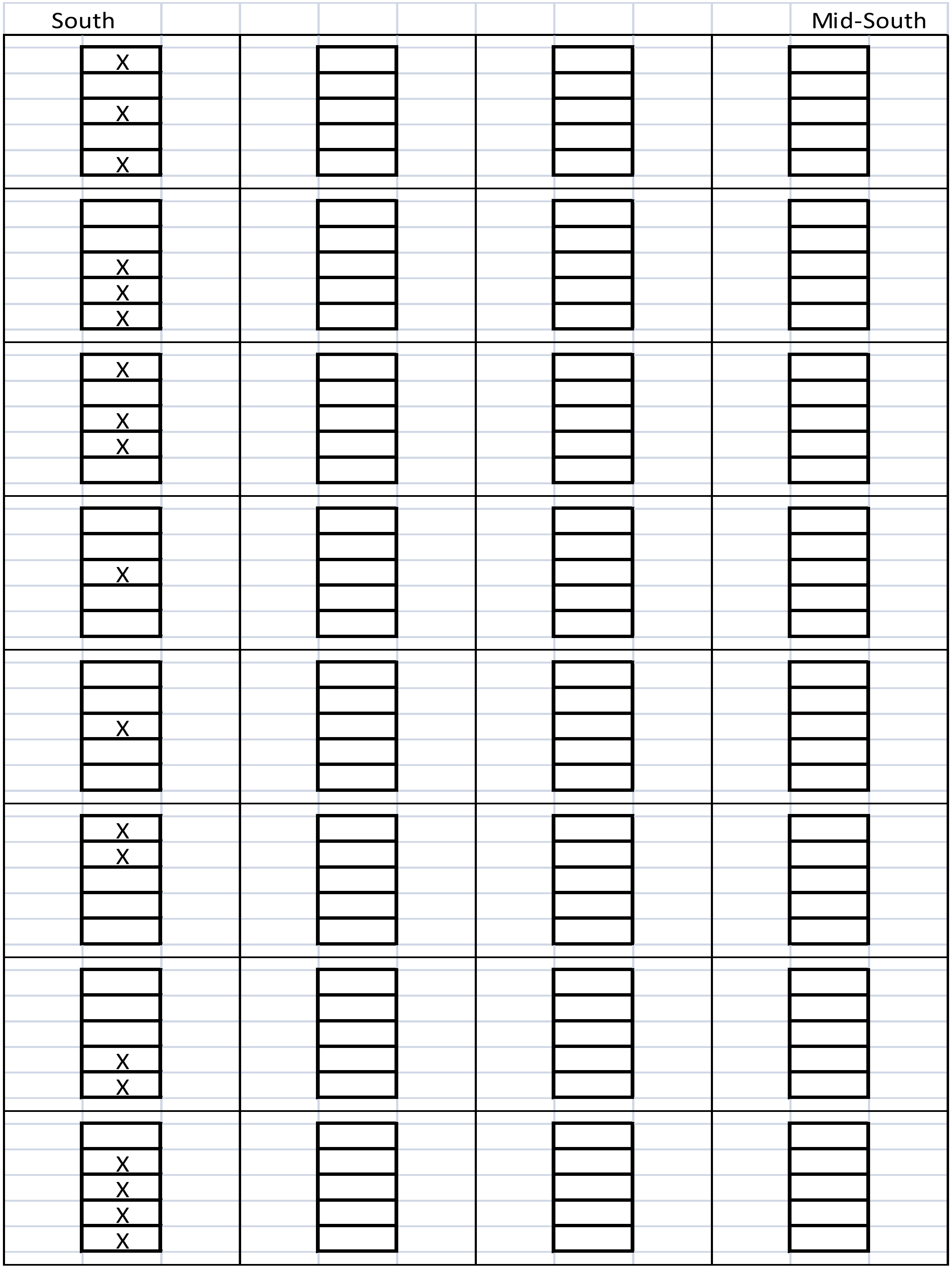

Figure E.126 – DIA10 – steel mass loss during inelastic test (1/3)

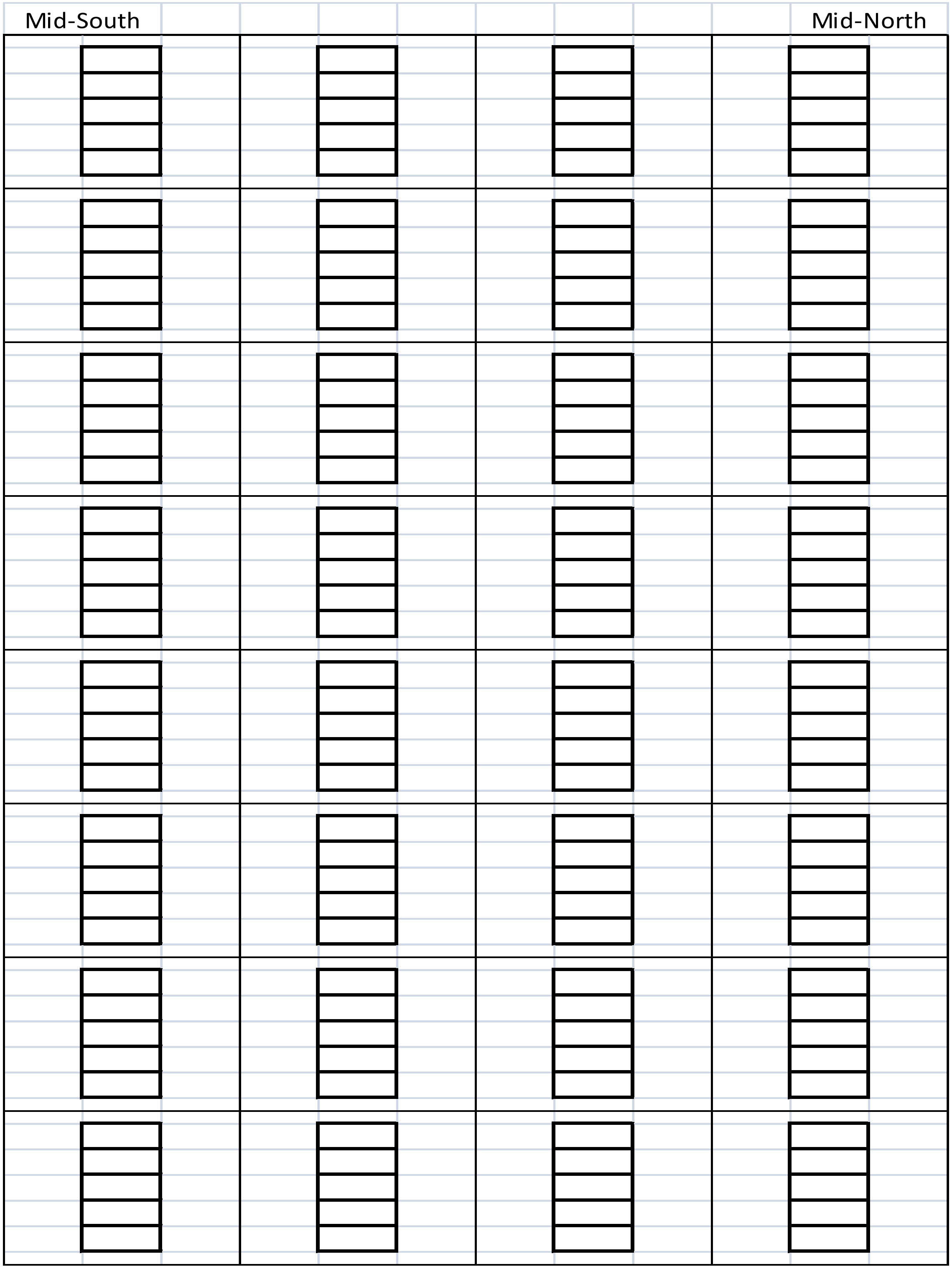

Figure E.127 – DIA10 – steel mass loss during inelastic test (2/3)

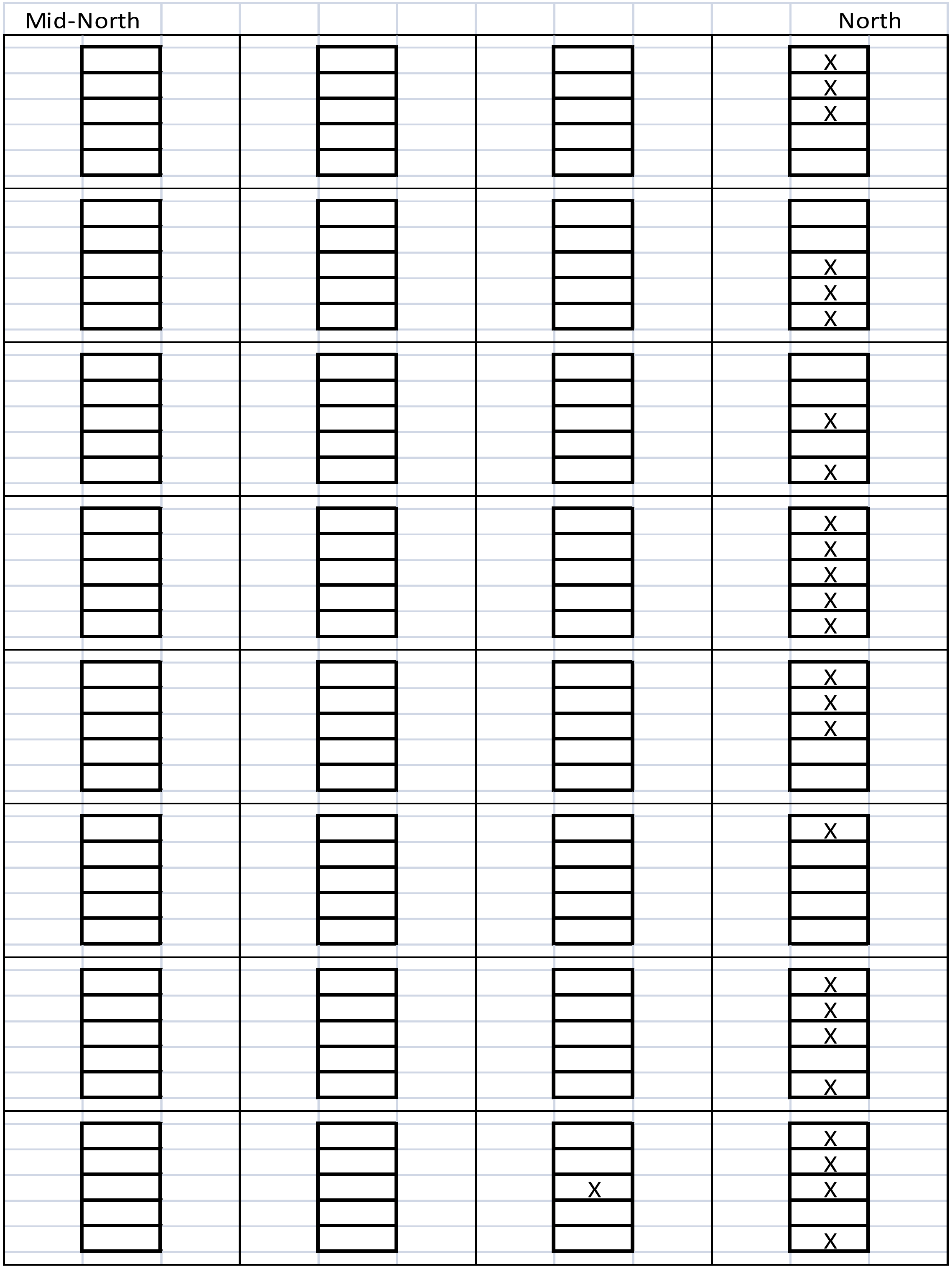

Figure E.128 – DIA10 – steel mass loss during inelastic test (3/3)

Table E.20 – DIA10R – list of testing protocols

BB		BF		SS3		SS1		SS2	
0	☑	3.2	☑	10	☑	5	☑	5	☑
250	☑	3.4	☑	15	☑	10	☑	10	☑
525	☑	3.5	☑	30	☑	20	☑	100	☑
1075	☑	3.6	☑	50	☑	30	☑		
1600	☑	3.7	☑	70	☑				
3200	☑	3.8	☑	90	☑				
5050	☑	3.9	☑	110	☑				
6000	☑	4	☑	130	☑				
8000	☑	4.2	☑						
10000	☑	4.4	☑						
20000	☑	4.6	☑						
40000	☑	4.8	☑						
60000	☑	5	☑						
80000	☑	5.2	☑						
100000	☑	5.4	☑						
120000	☑	5.6	☑						
		5.8	☑						

Notes

- Big actuator valves used for SS1-200 and SS1-80 and all larger amplitudes for those two loading protocols
- A frequency multiplier of 80% was used for SS2-80

	1	2	3	4	5	6	7	8	9	10	11	12	13	14	15	16	17	18	19	20	21	22	23	24	25
A																									
B	X																								
C	X																								
D																									
	X																								
E	X																								
F	X																								
G	X		O	O																					
H																									
I	X																								
J			O		O																				
K	X																								
L	X																								
M	X	O																							
N	X																								
O	X																								
P		O		O	O																				
Q	X																								
R	X																								
S	X		O																						
	X																								
T	X																								
U	X																								
V	X	O	O	O		O																			
	X																								
W	X																								
X	X																								
Y																									

Figure E.129 – DIA10R – record of fastener failure during inelastic test (1/3)

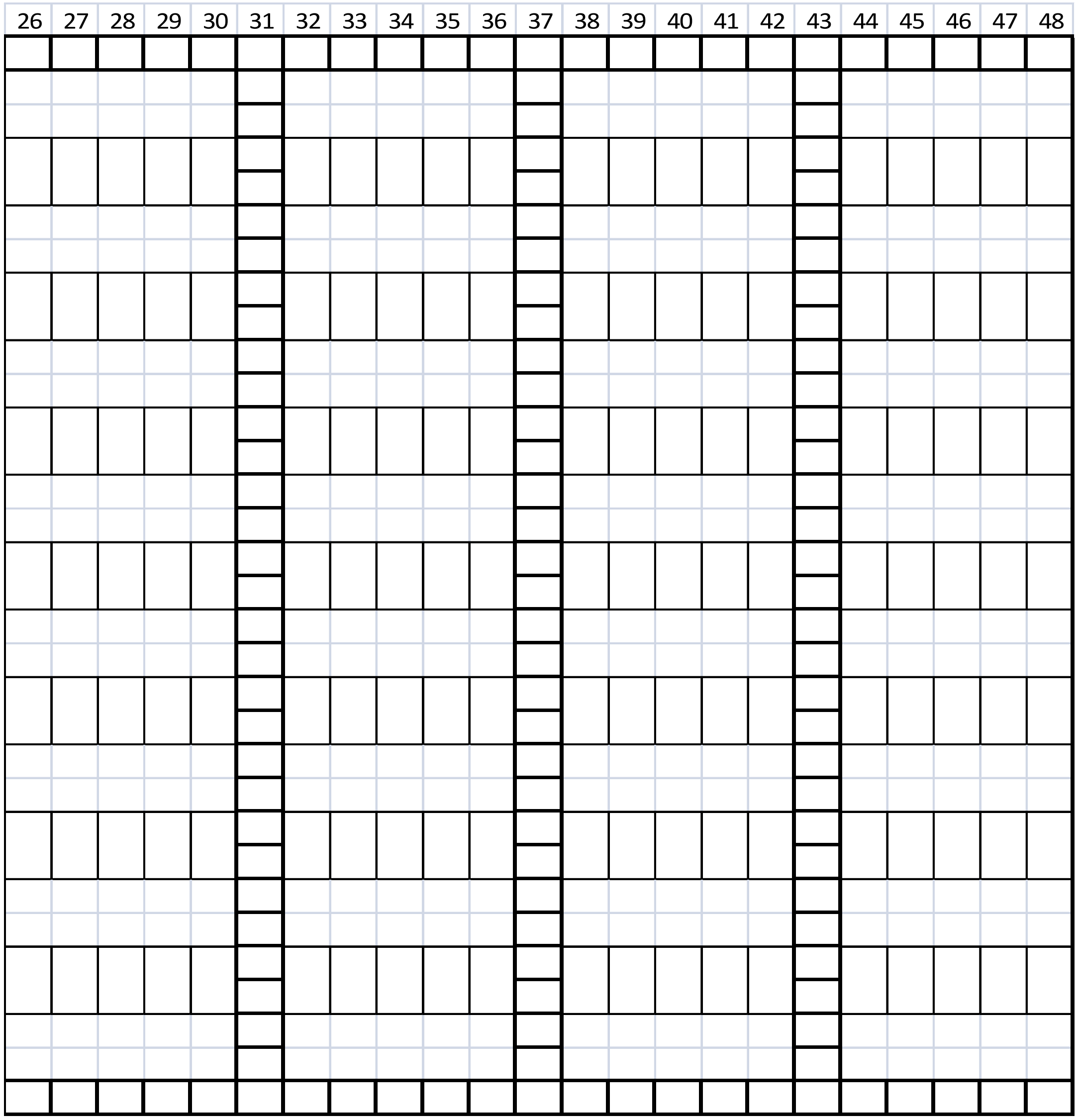

Figure E.130 – DIA10R – record of fastener failure during inelastic test (2/3)

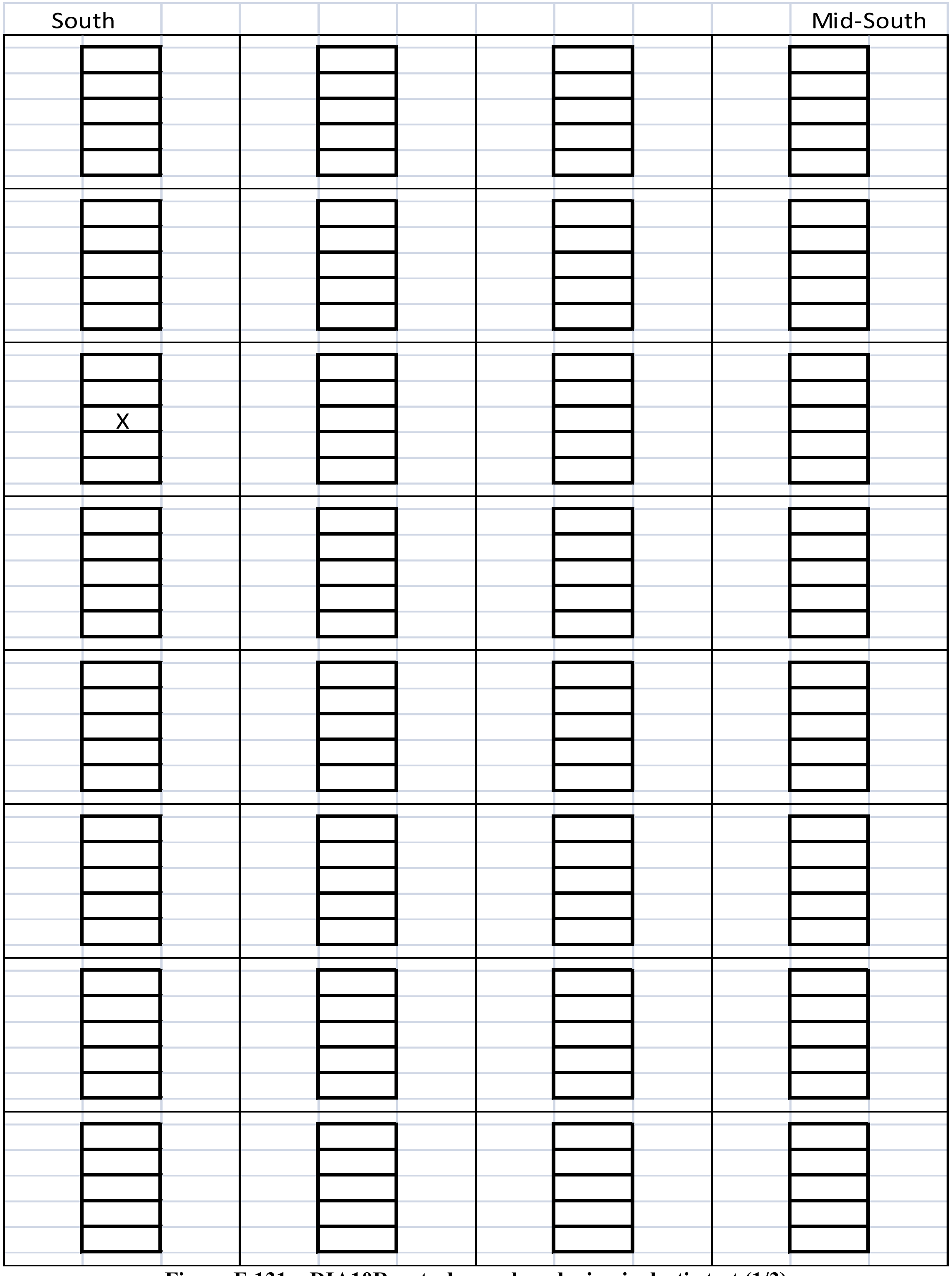

Figure E.131 – DIA10R – steel mass loss during inelastic test (1/3)

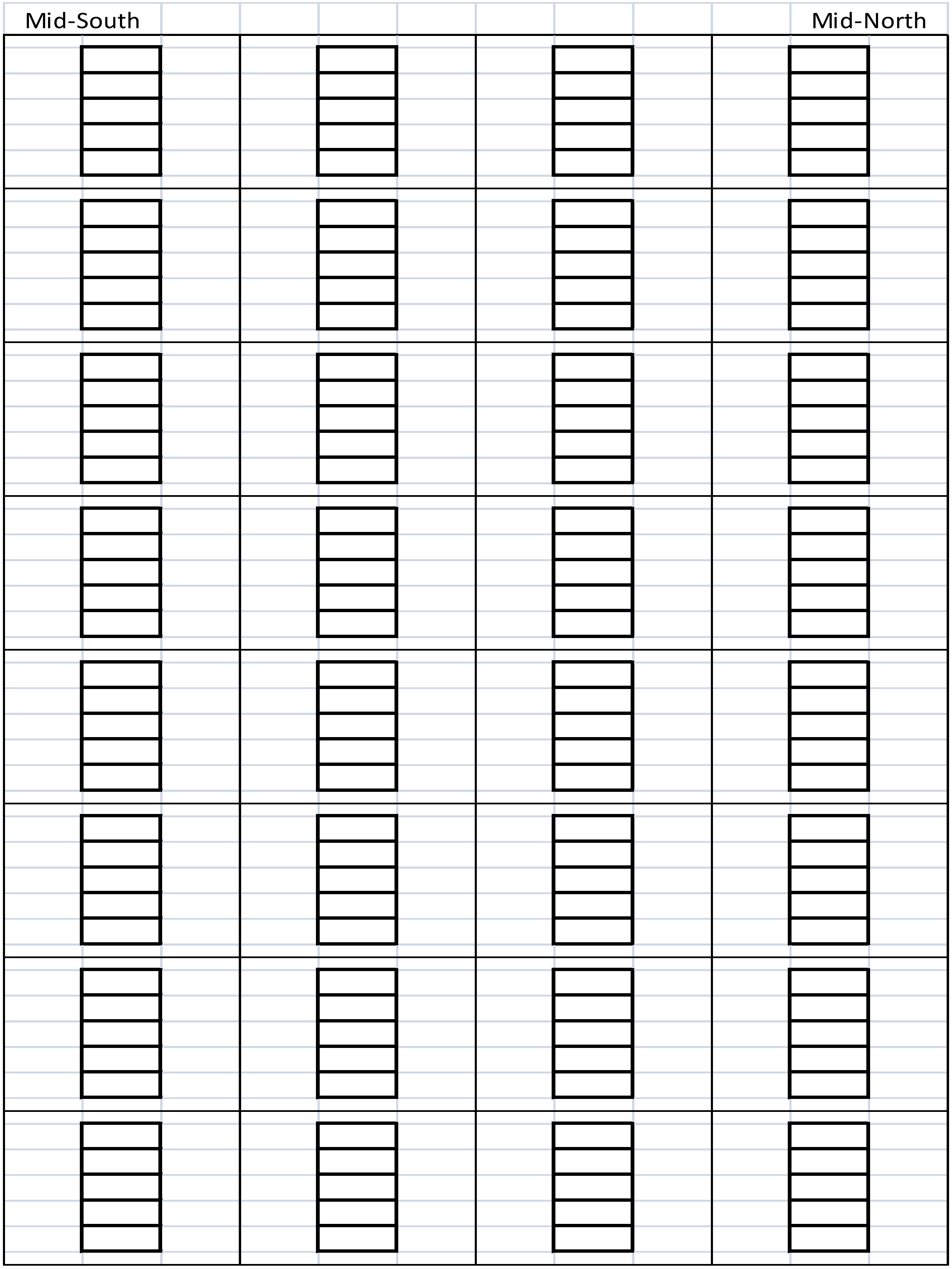

Figure E.132 – DIA10R – steel mass loss during inelastic test (2/3)

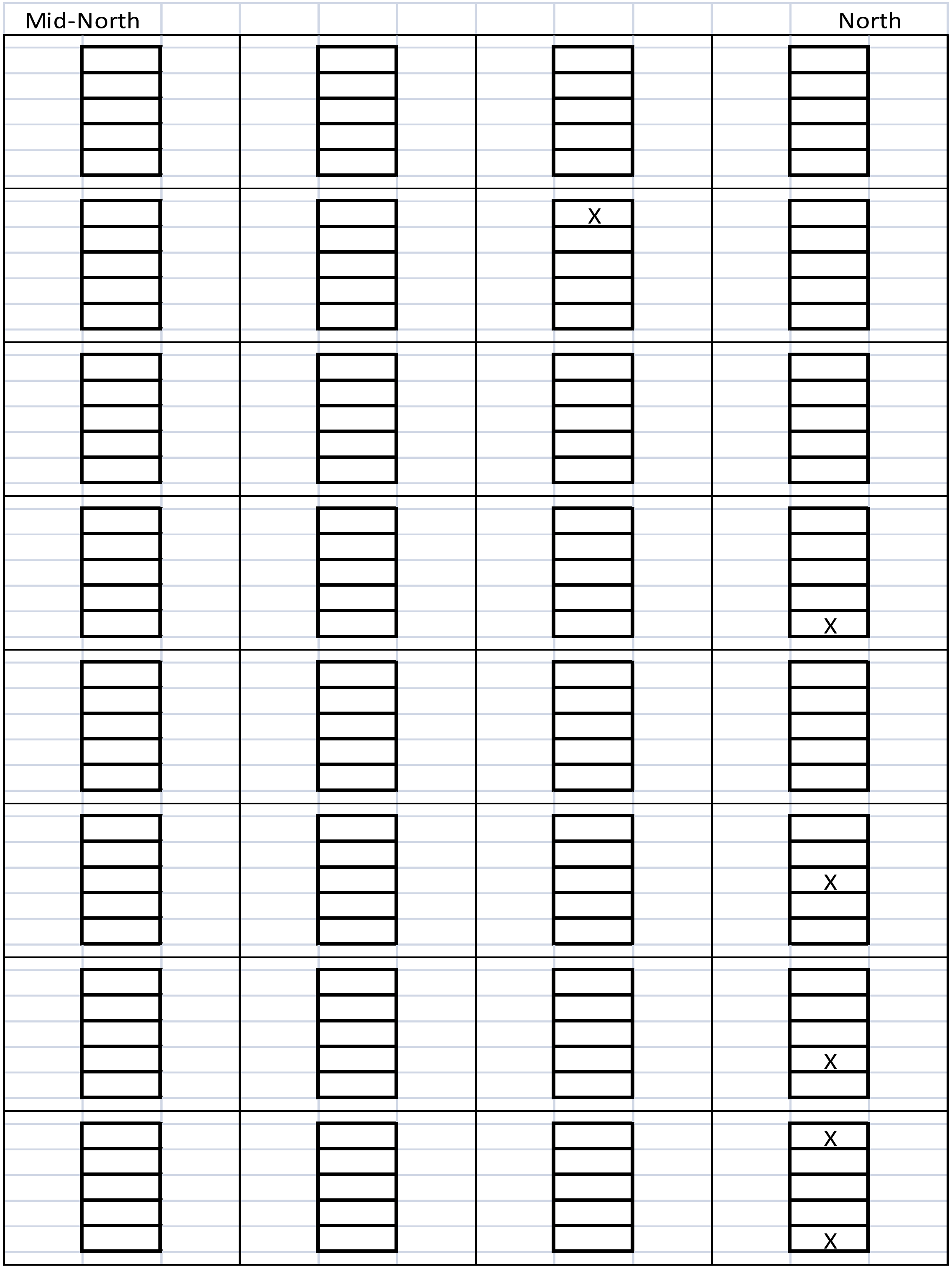

Figure E.133 – DIA10R – steel mass loss during inelastic test (3/3)

APPENDIX F: PHASE I & II – LOAD-DISPLACEMENT HYSTERESIS FOR NEW DIAPHRAGMS

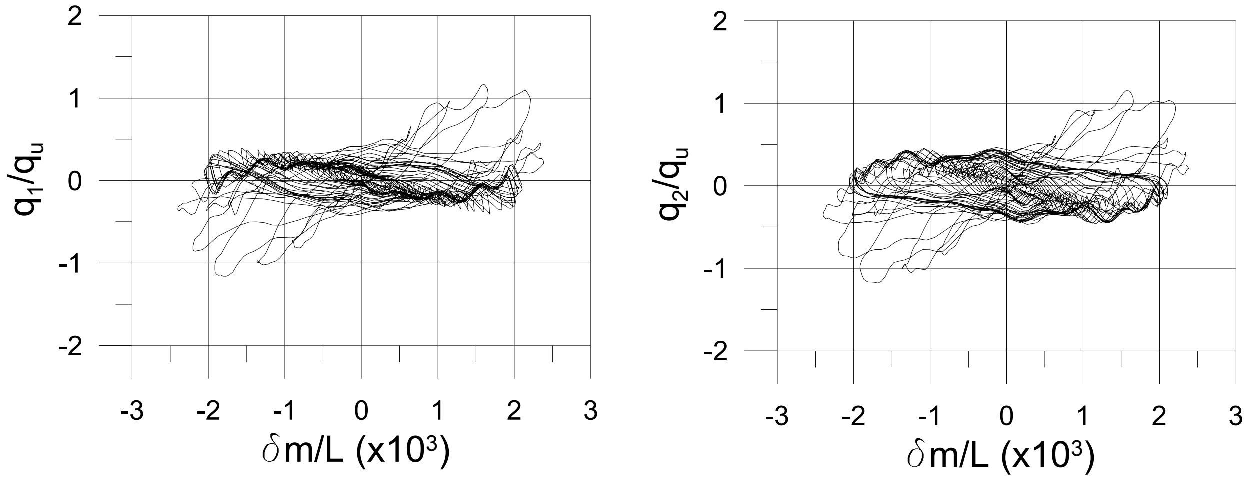

Figure F.1 – DIA1 – Hysteresis obtained from actuator 1 (right) and actuator 2 (left) load cell measurements and displacement at centre

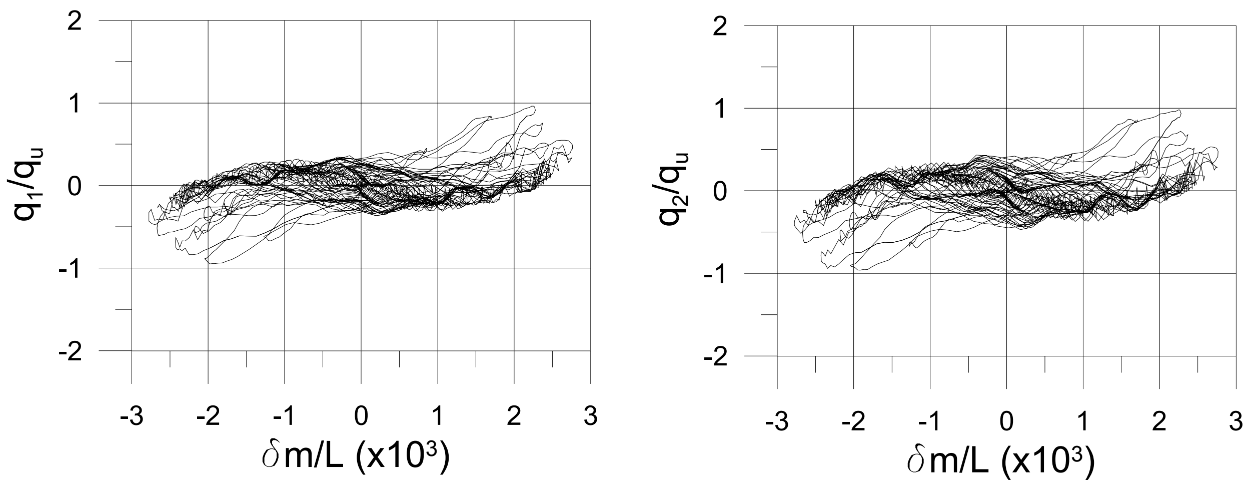

Figure F.2 – DIA2 – Hysteresis obtained from actuator 1 (right) and actuator 2 (left) load cell measurements and displacement at centre

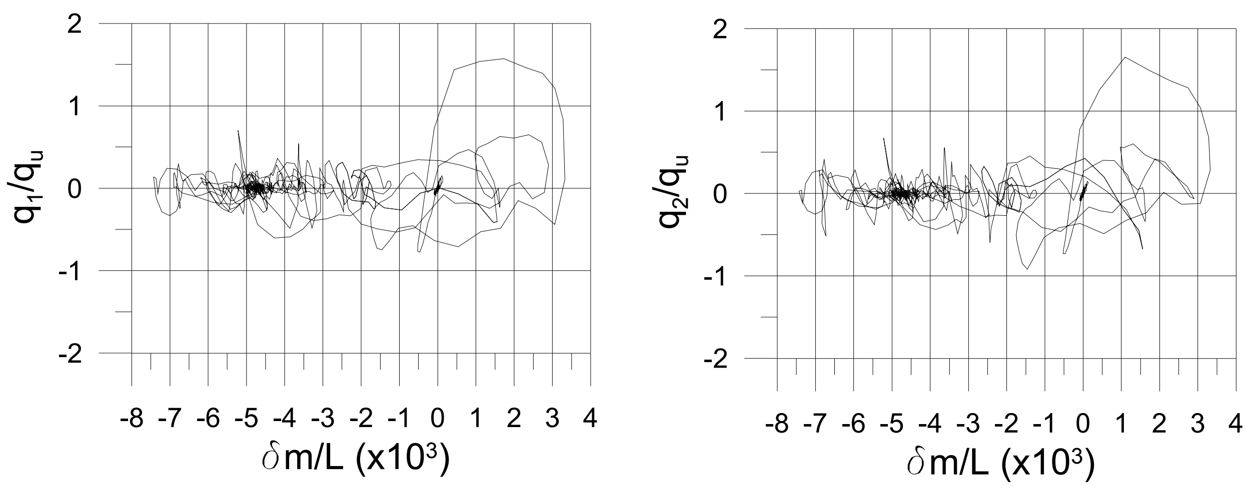

Figure F.3 – DIA3 – Hysteresis obtained from actuator 1 (right) and actuator 2 (left) load cell measurements and displacement at centre

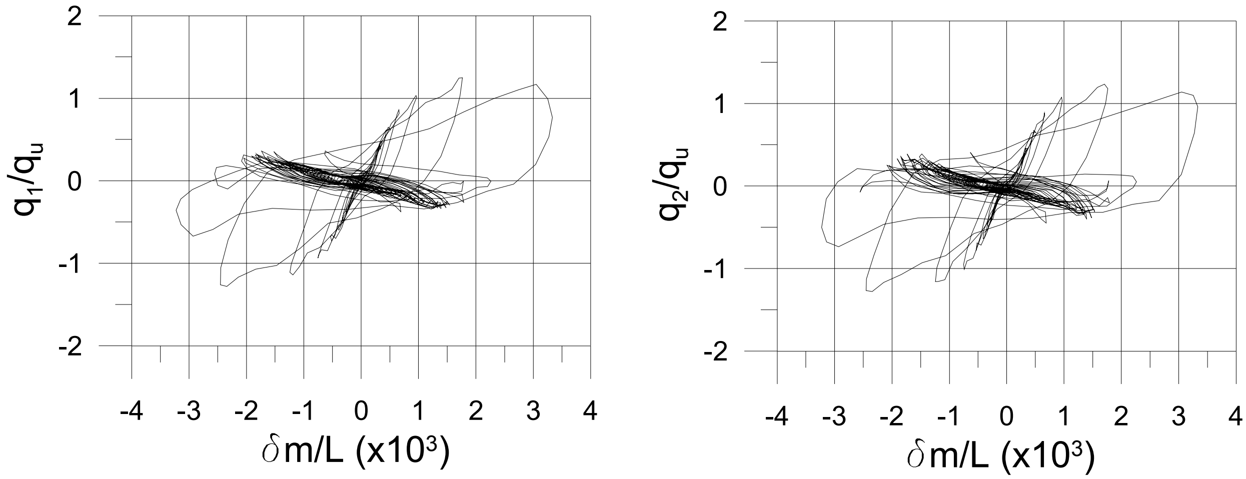

Figure F.4 – DIA4 – Hysteresis obtained from actuator 1 (right) and actuator 2 (left) load cell measurements and displacement at centre

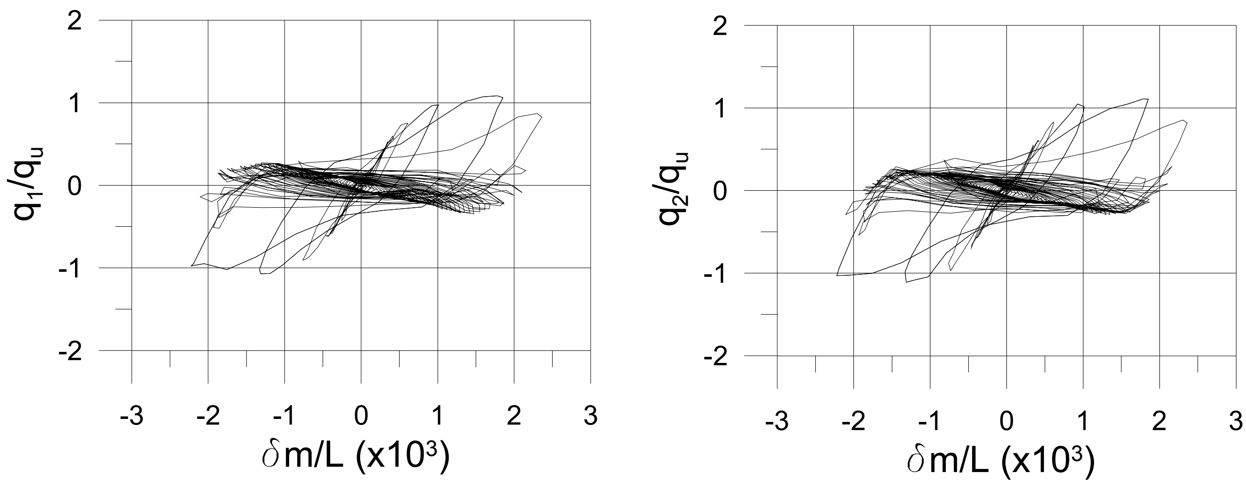

Figure F.5 – DIA5 – Hysteresis obtained from actuator 1 (right) and actuator 2 (left) load cell measurements and displacement at centre

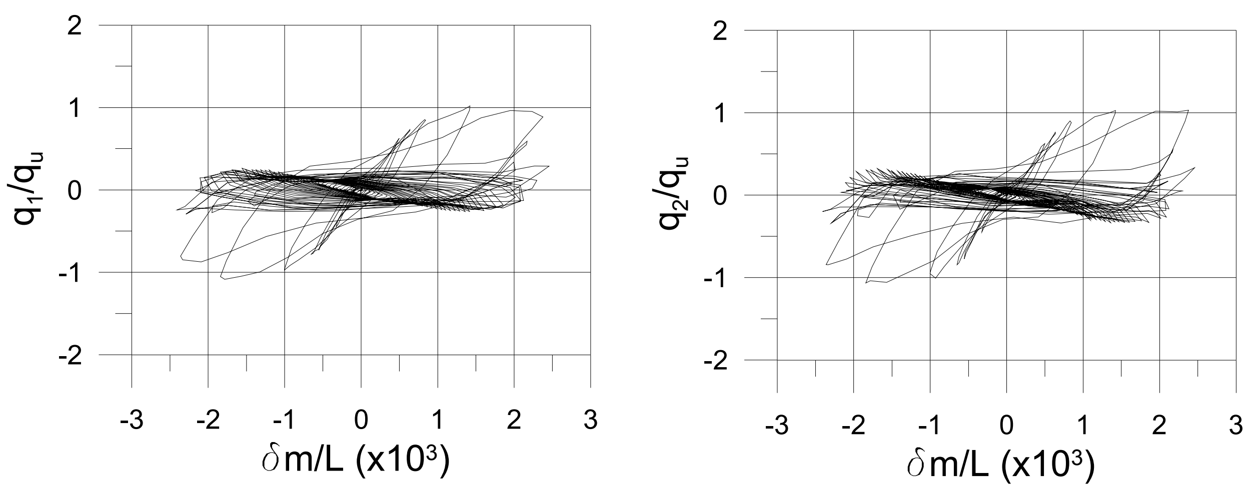

Figure F.6 – DIA6 – Hysteresis obtained from actuator 1 (right) and actuator 2 (left) load cell measurements and displacement at centre

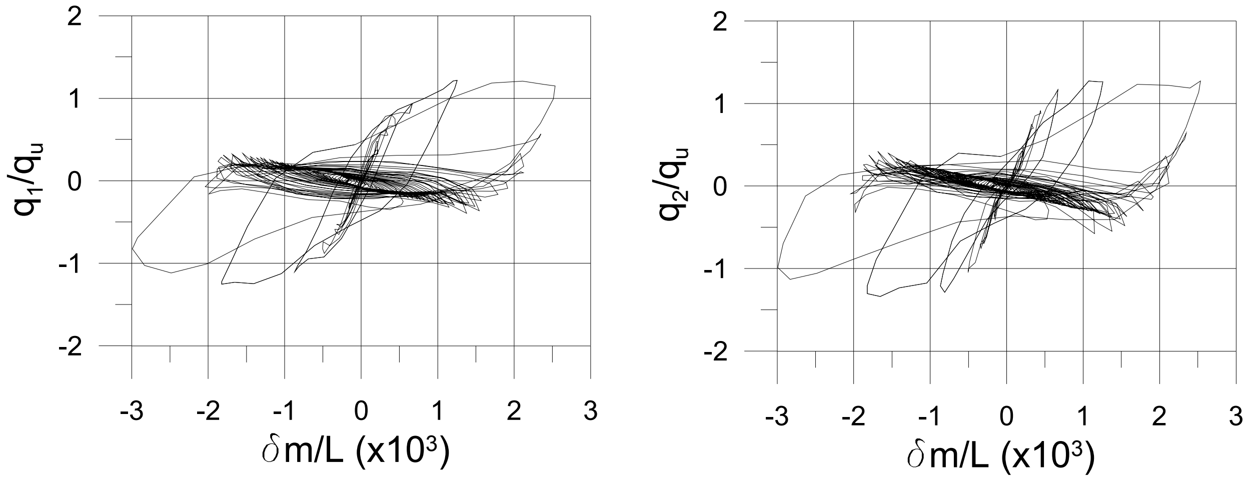

Figure F.7 – DIA7 – Hysteresis obtained from actuator 1 (right) and actuator 2 (left) load cell measurements and displacement at centre

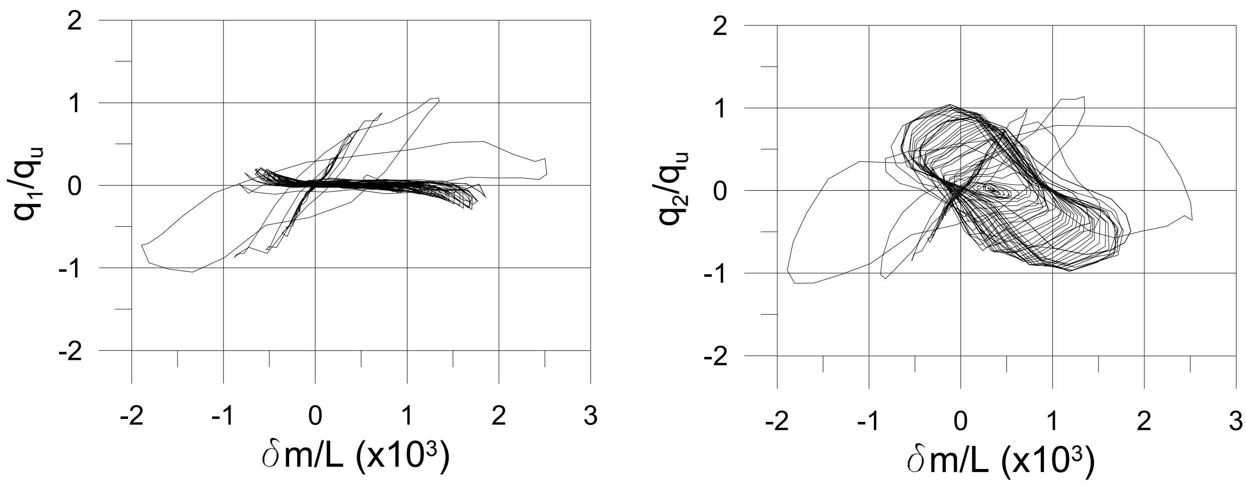

Figure F.8 – DIA8 – Hysteresis obtained from actuator 1 (right) and actuator 2 (left) load cell measurements and displacement at centre

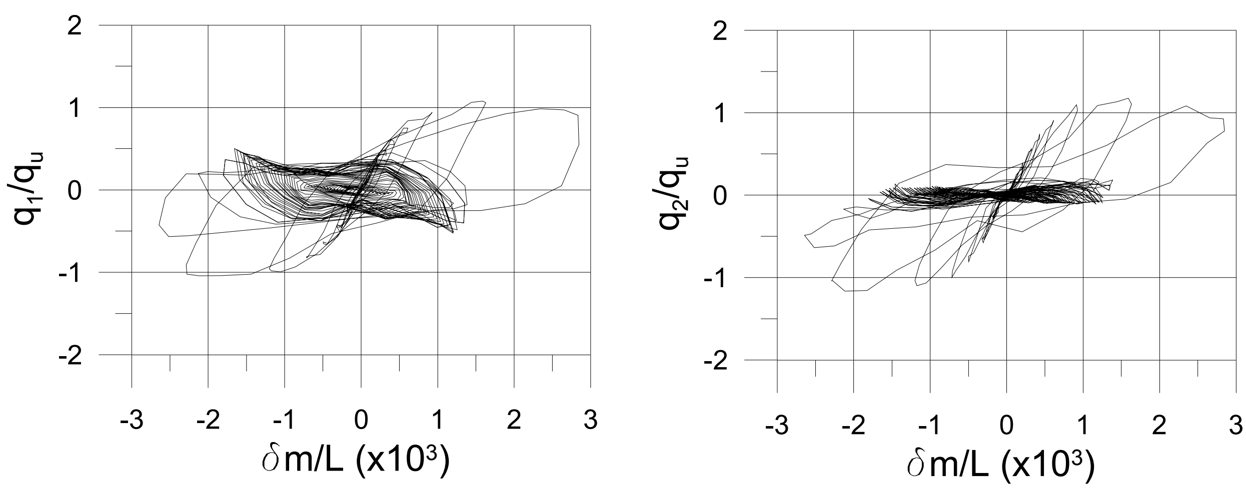

Figure F.9 – DIA9 – Hysteresis obtained from actuator 1 (right) and actuator 2 (left) load cell measurements and displacement at centre

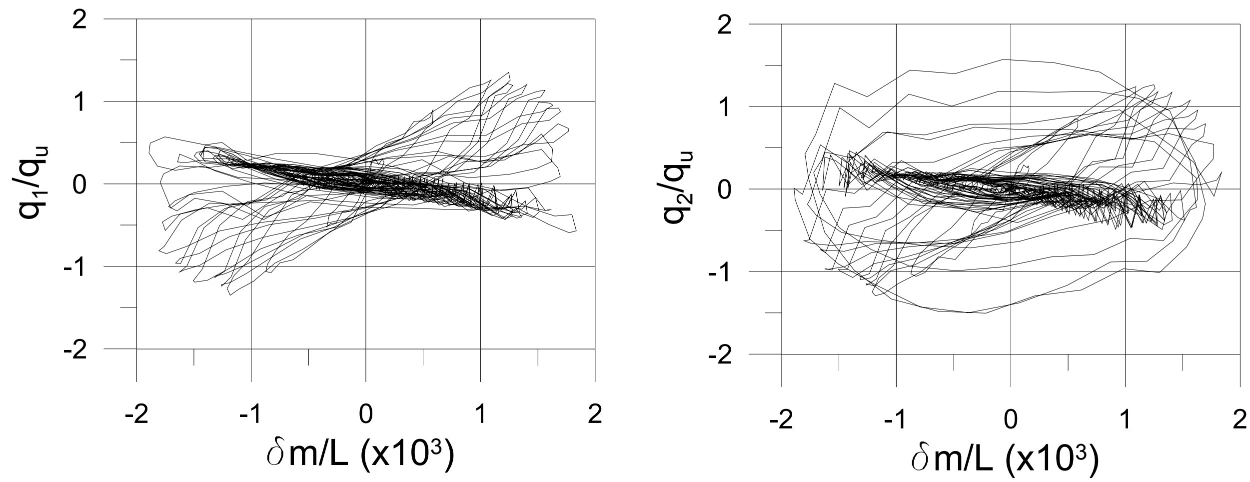

Figure F.10 – DIA10 – Hysteresis obtained from actuator 1 (right) and actuator 2 (left) load cell measurements and displacement at centre

APPENDIX G: PHASE I & II – LOAD-DISPLACEMENT HYSTERESIS FOR REPAIRED DIAPHRAGMS

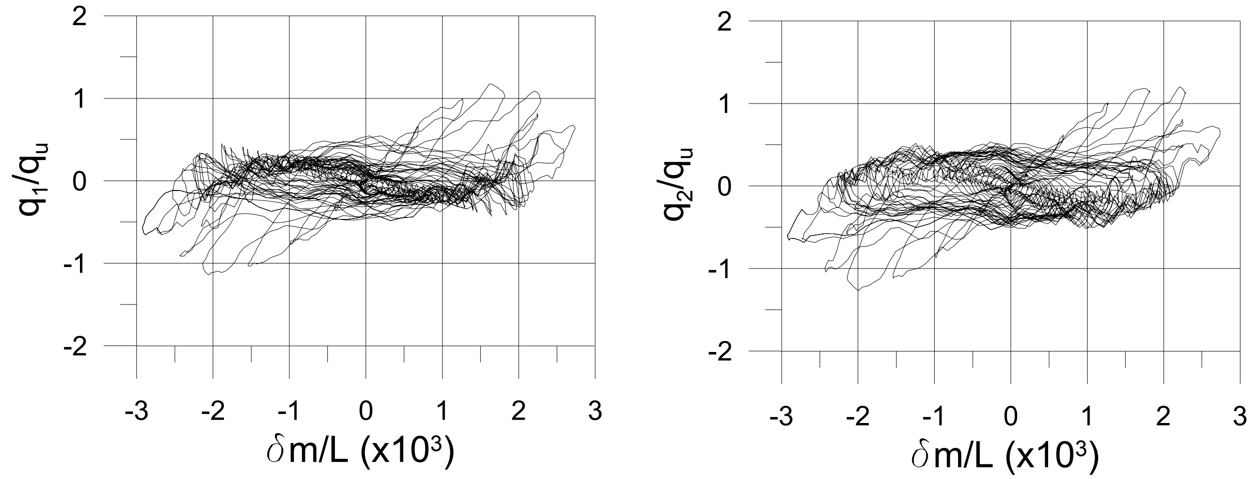

Figure G.1 – DIA1R – Hysteresis obtained from actuator 1 (right) and actuator 2 (left) load cell measurements and displacement at centre

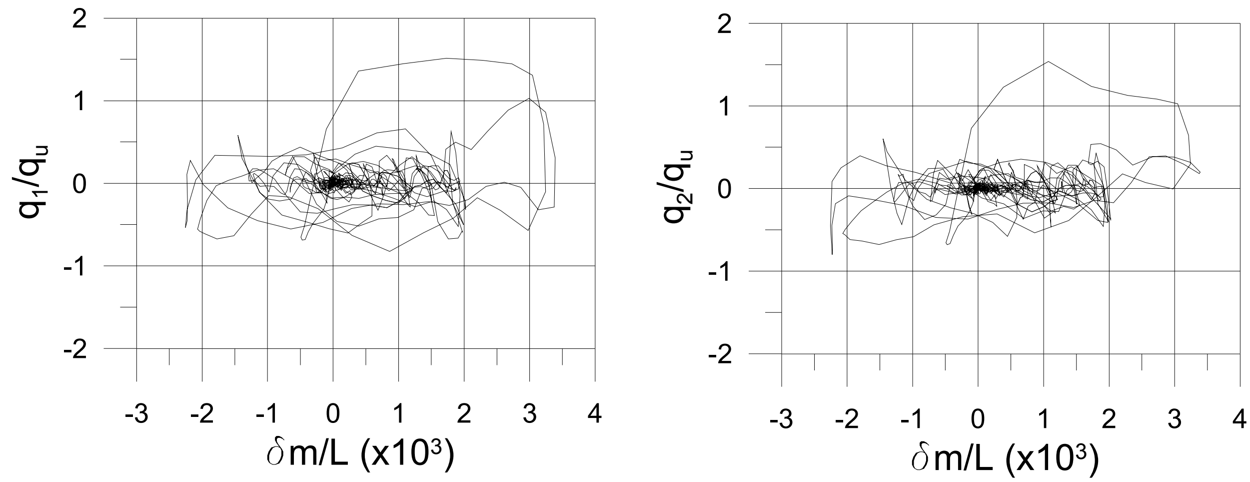

Figure G.2 – DIA3R – Hysteresis obtained from actuator 1 (right) and actuator 2 (left) load cell measurements and displacement at centre

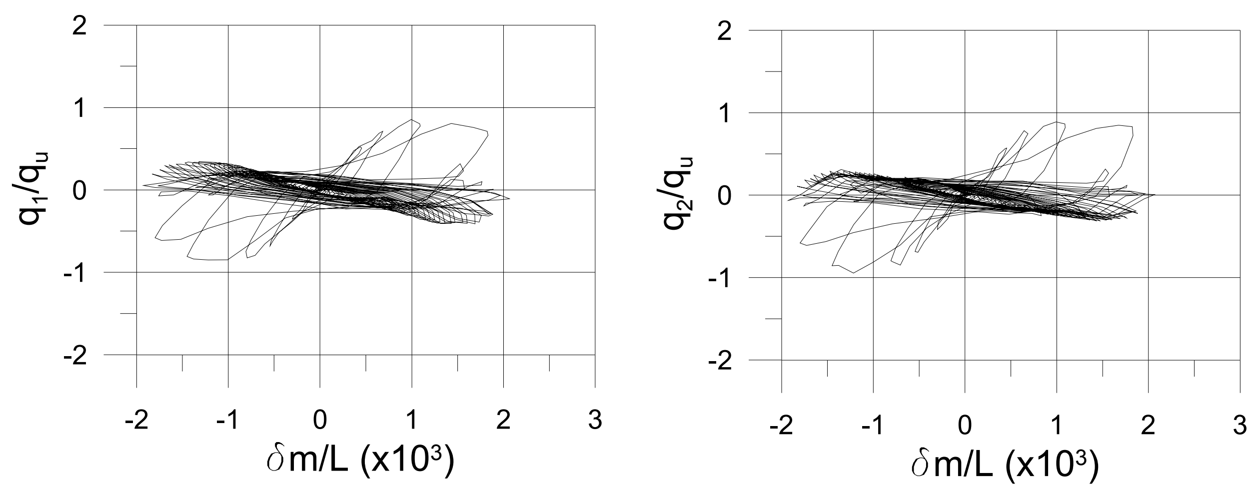

Figure G.3 – DIA4R – Hysteresis obtained from actuator 1 (right) and actuator 2 (left) load cell measurements and displacement at centre

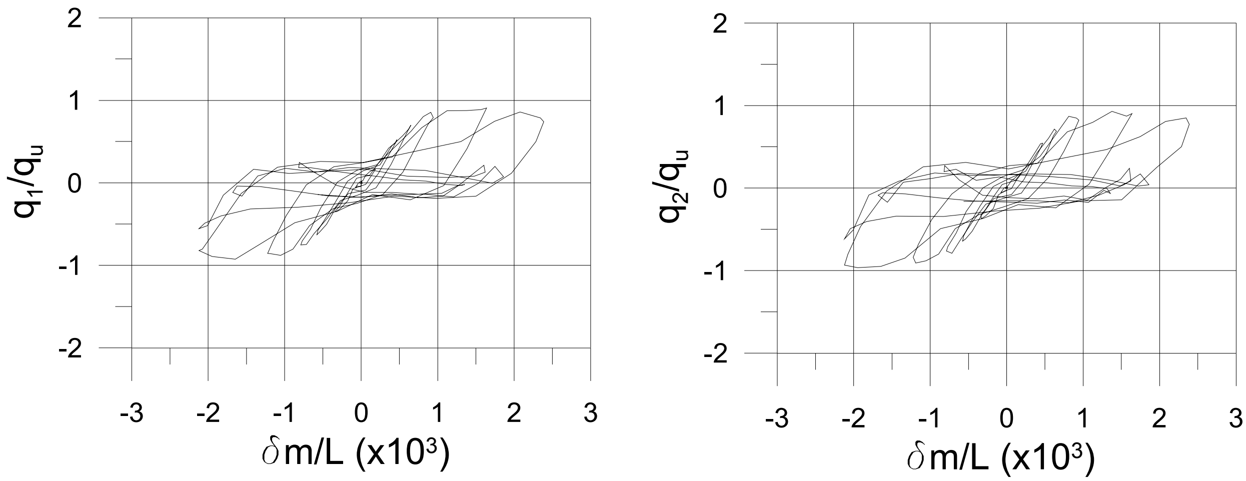

Figure G.4 – DIA5R – Hysteresis obtained from actuator 1 (right) and actuator 2 (left) load cell measurements and displacement at centre

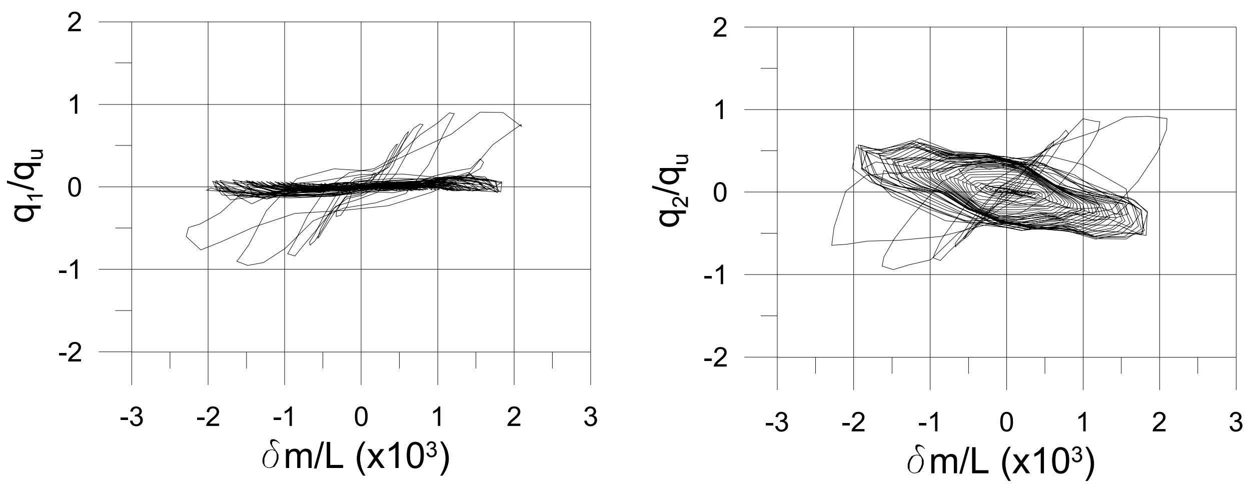

Figure G.5 – DIA6R – Hysteresis obtained from actuator 1 (right) and actuator 2 (left) load cell measurements and displacement at centre

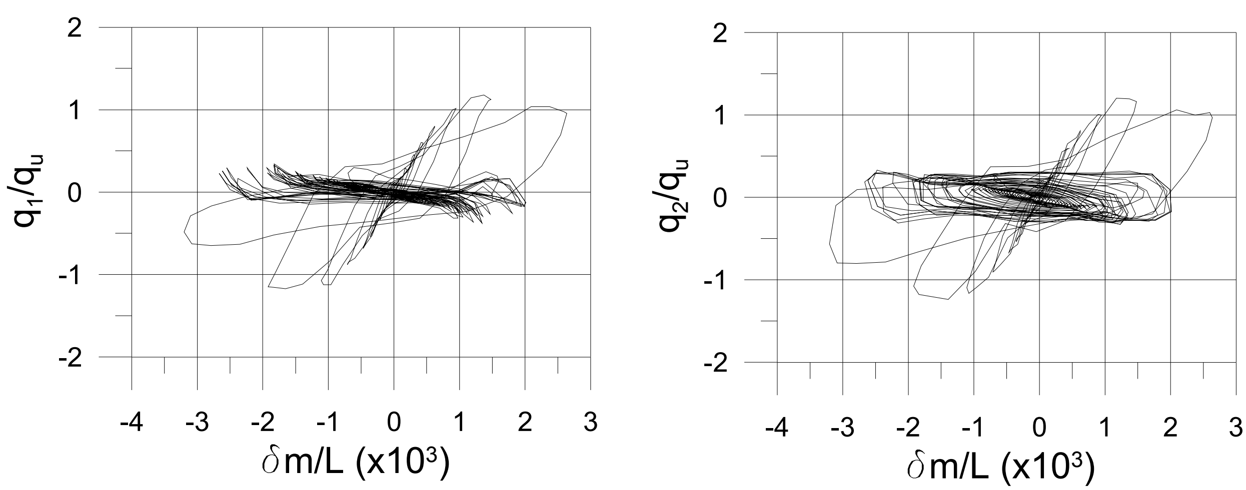

Figure G.6 – DIA7R – Hysteresis obtained from actuator 1 (right) and actuator 2 (left) load cell measurements and displacement at centre

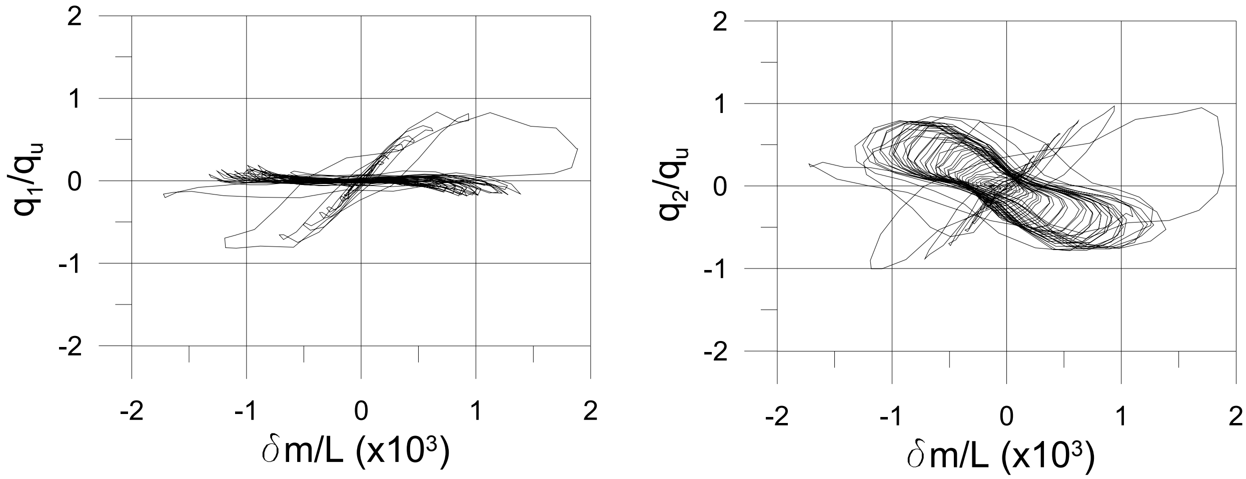

Figure G.7 – DIA8R – Hysteresis obtained from actuator 1 (right) and actuator 2 (left) load cell measurements and displacement at centre

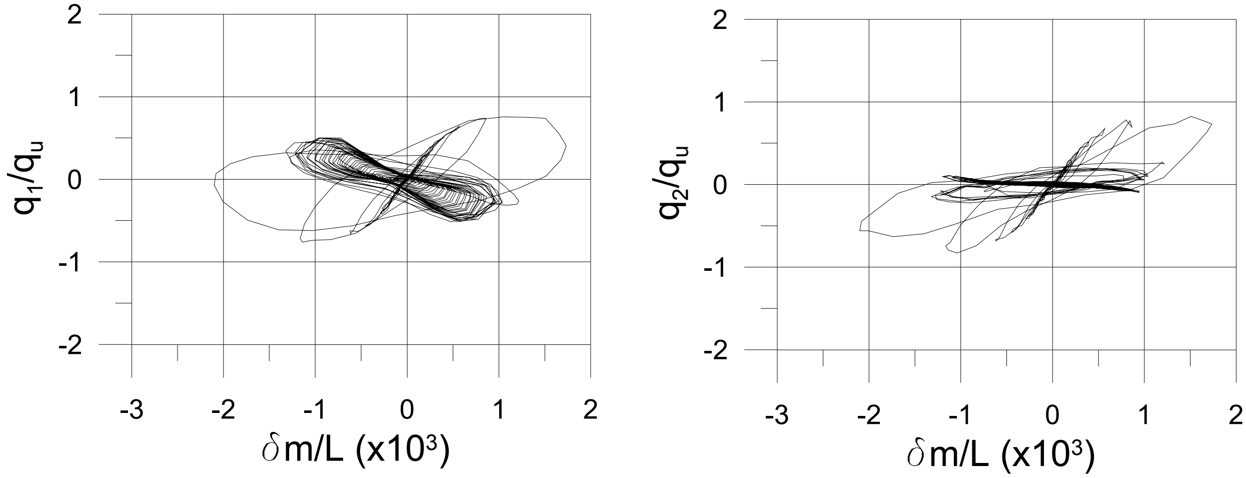

Figure G.8 – DIA9R – Hysteresis obtained from actuator 1 (right) and actuator 2 (left) load cell measurements and displacement at centre

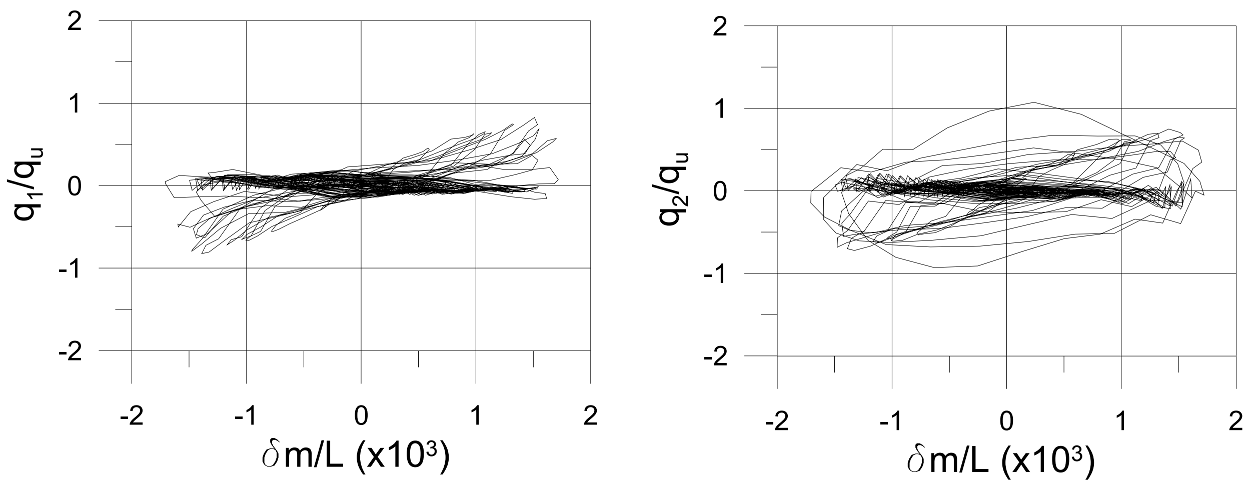

Figure G.9 – DIA10R – Hysteresis obtained from actuator 1 (right) and actuator 2 (left) load cell measurements and displacement at centre

APPENDIX H: PHASE I & II – SHEAR FORCE PROFILES AND DEFORMED SHAPES FOR NEW DIAPHRAGMS

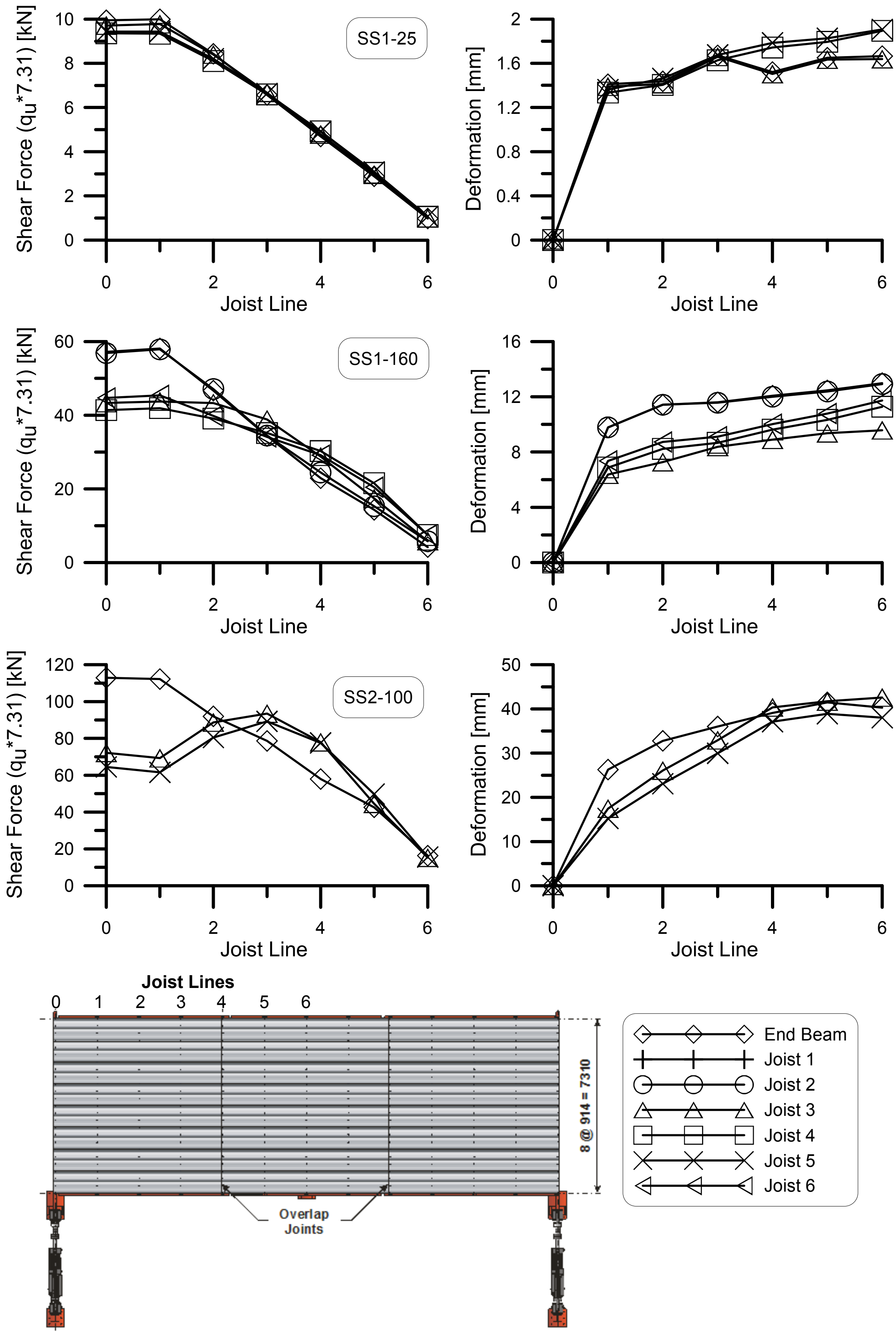

Figure H.1 – DIA1 – Shear force profile and deformation under SS1 and SS2

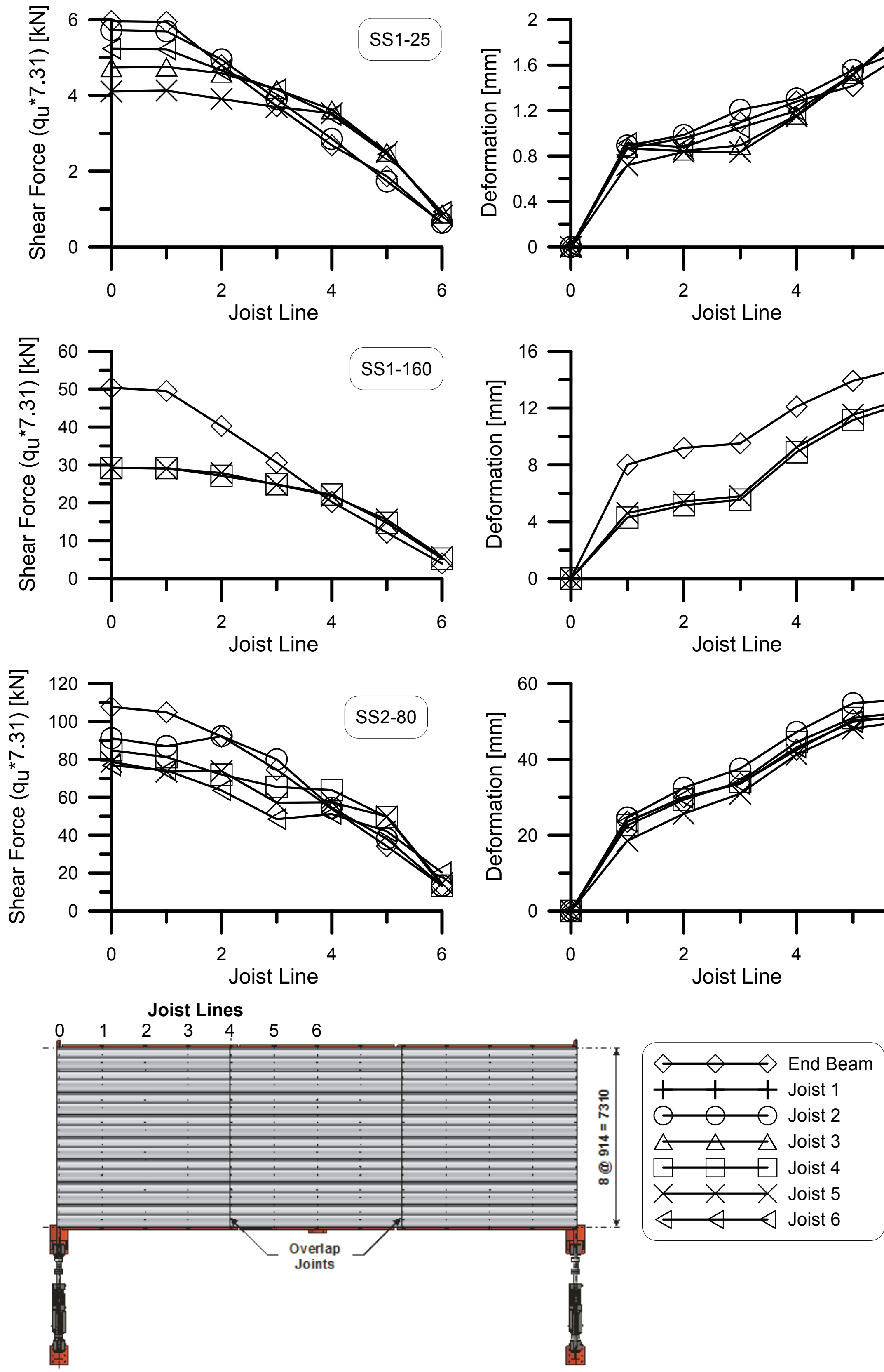

Figure H.2 – DIA2 – Shear force profile and deformation under SS1 and SS2

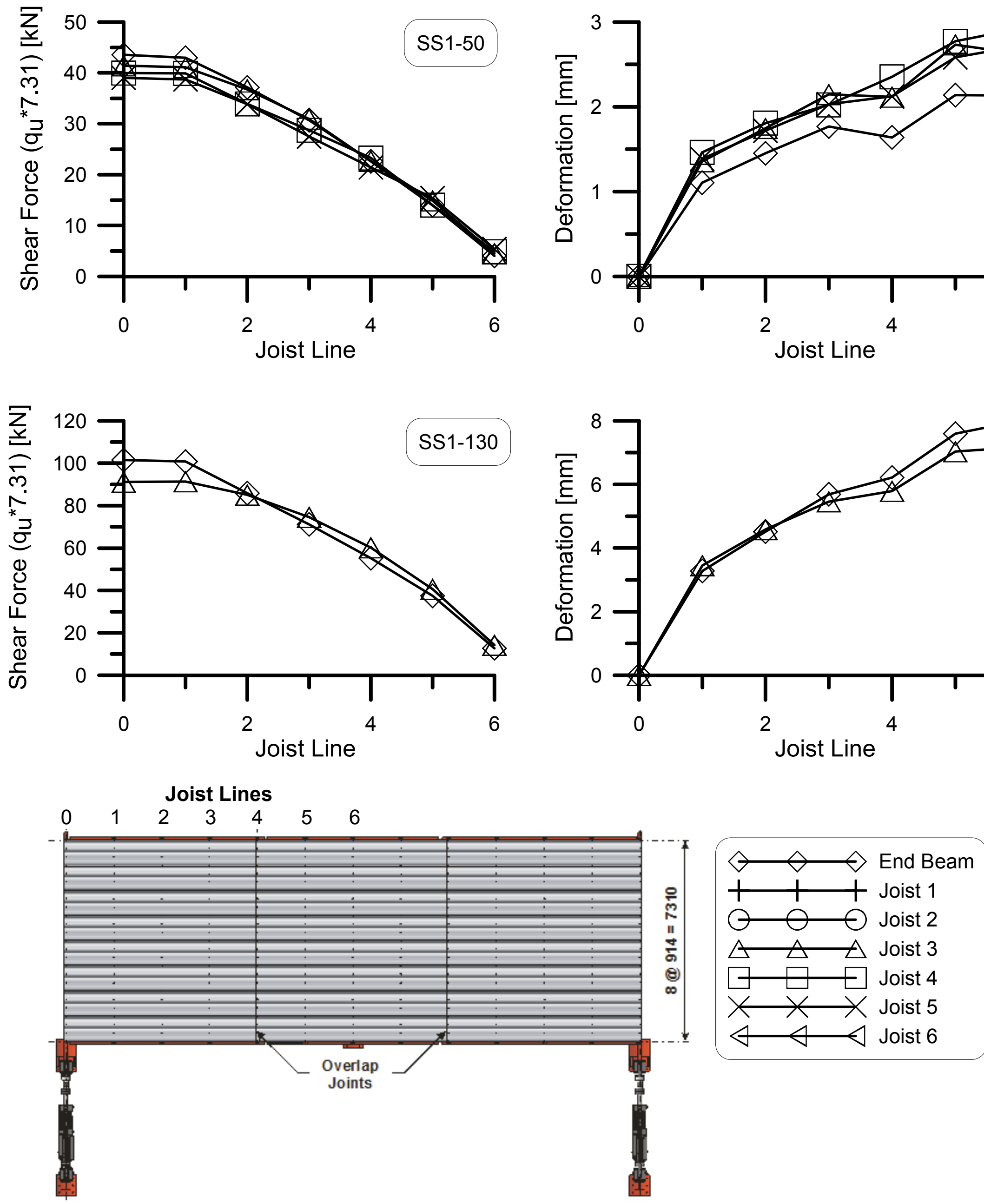

Figure H.3 – DIA3G – Shear force profile and deformation under SS1

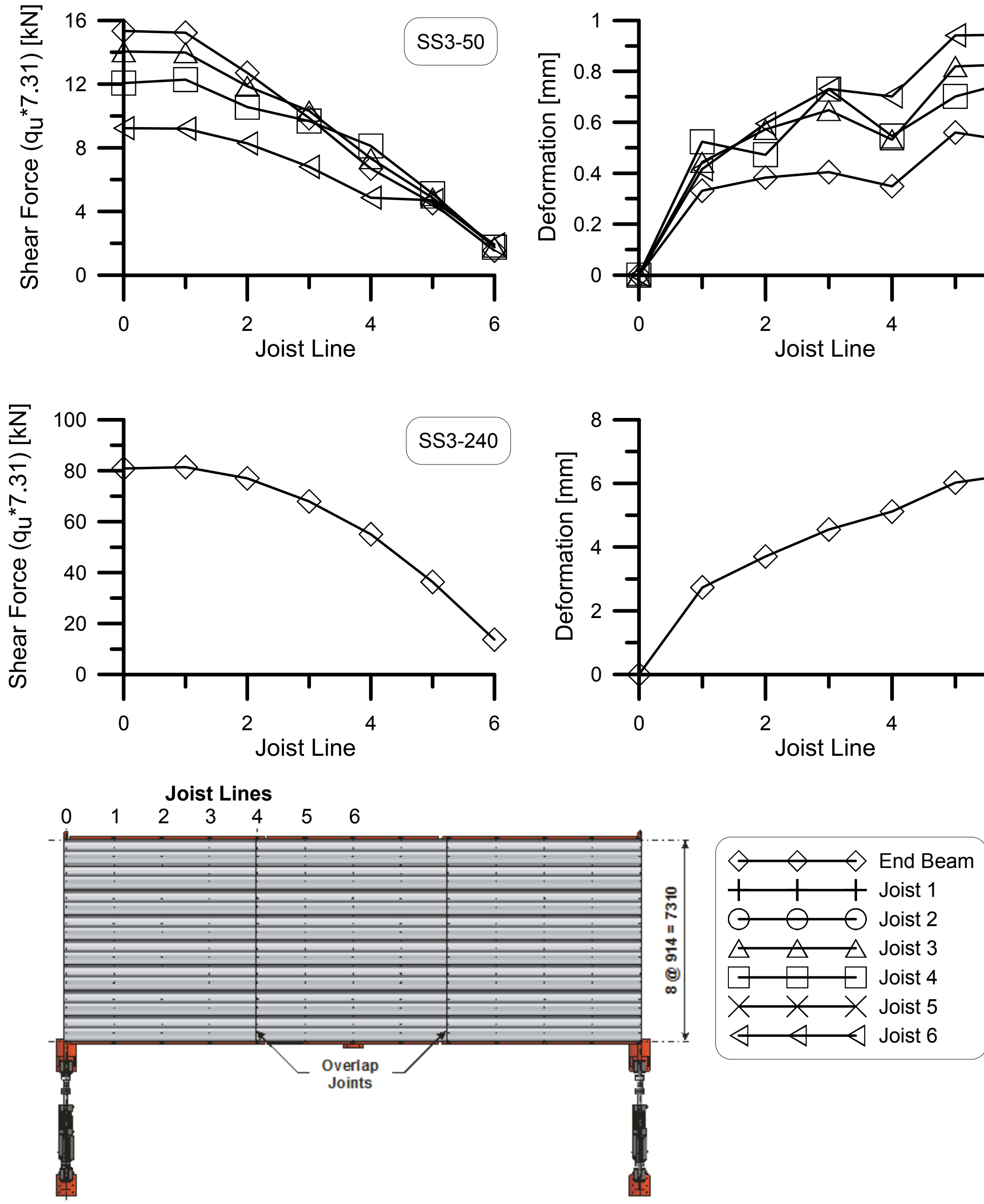

Figure H.4 – DIA3G – Shear force profile and deformation under SS3

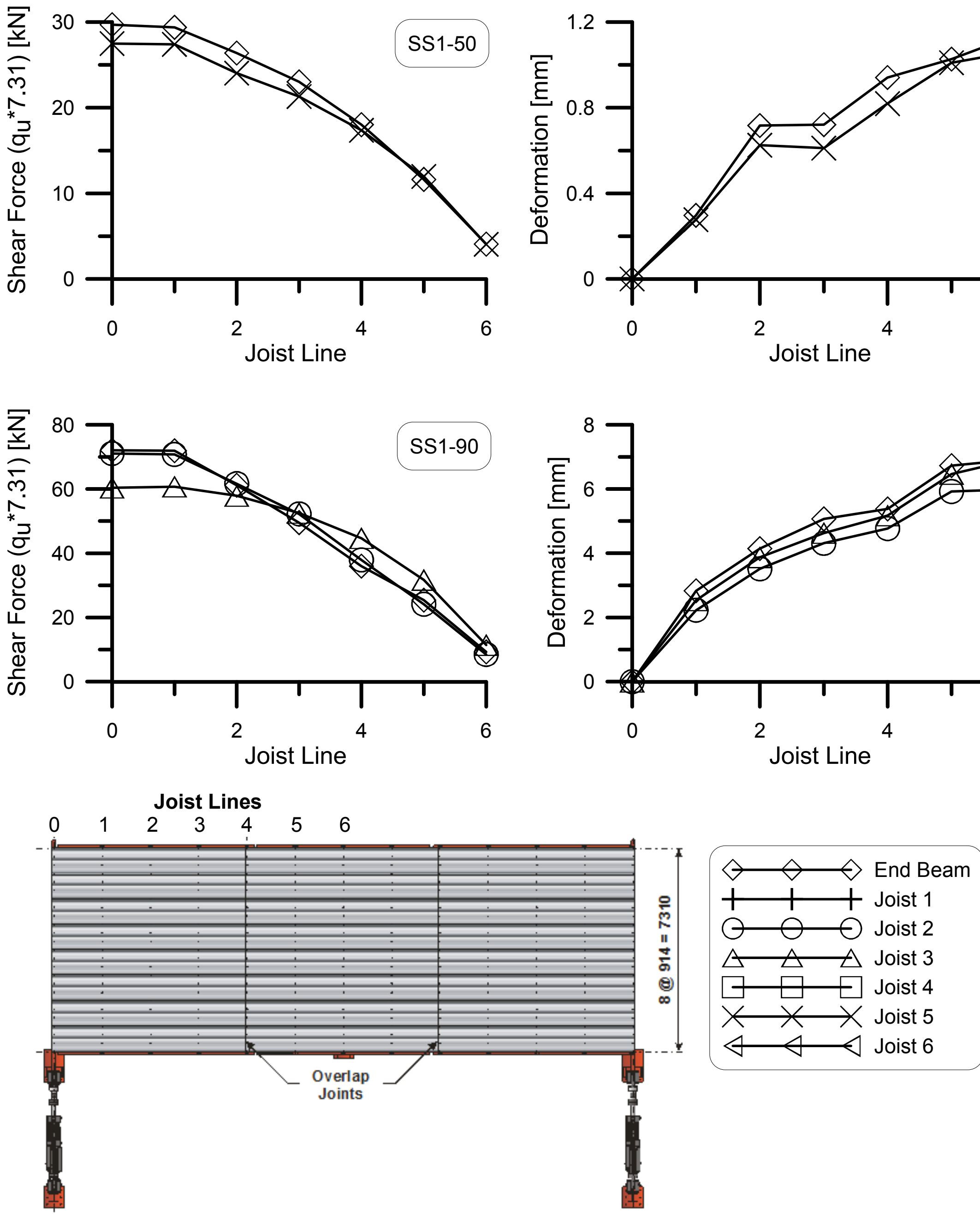

Figure H.5 – DIA3 – Shear force profile and deformation under SS1

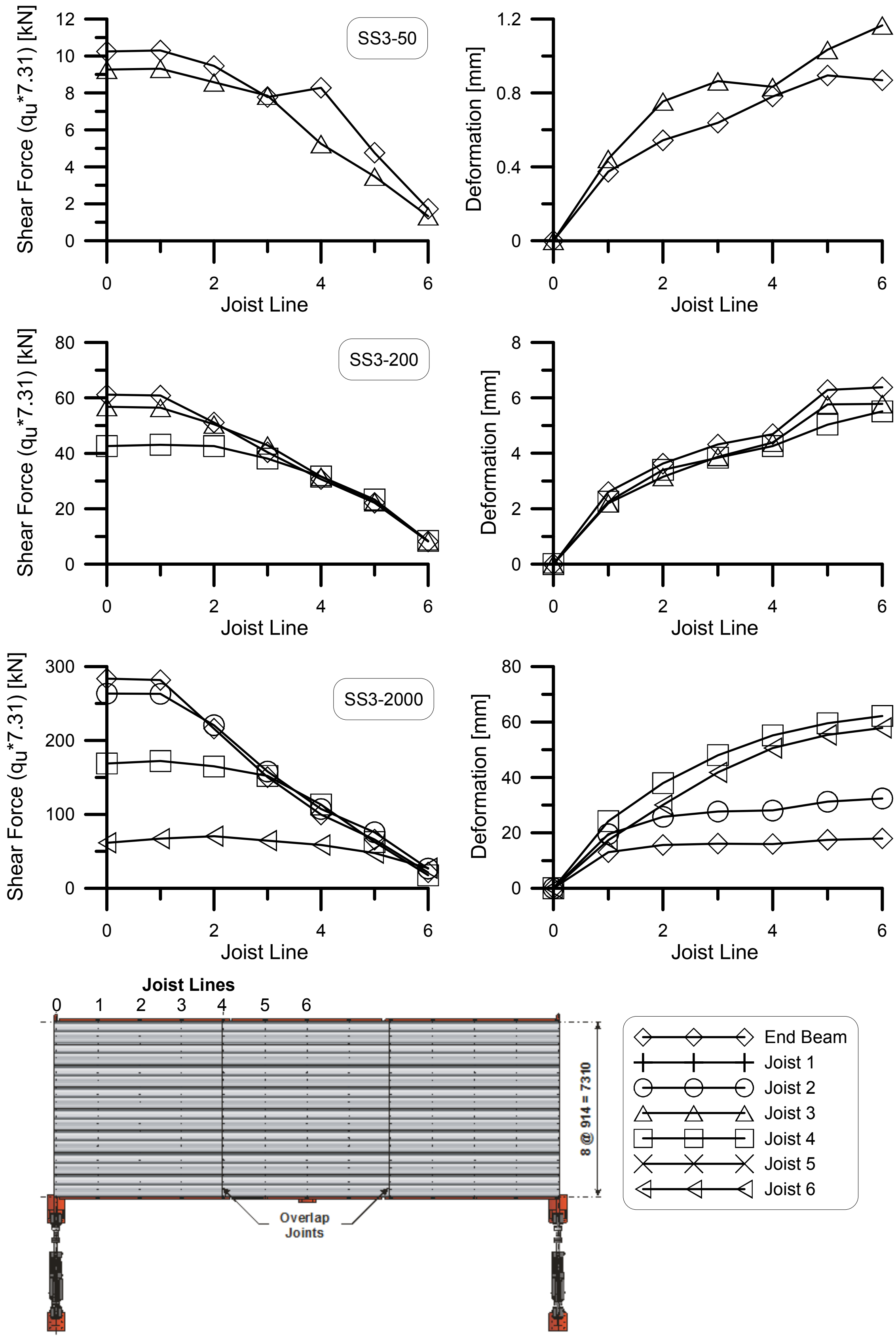

Figure H.6 – DIA3 – Shear force profile and deformation under SS2 and SS3

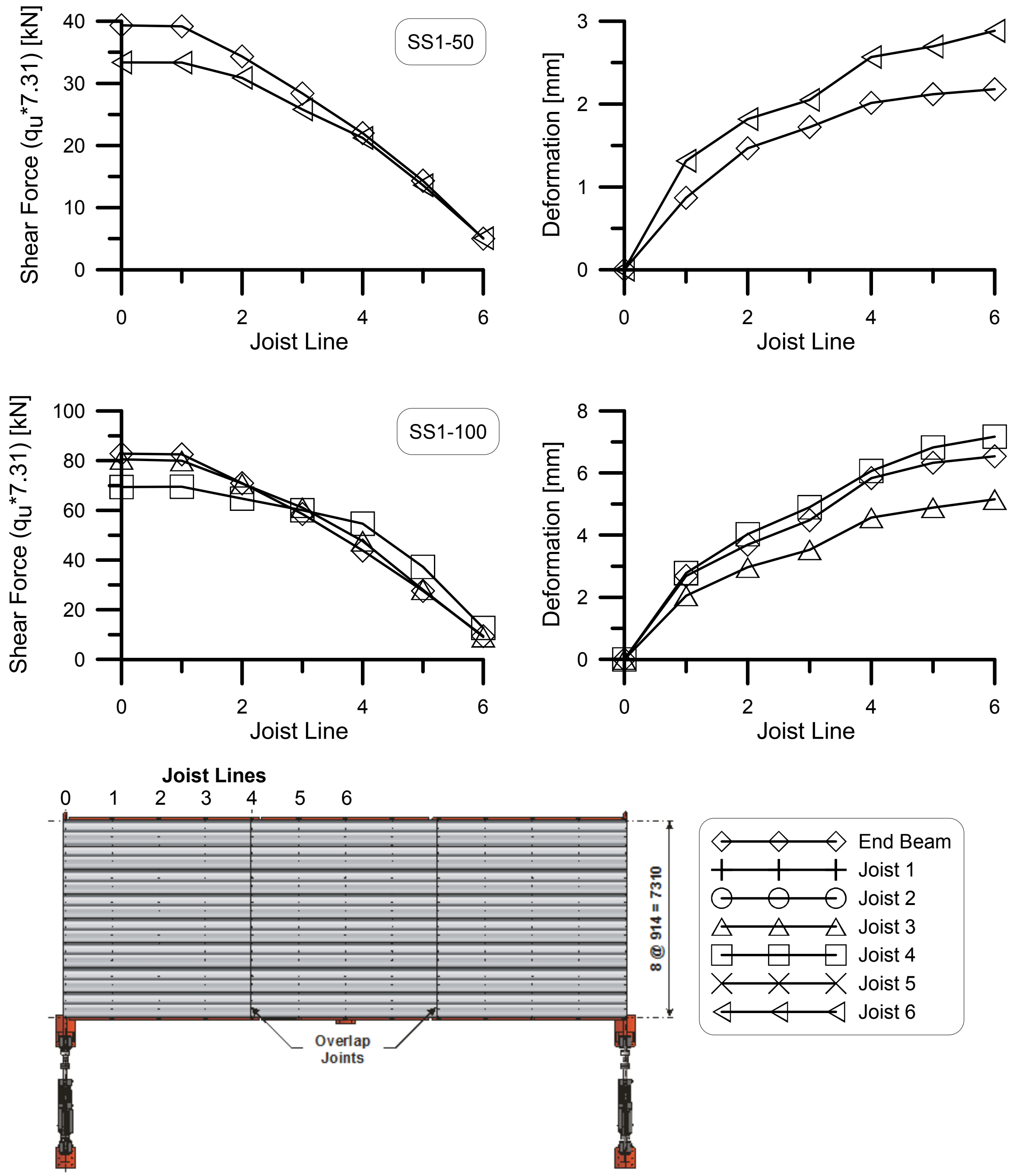

Figure H.7 – DIA4 – Shear force profile and deformation under SS1

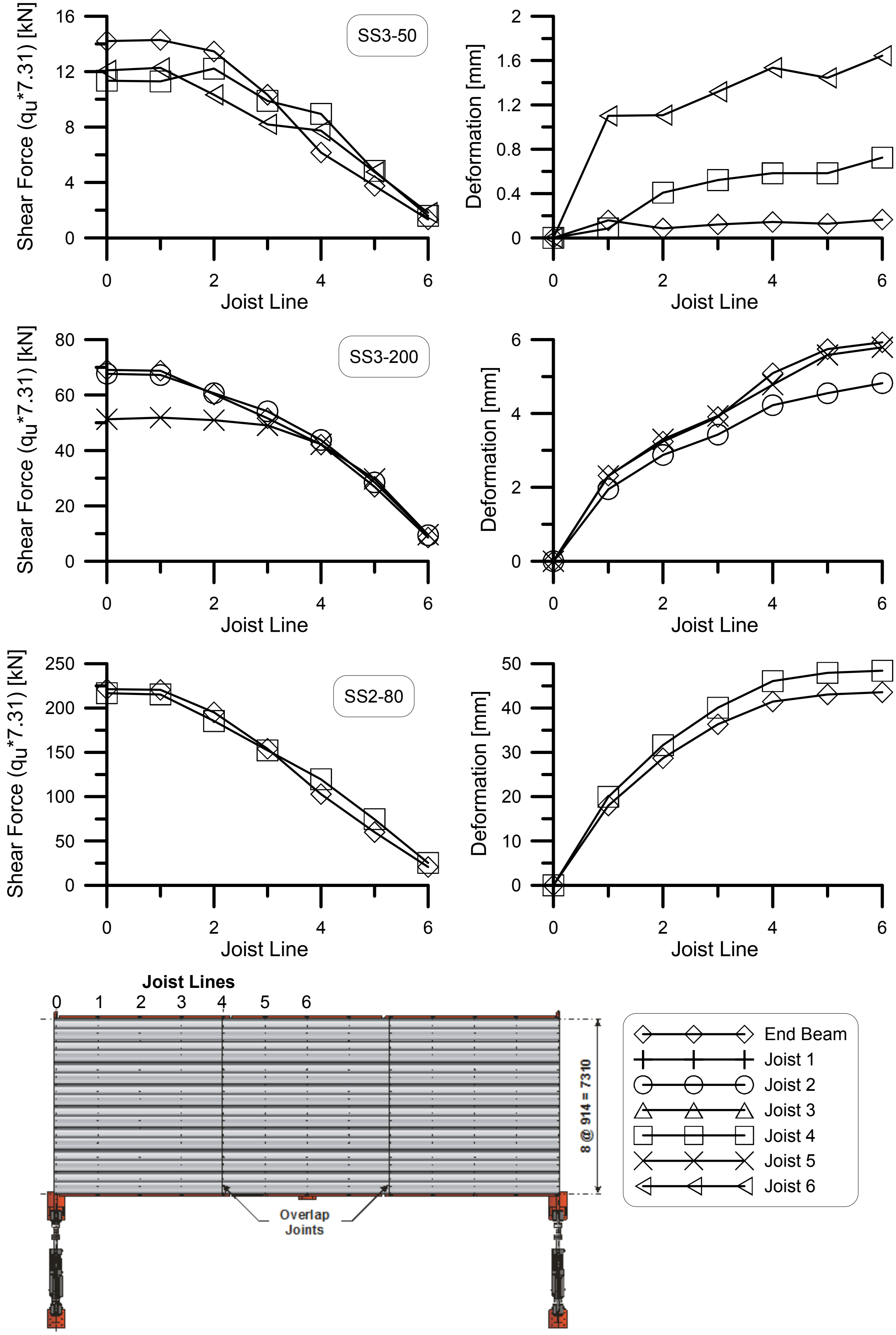

Figure H.8 – DIA4 – Shear force profile and deformation under SS2 and SS3

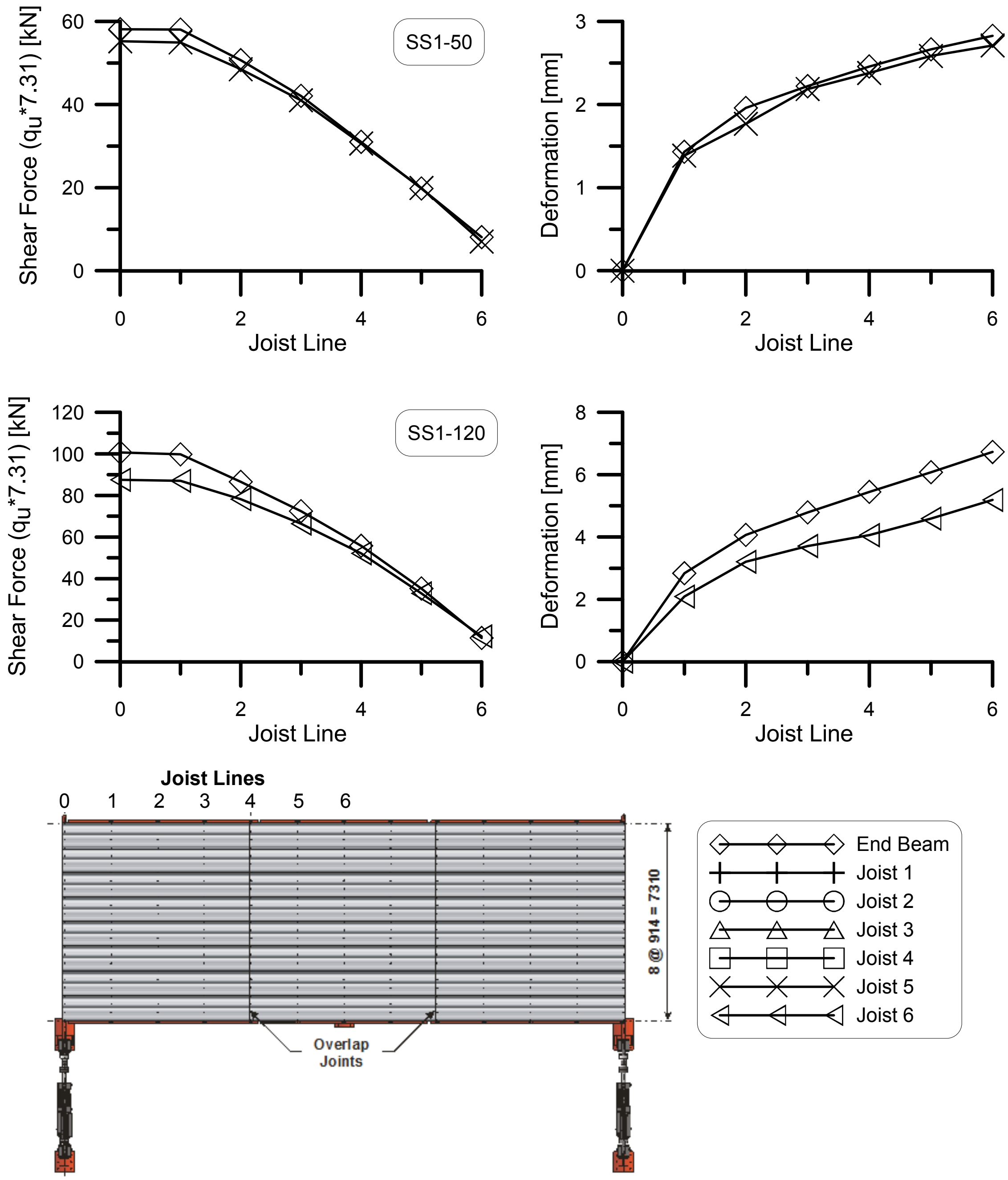

Figure H.9 – DIA5 – Shear force profile and deformation under SS1

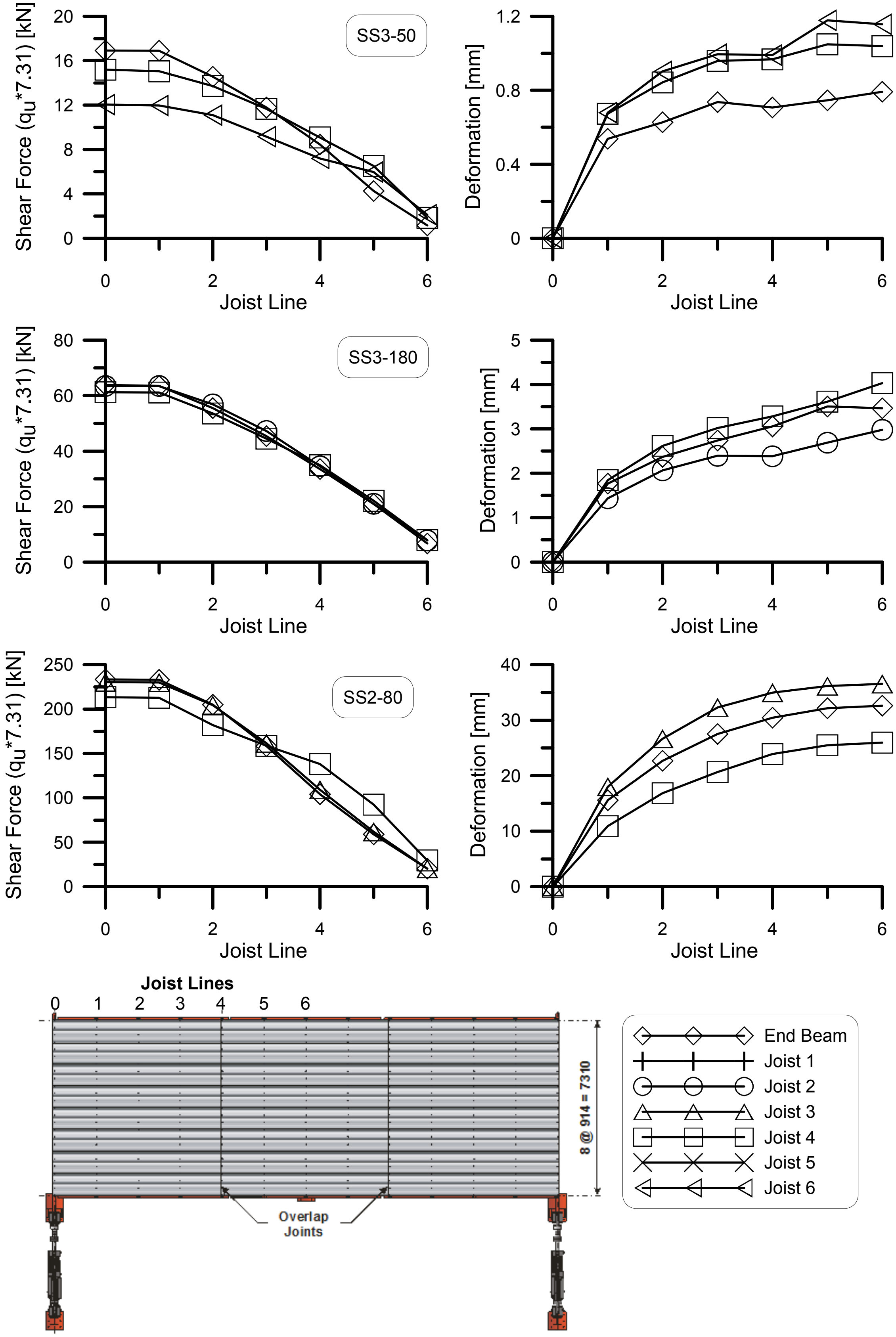

Figure H.10 – DIA5 – Shear force profile and deformation under SS2 and SS3

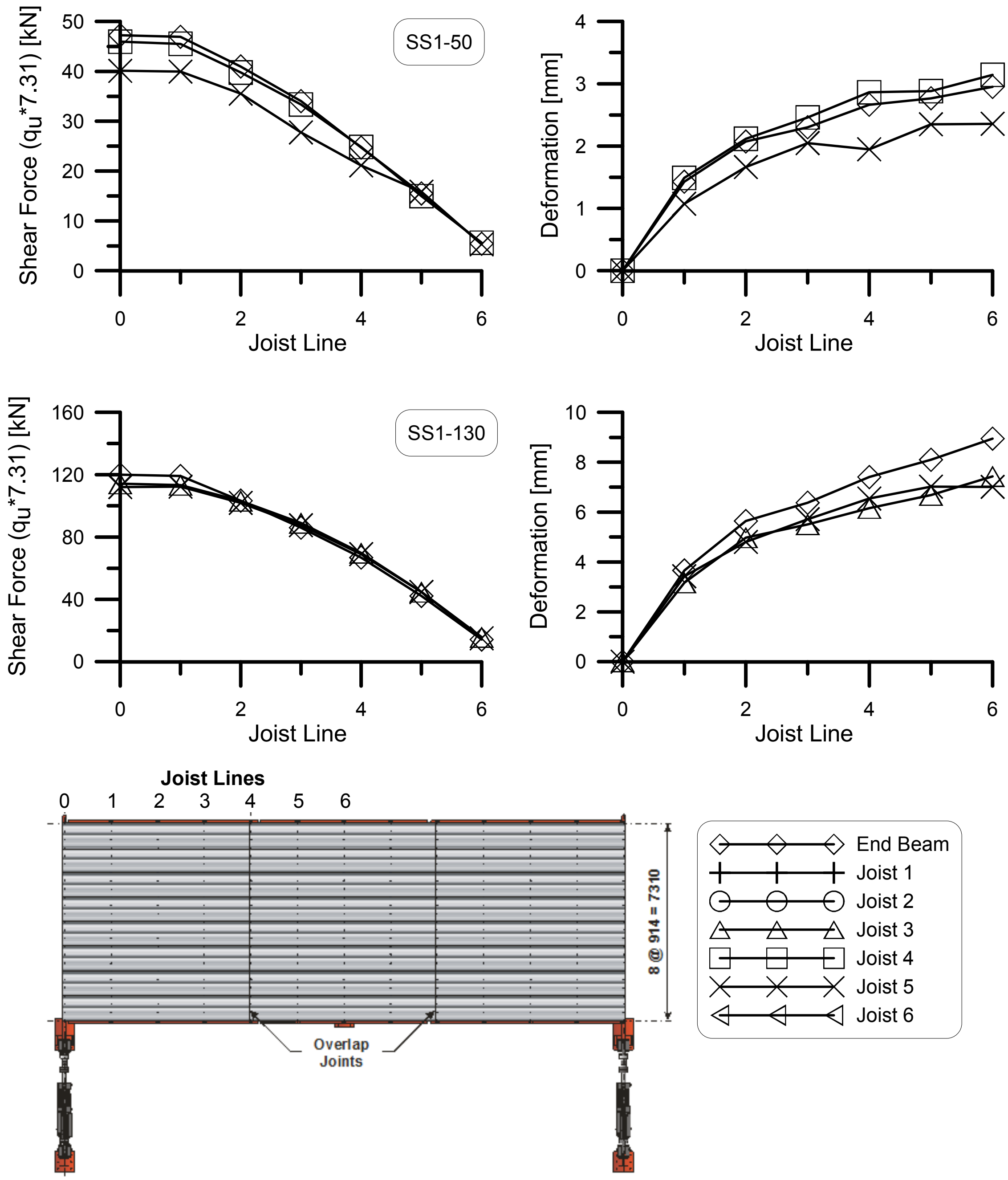

Figure H.11 – DIA6 – Shear force profile and deformation under SS1

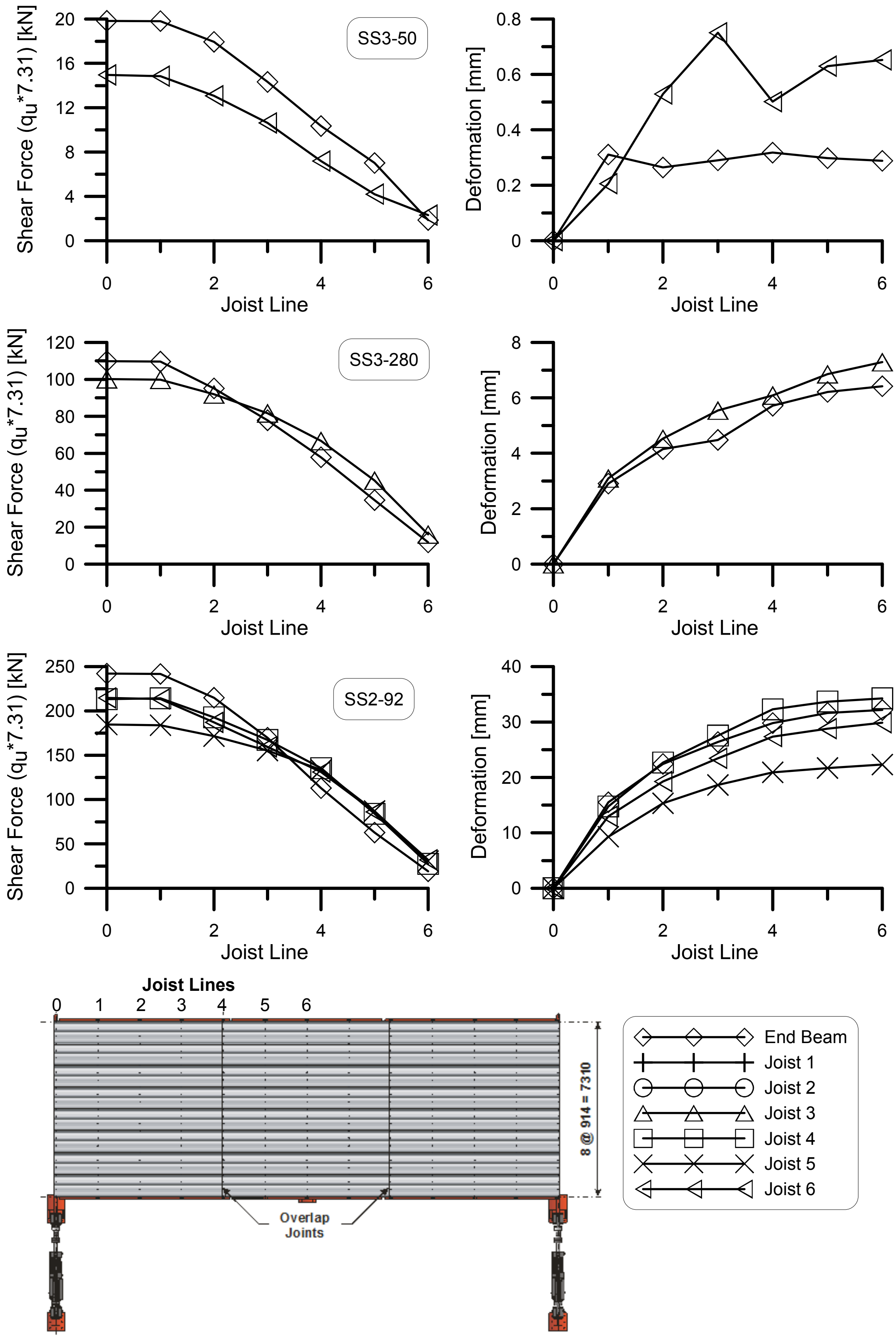

Figure H.12 – DIA6 – Shear force profile and deformation under SS2 and SS3

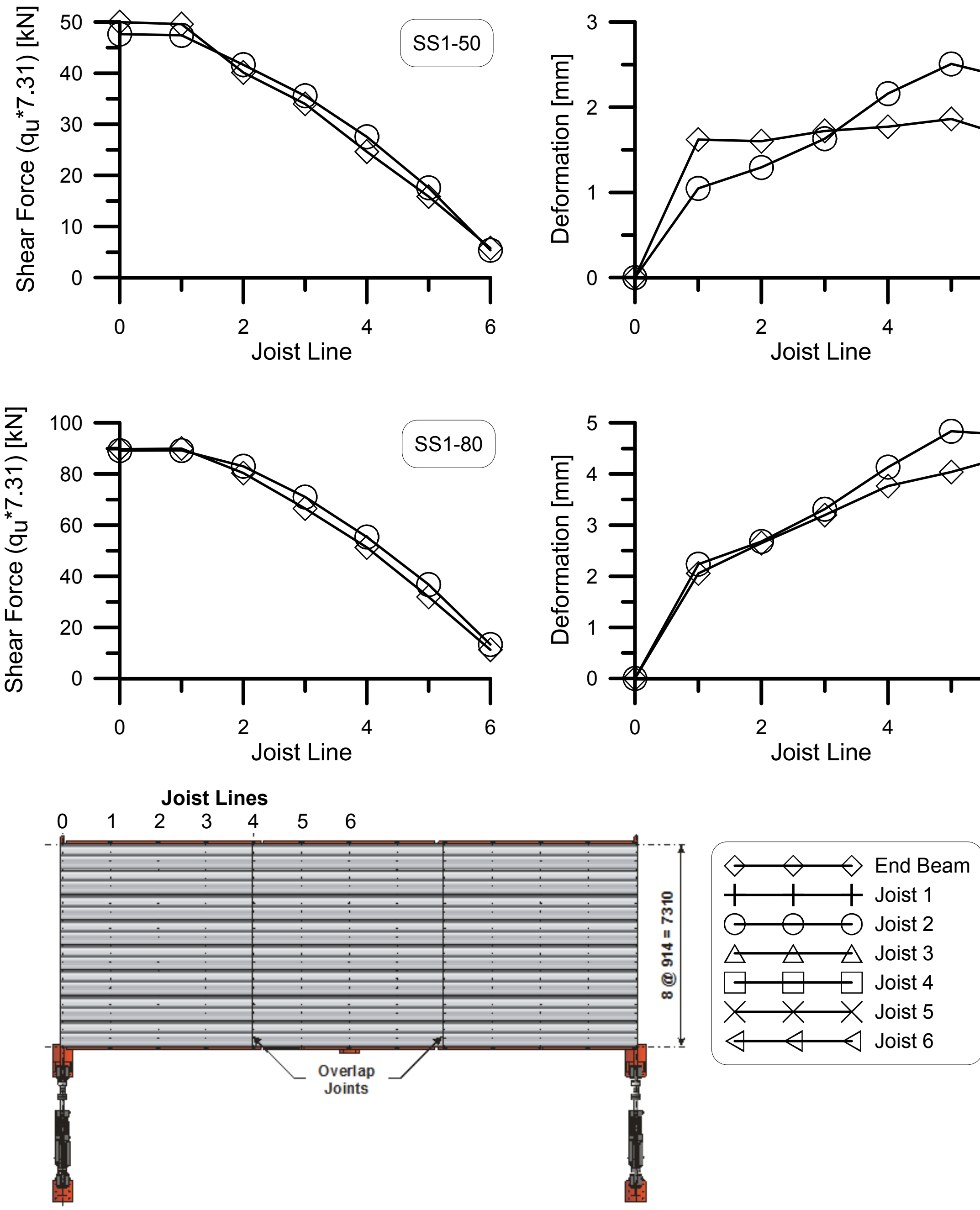

Figure H.13 – DIA7 – Shear force profile and deformation under SS1

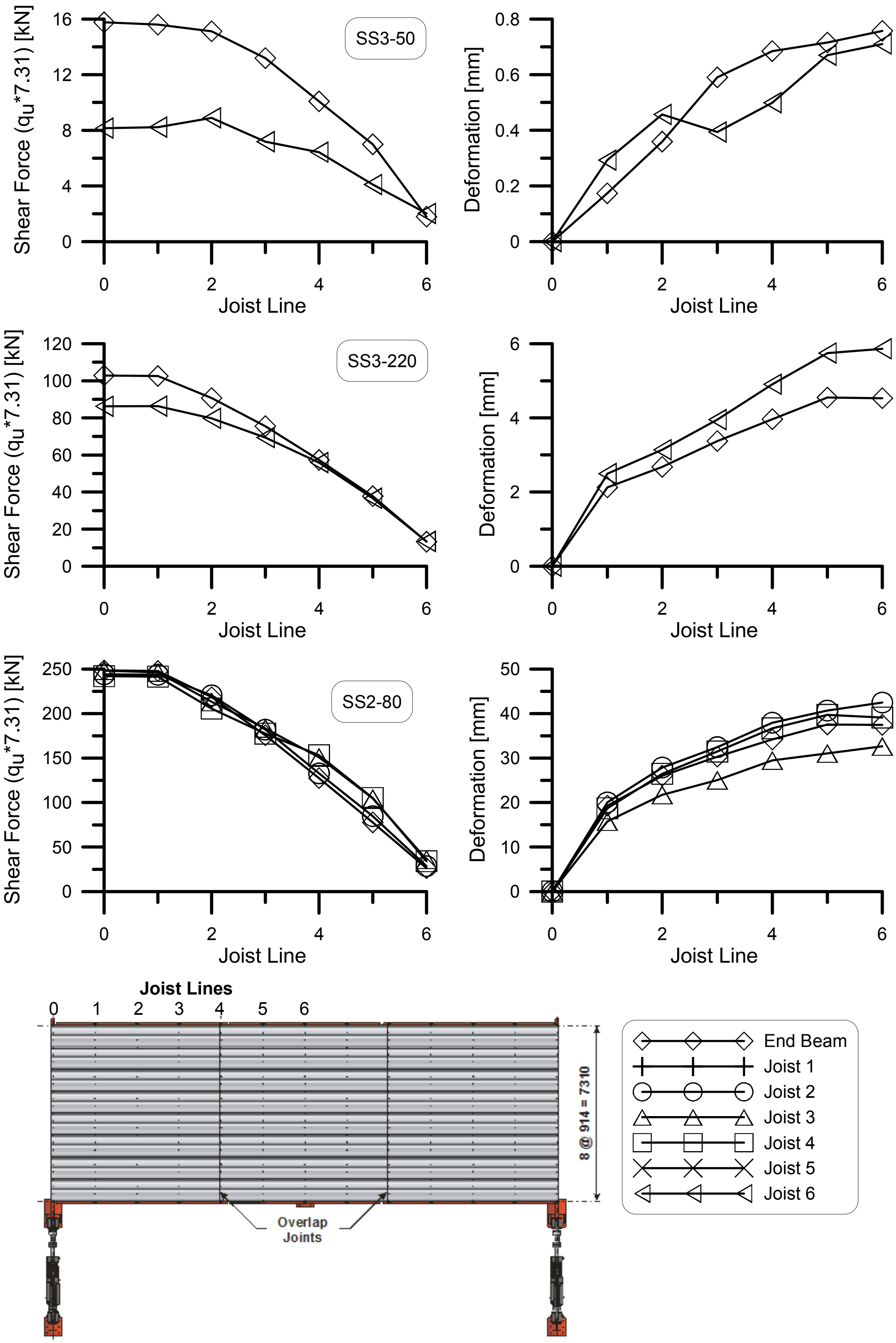

Figure H.14 – DIA7 – Shear force profile and deformation under SS2 and SS3

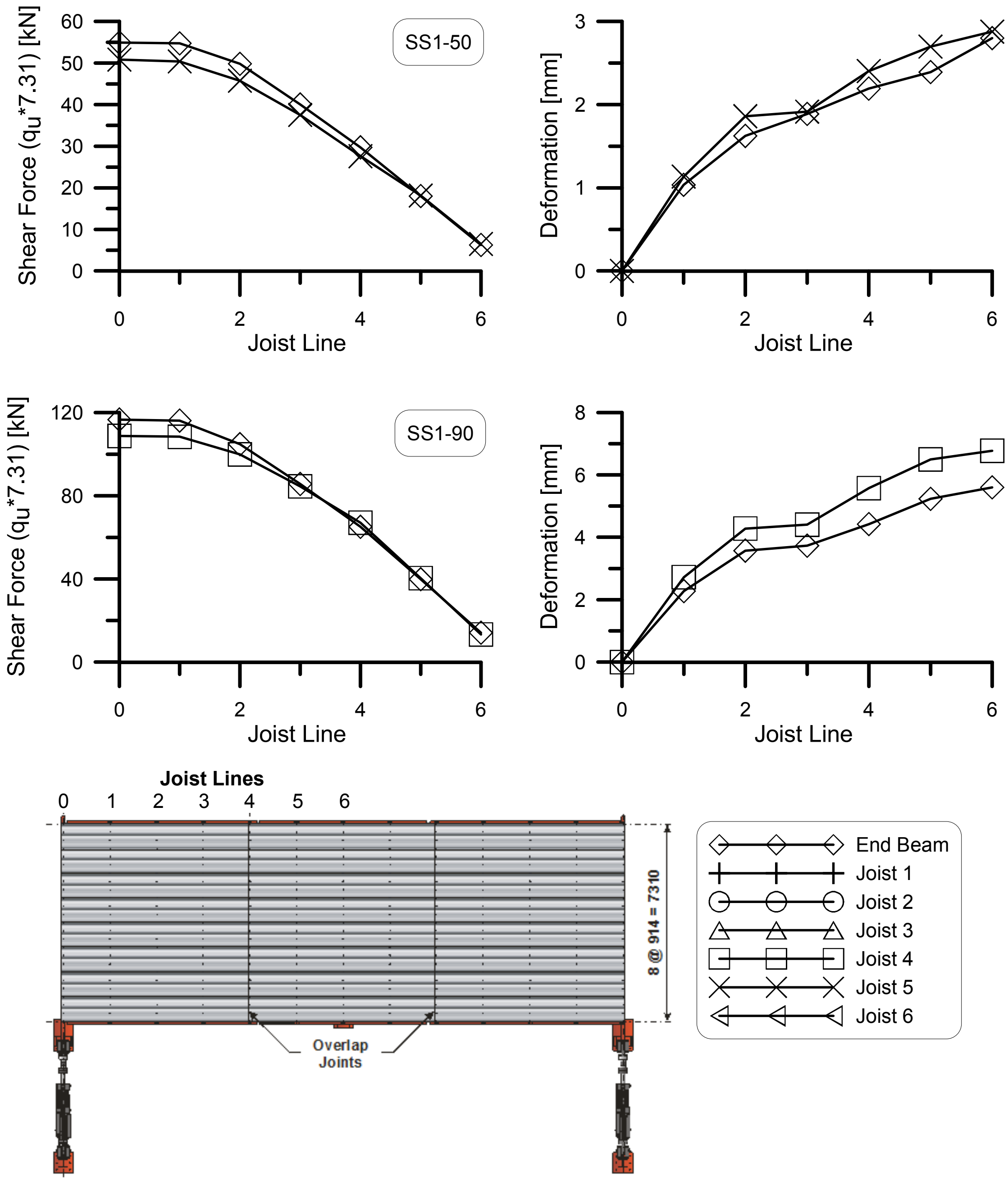

Figure H.15 – DIA8 – Shear force profile and deformation under SS1

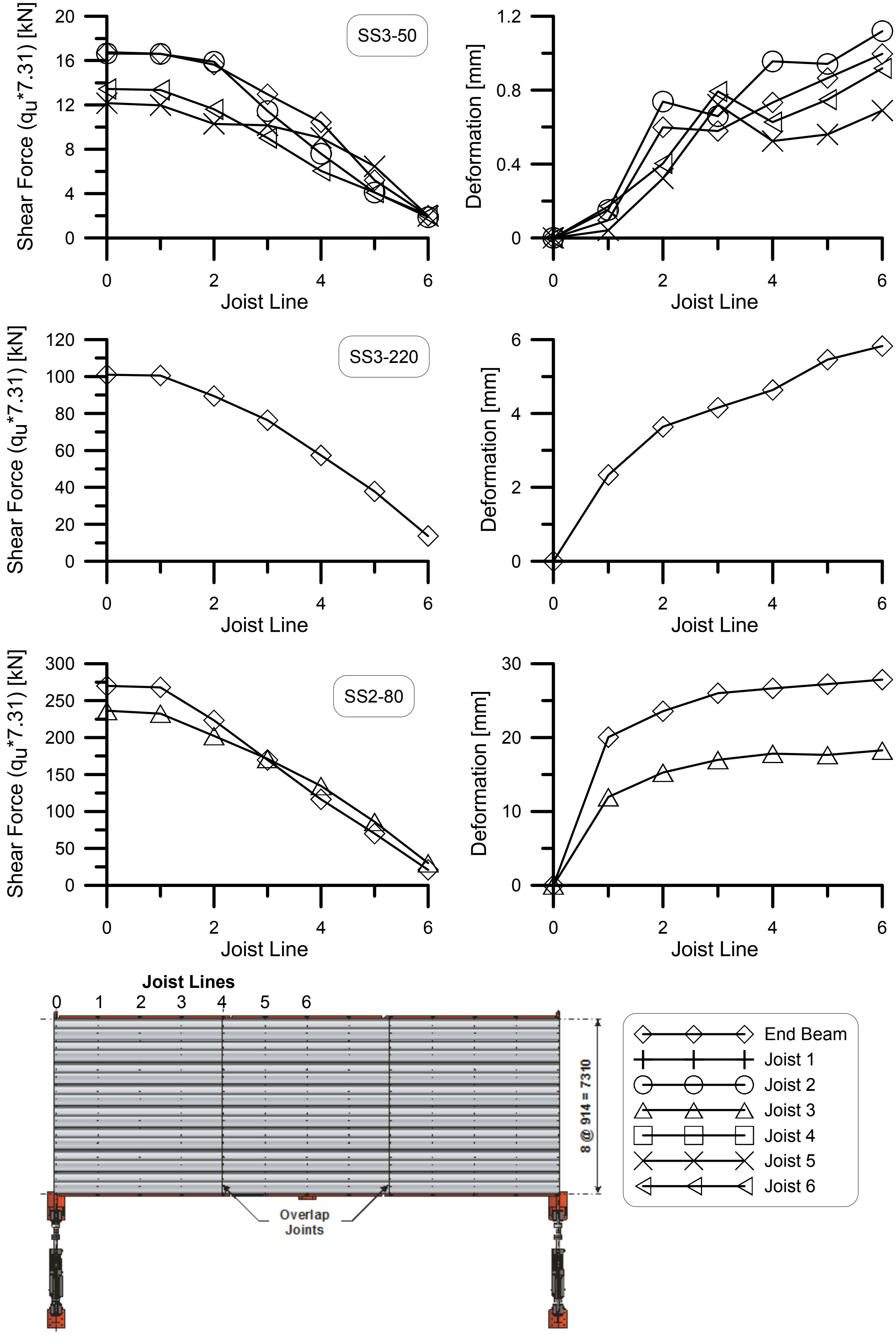

Figure H.16 – DIA8 – Shear force profile and deformation under SS2 and SS3

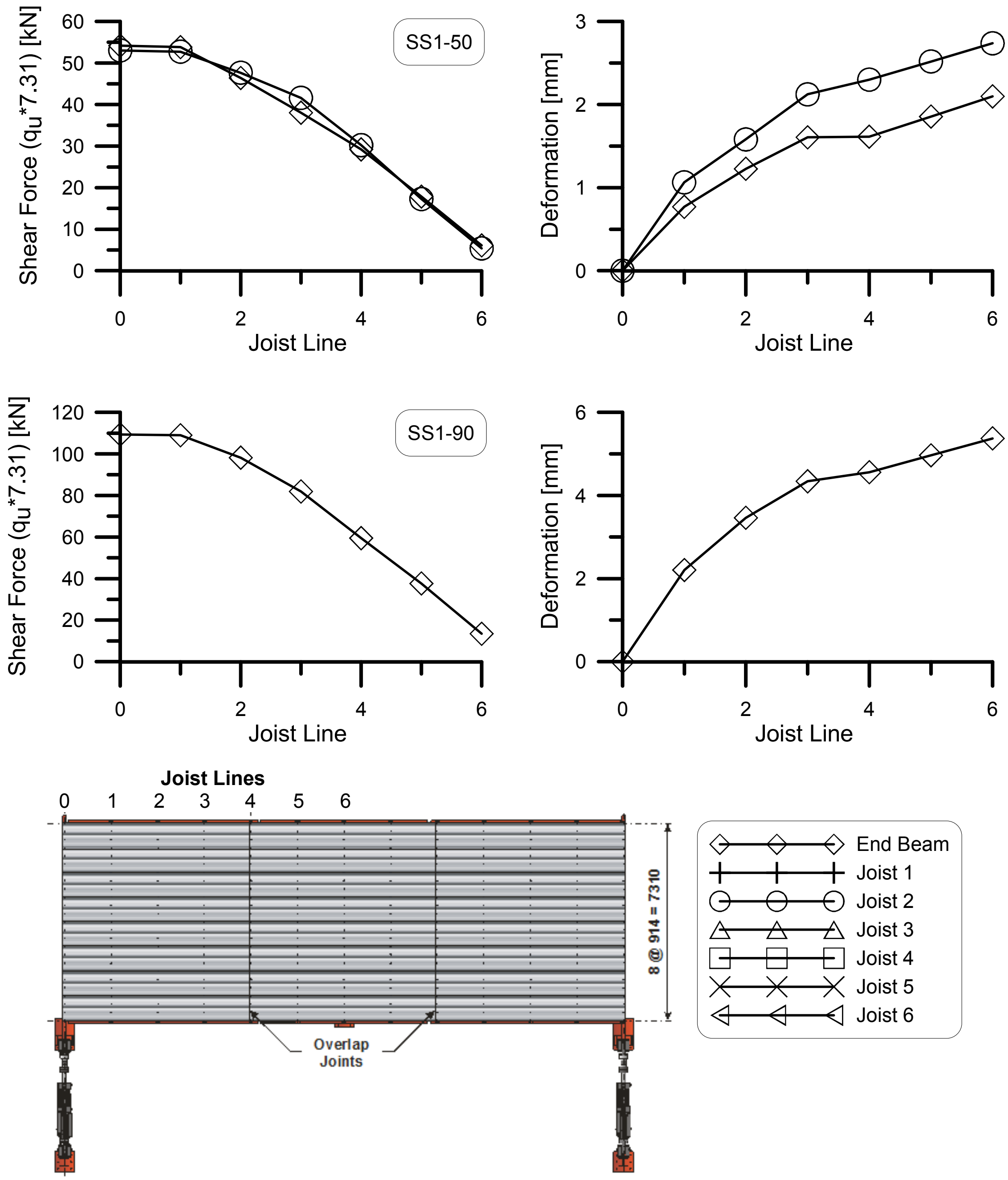

Figure H.17 – DIA9 – Shear force profile and deformation under SS1

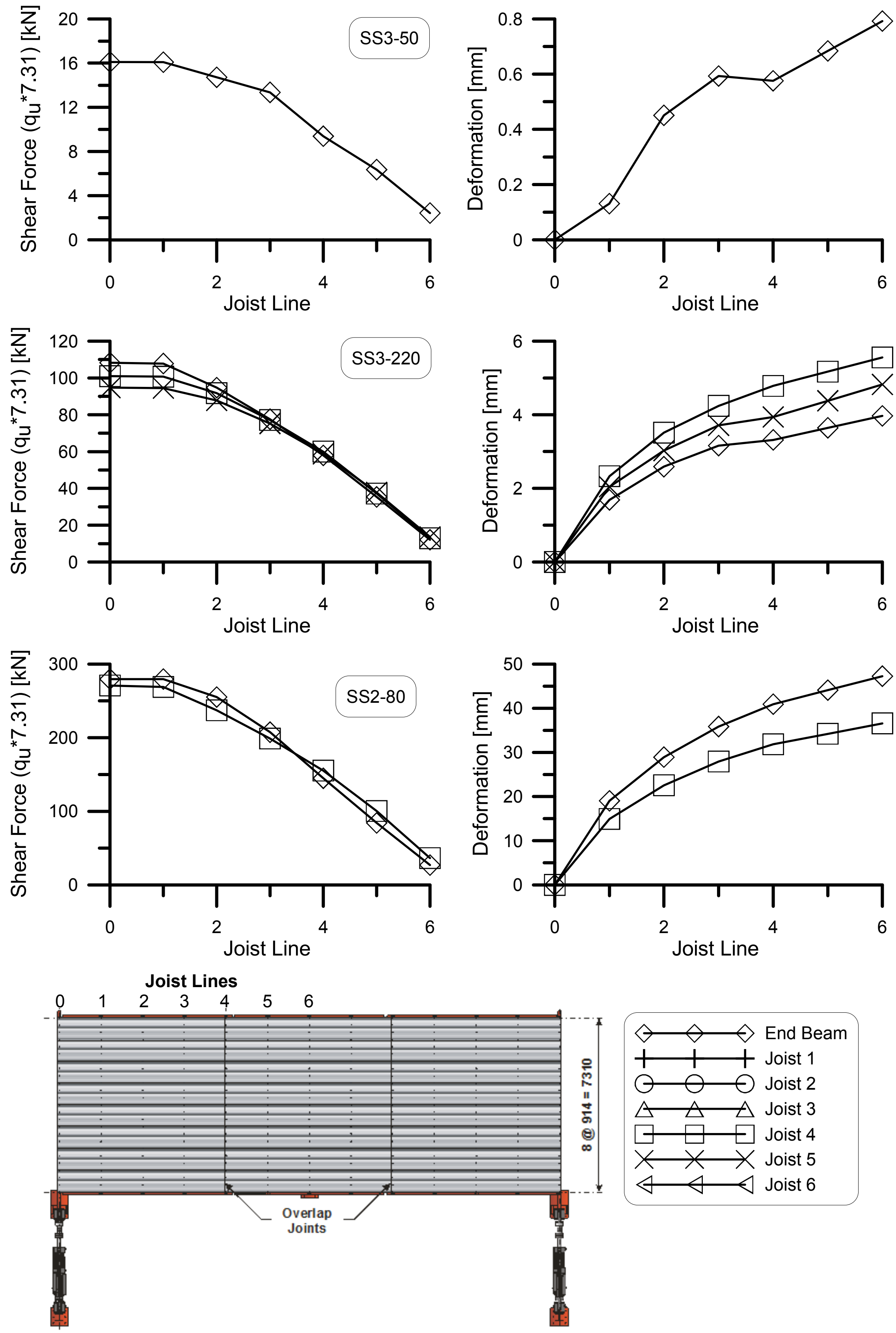

Figure H.18 – DIA9 – Shear force profile and deformation under SS2 and SS3

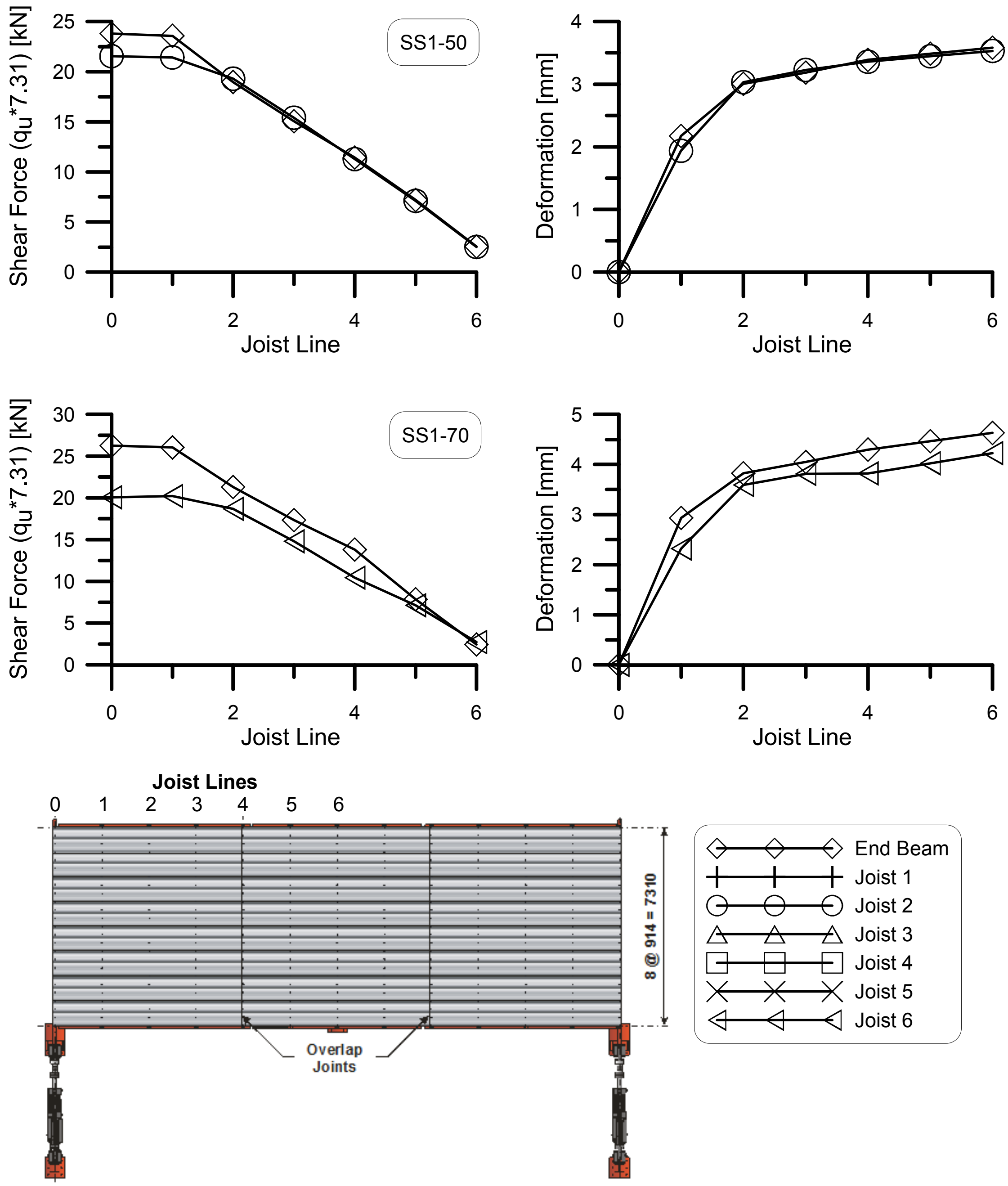

Figure H.19 – DIA10 – Shear force profile and deformation under SS1

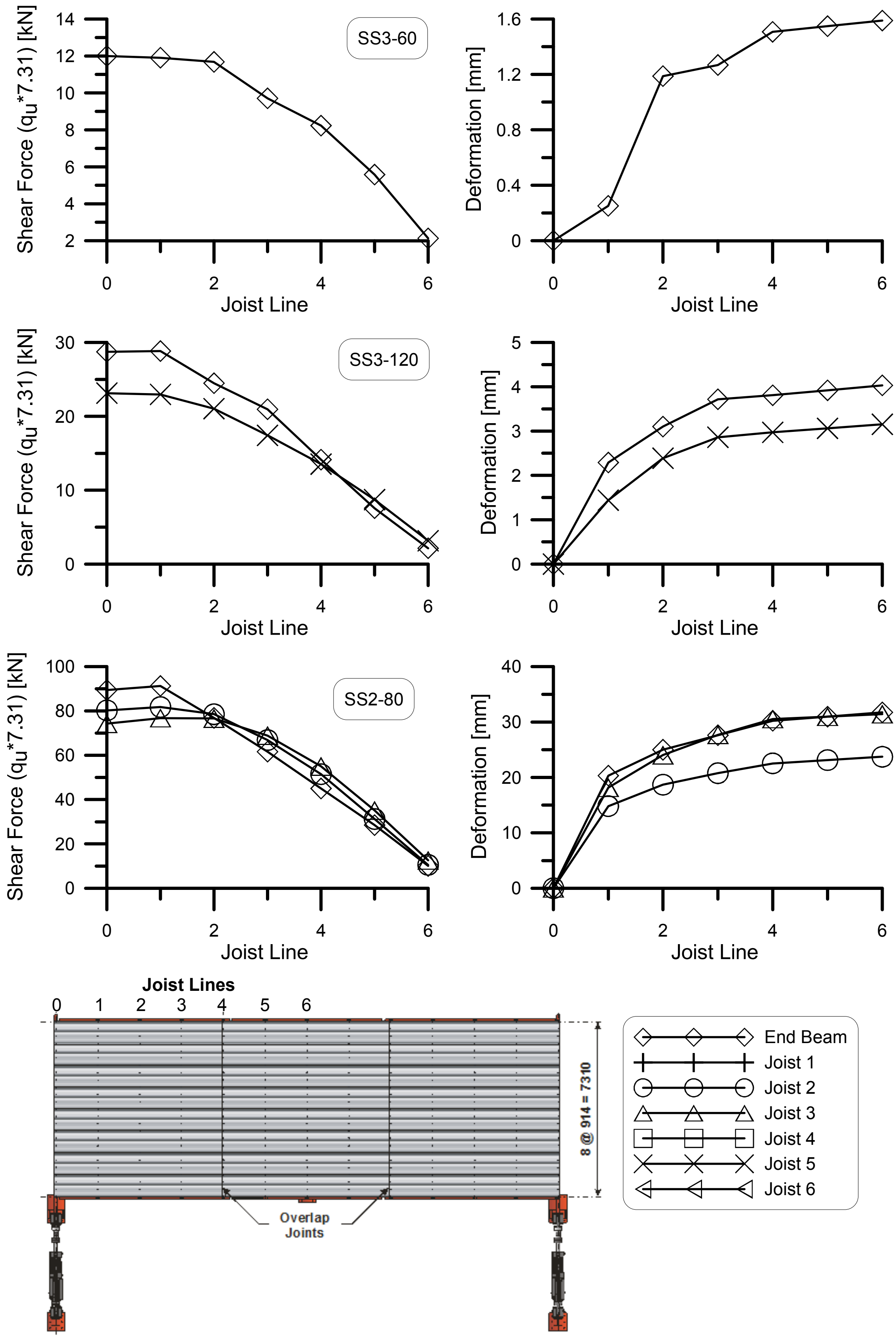

Figure H.20 – DIA10 – Shear force profile and deformation under SS2 and SS3

APPENDIX I: PHASE I & II – SHEAR FORCE PROFILES AND DEFORMED SHAPES FOR REPAIRED DIAPHRAGMS

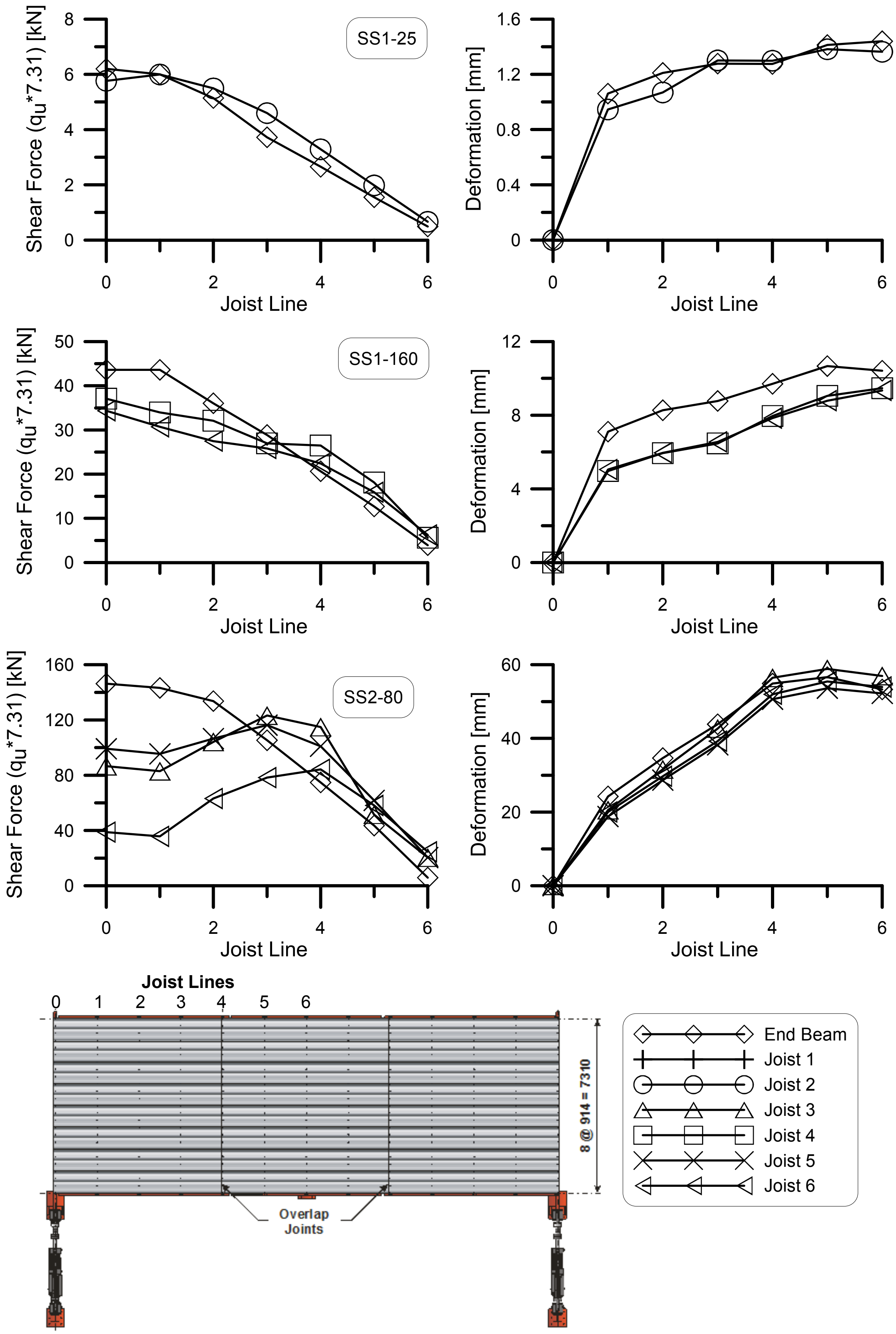

Figure I.1 – DIA1R – Shear force profile and deformation under SS1

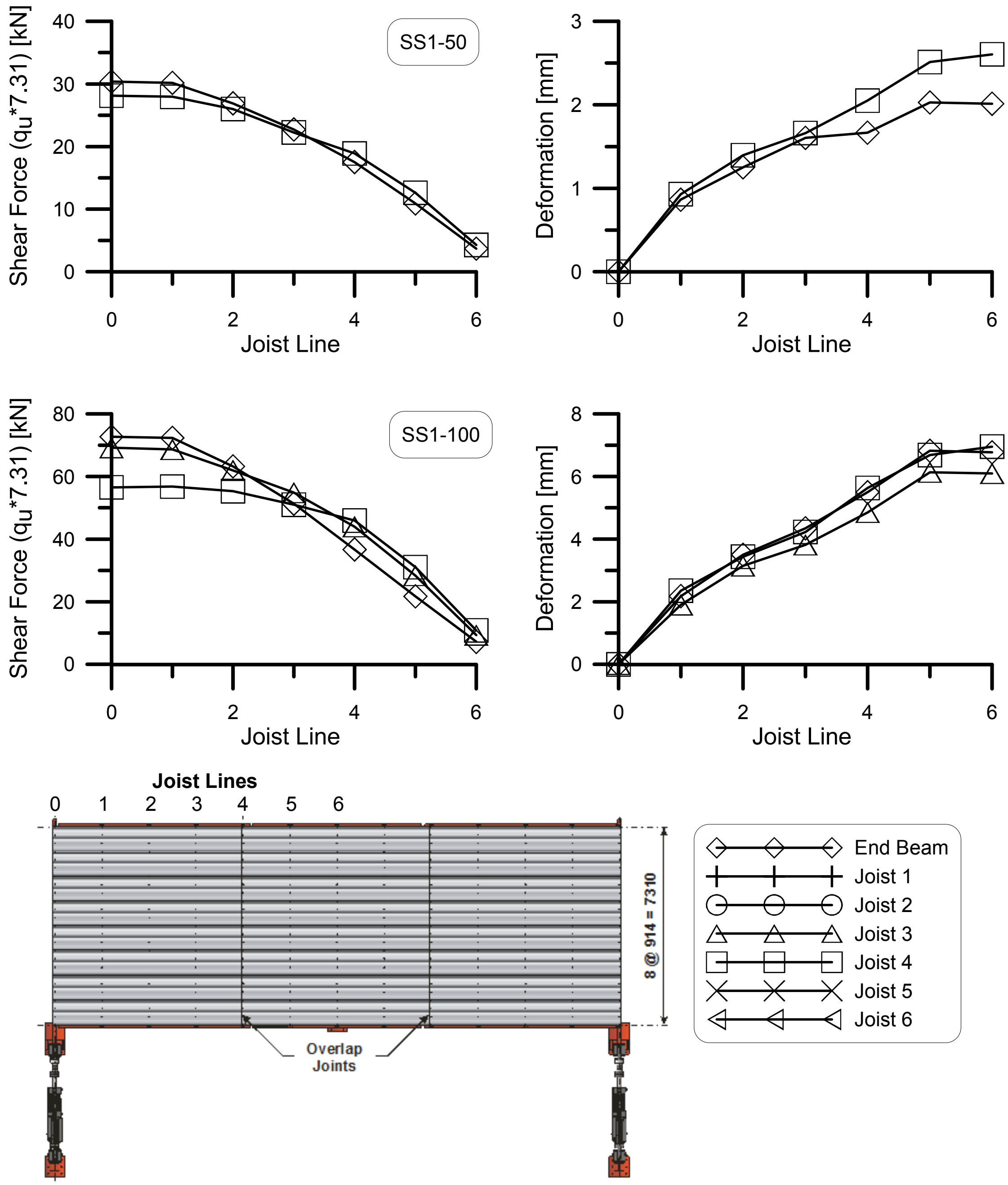

Figure I.2 – DIA3R – Shear force profile and deformation under SS1

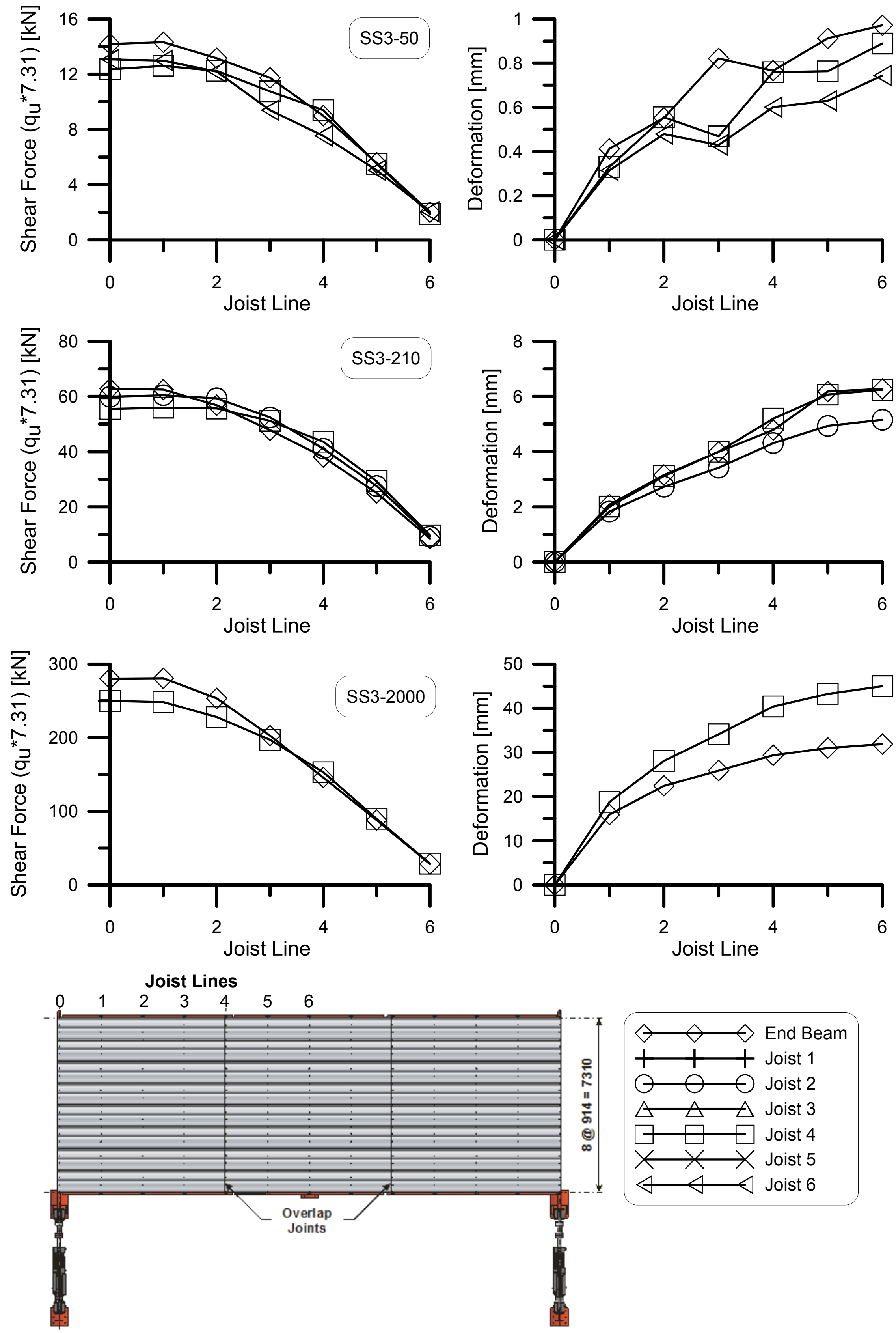

Figure I.3 – DIA3R – Shear force profile and deformation under SS2 and SS3

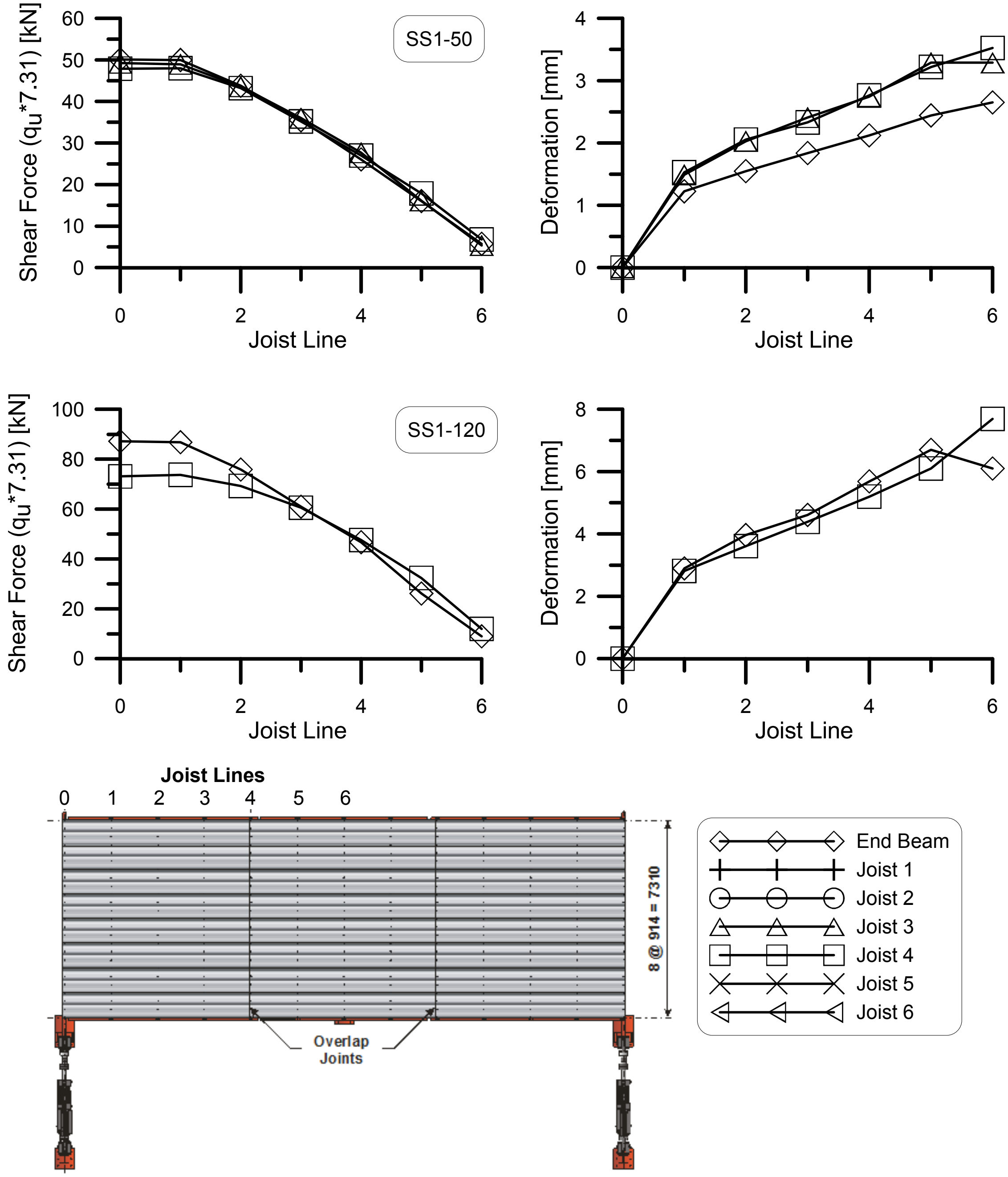

Figure I.4 – DIA4R – Shear force profile and deformation under SS2 and SS3

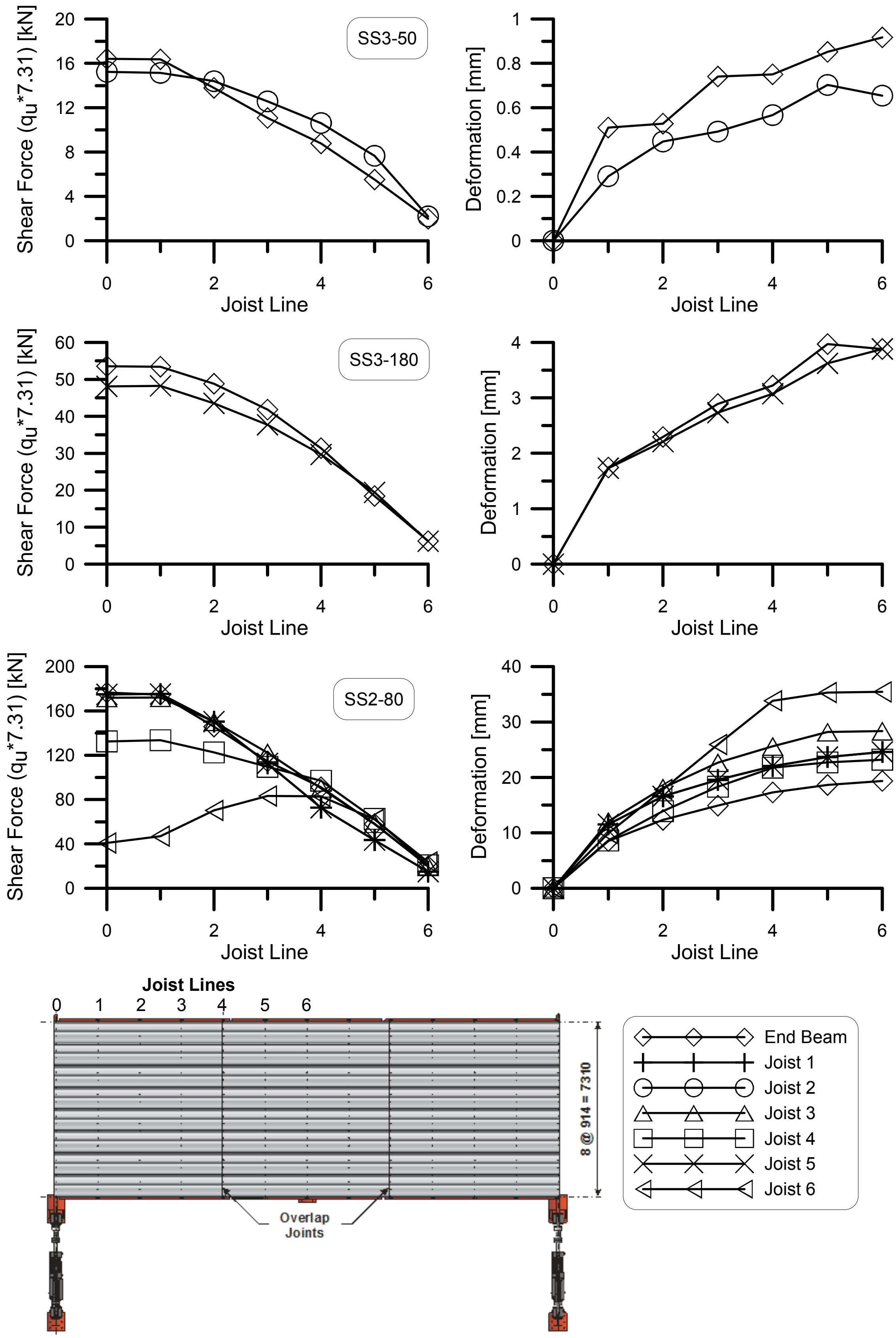

Figure I.5 – DIA4R – Shear force profile and deformation under SS2 and SS3

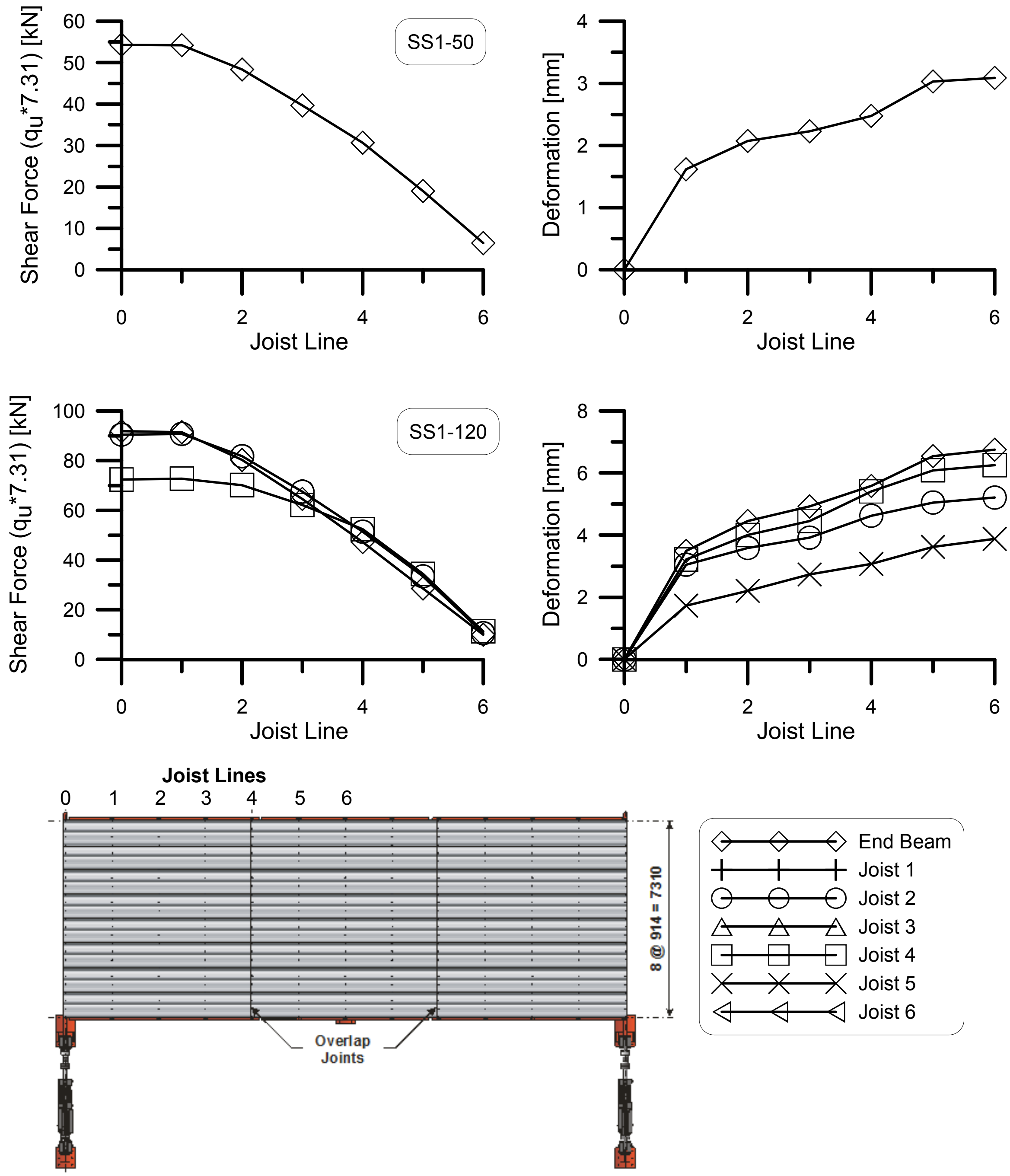

Figure I.6 – DIA5R – Shear force profile and deformation under SS2 and SS3

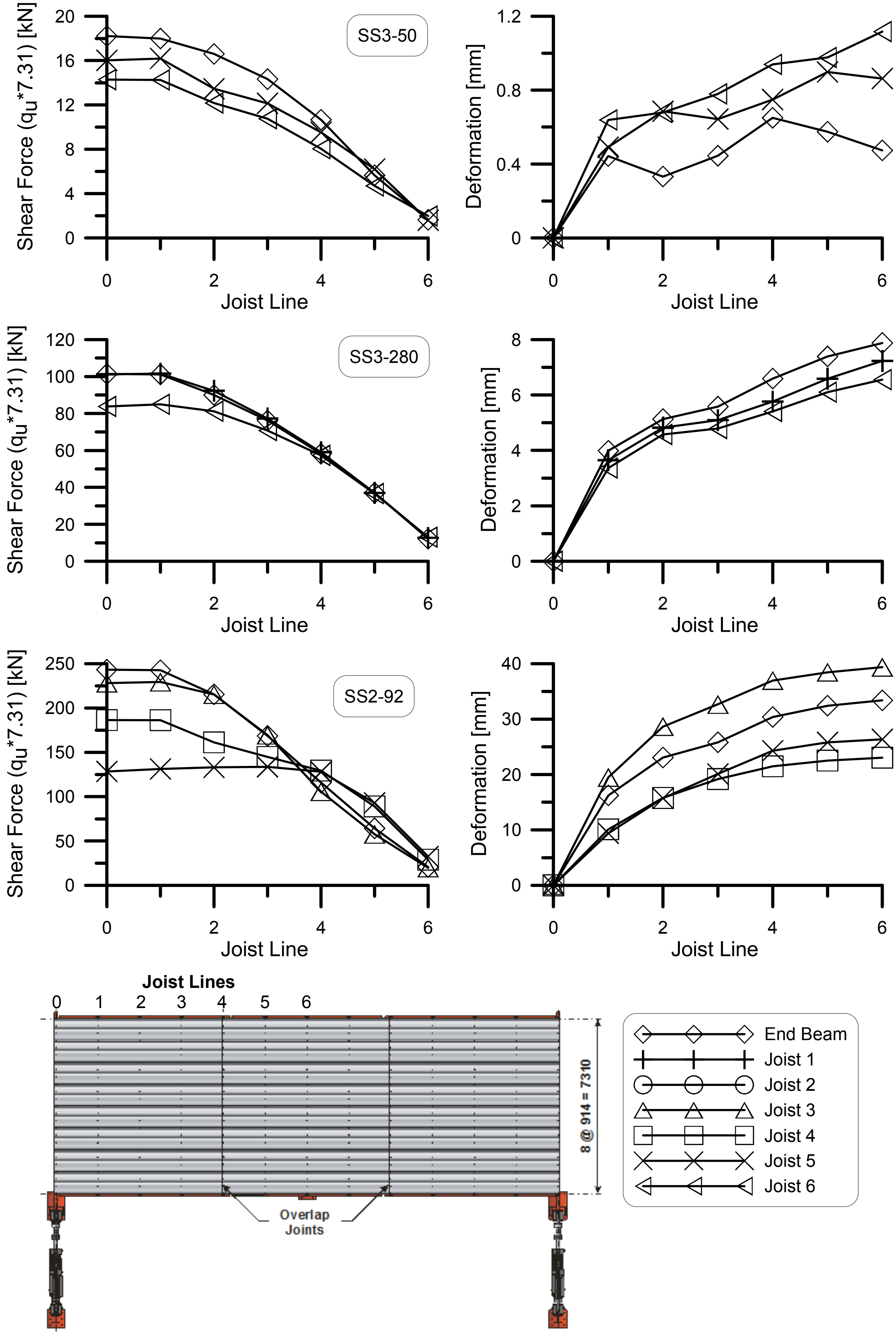

Figure I.7 – DIA5R – Shear force profile and deformation under SS2 and SS3

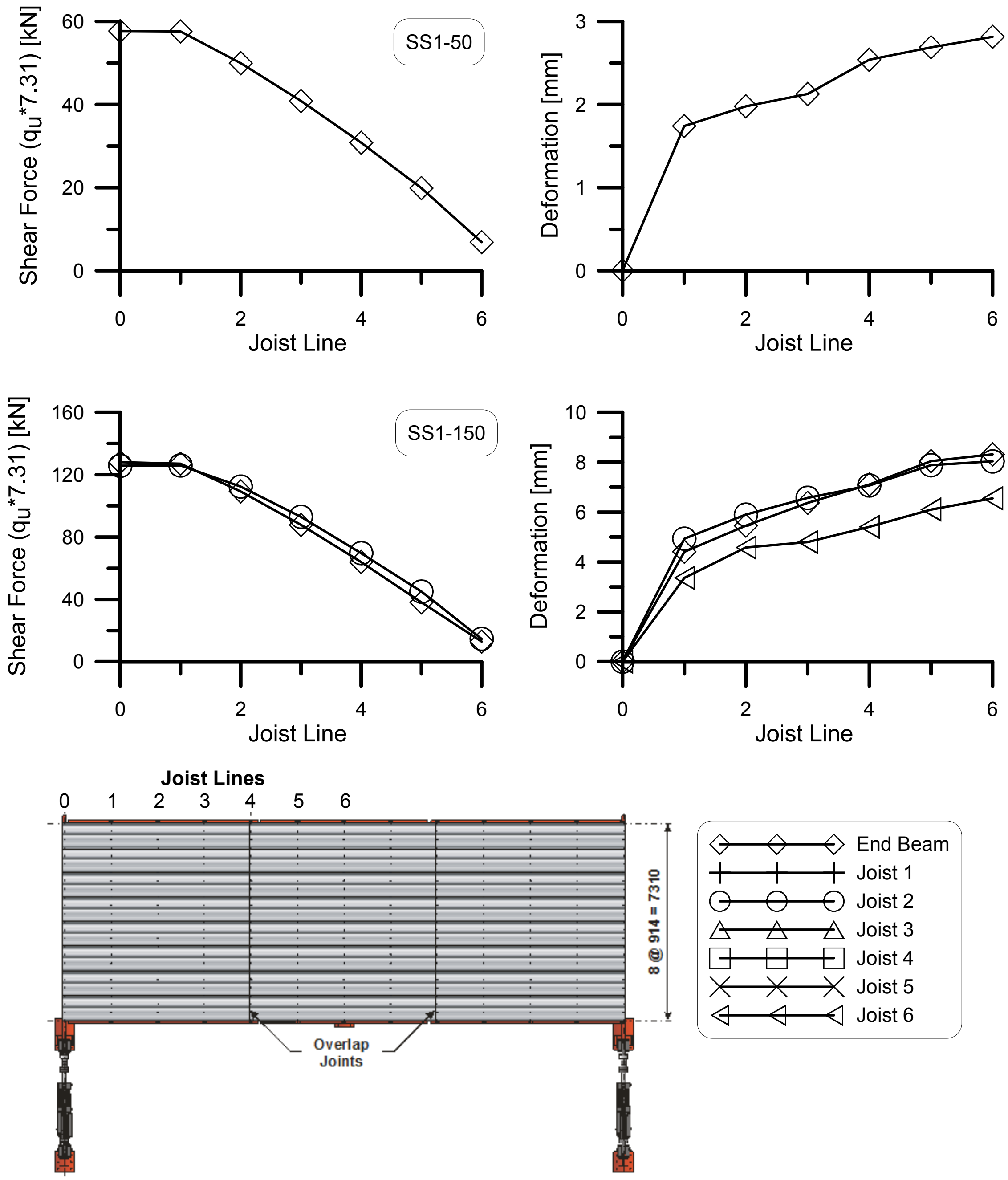

Figure I.8 – DIA6R – Shear force profile and deformation under SS2 and SS3

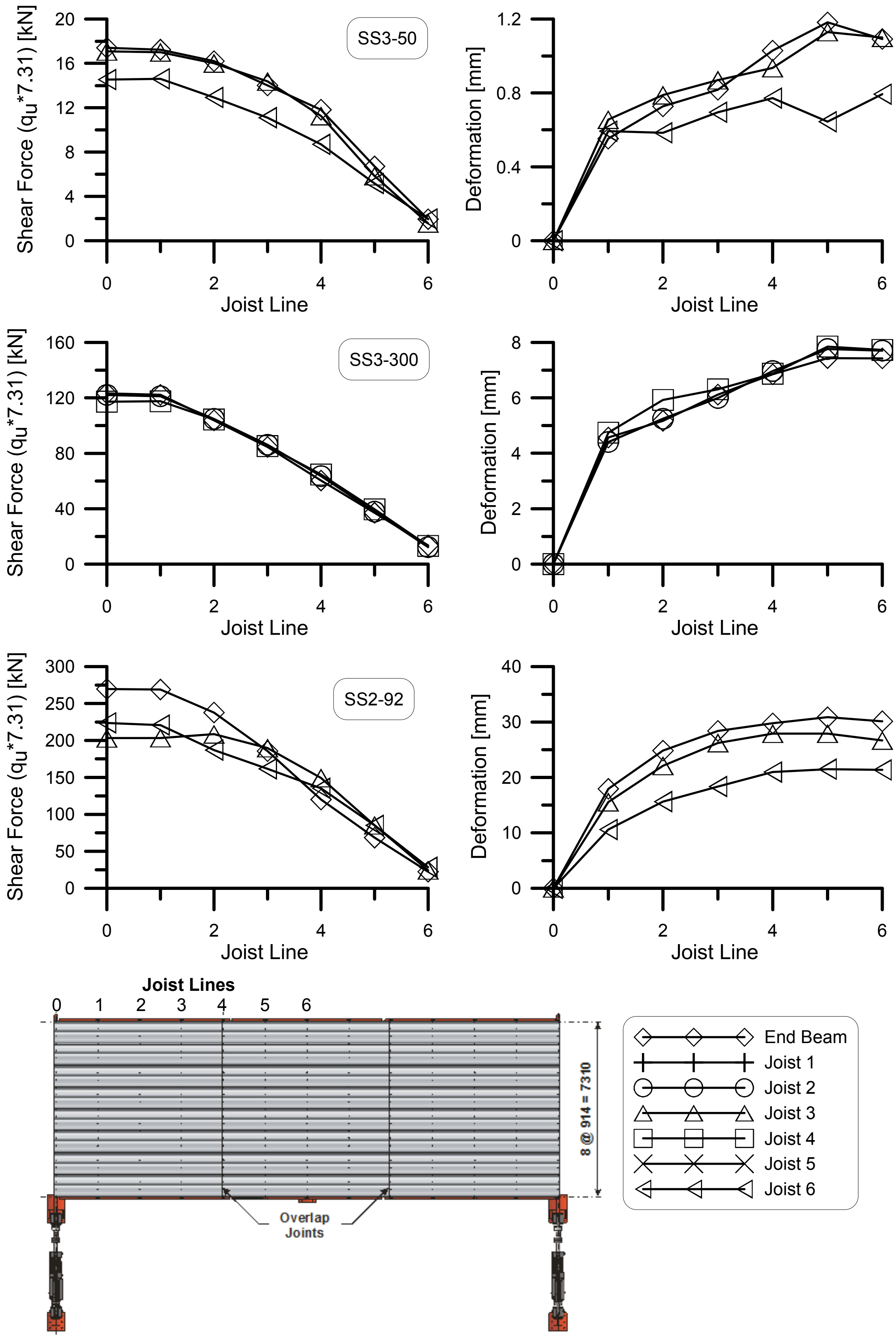

Figure I.9 – DIA6R – Shear force profile and deformation under SS2 and SS3

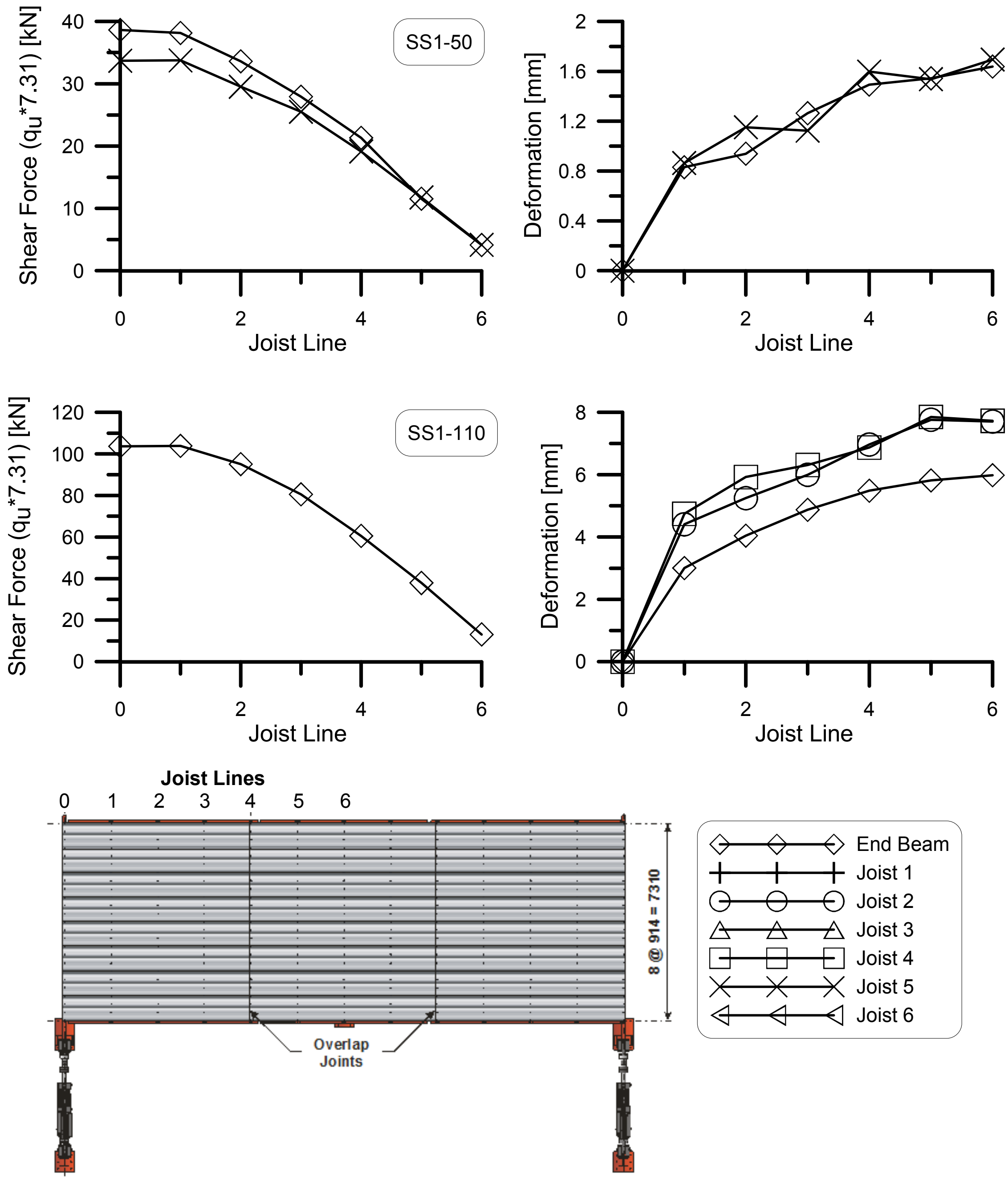

Figure I.10 – DIA7R – Shear force profile and deformation under SS2 and SS3

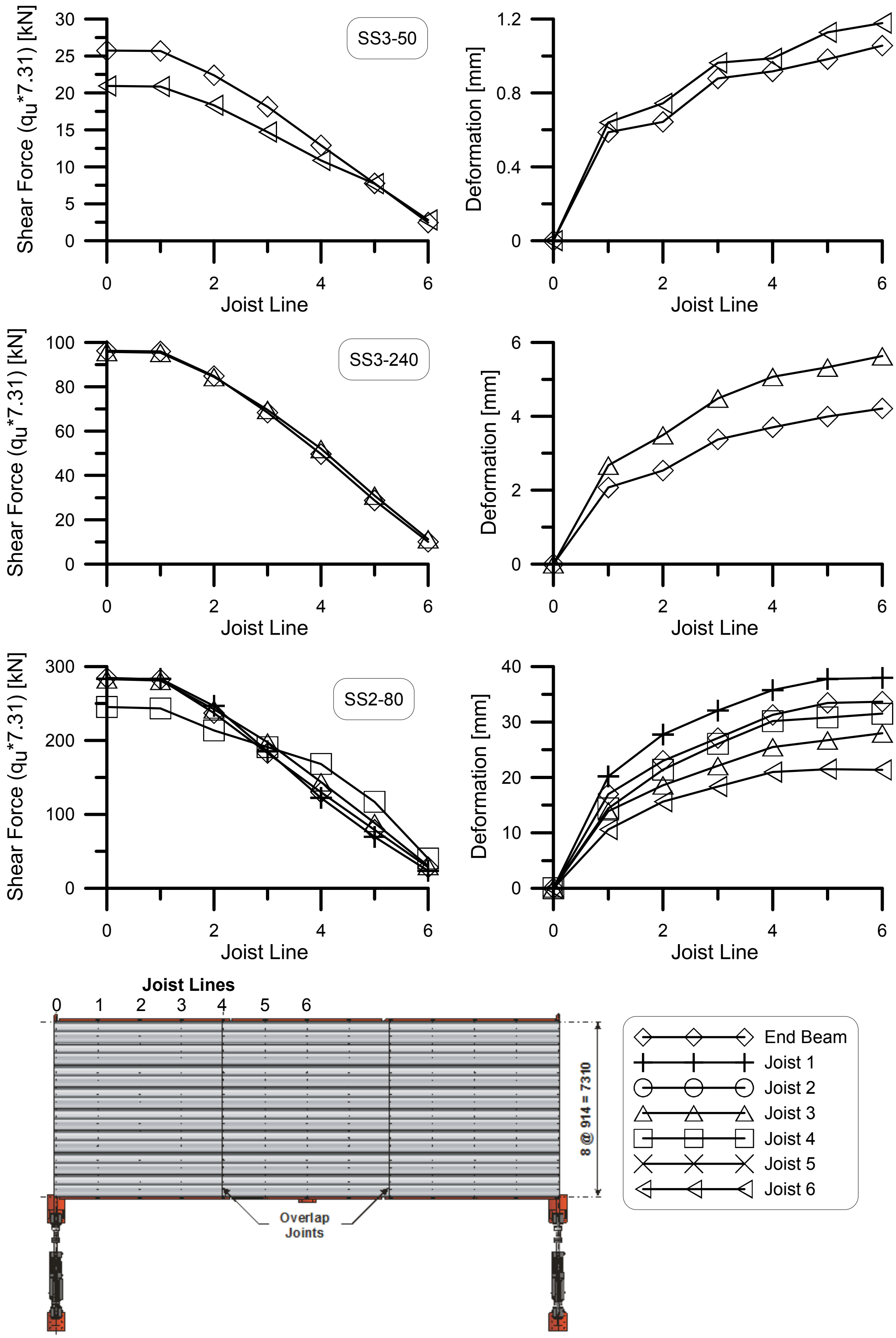

Figure I.11 – DIA7R – Shear force profile and deformation under SS2 and SS3

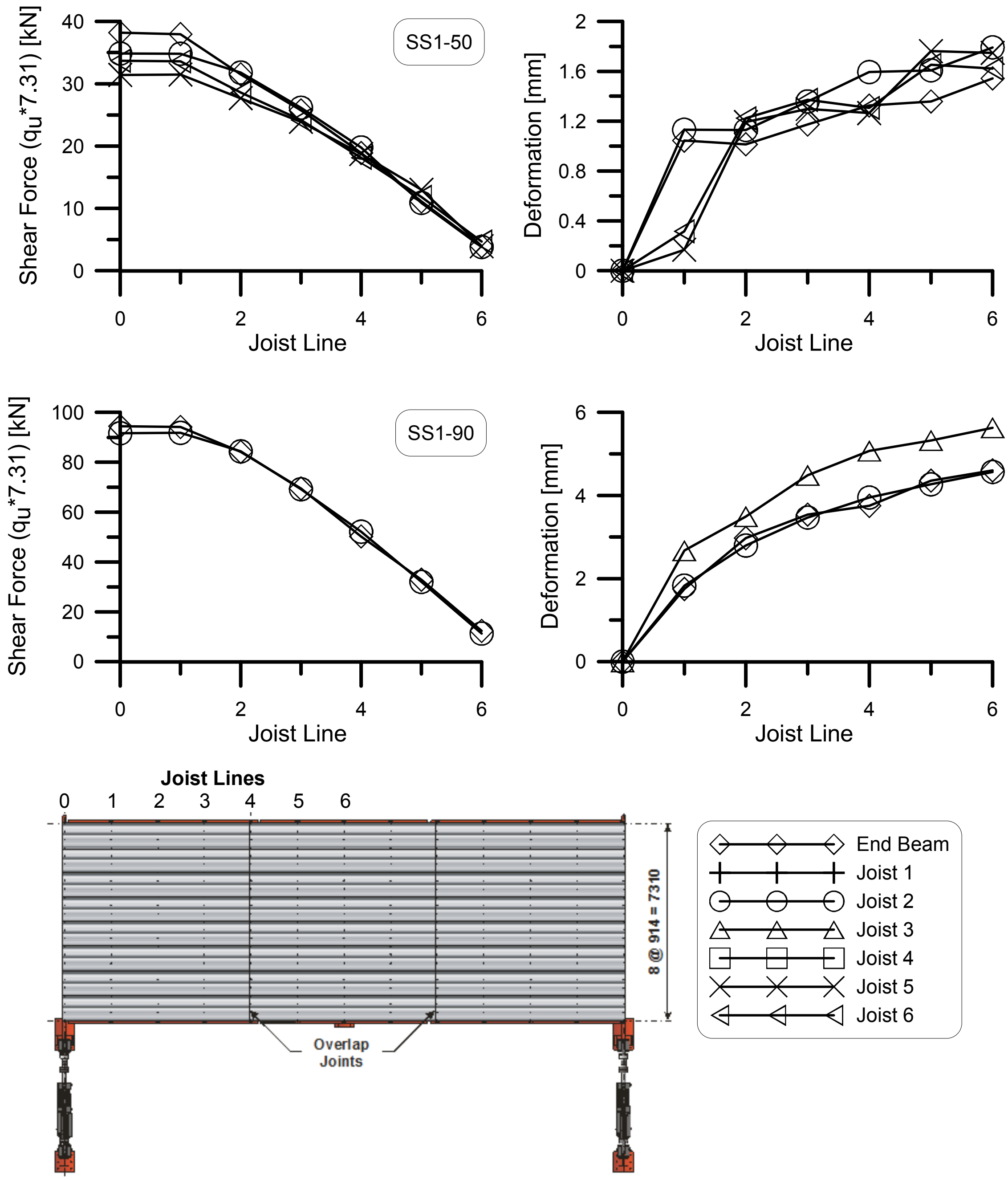

Figure I.12 – DIA8R – Shear force profile and deformation under SS2 and SS3

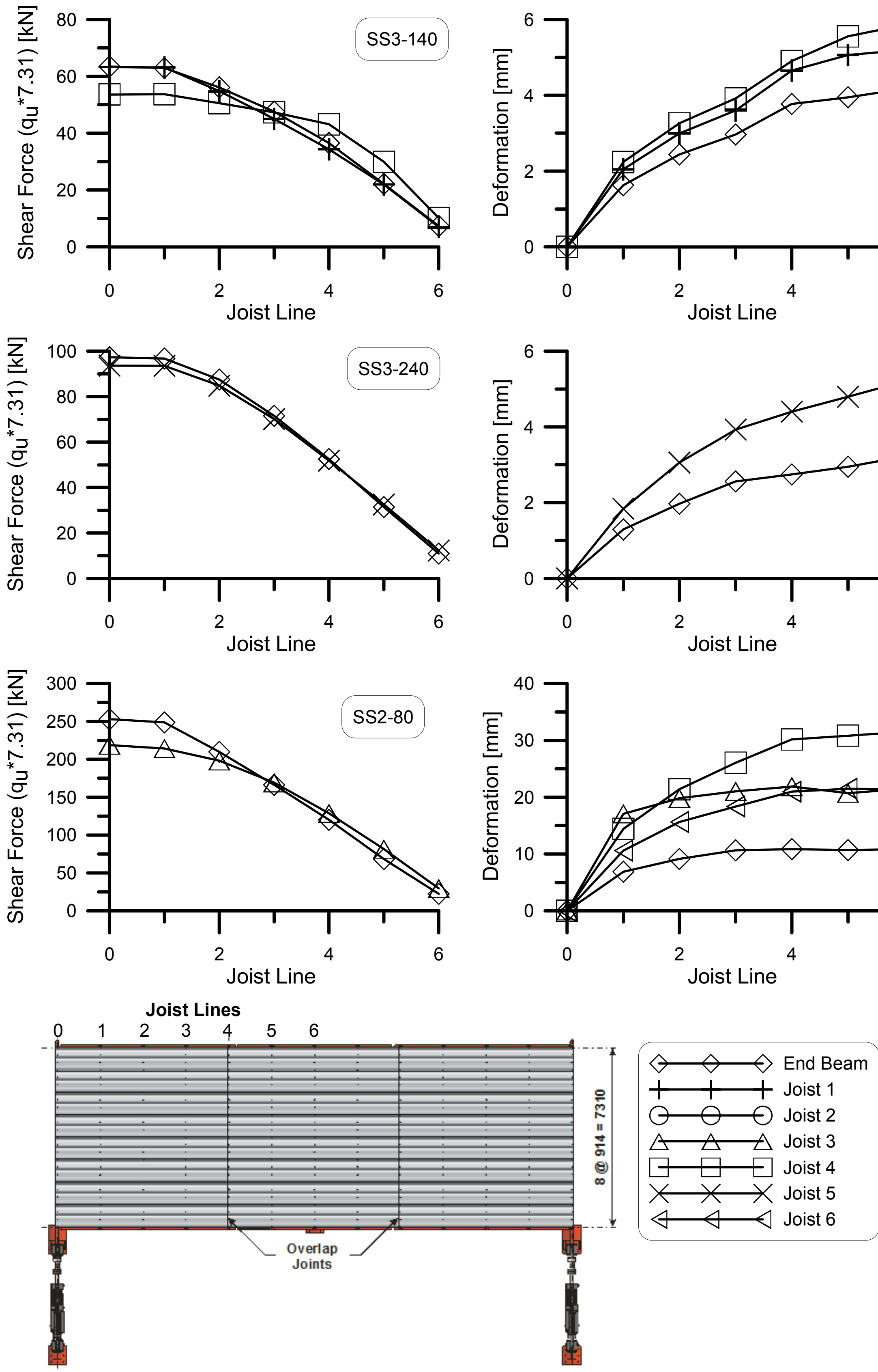

Figure I.13 – DIA8R – Shear force profile and deformation under SS2 and SS3

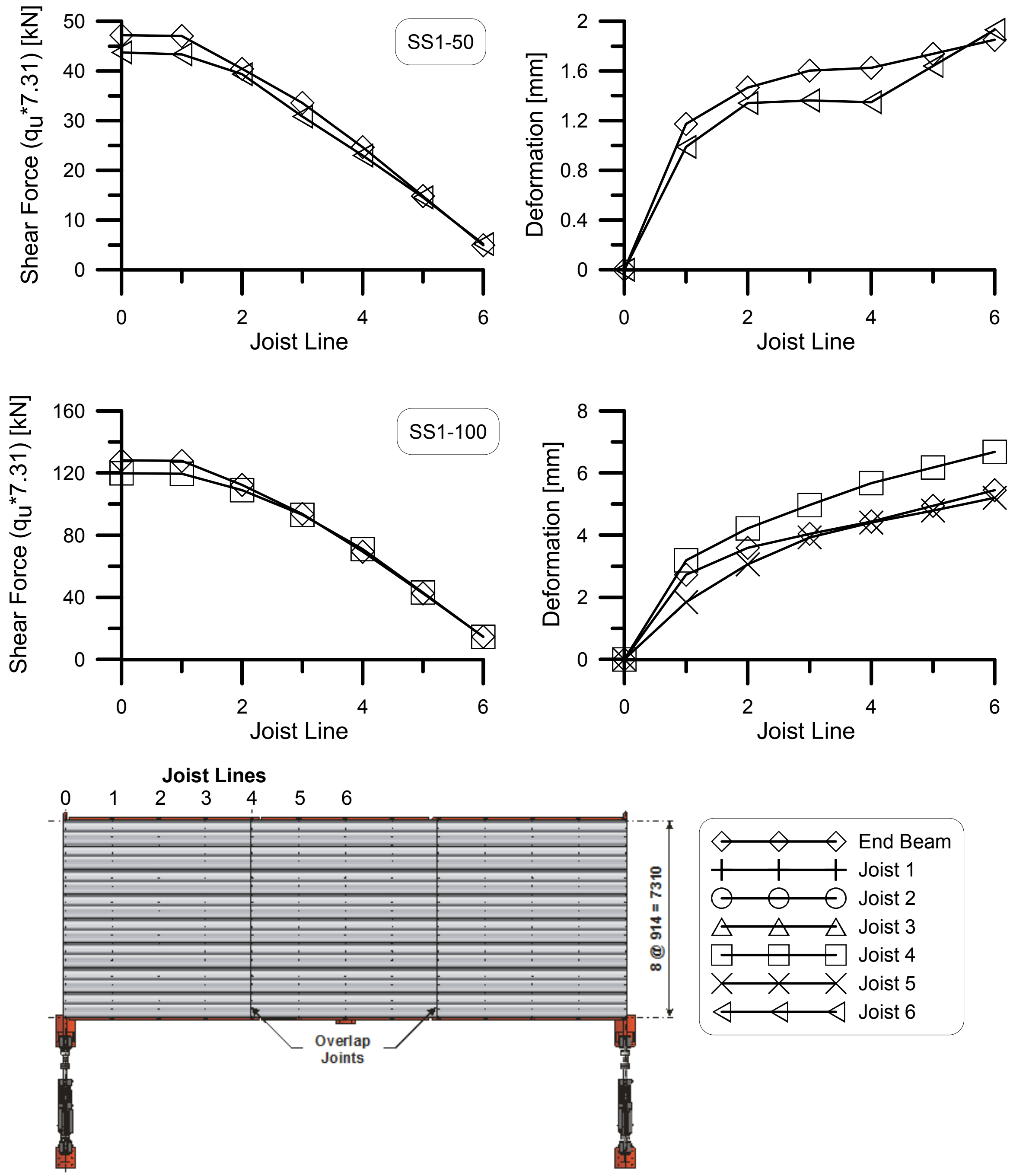

Figure I.14 – DIA9R – Shear force profile and deformation under SS2 and SS3

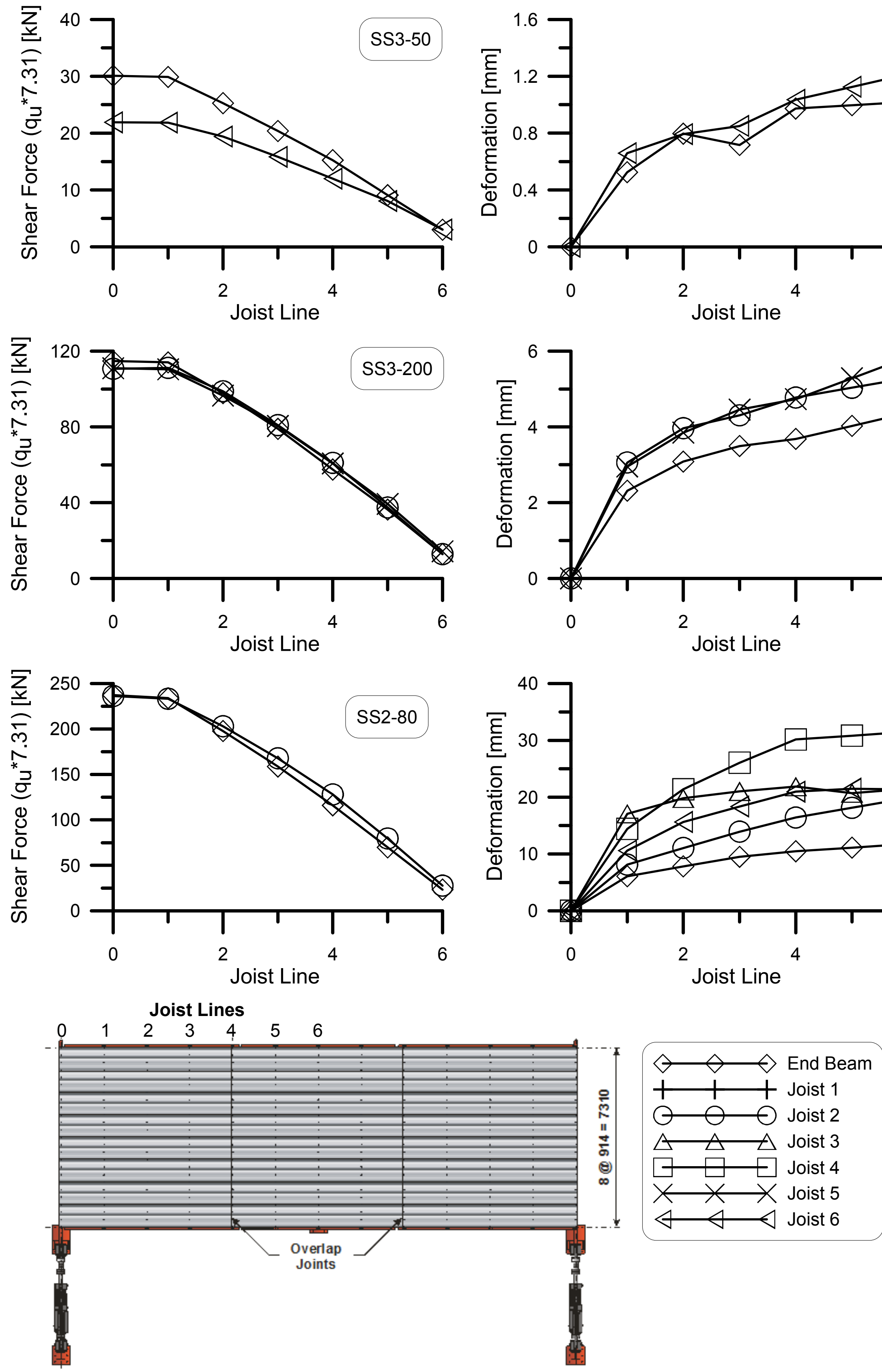

Figure I.15 – DIA9R – Shear force profile and deformation under SS2 and SS3

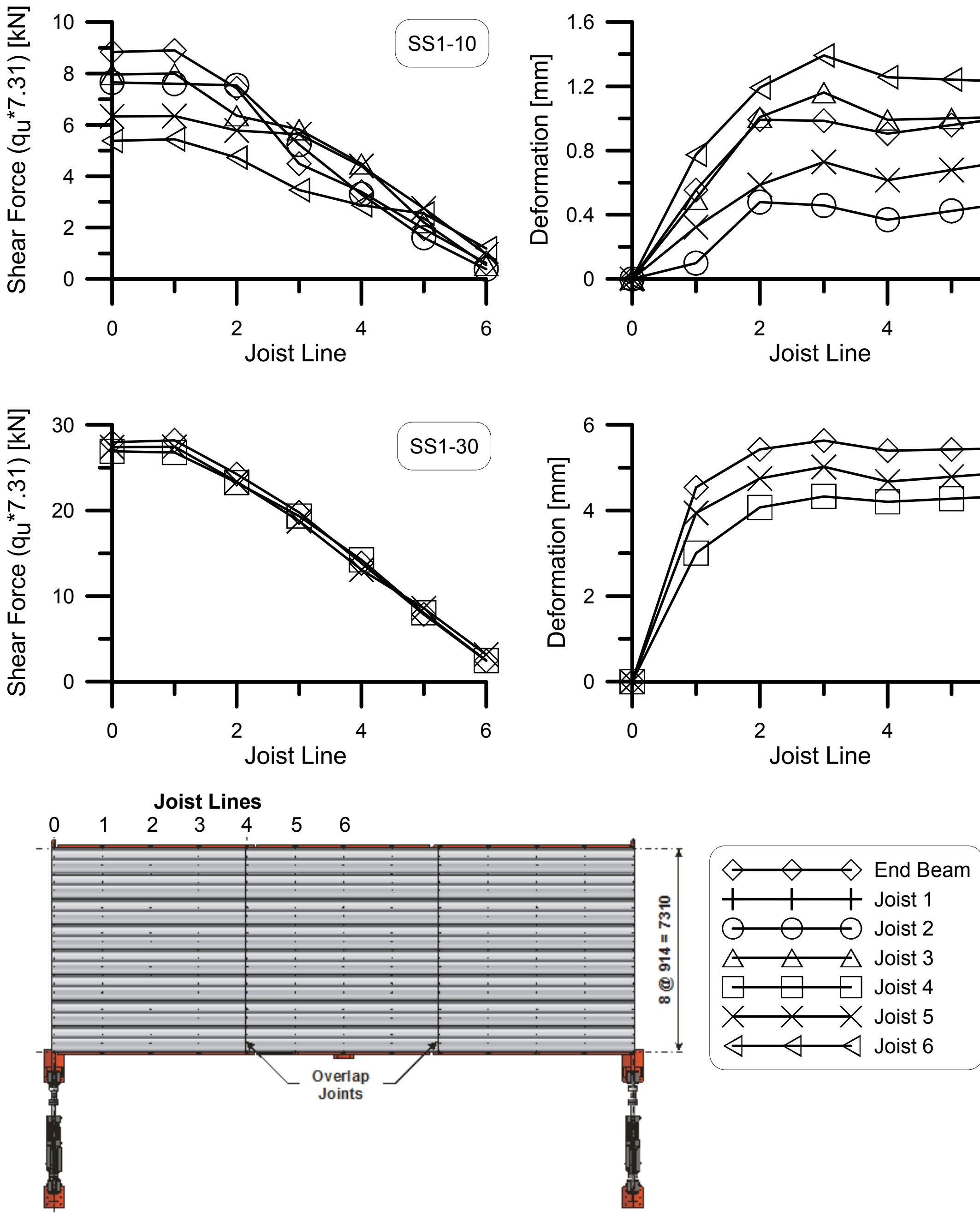

Figure I.16 – DIA10R – Shear force profile and deformation under SS2 and SS3

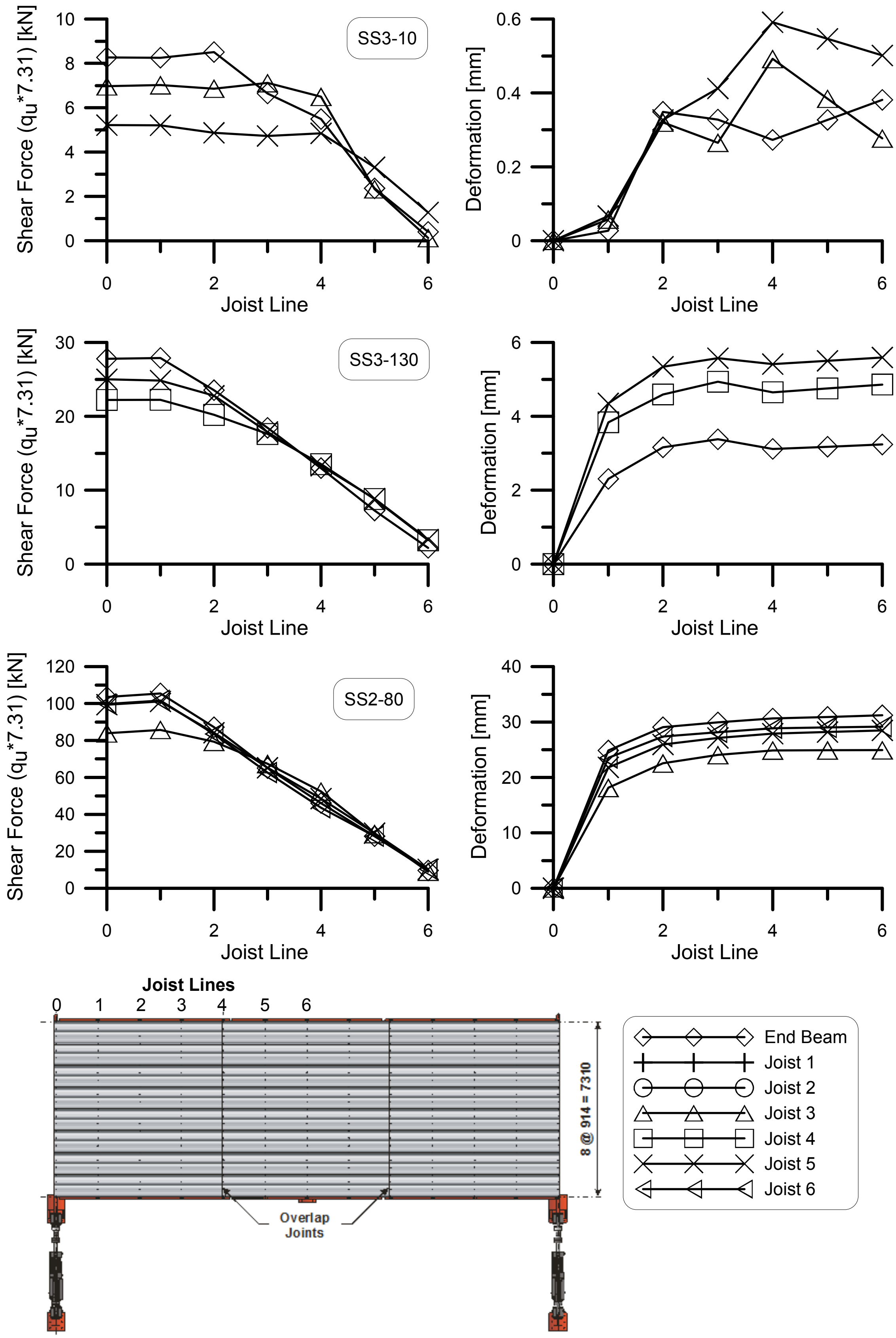

Figure I.17 – DIA10R – Shear force profile and deformation under SS2 and SS3

APPENDIX J: PHASE I & II – DAMPING

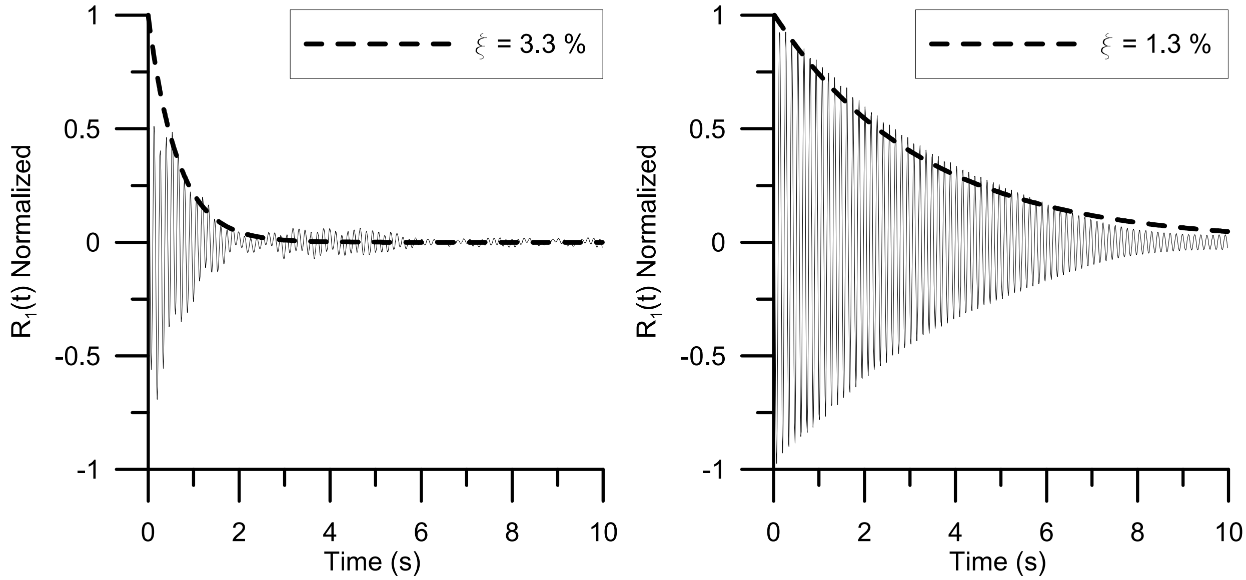

Figure J.1 – DIA4 (left) DIA5 (right) – Time free decay and estimated damping envelope

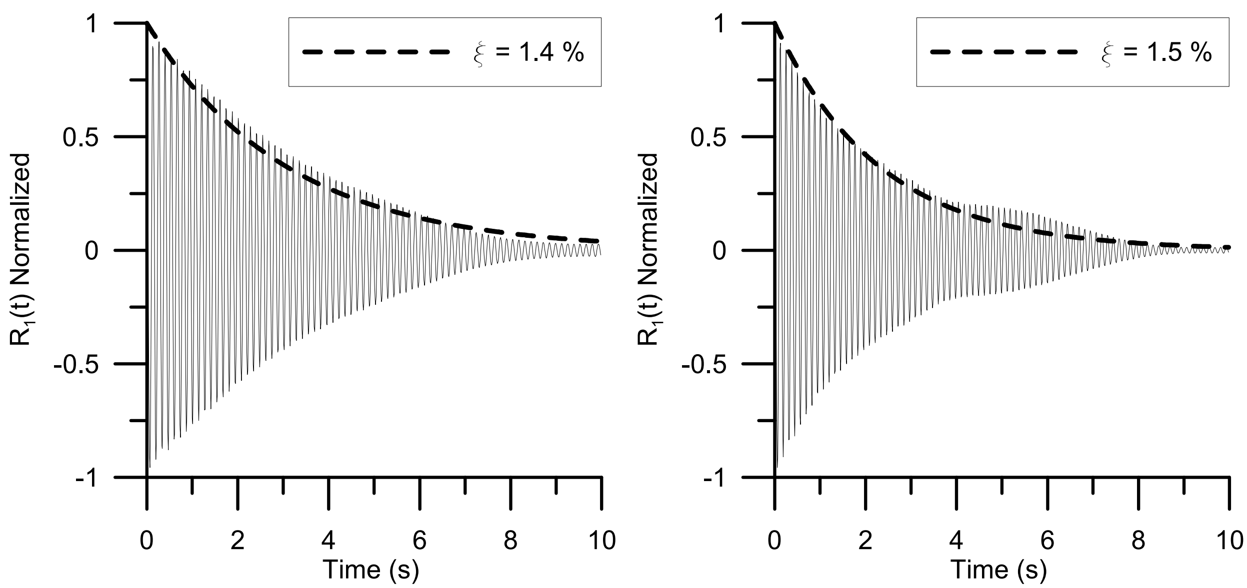

Figure J.2 – DIA6 (left) DIA7 (right) – Time free decay and estimated damping envelope

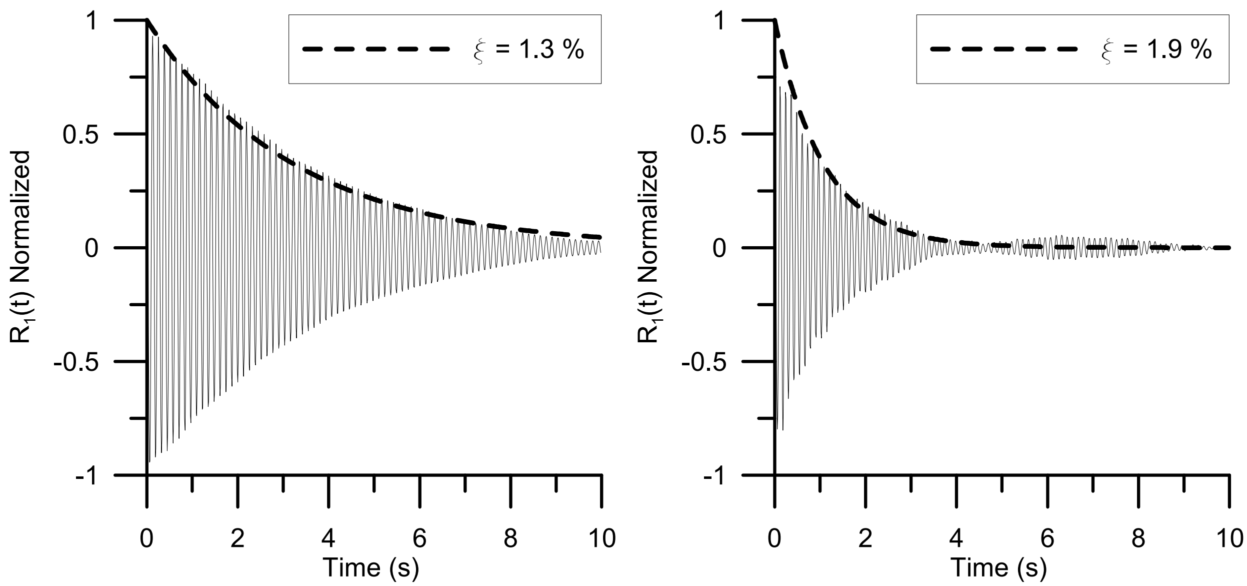

Figure J.3 – DIA8 (left) DIA9 (right) – Time free decay and estimated damping envelope